UNIVERSITÀ DEGLI STUDI DI VERONA

DEPARTMENT OF
Biotechnology

GRADUATE SCHOOL OF
Natural Sciences and Engineering

DOCTORAL PROGRAM IN
Biotechnology

Cycle / year: XXXIV/2018-2021

TITLE OF THE DOCTORAL THESIS

Photosynthetic Antenna Complexes: A Structure-Function Investigation of Light Harvesting and Photoprotection

S.S.D.: BIO/04

Coordinator: **Prof. Matteo Ballottari**

Tutor: **Prof. Roberto Bassi**
Co-Tutor: **Prof. Luca Dall'Osto**

Ph.D. Candidate: **Zeno Guardini**

Summary

List of Abbreviations:

ADP: Adenosine Diphosphate

ATP: Adenosine Triphosphate

ATPase: ATP synthase

Car: carotenoid

CET/F: Cyclic Electron Transport/Flow

Chl: chlorophyll

CRISPR: Clustered Regularly Interspaced Short Palindromic Repeats

Cyt *b6f*: cytochrome *b6f*

DBMIB: dibromothymoquinone

DCMU: 3-(3,4-dichlorophenyl)-1,1-dimethylurea

EM: Electron Microscopy

EMS: ethyl methyl sulfonate

ET: Electron Transport

FD: Ferredoxin

LET/F: Linear Electron Transport/Flow

LHC: Light Harvesting Complexes

Lhca: Light Harvesting Complexes of Photosystem I

Lhcb: Light Harvesting Complexes of Photosystem II

LHC: Light Harvesting Complex

LHCI: Light Harvesting Complex of Photosystem I

LHCII: Light Harvesting Complex of Photosystem II

Lut: Lutein

$NADP^+$: Nicotinamide Adenine Dinucleotide phosphate (oxidized form)

NADPH: Nicotinamide Adenine Dinucleotide phosphate (reduced form)

Neo: Neoxanthin

NPQ: Non Photochemical Quenching

OEC: Oxygen Evolving Complex

P680: Photosystem II Reaction Center

P700: Photosystem I Reaction Center

PAR: Photosynthetic Active Radiation

PBR: Photo Bio Reactor

PC: Plastocyanin

Pheo: Pheophytin

Pi: Inorganic Phosphate

PQ: Plastoquinone

PS: Photosystem

PsbS: Photosystem II subunit S

PSI: Photosystem I

PSII: Photosystem II

qE: energy dependent quenching

qI: inhibition depenedent quenching

qT: state transition dependent quenching

RC: Photosystem Reaction Center

ROS: Reactive Oxygen Species

RuBisCO: Ribulose-1,5-bisphosphate Carboxylase / Oxygense

VDE: Violaxanthin De Epoxidase

Vio: Violaxanthin

ZE: Zeaxanthin Epoxidase

Zea: Zeaxanthin

α- car: α- carotene

β- car: β- carotene

Abstract

Photosynthesis is the process that uses sunlight energy to convert inorganic CO_2 into sugars. This process is carried out by both microalgae and higher plants. During evolution, photosynthetic organisms developed several strategies to optimize the capture of light and funnel solar energy to the reaction centers (RC) of the photosystems (PS), which instead, remained essentially unchanged. Both PS, PSII and PSI, are equipped with a Light Harvesting system made of the so-called antenna proteins or Light Harvesting Complexes (LHC) aimed to increase the capture of solar radiation and transfer excitation energy, through pigment molecules, toward the RC. In general, a large antenna system is an advantage for plants, allowing for harvesting a larger fraction of the incident solar radiation, however under excess light conditions or when plants (or algae) are cultivated in dense canopies this may lead to a general loss of productivity. Indeed, under excess light conditions photosynthetic organisms intercept an excess of light that can easily result in the production of dangerous reactive oxygen species (ROS), responsible for damaging cell structures possibly causing cell death. On the other hand, the intensive cultivations forces plants, or algae to grow extremely closed to each other, thus determining self-shading effects that reduce light penetration within cultures. Under these conditions, the top of the canopy (or the external layer of algae cultures) is reached by strong radiation that could induce photooxidation while leaves in the inner part of the canopy (or in the inner layers of algae cultures) are exposed to suboptimal irradiances. Taken together, all these factors influence net productivity of cultures that, in field conditions, ranges around 1-2% of solar energy conversion into sugars, despite a theoretical yield of about 12%. This low yield is one of the few traits of cultures that is still far from its theoretical upper limits and has become a promising target toward improving crop yields. The engineering of LHC is a promising strategy to improve light management in algae cultures. Indeed, algal strains with a reduced antenna system showed better growth performances under intensive cultivation conditions; this is mainly due to the increased light penetration within the medium, allowing for a more homogeneous distribution of the light in the culture layers. On the plants side, recent studies revealed that a possible strategy towards the improvement of crop yield could be the tuning of photoprotective mechanisms to increase the fraction of solar radiation converted into biomass and reducing the amount dissipated as heat. These approaches, in both microalgae and higher plants, have been useful to improve yields. Yet many aspects need to be further clarified and there is still room for improvement towards the production of more productive strains that will be fundamental in the future to cope with the increasing food demand worldwide.

The aim of the thesis

The aim of this thesis is to understand the molecular basis of the mechanisms that regulate: i) light-harvesting, ii) photoprotection and iii) the role that LHC proteins plays in the supramolecular organization of thylakoid membranes in the chloroplasts. We focus our attention on two different species: the green microalga *Chlorella vulgaris,* a highly productive specie suitable as biofuels source and the model specie *Arabidopsis thaliana:* easy to transform, fully sequenced

and with a wide variety of knockout mutants already available, a useful trait for reverse genetics investigations.

We applied a direct evolution approach on *C. vulgaris* strains to increase high-light tolerance and resistance to photooxidation, while on *A. thaliana*, we applied a combination of CRISPR-Cas9 genome editing and site-directed mutagenesis to investigate the physiological and structural functions of specific LHC moieties and domains.

Chapter 3: The Light-Harvesting system as a target for improvement of algal growth in photobioreactors.

In Chapter 3 we focused on the microalga *C. vulgaris.* We treated cells with the mutagen ethyl methyl sulfonate (EMS) to induce random mutations. We selected mutant pale green colonies, thus allowing for a better light penetration under photobioreactor conditions (high-light and high cell density). The pale green phenotype was further submitted to mutation/selection for enhanced resistance to oxidative stresses or increased carotenoids content. To enhance the resistance of the strains to photooxidation, we treated the mutagenized population with Rose Bengal, a reagent that, upon illumination, produces singlet oxygen. The mutant strains we obtained, referred to as SOR (Singlet Oxygen Resistant), revealed improved growth performances under photobioreactor conditions, in both high and low light regimens. To increase carotenoids content, we selected the mutagenized population on a medium containing the herbicide Norflurazon, an inhibitor of the biosynthesis of carotenoids. We obtained the NFR (NorFlurazon Resistant) strains, pale green mutants that accumulate a higher content of carotenoids and are more tolerant to excess light conditions. Taken together, our results confirmed that the strategy to combine reduced antenna size and increased photo-tolerance is effective in the development of algal strains suitable for industrial applications, optimized for growth in photobioreactors.

Chapter 4: Physiological characterization of *Arabidopsis* mutants devoid of trimeric LHCII.

From chapter 4 we moved to the model specie *A. thaliana*. In this chapter, we applied genome editing to knock-out trimeric LHCII encoding genes producing Arabidopsis lines lacking trimeric LHCII (*koLHCII*) or both monomeric and trimeric PSII antenna complexes (*koLhcb*). In the first part of the Chapter (4.1) we investigated the genetic factors involved in the formation of the typical membrane organization of thylakoid of higher plants. In higher plants thylakoid are organized into appressed regions (grana) hosting PSII connected by linear membranes (stroma lamellae) where PSI are localized. This kind of organization has been achieved during evolution; indeed, the organization level of membrane increases from cyanobacteria to vascular plants. This special architecture seems to be developed to optimize the PSII repair cycle and avoid energy spillover between PSII and PSI. Recent structural studies proposed monomeric and trimeric Lhcb complexes as responsible for the stabilization of grana stacks. To verify this hypothesis, we applied CRISPR-Cas9-mediated genome editing to obtain *Arabidopsis* mutant lines that lack monomeric (Lhcb4-5), trimeric (Lhcb1-3), or both (Lhcb1-6) antenna complexes. It is worth noting that the chloroplasts of mutant lines lacking all the PSII antenna proteins (Lhcb1-6) completely

lost the typical stroma-grana organization. Our investigation confirmed that both classes of Lhcb are needed for the formation of grana stacks, with special roles played by the monomeric Lhcb5, mainly implicated in the stabilization of the stackings and Lhcb2 involved in the dynamic regulation of grana membranes induced by light.

In the second part of Chapter 4 we carried out the physiological characterization of the mutant lines produced in Chapter 4.1. This analysis confirmed the role of monomeric Lhcb proteins in Non-Photochemical Quenching (NPQ) activation, responsible for the fast activation of quenching reactions. On the other hand, trimeric LHCII confirmed its important role in heat dissipation, being responsible for the largest fraction of NPQ induction. The latter is a photoprotective mechanism activated by plants upon rapid exposure to excess light conditions. NPQ is switched on within seconds or minutes and allows for the dissipation as heat of up to 80% of the total excitation energy. Under excess light conditions the lumen of thylakoids accumulates protons, thus determining a drop in the pH, sensed by PsbS, that triggers the activation of qE, the fastest component of NPQ. PsbS is a pigment-less LHC-like protein. Since excited states depends on the presence of chlorophylls and quenching processes are mainly catalyzed by carotenoids, PsbS appers to be unable to directly perform quenching reactions of energy absorbed in excess. Indeed, this function is played by Lhc proteins. Although this aspect has been investigated for many years, several details are still under debate. One of these is the involvement of monomeric Lhcb complexes in the overall mechanism. In this study we tried to attribute the intrinsic photoprotective capacity of monomeric and trimeric Lhcb, thus revealing a higher photoprotection for the monomeric ones. In this chapter, we also produced multiple knockout mutants lacking LHCII (Lhcb1-3) and other NPQ activation components: PsbS (*npq4*), zeaxanthin (*npq1*), and lutein (*lut2*). This approach revealed that the NPQ mediated by monomeric Lhcb is fully dependent on zeaxanthin, while the role of lutein seems to be negligible, although further research in this field is needed. The lack of both LHCII and PsbS showed the presence of at least an additional quenching site within PSII, that we attributed to the core complex. Our results allowed us to draw an NPQ activation model comprising: PsbS, zeaxanthin, PSII-core, monomeric Lhcb (Lhcb4) and trimeric LHCII.

Chapter 5: *In vivo* site-directed mutagenesis of Lhcb4 chlorophyll binding sites

While results achieved in Chapter 4.2 highlighted how monomeric Lhcb are involved in the photoprotection of higher-plants and participate in the mechanism of NPQ, chapter 5 is dedicated to the *in vivo* site-directed mutagenesis of one of these, namely Lhcb4. Chlorophylls binding sites were targeted to verify their role in NPQ. According to literature, among monomeric Lhcbs, the most promising candidate in mediating quenching reactions is Lhcb4. For this reason, in chapter 5.1 and 5.2, we complemented *koLhcb4 Arabidopsis* plants with either wild-type or mutant versions of the *lhcb4.1* gene. Our analysis revealed that Lhcb4 is responsible for the activation of fast quenching reactions, which are catalyzed *in vivo* by a pigment cluster comprising chlorophylls *a*603-*a*609-*a*616 and the xanthophyll in site L2. Moreover, our mutational analysis on the protonatable residues of Lhcb4 exposed to the lumen ruled out the hypothesis that this protein can sense luminal ΔpH, a role that, to date seems to be unique for PsbS. In chapter 5.2 we describe the complementation of *koLhcb4 Arabidopsis* lines with mutant versions of the Lhcb4.1 protein

lacking chlorophyll *b614*. The lack of this specific chlorophyll determines the reorganization of the architecture of the thylakoid membranes. Indeed, we demonstrated that this chlorophyll acts as a docking site for the Lhcb6 subunit to the core complex. It was previously observed that the lack of Lhcb6 causes the formation of a crystal-like structure composed by PSII particles, ultimately determining an impairment in plastoquinone diffusion, electron transport and ΔpH formation. Phenotypical and microscopical investigations on *b614* lacking lines highlighted several similitudes between these lines and *koLhcb6* genotype. We concluded that the phenotypical traits observed in *b614* depleted lines were mainly due to the pleiotropic effects caused by the impaired accumulation of Lhcb6 rather than to the specific effect of deleting a single pigment.

Conclusions

My thesis is focused on the study of Lhcb proteins, with the aim to understand the molecular mechanisms which might lead to improving photosynthesis and ultimately increase the productivity of crops and microalgae. Results reported here are new and obtained, in cases, by procedures never previously implemented. These results allow asking more questions helpful for furtherly understanding Light harvesting and Photoprotection. We first report on the development of a successful strategy to enhance algal productivity in photobioreactors by combining enhanced resistance to excess light conditions with a better light penetration (pale-green phenotype), this is an important step towards the production of algal biofuels competitive with fossil energy sources. In a second step of the research, we contributed to clarify the genetic factors behind the formation of grana stackings in higher plants, a feature that puzzled scientists for more than 40 years. Last, but not least, we filled a gap in the knowledge of the mechanism of Non-Photochemical Quenching, by assessing the contribution of monomeric Lhcbs, and identifying a pigment cluster responsible for the activation of this mechanism *in vivo*. In the next years, the transgenic lines produced in this thesis will be a tool for the study of molecular events that mediate light harvesting and photoprotection and will constitute an *in vivo* expression platform for both the expression of individual Lhcb gene products in their wild type sequence or their targeted mutant versions.

1. Introduction

1.1 General Introduction

1.1.1 Oxygenic Photosynthesis:

Plants, green algae, and cyanobacteria are photosynthetic organisms; this means that they can convert solar energy into chemical energy. This key-biological process is responsible, directly, or indirectly, for the sustain of most of living organisms on earth. From a chemical point of view photosynthesis is a redox reaction where carbon dioxide (CO_2) is reduced and water (H_2O) is oxidized this leads to the production of sugars $(CH_2O)_n$ and oxygen (O_2) as a by-product. The evolution of photosynthetic organisms strongly contributed to the determination of the composition of the atmosphere of our planet. The overall reaction of photosynthesis is the following:

$$n CO_2 + n H_2O + \text{light} \rightarrow (CH_2O)_n + n O_2$$

In the latter reaction, water acts as an electron donor, and the sugars can be stored as chemical energy for cellular reactions.

Overall, photosynthesis can be organized into two main phases based on the dependence on light:

1- the light phase: solar energy is harvested and exploited to produce high-energy compounds ATP and reducing power (NADPH). In this phase, photosynthetically active radiation (PAR) is captured and converted into chemical bounds in accordance with the following reactions:

$$ADP + Pi + \text{energy} \rightarrow ATP$$

$$2NADP^+ + 2H_2O + \text{light} \rightarrow 2NADPH + O_2 + 2H^+$$

2-the dark phase: this phase does not depend on light as long as ATP and NADPH are available. These two chemicals are crucial to sustain CO_2 fixation into glyceraldeide-3-phosphate (GAP) the building block of a wide range of compounds including sugars, produced in plants chloroplasts through the Calvin-Benson-Bassham cycle (Bassham et al., 1950). The overall process of dark phase is here summarized:

$$3CO_2 + 9ATP + 6NADH \rightarrow GAP + 9ADP + 8Pi + 6NADP^+$$

The Chloroplast:

In eukaryotic photosynthetic organisms, photosynthesis takes places into specialized organelles called chloroplasts. These organelles originate from a primary endosymbiotic event between a protoeukariotic host and a cyanobacterium (Whatley and Whatley, 1981). Consistently with this, chloroplasts retain several prokaryotic features, such as their own genetic material, the plastome, organized into nucleoid and including about 120-130 genes, most of them involved in photosynthetic processes. Nevertheless, most of chloroplast proteins are nuclear encoded and need to be imported through the *envelope*, the double membrane layer surrounding the organelles. In more details, the envelope is composed of two membranes separated by a thin intermembrane space. The outer membrane is highly permeable, mainly involved in nonspecific transport for and from the chloroplast, while the inner membrane is responsible for specific transport and enzymatic activities. The volume defined by the envelope includes two compartments: the *stroma* and the lumen, separated by a membrane system, the thylakoids *(Fig. 1.1.1)*.

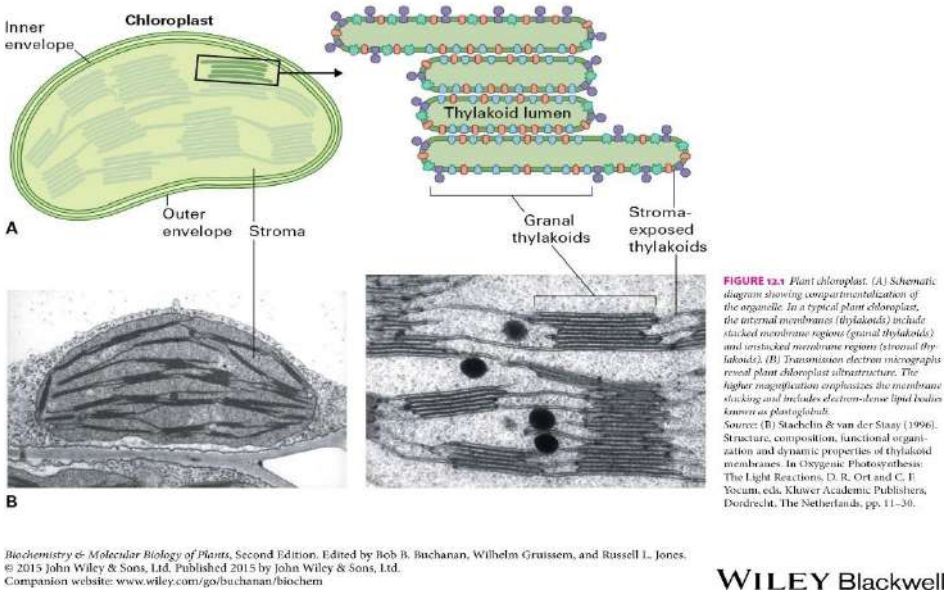

Fig. 1.1.1 | *Plant chloroplast. Source: (Buchanan et al., 2015)*

In land plants thylakoids membranes are organized into grana (appressed regions made of 5 to 20 membranes layers) and stroma lamellae: unstacked thylakoid membranes connecting grana to each other (Wietrzynski et al., 2020). Appressed regions are completely absent in cyanobacteria while algae present some regions with a grana-like structure but with a lower level of organization, thus suggesting the formation of grana as an evolutionary conquest of land plants (Liberton et al., 2011) (Fig. 1.1.2). One of the main functions of this high-level membrane organization is related to the need for a spatial segregation of PSII (grana) and PSI (stroma lamellae), known as lateral heterogeneity, allows avoiding spillover of excitation energy from PSII to PSI (Murata, 1969). The repair of PSII components damaged by excess light is composed of multiple steps localized in either grana or stroma membranes while functional PSII is localized in the grana partitions and moved to stroma membranes for repair (Theis and Schroda, 2016).

Also it has been suggested that cyclic and linear electron flow on the electron transport activities are related to the level of stacking (Armbruster et al., 2014).

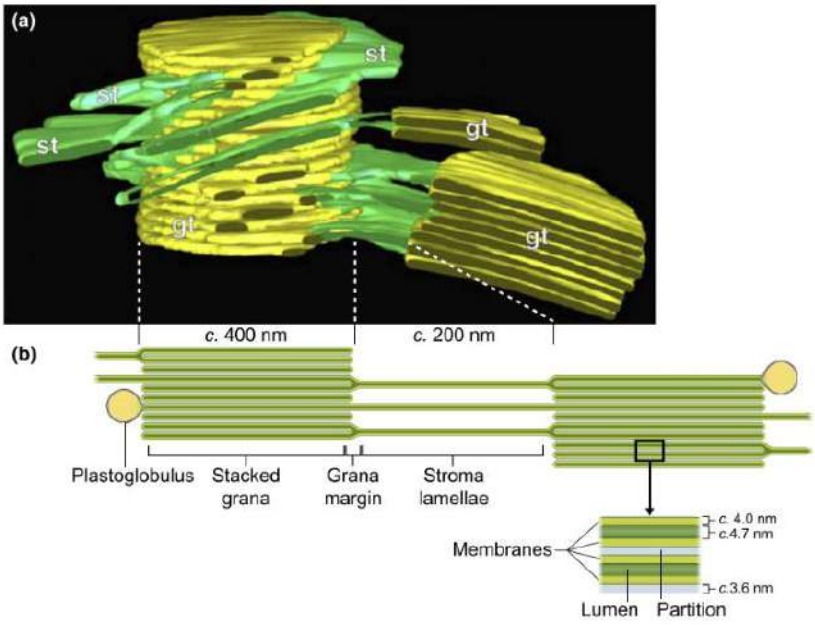

Fig. 1.1.2 | *Ultrastructure of the thylakoid membrane system. Source: (Kirchhoff, 2019)*

Stroma is the compartment where the soluble enzymes responsible for the dark phase take place, while thylakoids host the transmembrane complexes catalyzing the light-phase of photosynthesis. The light phase is catalyzed by four multiprotein complexes: photosystem II (PSII), cytochrome (Cyt) *b6f* and photosystem I (PSI), cooperating in the formation of a proton gradient through the thylakoid membrane while transferring electron from H_2O to $NADP^+$. Finally, ATP synthase (ATPase) converts the potential energy of the proton gradient into chemical energy by producing ATP from ADP and Pi. These complexes are unevenly distributed through thylakoids membrane, in fact, PSII mainly localized in grana and grana margins, PSI is only localized in stroma lamellae where also ATPase is preferentially found. Finally, Cyt *b6f* is located in both grana and stroma membranes (Olive and Vallon, 1991; Mustárdy and Garab, 2003) (Fig. 1.1.3).

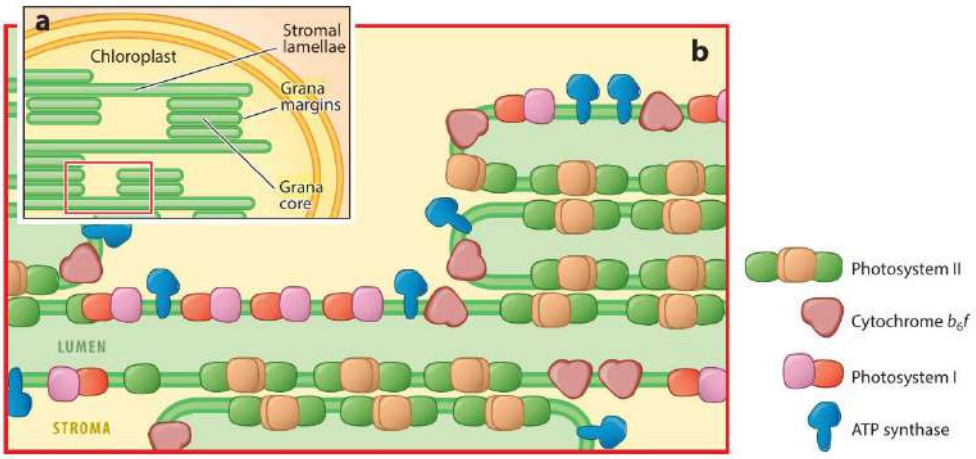

Fig. 1.1.3 | *Distribution of the electron transport chain component in the thylakoid membrane. Source: (Bassi and Dall'Osto, 2021)*

The Light Phase

The primary event in photosynthesis is light harvesting. Photons are captured by the antenna moieties of two multimeric complexes, namely the photosystem I (PSI) and the photosystem II (PSII). Their core moieties, instead, are in charge for charge separation, fueling electron transport. Photosystems are multimeric protein complexes binding chlorophylls (Chls), carotenoids (Cars) and other cofactors. Each photosystem is endowed with special chlorophylls called reaction centers (RCs), respectively P680 and P700 for PSII and PSI. Moreover, the light phase also needs the contribution of two other complexes: Cyt *b6f* and ATPase. When a photon is captured by the PSII the RC P680 undergoes charge separation to $P680^+$, one electron is transferred to a pheophytin molecule (pheo), then to a plastoquinone (PQ) at the Q_A site. The recovery of missing electrons in $P680^+$ restoring P680 for further charge separation is mediated by a tyrosine residue of the D1 subunit called Yz. Electrons derive from the Mn cluster of OEC. Water (the primary electron donor) is oxidized to a molecule of oxygen upon accumulation of 4 positive charges within OEC. Thus, four consecutive P680 charge separations events are needed to oxidize two water molecules producing O_2, releasing H^+ in the thylakoids lumen and restoring the manganese cluster to its reduced state. The electron in Q_A is then transferred at the Q_B site bound to a PQ molecule, which, working as double electron acceptor, becomes fully reduced and protonated from H+ in the stroma compartment after two cycles of photochemical turnover of the RC. The reduced plastoquinone (plastoquinol PQH_2) has a very low affinity for the Q_B site and is free to move in the hydrophobic environment of the membrane transferring the electrons to the second photosynthetic complex, the Cyt *b6f*. The oxidation of PQH_2 is coupled with the release of protons into thylakoid lumen, thus contributing with the formation of the transmembrane proton gradient. The Q_B -site is now free to bind a new PQ molecule from the PQ pool. Cyt *b6f* reduces plastocyanin (PC), a hydrophilic copper-binding protein that can diffuse in the lumen volume in order to give two electrons to the PSI. When photon excites PSI the charge separation of P700 is promoted with the electron being transferred through multiple e- transporters, including: a monomeric Chl a (A_0), a phylloquinone (A_1), Fe-S centers (F_X, F_A and F_B) and a ferredoxin (FD) on the stromal side. The flavoprotein ferredoxin- $NADP^+$ reductase (FNR) mediates the reduction of

$NADP^+$ to NADPH from 2 ferredoxin molecules. The last complex of the linear transport chain is the ATPase. It is composed by two main components: the F_0 domain, mediating protons translocation across the membrane and the F_1 domain responsible for the catalysis of ATP from ADP and Pi. The proton flux through the F_0 domain determines a conformational change in the tridimensional structure of the complex, allowing for the catalytic activity (Nelson and Yocum, 2006).

Linear electron transport (LET) describes the fate of an electron transferred from a molecule of water to one of NADPH through several redox reaction mediated by component of the photosynthetic transport chain. In photosynthetic organisms, other two modes of electron transport are present: pseudo-cyclic electron transport (PEF or water-water cycle, see section "Photoprotective Mechanisms") and cyclic electron transport (CET) (Allen, 2003). CET is a mechanism that can contribute significantly to photosynthetic electron transport under stress conditions (Clarke and Johnson, 2001; Golding and Johnson, 2003). CET shares some components with LET; PQ, Cyt *b6f*, PC, PSI, and FD and it is activated to balance the ATP:NADPH ratio according to metabolic demand. CET produces a ΔpH across the thylakoid membrane that drives the synthesis of ATP without the production of O_2 or NADPH (Heber and Walker, 1992). CET can occur following two alternative routes, the major one mediated by PGR5 and PGRL1 and a secondary one mediated by the NDH complex. Mutants for *ndh*, *pgr5* and *pgrl1* share a similar phenotype exhibiting higher sensitivity to drought and heat stress (Shikanai and Yamamoto, 2017) (Fig. 1.1.4).

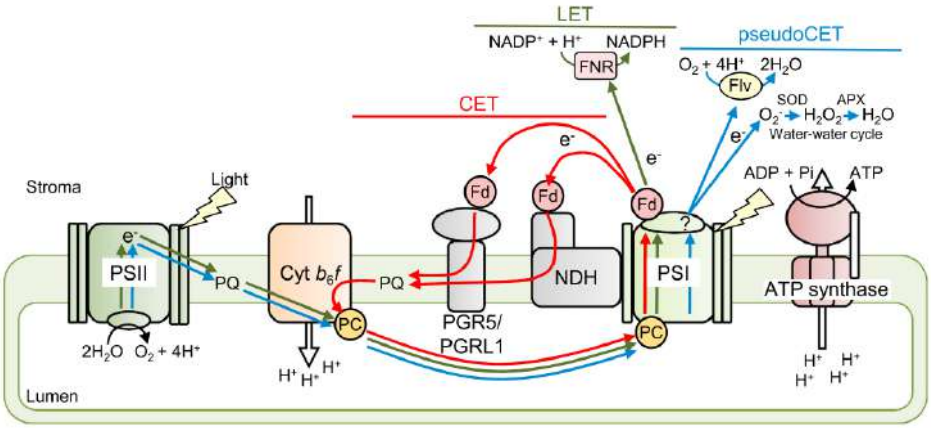

Fig. 1.1.4 | *Linear electron transport (LET) from water to $NADP^+$ is indicated by the green arrows. Two pathways of cyclic electron transport (CET) around PSI are indicated by the red arrows. The main CET pathway is mediated by the PGR5/PGRL1 complex, which interacts with PSI. On the other hand, the minor pathway depends on chloroplast NDH, which forms the supercomplex with PSI. The blue arrows indicate two pathways of pseudo-cyclic electron transport (pseudoCET).*
Source: (Shikanai and Yamamoto, 2017).

The Dark Phase.

During the dark phase, or light-independent phase, atmospheric CO_2 is fixed and reduced producing carbohydrates. This is possible thanks to the products obtained during the light phase: ATP and NADPH. The dark phase includes several reactions overall known as the Calvin-Benson-Bassham cycle (Bassham et al., 1950) that can be summarized as follows:

$$3CO_2 + 3RuBP + 3H_2O + 6ATP + 6H^+ + 6NADPH \rightarrow 6GAP + 6ADP + 6NADP+ + 6Pi$$

$$5GAP + 3ATP \rightarrow 3Ru5P + 3ADP$$

Overall, the pathway can be divided into three main phases: carboxylation, reduction and regeneration. The key enzyme in this process is the Ribulose-1,5-Bisfosphosphate-Carboxylase-Oxygense (RuBisCO), the most abundant protein in nature (Ellis, 1979). RuBisCO catalyzes the first reaction of the cycle in which three molecules of CO_2 and water react with three ribulose-1,5-bisfosphosphate (RuBP) to produce six molecules of 3-phosphoglycerate (3-PGA). 3-PGA is then reduced to glyceraldehyde 3-phosphate (GAP) consuming ATP and NAPH. During the regeneration phase, five GAP molecules are needed to restore RuBP to the original CO_2 acceptor with the consumption of more ATP. The remaining GAP molecule represents the net yield of the Calvin-Benson-Bassham cycle and is used to produce storage carbohydrates or other cellular components (Fig. 1.1.5).
The RuBisCO enzyme can also work as oxygenase and this leads to unwanted products that need to be detoxified via a process called photorespiration. (Whitney et al., 2011).

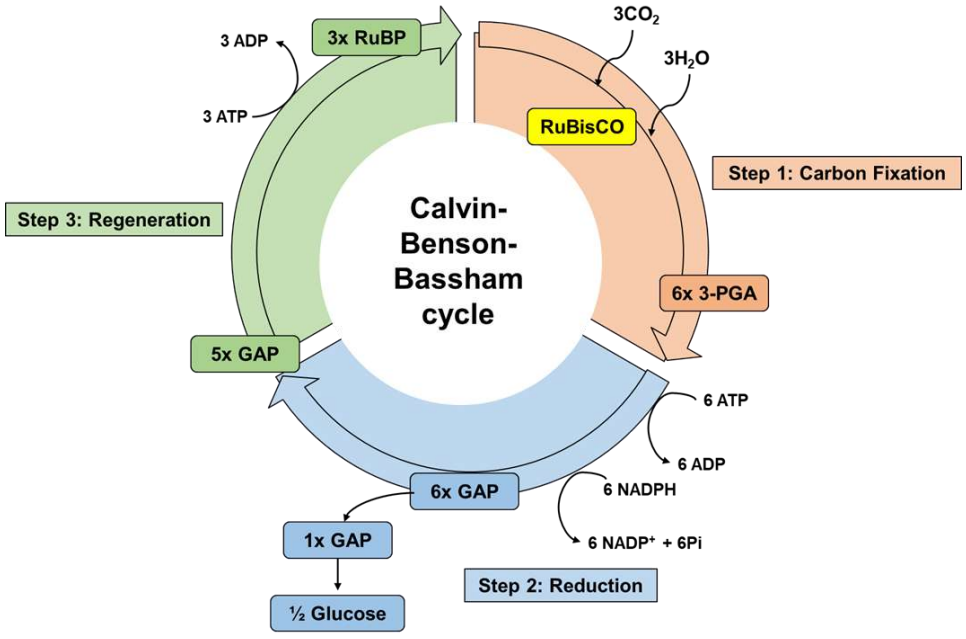

Fig. 1.1.5 | *Schematic representation of the Calvin–Benson–Bassham cycle (CBBc) reactions.*

1.1.2. Photosynthetic Pigments in higher plants:

Photosynthetic pigments, in higher plants, can be classified into two macro-categories: chlorophylls (Chl) and carotenoids (Car). And catalyze light absorption, charge separation, and energy transfer toward the RCs, both PSI and PSII.

Chlorophylls:

Chlorophylls are essential pigments for light harvesting and energy transfer. The general structure of chlorophylls is composed of a central magnesium ion (Mg^{2+}) surrounded by a tetrapyrrolic ring (porphyrin). A pivotal characteristic of this conformation is the presence of alternate C-C double bonds that favor light absorption and electron transfer. To bind the highly hydrophobic environment of the thylakoids membrane, the porphyrin ring is linked to a 20 C chain (phytol). Chl occurs in different forms depending on the different substitutions present on the porphyrin rings. Chl a is present in all photosynthetic organisms from higher plants to cyanobacteria (Björn et al., 2009), Chl a acts as electron donor in both photosystems. Chl b is the second most abundant chlorophyll in nature, it is virtually present in all higher plants, and green algae, constituting an complementary pigment for light harvesting and energy transfer (La Roche et al., 1996) *Chl c* and *d* are found mainly in red algae and bacteriochlorophylls in photosynthetic bacteria.

The characteristic of chlorophylls is the capacity to absorb light in the visible region; Chl a and b absorb light mainly in two regions: Soret (in the blue) and Q_Y (in the red) (Fig. 1.1.6). Q_Y transitions correspond to the transition of an electron from S_0 to S_1 (the first excited state) with a maximum at 640 and 670 nm for Chl b and Chl a, respectively, while Soret transitions correspond to higher energy states with a maximum at around 430 nm for Chl a and 470 nm for Chl b in organic solvent, given the high instability of S_2 (or even higher states) energy transfer between Chls occurs mainly from the Q_Y transition. These absorption properties are determined by different substitutions; Chl a binds to a methyl group ($-CH_3$) at the second pyrrolic ring, while Chl b binds to a formyl group (-CHO)(Strain et al., 1963; Chen and Blankenship, 2011).

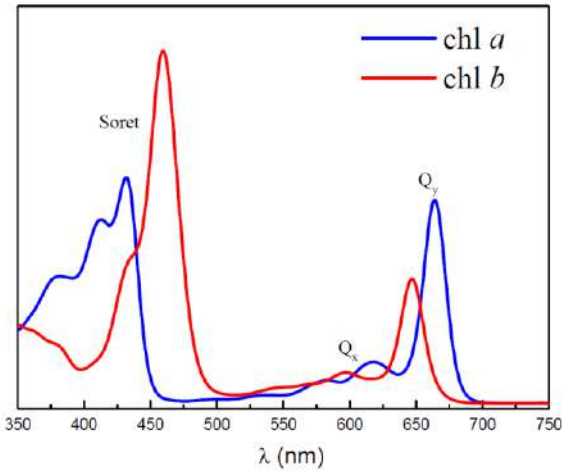

Fig. 1.1.6 | *Typical absorption spectrum of pure Chlorophyll a and b.*

Carotenoids:

Carotenoids are the second most abundant pigment class in plants. They are synthesized by several living organisms including plants, algae, fungi, bacteria, and some insects. Carotenoids are mainly lipophilic C40 tetraterpenes obtained from two isoprenoid units: isopentenyl diphosphate (IPP) and dimethylallyl diphosphate (DMAPP), together generating geranylgeranyl diphosphate (GGPP), the precursor of the entire carotenoid biosynthetic pathway. Carotenoids are classified into carotenes (oxygen-free carotenoids) and xanthophylls (hydroxylated or epoxidized carotenoids). In plants the most abundant carotenes is β-carotene (β-car) a low amount of α-carotene (α-car) is also present while the most abundant xanthophylls are lutein (Lut), violaxanthin (Vio), neoxanthin (Neo) and zeaxanthin (Zea). These pigments are embedded into the thylakoid membrane or bound to the photosystems and their antenna complexes (Nisar et al., 2015).
Carotenoids absorb light in the blue region of the visible spectrum (400-550 nm) (Fig. 1.1.7), thus appearing yellow, orange, or red to human eyes. Their spectral properties depend on the alternate C-C double bond extension of their hydrocarbon backbone (Britton et al., 2004; Fuciman et al., 2012). Carotenoid composition in the thylakoids is not constant: rather, changes responding to light conditions or during the acclimation of long-lasting stresses (Demmig-Adams et al., 1989).

Three xanthophylls; Vio, antheraxanthin and Zea are the actors of the so-called xanthophyll's cycle, consisting in the light-dependent de-epoxidation of Vio to Zea trough the intermediate antheraxanthin. Xanthophyll's cycle is mediate by two key enzymes: Violaxanthin De-Epoxidase (VDE) and Zeaxanthin Epoxidase (ZE). Under excess light conditions, the luminal enzyme VDE is activated by the low pH catalyzing the conversion of Vio into Zea (Gilmore and Yamamoto, 1991b). On the other hand, under limiting light conditions, VDE is inactive and ZE rapidly converts Zea to Vio, allowing for the continuation of carotenoids biosynthesis pathway. Xanthophyll's cycle is a key component in the activation of several photoprotective mechanism being Zea a positive regulator of thermal dissipation of excess energy, a ^{3}Chl* quencher and ROS scavenger (Niyogi et al., 1998; Holt et al., 2005; Dall'Osto et al., 2012).

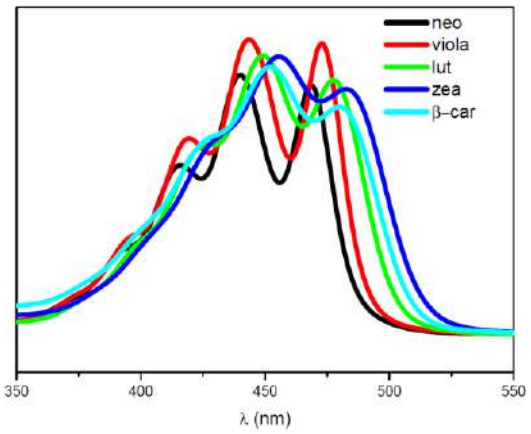

Fig. 1.1.7 | *Typical absorption spectrum of the most representative Carotenes and Xanthophylls.*

Light properties:

Light is electromagnetic radiation with both wave and particle properties. Electromagnetic waves are described by three main parameters: amplitude (A), frequency (ν) and wavelength (λ). Frequency and wavelength are inversely proportional according to the equation:

$$c = \lambda \nu$$

Where c is a constant, the speed of light in vacuum (3×10^8 m s^{-1}). Each wave is composed of an electric and a magnetic field moving in the same direction perpendicular to each other.

On the other hand, light is described, according to corpuscular theory, as a stream of discrete units of radiation (photons). Energy of each photon is proportional to frequency as described by Plank's equation:

$$E = h \nu = h \, n \, (c / \lambda);$$

where h is the Planck constant (6.626×10^{-34} J s).

The solar radiation is composed by photons with wavelengths, from 10^{-3} to 10^{-15} nm, including: X-rays, ultraviolet, visible light, infrared, microwave, and radio waves. Photosynthetic pigment can absorb a small fraction of the total solar radiation, photosynthetically active radiation (PAR) represents the fraction of solar energy suitable for photosynthesis includes wavelength ranging between 400 and 700 nm

Light Harvesting and Excitation Energy Transfer:

Plants antenna system evolved to harvest light and to mediate excitation energy transfer (EET) toward both PSI and PSII. For energy transfer events, an excited donor (D) and an acceptor (A) at the ground state (low energy state). Energy transfer could occur, within picoseconds, in two ways; a resonant mechanism (Förster, 1948) or electron exchange (Dexter, 1953). Considering the Förster mechanism, the emission spectrum of the D molecule partially overlaps with the absorption spectrum of a nearby A molecule (30-100 Å). The excited donor molecule transfers excitation through dipole-dipole interaction by resonance without emitting light (Pearlstein, 1982). Excitation energy transfer between chlorophylls is probably mediated by Förster mechanism (Förster, 1965) and is under the control of three main parameters:

- Energy level of electron transition of D and A molecules (spectral superimposition of D emission and A absorption)
- Distance between D and A
- Dipole moment orientation of D and A

In a typical Chls network within light-harvesting system pigments distance is compatible with Förster mechanism. The protein environment influences pigment orientation and slightly changes energy levels inside chromophores. These characteristics together with the Stoke's shift phenomenon (absorbed energy has always a smaller wavelength respect to emitted energy)

contributes to funneling excitation energy in only one possible way, from Chls b to Chl a (lowest energy).
Dexter energy transfer involves electron exchanges between molecules through covalent bonds. In this case, an electron at the excited state of the D molecule moves to the excited state of the A molecule, while a ground state electron from the A molecule is transferred to the ground state of the D. In the primary stages of photosynthesis exchanges between pigments bound to light-harvesting system convey energy to the RCs.

1.1.3. Photosynthetic Machinery: Pigment binding Complexes:

Photosystems are multimeric pigment binding complexes embedded into the thylakoid membrane; they are able to carry on the primary events of photosynthesis, namely: light absorption and charge separation. Both PSs are endowed with a peripheral Light Harvesting system, aimed to enlarge PS cross-section allowing for enhancing light capture and transfer excitation energy to the core complex. Core subunits of both PSs are encoded by genes in the plastome defined as Psa and Psb for PSI and PSII respectively, in particular PsaA and PsaB for PSI and D1, D2, CP43 and CP47 for PSII constitute the core complexes and are extremely conserved among photosynthetic organisms. The peripheral antenna system is encoded in the nucleus for both PSs. Photosystem antenna complex is composed by several different proteins belonging to LHC family called Lhca/LHCI and Lhcb/LHCII for PSI and PSII respectively (Jansson, 1999). Antenna systems can vary greatly between different organisms and under contrasting environmental conditions.

Photosystem I:

PSI is a thylakoid-membrane-embedded-multimeric complex catalyzing electron transfer from the plastocyanin (PC) in the luminal side to the ferredoxin in the stromal side, thus being defined as plastocyanin-ferredoxin oxidoreductase. Its core complex is composed by 15 subunits known as PsaA–PsaP and encoded by both nuclear and plastid genes. Core complex is bound to a peripheral antenna system defined LHCI or Lhca; in higher plants PSI-LHCI supercomplex binds a total of 19 protein subunits and 174 Chl a molecules and 19 Cars (Scheller et al., 2001; Qin et al., 2015)
In more detail, the PSI core complex coordinates 98 Chl a molecules and 20 β-cars units. Among all the subunits only PsaA/B and C are directly involved in the binding of electron transport mediating co-factors namely the special Chl pair P700, A_0 (a Chl a molecule), A_1 (phylloquinone) and three iron-sulfur clusters. PsaD and PsaE are involved in the formation of a suitable docking site for the ferredoxin in the stromal side (Jordan et al., 2001; Ihnatowicz et al., 2004), PsaF and PsaN are in charge for the binding of plastocyanin (Farah et al., 1995; Haldrup et al., 1999, 2000), LHCI can interact with the core-complex thanks to PsaF, PsaK and PsaG subunits that at the same time play a crucial role in the stabilization of the supercomplex (Ben Shem et al., 2003; Haldrup et al., 2000) Lastly PsaH, PsaI, PsaL, and PsaO can interact with LHCII, stabilizing the PSI-LHCII binding during state transitions (Jensen et al., 2004). Photosystem I works as an almost perfect

"Einstein photochemical machine" (Nelson and Ben-Shem, 2004) it reaches a quantum efficiency value close to one, not reproduced by any artificial system so far.

PSI Antenna System:

The PSI antenna system is composed of 4 Lhca subunits (Lhca1-4) with a molecular mass ranging from 20 to 24 kDa coordinating Chl a, Chl b, Lut, Vio, and β-car (Croce et al., 2002b) (Fig. 1.1.8). All Lhca share a common structure characterized by 3 transmembrane helices (A, B, and C) and an amphipathic helix (D) on the luminal side of the membrane, these structural features are also shared with PSII light harvesting complexes (Qin et al., 2015). For each supercomplex a single copy of Lhca1-4 proteins is present (Ballottari et al., 2004). Lhca are assembled into heterodimers Lhca1/4 and Lhca2/3 and their binding to the core-complex is strongly cooperative (Morosinotto et al., 2005a; Wientjes et al., 2012). In *A. thaliana* two additional Lhca encoding gene are present; *lhca5* and *lhca6* but their expression level has been shown being very low in several condition and protein accumulation is not stochiometric with core complex (Jansson, 1999; Klimmek et al., 2006). Lhca proteins (or LHCI) form a single layer bound to the core complex; this bound is strengthened by the presence of linker chlorophylls and probably linker carotenoids (Caffarri et al., 2014). It has been observed that light-harvesting capacity of PSI can be increased, depending on light conditions and light quality, by recruiting LHCII as additional antenna to balance energy excitation between PSI and PSII (Allen, 1992; Galka et al., 2012).
The movement of LHCII towards the thylakoid membrane from PSII to PSI is defined as the 'state transition' and is triggered by the LHCII specific kinase STN7 (Bellafiore et al., 2005).

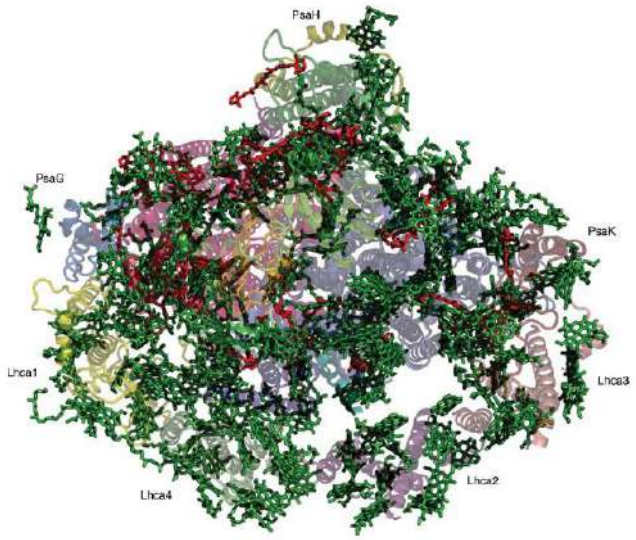

Fig. 1.1.8 | *A view of the structure of plant photosystem I from the stromal side. Source: (Nelson and Yocum, 2006)*

Photosystem II:

PSII is a multi-protein super complex catalyzing the oxidation of water and the reduction of plastoquinone. PSII binds several co-factors including: Chl, Cars, quinones, iron, sulfur, and manganese. The overall structure of PSII comprises a dimeric core complex surrounded by a layer of monomeric antenna proteins (CP29/Lhcb4, CP26/Lhcb5 and CP24/Lhcb6) and an external layer of trimeric LHCII proteins (Lhcb1, Lhcb2, and Lhcb3). The core of PSII is composed of four main transmembrane subunits (D1/PsbA, D2/PsbD, CP43/PsbC and CP47/PsbB) and twelve intrinsic low molecular weight subunits (PsbE, PsbF, PsbH, PsbI, PsbJ, PsbK, PsbL, PsbM, PsbTc, PsbW, PsbX, and PsbZ) and four extrinsic subunits exposed on the luminal side (PsbO, PsbP, PsbQ and PsbTn) (Shi et al., 2012; Wei et al., 2016) (Fig. 1.1.9).

D1 and D2 proteins constitute the reaction center, a heterodimeric structure binding 6 Chl a, 2 pheophytin a, plastoquinones Q_A and Q_B and 2 molecules of β-car. Two of the six chlorophylls constitute the P680 reaction center, two are part of the electron transport chain and the two are involved in the energy transfer with CP43 and CP47 the inner antenna system of PSII binding most of Chl a and β-car molecules in the core-complex.

D1/D2 dimer is also connected with the so-called "oxygen-evolving-complex" (OEC) a heterotrimeric subunit composed by the extrinsic proteins: PsbO/OEE1, PsbP/OEE2 e PsbQ/OEE3 (Hankamer et al., 2001). In the OEC a cluster of 4 Mn^{2+} ions are located, together with other cofactors such as Cl and Ca^{2+}, playing a fundamental role in the water splitting reaction providing electrons for P680 to replace electron loss due to charge separation (Joliot, 2003)

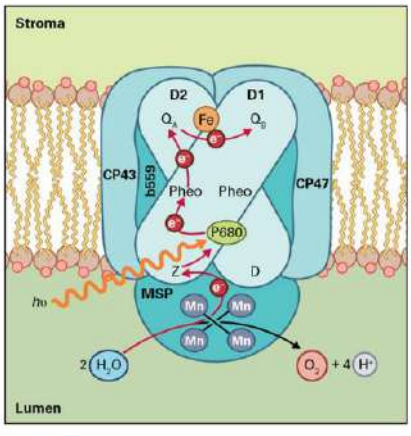

FIGURE 12.11 *Schematic diagram of the reaction center core of monomeric PSII. The D1 and D2 proteins bind most of the cofactors involved in charge separation and electron transport. Electrons are transferred from P680 to pheophytin (Pheo) and subsequently to two plastoquinone molecules, Q_A and Q_B. The nonheme iron (Fe) does not have a direct role in electron transfer. P680⁺ is reduced by Z, a tyrosine residue in the D1 subunit. Also indicated is the oxidation of water by the Mn cluster, which is bound to the luminal side of the complex and stabilized by a peripheral protein, PsbO (labeled as MSP). CP43 and CP47 are chlorophyll a–binding core antenna proteins. D1 is susceptible to photooxidative damage and undergoes active turnover (see Chapter 10, Box 10.B).*

Fig. 1.1.9 | *Schematic diagram of the reaction center core of monomeric PSII. Source: (Buchanan et al., 2015)*

PSII Antenna System:

PSII antenna system is composed of several kinds of Chl a/b–xanthophylls binding proteins (Lhcb/LHCII). From a structural point of view, they all share a common structure (as for Lhca proteins) characterized by three transmembrane alpha helices and a fourth amphipathic helix on the luminal side. The main role of Lhcbs proteins is the light harvesting; in fact, they are in charge of the light capture and efficiently transfer excitation energy to the PSII reaction center. Moreover, LHCII are involved in other several fundamental roles in plant physiology such as: photoprotection (this will later be discussed in detail), short and long stress acclimation, and energy balance between the two PSs (state transitions). Lhcb proteins can be classified as monomeric (or minors) forming an antenna layer in close contact with the PSII-core, namely: Lhcb4/CP29, Lhcb5/CP26 and Lhcb6/CP24, these three proteins are present in stoichiometric 1:1 ratio with the core complex and work as a bridge between the core and a second layer of antennas major LHCII (present in three distinct isoforms: Lhcb1, Lhcb2 and Lhcb3) organized into trimers, by far the most abundant transmembrane pigment-binding protein in nature (Su et al., 2017).
In *Arabidopsis thaliana, lhcb* is a complex gene family composed by 14 genes, 5 of them encoding for Lhcb1, the most abundant LHCII subunit (*lhcb1.1-1.5*), Lhcb2 is encoded by two highly homologous genes (*lhcb2.1* and *lhcb2.2*) and a third slightly different one *lhcb2.3*, Lhcb3 is encoded by a single gene such as Lhcb5 and Lhcb6 while Lhcb4 is encoded by two genes with a similar expression level (*lhcb4.1* and *lhcb4.2*) and by *lhcb4.3* which is very lowly expressed in moderate light conditions (Jansson, 1999). In recent years the role of Lhcb4.3 has been further investigated, suggesting a protective role in stress conditions, such as cold or high-light (Albanese et al., 2019). Consistently, Grebe and co-workers demonstrated the presence of lhcb4.3 in Pinaceae family as unique CP29-like antenna of PSII (Grebe et al., 2019), the unique characteristics of lhcb4.3 led to the suggestion by (Klimmek et al., 2006) of renaming the gene as *lhcb8*. The major LHCII is composed of heterotrimeric combinations of Lhcb1, Lhcb2, and Lhcb3 distributed in a non-equimolar composition, being Lhcb1 found in larger amount (Caffarri et al., 2004; Dekker and Boekema, 2005).

Monomeric Lhcb:

Among monomeric antenna protein CP29 is the largest: it is composed by 256-258 residues in its mature form *in A. thaliana*. The crystal structure of PSII-supercomplex helped to shed light on tridimensional features of CP29, with regards to pigment composition and organization (Pan et al., 2011). CP29 is characterized by 9 Chl a, 4 Chl b and three xanthophylls: a lutein in the L1 site, a neoxanthin in the N1 site and a violaxanthin in the L2 site, recent data also confirmed the presence of a promiscuous Chl a/b site (site a1) (Fig. 1.1.10). CP29 plays a fundamental role acting as a bridge between CP47 (core complex) and peripheral trimeric LHCII. Structural analysis suggested the presence of hydrophobic interaction between α-helices of CP29 and CP47, thus contributing to the structural stability of the PSII supercomplex. Some Chl of CP29 (Chl *a*616, Chl *a*609, Chl *a*603 and Chl *b*607) can directly interact with Chl of CP47 allowing for an efficient energy transfer between external antenna system and the core complex.

The second largest monomeric antenna protein is CP26. In *A. thaliana* CP26 is composed by 243 residues, according to the most recent cryo-EM structure it binds 13 Chl molecules and 3 xanthophylls, a lutein in the L1 site a neoxanthin in the N1 and a lutein or a violaxanthin at the L2 (Caffarri et al., 2007).
The last monomeric antenna is CP24, composed of 211 aminoacids in mature form of *A. thaliana*, and is the smallest among monomeric Lhcbs. The recent crystal structure described the binding of 6 Chl a, 5 Chl b, two xanthophylls (Lut and Vio) and probably one β-car. Unlike CP29 and CP26, CP24 does not bind neoxanthin, probably due to the absence of a Tyr residue that stabilizes the N1 site (Su et al., 2017). CP24 is linked to the PSII supercomplex by interacting with CP29, as confirmed by its absence in koCP29 mutants (De Bianchi et al., 2011).

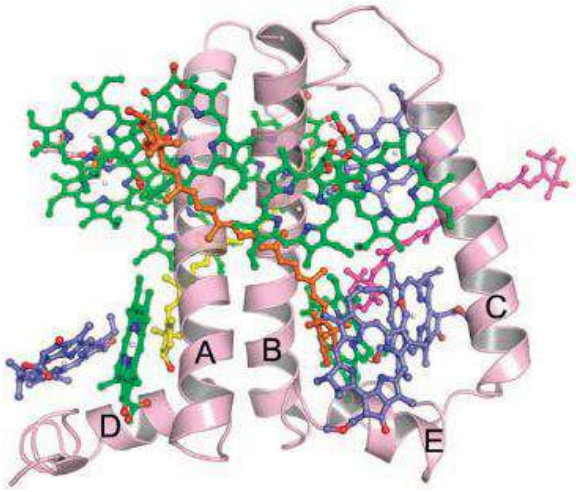

Fig. 1.1.10 *| Stereo view of the overall structure of CP29. Green, Chl a; blue, Chl b; yellow, Lut; orange, Vio; magenta, Neo; light pink, G3P Source: (Pan et al., 2011)*

Trimeric Lhcb:

Trimeric LHCII is the most abundant antenna protein in plants. It binds up to the 65% of total Chls in higher plants (Kouřil et al., 2013; Su et al., 2017) and up to the 50% of total protein in thylakoid membrane. LHCII is organized into heterotrimers made by non-equimolar ratio of its three isoforms: Lhcb1, Lhcb2 and Lhcb3. In *A. thaliana,* LHCII is encoded by 9 homologous nuclear genes (Jansson, 1999). Each trimer binds a total of 28 Chl a, 12 Chl b, and 12 xanthophylls. The monomeric structure of LHCII is characterized by 3 transmembrane helices binding 8 Chl a 6 Chl b and four xanthophylls (2 Lut at L1 and L2 site 1 Neo at the N1 site and 1 violaxanthin at the external V1 site). In *A. thaliana* mature version of Lhcb1, Lhcb2 and Lhcb3 are 232, 228 and 223 aminoacids long respectively. Different trimeric structures can be classified as S or M trimers according to their binding capacity to the core complex (S=strongly bound, M=mildly bound) (Fig. 1.1.11). The S-trimers interact with CP26 and CP43, while the M-trimers are bound to CP24 and CP29 (Caffarri et al., 2009).

Quantitative biochemical analysis and immune-titolations revealed that the average number of trimers for each core is higher than four. These extra LHCII trimers are defined L-trimers (loosely bound) and are easily detached from the core upon solubilization with mild detergents.
Lhcb1 and Lhcb2 are the most abundant components, while Lhcb3 is present in a lower amount and can be found in the LHCII-M and L-trimers only. Lhcb3 is absent in the S-trimer while its presence in mobile trimers during state transitions is still controversial (Galka et al., 2012).
Trimeric structure is allowed and maintained by two stretches of highly conserved domains, the first at the N-terminus (WYxxR) and the second the C-terminal (W) as biochemically investigated by Harald Paulsen's group in the middle '90s (Hobe et al., 1995; Kuttkat et al., 1996) and then confirmed by more recent structural studies (Fig. 1.1.11) (Pan et al., 2013; Su et al., 2017).

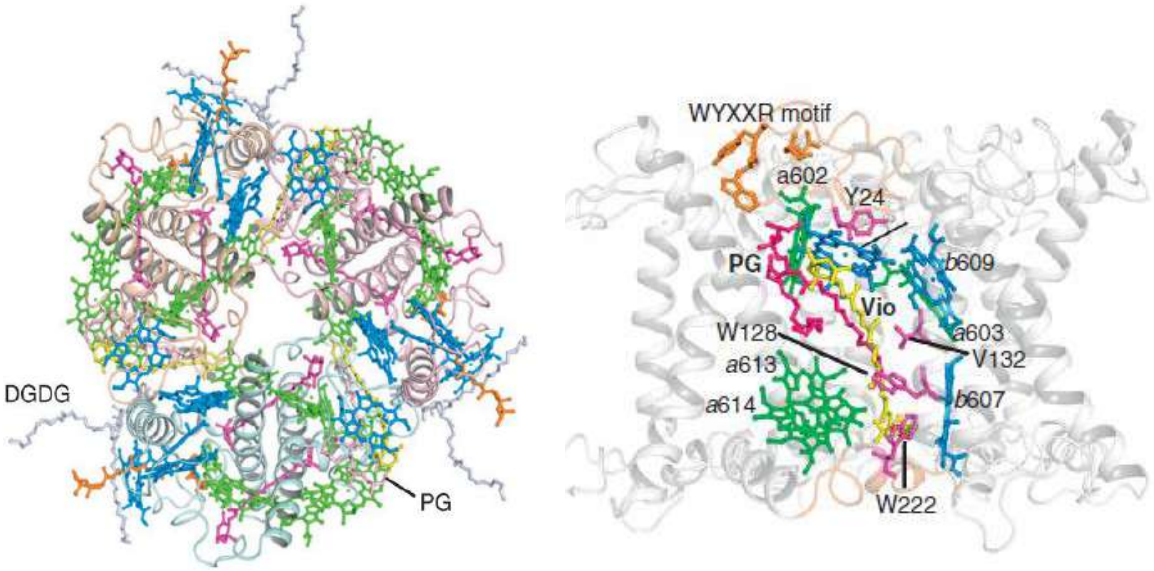

Fig. 1.1.11 | ***Left panel:*** *Tridimensional structure of trimeric LHCII*
Right panel: *Focus on trimerization site and V1 site. Source: (Pan et al., 2013)*

Architecture of PSII-supercomplexes:

The largest supercomplex observed so far in *A. thaliana* by EM is composed of a dimeric core (C_2) two S-trimers (S_2) bound to the CP43 and CP26 side and two additional M-trimers (M_2) bound to the CP29 and CP24 side (Fig. 1.1.12). This kind of supercomplex has been described as $C_2S_2M_2$ (Dekker and Boekema, 2005). The presence of CP24 and Lhcb3 has been shown to be necessary for the accumulation of M-trimers (Kovács et al., 2006) while the absence of CP26 completely abolishes the formation of $C_2S_2M_2$ and reduces the presence of smaller supercomplexes (C_2S_2, C_2S_2M and C_2SM) (Caffarri et al., 2009). The absence of CP29 does not impede the possibility of $C_2S_2M_2$ assembly, but in koCP29 mutants a very low number of supercomplexes have been detected displaying an empty space in the CP29 region (De Bianchi et al., 2011). Recently $C_2S_2M_2$ cryo-EM structure has been obtained at 2.7 Å resolution showing the homodimeric structure of

the PSII-LHCII supercomplex, confirming the localization of S and M-trimers in proximity of CP26/CP43 and CP29/CP47 respectively (Su et al., 2017).
It is important to remember that the structure of PSII-supercomplex is a highly dynamic system that needs to be re-modulated according to changing environmental conditions such as increasing the antenna dimension in low-light and reducing it in low-light conditions. (Ballottari et al., 2007; Grinzato et al., 2020).

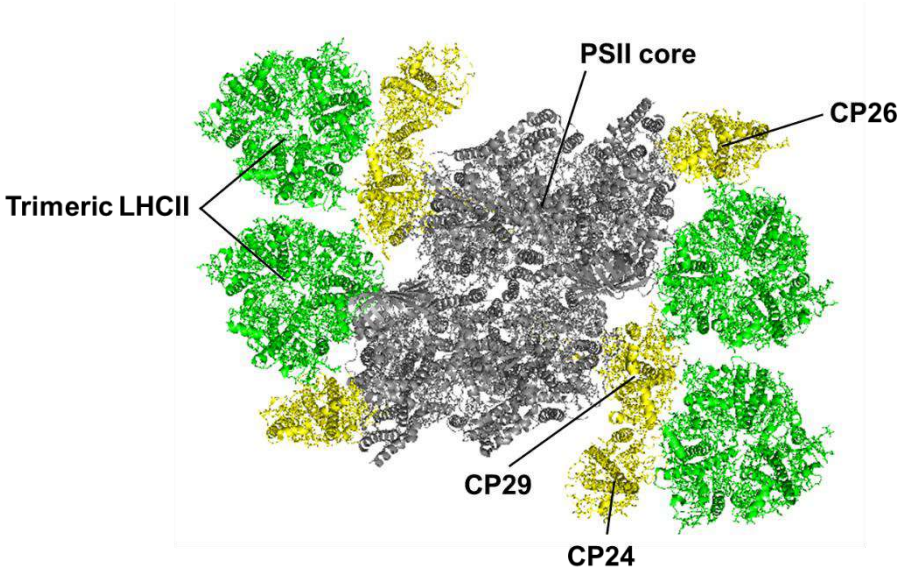

Fig. 1.1.12 | *Schematic representation of $C_2S_2M_2$ supercomplex made with PyMOL. Based on (Su et al., 2017).*

1.1.4. Photooxidative stress and Photoprotection mechanisms

Generation of Oxygen-Reactive Species:

In previous sections, we reported on light harvesting. However, in cases, plants could be exposed to excess photons that cannot be managed by the photosynthetic apparatus. This scenario is called "excess light conditions" (EL) and can vary depending on other factors such as cold, drought, high salinity and nutrient deficiency which can exacerbate the effect of EL.
The tuning of light-harvesting capacity, in response to changing environmental conditions, is fundamental for photosynthetic organisms to balance light reactions with downstream metabolism. To this end, autotrophic organisms developed regulatory mechanisms to rapidly switch between the "conservative" and "dissipative" states respect to excitation energy. Typically, photosynthesis displays a light saturation curve that can be divided into three phases: (i) at low irradiance, light is the limiting factor and photosynthesis rate linearly increases with light intensity; (ii) at higher irradiance the limiting factor becomes CO_2 (the substrate) and photosynthetic rate increases non-linearly with light intensity; (iii) at saturating light, the use of ATP and NADPH is limited by the low turn-over rate of RuBisCO. In these conditions photosystems dissipate excess energy into heat leading to a decrease of photosynthetic rate, reaching a plateau. If this state is maintained, photoinhibition occurs causing a drastic decrease in photosynthetic efficiency (Oberhuber et al., 1993).
Excess light conditions could lead to overexcitation of PSs, generating potentially dangerous reactive species such as singlet oxygen ($^1O_2$) or other oxygen reactive species (ROS) capable of oxidizing lipids, proteins and pigments, inducing photooxidative damage (Prasil et al., 1992; Tjus et al., 1998, 2001).
ROS are continuously produced in photosynthetic apparatus, and Chls play a crucial role in that, acting as potential photosensitizers. The main ROS generating centers are: Lhcbs, PSII-RC and PSI. When photosynthesis is saturated PQ is fully reduced to PQH_2, thus Q_A cannot further reduce PQH_2 so one electron recombines with $P680^+$ forming $^1P680^*$ which undergoes transition to its triplet state ($^3P680^*$) (Melis, 1999). Also, PSII antenna system sun-light absorption excites Chl to the singlet state ($^1Chl^*$) that can be converted into triplet state ($^3Chl^*$) by intersystem crossing (ISC) before excitation energy is captured by RCs (Krieger-Liszkay, 2005). Under EL conditions, the probability of Chl singlet state being accumulated is higher. Increasing the lifetime of ($^1Chl^*$) favors the formation of the ($^3Chl^*$) by ICS. The latter is a long-lasting reactive specie (time scale of ms) which can react with molecular oxygen producing dangerous $^1O_2$ (Havaux and Tardy, 1996). PSI can also produce ROS, although $P700^+$ has a lower oxidizing power compared to $P680^+$ (Asada et al., 1974). When the electron accepting capacity of PSI is saturated, ferredoxin electrons can interact directly with the superoxide radical anion (O^{2-}) that produces oxygen (Tikkanen and Grebe, 2018). O^{2-} is a short-living reacting specie and rapidly reacts with water forming H_2O_2 or OH●, two aggressive reactive species.

Photoprotective Mechanisms:

To avoid detrimental effects of ROS, plants evolved several photoprotective mechanisms to cope with EL conditions at different time scales; these mechanisms can be distinguished based on their function (Niyogi, 1999),

Short-term photoprotective mechanisms include the following:

- Photochemical Quenching: the charge separation in RC acts as a direct quencher of excited states.
- ROS detoxification: ROS are detoxified thanks to the action of antioxidant molecules (such as Cars, tocopherol, or ascorbic acid) and detoxifying enzymes as Superoxide Dismutase (SOD).
- Water-water cycle: when PSI is saturated ferredoxin can directly interact with oxygen producing superoxide, this ion is converted into H_2O_2 by SOD and then to water by Catalase (Asada, 1999).
- Non Photochemical Quenching (NPQ): when PSII is saturated plants can dissipate excess energy as heat, thus contributing to lower excitation pressure on PSII RC (see also section: "*Non Photochemical quenching: Excess energy dissipation*") (Niyogi, 1999).

Long-term photoprotective mechanisms include:

- Antenna size modulation: plants can produce or degrade LHC protein to adapt light absorption based on quantity and quality of absorbed light (Escoubas et al., 1995).
- Modulation of enzyme biosynthesis: Calvin cycle, ATP production, and electron transport chain protein amount can be modulated depending on the growth conditions (Moejes et al., 2017).
- Chloroplast movement: chloroplasts can move in a plant cell to avoid excess light that could damage organelle functionality (avoidance) or, on the other hand, maximize the absorption surface under limiting light conditions (accumulation) (Wada, 2013).
- Heliotropism: the movement of leaves in a way to optimize light interception (Ehleringer and Forseth, 1980).

Non Photochemical Quenching: Excess Energy Dissipation

As mentioned above, the formation of $^3Chl^*$ states is an intrinsic property of Chls, leading to the production of ROS in the close proximity of PSII-RC or the PSII antenna system. In more details, deexcitation of $^1Chls^*$ excited states can follow three competitive ways: (a) photochemistry (qP), (b) it can be reemitted as fluorescence (F), or (c) dissipated as heat (qN/NPQ). In limiting light conditions most of the excitation energy is used to drive photosynthesis and produce ATP, a low percentage (about 1-2%) is emitted as fluorescence and only a small amount is dissipated as heat. In EL, when electron transport chain is saturated, photochemistry is virtually blocked and excess energy is dissipated as heat thus shortening $^1Chl^*$ lifetime and avoiding (or reducing) ROS formation. NPQ can be monitored *in vivo* as a light-dependent leaves Chls fluorescence quenching, thanks to special fluorimeters (PAM=Pulse Amplitude Modulation system) (Fig. 1.1.13) (Brooks and Niyogi, 2011). Several processes contribute to NPQ amplitude, affecting fluorescence rise and decay, these can be organized into: Energy dependent quenching (qE, with half-time of about 1 minute), intermediate quenching component (qZ, qM half time of 10-30 minutes) and the photoinhibitory quenching (qI, half time of hours). In recent years, qI has been dissected into two components: qI itself, caused by photoinhibition and photodamages, and qH, a sustained photoprotective slow-relaxing quenching component (Malnoë et al., 2018).

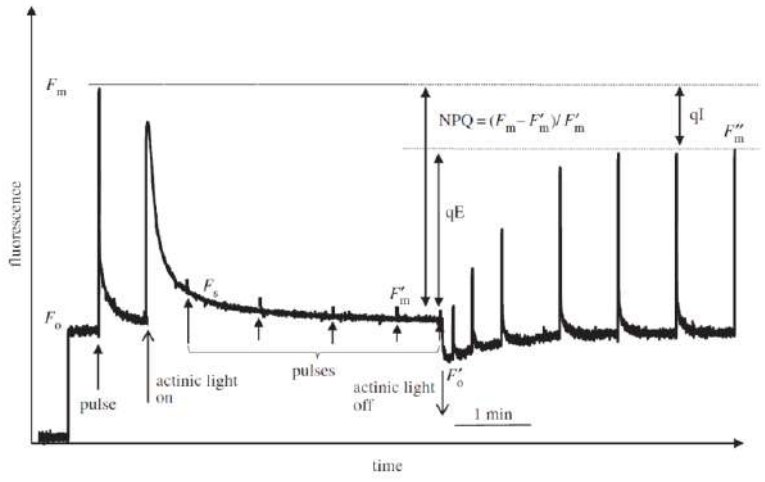

Fig. 1.1.13 | *Typical PAM fluorescence trace on Arabidopsis leaf showing induction and relaxation of NPQ. Source: (Ruban, 2017).*

The Energy Quenching (qE)

In excess light conditions, when electron transport chain is saturated, thylakoids ATPase cannot produce ATP due to the lack of its substrates ADP and Pi. Thus, the protons accumulated in the lumen as a result of ET cannot return to the stroma and causes hyper acidification of the lumen. Lumen acidification is the trigger for qE induction, which is activated in a time scale of about 20-60 seconds, fast enough to cope with natural sunlight fluctuation (Müller et al., 2001). The need for lumen acidification in qE induction has been demonstrated by treating plants with nigericin,

an ionophore drug inhibiting ΔpH formation, thus preventing qE formation (Takahashi et al., 2009). A low pH in the lumen has been shown to activate at least two events: the xanthophyll cycle (VDE conformational changes are induced by acidic conditions, thus determining Vio conversion into Zea) (Adams et al., 1996) and the protonation of specific lumen- exposed residues of PsbS, a pigmentless protein belonging to the LHC family (Dominici et al., 2002). PsbS is able to sense pH thanks to two Glu residues (Glu-122 Glu-226) arranged symmetrically and exposed to the lumenal surface of thylakoids, site-directed mutagenesis on these two residues completely abolished qE induction, as observed in the koPsbS *Arabidopsis* mutant (*npq4-1*) (Li et al., 2004). The precise location of PsbS is still under debate; it is localized in the grana but is not present in the C_2S_2 supercomplex and neither in the $C_2S_2M_2$ (Nield et al., 2000; Caffarri et al., 2009). Bergantino and co-workers showed the existence of reversible interactions, involved in NPQ control, between PsbS and PSII-antenna proteins (Bergantino et al., 2003), consistently, in more recent years similar evidence have been reported by (Sacharz et al., 2017).

As shown in several studies, Lhcb proteins are the best candidates for hosting qE quenching sites. The *A. thaliana ch1* mutant (knock-out for the Chl *a* oxidase gene) cannot build up PSII-antenna proteins (Lhcbs cannot be correctly folded in the absence of Chl *b*), exhibits a strong reduction in qE activation and an increased level of peroxidation under EL conditions due to the lack of a rapid photoprotective response. (Havaux et al., 2004). The contribution of single Lhcb moieties in qE activation has been widely studied thanks to reverse genetic approaches. The availability of insertional knockout lines for *lhcb4*, *lhcb5* and *lhcb6* showed the fundamental role played *in vivo* by Lhcb4 / CP29 in NPQ fast activation, while Lhcb5 / CP26 and Lhcb6 / CP24 appear not to be involved in the mechanism (De Bianchi et al., 2008, 2011). In 2014, an RNA interference analysis was applied to knock down the main components of LHCII, namely Lhcb1 and Lhcb2, showing a dramatic decrease in qE in the *amiLhcb1* lines and negligible effects in *amiLhcb2* (Pietrzykowska et al., 2014), *kolhcb3* mutant did not show significant effects on qE (Andersson et al., 2003).

However, no single Lhcb mutant showed a complete depletion of qE showing redundancy in LHCs gene family.

In 2017, Dall'Osto and colleagues produced the *NoM* mutant, a triple knockout mutant unable to accumulate the Lhcb4, Lhcb5, and Lhcb6 proteins that showed slower qE kinetics compared to WT suggesting the role that monomeric antenna proteins play in NPQ activations (Dall'Osto et al., 2017). However, very recently, the production of the *NoLHCII* mutant, produced by crossing the *amiLhcb1* and *amiLhcb2* lines, retaining all monomeric antenna proteins and about 5% of trimeric LHCII showed qE kinetics very similar to *ch1*, proposing LHCII as a unique quenching site between the outer antenna of PSII (Nicol et al., 2019). All this contrasting evidence contributed to the definition of different NPQ activations models designed to settle the role of Lhcb, PsbS, xanthophylls and RCs.

The two main hypotheses proposed so far are based on the dependence or independence of qE activation on monomeric Lhcb proteins:

- **Multiple Quenching sites model:** Under EL light conditions, protonated-PsbS displays affinity for CP29 leading to the disassembly of the $C_2S_2M_2$ supercomplex in C_2S_2 and CP24-LHCII (Betterle et al., 2009) both able to interact with PsbS thus creating two quenching sites, the first activated within a few minutes in monomeric antennae and a second one in peripheral LHCII (Dall'Osto et al., 2017).
- **LHCII-only dependent model:** This model is based on the property of LHCII to encounter aggregation at low pH *in vitro,* thus determining a fluorescence quenching (Horton et al., 1991). In EL conditions, ΔpH acts as a trigger for LHCII aggregation, with PsbS acting as a catalyst for the process not being directly involved in quenching (Townsend et al., 2018; Ruban and Wilson, 2020).

Moreover, other important open questions about qE mechanisms concern the biophysical mechanism involved. The principal quenching mechanisms proposed are the following:

- Chl-Chl interactions acting as quenchers (Müller et al., 2010; Wahadoszamen et al., 2012).
- Formation of short living Chl-xanthophyll excited states, suited as a trap for singlet Chl states (Ruban et al., 2007; Bode et al., 2009; Van Oort et al., 2015).
- Charge transfer Chl-Zea, excess energy leads to the formation of a Zea-radical cation ($Zea^{\bullet+}$) in one of the LHC subunits, due to charge separation event between Zea and Chl *a*, when the two molecule reach the ground state excess energy is dissipated as heat (Holt et al., 2005).

Xanthophylls and qE modulation:

As briefly mentioned in the previous paragraph xanthophylls play a crucial role in qE activation and regulation even if detailed biophysical mechanisms are still under debate. In plants, the Car composition is continuously modulated to cope with changing environmental conditions, the fastest mechanism is the xanthophyll cycle (see Section "*Carotenoids*") allowing Vio accumulation under LL conditions and Zea in EL. In plants, Zea is a positive modulator of qE and the *Arabidopsis* mutant *npq2*, constitutively accumulating Zea, presents faster qE kinetics, thus implying the requirement of Zea for qE full activation (Niyogi et al., 1998; Li et al., 2002b) (Fig. 1.1.14).
Lut is also involved in qE kinetics, *lut2 Arabidopsis* mutant, unable to produce Lut, presents a reduced NPQ amplitude while Lut hyper-accumulation in the *szl1* x *npq1* mutant partially compensate the lack of Zea (Li et al., 2009b).

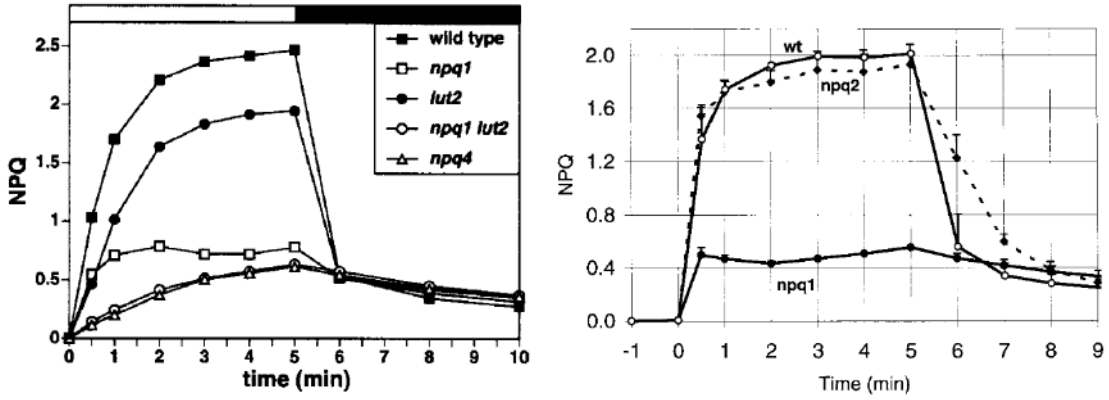

Fig. 1.1.14 | ***Left Panel:*** *NPQ phenotypes of Arabidopsis mutants. Source: (Niyogi et al., 2001).* ***Right Panel:*** *Time Courses for Induction and Relaxation of NPQ in Leaves of the Wild Type, npq1, and npq2. Source: (Niyogi et al., 1998)*

Zeaxanthin dependent Quenching qZ:

Zeaxanthin is responsible for a slower NPQ component occurring in parallel with the reconversion of Zea into Vio, in timescale of about 10 to 60 minutes (Nilkens et al., 2010). In *Arabidopsis*, Zea-dependent quenching is independent on PsbS and is probably due to Zea binding to monomeric Lhcbs, with CP26 being essential for the establishment of this slow component (Dall'Osto et al., 2005).

Chloroplast Movement qM:

This component does not actually promote a thermal dissipation; in fact, chloroplast re-location during EL conditions determines a decrease in light absorption (avoidance) increasing leaves transmittance (%T). The process is triggered by a blue-light photoreceptor (PHOT2) under blue or withe actinic light (Wada and Kong, 2018). Red light is not capable of induce qM, therefore, the use of red actinic light is preferable in NPQ measurements to avoid the contribution of chloroplast movement. (Fig. 1.1.15) (Cazzaniga et al., 2013; Dall'Osto et al., 2014b).

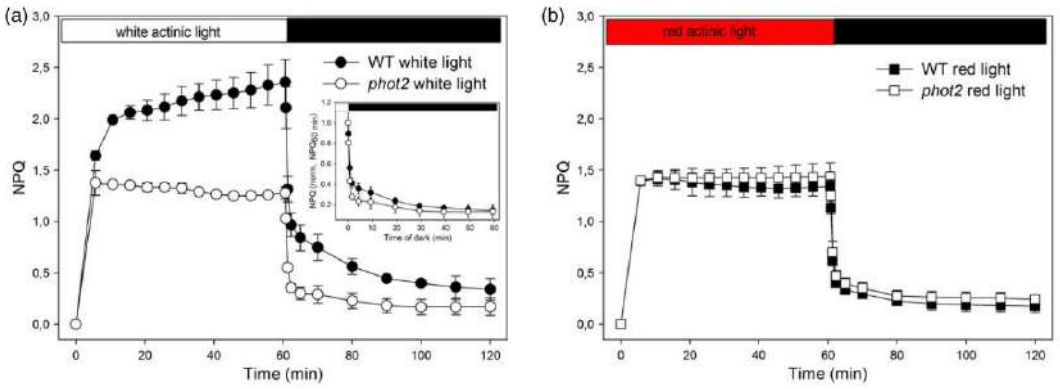

Fig. 1.1.15 | *Kinetics of formation and relaxation of photoprotective energy dissipation in WT and phot2 leaves. (a, b) NPQ kinetics were measured on WT and phot2 leaves upon illumination with either white actinic light (400 µmol photons m^{-2} sec^{-1},22°C (a), or red actinic light (350 µmol photons m^{-2} sec^{-1}, 600 < λ<750 nm, 22°C (b). Inset, kinetics of NPQ dark recovery in WT and phot2, after normalization to NPQ values at the end of the white light window. Source: (Cazzaniga et al., 2013).*

State Transitions qT:

PSII and PSI have different performances concerning the capture of light, depending on the quantity and, more important, the quality of incident light. In more detail, PSII presents a broader absorption peak in the blue and red spectrum while PSI presents a far-red region. In shading or canopy conditions, photon absorption rate of PSI and PSII is uneven, in these conditions state transitions (qT) are activated to balance energy distribution between the two PSs (Rochaix, 2007). State transitions are caused by the movement of LHCII trimers from PSII (state 1) to PSI (state 2) mediated by the phosphorylation of LHCII by the kinase STN7 (STT7 in algae) (Fig. 1.1.16)(Bellafiore et al., 2005). Knockdown of specific LHCII moieties proved the involvement of Lhcb2 isoform in the activation of state transitions (Pietrzykowska et al., 2014). During years contribution of qT in NPQ has been revised considering NPQ kinetics of *A. thaliana stn7* mutant, identical to WT, (Bellafiore et al., 2005) and observing that qT is only possible under LL conditions, and it is mainly involved in long-term acclimation (Tikkanen et al., 2012; Wientjes et al., 2013).

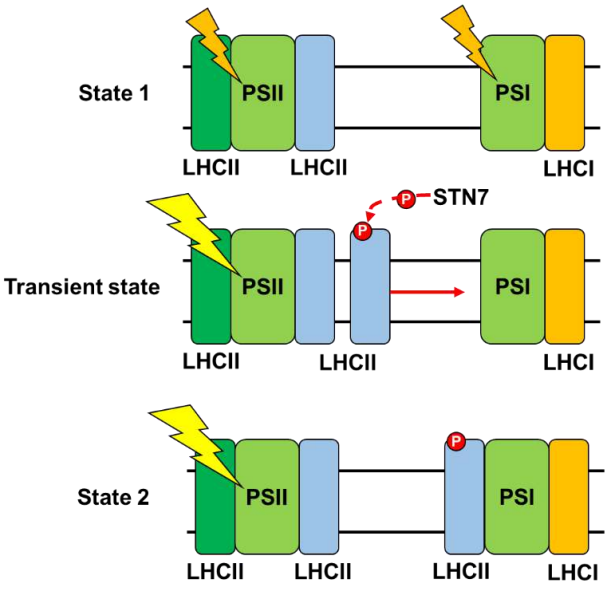

Fig. 1.1.16 | *Schematic representation of the regulation of state transitions.*

Sustained Quenching qH:

A sustained decrease of fluorescence in PSII external antenna system. qH is independent on other types of NPQ such as PsbS, pH, or Zea-mediated. qH has been shown to be catalyzed by a chloroplast lipocalin (LCNP), a soluble protein of about 29 kDa located in the thylakoid lumen whose expression is up regulated under stress conditions such as drought or EL (Malnoë, 2018). LCNP-dependent mechanism is controlled by the action of SOQ1 (Suppressor of Quenching 1) a transmembrane protein that negatively regulates qH induction (Fig. 1.1.17). The double mutant

ch1 x *soq1* showed NPQ kinetic indistinguishable compared with *ch1* indicating that SOQ1-mediated quenching reactions are localized in PSII-peripheral antenna complexes (Malnoë et al., 2018).. Further genetic analyses identified ROQH1 (Relaxation of qH 1), an atypical short-chain dehydrogense-reductase localized in the stroma membranes, that contributes to the maintenance of light harvesting efficiency acting antagonistically with LCNP, protecting the photosynthetic apparatus under low temperature and EL conditions (Amstutz et al., 2020). The precise role of individual PSII antenna in the mechanism remains an open question.

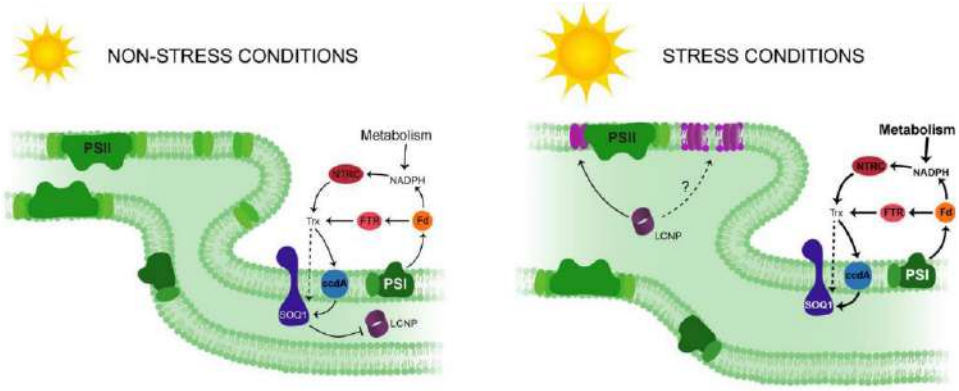

Fig. 1.1.17 | *Model for qH. Under non-stress conditions, SOQ1 inhibits LCNP activity. Under stress conditions, such as cold and high light, LCNP is active, and quenching sites indicated by purple color are produced in the peripheral antenna of PSII. Source: (Malnoë, 2018).*

Photoinibitory quenching (qI):

The slowest quenching component. qI is often associated with the repair cycle of PSII D1 subunits and, in general, involves the decrease of PSII RC activity due to photodamage (Aro et al., 1993). qI relaxation is very slow, in the time scale of hours, and correlates with the *de novo* biosynthesis of PSII components (Niyogi, 2000). Recently, (Nawrocki et al., 2021), proposed a model to describe the formation of qI site mediated by ROS attack to PSII RC, thus determining the closure of the RC and the formation of quenching sites, which are lost upon FtsH (a thylakoid protease)-mediated PSII degradation.

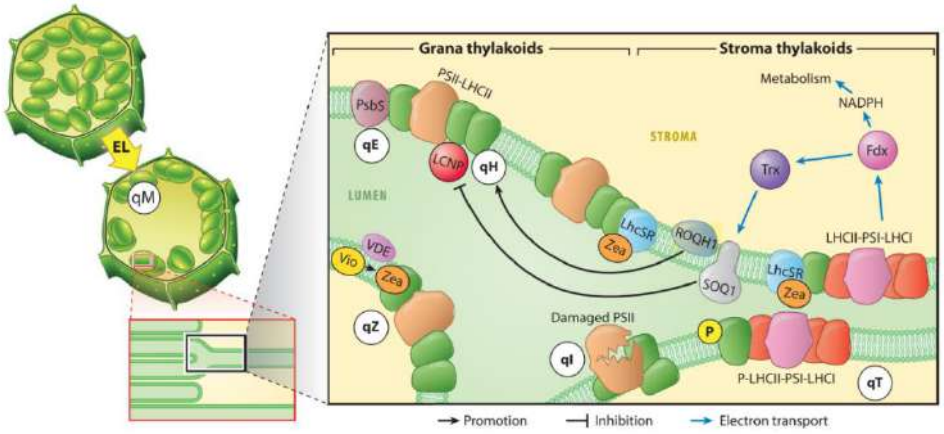

Fig. 1.1.18 | *Model for the localization of different EL-induced photoprotective processes at the cellular and molecular level. Source: (Bassi and Dall'Osto, 2021)*

1.1.5 Genome Editing as a tool to investigate Photoprotective Mechanisms:

CRISPR-Cas9 mediated genome editing:

The CRISPR-Cas9 mechanism was first observed in prokaryotes, acting as an immune system to protect bacteria from viral invasions (Deltcheva et al., 2011; Jinek et al., 2012). The acronym CRISPR stands for: "Clustered Regularly Interspaced Short Palindromic Repeats", short repeated genomic sequences separated by spacers derived from the integration of external plasmids or viruses (Mojica et al., 2005). The immunological response is mediated by an RNA-guided-DNA interference, and the CRISPR sequence is transcribed into an RNA molecule (pre-crRNA) and then processed to anneal with a non-coding RNA sequence (tracrRNA). The hybrid RNA molecule (crRNA-tracrRNA) recruits the Cas9 protein and guides it near the target DNA sequence. A short sequence, typically NGG, flanking the target sites allows for correct recognition; it is known as the protospacer adjacent motif (PAM) (Fig. 1.1.19 upper panel). When DNA is correctly recognized by the RNA-Protein complex is cleaved by two distinct DNAse domains (HNH and RuvC) inducing the formation of a double-strand brake (DSB). The CRISPR-Cas9 tool is based on the synthesis of a single RNA molecule mimicking the hybrid crRNA-tracrRNA, the single-guide RNA (sgRNA). The power of this tool is the ease to produce specific sgRNA targeting desired sequencing to induce DSB. Once produce DSB can be repaired by the organism by following two independent mechanisms: homology-direct repair (HDR) through the exploiting of homologous sequencing (low error rate) or non-homologous-end-joining (NHEJ) that could result in the production of errors or the random insertion/deletion of nucleotides (Fig. 1.1.19 lower panel) (Doudna and Charpentier, 2014). At its very basic level CRIPR-Cas9 allows for the knock-out of genes, but it is also possible to exploit the system to precisely integrate sequences in desired loci within genome (Kim et al., 2020).

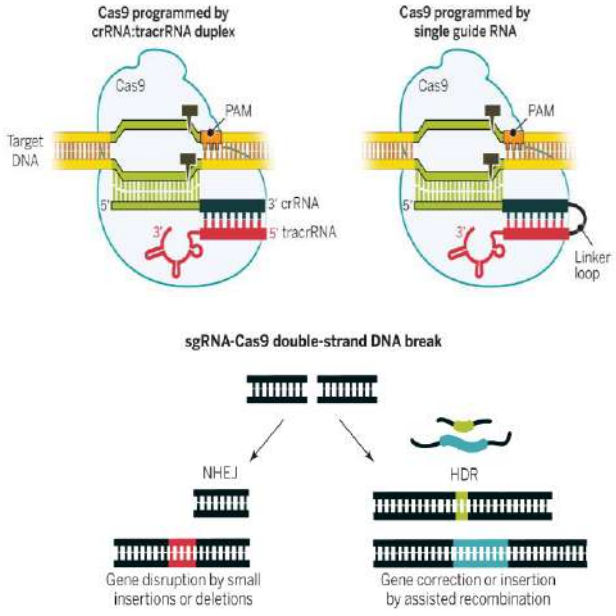

Fig. 1.1.19 **|** ***Upper panel:*** *The structure of S. pyogenes Cas9 in the unliganded and RNA-DNA–bound forms.*
Lower panel: *Different strategies for introducing blunt double-stranded DNA breaks into genomic loci, which become substrates for endogenous cellular DNA repair machinery that catalyze nonhomologous end joining (NHEJ) or homology-directed repair (HDR). Source: (Doudna and Charpentier, 2014).*

Genome editing to study NPQ:

Over the years several studies aimed to find NPQ quenching sites. Several approaches have been used, from *in vitro* investigation of recombinant LHC protein to *in vivo* treatment of plants with drugs that interfere with specific physiological events, such as the use of lincomycin, an inhibitor of chloroplast ribosomes, used to obtain plants with a reduced level of RC (Ruban and Wilson, 2020). In the last decades the availability of insertional knockouts for most of PSII subunits lead to the possibility of reverse genetics approaches.

As already mentioned in section "*The Energy Quenching (qE)*", all these studies contributed to the production of different and incompatible activation models for qE. This is probably due to the redundancy of functions typical of the LHC family, but also mainly to the fact that a real complete knock-out mutant for LHCII (the main quencher) is impossible to achieve via classical crossing methods; this is due to the high number of LHCII encoding genes (9 in total) (Jansson, 1999) and their clustered organization in the genome.

The incoming of the CRISPR-Cas9 era deeply changed the approach of molecular biologists (Doudna and Charpentier, 2014) paving the way for fine interventions at genetic level exploiting a user-friendly and almost ready to use tool. The technology was soon exported to plant biology and, after the optimization of plant versions of Cas9 gene driven by increasingly effective promoters, allowed for the inactivation of multiple genes in a single transformation event directly in the first or second transgenic generation (Ordon et al., 2017). This approach has recently been successfully applied to delete all five genes encoding Lhcb1, the most abundant isoform of LHCII, a first step towards the production of a genotype completely devoid of LHCII (Ordon et al., 2020).

This chapter has been published as chapter 7 in the book: "Photosynthesis in Action: Harvesting Light, Generating Electrons, Fixing Carbon". DOI: 10.1016/B978-0-12-823781-6.00005-8. Academic Press. 2022. ISBN: 9780128237816

Introduction

1.2 Improving Light Harvesting

CHAPTER

7

Improving light harvesting

Zeno Guardini, Rodrigo L. Gomez, and Luca Dall'Osto

Department of Biotechnology, University of Verona, Verona, Italy

Abstract

The family of Light-Harvesting Complexes (LHCs) includes integral membrane proteins, which combine with the core complexes of both photosystems and form a flexible peripheral antenna system in order to enhance the absorption of light quanta and provide protection against excess light stress. Following their first appearance, LHCs underwent evolutionary diversification into a large protein family and this differentiation was a crucial event in the adaptation of photosynthetic organisms to changing light environments and the colonization of different ecological niches. Indeed, plants and algae undergo highly variable irradiance and spectral quality in space and time, which probably shaped the evolution of a plethora of processes to counteract these fluctuations and finely adjust light-use efficiency. Many of these mechanisms are hosted by LHCs. Consistently, multiple findings have suggested that the crucial point in enhancing the efficiency of photosynthesis is the optimization of the light-harvesting process. In this chapter, developing and promising approaches will be presented for a prospective redesign of antenna systems.

Key Words: Light-harvesting complexes, antennae, LHC, crops, microalgae, non-photochemical quenching (NPQ), pigments, antenna size, chloroplast photorelocation, excess light, photoprotection, photoinhibition.

1.2.1 Functional architecture and molecular physiology of light harvesting in plants and green algae

'Net primary production' is the difference between carbon (CO_2) fixed into sugars during photosynthesis and carbon released by respiration (Clark et al., 2001), that is, it represents the energy stored in plant material that becomes available as a source of food, feed and fibre. Sunlight, the driving force of photosynthesis, is a diffuse energy source that must be concentrated before conversion into chemical form can occur. So light harvesting is a fundamental step in net primary production, indeed it has been identified as a target for synthetic improvement of biomass and bioenergy production in plants and algae.

In each photosystem (PS), sunlight is absorbed by chlorophylls (Chl) and excitation energy is rapidly transferred to a reaction centre (RC). There, a charge separation event fuels the electron transport chain and promotes water oxidation and $NADP^+$ reduction, generating a trans-membrane proton motive force used for ATP synthesis (Nelson and Ben-Shem, 2004). Each PS is made up of a core complex that houses the RC and an array of membrane-embedded light-harvesting complexes (LHCs), shaping a modular antenna system that surrounds the core. Together, these elements form a so-called supercomplex (Figure 1.2.1) (Croce and van Amerongen, 2020).

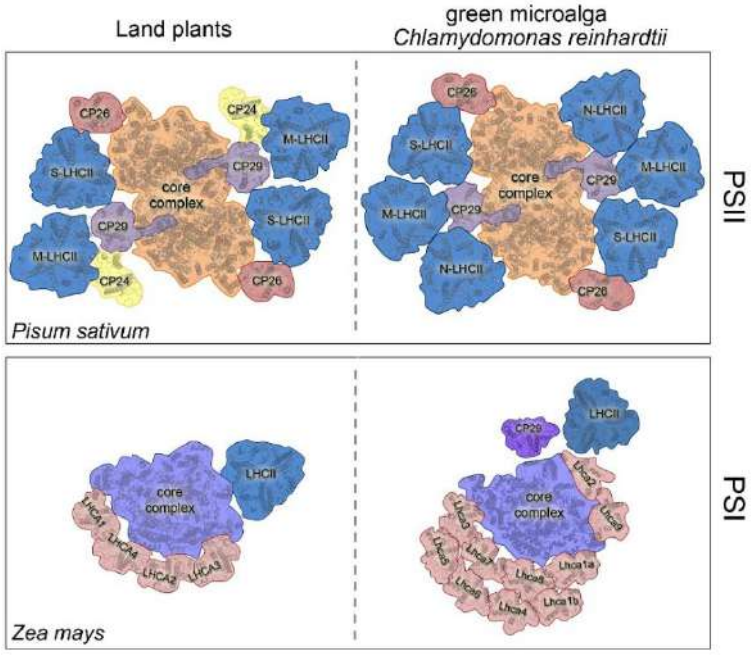

Fig. 1.2.1 | *Models of the supramolecular organization of Photosystems in land plants and green microalga C. reinhardtii.* *(upper part) PSII supercomplex of plants (left panel) and green algae (right panel). Models were assembled based on the 3D structures of P. sativum $C_2S_2M_2$ (Su et al., 2017) (PDB 5XNM) and C. reinhardtii $C_2S_2M_2N_2$ (Shen et al., 2019b) (PDB 6KAF). (lower part) PSI supercomplexes of land plants (left panel) and C. reinhardtii (right panel). Models were assembled based on the 3D structures of Z. mays PSI-LHCI-LHCII (Pan et al., 2018)(PDB 5ZJI), C. reinhardtii PSI-LHCI (Suga et al., 2019) (PDB 6JO5) and the projection map of algal PSI upon state transitions (Drop et al., 2014). The structures of CP29 and LHCII (Shen et al., 2019b) (PDB 6KAF) were used.*

Evolution generated a wide group of photoautotrophs, ranging from cyanobacteria to higher plants. These optimized the photosynthesis process, making it possible to occupy the most diverse ecological niches, which occurred along with the enlargement of the LHC super-family (Dall'Osto et al., 2015), in contrast with the high level of conservation in the composition of core complexes (Neilson and Durnford, 2010). Antenna subunits comprise about 40% of the protein content in the thylakoid membrane. They all share common structural motifs, with membrane-spanning regions hosting many Chl-binding residues (Pan et al., 2011).

In addition to enlarging the absorption capacity of the supercomplexes, antenna systems regulate light-use efficiency and provide an enhanced level of photoprotection. Indeed, while the efficiency of energy conversion is maximal under moderate irradiance levels, photosynthesis is hampered under excess light (EL) conditions. In these cases, the concentration of Chl singlet excited states (^{1}Chl*) in the photosynthetic machinery exceeds the capacity to use this energy, a phenomenon known as over-excitation. Under these conditions, the probability of the spontaneous formation of Chl triplets (^{3}Chl*) increases, leading to the release of singlet oxygen ($^1O_2$) (Figure 1.2.2), a reactive oxygen species (ROS) which might act as damaging agent as well as signaling molecule (Dogra and Kim, 2020).

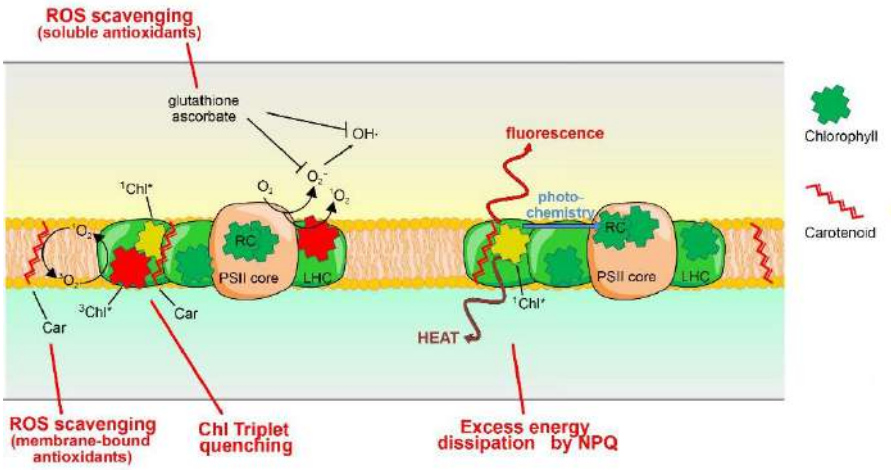

Fig. 1.2.2 | Photoprotective mechanisms of PSII. *(left) In pigment-binding complexes, the transition $^1Chl^* \rightarrow {}^3Chl^*$ leads to $^1O_2$ release, and possibly the univalent reduction of O_2 produces O_2^- and OH·. Carotenoid (Car) scavenge ROS and modulate $^3Chl^*$ yield. Other antioxidant system include the soluble compounds glutathione and ascorbate. (right) NPQ mechanism regulates $^1Chl^*$ lifetime. Light absorbed by the PSII can be used for driving photosynthetic electron transport, or can be lost as fluorescence or heat. Since these processes are in competition with each other, an increased efficiency of a process leads to a decreased efficiency of the two others. The mechanism of NPQ accounts for light-induced excitation decay by heat loss.*

Molecular safety valves are built-in LHC proteins which catalyze detoxification of $^1O_2$ or prevent its formation by quenching ^{1}Chl* excited states (see above) (Li et al., 2009b). The evolutionary selection of LHCs that are more efficient in their photoprotective responses was probably crucial during transition from an aquatic to a land environment, in which a concomitant increase in O_2 concentration led to a higher risk of $^1O_2$ formation and photodamage (Triantaphylidès et al., 2008). The evolution of photosynthesis therefore occurred together with the diversification of LHC on multiple isoforms, which gave rise to a genetic complexity within a conserved supramolecular assembly. These events were important during evolution and led to a number of gene products tuned to a different balance between light harvesting and photoprotection capacity.

LHCII, the major antenna of higher plants (Liu et al., 2004), has three membrane-spanning helices, connected by both stroma- and lumen-exposed loops, and two amphipathic helices exposed to the lumen. The complex binds 4 carotenoids, 8 Chl *a* and 6 Chl *b* molecules. More recently, a cryo-electron microscopy structure resolved at 2.7 Å showed that the PSII supercomplex from *Pisum sativum* is comprised of a dimeric core-complex (C_2), and each half of the core binds the so-called trimeric antenna LHCII-S (strongly-bound, named for their resistance to detachment by detergents) and one copy of each monomeric antenna proteins Lhcb4 (CP29), Lhcb5 (CP26) and Lhcb6 (CP24). The latter coordinates additional LHCII-L (loosely bound) trimers which accumulate in LL conditions. The whole supercomplex is thus labelled $C_2S_2M_2L_2$ (Su et al., 2017). In the green alga *Chlamydomonas reinhardtii*, an additional trimeric LHCII (LHCII-N) occupies the position of CP24, which is present in the higher plants PSII–LHCII but absent in this species (Figure 1.2.1) (Shen et al., 2019b).

The core complex of PSI is also endowed with a peripheral antenna system called LHCI (Light-Harvesting Complex of PSI), which, in plants, consists of four antenna proteins (Lhca1-4), one copy each per supercomplex (Figure 1.2.1) (Pan et al., 2018). The study of the PSI-LHCI supercomplex in organisms other than higher plants found differences in organization: a recent 3D structure of PSI supercomplex from the green alga *Chlamydomonas reinhardtii* revealed 10 LHCI subunits distributed between two different locations of the supercomplex (Figure 1.2.1) (Suga et al., 2019). LHCII is also known to move from PSII and bind to PSI, increasing its light-harvesting capacity. Beside the more abundant members, the LHC super-family includes other proteins that share sequence similarity with the formers yet having significant functional differences, namely PsbS, LhcSR and light-harvesting-like (LIL) proteins.

PsbS is a four-helix protein which is essential for both the photoprotective mechanism of excess energy dissipation NPQ (Non-Photochemical Quenching, see above) and the EL-dependent reorganization of the antenna system within PSII in plants. On the other hand, PsbS protein is transiently expressed in *C. reinhardtii* under EL acclimation (Tibiletti et al., 2016; Redekop et al., 2020).

LhcSR is also essential for NPQ but in green algae and mosses, since plants lack ortholog of *lhcsr* genes. In *C. reinhardtii*, LhcSR was first described as a stress-related protein, the transcripts of which accumulate in response to EL conditions (Tokutsu et al., 2019).

LIL can be found in both plants and algae. This class includes proteins which differ in their number of transmembrane segments: three-helix early light-inducible proteins (ELIPs), one-

helix proteins (OHPs) and stress-enhanced proteins (SEPs) (Rochaix and Bassi, 2019). LILs are probably involved in photoprotection rather than light harvesting (Li et al., 2019b).

Why do photosystems need to equip themselves with an outer antenna system? In addition to light harvesting, the specific properties of the LHCs are the ability (i) to actively regulate PSII light-use efficiency, and (ii) to catalyze photoprotective reactions. Indeed, fluctuations of light quality and quantity on a daily as well as seasonal basis give rise to changes of excitation pressure on plant PSII, which may overwhelm the capacity for photochemical quenching of ^{1}Chl*, thereby leading to increased $^1O_2$ release (Krieger-Liszkay et al., 2008; Roach et al., 2020) (Figure 1.2.2).
We can think of PSII as an engine: when sunlight is too abundant, it's like an increase in pressure that turns on a "safety valve" and gets rid of the excess excitation energy. Activation of photoprotective safety systems is therefore required in order to either detoxify ROS or limit their release into the chloroplast. LHC proteins have an irreplaceable role in all these processes. Lhcb proteins actively participate in down-regulation of the ^{1}Chl* lifetime through the process of NPQ, which is rapidly activated (timescale in seconds) to preserve PSII activity (Figure 1.2.2) (Ruban, 2016). NPQ allows excess excitation energy to be safely dissipated as heat, and is located within the PSII antenna system: indeed, the depletion of LHC proteins in plant mutants, such as *ch1* in the model plants *Arabidopsis thaliana*, leads to impaired NPQ activation and a dramatic increase in photodamage as well as a decline in the photosynthetic yield (Havaux et al., 2004). Additional regulation mechanisms under natural fluctuating light environments include the reversible migration of phosphorylated LHCII trimers between PSII and PSI (timescale in minutes), triggered by photosynthetic electron chain over-reduction, thereby balancing excitation distribution of PSs through the so-called state I – state II transition (ST) (Pesaresi et al., 2011). In the green alga *C. reinhardtii*, the amplitude of ST is far larger than in higher plants: the migration of CP26 and CP29 to PSI, in addition to that of LHCII, results in the dissociation of PSII supercomplexes and the enlargement of the PSI antenna (Tokutsu et al., 2009). Additional photoprotective mechanisms include long-term (timescale in days) photoacclimatory responses through the re-programming of gene transcription and protein turnover, leading to stoichiometric reduction of the trimeric LHCII complement (Flannery et al., 2021), thus relieving chronic over-excitation on the PSII.
Analysis of isolated LHC has been largely used as an *in vitro* system for studying NPQ and incorporates a multitude of different models. However, data derived mainly from *in vitro* measurements might not reflect the *in vivo* situation. To gain a deeper understanding, *Arabidopsis thaliana* plants lacking one or more Lhcbs have been produced, using a reverse genetic approach, and then characterized (Pietrzykowska et al., 2014; Dall'Osto et al., 2017). While findings supporting a reversible, conformational switch between unquenched and quenched states of LHCII units have been provided, there was no common agreement on the molecular events that lead to NPQ in plants. Major questions concern the interacting partners of PsbS and the localization of the quenching site(s) within the antenna of PSII (Sacharz et al., 2017; Dall'Osto et al., 2017; Townsend et al., 2018; Nicol et al., 2019; Guardini et al., 2020). Moreover, the high degree of conservation through evolution of LHC subunits and their spectroscopic peculiarities suggest specific functional roles for the different members of the system. The outer PSI antenna system

displays pigment organization similar to the other members of the LHC family, but regulation of light harvesting is different in PSI compared to PSII. Exposure to sustained over-excitation did not change the PSI core:LHCI, while the long-term decrease of LHCII content is a common response under EL. Instead, compensation for excitation unbalance between PSs is reached by binding LHCII as PSI additional antenna (Bos et al., 2017) and by the long-term modulation of PSI:PSII ratio (Ballottari et al., 2007; Bonente et al., 2012). Lhca subunits display peculiar spectroscopic features including the so-called "red spectral forms", that is, Chls with energy levels lower than the PSI RC. It is possible that red Chls provide preferential absorption of far-red (FR) photons transmitted under a canopy. Indeed, the characterization of the *Arabidopsis* KO mutant devoid of all PSI antenna subunits indicates that Lhca optimizes the photosynthetic electron transport by maintaining high PSI activity, by harvesting FR photons not absorbed by the PSII antenna (Bressan et al., 2018). These peculiar spectral properties possibly contributed to land colonization by plants and their adaptation to life under canopies.

1.2.2 Biological constraints in light-use efficiency

Land plants

Why might enhancing light harvesting and light-use efficiency be critical to improving the yields of the major crops? To understand this point, we could consider a formula for the so-called harvestable yield 'Y', defined as the yield that a crop can achieve under optimal conditions without suffering any biotic or abiotic stresses. The original equation proposed by Monteith (Monteith JL, 1977), and adapted by (Zhu et al., 2010), can be expressed as follows:

$$Y \propto S_{total} \cdot \varepsilon_i \cdot \varepsilon_c \cdot \varepsilon_p$$

where

- S_{total} is the total incident sunlight during the growing season;
- ε_i is light interception efficiency of photosynthetically-active radiation (PAR, 350–730 nm), which depends on leaf absorbance, growth rate of the culture, conformation of the canopy;
- ε_c is the conversion efficiency, that is, the total C assimilation, net of respiratory losses;
- ε_p is the harvest index, that is, the ratio of grain yield to total biomass produced by the crop.

Multiplying S_{total} by the constant 0.487, which takes into account the fraction of PAR that is either not absorbed or transmitted by leaves, the equation gives the harvestable yield in MJ m^{-2}, which can be converted into mass yield, based on the energy content of the harvested grain (Zhu et al., 2010).

In the context of the former equation, an increase in biomass yield can result from an increase in any of the terms. A number of findings suggest that the term ε_c can be further improved. For example, in soybean, an important dicotyledonous crop, artificial elevation of CO_2 concentration increased biomass yield by 18% over the growing season (Bernacchi et al., 2002), thereby (i) showing that enhancing photosynthesis in a crop does result in an increase in yield, and (ii) suggesting that genetic improvements might lead to similar results without increasing [CO_2].

What is the theoretical maximum value of ε_c in higher plants? Detailed analyses of the efficiency of energy transduction, through a series of steps from the absorption of light to the biosynthesis of carbohydrates, are available and can be summarized as follow:

1. Only photons in the waveband 350–730 nm can be used to fuel photosynthesis at high efficiency, moreover the weaker absorbance of Chl in the green region and reflection further reduces the interception of PAR to approximately 90% (Zhu et al., 2008).
2. Blue photons (350-450 nm) are more energetic than red photons (650-740 nm) and lead to higher excited states of Chls. However, they relax rapidly, before catalyzing photochemistry in the RC, thereby resulting in a further ~10% loss of energy as heat (Tredici, 2014).
3. In the RC of each photosystems, thermodynamic limits reduce the efficiency of photochemistry and charge separation, resulting in an energy loss of ~14% (Zhu et al., 2010).
4. Further energy losses are associated with photosynthetic electron transport, carbohydrate biosynthesis and mitochondrial respiration, with the result that the theoretical maximum conversion efficiencies of PAR into biomass are 4.6% in C3 crops and 6.0% in C4 crops, and 5.4% in microalgae mass cultures (see (Zhu et al., 2010; Tredici, 2014) for further details).

In addition to the theoretical calculation, values of ε_c can be determined in the field by measuring the accumulation of biomass in crops compared to the total amount of radiation intercepted by plants. This value is dependent on a number of factors, such as temperature and irrigation, while optimal nitrogen fertilization strongly increases ε_c. Interestingly, the maximal ε_c values were found to be about a third of the theoretical for most of the species considered, even in healthy crops with optimized spacing and good nutrition (Slattery and Ort, 2015).

Productivity in field crops is limited by a number of intrinsic features within the photosynthetic mechanism (Ort et al., 2015). In this chapter, we will only consider inefficiencies concerning light capture and the use of excitation energy to fuel charge separation.

Three distinct phases can be identified in a typical leaf CO_2 assimilation rate in response to sunlight intensity (Figure 1.2.3): (1) under low light, there is a linear increase of the photosynthetic rate with irradiance, that is, light is the limiting factor; (2) under higher irradiance, the photosynthetic rate undergoes inflection and rises in a non-linear way as a function of light; (3) when the light intensity is increased further, the assimilation rate reaches a plateau (Ye et al., 2013).

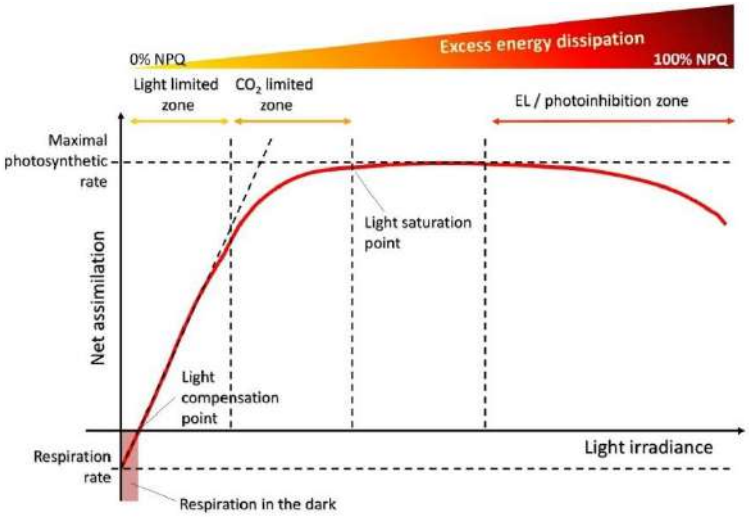

Fig. 1.2.3 | Light response curves for photosynthesis. *The light compensation point is the minimum irradiance at which the organism displays a gain of fixed carbon. The net assimilation rate displays a linear rise in response to increased light, within the range of light limitation. At higher light irradiances, saturation occurs as the efficiency of the photosynthetic mechanism is reduced, to which the activation of NPQ processes contributes. Under excess light, photosynthesis can decline as a result of photoxidative stress.*

The slope of the initial, linear rise represents the amount of CO_2 molecules that can be fixed per photon absorbed. Under low light, a large fraction of the photons captured (more than 80% of the absorbed PAR) can be used while, at higher irradiance, this value rapidly falls. For example, at 50% of full sunlight, about 25% of the absorbed photons are used but, under full sunlight, this value drops to less than 15% (Oberhuber et al., 1993).

In the case of plants placed close together, the light levels inside the canopy are extremely uneven: light intensity declines toward the base of a crop and forms a gradient (Zhi et al., 2014). Consequently, in the lower parts of the crop, irradiance is too low to sustain C assimilation. Most light is absorbed by the upper leaves, leading to light saturation: in this part of the plants, the major limitation on efficient light utilization is that leaves readily absorb more photons than they can productively use. Therefore, under EL conditions, PSII (which is usually highly efficient in PAR absorption) switches to a photoprotective state: the NPQ mechanism gets rid of the potentially harmful excess excitation energy as heat while PSII limits the production of ROS and preserves photosynthetic capacity (Niyogi, 2000). Such photoprotective energy dissipation occurs in the outer antenna system and competes with photochemistry in the de-excitation of the ^{1}Chl* states. The NPQ process involves the reversible activation of the xanthophyll cycle, which is dependent on the enzymes violaxanthin de-epoxidase (VDE) and zeaxanthin epoxidase (ZEP), and the sensing of changes in the lumen pH by the protein sensor PsbS (Li et al., 2009b; Steen et al., 2020). NPQ induction occurs over a time scale of seconds to minutes and is therefore a rapid response, independent of acclimatory changes in gene expression. Photoprotection is vital for the photosynthetic apparatus: if EL cannot be dissipated safely, oxidative damage of PSII occurs, which results in reduced photosynthetic efficiency, requiring the replacement of the damaged components before quantum yield efficiency can be restored (Li et al., 2002a).

On the other hand, activation of a dissipative channel decreases the quantum yield of PSII and so leads to a corresponding decrease in carbon assimilation. However, the light environment in a canopy is uneven and so plants are exposed to unpredictable extremes of high and low irradiance over the course of a day, for example, leaves that are higher in the canopy or due to passing clouds. Accordingly, plants must adapt to this intermittent shading (Külheim et al., 2002).
It is worth noting that the recovery of C assimilation from the dissipative state to the high-efficiency state is slower than the rate of light fluctuations: activation of a dissipative reaction inevitably leads to a substantial delay in quantum yield recovery and so to reduced CO_2 uptake.
Keep in mind the metaphor of PSII as an engine: NPQ dissipates excitation pressure under high light levels but, in the shade, the pressure in the engine decreases and NPQ also declines, but not quickly enough. The system therefore leaks, as if a lid had been left open, and the engine cannot run as efficiently.
Algorithms were deployed to predict photosynthetic dynamics in a model canopy and these simulations forecast that the delayed recovery of the photosynthetic efficiency on a decrease in irradiance would cause average losses in canopy carbon gain in the order of 15%, due solely to the constantly changing incident radiation on each leaf over the course of a day (Zhu et al., 2004).

Green microalgae

From the perspective of using sunlight and CO_2 to produce high-added value compounds and biomass through the mass cultivation of photoautotrophs, microalgae farming has garnered increasing interest in the last decades. Commercial production of algae on an industrial scale has been proclaimed as an environmentally-sustainable strategy for energy-rich feedstock production (Yen et al., 2013). Microalgae include a large group of photosynthetic, unicellular, eukaryotic organisms; in particular, green microalgae (class Chlorophyceae) include genera that are among the most widely used for massive cultivation, such as *Chlorella vulgaris, Dunaliella salina* and *Haematococcus pluvialis*. Microalgae are a source of genetic and metabolic diversity, since they include species adapted to diverse environmental conditions (Gimpel et al., 2015). Production in industrial-scale photobioreactors (PBRs) and biorefinery processes can yield a large variety of resources, such as bioactive compounds, recombinant proteins, wastewater treatment and biofuels, livestock feed, fertilizer and biostimulants (Benedetti et al., 2018).
The photosynthetic apparatus of green microalgae is similar to that of plants but the light-use efficiency of algae is appreciably higher. Many reasons contribute to such a high performance level:
(i) microalgae lack heterotrophic organs, the maintenance of which is costly, and the unicellular organization makes the whole biomass fully photosynthetically active;
(ii) algae have a short doubling time (a few hours) and are metabolically flexible, which means they undergo a metabolic shift on changes in environmental conditions, either from autotrophy to heterotrophy (using organic compounds as a source of C and energy) or to mixotrophy (carrying out photosynthesis as the main energy source and using both organic molecules and carbon dioxide as the C source) (Xie et al., 2020);
(iii) microalgae do not require fertile land and can grow on wastelands in brackish water or even sea water, so their cultivation would not compete with conventional crops (Abdel-Raouf et al., 2012);

(iv) different species can be selected for specific growth conditions, suited to even harsh climate (Treves et al., 2013).

Although several industrial applications of microalgae have been proposed, the only successful exploitation of their potential is, so far, the production of carotenoids. Production of high-value compounds is currently undertaken in small-scale cultivations, the operating costs of which will need to be reduced if they are to be competitive with other feedstocks (Borowitzka, 2013).

The overall cost of a biorefinery depends on the cellular content of the bioproduct and the growth rate of the culture, the latter being determined by the efficiency with which light is used to drive photosynthesis.

Calculations provided both the theoretical maximum of sunlight conversion efficiency and the productivity of microalgae, which are equal to 8–10% solar-to-biomass and 280 ton of dry biomass per ha per year, respectively (Chisti, 2007; Weyer et al., 2010). In contrast, outdoor mass cultivation of wild type strains recorded maximal productivity of around 80-100 ton of dry biomass per ha per year (Rodolfi et al., 2009). As has been shown in plants, overcoming this productivity gap is essential in order to exploit the full potential of microalgae.

Regulation of light harvesting is crucial for algal cells to balance light reactions and downstream biochemical processes. In a dilute culture of *C. vulgaris*, light saturation is reached at around 1000 μmol photons m^{-2} s^{-1} (Dall'Osto et al., 2019). At this irradiance, algae protect themselves from excess illumination by triggering NPQ in order to prevent the over-excitation of the RC. Moreover, algae can experience very high light, saturating photoprotective mechanisms. In this way, EL is mainly dissipated rather than contributing to biomass accumulation, or can even cause the release of ROS, which inhibits the photosynthetic machinery impairing biomass productivity (Figure 1.2.3).

A peculiar trait of microalgae is the size of the antenna systems in both photosystems, which are larger than they are in plants and cause uneven light distribution within the culture (Formighieri et al., 2012). These large antenna systems were selected by evolution as a favorable trait since, in natural environments, light is often a limiting factor for the growth, thus implying the need of maximizing light-harvesting capacity (Ort et al., 2011). Nevertheless, such a large antenna strongly contributes to the gap between theoretical and real productivity. Unlike in the natural environment, industrial cultures in PBRs need to reach a high biomass concentration per volume of installed facility (Freudenberg et al., 2021). This inevitably results in high optical density, determining a light shortage in the deeper layers of the cell suspension (Pandey et al., 2015). On the other hand, cells in the outermost layers absorb most of the photons, leading to the saturation of photosynthesis, dissipation of excitation energy and/or photoinhibition. The innermost layers fall below the compensation point of photosynthesis, while respiration consumes energy. It transpires those dense algal cultures suffer both photo-deprivation and photo-inhibition, thereby reducing the overall light-to-biomass conversion efficiency to below its theoretical value. Regulated mixing of biomass may relieve the effects of light gradients, while too rapid cycles between dark and over-saturating irradiance have a deleterious effect on the photosynthetic yield (Sforza et al., 2012). Modelling of the photosynthesis light-response curve in a culture suggests that the optimal setting of optical density (OD) should minimize shading while enhancing light absorption and net photosynthesis (Formighieri et al., 2012).

In conclusion, observations reported in this section suggest that the modulation of light reactions is one of the key factors in controlling biomass yield at both saturating and sub-saturating irradiance and is worthy of consideration as a domestication strategy aimed at improving productivity in both plants and algae.

1.2.3 Targets for improved light harvesting: the "cooperative interaction" concept

The inefficiencies listed in the previous chapter are inherent to the mechanism of photosynthesis. Much of our current knowledge about these biological constraints comes from studies on model plants and algae, in which key steps of the photosynthetic mechanisms have been altered, resulting in changes to the capacity of light harvesting or biomass production. Advances in our understanding of the functional and molecular details of these processes have paved the way for a challenging and exciting prospect, namely the manipulation of specific pathways to enhance the photosynthetic productivity of either crop plants or microalgal strains for industrial applications. The "cooperative interaction" concept underpins the "smart" populations of photosynthetic organisms, optimized in order to interact cooperatively in accessing a widely diffuse resource such as sunlight (Ort et al., 2015). The final aim is to improve the light-harvesting capacity of the population as a whole, rather than of the individual organism, the biotechnological equivalent of the sentiment "There is strength in numbers".
Genetic engineering approaches based on detailed knowledge of potential cooperation within the population is required. Light irradiance and spectral range vary minute by minute in a plant canopy or a microalgal culture, depending on passing clouds, the wind altering the shading offered by the uppermost leaves (Külheim et al., 2002; Zhi et al., 2014), or convective fluxes of microalgal cells within a PBR (Sforza et al., 2012). Such events lead to a significant portion of the population become increasingly shaded.
Which biophysical traits could be engineered to create a "smart" population with improved productivity?

Lowering cell absorptivity

The antenna size, that is, the number of pigments associated with each RC, is an important trait for the efficiency of photosynthesis. Indeed, under excess irradiance, cells absorb more light than can be used by downstream metabolic processes. This means they have an antenna with excess capacity. It was therefore predicted that reducing leaf Chl content would be a promising approach in enhancing light-use efficiency (Formighieri et al., 2012) since it would improve light distribution inside the canopy (Figure 1.2.4).

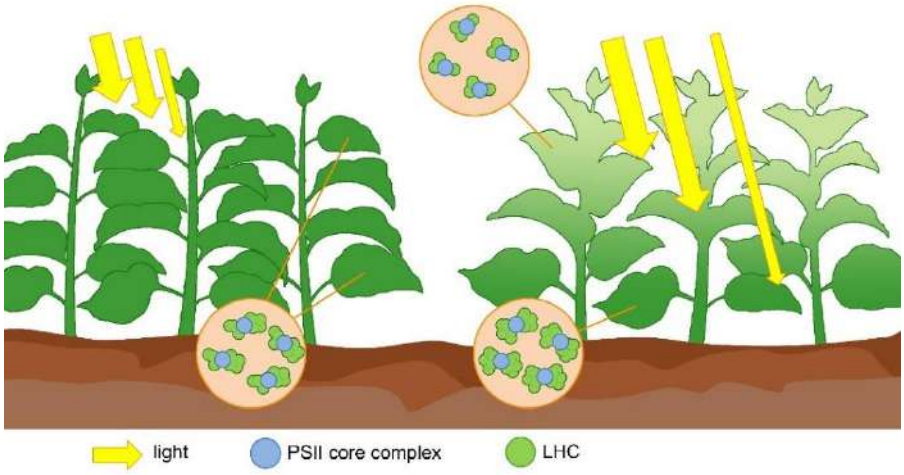

Fig. 1.2.4 | Potential molecular mechanisms of plants to be targeted for improved productivity. *The light environment inside a canopy is highly heterogeneous. Light declines toward the base of a crop canopy, generating gradients in the red to far-red ratio (R/FR), while cloudiness and shading by adjacent vegetation moved by the wind generate irregular fluctuations in the PAR. In a typical canopy (left), most light is absorbed by the leaves in the upper layers. A canopy with optimized light harvesting (right) would have upright, paler green leaves in the upper portions of the canopy and horizontal, darker leaves at the base. The light harvesting capacity would also be improved through a reduced antenna cross-section per photosystem in the upper leaf layers. The Chl b biosynthesis and/or the expression of LHC components could be regulated by the R/FR ratio.*

However, strategies to improve light penetration must ensure that lines with truncated antenna are not photosynthetically impaired in ways other than in reduced LHC content. Indeed, in higher plants, the depletion of a sub-group of LHCs, the so-called monomeric LHC, strongly affects the PSII light-harvesting efficiency and therefore the photoautotrophic growth, thereby cancelling out the benefits from optical density reduction (van Oort et al., 2010). Although they share some common features, LHC proteins are not all the same.
Even microalgae in mass cultures, suffer from uneven light distribution within the PBR. In the outer layers, light intensity leads to saturation (and possibly photoinhibition), while cells deeper in the culture suffer from light limitation, thus resulting in an overall decrease of productivity.
It has been proposed that a promising approach for the improvement of productivity in mass culture would be to target genes required for the synthesis of antenna pigments or their ligand LHC.

Decreasing photoprotective energy loss

In addition to considering antenna size, an increase in the quantum yield of PSII could be achieved by decreasing photoprotective energy loss in the photosynthetic apparatus. While excess energy must be carefully dissipated in order to avoid photooxidative stress (Figure 1.2.2), over-activation of NPQ brings about a significant loss in efficiency. Fine-tuning of photoprotective responses would allow a greater proportion of absorbed photons to be converted to biomass. Significantly, the relative weight of other photoprotective components, such as the

antioxidant carotenoids, must be considered in engineered cell lines. Indeed, the optimized accumulation of photoprotective pigments could compensate for the lack of defenses and preserve PS through the effects of photooxidation (Havaux et al., 2007).

Enhancing light capture

Not all the solar energy that reaches the Earth's surface is absorbed by the chromophores associated with photosystems. Usable PAR lies in the wavelengths ranging from 350– 730 nm, therefore comprising less than 50% of the incident solar radiation (Zhu et al., 2008). Moreover, because of the weaker absorbance of Chls and carotenoids in the green band, even the interception of usable PAR is not optimal.

However, the spectrum of absorbed PAR has been extended beyond these wavelengths in biological systems other than plants and green algae. Photosynthetic pigments such as Chl *f* (λ_{max} 706 nm), Chl *d* (λ_{max} 710 nm), and bacteriochlorophyll (λ_{max} approximately 700–1000 nm) absorb in the far-red wavelengths (Figure 1.2.5) (Chen and Blankenship, 2011; Nürnberg et al., 2018).

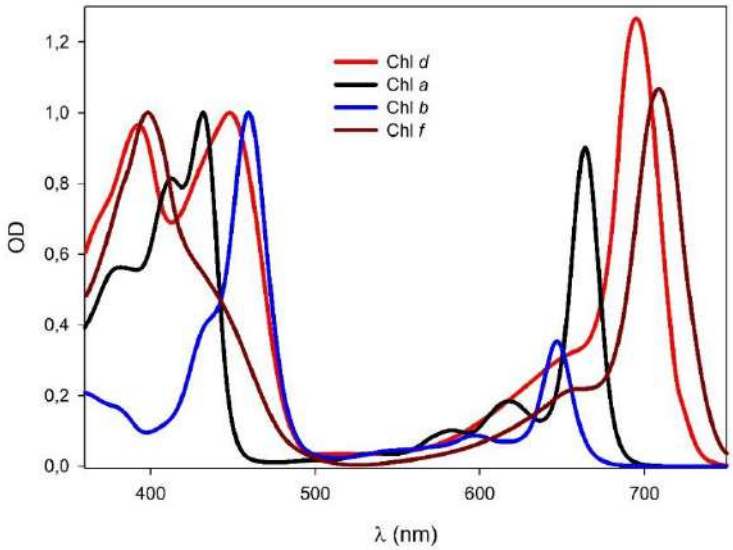

Fig. 1.2.5 | Absorption spectra of Chl a, b, d and f in organic solvent. *Each spectrum has been normalized at its Soret (blue region) peak.*

These pigments could potentially be engineered in plants or algal species. In addition, phycobilisomes, the antenna subunits of cyanobacteria, efficiently absorb green wavelengths (550–560 nm) and could also therefore be expressed in green microalgae in order to increase the efficiency of PAR absorption (Puzorjov and McCormick, 2020). This strategy could be combined with the optimization of LHC composition by expressing antenna isoforms that are more suited to either light-harvesting or photoprotection.

Sensing the ratio of red to far-red radiation

A peculiar feature of plants is their ability to sense the ratio of red (R) to far-red (FR) radiation. This becomes particularly important for high density cultivations. Leaves readily absorb R wavelengths but transmit most FR radiation so the light environment deeper under the canopy is enriched in FR components. The phytochrome mediates the sensing of the R/FR ratio, promoting downstream signalling, which modulates plant architecture (de Wit et al., 2016). This regulatory mechanism could be used to optimize the expression of molecular targets within the canopy, aimed at optimizing photosynthesis under the prevailing light conditions. Chl *d* or Chl *f*, with greater red-shift than Chl *a*, could be expressed differently in the lower leaves of the canopy, thereby increasing their capacity to intercept FR photons. The expression of light-harvesting systems could also be modulated by the R/FR ratio. Upper leaves, which receive the most R light, would synthesize PSs with a smaller antenna, thereby enabling a higher quantum yield, while the lower leaves in limiting light, would accumulate PS with increased antenna size and improved performance in the interception of photons (Figure 1.2.4).

Light-harvesting capacity might also be influenced by optimizing the antenna composition, such as by targeting mutations in the protein sequence of the wild type LHC, in order to modulate protein–protein and/or pigment-protein interactions and shift the absorption maximum of specific chromophores to longer wavelengths (Morosinotto et al., 2005b).

Optimized variation in leaf angle

In conditions of high plant density, half of the crop's photosynthesis takes place in the shade, so the reach of a more uniform distribution of sunlight inside the canopy would result in productivity boost. This could be obtained by optimizing the variation of the leaf angle (Ding et al., 2011), turning leaves in vertical in the upper portion of the canopy (under high light conditions) and those deeper in the canopy (low light conditions) turned horizontal (Figure 1.2.4). This would optimize the distribution of sunlight by avoiding the saturation of the upper leaves and increasing the irradiance that reaches the lower leaves.

Many of the aforementioned approaches remain on the drawing board and will require extensive research work and experimental validation. Of course, there are trade-offs with all possible mutations: although a number of biophysical traits could be identified as targets for genetic engineering, there is no one mutation that surely can solve all problems. Light harvesting in both crops and algae cultures should be viewed as part of a much more complex system, including not only the light reactions, but also a complex network of regulatory and acclimation processes. Thus, such manipulations should tailor to match growth conditions, locations and seasons. Nevertheless, models were presented which demonstrate the impact of genetic manipulations in a way that produces useful outcomes (Long et al., 2006), and some promising results have already been obtained (see further sessions).

1.2.4 Optimization of light harvesting in plants through genetic engineering

Over the last half century, the so-called "Green Revolution" in agriculture, a domestication strategy based on breeding and phenotypic selection, has managed to boost crop productivity (Langridge, 2014). This increase in crop yield was attained mainly by increasing the amount of biomass set aside for grain, that is, the harvest index ε_p, now considered close to its upper limit. More recently, several theoretical models have been drawn up to find new ways of enhancing crop productivity. Moreover, selected targets in the photosynthetic machinery have been manipulated by genetic engineering, in order to optimize light collection and select lines that can be used under specific light conditions.

As previously discussed, the high Chl pigment content of leaves leads to uneven light distribution within the canopy with the upper leaves shading those beneath, thereby reducing the system's efficiency. In simulations of canopy photosynthesis, the reduction of Chl content per leaf was found to be a promising approach to improving canopy performance (Ort et al., 2011). Then, transgenic plants bearing small antenna systems were produced and characterized. In many cases, the results were consistent with the predictions of the modelling. For example, transgenic tobacco, the biogenesis of the peripheral antenna of which was altered, displayed a truncated light-harvesting system and resulted in plants with higher biomass yield under high-density planting conditions (Kirst et al., 2017). Similar results were obtained in rice and *Arabidopsis thaliana* mutant lines with reduced Chl content (Gu et al., 2017; Jin et al., 2016). In other species, the outputs differed: photosynthetic efficiency was investigated in soybean mutants with pale-green phenotypes, and despite a significant (-50%) Chl depletion, the enhancement on biomass accumulation was very limited (Sakowska et al., 2018). While this result suggests that soybean significantly overinvests in Chl biosynthesis, the reduced pigment content failed to translate into higher yield from canopy-level processes. As previously shown, LHCs participate in the photoprotection of the photosynthetic apparatus so their reduction must be carefully calibrated. To this end, *Camelina sativa* plants were engineered to incorporate a range of reduction in Chl *b* levels, and so in LHC content, in order to pinpoint the efficiency threshold. Interestingly, plants with slightly reduced antenna size (Chl *a*/*b* ratio ~ 5.0) displayed enhanced biomass yield compared to wild type plants (Chl *a*/*b* ~ 3.0) but further reductions in this optimal antenna size impaired both light-stress tolerance and plant productivity (Friedland et al., 2019).

Recently, Kromdjik and colleagues (Kromdijk et al., 2016) produced tobacco plants that had been genetically-modified to use light more efficiently, by targeting three of the gene products that plants use to catalyze NPQ. In particular, two enzymes, violaxanthin de-epoxidase and zeaxanthin epoxidase, were over-expressed to boost the xanthophyll cycle needed to maximize NPQ, together with the regulatory subunit PsbS, which enhances the rate of NPQ formation. Engineered plants were able to bounce back from a "dissipative" into a "productive light-harvesting" state faster than the wild type, resulting in a 14-20% increase in the productivity measured in open field experiments. These results first displayed a genetic-engineering approach by targeting the regulatory mechanisms of light harvesting and succeeded in boosting the efficiency of photosynthesis, thereby potentially offering the opportunity for similar gains across major food crops. The finding is important because it confirmed that regulatory pathways of

photon capture are not optimized for maximum yield: plants prefer to produce less in exchange for a lower risk of being damaged by too much light. This implies that there may be significant room for further improvements. For example, it will be possible to dynamically down-regulate the dissipative reactions in order to make plants grow faster under lower light conditions, such as in greenhouses (Figure 1.2.6), or to reinforce the photoprotective responses to enable plants to grow in hostile environments (Davison et al., 2002), where EL is accompanied by other stress factors, such as cold or drought.

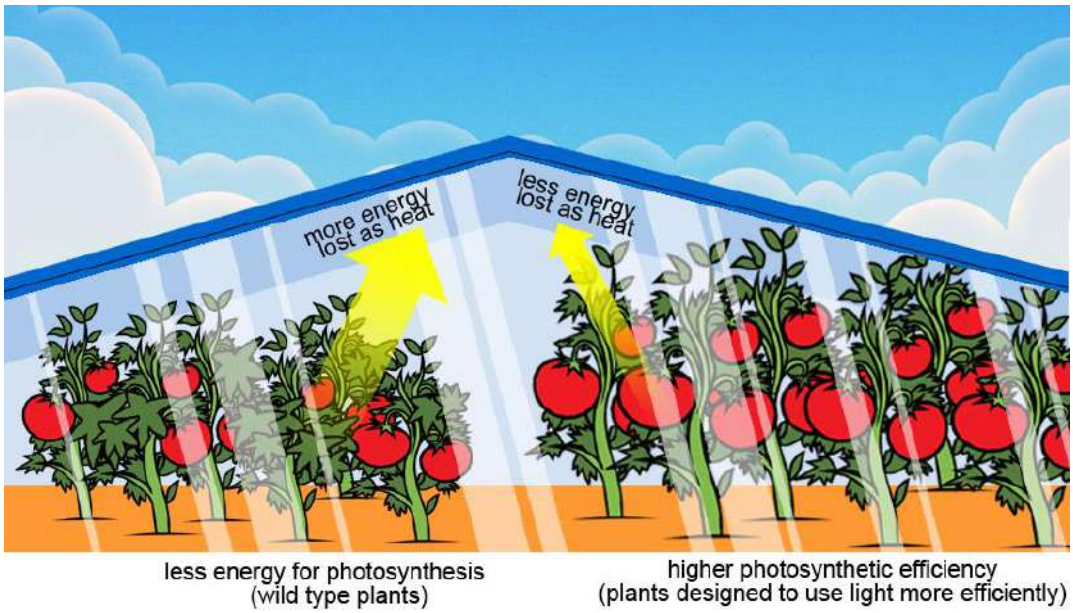

Fig. 1.2.6 | Genetic engineering of the light reactions of photosynthesis can potentially enhance crop productivity. *Recent experimental findings give weight to the idea that photosynthetic efficiency is a trade-off between energy used in growth and energy lost (Kromdijk et al., 2016). Crops of the future might be genetically tailored for high yield in specific environments. For example, plants intended for highly controlled environments such as a greenhouse could be engineered to eliminate photoprotective responses in favors of maximum productivity.*

Light is not only the essential energy source absorbed by the Chl-binding complexes that drive photosynthesis. It also participates in the coordination of a number of cellular processes that enhance photosynthetic performance. Phototropins (PHOT) are blue-light receptors that mediate a large number of responses that optimize light absorbance, such as phototropism, stomatal opening, chloroplast movement and leaf flattening (de Wit et al., 2016). Light-induced chloroplast movements are a regulatory mechanism for light harvesting. Chloroplasts are induced to move towards a weakly-illuminated area of cells to promote efficient photon capture, the so-called "accumulation response"; in contrast, they move away from high light levels, that is, the "avoidance response" (Figure 1.2.7) (Suetsugu and Wada, 2007).

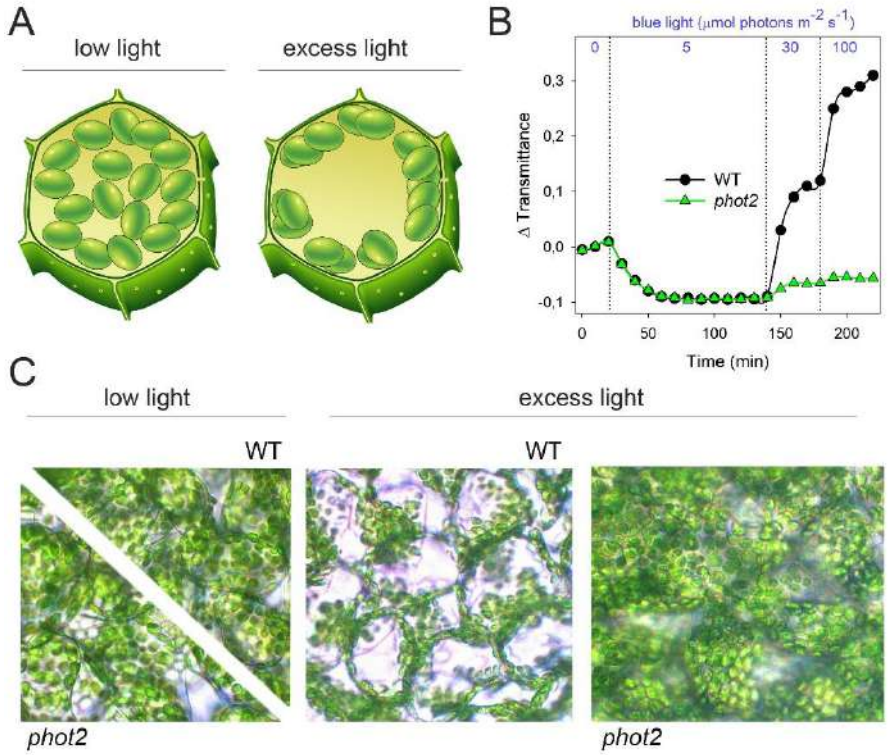

Fig. 1.2.7* | *Chloroplast movements in leaves. *(A) Schematic drawing of chloroplasts photorelocation. Chloroplasts can change their distribution within the cell in response to the intensity of the incident light, moving from positions yielding maximum light absorption to others in which light absorption is minimized. (B) Time course of changes in the leaf transmittance induced in WT and phot2 leaves by blue light at different intensities. Blue light at 5 µmol photons m^{-2} s^{-1} promotes accumulation response in both genotypes, while avoidance response can be observed at higher irradiance only in WT leaves. (C) Distribution of chloroplasts in the mesophyll cells of wild type and phot2 Arabidopsis, as determined by light microscopy. Leaves were dark-adapted for 1 h (left panel) and then irradiated with white light at 400 µmol photons m^{-2} s^{-1} for 30 minutes (right panels).*

Under low light conditions, the accumulation response induces the alignment of the chloroplasts on the upper surfaces of the mesophyll cells while, under EL conditions, chloroplasts align along the sides of cells, producing an "escape" response (Wada et al., 2003). Chloroplast movements affect leaf absorbance: as they accumulate, light harvesting capacity is maximized. Under EL, on the other hand, leaf absorbance of the upper cell layers is minimized, thereby providing protection against photodamage, and leaf photosynthesis is maximized due to greater light penetration within the mesophyll cell layers (Figure 1.2.7). Under natural conditions, the chloroplast distribution constantly changes and the balance between accumulation and avoidance responses adjusts the trade-off between light harvesting and photoprotection.
In *Arabidopsis thaliana*, the accumulation response is regulated by both phototropins PHOT1 and PHOT2, the avoidance response by PHOT2. The importance of these physiological responses has been investigated by using *Arabidopsis* KO mutants devoid of phototropin-mediated responses. The *phot1* plants displayed a reduced growth rate because of attenuated chloroplast accumulation

(Goh et al., 2009). Several research groups demonstrated that chloroplast avoidance response limits photoxidative stress of plants under strong or fluctuating irradiances (Kasahara et al., 2002; Sztatelman et al., 2010; Davis and Hangarter, 2012; Cazzaniga et al., 2013; Gotoh et al., 2018; Shang et al., 2019), thus suggesting this mechanism is critical for photoprotection in long-term (hours) EL conditions. In contrast, a recent report showed chloroplast movements did not play role in preventing PSII RC inactivation in shorter-term high light (Wilson and Ruban, 2020).

However, it is widely believed that the accumulation response is required for efficient light capture under weak light conditions. The light threshold for triggering the avoidance response is low (<100 μmol photons m^{-2} s^{-1}) so it might become activated even in leaves lying deeper under the canopy (Dutta et al., 2015). This may happen because the process is not optimized for maximum yield: in other words, plants may "prefer" to limit productivity in return for greater safety when there is too much light.

In a recent report, Gotoh and coworkers demonstrated that the chloroplast accumulation response is essential for efficient photosynthetic performance in *Arabidopsis*: *phot2* mutation enhanced leaf photosynthesis and increased plant biomass production under a wide range of light conditions (Gotoh et al., 2018). Therefore, the chloroplast accumulation response was seen as a potential physiological target that could be engineered to enhance light harvesting and biomass yield. It should be noted, however, that *phot2* plants are susceptible to very high light levels (1500-1800 μmol photons m^{-2} s^{-1}), that is, the level of irradiance that the upper leaves of a canopy can easily experience in field conditions in central/south Europe (https://ec.europa.eu/jrc/en/PVGIS/tools/daily-radiation). Therefore, caution should be applied in the suppression of the avoidance response since it might increase leaf photosensitivity and cancel out the benefits for biomass production.

In a recent work, Hart and collaborators (Hart et al., 2019) deployed protein engineering to improve the performance of phototropins and thereby light-use efficiency.

They suggested that the modulation of phototropin activity might offer a new opportunity to enhance the efficiency of light capture. Site-directed mutation on LOV domains of PHOT1 and PHOT2 succeeded in modulating the photocycle lifetime of *Arabidopsis* phototropins. These variants were used either to speed up or slow down photoreceptor activation *in vivo*. In this way, slowing the phototropin photocycle enhanced light harvesting responses, while accelerating it reduced phototropin's sensitivity for chloroplast accumulation movement. As a consequence, plants engineered to have increased responsiveness of PHOT1 or PHOT2 displayed higher biomass productivity under low light conditions. The explanation for this is that plants carrying engineered receptors exhibited more rapid chloroplast movement responses, together with enhanced leaf positioning and expansion (mechanisms regulated by PHOTs), resulting in improved biomass accumulation under light-limiting conditions. This finding shows that PHOTs proteins constitutes a promising new target for manipulating plant growth and optimizing photosynthetic light harvesting, particularly under suboptimal light regimes.

1.2.5 Engineering of the light-harvesting system in green algae

As stated in the previous section, the high OD of cells is a condition that limits PAR penetration in the culture and this uneven light distribution accounts for the gap between the theoretical and real biomass productivity of industrial PBRs. Biomass production using wild type algal strains, endowed with features hampering high cell density, such as elevated optical density of cells, is therefore as unviable as farming with ancestral crop varieties, which in most cases showed reduced yields (Ritchie and Roser, 2013).

Microalgae biotechnology may take advantage of a domestication approach, similar to that adopted for modern crops, through the selection of strains carrying the desired traits by implementing new alleles through random mutagenesis or genetic engineering, which is expected to improve light harvesting capacity and therefore the biomass yield in industrial production systems.

Random mutagenesis has been widely employed to study the molecular basis of cellular processes and for strain improvement, thus is recognized as a powerful tool in mutation breeding. This is the "forward genetic" strategy, which is of particular relevance for algal biotechnology since it generates mutant lines, thereby avoiding restrictions on GMO for outdoor PBRs (Snow and Smith, 2012).

Attempts to genetically improve microalgae, aimed at enhancing light-use efficiency, relied on random mutagenesis and the screening of favourable traits. The latter requires efficient selection strategies for strains with a higher biomass yield. A number of approaches succeeded in enhancing light-harvesting capacity and are illustrated below.

Due to the adverse effect of high OD on large-scale culture, mutants carrying smaller antenna size were regarding as performing better in light transmittance than wild type strains (Figure 1.2.8).

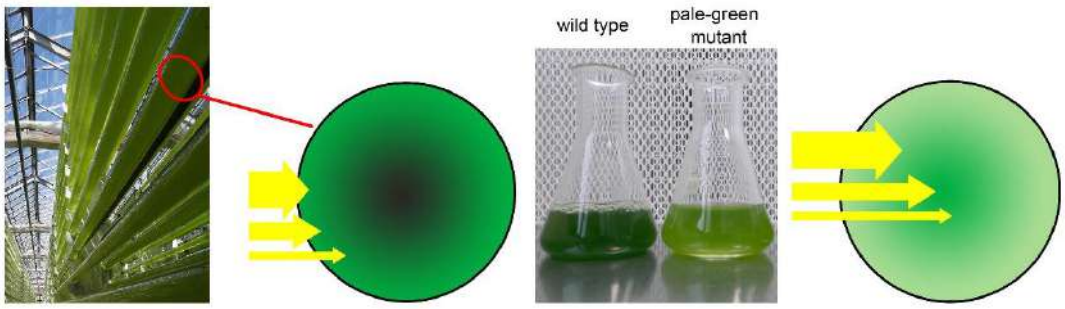

Fig. 1.2.8 | Light distribution and photosynthetic activity in algal cultures. *Light penetration and distribution inside a PBR (yellow arrows) is limited by the high optical density of the cells. Mutations that decrease Chl concentrations of cells without disrupting photoprotective responses enable increased productivity of the shaded layers and lower energy losses in the cells exposed to full light, thereby increasing overall light-use efficiency. Note that the two cultures in the flasks have the same cell concentration.*

Mutagenesis and the selection of the model green alga *Chlamydomonas reinhardtii* were used to isolate strains with a truncated light-harvesting system (Perrine et al., 2012; Kirst et al., 2012). All these strains displayed higher biomass productivity than the wild type in laboratory-scale PBRs. A random mutagenesis approach was applied to a thermotolerant, fast-growing strain of *Chlorella sorokiniana*, then pale-green mutants were selected by imaging Chl fluorescence since a reduced Chl content per unit cell decreases the emission of colonies. Mutants were able to perform photosynthesis more efficiently than wild types, and displayed reduced photoinhibition under EL conditions. The enhancement of photosynthetic productivity was confirmed in both bench-scale and outdoor PBRs (Cazzaniga et al., 2014). Similar results were obtained with oleaginous microalga *Nannochloropsis gaditana* strains with lower cellular pigment content (Perin et al., 2015). Finally, simultaneous down-regulation of three LHC subunits (LHCMB1, 2 and 3) in *C. reinhardtii* resulted in improved (+165%) light-to-biomass conversion yield (Oey et al., 2013).
In addition to random mutagenesis, genetic manipulation approaches include the transfer of genes identified in other species in order to generate strains with desirable productive features (Figure 1.2.9).

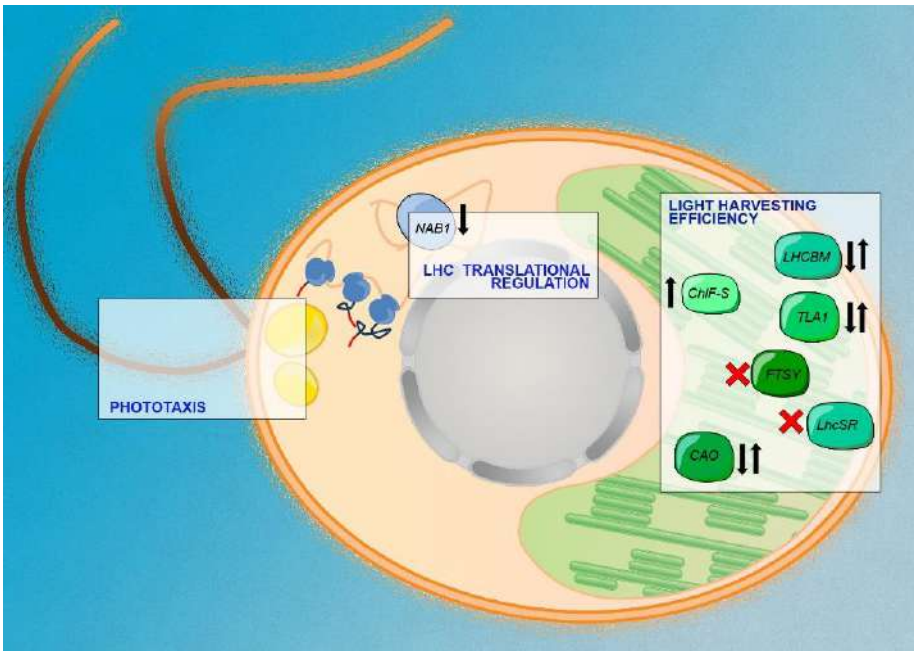

Fig. 1.2.9 | Antenna-related traits to be introduced into genetically-modified C. reinhardtii cells. *The diagram displays a number of genetic strategies, aimed at enhancing productivity in the mass culture of microalgae. Traits that may result in higher productivity include increased light-use efficiency, enhanced light absorption and improved phototaxis. Up and down arrows mean up- and down-regulation, respectively, and refer to the expression level of the corresponding endogenous enzyme. A red cross means in vivo loss of function. Abbreviations: Chl-f S chlorophyll f synthase, CAO chlorophyll a oxygenase, FTSY chloroplast signal recognition particle, LHCBM / LhcSR light harvesting complexes, NAB1 RNA-binding protein, TLA1 truncated light-harvesting antenna 1.*

The implementation of a biosynthetic pathway of additional chromophores, such as phycobilins or chlorophylls with peculiar spectral properties, has been proposed to enhance light harvesting over the entire PAR spectrum in genera of industrial interest. For example, Chl *f* expression in microalgae may expand the spectral range used for photosynthesis (Zamzam et al., 2020) and confer advantages for mass culture, which suffers from unfavourable sieve-effects at high cell densities. Recently, the enzyme catalyzing the synthesis of Chl *f* has been identified in the cyanobacterium *C. fritschii*, and the heterologous expression of Chl *f* synthase in *Synechococcus* sp. succeeded in accumulating this chromophore (Shen et al., 2019a). However, the feasibility of this approach in improving light harvesting capacity, which assumes a correct binding of the new pigment to the existing pigment scaffolds, still awaits experimental confirmation.

As previously discussed, a high photosynthetic efficiency can be attained only in low irradiance and a stable light environment, which enable most absorbed photons to be efficiently converted into chemical energy. Outdoors, however, the efficiency drops due to rapidly fluctuating light, which easily exceeds the photosynthetic capacity. As shown in plants, microalgae also evolved mechanisms for regulating the efficiency of light harvesting, which could be the targets of domestication programs. A number of microalgal species of industrial interest, for example, *C. reinhardtii* and *Haematococcus pluvialis*, trigger rapid phototactic responses. In order to optimize its position in the water column, algae use flagella to move towards or away from a light source. Physiological characterization confirmed that phototaxis confers a fitness advantage and is affected by photosynthetic electron transport (Wakabayashi et al., 2011). In the attempt to select mutants with improved light-use efficiency, Kim and coworkers analyzed a *C. reinhardtii* mutant population for rapid phototaxis response and identified strains with enhanced photoautotrophic growth (8.1-fold increases) compared to the wild type (Kim et al., 2016).

Photosynthetic organisms dynamically regulate the amplitude of dissipative reactions of PSII (see section 1.2.4). By balancing the excitation energy partition between photochemistry and heat dissipation, they optimize fitness in a rapidly changing light environment. The slow relaxation rate of the NPQ response on high- to low-light transition was shown to reduce the biomass yield in microalgae, consistent with recent findings in plants. Indeed, the deletion of the OCP protein, responsible for NPQ activation in cyanobacteria, resulted in 30% more biomass productivity in mass cultures of *Synechocystis* compared to wild type strains (Peers, 2011). The random insertional mutagenesis and TILLING (Targeting Induced Local Lesions IN Genomes) approach, coupled with fluorescence imaging selection, produced *C. reinhardtii* mutants specifically devoid of *lhcsr* genes (Peers et al., 2009). An initial report argued that biomass yield is modulated by LhcSR protein accumulation and, indeed, *C. reinhardtii* strains lacking the two *lhcSR3* genes were found to be more productive than the wild type, therefore supporting down-regulation of NPQ as a strategy for also improving light-use efficiency in microalgae. However, more recent results reported no significant differences in biomass yield between *C. reinhardtii* wild type and a mutant devoid of all LhcSR isoforms, over a wide range of light regimes (Cantrell and Peers, 2017; Barera et al., 2021).

Recently, a novel approach based on CRISPR-Cas9 genome editing technology has been successfully developed in *C. reinhardtii*, enabling the selective deletion of gene functions (Baek et al., 2016). This was achieved using a DNA-free CRISPR-Cas9 method and the outcome was the

FTSY and *ZEP* double KO, which led to pale-green strains displaying enhanced light-use efficiency.

As previously described, a truncated antenna size led to increased productivity in green microalgae so proteins involved in the biogenesis of the light-harvesting systems are potential candidates for increasing biomass yield. Truncated light-harvesting antenna 1 (*TLA1*) is a nuclear gene involved in the regulation of both PSI and PSII outer antenna in *C. reinhardtii*. TLA1 over-expressing strains displayed a larger antenna size for both photosystems and a lower Chl *a*/*b* ratio respect to the wild type, while its down-regulation resulted in the opposite phenotype (Mitra et al., 2012). As in plants, LHCII is the major light-harvesting protein associated with PSII in *C. reinhardtii*. It is nuclear-encoded, and its regulated expression finely tunes the antenna cross-section to the light environment. LHCII translation efficiency is regulated by NAB1, a cytosolic RNA-binding subunit which works as translational repressor. Under limiting light, a specific nitrosylation makes the regulator less active and thereby promotes the accumulation of LHCII and larger antenna (Berger et al., 2016). The transformation of algae with a permanently active variant of NAB1 succeeded in reducing antenna size and improved both photosynthetic efficiency at saturating light intensity and growth rate compared to wild type strains. Recently, the expression of CAO (Chl *b* biosynthetic enzyme) coupled with a NAB1 translational repressor binding site created a translational control system for dynamically tuning the antenna size in *C. reinhardtii*. In these engineered strains, Chl *b* synthesis (and therefore LHC biogenesis) was continuously adjusted depending on the light conditions. Strains expressing such light-regulated antenna systems displayed higher photosynthetic rates and twice the biomass yield than the parental strains (Negi et al., 2020).

1.2.6 Concluding remarks

(i) Population growth, by increasing demands for global food production and a sustainable bioeconomy, makes it increasingly important to generate photosynthetic organisms that will meet these needs.

(ii) Theoretical estimation and findings in the field lend support to the engineering of light-harvesting systems as a viable strategy to significantly increase the productivity of both crops and algae. One of the most striking results in this field was recently obtained with transgenic tobacco. By increasing the expression of genes involved in the regulation of light-harvesting efficiency, scientists saw increases of 14-20 percent in the productivity of modified tobacco plants in field experiments. These results are strong evidence that genetic manipulation of the mechanisms involved in photon capture can bring about a significant (and possibly unprecedented) increase in crop productivity. Interestingly, engineering the regulatory switch of the antenna also affected the intracellular signaling and stomatal opening in tobacco lines, resulting in improved efficiency of water use under field conditions (Głowacka et al., 2018).

(iii) The future development of more productive cultivars will require the implementation of different approaches, including complex modelling, breeding, gene transfer and measurements under real conditions. Continuous research efforts provided a wide array of molecular tools that can be suited for the prospective redesigning of light-use efficiency in plants. Moreover, several

structural and functional properties related to light perception have been identified as potential targets for optimization. Further research is required to furnish direct proof, through genetic manipulation, of the effectiveness of these productivity targets.

(iv) In green algae, investigating the mechanisms underpinning light-use efficiency lags behind work on terrestrial plants, and a number of challenges have yet to be overcome. Currently, many of the proposed targets have not been tested in algal species of industrial interest. While a large array of molecular tools for genetic engineering are available for a model species such as *Chlamydomonas*, difficulties in efficiently transforming other industrially-relevant species, such as *Chlorella* or *Dunaliella*, still limit the development of algal biotechnology. However, our knowledge is rapidly improving through the application of next-generation molecular techniques. In a future "green revolution" of microalgal biorefineries, boosting light-use efficiency by addressing the constraints of the wild type antenna system, will be a crucial step.

This chapter has been accepted for publication as chapter 2 in: "Methods in Enzymology" ISBN 0076-6879. doi.org/10.1016/bs.mie.2022.04.006"

Introduction

1.3 Assessing photoprotective functions of carotenoids in photosynthetic systems of plants and green algae

Assessing photoprotective functions of carotenoids in photosynthetic systems of plants and green algae

R. Caferri†, Z. Guardini†, R. Bassi*, and L. Dall'Osto*
Dipartimento di Biotecnologie, Università di Verona, Verona, Italy
*Corresponding authors: e-mail address: roberto.bassi@univr.it; luca.dallosto@univr.it

Abstract

Carotenes and xanthophylls act as photoreceptors in the photosystems of plants and algae by absorbing light energy which drives photosynthetic electron transport. Moreover, these carotenoid pigments protect chloroplasts from excess light and from reactive species generated during oxygenic photosynthesis. These pigments share similar spectral properties, a feature which contrasts with the extreme level of conservation of their relative composition and abundance in leaves across taxa. Such a conservation through evolution suggested each carotenoid species had a peculiar role, which indeed has been investigated by different approaches. These studies included the purification of individual carotenoid-binding proteins and their characterization in vitro. In a complementary approach, plant and algal mutants devoid of selected carotenoid species have been produced. The physiological characterization of these mutants revealed that the integrated contributions of all carotenoid species provide the most efficient response to photooxidative stress. In this chapter, we provide step-by-step guides for characterizing the in vivo antioxidant activity of carotenoids in plants and green algae, and methods for quantifying the effect of photooxidative stress in genotypes with altered carotenoid composition or impaired defense mechanisms.

1.3.1. Introduction – Functions of carotenoids in the photosynthetic apparatus

Carotenoids form a large group of C40 pigments, widely distributed among taxa, characterized by an extended conjugated double-bond system which gives rise to a high molar extinction coefficient and provides strong antioxidant properties (Britton, 2022, Britton et al., 2004; Fuciman et al., 2012; Britton, 2022). The structural diversity within this group broadened during evolution (Sandmann, 2021; Takaichi, 2011), likely depending on the many functions of carotenoids: they color flowers and fruits, insects and marine invertebrates, and are substrates for the synthesis of vitamins, hormones, and volatile products (Maoka, 2020). These pigments are marketed as dietary supplements, nutraceuticals, as strong antioxidants, feed colorants, and additives to cosmetic formulations (Leu and Boussiba, 2014). In photosynthetic tissues, carotenoids mediate energy capture and transfer and protect membrane lipids from peroxidative damage. Moreover, photooxidative stress dramatically increases the release of β-cyclocitral, an oxidized by-product of β-carotene, that in plants works as a retrograde signal for acclimation to excess light (D'Alessandro and Havaux, 2019).

In the photosynthetic apparatus of land plants and green algae, a minor fraction of carotenoids is found as free pigment in the lipid phase of thylakoid membranes (Dall'Osto et al., 2010), while most of carotenoids are located within specific sites of the photosystems (PS): β-carotenes are bound to the core complexes of both PSII and PSI, while the oxygenated derivatives called xanthophylls are bound to the light-harvesting complexes (LHC) which constitute the peripheral antenna of the PS (Su et al., 2017; Pan et al., 2018). In the LHC, the pigment moiety includes the chlorophylls (Chl) *a* and *b*, and four major xanthophyll species: the β,β–xanthophylls, violaxanthin and neoxanthin, and the β,ε-xanthophyll, lutein; zeaxanthin, which is synthesized from violaxanthin under excess light, can also bind to LHC (Caffarri et al., 2001; Dall'Osto et al., 2005).

Besides their role in light harvesting and as structural determinants of PS architecture, carotenoids have a crucial role for providing photoprotection (Naqvi et al., 1997). Indeed, oxygenic photosynthesis is particularly prone to oxidative damage due to (i) the photosensitizing action of porphyrins and (ii) reduction of oxygen by univalent electron carriers. Environmental conditions which unbalance the ratio between energy capture and utilization, raise the probability of Chl triplet state (^{3}Chl*) formation from excited Chl (^{1}Chl*), and singlet oxygen ($^1O_2$) release, while direct reduction of O_2 generates superoxide radicals (O_2^-) and H_2O_2. Due to their high reactivity, these reactive oxygen species (ROS) harm proteins, pigments and lipids, leading to increasing oxidative damage in the chloroplasts, and ultimately to a depression of photosynthetic yield (Niyogi, 1999; Fischer et al., 2013). Carotenoids mediate a number of photoprotection mechanisms, being active in (i) preventing over-excitation of reaction centers by quenching ^{1}Chl* states (Niyogi et al., 1998; Dall'Osto et al., 2017), (ii) de-activating ^{3}Chl* thus limiting ROS release (Mozzo et al., 2008), and (iii) detoxifying ROS (Havaux et al., 2004). The crucial role of carotenoids in photoprotection was revealed by the photosensitivity of carotenoid-less algae, which were incapable of autotrophic growth (Herrin et al., 1992; Trebst and Depka, 1997). In the last decade, efforts have been devoted to studying the specific *in vivo* role of each carotenoid species, by the isolation and characterization of *Arabidopsis thaliana* and *Chlamydomonas reinhardtii* mutants with altered carotenoid compositions. Such a genetic

dissection, besides improving our understanding of the carotenoid biosynthetic pathways, showed that these mutants were impaired in photoprotection. Thus, depletion of carotenes brought about stronger photoinhibition of PSI compared to PSII (Cazzaniga et al., 2012), lack of lutein, violaxanthin and/or zeaxanthin impaired the photoprotection capacity under excess light (EL) conditions (Niyogi et al., 2001; Dall'Osto et al., 2006, 2012, 2007b; Baroli et al., 2004), while a mutant devoid of all xanthophylls revealed unprecedented levels of photosensitivity (Dall'Osto et al., 2013). Interestingly, the characterization of these mutants showed that the photochemical features and the peculiar functions of individual xanthophyll species are shaped by their binding to LHC subunits. For example, lutein which is bound to site L1 of all LHCs, maximizes ^{3}Chl* quenching (Dall'Osto et al., 2006). Violaxanthin-less and neoxanthin-less mutants revealed ROS scavenging as a constitutive mechanism in LHC photoprotection (Dall'Osto et al., 2007a, 2007b). Zeaxanthin, which replaces violaxanthin in LHC under EL, (i) enhances ^{1}Chl* quenching, (ii) protects thylakoid membrane lipids against photooxidation, and (iii), modulates ^{3}Chl* yield (Dall'Osto et al., 2012).

Here we provide a series of step-by-step procedures for the detection and quantification of photooxidative damage in either leaves or algal suspensions: we include assays for evaluating the extent of Chl bleaching and lipid peroxidation following the release of ROS, and quantifying the extent to which each PS is being damaged by EL.

1.3.2. *In vivo* photobleaching assay

In photosynthetic organisms, exposure to EL conditions for a prolonged time enhances $^1O_2$ release and oxidative damage, including bleaching of Chl. This phenomenon is known as photobleaching, and its rate can be evaluated by determining the time course of Chl content in a leaf or algal cell throughout the treatment. This method allows an indirect evaluation of the role carotenoids play in photoprotection (Formaggio et al., 2001; Dall'Osto et al., 2006): organisms with a different carotenoid complement show different capacity to detoxify $^1O_2$ which, in turn, reflected the ability to preserve Chl from photodestruction.

This method quantifies the Chl and carotenoids content of acetone extracts of leaves or algae, by spectral deconvolution as described in (Croce et al., 2002a) or by measuring absorption at specific wavelengths, as reported in (Porra et al., 1989).

Reference papers: (Porra et al., 1989; Croce et al., 2002a; Dall'Osto et al., 2006)

Material

Liquid nitrogen

Acetone for spectroscopy

Na_2CO_3

Equipment

Micropipettors, tips

1.5 mL polypropylene tubes

Pestles for 1.5 mL tubes

Benchtop microcentrifuge

Light source (e.g. high-power LEDs panel, white light, reaching irradiances of at least 1,500-2,000 μmol photons m^{-2} s^{-1})

UV-VIS spectrophotometer

Cuvette, 10 mm light path

Method

Light treatment

Duration: 8-14 hours.

Plant tissue

- Prepare leaf disks, by cutting fully-developed leaves with either a hole puncher (Ø ~ 8-10 mm) or the lid of a microcentrifuge tube. Be careful in sampling the same area for each leaf disc; 4-6 disks per time point are enough.
- Put the leaf disks on a wet filter paper and adapt to darkness for 1 hour. Then expose the leaf disks to EL conditions. Usually, irradiances (measured at the leaf surface) around 1,800-2,000 μmol photons m^{-2} s^{-1} at 20-25 °C, or around 800-1,200 μmol photons m^{-2} s^{-1} at 5-10 °C, are enough to promote Chl bleaching within 8-14 hours of treatment.
- Sample every 60-120 min by freezing leaf disks in liquid nitrogen. If needed, store samples at -80 °C until ready to be processed.

Microalgae

- Grow cells (e.g. *Chlamydomonas reinhardtii*) to exponential phase (typically ~$2 \cdot 10^6$ cells/mL in *C. reinhardtii*) in 50 mL or more of minimal medium (TP medium, see (Kropat et al., 2011, or HS medium, see (Sueoka, 1960))). Cultures are maintained in flask at 25°C, under constant shaking (~150 rpm), illuminated with 70-100 μmol photons m-2 s-1 provided by warm-white fluorescent lamps, with a photoperiod of 16:8 light:dark. Cell density can be measured using either a hemocytometer (e.g. Neubauer improved cell counting chamber) or an automated cell counter (e.g. Invitrogen Countess 3™).

- Algal cultures are centrifugated 3,000 × *g* for 5 min at RT in 50 mL tubes and resuspended in fresh medium to reach a final concentration of ~$5 \cdot 10^7$ cells/mL.

- Aliquots of *C. reinhardtii* cell suspensions (1-5 mL, ~$5 \cdot 10^7$ cells/mL) are transferred to 24-well plates, dark-adapted for 1 hour, and then expose to EL. Shaking (~150-200 rpm) should be maintained during irradiation.

- Sample every 60-120 min aliquots corresponding to 1-$4 \cdot 10^5$ cells, 4 to 6 replicates per time point.

- Centrifuge cells at 3,000 × *g* for 10 min at 4 °C, discard the supernatant, if needed, store samples at -80 °C until ready to be processed.

Pigment extraction

Duration: 2 hours to overnight

Plant tissue

Grind the tissue to fine powder in liquid nitrogen with a pestle.

Immediately add 1 mL of ice-cold 80% aqueous acetone buffered with a small amount of Na_2CO_3 (2-3 g per 50 mL acetone are enough).

To improve extraction yield, incubate samples in ice for 1 hour to overnight.

Pellet down cell debris at 20,000 × *g*, 4 °C for 10 min, then transfer the supernatant to a clean 1.5 mL tube. Upon a complete extraction, pellet should appear white.

Microalgae

Resuspend the pellet in 1 mL of ice-cold 80% acetone buffered with a small amount of Na_2CO_3 (2-3 g per 50 mL acetone are enough).

To improve extraction yield, incubate on ice for 1 hour to overnight.

Pellet the debris at 20,000 × *g*, 4 °C for 10 min and then transfer the supernatant to a new 1.5 mL tube. The remaining pellet should appear white.

Some algal strains (e.g. *Chlorella spp*, *Nannochloropsis spp)* are refractory to this extraction procedure, mainly due to their resistant cell wall. In this case resuspend the cell pellet in 100 μL of pure DMSO at 55°C, vortex for 30 sec, then incubate tubes at 55 °C for 2 min, cool down samples to RT then add 900 μL of 90% ice-cold, aqueous acetone.

Pellet down cell debris at 20,000 × *g*, 4 °C for 10 min and then transfer the supernatant to a clean 1.5 mL tube.

The remaining pellet should appear completely white; in case of incomplete extraction, treat again the pellet by the same procedure.

Absorption spectra

A number of methods can be used to quantify Chl content in acetone extracts by absorption spectroscopy. These include the calculation developed by Porra and co-workers (Porra et al., 1989):

Record absorption of acetone extracts at 646.6, 663.6 and 750 nm.

Apply the following equations to obtain Chl concentration (in μg/mL) of the sample:

$$\text{Chl } a = 12.25 \cdot A^{(663.6\text{ nm} - 750\text{ nm})} - 2.55 \cdot A^{(646.6\text{ nm} - 750\text{ nm})}$$

$$\text{Chl } b = 20.31 \cdot A^{(646.6\text{ nm} - 750\text{ nm})} - 4.91 \cdot A^{(663.6\text{ nm} - 750\text{ nm})}$$

$$\text{Chl } a + b = 17.76 \cdot A^{(646.6\text{ nm} - 750\text{ nm})} - 7.34 \cdot A^{(663.6\text{ nm} - 750\text{ nm})}$$

Alternatively, (Croce et al., 2002a) proposed a Chl content determination based on the fitting of the absorption spectra of the acetone extracts with the spectra of individual pigments:

Record the spectra of the acetone extracts in the visible range from 600 to 750 nm.

To fit the experimental spectra in terms of Chl spectral forms, spectra of Chl *a* and Chl *b* can be obtained by pure standards in 80% aqueous acetone.

Combine spectra of the standards to obtain a fit of the spectrum of the acetone extracts from leaves or microalgae. It can be carried out by a software, e.g. based on Microsoft Excel and Visual Basic utilities, which uses the "solver" module of Excel to find the least-squares solution of the polynomial combination that best fits the spectrum in the selected region, thus determining both the Chl content and the Chl *a*/*b* ratio.

Once determined the Chl composition of each extract, this value can be normalized to leaf area in the case of plant material, or to the number of cells in the case of microalgal samples. These values will allow to assess the kinetic of Chl photobleaching during the treatment (Figure 1.3.1).

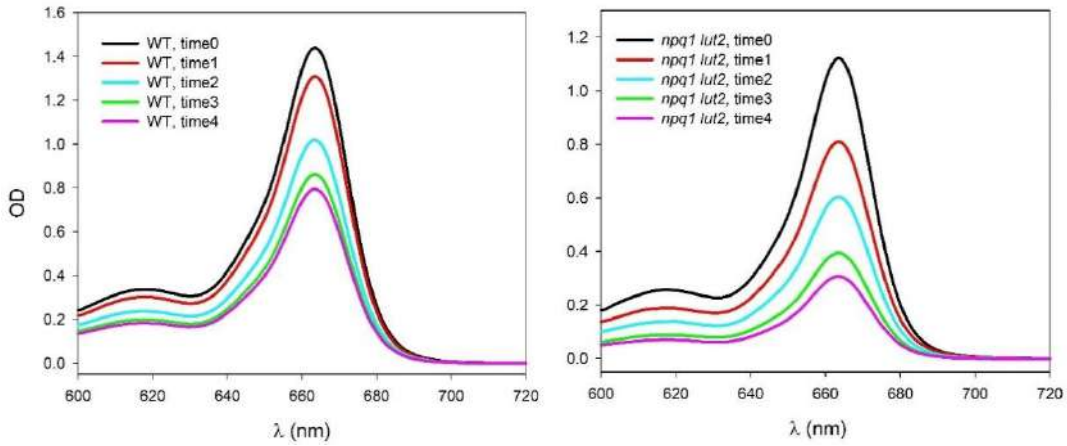

Fig. 1.3.1 | Photobleaching of Arabidopsis thaliana leaves, WT (left panel) and the npq1 lut2 mutant (right panel), altered in the xanthophyll content. *Panels show the absorption spectra in the visible range (600 to 720 nm) of acetone extracts from leaves collected at different time points.*

1.3.3. *In vivo* detection of ROS release

In addition to quantify the damages $^1O_2$ causes to the photosynthetic machinery, the capacity for detecting $^1O_2$ in intact plants tissues allows to follow the early events of photooxidative stress and locate the site of production of this ROS. However, in biological systems, $^1O_2$ has a short half-life (around 3 μs) which make detection difficult. Recently, a number of fluorescence probes highly sensitive to different ROS have been developed, which can be vacuum-infiltrated into leaves or added to algal suspensions and used to detect ROS release *in situ*. Singlet Oxygen Sensor Green (SOSG) is a highly selective probe for $^1O_2$, suitable for routine analysis *in vivo*. SOSG molecule is composed by a fluorophore and an anthracene-derived moiety acting as a quencher. The reaction with $^1O_2$ converts SOSG into the endoperoxide derivative (SOSG-EP) and removes the quenching by anthracene moiety, thus enhancing a green fluorescence with excitation and emission maxima at ~500 and ~525 nm respectively (Kim et al., 2013) (Figure 1.3.2). The following protocol describes a step-by-step procedure to assess the kinetic of $^1O_2$ release in leaves and algal cultures exposed to EL.

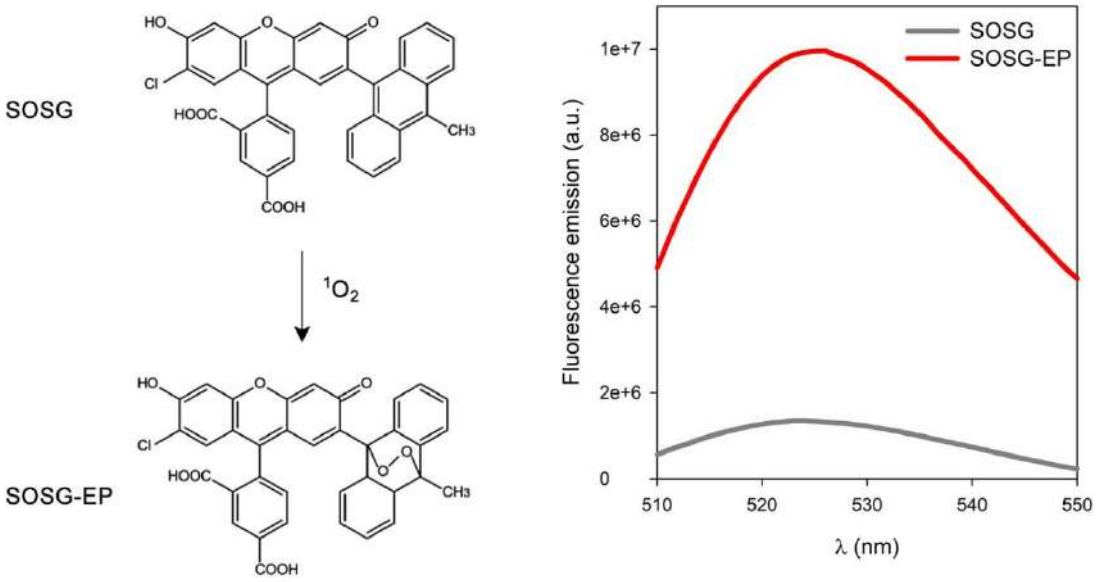

Fig. 1.3.2 | SOSG activation upon reaction with $^1O_2$. *(left panel) SOSG is a fluorescence probe highly selective for $^1O_2$: in presence of this ROS, the formation of an endoperoxide in the anthracene-derived functional group relieves the quenching on the emitting moiety. The probe can be vacuum-infiltrated into leaves, and used to follow the kinetic of $^1O_2$ release in situ, by exciting sample at 480-500 nm while monitoring emission at 525-530 nm (right panel).*

Reference papers: (Flors et al., 2006; Barera et al., 2021; Dall'Osto et al., 2012)

Material

- SOSG (S36003, Invitrogen®)
- Methanol
- Infiltration Buffer: 100 mM sorbitol, 5 mM $NaHCO_3$, 20 mM HEPES, pH 7.0

Equipment

- Micropipettors, tips
- 50 mL plastic syringe, without needle, equipped with a 2-way valve
- 15 mL tubes
- High-power red light source (e.g. high-power LED panel reaching irradiances around 1,200 μmol photons m^{-2} s^{-1} producing red light, $\lambda > 600$ nm); or high-power white light sources equipped with long-pass edge interference filter (600 nm)
- 24-wells plate
- Spectrofluorometer equipped with an optical fiber, or microplate spectrofluorometer

Method

Plant sample (optimized on *Arabidopsis thaliana*)

- Prepare SOSG stock solution by dissolving SOSG in methanol at a final concentration of 5 mM.
- Prepare 20 mL of working solution by diluting SOSG in Infiltration Buffer to 200 μM final concentration.
- Detach leaves from plants that have been dark-adapted for at least 30 min; the following procedure can be applied to whole leaves as well as to leaf disks (refer to dedicated section on leaf disk preparation).
- Remove the plunger of the 50 mL syringe, close the 2-way valve, and pour 20 mL of the SOSG working solution into the syringe barrel, together with the leaves.
- Replace the plunger, taking care not to crush the leaves.
- Open the 2-way valve, push the plunger until most of the air is left in the barrel.
- Close the valve, then create a negative pressure by drawing back the plunger and maintain for 5-10 sec while swirling the leaves in the solution, to ease infiltration of the solution into the air spaces of the leaf mesophyll. If the procedure succeeded, leaves should sink and appear translucent. If necessary, repeat the procedure a few times.
- Release the vacuum, recover the working solution into a tube (the syringe and the working solution can be re-used for many samples of vacuum-infiltration), transfer leaves onto a filter paper wetted with water.
- Record the fluorescence emission of each sample, $\lambda_{excitation}$ 480 nm, $\lambda_{emission}$ 530 nm.
- Expose samples to red, excess light ($\lambda > 600$ nm), since illumination with $\lambda < 600$ nm causes photosensitization of SOSG, leading to SOSG-EP formation (Prasad et al., 2018). Irradiances around 1,000-1,200 μmol photons m^{-2} s^{-1} at 20-25 °C, or around 400-500 μmol photons m^{-2} s^{-1} at 5-10 °C, are enough to promote $^1O_2$ release.

- Record fluorescence emission of each sample at time zero and with 30-60 min intervals, for at least 4-5 time points. Use at least 8 leaves / leaf discs for each genotype. Include at least 4 samples as negative control (leaves / leaf discs infiltrated with the Infiltration buffer, without SOSG).

Algal sample (optimized on *Chlamydomonas reinhardtii*)

- Prepare SOSG stock solution by dissolving SOSG in methanol at a final concentration of 5 mM.
- Transfer aliquots of *C. reinhardtii* cell suspensions (1-5 mL, ~$5 \cdot 10^7$ cell/mL), from cultures in late exponential growth phase, to a 24-well plate, then maintain shaking (~150-200 rpm) with illumination (refer to dedicated section on cultivation of microalgae).
- Add SOSG stock solution to 100 μM final concentration.
- Incubate samples in the dark at RT for 30 min, maintaining continuous shaking (~150-200 rpm).
- Record the fluorescence emission of each sample, $\lambda_{excitation}$ 480 nm, $\lambda_{emission}$ 530 nm.
- Expose samples to red, excess light (λ > 600 nm), since illumination with λ < 600 nm causes photosensitization of SOSG, and SOSG-EP formation (Prasad et al., 2018). Irradiances around 800-1,000 μmol photons m^{-2} s^{-1} at 20-25 °C, or around 400-500 μmol photons m^{-2} s^{-1} at 5-10 °C, are sufficient to promote $^1O_2$ release.
- Record fluorescence emission of each sample at 30-60 min intervals; take at least 5 time points. At the end of each measurement, return the samples to EL. Use a timer when taking measurements so that the time of light exposure and the interruptions for measurement are the same for all samples. Use at least 8 samples for each genotype. Include at least 4 samples as negative control (algal suspension without SOSG).

1.3.4. Assess the sensitivity to exogenously-added ROS

To test the capacity of carotenoids to scavenge ROS, leaves or algae can also be exposed to exogenous pro-oxidants. Photosensitizing dyes are molecules that generate $^1O_2$ upon illumination. This class of dyes includes the water-soluble rose bengal (RB), neutral red (NR) and methylene blue (MB). Methyl viologen (MV) and metronidazole (MZ) can be reduced via photosynthetic electron transport to produce active forms which can catalyze reduction of O_2 to superoxide anion ($O_2^{\cdot-}$). Exogenously-added hydrogen peroxide (H_2O_2) and *tert*-butylhydroperoxide (*t*-BOOH) act directly as oxidizing molecules or indirectly through the formation of hydroxyl radicals (OH*). ROS released by dyes causes cellular sensitivity which can be assessed by quantifying the reduction of Chl content over time or the reduction in growth rates. Here we propose a protocol for the evaluation of photoprotection activity of carotenoids when exogenous pro-oxidants are added, at a sub-lethal dose, to the growth medium of algae or vacuum-infiltrated into leaves.

Reference papers: (Fischer et al., 2012; Dall'Osto et al., 2007a; Baroli et al., 2004)

Material

- Rose bengal B (RB), Na salt (R3877, Sigma-Aldrich)
- Metronidazole (MZ) (M1547, Sigma-Aldrich)
- Hydrogen peroxide (H_2O_2), 30% (w/w) (8.22287, Sigma-Aldrich)
- Methyl viologen dichloride hydrate (MV) (856177, Sigma-Aldrich)
- Infiltration Buffer: 100 mM sorbitol, 5 mM $NaHCO_3$, 20 mM HEPES, pH 7.0
- Liquid nitrogen
- Acetone for spectroscopy
- HS medium (Sueoka, 1960): 5 g/L NH_4Cl, 0.2 g/L $MgSO_4 \cdot 7H_2O$, 0.1 g/L $CaCl_2 \cdot 2H_2O$, 14.4 g/L K_2HPO_4, 7.2 g/L KH_2PO_4, 50 mg/L EDTA, 22 mg/L $ZnSO_4 \cdot 7H_2O$, 11.4 mg/L H_3BO_3, 5.06 mg/L $MnCl_2 \cdot 4H_2O$, 1.61 mg/L $CoCl_2 \cdot 6H_2O$, 1.57 mg/L $CuSO_4 \cdot 5H_2O$, 1.1 mg/L $(NH_4)_6Mo_7O_{24} \cdot 4H_2O$, 4.99 mg/L $FeSO_4 \cdot 7H_2O$.
- Plant agar (P1001, Duchefa)

Equipment

- Micropipettors, tips
- 50 mL tubes
- Petri dishes, Ø 60 mm and Ø 100 mm
- Syringe filters 0.22 μm
- 50 mL plastic syringe, without needle, equipped with a 2-way valve
- Light source (e.g. warm-white LED panel reaching irradiances around 1,000 μmol photons m^{-2} s^{-1}) equipped with green bandpass filter (500-550 nm); or green light system (e.g. green LED panel reaching irradiances around 100-120 μmol photons m^{-2} s^{-1}, 500 nm $< \lambda <$ 550 nm).

<u>Method</u>

Plant samples (optimized on *Arabidopsis thaliana*)

- Prepare 50 mL of Infiltration Solution containing 50 μM RB, or 250 μM MZ, or 250 mM H_2O_2.
- Harvest leaves from plants dark-adapted for at least 30 min; the following procedure can be applied to whole leaves as well to leaf disks.
- Use a pro-oxidant containing buffer to vacuum-infiltrate leaves or leaf disks (see paragraph 3 of this chapter). Remove excess solution form leaves by kindly pressing between two layers of filter paper.
- Freeze 4-5 samples in liquid nitrogen and store them at -80 °C, to be used as reference samples (time 0, untreated with light).
- Pour 10 mL of Infiltration Solution in a Ø 60 mm Petri dish and let leaf samples floating.
- Start the light treatment:
    - samples infiltrated with RB: expose leaves to green light (500 nm $< \lambda <$ 550 nm, 100 μmol photons m^{-2} s^{-1}, RT) for 6 hours. The wavelength range was chosen to excite the dye (A_{max} at 520 nm) while minimizing light absorption by leaves;

    - samples infiltrated with MZ: expose leaves to white light (100 μmol photons m^{-2} s^{-1}, RT) for 6 hours;
    - samples infiltrated with H_2O_2: maintain in the dark for 6 hours.
- Collect leaves with 1-2 hours intervals, at least 3-4 time points. Freeze samples in liquid nitrogen.
- Quantify Chl content of each sample (see paragraph 2 of this chapter).
- The effect of exogenous pro-oxidants can be quantified by following the decrease of Chl content over time, upon normalization to the leaf area.

Algal samples (optimized on *Chlamydomonas reinhardtii*)

- Grow a culture in minimal medium, to exponential phase.
- Autoclave HS medium containing 1.5% (w/v) plant agar. Let it cool until ~65 °C, then add the filter-sterilized pro-oxidants: RB 2.5 μM or MV 0.5 μM or MZ 2 mM or H_2O_2 0.5 mM.
- Pour the medium in Petri dishes Ø 100 mm.
- Spot 20 μL of a serial dilution of algae suspension onto solid medium, at different cell loading (e.g. $2{\cdot}10^5$, $2{\cdot}10^4$, $2{\cdot}10^3$, $2{\cdot}10^2$ and $2{\cdot}10^1$ cells/spot).
- Maintain plates for 7-10 days at 50 μmol photons m^{-2} s^{-1} continuous light, 25 °C.
- Compare growth of mutants respect to WT: strains with impaired resistance to oxidative stress will show retarded growth vs WT strains (Figure 1.3.3).

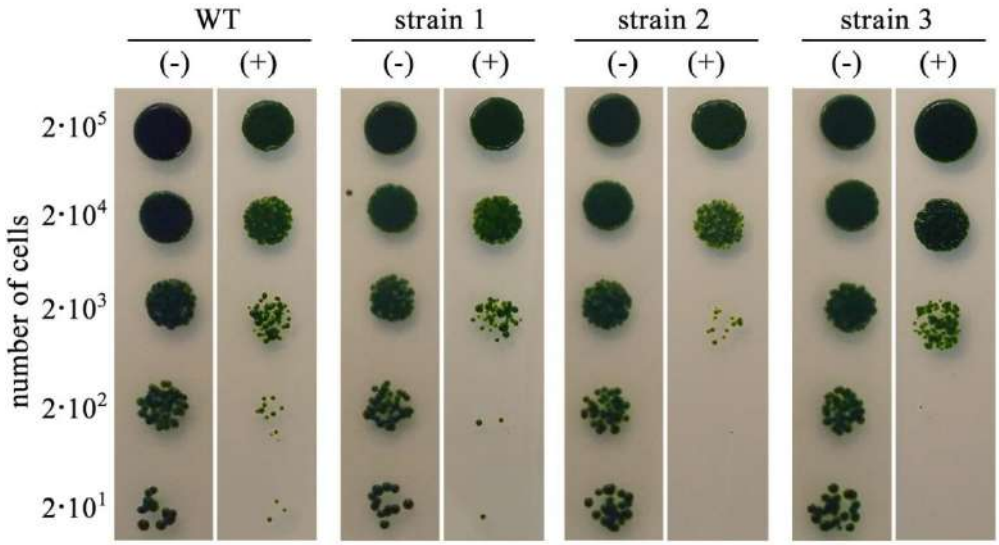

Fig. 1.3.3* | *Assess sensitivity to exogenously added pro-oxidant. *Chlamydomonas reinhardtii mutant strains were isolated as a $^1O_2$-sensitive mutant by growth on solid medium either containing rose bengal (RB 3 μM) (+) or not (−). The number of cells spotted is indicated in the left border.*

1.3.5. Protein carbonylation assay

Photosynthesis involves highly reactive intermediates and inevitably produces potentially damaging byproducts in the chloroplasts. In particular, the acceptor side of PSI has a redox potential low enough to reduce O_2 to the superoxide anion radical $O_2^{\cdot-}$. The latter is mostly deactivated to H_2O_2 and then to H_2O by the scavenging enzymes Superoxide Dismutase and Ascorbate Peroxidase (Asada, 1999), however the Fe^{2+}-catalyzed Fenton reaction can convert H_2O_2 to the hydroxyl radical $OH^{\cdot}$, the most reactive species of those derived from activated oxygen. Under photooxidative conditions, high levels of $OH^{\cdot}$ in the chloroplasts trigger the oxidation of diverse cellular components, including proteins. Protein carbonylation is a common ROS-mediated, post-translational modification of the side chains of Lys, Pro, Arg, Thr, and sometimes Trp, which get cleaved by $OH^{\cdot}$ and form carbonyl groups (Johansson et al., 2004). High protein carbonylation is associated with enhanced ROS release under EL, thus carbonylated proteins are good indicators of chloroplast photooxidative stress.

The method proposed here uses DNPH (2,4-dinitrophenylhydrazine), a specific probe which reacts with protein carbonyls to produce protein-conjugated dinitrophenylhydrazones, which can be detected and quantified by immunotitration, through a two-steps incubation with primary rabbit α-dinitrophenyl antibody and secondary goat anti-rabbit IgG, HRP-conjugate.

Reference papers: (Colombo et al., 2016; Laemmli, 1970)

Material

- Acetone
- Liquid nitrogen
- Chemicals for derivatization of proteins
    - 10 mM DNPH in 2 N HCl (note: prepare fresh DNPH solution, since reactivity decreases over time, and maintain the solution at RT, protected from light)
    - 2 N HCl
    - 20% (w/v) TCA (trichloroacetic acid), ice cold
    - 1:1 (v/v) ethanol:ethyl acetate
- Sample buffer (2X): 125 mM TRIS/HCl (pH 6.8); 20% (w/v) Glycerol; 2% (w/v) SDS; 5% (v/v) 2-mercaptoethanol
- Solutions for SDS-PAGE (sodium dodecyl sulfate – polyacrylamide gel electrophoresis) (Laemmli, 1970):
    - Stacking gel: 4.0% (w/v) acrylamide, 0.11% (w/v) bisacrylamide, 125 mM TRIS/HCl pH 6.8
    - Separation gel: 15.0% (w/v) acrylamide, 0.41% (w/v) bisacrylamide, 375 mM TRIS/HCl pH 8.8
    - Cathode buffer: 25 mM TRIS, 200 mM glycine, 0.1% (w/v) SDS
    - Anode buffer: 25 mM TRIS, 200 mM glycine

    - TEMED (N,N,N',N'-Tetramethylethylenediamine, T9281 Sigma-Aldrich), APS (ammonium persulfate, A3678 Sigma-Aldrich).
- Solutions for Western blotting:
    - PBS (phosphate buffered saline) solution (10X): 1.37 M NaCl, 27 mM KCl, 15 mM KH_2PO_4, 81 mM Na_2HPO_4
    - PBS-T: PBS 1X, 0.2% (w/v) Tween 20 (P1379, Sigma-Aldrich)
    - Blocking solution: PBS 1X, 0.2% (w/v) Tween 20, 5% (w/v) powdered nonfat milk
    - anti-DNP (dinitrophenyl) primary antibody, from rabbit (e.g. Invitrogen A-6430, Dinitrophenyl-KLH Polyclonal Antibody)
    - anti-rabbit HRP (horseradisch peroxidase)-conjugated secondary antibody, from goat (e.g. Invitrogen **G-21234**)
    - ECL (enhanced chemiluminescence) Western blotting detection kit (e.g. Pierce® ECL Western Blotting Substrate)
- Coomassie blue staining solution: 0.025% (w/v) Coomassie brilliant blue R-250, in 40% (v/v) methanol and 8% (v/v) acetic acid
- Destaining solution: 50% (v/v) methanol, 8% (v/v) acetic acid

Equipment

- Electrophoresis unit, Blotting unit and power supply (e.g. Bio-Rad Mini-PROTEAN®)
- Microcentrifuge
- Orbital shaker
- Micropipettors, tips,1.5 mL polypropylene tubes
- PVDF membrane (e.g. Amersham Hybond® P 0.45)
- Imaging System (e.g. Bio-Rad ChemiDoc® Touch), or X-ray films
- Plastic box (LxW ~20x15 cm is enough for processing mini-gels)

<u>Method</u>

- Detached leaves or leaf disks (cut with a hole puncher, Ø ~ 8-10 mm) should be placed on wet paper (refer to section 2.3.2 on leaf disk preparation), or
- aliquots of *C. reinhardtii* cell suspensions (2 mL, ~$5 \cdot 10^7$ cell/mL) are transferred in 24-well plates, maintained on shaking (~150-200 rpm) (refer to section 2.3.3 on cultivation of microalgae).
- Expose plants, detached leaves, leaf disks or microalgal suspensions to EL conditions. Usually, irradiances around 1,800-2,000 μmol photons m^{-2} s^{-1} white light at 20-25 °C, or around 800-1,200 μmol photons m^{-2} s^{-1} white light at 5-10 °C, are enough to induce protein carbonylation within 4-8 hours of treatment.
- Harvest samples in 1.5 mL tubes:
    a) for *Arabidopsis thaliana*, collect at least 3 leaf disks/genotype, then freeze in liquid nitrogen; if needed store samples at -80 °C until ready to be processed;
    b) for *Chlamydomonas reinhardtii*, collect a volume corresponding to 2-4·10^7 cells, at least 3 sampling/genotype, then centrifuge each sample at 3,000 × *g* for 10 min at

4 °C, discard the supernatant; if needed store samples at -80 °C until ready to be processed.

- Grind samples:
    a) for *Arabidopsis thaliana*, grind frozen disks with a 1.5 mL-tube pestle, then add 250 µL Sample buffer, mix by repetitive pipetting;
    b) for *Chlamydomonas reinhardtii*, grind the sample directly in 250 µL of Sample buffer in a 1.5 mL-tube pestle, mix by repetitive pipetting.
- Centrifuge samples at 20,000 × *g* for 10 min at RT, to pellet debris.
- Transfer 200 µL of the supernatant to a new 1.5 mL-tube.
- Add 50 µL of 10 mM DNPH solution.
- Mix samples by repetitive pipetting, then incubate in the dark at RT for 60 min, occasionally swirling.
- Add 300 µL of 20% TCA solution, incubate on ice for 15 min.
- Centrifuge samples at 10,000 × g for 5 min at 4 °C, then discard the supernatant.
- Wash the pellet with 500 µL of 20% TCA solution, mix by vortexing.
- Centrifuge samples at 10,000 × g for 5 min at 4 °C, then discard the supernatant.
- Wash protein pellets with 1 mL of ethanol:ethyl acetate solution; mix by vortexing to remove any traces of DNPH.
- Wash the pellet with 500 µL of 20% TCA solution, then mix by vortexing.
- Centrifuge samples at 10,000 × g for 5 min at 4 °C, then discard the supernatant.
- Repeat the last two steps at least twice.
- Vacuum-dry the pellets for about 5 min to remove traces of solvents.
- Resuspend protein pellets in 200 µL of 1X Sample buffer containing 0.02% (w/v) Bromophenol Blue and incubate at 95 °C for 5–10 min to complete the resuspension.

A positive control of oxidized proteins, to be included in the SDS-PAGE, can be prepared as follows: collect 200 µL of protein extract in sample buffer, add 200 µL of 50 mM HEPES pH 7.1, 50 mM sodium ascorbate, 200 µM $FeCl_3$; incubate the sample at 37 °C for 5 hours; dialyze the sample against 50 mM HEPES pH 7.0, 1 mM EDTA. Proteins will be oxidized by the treatment, thus the sample can be used to validate the immunotitration (see following procedure).

- Separate 20 µL of DNPH-labelled protein samples by SDS-PAGE in a 15% gel according to standard techniques (Laemmli, 1970).
- Soak a PVDF filter (that matches the gel size) in pure methanol for 10 min.
- Transfer the proteins from the gel to a PVDF membrane by electroblotting, using a transfer unit.
- Disassemble the transfer unit, then wash the PVDF membrane for 15 min in 50-100 mL PBS-T, with gentle agitation in an orbital shaker.
- Incubate the membrane for 60 min in 50-100 mL Blocking solution.
- Wash the membrane twice with 50-100 mL PBS-T, 10 min each.
- Incubate the membrane with primary antibody in Blocking solution, for 2 hours at RT, with gentle agitation. Use a minimum of 8-10 mL for a 40-50 cm^2 membrane. Antibody dilution is highly variable, being dependent on the amount of protein loaded and the

level of protein carbonylation. In the case of A-6430 primary antibody, try 1:35,000 dilution, if necessary, increase antibody concentration for a second attempt of immunodetection performed on the same membrane.

- Wash the membrane twice, with 50-100 mL PBS-T, 10 min each.
- Incubate the membrane with secondary antibody in 50-100 mL Blocking solution, for 1 hour at RT, with gentle agitation. Dilute the antibody in PBS-T according to manufacturer's instructions.
- Wash the membrane twice, with 100 mL PBS-T, 10 min each.
- Detect the antigen with ECL solutions, according to manufacturer's instruction. Follow chemiluminescence development by exposing the membrane to X-ray film or by CCD (charge-coupled device) imaging.

Stain PVDF membrane with Coomassie blue

- Wash the membrane with water, three times for 5 min each, to remove all ECL reagents.
- Stain membrane with 50 mL Coomassie blue solution for 5 min.
- Destain membrane with 50 mL methanol/acetic acid solution for 5 min.
- Rinse with water 3-4 times, then air dry.
- The degree of protein oxidation can be assessed by the intensity of the immunodetected bands normalized to the optical density of the same bands stained with Coomassie blue.

1.3.6. Detect and quantify lipid peroxidation

$^1O_2$ is highly reactive against a large group of molecules, including polyunsaturated fatty acids (PUFAs); once initiated, lipid peroxidation proceeds as radical chain reactions which impair the stability of membranes (Alché, 2019), leading to a decline in the photosynthetic yield. Two types of reactions result in $^1O_2$-mediated lipid peroxidation: (i) radicals or enzymes such as lipoxygenases catalyze hydrogen abstraction from the PUFAs, followed by the reaction with $^1O_2$, or (ii) $^1O_2$ adds to a double bond of PUFAs. In both cases, the reaction leads to the production of PUFA hydroperoxides (Montillet et al., 2004). Malondialdehyde (MDA) is formed by spontaneous oxidation or enzymatic degradation of the PUFA hydroperoxides, and has been commonly used as a biomarker for lipid peroxidation (Davey et al., 2005) (Figure 4). Moreover, plant cells subjected to photooxidative stress will produce compounds such as $^1O_2$ and excited carbonyls of peroxylipids. They both generate a faint light when decaying back to their ground state: the phenomenon is called chemiluminescence. This flux of photons can be boosted by increasing the temperature of the samples. Thus, taking advantage of this mechanism, thermoluminometry represents a highly sensitive technique to quantify *in vivo* lipid peroxidation: samples get slowly heated, and luminescence appears as successive bands, related to the nature and the concentration of different emitting species (Havaux, 2003). In particular, (Ducruet and Vavilin, 1999) showed that the band (called HTL2) observed in plants and algae at high temperature (120-140 °C) is increased by photooxidative stress and has been ascribed to triplet carbonyls generated by lipid peroxidation and/or upon thermolysis of lipid hydroperoxides. The

HTL2 amplitude correlates with lipid hydroperoxide content of a sample as determined by biochemical methods (Vavilin and Ducruet, 1998; Havaux and Niyogi, 1999).

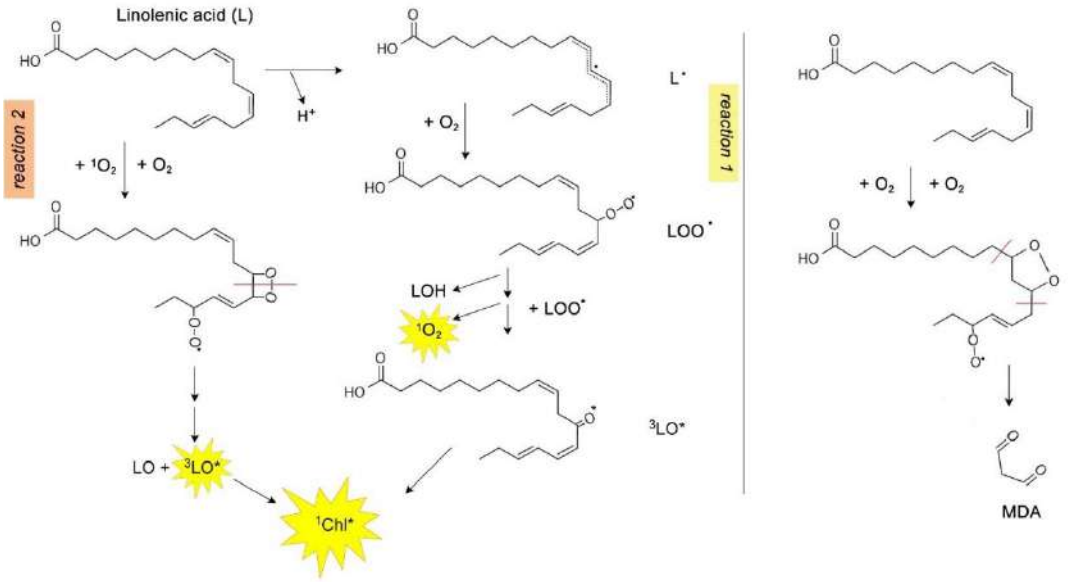

Fig. 1.3.4 | Reactions of lipid peroxidation. *(left panel) Lipid peroxidation starts when a radical species abstracts a hydrogen atom from the carbon chain of a fatty acid (reaction 1). The resulting radical species (L·) reacts with O_2 to form lipid hydroperoxides (LOOH), through an intermediate peroxyl radical (LOO·). The latter can also produce triplet excited carbonyl ($^3LO^*$) and $^1O_2$. Additionally (reaction 2), $^1O_2$ can react with unsaturated fatty acids leading to dioxetanes formation, which spontaneously produce $^3LO^*$. $^1O_2$ and $^3LO^*$ deactivation emits photons, either directly or after excitation transfer to Chl (Prasad and Pospíšil, 2011). (right panel) Mechanism for the formation of malondialdehyde (MDA) from α-linolenic acid (Tsikas, 2017).*

Biochemical assessment of lipid peroxidation

Reference papers: (Havaux et al., 2005; Davey et al., 2005)

Material

Liquid Nitrogen

n-butanol

Buffer 1 (extraction buffer):

175 mM NaCl

50 mM Tris-HCl, pH 8.0

0.01% (w/v) butylated hydroxytoluene (from a stock 10% in ethanol)

Buffer 2 (reaction buffer):

0.5% (w/v) thiobarbituric acid

20% (w/v) trichloroacetic acid

Buffer HPLC:

50 mM KH_2PO_4, pH 7.0

35% (v/v) HPLC-grade methanol

Equipment

- HPLC system which include injector, pumps, optical detector in the visible region
- Analytical reverse-phase C18 column (e.g. Synergi® 4 μm Hydro-RP 80Å LC column 250 x 4.6 mm)
- Block heater
- Microcentrifuge
- Micropipettors, tips
- 1.5 mL polypropylene tubes, pestles for 1.5 mL tubes

Method

- Expose plants, detached leaves, leaf disks or microalgal suspensions to EL conditions. The method has been optimized for the model species *Arabidopsis thaliana* and *Chlamydomonas reinhardtii*. Usually, irradiances around 1,800-2,000 μmol photons m^{-2} s^{-1}

white light at 20-25 °C, or around 800-1,200 μmol photons m^{-2} s^{-1} white light at 5-10 °C, are enough to induce lipid peroxidation within 8-12 hours of treatment.

a) Detached leaves or leaf disks (cut with a hole puncher, Ø ~ 8-10 mm) should be placed on wet filter paper (refer to section 2.3.2 on leaf disk preparation), or
b) aliquots of *C. reinhardtii* cell suspensions (1-5 mL, ~$5 \cdot 10^7$ cell/mL) are transferred to 24-well plates, then stirred while illuminated (refer to section 2.3.3 on cultivation of microalgae).

- Harvest samples in 1.5 mL tubes:
  a) for *Arabidopsis thaliana*, collect at least 5 leaf disks, transfer in 1.5 mL tube, then freeze them in liquid nitrogen; if needed, store samples at -80 °C until ready to be processed;
  b) for *Chlamydomonas reinhardtii*, quantify cell number using either a hemocytometer (e.g. Neubauer improved cell counting chamber) or an automated cell counter (e.g. Invitrogen Countess 3TM) and collect a volume corresponding to 1-4·10^5 cells; add butylated hydroxytoluene at a final concentration of 0.01% (w/v) to terminate lipid peroxidation chain reactions, then centrifuge cells at 3,000 × *g* for 10 min at 4 °C, discard the supernatant; if needed store samples at -80 °C until ready to be processed.
- Grind samples:
  a) for *Arabidopsis thaliana*, grind frozen disks with a 1.5 mL-tube pestle, then add 250 μL Buffer 1 and vortex for 5 sec;
  b) for *Chlamydomonas reinhardtii*, use a 1.5 mL-tube pestle to grind the sample in 250 μL of Buffer 1.
- Add 200 μL Buffer 2 and vortex for 5 seconds.
- Punch a hole into the tube cap with a needle, then heat the samples in the block heater at 95 °C for 25 min.
- Centrifuge the samples for 20 min at 20,000 × *g*, at RT.
- Transfer 200 μL to a new tube.
- Induce the partition of the MDA-$(TBA)_2$ (Figure 5) adduct out of the reaction buffer by adding 200 μL of *n*-butanol and vortexing for 30 sec.
- Centrifuge the samples for 1 min at 20,000 × *g* at RT, to separate the phases.
- Transfer the supernatants (*n*-butanol phase) to a vial for HPLC, then inject 50 μL into the HPLC.

Prepare a standard of MDA (for comparison with samples being tested for lipid peroxidation, which is indicated by MDA accumulation) for injection into the HPLC. MDA is not commercially available, but is released from 1,1,3,3-tetraethoxypropane (T9889, Sigma-Aldrich) by acid-catalyzed hydrolysis:

- Prepare standard samples by diluting the stock solution of 1,1,3,3-tetraethoxypropane in Buffer 1, to have a range of substrate concentrations (e.g., 0, 10, 30, 90, 200, 300, 700, 1,500 ng/mL), and bring the final volume of all samples to 250 μL.
- Add 250 μL Buffer 2 and vortex for 5 sec.

- Punch a hole into the tube cap with a needle, then heat the samples in the block heater at 95 °C for 25 min.
- Centrifuge the samples for 20 min at 20,000 × *g*, at RT.
- Transfer 200 µL to a new tube.
- Partition the MDA-$(TBA)_2$ adduct out of the reaction buffer by adding 200 µL of *n*-butanol and vortexing for 30 sec.
- Centrifuge the samples for 1 min at 20,000 × *g*, at RT to separate the phases.
- Transfer the supernatants (*n*-butanol phase) to a vial for HPLC, then inject 50 µL into the HPLC.

HPLC analysis:

- Elute the column isocratically with 35% methanol in 50 mM KH_2PO_4 (pH 7.0) at 0.8 mL/min.

Under these conditions, analyses last about 10 min. Record absorption spectra over the 400–600 nm range.

- The identity of the MDA-$(TBA)_2$ peak is confirmed by co-elution with standard samples (prepared using a range of 1,1,3,3-tetraethoxypropane concentrations) and by its characteristic absorption spectrum with maximum at 532 nm. By using the samples for calibration, the MDA-$(TBA)_2$ content in ng for each extract can be easily determined.
- At the end, purge the machine with double-distilled water for 20 min at a 3 mL/min flow rate in order to clean it from the excess of salts of this assay.

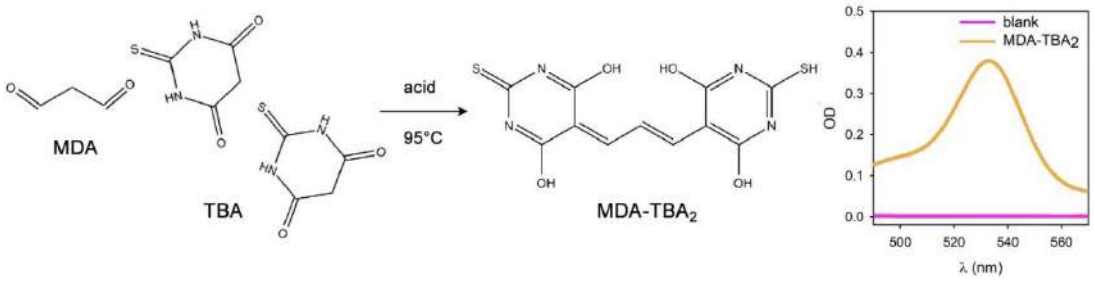

Fig. 1.3.5* | *Reaction involved in the thiobarbituric acid (TBA) assay. *(left panel) One MDA molecule reacts with two TBA molecules at 95°C, to form the MDA-$(TBA)_2$ adduct, which (right panel) absorbs with a peak at 532 nm.*

Biophysical assessment of lipid peroxidation

Reference papers: (Ducruet, 2003; Havaux, 2003)
Material

High purity N_2 gas

Glycerol

Filter paper

Equipment

Thermoluminescence can be measured in algae and leaves by devices which simultaneously regulate sample temperature by a linear warming and detect a low far-red emission ($\lambda > 700$ nm). Easy-to-use instruments are commercially available (e.g. PSI Thermoluminescence System® TL 6000/ET) or can be a home-made, low-cost device as that described by (Ducruet, 2003) (Figure 6).

Method

- Expose plants, detached leaves, leaf disks or microalgal suspensions to EL conditions. The method has been optimized for the model species *Arabidopsis thaliana* and *Chlamydomonas reinhardtii*. Usually, irradiances around 1,800-2,000 μmol photons m^{-2} s^{-1} white light at 20-25 °C, or around 800-1,200 μmol photons m^{-2} s^{-1} white light at 5-10 °C, are enough to induce lipid peroxidation within 8-12 hours of treatment.

a) detached leaves, or leaf disks (cut with a hole puncher, Ø ~ 8-10 mm) should be placed on wet paper (refer to section 2.3.2 on leaf disk preparation), or

b) aliquots of *C. reinhardtii* cell suspensions (1-5 mL, ~$5 \cdot 10^7$ cell/mL) (refer to section 2.3.3 on cultivation of microalgae) are transferred to 24-well plates on shaking (~150-200 rpm), while illuminated.

Collect samples:

a) for *Arabidopsis thaliana*, collect leaves/leaf disks throughout the treatment, and analyze immediately;

b) for *Chlamydomonas reinhardtii*, quantify cell number using either a hemocytometer (e.g. Neubauer improved cell counting chamber) or an automated cell counter (e.g. Invitrogen Countess 3™) and collect a volume corresponding to 1-4·10^5 cells throughout the treatment. Deposit then the suspension onto a disk of filter paper, then analyze immediately.

- In both cases, put the sample in contact with the heating surface of the TL instrument, by using a metal grid. A drop of glycerol in between the metal surface and the sample will help heat transfer.

- To perform TL measurement in a dry environment and to detect the amplitude of the HTL2 band, gaseous N_2 should be flushed in the chamber throughout the heating, in order to desiccate the sample and also to prevent oxidative reactions induced by high temperature.

- Record TL trace by increasing temperature of the sample from 30 °C to 160 °C – set a heating rate of 0.1 °C/sec.

The changes in leaf Chl content during the treatment should be quantified in the same batch of samples exposed to EL: thus, for each sample collected for recording TL trace, another one must be frozen in liquid nitrogen before assessing Chl content (refer to section 2.3.7 on quantification of Chl content in acetone extracts). The reason for doing this is because in photosynthetic tissues, the HTL2 luminescence band originates from excited carbonyls and oxygen species which transfer their excitation to Chls, thus generating Chl*. The HTL signal measured in the far-red region (λ > 700 nm) is predominantly emitted by Chl, and therefore the signal should be normalized to the Chl concentration of the sample, to more accurately quantify lipid hydroperoxides.

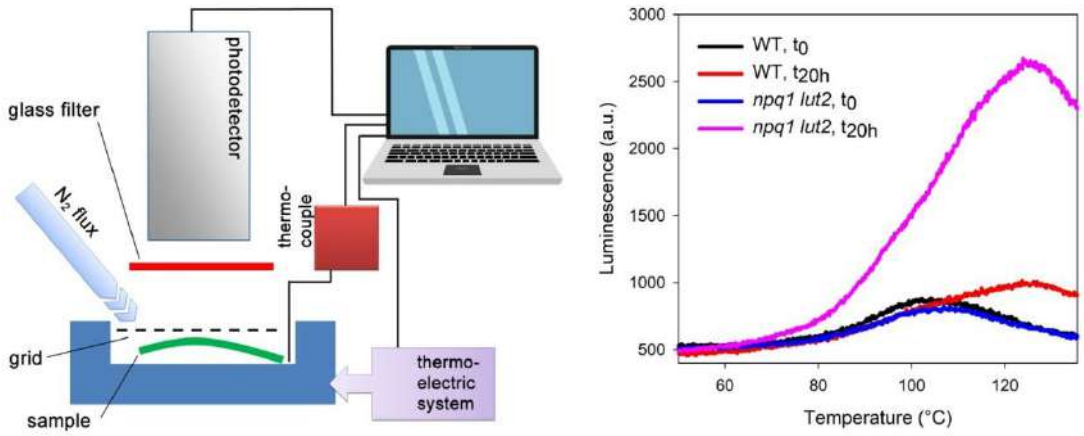

Fig. 1.3.6 | Detection and quantification of lipid peroxidation in vivo by thermoluminescence. *(left panel) Major elements of equipment for thermoluminescence (TL) analysis. Leaf luminescence is measured by a photomultiplier, while the sample is maintained in contact with a thermoelectric Peltier through a metal grid. The temperature of the sample is linearly increased from 30 °C to 160 °C, 0.1 °C/sec. A glass filter on the photodetector is used to select red photon emission. Since the HTL2 band becomes evident in dehydrated samples, the TL measurements are carried out by maintaining the sample in a dry atmosphere, e.g., under a constant flux of gaseous N_2. (right panel) HTL2 band measured under 'dry' conditions, for Arabidopsis thaliana genotypes WT and npq1 lut2, exposed to photooxidative conditions (800 µmol photons m^{-2} s^{-1} at 8 °C, for 20 hours). These two genotypes largely differ in photosensitivity: npq1 lut2 plants are deficient in lutein and zeaxanthin, carotenoid which enhance photoprotection of the chloroplast.*

1.3.7. Measurement of PSI and PSII photoinhibition

Photooxidative damage to both PSII and PSI decreases their photochemical quantum yield, thus leading to a decline in the maximum rate of photosynthesis. PSII is a major target of ROS-dependent damage: generation of $^1O_2$ within both LHCs and reaction can result in damage to subunits involved in the charge separation events, especially the D1 protein (Jarvi et al., 2015). On the other hand, PSI photosensitivity is enhanced at low temperature, due to less efficient enzymatic detoxification of ROS generated at the acceptor side (Sonoike, 2011); in addition, over-reduction of the electron transport chain occurs under conditions in which linear *vs* cyclic electron transport are unbalanced, such as fluctuating light, leading to enhanced ROS release and damage to PSI iron-sulfur centers (Suorsa et al., 2012).

The quantum yield of PSs can be investigated *in vivo* by measuring the fluorescence emitted by PSII and the absorption changes of the reaction center of PSI (P700). PSII quantum yield can be assessed by using a Chl fluorometer, e.g. the "Dual-PAM" (Pulse Amplitude Modulation) fluorometer (Waltz, Germany). This instrument measures the Chl fluorescence of a sample in a non-destructive way, and it is equipped with (i) a measuring light to assess the fluorescence yield of dark-adapted samples, (ii) a detection system able to distinguish between Chl fluorescence emitted by measuring light and ambient or actinic light, and (iii) a saturating light inducing fast changes in Chl fluorescence yield.
The measuring light of the PAM induces the basal level of PSII fluorescence, called F_0. The maximal level of fluorescence (F_m) is then obtained by a saturating pulse (4,500-10,000 μmols photons m^{-2} s^{-1}) which causes the closure of PSII reaction centers. The PSII quantum efficiency is calculated as $F_v/F_m=(F_m-F_0)/F_m$. Treatments with EL and low temperature induce PSII photoinhibition, since they increase the proportion of "closed" PSII unable to undergo charge separation. This results into a lower PSII quantum efficiency.
PSI quantum yield cannot be evaluated by Chl fluorescence analysis (PSI fluorescence yield is too low at RT). Rather, PSI quantum yield can be calculated by analyzing the absorption changes recorded at 830 nm, being the $\Delta Abs_{830\ nm\ -\ 875\ nm}$ related to the oxidation of P700 ($P700 \rightarrow P700^+$).
In the Dual PAM, the redox state of P700 is measured with a dual wavelength unit (830 – 875 nm). The $P700^+$ signal (P) can vary between a minimum (P700 fully reduced) and a maximum (P700 fully oxidized). The maximum value, known as P_m, is determined through a saturating pulse of far-red light which transiently oxidizes all PSI reaction centers thus assessing the maximum photoxidizable P700. Treatment with EL at chilling temperature increases the proportion of non-oxidable (damaged) PSI (Zhang and Scheller, 2004); thus, the photoinhibition rate can be quantified by following the photo-oxidizable P700 throughout the stress treatment.
.

Note: decrease in the P700 oxidation ratio could be caused not only by photoinhibition but also by the over-reduction of PSI acceptor side, which promotes a charge recombination of P700, or by an imbalance in the cyclic vs. linear electron flow. In these cases, $P700^+$ level can be restored by treating cells or vacuum-infiltrate leaves with Dibromothymoquinone (DBMIB, an inhibitor of plastoquinol oxidation) and methyl viologen (MV, an artificial electron acceptor from PSI).

Here we report an effective method to evaluate PSI and PSII photoinhibition, induced by a combination of EL and low-temperature stresses, using simple PAM protocols optimized to assess PSI redox state and PSII quantum efficiency.

Reference papers: (Baker, 2008; Zhang and Scheller, 2004)

Material:

- Methyl viologen (MV), stock solution 1 M in water
- Dibromothymoquinone (DBMIB), stock solution 50 mM in ethanol

Equipment

- Dual-PAM
- Optical unit and, for microalgae, cuvette with 10 mm light path + cuvette stirrer
- High-light system (e.g. high-power LED panel, white light, reaching irradiances around 1,500-2,000 μmol photons m^{-2} s^{-1})

Method

Light treatment

Duration: 6-10 hours.

- Prepare 5-7 plants per genotype, or *C. reinhardtii* cell cultures in the exponential phase, in minimal medium.
- Record F_v/F_m and P_m values, from samples dark-adapted for 30 min. These values constitute the maximal PSII and PSI quantum efficiency, respectively. In healthy plants F_v/F_m reaches a value of about 0.8, while in algae it is more variable, for *Chlamydomonas* is around 0.7.
- Expose the samples to EL conditions. Usually, irradiances around 500-800 μmol photons m^{-2} s^{-1} at 5-10 °C, are enough to promote photodamage on PSs:
    a) detached leaves, or leaf disks (cut with a hole puncher, Ø ~ 8-10 mm) should be placed on wet paper, or
    b) aliquots of *C. reinhardtii* cell suspensions (1-5 mL, ~$5 \cdot 10^7$ cell/mL) are transferred in 24-wells plate, stirring should be maintained during treatment. Dilute an aliquot of cells to $2 \cdot 10^6$ cell/mL prior each measurement.

Note: to avoid overheating of samples, light system can be equipped with infrared suppressor filters.

Measure PSI and PSII photoinhibition

- Treat samples with 50 μM DBMIB and 1 mM MV. Leaves can be vacuum-infiltrated with the inhibitor solution using a syringe (see paragraph 3 of this chapter), while chemicals can be added directly to the aliquots of algal suspension, prior to measurement.
- Set the Dual-PAM with the function "Fluo+P700 measuring mode".
- Record F_v/F_m and P700 signal every 30-60 min. Measure:
    a) 4 to 6 leaves per time point or

b) 4 to 6 algal replicates for each genotype per time point.

- Determine PSII and PSI photoinhibition rate by plotting the decay kinetics of F_v/F_m and photo-oxidizable P700.
- Discard samples once measured.

1.3.8. Conclusions

The protocols here reported describe how to assess *in vivo* the photoprotection ability of plants and algae. These methods allow for a quantitative description of a diverse range of biochemical modifications induced by EL stress, including Chl bleaching, lipid peroxidation, and oxidative events on proteins. Beside quantifying MDA as a convenient biomarker for lipid peroxidation, we provided protocols for detecting thermoluminescence bands at high temperature, as a non-invasive, probe-independent method for quantifying lipid oxidative damage in plant cells. While more suitable for *in vivo* routine analysis, these protocols could be easily adapted to the characterization of purified photosynthetic complexes: e.g. strong illumination of Chl-binding subunits promotes ^{3}Chl* formation and $^1O_2$ release, the latter causing bleaching of bound Chl, with kinetics inversely dependent on the antioxidant efficiency of Car in the complexes. Moreover, the photoprotection capacity of mutant LHCs, e.g. binding different Car complements, can be compared by quantifying the amount of ROS released upon illumination, in the presence of sensitive and highly selective fluorescence probes.

Acknowledgments

This work was supported by MIUR through the grant PRIN 2017(201795SBA3_002, to L.D.) and by University of Verona (Funds for basic research, to R.B.).

2. Aim of the Thesis

The aim of this thesis is the *in vivo* functional analysis of Lhcbs, the Light Harvesting Complexes (LHC) of PSII. Lhcb subunits mediate the capture of photons and transfer excitation energy to the reaction centers of the PSII (Nelson and Ben-Shem, 2004) where the photochemical reactions take place. In an ever-changing environment, LHCs play a pivotal role in optimizing the capture of light, and moreover they act as photo-protecting factors in the photosynthetic membranes. Indeed, the light environment in a cultivation setting is highly heterogeneous: top layers of crop canopies as well as upper layers of massive microalgal cultures absorb sunlight far in excess of what required to saturate photosynthesis, while lower leaves/culture layers are often light-limited. Excess light is dissipated via the non-photochemical quenching (NPQ) mechanisms, which evolved in the LHC system to regulate light-harvesting while preventing photo-oxidative damage.

Engineering the LHC systems was identified as having a potential to improve productivity of both crops and microalgal cultivation (Ort et al., 2015) the photosynthetic yield is one of the physiological traits of cultures that is still far from its upper limit (Zhu et al., 2008, 2010), and the antenna system is pivotal in regulating light-use efficiency.

Recent results showed that redesign of light-harvesting capacity is a promising route. The isolation of pale green algal strain, having reduced LHC content, was found as an effective strategy to increase light penetration within cultures and to boost carbon assimilation (Melis, 2009; Ort et al., 2011) and promising results were obtained in plants with reduced Chl content (Gu et al., 2017). Moreover, regulation of NPQ response yielded into increased CO_2 uptake and biomass yield in tobacco (Kromdijk et al., 2016).

For all these reasons, a functional characterization of the copious members of Lhcb subfamily, which likely retain distinct and peculiar function in vivo, is therefore an essential step in the synthetic biology of the light-harvesting system.

To optimize the growth in PBRs conditions of the green microalga *Chlorella vulgaris*, we produced and analyzed mutant strains with a reduced content of LHC and enhanced resistance to photooxidative stress. Through sequential rounds of mutagenesis by ethyl-methyl-sulfonate, we identified pale green strain with an enhanced resistance to oxidative stress (resistant to $^1O_2$) or with an increased Car complement (chapter 3).

To investigate the physiological role of Lhcb protein family, we moved our attention on *Arabidopsis thaliana*, the model specie for plant biology. In chapter 4 and 5 we applied a combination of reverse genetics and site-directed mutagenesis to investigate the photoprotective properties of specific Lhcb complexes, as well as and their roles in regulating thylakoids structure and dynamics. In chapter 4 we used a CRISPR-Cas9 based genome editing to obtain mutants devoid of specific Lhcb complexes. EM analysis highlighted the role of specific subunits in modulating thylakoids architecture. In chapter 5 we applied a strategy of *in vivo* site-directed mutagenesis to produce mutant lines accumulating either wild type or mutant version of the monomeric Lhcb4. A chl-xanthophyll cluster, catalyzing the fast-quenching response within Lhcb4, has been identified.

3. The Light-Harvesting system as a target for improvement of algal growth in photobioreactors

In recent years, due to the need to find alternatives to fossil fuels, the production of biodiesel from microalgal oil has become an interesting renewable source of biofuels that do not compete with food crops for water and arable lands (Hambourger et al., 2009; Sivakumar et al., 2012). Despite these relevant advantages, large-scale cultivation of microalgae suffers of some major drawbacks: the high cost of management for industrial-scale photobioreactors (PBR), limits in microalgae productivity in large-scale conditions, the low light-use efficiency in high-density cultures and difficulties in maintenance of axenic conditions (Benedetti et al., 2018). In chapter 1.2 of the introduction, we discussed that a possible strategy to improve microalgal cultivation in photobioreactors (PBR) is the production of pale green strains. Pale green strains are characterized by a truncated Light-Harvesting system, this allows for a better light penetration within the PBR, thus determining an increased light availability in the inners layers of the liquid column, resulting in higher productivity in terms of biomass (Kirst et al., 2012). Direct evolution of microalgae of economic interest (e.g. *Chlorella sorokiniana* and *Nannochloropsis gaditana*), produced pale-green strains with an increased biomass yield (Cazzaniga et al., 2014; Perin et al., 2015). In this chapter we applied the same strategy to the green alga *Chlorella vulgaris*. We selected pale-green strains upon the application of ethyl methyl sulfonate (EMS) mutagenesis. Moreover, to further improve the performances of our strains under PBR conditions we applied additional rounds of mutagenesis to produce algal lines with an enhance resistance to excess light. The treatment of mutagenized population with Rose Bengal (induces ROS release in the medium) or Norflurazon (an herbicide inhibiting carotenoids biogenesis), allowed us to isolate Singlet-Oxigen-Resistant lines (SOR) (Dall'Osto et al., 2019) and Norflurazon-Resistant line (NFR) (Guardini et al., 2021). These lines resulted in an enhanced growth in photobioreactor conditions when compared to both the wild-type and the PG-14, a pale-green *Chlorella* mutant previously isolated in the lab. These results will be discussed in the next chapters: 3.1 and 3.2.

3.1 Combined resistance to oxidative stress and reduced antenna size enhance light-to-biomass conversion efficiency in *Chlorella vulgaris* cultures

Dall'Osto *et al. Biotechnol Biofuels* (2019) 12:221
https://doi.org/10.1186/s13068-019-1566-9

Biotechnology for Biofuels

RESEARCH Open Access

Combined resistance to oxidative stress and reduced antenna size enhance light-to-biomass conversion efficiency in *Chlorella vulgaris* cultures

Luca Dall'Osto[1†], Stefano Cazzaniga[1†], Zeno Guardini[1], Simone Barera[1], Manuel Benedetti[1], Giuseppe Mannino[2], Massimo E. Maffei[2] and Roberto Bassi[1*]

Abstract

Background: Microalgae are efficient producers of lipid-rich biomass, making them a key component in developing a sustainable energy source, and an alternative to fossil fuels. Chlorella species are of special interest because of their fast growth rate in photobioreactors. However, biological constraints still cast a significant gap between the high cost of biofuel and cheap oil, thus hampering perspective of producing CO_2-neutral biofuels. A key issue is the inefficient use of light caused by its uneven distribution in the culture that generates photoinhibition of the surface-exposed cells and darkening of the inner layers. Efficient biofuel production, thus, requires domestication, including traits which reduce optical density of cultures and enhance photoprotection.

Results: We applied two steps of mutagenesis and phenotypic selection to the microalga *Chlorella vulgaris*. First, a pale-green mutant (PG-14) was selected, with a 50% reduction of both chlorophyll content per cell and LHCII complement per PSII, with respect to WT. PG-14 showed a 30% increased photon conversion into biomass efficiency vs. WT. A second step of mutagenesis of PG-14, followed by selection for higher tolerance to Rose Bengal, led to the isolation of pale-green genotypes, exhibiting higher resistance to singlet oxygen (strains SOR). Growth in photobioreactors under high light conditions showed an enhanced biomass production of SOR strains with respect to PG-14. When compared to WT strain, biomass yield of the pale green + sor genotype was enhanced by 68%.

Conclusions: Domestication of microalgae like *Chlorella vulgaris*, by optimizing both light distribution and ROS resistance, yielded an enhanced carbon assimilation rate in photobioreactor.

Keywords: Microalgae, Chloroplast, Biofuel, Excess light, Photoprotection, Singlet oxygen, Biomass

Background

The rapid burning of fossil fuels impacts on Earth's climate making the search for carbon-neutral fuels solutions urgent. Liquid fuels derived from photosynthetic organisms represent a renewable alternative to fossil fuels and a source of sustainable energy (Hambourger et al., 2009; Sivakumar et al., 2012). Mass cultures of microalgae in photobioreactors (PBRs) are a promising source of biomass for biofuel production on a large scale, due to the high productivity and lipid content, far exceeding the best crops (Chisti, 2008; Jones and Mayfield, 2012; Benedetti et al., 2018). In both microalgae and land plants, photosynthetic reactions are carried out by membrane supercomplexes and soluble enzymes (Nelson and Ben-Shem, 2004); yet, of species can accumulate high level of lipids, up to over 50% of their dry biomass (Scott et al., 2010). After oil extraction, the residual lipid-free biomass can be used as bio-stimulant and fertilizer or fermented to produce biogas (Passos et al., 2014). Microalgae are also useful for wastewater bioremediation and CO_2 mitigation because of their high capacity to recover nitrogen, phosphorus and heavy metals from industrial, municipal and agriculture wastes (Christenson and Sims, 2011; Pittman et al., 2011). Among microalgae species, members of the genus *Chlorella* gained importance as robust biomass accumulating strains, allowing for sustainable industrial productions of high-value products and biofuels (Münkel et al., 2013). Under high irradiance or nutrient (N, P) deficiency, *Chlorella* mass cultures increase their neutral lipid content (Rodolfi et al., 2009) in the form of triacylglycerols, which serve as cellular storage molecules, thus making these organisms promising candidates for lipid-based biofuels production. Potential coupling of oil production with either wastewater bioremediation or CO_2 abatement technologies to industrial applications may decrease the cost of biofuel production as well as provide significant environmental benefits (Pittman et al., 2011).

Production of biofuels from microalgae, however, still suffers from limitations, hampering cost effectiveness. These include the costs for PBRs construction and management, water pumping and mixing, axenic practices for preventing contamination of monocultures, harvesting biomass and lipid extraction (Benedetti et al., 2018). In addition, there are physiological limitations such as low efficiency of light use, especially under high irradiance. The maximal theoretical efficiency of photosynthetically active radiation (400–700 nm) (PAR) solar energy conversion into biomass is about 27% (Weyer et al., 2010). However, such values are only observed at low light intensity in laboratory-scale growth trials, while efficiency drops below 6% in outdoor cultures at full sunlight intensities (Rodolfi et al., 2009). Limits in biomass yield can be ascribed to a number of factors (Stephenson et al., 2011), including (i) light-saturation effect, (ii) inhomogeneous light distribution within a mass culture and (iii) photoinhibition.

The light-saturation effect becomes evident when considering the light response curves for photosynthesis compared with the rate of light absorption (Li et al., 2009b). In low-light conditions, photosynthetic rates increase with increasing irradiance, and the rate of photon absorption is correlated with that of electron transport from water to CO_2; at higher irradiance, the photosynthetic rate increases non-linearly with respect to light intensity, reaching light saturation (Pmax). Within saturation range, excess energy is dissipated into heat. At even higher fluency, net assimilation decreases due to oxidative photoinhibition.

Within the light limited range, energy is efficiently used for photosynthesis. When light irradiance overcomes the rate of downstream biochemical reactions, excess absorbed energy is wasted as heat, thus impairing lightto-biomass conversion efficiency (Ruban et al., 2012). Additional energy loss derives from the inhomogeneous light distribution in the algal culture. The high optical density of algal cells at the surface causes a steep light gradient which leaves inner layers below compensation point with respiration causing energy loss. The high Chl content per cell maximizes the photon capture in the natural environment, with limiting light and low cell density. To this aim, large arrays of antenna complexes (Light-harvesting complexes, LHCs), binding chlorophylls (Chl) and carotenoid (Car) in quasi-molar concentration, enhance exciton supply to reaction centers, hosting photochemical reactions (Van Amerongen and Croce, 2013). However, large antenna systems do not enhance overall productivity in a PBR because the high optical density readily leads to saturation of photosynthesis in the surface layers, while the inner space becomes light limited. The resulting inhomogeneous light distribution impairs productivity (Formighieri et al., 2012). Upon sustained over-excitation experienced by cells of surface layers, increase in lifetime of Chl singlet excited states (^{1}Chl*) and intersystem crossing to the Chl triplet state (^{3}Chl*) occur. Moreover, reaction with molecular oxygen (O_2) yields singlet oxygen ($^1O_2$) hence photoinhibition of PSII, a complex highly susceptible to light damage (Aro et al., 1993; Krieger-Liszkay et al., 2008). Algal cells rapidly shift between layers with low vs. high irradiance due to mixing, which impairs the light acclimation capacity of their photosynthetic apparatus.

Domesticating microalgae for enhanced growth rate in PBRs requires introduction of traits alleviating these physiological constraints to (i) optimize the optical density per biomass unit and, (ii) increase the resistance to photo-oxidation (Benedetti et al., 2018). Decreasing overall absorption of photosynthetic active radiation (PAR) per cell (Kirst et al., 2012) improves light distribution in PBR so that cells facing the surface absorb less photons, while those in inner layers become net contributors to carbon fixation (Cazzaniga et al., 2014). Increasing resistance to photo-oxidative damage is expected to decrease photoinhibition. Indeed, preventing photoinhibition was reported to increase fitness (Külheim et al., 2002) and provide carbon gain (Zhu et al., 2004). However, it is unclear whether manipulation of photoprotection traits might have beneficial effects for mass culture in PBR environment once weighted against the metabolic cost these processes have in algae. In this work, we report on the construction of *Chlorella vulgaris* strains combining enhanced light transmittance and resistance to oxidative stress by two steps of mutagenesis followed by phenotypic selection. The first selection round yielded the pale-green PG-14 strain with increased photon use efficiency and higher biomass productivity in PBR. Further mutagenesis/selection allowed to select pale-green strains with increased tolerance to $^1O_2$ (SOR strains). Selected SOR strains in PBR under strong irradiances showed further enhancement in productivity with respect to PG-14. Overall, these results show that resistance to oxidative stress is an important component of algal productivity. In addition, the traits responsible to improved optical properties can be combined with those providing oxidative stress resistance for the construction of domesticated algal strains with improved biomass yield for growth in PBRs.

Results

Isolation of PG-14, a pale-green mutant of *Chlorella vulgaris*

Chlorella vulgaris mutants that exhibited a pale-green (PG) phenotype with respect to WT were visually screened following EMS mutagenesis (Figure S3.1.1A, B). Approximately 25,000 mutagenized lines were visual screened, and seven independent mutants were identified as putatively affected in Chl content per cell. All these mutants were capable of phototrophic growth and displayed different levels of depletion in Chl (Figure S3.1.1C). Among the identified strains, p1–14 showed the highest growth rate in batch conditions (Figure S3.1.2). It was, therefore, selected for further analysis and renamed as PG-14.

Pigment composition of both mutant and WT strains was determined after 5 days of growth, as shown in Table 3.1.1. PG-14 showed a significant reduction of Chl content per cell (− 50%) when grown in minimal medium. The Chl a/b ratio was significantly higher in the mutant, with a value of 4.12 vs. 2.67 in WT, whereas the Chl/Car ratio was significantly lower in PG-14 (2.25) with respect to the WT (4.03). These data suggest a depletion in the Chl b-rich antenna complexes (LHC) in PG-14.

Stoichiometry of pigment-protein complexes and photosynthetic electron transport

To determine whether the capacity of the antenna system to transfer absorbed energy to RCs was affected by the mutation, Chl fluorescence analysis was used to quantify the PSII operating efficiency. No significant differences were observed in Fv/Fm between PG-14 and WT (Table 3.1.1), suggesting that the maximal quantum yield of PSII photochemistry was not impaired in the pg mutant. Functional antenna size of PSII was measured on cell suspensions in the presence of DCMU, by estimating the rise time of Chl a fluorescence (Fig. 3.1.1a). The T2/3 of the Chl fluorescence rise is inversely related to the functional antenna size of PSII [25] and was reduced by ~ 35% in PG-14 with respect to WT (Table 3.1.1).

These results were further confirmed through biochemical estimation of PSII antenna size. The level of selected thylakoid proteins was determined by immunetitration on thylakoids and expressed relative to WT once normalized to the PSII core complex (CP43) content (Fig. 3.1.1b). The LHCII abundance was reduced in the PG14 mutant to ~ 61% with respect to the WT level, while the PSI/PSII ratio was the same in both genotypes.

Table | 3.1.1 Pigment content, PSII maximum quantum yield (Fv/Fm) and PSII functional antenna size of WT and mutants PG-14

genotype	Chl / cell (pg)	Chl *a* / *b*	Chl / Car	F_v / F_m	PSII antenna size ($T_{2/3}^{-1} \cdot 10^3$, ms^{-1})
WT	0.26 ± 0.03[a]	2.67 ± 0.22[a]	4.03 ± 0.22[a]	0.67 ± 0.03[a]	6.74 ± 0.49[a]
PG-14	0.13 ± 0.02[b]	4.12 ± 0.30[b]	2.25 ± 0.13[b]	0.69 ± 0.05[a]	4.40 ± 0.27[b]
SOR-1	0.13 ± 0.02[b]	4.12 ± 0.20[b]	2.24 ± 0.17[b]	0.67 ± 0.03[a]	4.17 ± 0.21[b]
SOR-5	0.11 ± 0.03[b]	3.96 ± 0.31[b]	2.24 ± 0.05[b]	0.66 ± 0.03[a]	4.37 ± 0.23[b]
SOR-6	0.13 ± 0.03[b]	4.20 ± 0.12[b]	2.25 ± 0.07[b]	0.66 ± 0.05[a]	4.29 ± 0.30[b]

Parameters were measured on dark-adapted cell suspension of WT, PG-14 and SOR strains, upon 7 days of photoautotrophic growth in BG-11 medium in low light (conditions (100 μmol photons m^{-2} s^{-1}, 25 °C ANOVA test, $p < 0.05$). Data are expressed as mean ± SD, $n > 4$. For each parameter measured, significantly different values among genotypes are marked with different letters

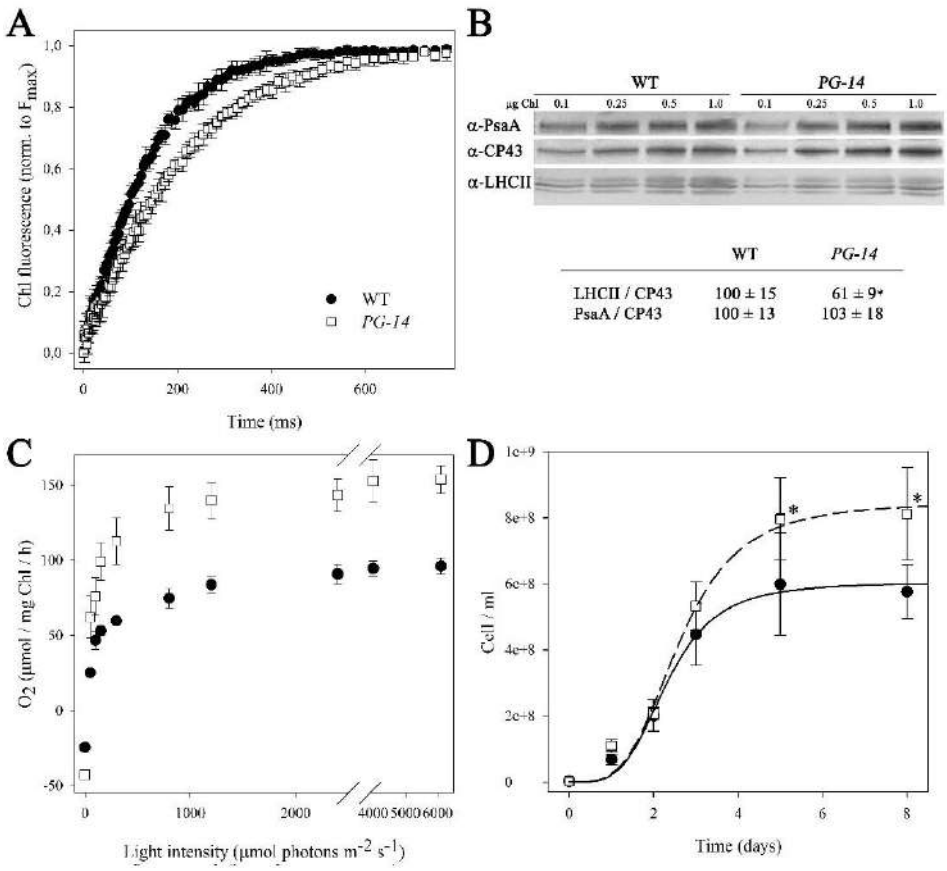

Fig. | 3.1.1 Characterization of pale-green-14 (PG-14) mutant of Chlorella vulgaris. a *PSII functional antenna size. Variable Chl fluorescence was induced with a green light (15 μmol photons m^{-2} s^{-1}), on dark-adapted cells of WT and PG-14, in BG-11 medium supplemented with 50 μM DCMU. Data are expressed as mean ± SD, n = 10. The reciprocal of time corresponding to two-thirds of the fluorescence rise (T2/3) was taken as a measure of the PSII functional antenna size (see Table 3.1.1).* ***b*** *Immunoblotting used for the quantification of photosynthetic subunits. Immunotitration was performed with antibodies directed against individual gene products: LHCII, the major light harvesting complex of PSII; the PSII core subunit PsbC (CP43); the PSI core subunit (PsaA). The amount of Chls loaded for each lane is shown. Values significantly different (Student's t test, $p < 0.05$) with respect to the WT are marked with asterisks.* ***c*** *Light-saturation curves of photosynthesis. Measured cultures (panels* ***a–c****) were grown in minimal BG-11 medium at 100 μmol photons m^{-2} s^{-1}, in shaken flasks (120 rpm) illuminated from the top, photoperiod of 16/8 h light/dark, 25 °C. d Growth curves of wild type and PG-14 mutant under autotrophic conditions. All experiments were performed in 1-L cylinders, illuminated with 1400 μmol photons m^{-2} s^{-1}, 25 °C. Growths were performed in a semi-batch system fed with air/CO2 mix; the CO2 supply was modulated to keep the pH of the medium always below 7.1. Data are expressed as mean ± SD, n = 4*

To investigate the functional properties of the photosynthetic machinery of the PG-14 mutant, the light saturation curve of photosynthesis was measured in photo-autotrophically grown cells (Fig. 3.1.1c). The rate of O_2 release was shown to increase as a function of irradiance within the range of light intensities between 0 and 1000 μmol photons m^{-2} s^{-1}. The increase was linear for both WT and PG-14 at irradiances below 150 μmol photons m^{-2} s^{-1}. The slope of the linear regressions of O_2 yield vs. light intensity for WT and PG-14 was 0.84 ± 0.21 and 1.32 ± 0.35, respectively, implying that the quantum yield of photosynthesis was significantly higher in the mutant with respect to WT. The light intensity for half-saturation of photosynthesis was similar in the two strains, at approximately 100 μmol photons m^{-2} s^{-1} (Table 3.1.2); irradiances higher than 1000 μmol photons m^{-2} s^{-1} were saturating for the O_2 production in both WT and the PG-14 mutant (Fig. 3.1.1c). In WT, the maximum rate of light-induced oxygen evolution Pmax (photosynthesis net respiration) was reached at 2000 μmol photons m^{-2} s^{-1} and was equal to 96 ± 5 μmol O_2 mg Chl $^{-1}$ h^{-1}. PG-14 cells showed a significantly higher Pmax, i.e. (155 ± 11) (Table 3.1.2). Owing to the normalization of O_2 production rate on Chl content, Pmax is a measure of the Chl productivity for the two strains. The dark respiration rate was 25 ± 3 μmol O_2 mg C hl^{-1} h^{-1} in the WT vs. 43 ± 3 in PG-14 (Table 3.1.2), while it was the same in WT and mutant on a per cell basis. Altogether, these results imply that the PG-14 mutant possesses an enhanced photosynthetic productivity with respect to the WT. To verify this hypothesis, growth rate and biomass productivity analysis were performed. Photoautotrophic growth was monitored over a period of 8 days in a lab-scale photobioreactor, a semi-batch cultivation system composed of 1-L glass cylinders exposed at a light intensity of 1400 μmol photons m−2 s−1. The system was fed with a flux of air and CO2, whose relative abundance was regulated by the pH of the medium in order to keep it within the range 6.8–7.2. The PG-14 culture reached a cell concentration of ~ $8.1 \cdot 10^8$ cell mL^{-1} at day five vs. $6.0 \cdot 10^8$ cell mL^{-1} obtained in the WT (Fig. 3.1.1d), with a specific growth rate (μ) of the mutant which was significantly higher than the WT (2.00 day^{-1} for PG-14 and 1.87 day^{-1} for WT, Table 3.1.3). Moreover, the mutant showed a higher mean biomass productivity, equal to 550 mg L^{-1} day^{-1}, which was significantly higher (+28%) with respect to that in the corresponding WT (Table 3.1.3).

Table | 3.1.2 Photosynthesis and respiration rates

Parameters	WT	*PG-14*	*SOR-1*	*SOR-5*	*SOR-6*
Half-saturation intensity (µmol photons m^{-2} s^{-1})	110 ± 24[a]	96 ± 41[a]	128 ± 6[a]	124 ± 9[a]	118 ± 29[a]
P_{max} (µmol O_2 mg Chl^{-1} h^{-1})	96 ± 5[a]	155 ± 11[b]	146 ± 8[b]	143 ± 7[b]	150 ± 3[b]
Respiration (µmol O_2 mg Chl^{-1} h^{-1})	25 ± 3[a]	43 ± 3[b]	40 ± 5[b]	47 ± 7[b]	42 ± 6[b]
Respiration (fmol oxygen $cell^{-1}$ h^{-1})	6.4 ± 0.8[a]	5.5 ± 0.4[a]	5.2 ± 0.6[a]	5.6 ± 0.8[a]	5.4 ± 0.8[a]
P_{max}/respiration (relative units)	3.9 ± 0.4[a]	3.6 ± 0.2[a]	3.7 ± 0.6[a]	3.1 ± 0.5[a]	3.6 ± 0.5[a]

Parameters were measured on dark-adapted cell suspension of WT, PG-14 and SOR strains, upon 7 days of photoautotrophic growth in BG-11 medium in low light conditions (100 µmol photons m^{-2} s^{-1}, 25 °C). O_2 evolution/consumption was measured with a Clark-type oxygen electrode (Oxygraph, Hansatech). Data are expressed as mean ± SD (n > 4). For each parameter measured, significantly different values among genotypes (ANOVA test, p < 0.05) are marked with different letters.

Isolation of pale-green, singlet oxygen-resistant strains When experiencing excess light (EL) conditions, microalgae activate acclimatory responses involving induction of genes encoding products conferring enhanced tolerance to $^1O_2$ stress (Li et al., 2009b).

Table | 3.1.3 Growth parameters of WT, PG-14 and SOR strains, cultured in air/CO_2 bubbling system

	lab-scale, indoor PBR			
	1,400 µmol photons m^{-2} s^{-1}		50 µmol photons m^{-2} s^{-1}	
genotype	Mean increase of biomass (g l^{-1} day^{-1})	µ (day^{-1})	Mean increase of biomass (g l^{-1} day^{-1})	µ (day^{-1})
WT	0.43 ± 0.03[a]	1.87 ± 0.08[a]	0.059 ± 0.023[a]	0.94 ± 0.09[a]
PG-14	0.55 ± 0.02[b]	2.00 ± 0.07[b]	0.024 ± 0.004[b]	0.85 ± 0.13[a]
SOR-1	0.58 ± 0.03[b]	1.97 ± 0.04[a,b]	0.059 ± 0.008[a]	0.94 ± 0.08[a]
SOR-5	0.70 ± 0.03[c]	2.07 ± 0.03[c]	0.048 ± 0.002[c]	0.94 ± 0.09[a]
SOR-6	0.72 ± 0.04[c]	2.09 ± 0.03[c]	0.049 ± 0.015[c]	0.94 ± 0.08[a]

Biomass increase was measured by the determination of dry biomass accumulated after the cultivation period, divided by the number of days of cultivation (see Fig. 3.1.6). µ, specific growth rate, was calculated from the slope of logarithmic cell concentration curve. Growth was performed under autotrophic conditions, in 1-L cylinders, illuminated with either 1400 or 50 µmol photons m^{-2} s^{-1}, 25 ° C. Data are expressed as mean ± SD, n > 3. For each parameter and condition measured, (significant different values among genotypes (ANOVA test, p < 0.05) are marked with different letters.

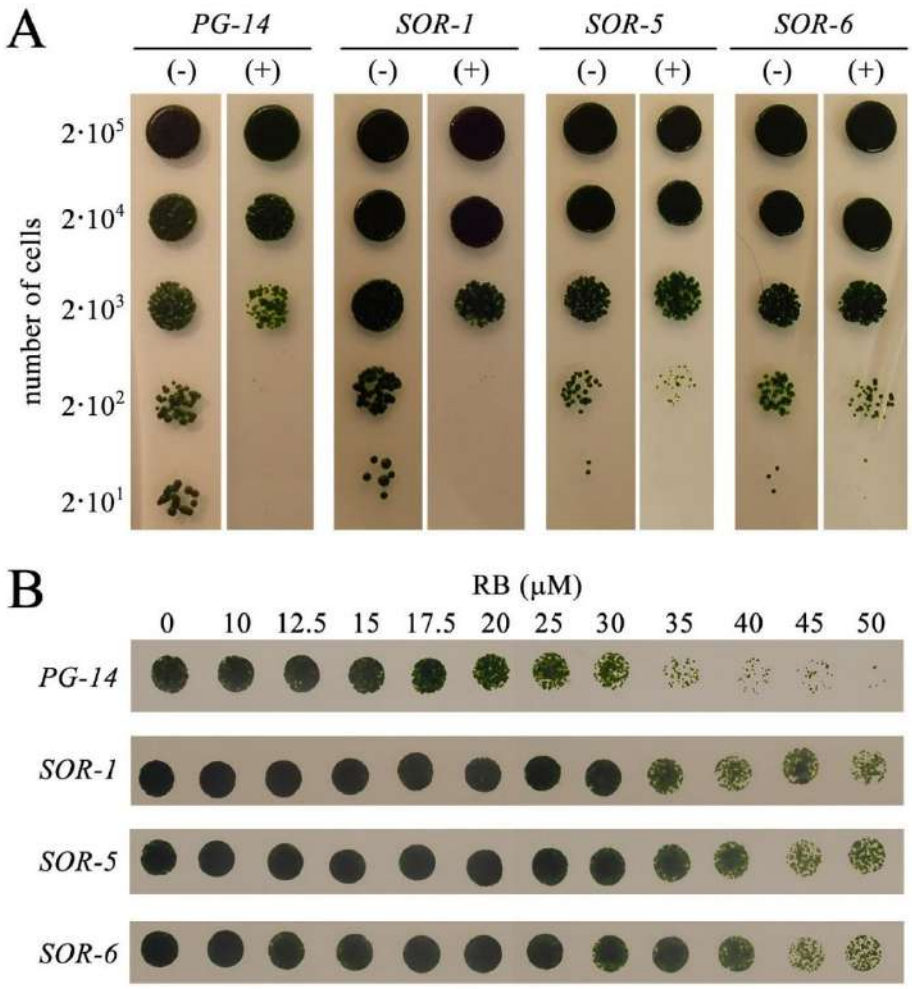

Fig.* | *3.1.2 Isolation of singlet-oxygen-resistant (SOR) lines of C. vulgaris.
a *SOR-1, SOR-5 and SOR-6 strains were isolated as a $^1O_2$-resistant mutant by growing on solid TAP medium either containing (+) or not (−) of Red Bengal (RB 12 μM). The amount of cells spotted is indicated in the left border.* ***b*** *Quantitative analyses of the resistance of SOR strains to oxidative stress. Cells were grown in liquid cultures with increasing concentration of RB (0–50 μM) for 24 h, then were spotted on TAP-agar for recovery. Plates were illuminated with 100 μmol photons m^{-2} s^{-1}, photoperiod of 16-/8-h light/dark, 25 °C.*

To identify mutants with constitutively activated acclimation, we performed a screening for lines showing an increased tolerance to exogenous $^1O_2$. The PG-14 strain was mutagenized by EMS and plated onto agar containing the $^1O_2$-photosensitizer Red Bengal (RB) used at the minimal concentration (12 μM) needed to inhibit growth of WT cells. Plates were exposed to a light–dark cycle (16:8 h) for 10 days, at which point 18 RB-resistant clones were isolated. To verify increased $^1O_2$ resistance, colonies were picked to liquid medium in microtiter plates, and then re-evaluated for $^1O_2$ tolerance by spotting cells in agar plates containing 12 μM RB (Fig. 3.1.2a). The three clones which passed the second screen were named as singlet oxygen resistant (SOR) mutants. No significant difference in the growth rates with respect to the parental line PG-14 on control agar conditions were observed with these three mutant strains (Fig. 3.1.2a). RB significantly impaired growth of all genotypes; however, the effect was far more severe in the PG-14 strains with respect

to SOR mutants. The $^1O_2$ resistance of the three SOR clones was quantified (Fig. 3.1.2b): cultures of SOR-1, -5 and -6 and the parental strain PG-14 were exposed to increasing concentrations of RB (0–50 μM) in liquid cultures for 24 h, upon which, cells were spotted on agar plates. All SOR strains showed higher survival rates at high RB concentrations (≥ 25 μM) with respect to the parental strain. PG-14 and SOR mutants showed the same phenotype as for the Chl/cell, Chl a/b and Chl/Car ratios (Table 3.1.1), suggesting that the size of LHC antenna system was similar to the parental line PG-14. This was confirmed through immunotitration: both LHCII content and PSI/ PSII ratio of SOR mutants were the same as measured in PG-14 (Fig. 3.1.3a). No significant differences were observed in both PSII operating efficiency (Fv/Fm) and functional antenna size of PSII, with respect to the corresponding parental line (Fig. 3.1.3b, Table 3.1.1). In both SOR and PG-14 strains, the light-saturation curves of photosynthesis (Fig. 3.1.3c) showed similar values for the maximum rate of light-induced oxygen evolution (Pmax), half-saturation intensity for photosynthesis and dark respiration rates on a per cell basis (Table 3.1.2), thus indicating that the SOR mutant strains maintained the reduction in antenna size and the enhanced photosynthetic productivity previously shown in PG-14 cells.

Sensitivity to photooxidative stress of SOR strains

Under strong light, microalgae undergo photooxidative stress (Li et al., 2009b). Under such conditions, enhanced release of $^1O_2$ leads to bleaching of pigments, lipid oxidation and a decrease of photosynthetic efficiency. Mechanisms evolved by photosynthetic organisms to limit photooxidative damage and acclimate to changes in the light environment include increasing Car pool size and a specific acclimation response enhancing $^1O_2$-resistance. Therefore, the mutant strains SOR, with a constitutive up-regulation of protective mechanisms are expected to better perform under photooxidative stress conditions, by limiting pigment-protein damage and ultimately, photoinhibition.

The sensitivity to EL stress of WT, PG-14 and SOR mutant strains was assessed upon transfer of cells from control conditions to HL at 25 °C, then a time-course lipid peroxidation and pigment bleaching was measured (Fig. 3.1.4). When cells were exposed to 1400 μmol photons m^{-2} s^{-1} for 24 h, malondialdehyde production was 1.5 times higher in both WT and PG-14 cells with respect to SOR (Fig. 3.1.4a) strains, implying a significantly lower level of lipid peroxidation in the latter. We further examined liquid cultures of the WT and the mutants, at various times after transfer of low light grown cells to extremely high irradiances (14,000 μmol photons m^{-2} $s^{-1,}$ at 25 °C). In both WT and PG-14 cell suspensions, the Chl content decreased progressively upon exposure to HL until it reached ~ 40% of the initial value, after 2-h treatment (Fig. 3.1.4b). The rate of Chl bleaching was three times faster in WT or PG-14 with respect to SOR strains (Fig. 3.1.4b).

To assess whether the SOR mutations affect the composition of the photosynthetic machinery, we determined the accumulation level of selected chloroplast proteins relative to the WT by immunotitration in EL grown cells (Figure S3.1.3). LHCII content was reduced in all mutants, ranging between 45 and 60% with respect to WT on a Chl basis. On the other hand, the PSI: PSII ratio was similar in all genotypes. Cytochrome f complex and ATP synthase (β subunits) were present in higher amounts in all mutants with respect to the WT. Rubisco was increased in all

mutants (× 1.5–2 with respect to the WT level), with the only exception of SOR-1 strain, whose Rubisco content accounted to 70% of the control strain (Figure S3.1.3).

The antioxidant properties of the algal biomass are related to the efficiency of the detoxification mechanisms. To assess the antioxidant capacity of the extracts from WT and mutant lines, we resorted to more than one method, since the activity of an extract depends on its composition, polarity of extraction solvents and type of assay used.

FRAP assay measures the capacity of an antioxidant in the reduction of the oxidant Fe^{3+} ion. When tested by FRAP, the levels of antioxidant activity of the different samples were as follows: SOR ≥ PG-14 > WT (Fig. 3.1.5a). ABTS (2,2′-azino-bis(3-ethylbenzothiazoline-6-sulphonic acid) assay, which requires a buffered aqueous solution, yielded very high scavenging activity in PG-14 extracts; while all other mutants showed a significantly ($p < 0.05$) lower activity, even though far higher than the WT (Fig. 3.1.5b).

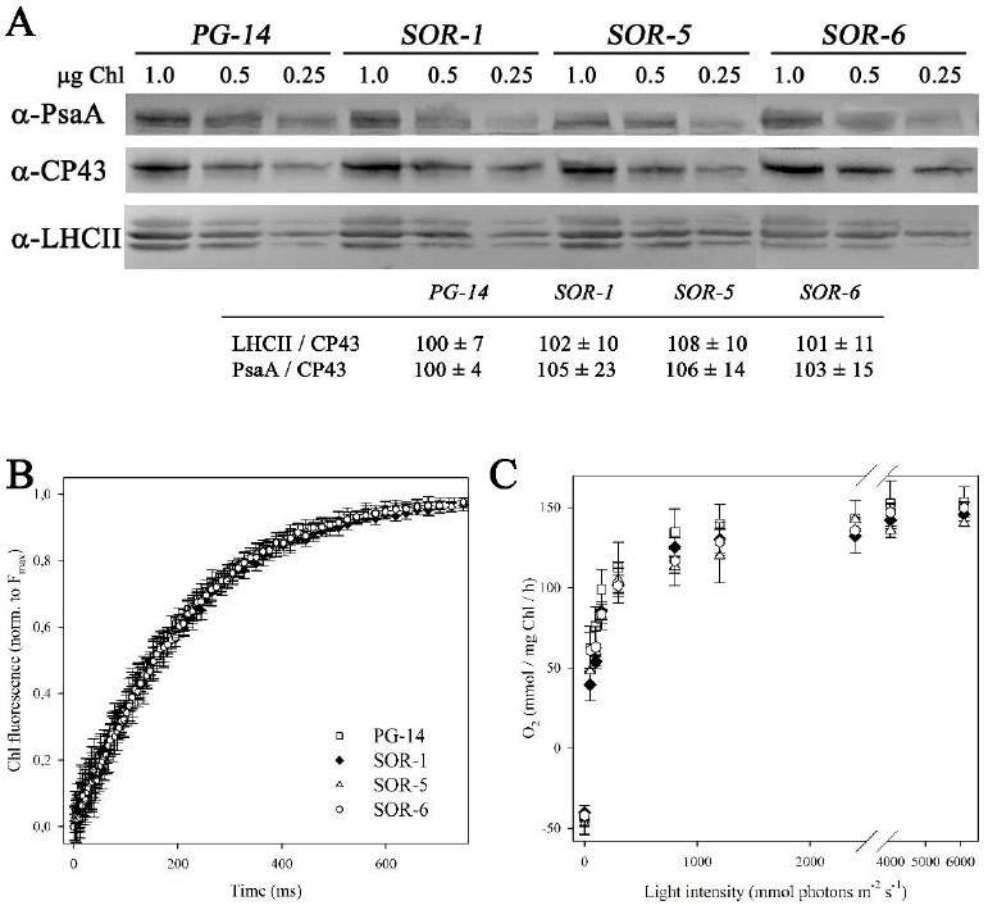

Fig. | 3.1.3 Photosynthetic characterization of SOR strains. a *Immunoblotting titration of photosynthetic subunits in thylakoid membranes. PSII biochemical antenna size (LHCII/CP43 ratio) and PSI/PSII ratio (PsaA/CP43) are shown in the table. The amount of Chls loaded for each lane is shown.* ***b*** *PSII functional antenna size. Variable Chl fluorescence was induced on dark-adapted cells of PG-14 and SOR mutant lines, in BG-11 medium supplemented with 50 µM DCMU. Data are expressed as mean ± SD, n = 10. See Table 3.1.1 for quantitative description of antenna size. c Light-saturation curves of photosynthesis. Data are expressed as mean ± SD, n = 4*

Cultivation of WT and mutant strains in laboratory-scale photobioreactor

The above results show that the mutant strains SOR have both enhanced efficiency of light energy conversion and higher tolerance to conditions of EL with respect to PG-14 and WT strains, suggesting that they could have an enhanced light-to-biomass conversion yield. To verify such increased yield, growth rate and biomass productivity were further assessed in SOR lines. Photoautotrophic growth was monitored over a period of 6 days in the lab-scale 1L PBR at 1400 uE. Both the SOR-5 and SOR-6 cultures reached a cell concentration of about 6.8 10^8 cell mL^{-1} at day six vs. $5.1 \cdot 10^8$ cell mL^{-1} in the PG-14 (Fig. 3.1.6a), with a specific growth rate (µ) higher than for PG-14 (Table 3.1.3). Moreover, these mutants showed a higher mean biomass productivity, equal to 700 mg L^{-1} day^{-1} , that was significantly improved (+30%) respect to the corresponding value for the PG-14 (550 mg L^{-1} day^{-1}) (Table 3.1.3). The SOR-1 mutant did display a faster growth

rate (Fig. 3.1.6a); however, it did not show any significant enhancement in biomass productivity (580 mg L^{-1} day^{-1}) with respect to PG-14 (Table 3.1.3).

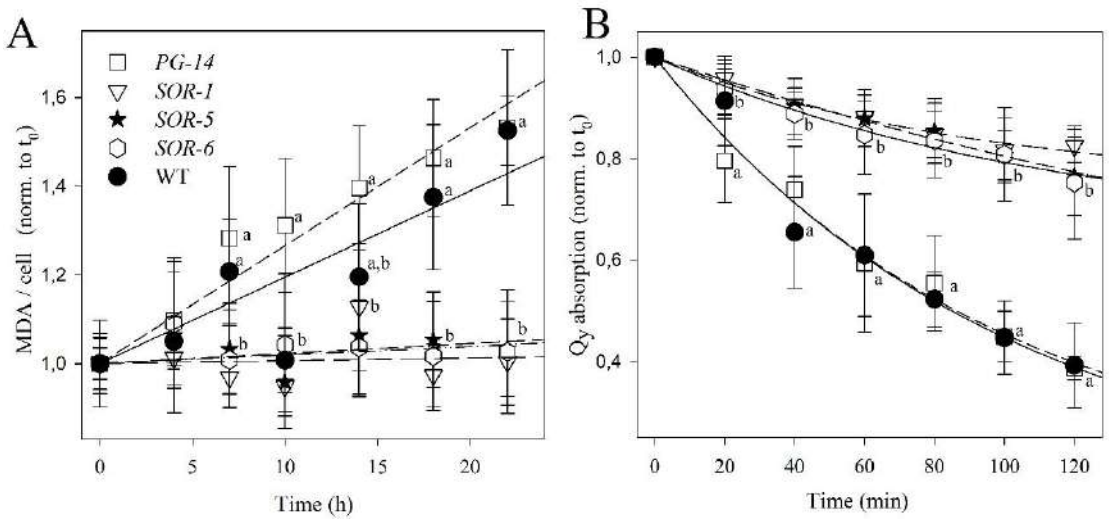

Fig. | 3.1.4 Photooxidation of C. vulgaris WT, PG-14 and SOR mutant genotypes under photooxidative stress. *a Cell suspensions were treated with 1400 µmol photons m−2 s−1 at 20 °C, and kinetics of malondialdehyde (MDA) formation were followed. MDA is an index of membrane lipid peroxidation, and was quantified by HPLC as thiobarbituric reactive substances. (B) Cell suspension of WT and mutant strains were treated with strong white light (14,000 µmol photons m^{-2} s^{-1}, 20 °C) and the amount of Chl was evaluated by measuring the absorption area in the region 600–750 nm. See "Materials and methods" for details. Symbols and error bars show mean ± SD, n = 4. Values marked with the same letters are not significantly different from each other within the same time point (ANOVA, p < 0.05)*

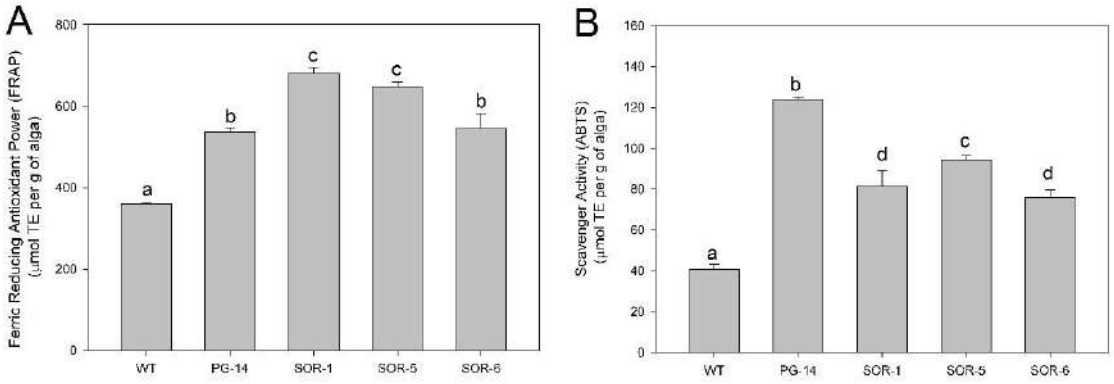

Fig. | 3.1.5 Comparison of antioxidant activity of whole-cell extracts from C. vulgaris WT and mutants PG-14 and SOR. *Antioxidant activity was measured by FRAP (a) and ABTS (b) assays. Within each panel, different letters indicate significant (ANOVA test, $p < 0.05$) differences. The values are the mean of 3 replicates, metric bars indicate SD.*

Among the mechanisms possibly underlying the higher biomass yield of SORs, the most relevant is the Non-Photochemical Quenching (NPQ), which catalyzes dissipation, as heat, of the light energy absorbed in excess. In WT, PG-14 and SOR genotypes, NPQ amplitude was measured at steady-state photosynthesis over a range of irradiances, showing differences mostly negligible (Fig. 3.1.7a). Moreover, recovery of Fv/Fm upon photoinhibition (Fig. 3.1.7b) showed that all strains had the same behavior, implying that the higher growth of mutants was due to enhanced PSII repair.

The enhanced growth of the three SOR strain in HL is consistent with their truncated antenna system and resistance to ROS. However, it is unclear whether it is also due to enhanced efficiency in light-use efficiency. To explore this possibility, we grew these strains as well as WT and PG-14 in limiting-light conditions (Fig. 3.1.6b). At 50 µmol photons m^{-2} s^{-1}, PG-14 had a lower grow rate with respect to WT as expected from its reduced antenna size. The three SOR mutants had a growth kinetic and final biomass yield similar to WT, despite they had a reduced antenna size, similar to PG-14 (Fig. 3.1.6b, Table 3.1.3). These results are consistent with enhanced growth rate of SOR mutants being caused not merely by enhanced ROS resistance plus enhanced growth penetration in the culture, but also by enhanced light-use efficiency in low light.

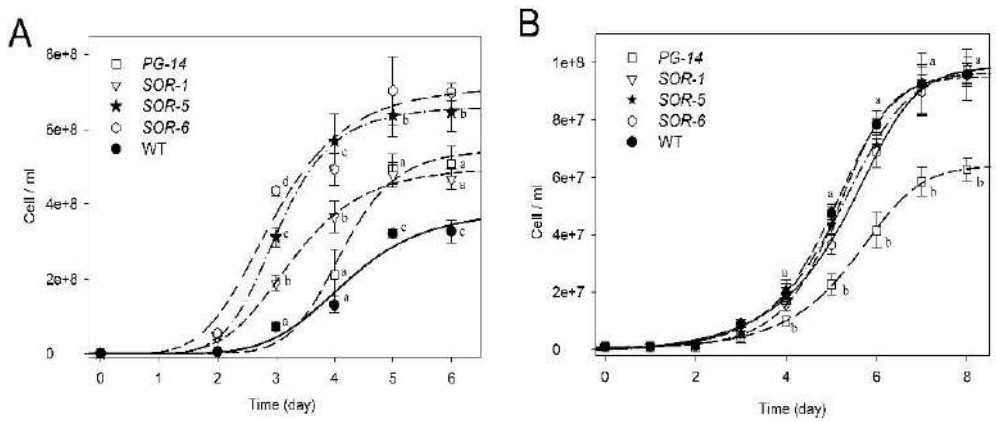

Fig. | 3.1.6 Growth curves of WT and mutant strains. *Growth of WT, PG-14 and SOR strains was performed under autotrophic conditions, at 25 °C, in 1-L cylinders, illuminated with either 1400 µmol photons m^{-2} s^{-1} (panel a) or 50 µmol photons m^{-2} s^{-1} (panel b). Cultures were maintained in a semi-batch system fed with air/CO_2 mix; CO_2 supply was modulated in order to keep the pH of the medium always below 7.2. Symbols and error bars show mean ± SD, n ≥ 6. Values marked with the same letters are not significantly different from each other within the same time point (ANOVA, $p < 0.05$)*

Investigation of lipid production as a response to nitrogen starvation

Lipid yield is a key parameter to be considered when aiming to produce biofuels. Stress factors, such as excess light (Damiani et al., 2010; Solovchenko et al., 2011) and nitrogen starvation (Hu et al., 2008; Bona et al., 2014), trigger lipid accumulation in algae. ROS likely participate as molecular mediators of stresses in algae as suggested by the correlation between lipid content and intracellular ROS level in *C. vulgaris* (Menon et al., 2013). Because of this relation, the higher resistance to oxidative stress observed might prevent oil productivity by impairing ROS cross-talk signals. We, therefore, evaluated the lipid productivity in our selected mutants, under a two-stage cultivation protocol, in which microalgae were first grown in the standard BG-11 medium to achieve high cell density and then transferred to a modified BG-11 medium with limiting N source. At the end of growth phase, oil content per DW was determined gravimetrically. Dry biomass from WT contained ~ 25% oil, in accordance with previous quantification in the same species (Rodolfi et al., 2009); N-deprivation brought about oil content of PG-14 and SORs to the same level than WT cells (Table 3.1.4). The fatty acid content and composition of oil fraction were also determined: dry biomass from PG-14 and SOR mutants were enriched in fatty acids than the WT as follows: PG-14 > SOR5/6 > B1; EL grown WT strain showed high relative amounts of C16:0 fatty acids (~ 18% of total acyl chains) and high proportions of mono-unsaturated C18:1 (~ 28%) and di-unsaturated C16:2 and C18:2 fatty acids (~ 44%), which overall accounts for more than 90% of total acyl chains in *C. vulgaris*. Comparison of the fatty acid profiles of the mutant strains revealed that the C16:2 content was reduced in all mutants (− 15/− 35% vs. WT); while the C16:0 content was essentially unaffected. PG-14 and SOR mutants underwent changes in the C18 composition, with a significant increase of C18:1 in PG-14 and SOR mutants vs. WT and a corresponding decrease of C18:2 acyl chain (Table S3.1.1).

Discussion

Reduction of antenna size improves light-use efficiency limiting factors for large-scale algal biomass production include the inefficient use of photons under mass culture conditions, due to high optical density of the cell suspension and the generation of steep light gradients. Biomass productivity can be improved by engineering optical properties of strains. Previous work targeted genes, such as TLA1 (Melis, 2009; Mitra et al., 2012), which control antenna size in the model species *C. reinhardtii*, yielding enhanced productivity. A forward-genetic approach was adopted in species with a high market interest, such as *C. sorokiniana* and *N. gaditana*, involving random mutagenesis and screening for desired traits. Truncated antenna mutants were selected for both species, and exhibited increased photon use efficiency and biomass yield in dense cell suspensions, which are typical of industrial PBRs (Cazzaniga et al., 2014; Perin et al., 2015). In this work, we used a similar approach with *Chlorella vulgaris*, a robust, interesting species for industrial applications.

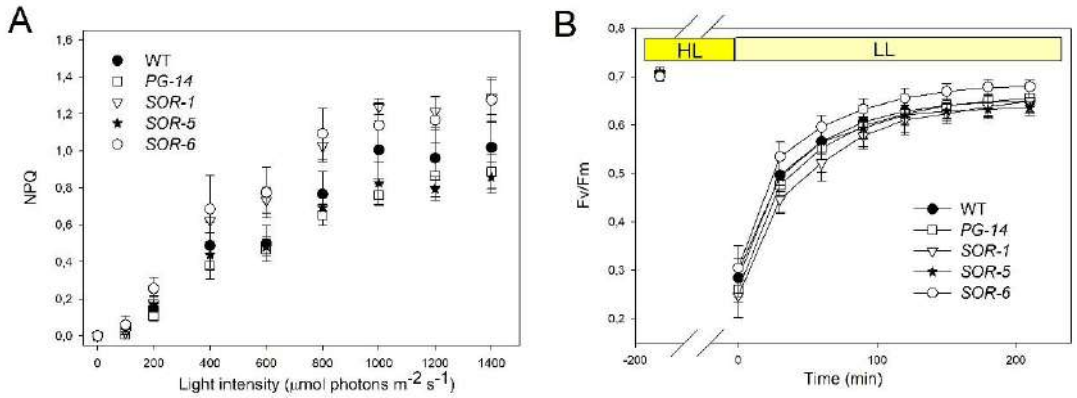

Fig. | 3.1.7 Analysis of room temperature chlorophyll fluorescence during photosynthesis under EL. a *Chlorophyll fluorescence was monitored at 24 °C in dark-adapted cultures. Cell suspensions were illuminated for 20 min and the thermal energy dissipation (NPQ) was determined during steady-state photosynthesis. Symbols and error bars show mean ± SD (n = 4).* ***b*** *PSII repair efficiency was quantified on WT, PG-14 and SOR strains plants by measuring Fv/Fm (PSII photoinhibition) recovery in low light (LL—20 µmol photons m−2 s−1, 24 °C) after photoinhibitory treatment (HL—1800 µmol photons m−2 s−1, 24 °C, 3 h) that reduce the Fv/Fm value to ~ 0,3 in all genotypes. Data are expressed as mean ± SD (n = 4)*

genotype	Total oil content (% DW)
WT	25.1 ± 2.7[a]
PG-14	23.2 ± 0.8[a]
SOR-1	22.2 ± 2.3[a]
SOR-5	21.9 ± 2.2[a]
SOR-6	27.5 ± 2.6[a]

Table | 3.1.4 Lipid content of algal biomass
Total lipid content was determined gravimetrically on the dry biomass, from WT and mutant cultures grown for 7 days in standard, nutrient-rich BG-11 medium at 1400 µmol photons m^{-2} s^{-1} 25 °C, and then moved for further 4 days of growth in modified BG-11 medium with limiting N source. Data are expressed as mean ± SD, n = 4. Significant different values in oil content among genotypes (ANOVA test, $p < 0.05$) are marked with different letters.

In a first screen, we searched for pale-green phenotype to establish a background strain for further domestication by incorporating the low optical density trait (Kirst et al., 2012; Mitra et al., 2012; Cazzaniga et al., 2014), thus increasing light penetration and light-to-biomass yield. Among seven pale-green mutants recovered from screening 25,000 colonies, a range of reduction in Chl content between 25 and 60% with respect to WT strain was obtained (Figure S3.1.1C). Clearly, reduction of Chl content per se was not sufficient for improving light-use efficiency in all strains (Figure S3.1.2). In fact, four mutants (p1–14, p1–43, p1–47 and p2–77) showed a productivity higher than WT, while the others performed similar to the control genotype despite their pg phenotype. Strains p2–25 and p2–36 had a similar Chl content per cell as PG-14 and yet performed differently. This is consistent with the previous reports with two low Chl/cell mutants in *Cyclotella* sp. (Huesemann et al., 2009) whose productivity respect to WT was not improved in PBRs. Indeed, random mutagenesis may well affect multiple genes, thus influencing cell metabolism and impairing growth. Therefore, a full photosynthetic characterization of mutants obtained by chemical/UV mutagenesis is needed to ensure that pale-green mutants are not affected in their photosynthetic performance other than by reducing their LHCII content (Polle et al., 2003; Cazzaniga et al., 2014). We chose PG-14 based on its defect in PSII antenna size, consisting in a LHCII content of 61% with respect to WT (Fig. 3.1.1b). Fluorescence induction in cells infiltrated with DCMU confirmed that PG-14 had a marked reduction of the PSII functional antenna size as compared to WT (Fig. 3.1.1a). In contrast, the PSII: PSI ratio was unaffected with respect to WT level (Fig. 3.1.1b).

Photosynthetic yield was significantly enhanced in PG-14 vs. WT. Indeed, the Pmax of PG-14 was 60% larger than in WT at saturating irradiances (Table 3.1.2), implying that the undercut in antenna size did not negatively impact on photosynthesis. These results are consistent with those reported for *C. reinhardtii* mutants tla1 (Polle et al., 2003) and tla3 (Kirst et al., 2012).

Owing to the double light-harvesting and photoprotective function of LHC proteins, it is relevant to consider whether mutations increase susceptibility to photoinhibition (Krieger-Liszkay et al., 2008) as observed in the *ch1* mutation (Dall'Osto et al., 2010), by preventing LHC assembly, which leads to overproduction of $^1O_2$ and enhanced photooxidation (Dall'Osto et al., 2012).

The light-saturation curve of photosynthesis showed no decline of O_2 evolution even at very high light intensity (6000 μmol photons m^{-2} s^{-1}, Fig. 3.1.1c), whereas the lipid peroxidation and rate of Chl photobleaching were the same in PG-14 and WT cultures exposed to high light (Fig. 3.1.4). We conclude that 50% loss of LHC per PSII does not significantly affect photo-tolerance of *C. vulgaris* cells under the tested growth conditions. Finally, cell growth rates and biomass yield were measured in the long-term cultivation of dense algal suspensions under very high irradiance (1400 μmol photons m^{-2} s^{-1}). During 8 days of growth, PG-14 showed a significant increase of productivity with respect to WT, both as biomass increment per day and maximal level of biomass reached at the end of the growth period (Fig. 3.1.1d, Table 3.1.3). In conclusion, characterization of *C. vulgaris* PG-14 strain confirmed that selection for reduced optical cell density is a viable strategy to obtain higher productivity.

Enhanced resistance to oxidative stress differently affects the growth rate

How do the SOR mutations contribute to the increased growth rate relative to PG-14? Photosynthetic organisms have evolved a number of photoprotective mechanisms to limit photooxidative damage (Li et al., 2009b), the latter being an unavoidable consequence of the presence of highly reactive intermediates during oxygenic photosynthesis. These mechanisms are active in (i) preventing over-excitation of reaction centers by quenching either ^{1}Chl* (Ruban et al., 2012) or ^{3}Chl* states (Dall'Osto et al., 2012), thus avoiding ROS formation, or (ii) detoxifying ROS (Havaux et al., 2007). The first class includes the activation of energy dissipation into heat thus relieving the excitation pressure on PSII (Ruban et al., 2012), and long-term physiological acclimation processes, some of which induce the re-organization of the photosynthetic apparatus (Li et al., 2009b) upon triggering by signal pathways activated by oxidative products (Ramel et al., 2012). The antioxidant defence mechanisms include enzymatic- (APX, SOD, CAT, etc.) and non-enzymatic antioxidants (carotenoids, tocopherols, ascorbate, glutathione) (Erickson et al., 2015); in particular, the thylakoid-bound antioxidants carotenes and xanthophylls play an irreplaceable role as structural components of the photosynthetic apparatus and photoprotective molecules, crucial in both quenching $^1O_2$ and inhibiting lipid peroxidation (Dall'Osto et al., 2014a).

Among the first class of mechanisms, possibly underlying the higher biomass yield of SORs, NPQ is the most relevant. NPQ catalyzes dissipation, in form of heat, of the light energy absorbed in excess. In microalgae, the mechanism is activated by LhcSR (light-harvesting complex stress-related) protein (Peers et al., 2009). In WT, PG-14 and SOR genotypes, NPQ amplitude was measured at steady-state photosynthesis over a range of irradiances, showing differences mostly negligible (Fig. 3.1.7a), consistent with the similar LhcSR content in all the strains (Figure S3.1.3). Thus, we conclude that the differences in growth of SOR lines were not due to enhanced NPQ.

The antioxidant activity of PG-14 and SOR mutants was in general higher than the WT, irrespective of the antioxidant assay used. SOR-1 showed the highest antioxidant power when tested with FRAP, a reagent that evaluates the antioxidant activity by reducing a metallic ion (Fig. 3.1.5a). This assay has been used to evaluate both lipophilic substances such as tocopherol as well as more polar antioxidants as ascorbic acid (Benzie and Strain, 1996). On the other hand, PG-14 showed the highest antioxidant activity with the ABTS assay (Fig. 3.1.5b). The latter assay reacts

with both phenolic compounds and carotenoids (Re et al., 1999) and correlates with the higher content of carotenoids of this mutant with respect to WT (Table 3.1.1). However, since the carotenoid level of all mutants is not significantly different (Table 3.1.1), other compounds (e.g., phenolics or other natural antioxidants) might be more abundant in PG-14 cells than SOR mutants. Lower MDA accumulation and higher resistance to photobleaching in EL (Fig. 3.1.5) suggest either a reduced $^1O_2$ release of SOR vs. PG-14 and WT, or a more effective scavenging activity of $^1O_2$ in the chloroplasts, being this ROS unstable and suggested as unable to leave the plastid compartment (Gorman and Rodgers, 1992). Reduced $^1O_2$ release within the chloroplasts appears unlikely, being content of the major photosynthetic components identical in PG-14 and SOR strains (Figure S3.1.3). Regarding the antioxidant capacity, it is worth noting that SOR-6 cells, namely the fastest-growing strain, did not show higher antioxidant ability than the control genotype PG-14, with both methods used; the other two SOR strains showed a slightly higher antioxidant capacity when probed by FRAP methods, while lower capacity than PG-14 when probed by ABTS. Similar results were obtained with other two antioxidant assays, namely DPPH and Folin–Ciocalteau (data not shown). In an attempt to reconcile such contrasting results, it can be hypothesized the antioxidant assays here chosen is more sensitive to specific ROS, thus might have underestimated the contribution of $^1O_2$-specific detoxification mechanisms, although more active in SOR mutants. Alternatively, the scavenging potential of SOR cells might not be the main factor improving photosynthetic performance in EL.

The higher resistance of SOR strains to photooxidative stress was not due to enhanced capacity for PSII repair process: indeed, the recovery of Fv/Fm (quantum yield of PSII) upon photoinhibitory treatment showed that all genotypes showed a similar behavior (Fig. 3.1.7b).

Interestingly, these mutants showed a biomass productivity significantly higher with respect to the corresponding value for the PG-14 even when grown in limiting-light conditions (50 μmol photons m^{-2} s^{-1}), showing biomass productivities similar to WT culture (Fig. 3.1.6b, Table 3.1.3). Similar results were obtained in growth assay carried out at lower irradiance (20 μmol photons m^{-2} s^{-1}, data not shown). These results are unexpected in mutants with truncated light-harvesting antenna size, in which photosynthetic efficiency decreases at sub-saturating irradiances due to limitation in PSII cross section.

Indeed, enhanced growth in low light despite truncation in antenna size suggests that the enhanced light-use efficiency is obtained in SOR genotypes, and contributes to the enhanced biomass production. Clearly, this is not due to enhanced PSII repair not to decreased NPQ with respect to WT and PG-14, and its nature is unclear based on present results. Hypothesis includes altered thylakoid architecture, change in composition or relative abundance of LHC proteins, altered kinetic in the remodeling of photosynthetic membranes in response to illumination (Clausen et al., 2014) or up-regulation of plastidial regulatory elements (Brooks et al., 2013; Malnoë et al., 2018). The elucidation of this mechanism will be the object of further analysis including identification of mutations and physiological analysis of these genes, to identify genetic elements potentially useful for enhancing primary productivity.

Alternatively, higher biomass yield in EL might not be exclusively due to either improved antioxidant networks or enhanced light-use efficiency in SOR strains. (Ledford et al., 2007) showed that activation of stress response upon $^1O_2$ induction was effective in increasing resistance to oxidative stress in *C. reinhardtii* without altering antioxidant levels. Indeed,

depending on its concentration, $^1O_2$ may either cause oxidative damage or act as "second messenger" in cell signal transduction. In algae, similar to reports on plants (Triantaphylidès et al., 2008), PSII is the cellular major source of $^1O_2$. However, due to its high reactivity and short lifetime, $^1O_2$ is not considered as directly involved in chloroplast-to-nucleus signaling; rather, plant cells perceive $^1O_2$ as signal which controls a number of stress-response mechanisms (Zhang et al., 2014): in Arabidopsis, EXECUTER proteins (EX1 and EX2) are involved in the regulation of the $^1O_2$-mediated genetic response (Op Den Camp et al., 2003; Kim et al., 2012); in *Chlamydomonas*, specific responses to $^1O_2$ vs. other ROS was attributed to specific promoter regions (Shao et al., 2007; Fischer et al., 2009)(Fischer et al., 2009). Moreover, a moderated $^1O_2$ release under EL stress affects susceptibility of *C. reinhardtii* cells to subsequent, more severe stresses (Ledford et al., 2007). In plants, induction of stress acclimation allowed higher protection against PSII photoinhibition upon harsher conditions: acclimation activates a subset of $^1O_2$-responsive genes in WT plants, while represses them in *ex1*/*ex2* plants. However, the extent of photosensitivity in WT and *ex1*/*ex2* plants was the same upon acclimation (Kim et al., 2012), thus suggesting that it relies on extensive cross-talk with different stress-related signaling pathways.

A set of plastid-derived signals were found to be involved in the adaptation of cell physiology to the changing environmental conditions: these include tetrapyrroles, metabolites such as 3-phosphoadenosine5-P (PAP) and methylerythritol cyclo-PP, ROS and cleavage products of carotenes and/or phytofluene, as well the redox state of stroma and the organellar gene expression (reviewed in (Bobik and Burch-Smith, 2015; Kleine and Leister, 2016)). Under photooxidative stress, oxidized derivatives of β-carotene such as β-cyclocitral (β-CC), β-ionone and dihydroactinidiolide (dhA) act as signaling molecules, inducing transcriptomic responses associated with enhanced resistance to photoxidative stress (Ramel et al., 2012; Shumbe et al., 2014; D'Alessandro and Havaux, 2019). Release of carotenoid oxidation products was reported not only in plants but also in cyanobacteria (García-Plazaola et al., 2017), while the small zinc finger proteins MBS were shown to mediate the $^1O_2$-dependent transcriptomic response in both *Chlamydomonas* and plants, thus suggesting these sensing mechanisms are ubiquitous in the green lineage.

The task of identifying the signaling pathway affected in SOR mutants is complex due to integration of multiple signaling cascades whose components are still poorly understood and involving considerable cross-talk aimed at sustaining cell homeostasis during stress responses as shown by interaction between elements of PAP and β-CC retrograde signaling. Such interactions promote gene reprogramming and enhance tolerance to photoinhibition as shown by the positive effect of pre-treatment with either PAP or β-CC before stress treatment (Shumbe et al., 2014, 2017). We speculate that higher phototolerance in SOR mutants might be related to a constitutive activation of one or more of the above-mentioned signal transduction pathways. High-productivity phenotype of SORs suggests that multiple defense processes might be affected, possibly due to mutations in global regulators of photoprotection response in algal cell. Future identification of these mutations will possibly allow pinpointing new components of $^1O_2$-mediated signaling control and their role in different cellular protection mechanisms.

Influence of ROS-resistance traits on stress-induced lipid production

While excessive ROS release causes irreversible damage to cellular structures, ROS formed under mild photooxidative stress conditions promote lipid accumulation in oleaginous microorganisms (Yilancioglu et al., 2014), possibly by a complex signaling pathway that triggers up-regulation of the enzyme ACCase and increases C flux into the pathway of fatty acid biosynthesis (Guarnieri et al., 2011). Indeed, (Menon et al., 2013) found that intracellular lipid content in *C. vulgaris* is correlated with hydroxyl radical levels. Moreover, oxidative stress perception by the endoplasmic reticulum promotes lipid droplets formation (Jacquier et al., 2011). Overall, direct experimental evidence of an association between ROS and intracellular lipids are still scarce, and details on the molecular mechanisms of ROS-mediated lipid accumulation are missing. However, if ROS are obligate mediators of lipid accumulation by complex signaling pathways, then we might expect an altered lipid yield in an individual mutant possibly affected in such stress-response pathways. Quantification of oil content, upon short-term nitrogen-starvation treatment of cultures, ruled out the hypothesis: indeed, oil content was essentially the same in all strains analyzed, while fatty acid content of dry biomass was significantly higher in all mutants than WT. We only measured a decrease of C16:2 acyl chain fraction in mutant strains vs. WT; a significant increase of C18:1 acyl chain in mutants vs. WT and a corresponding decrease of C18:2 acyl chain, the most abundant PUFA of C. vulgaris, was also shown. These results contrast with former evidence that higher ROS release obstructs PUFA biosynthesis (Sun et al., 2018): indeed, kinetic of MDA formation in EL suggests PUFA peroxidation is lower in SOR vs. WT and PG-14 strains. Rather, such a change in lipid composition points again to an altered signaling cues in SORs with respect to control genotypes.

Conclusions

Our results show that domestication of WT strains, by both modulating antenna size to improve light penetration and enhancing resistance to excess light, is an effective strategy in the development of microalgal strains optimized for mass culture and these effects are additive towards a higher biomass productivity and stress resistance. Further work will be undertaken for the identification of genes affected in the SOR mutants by DNA and RNA sequencing. Owing to the impossibility of carrying on genetic crossing in Chlorella, pyramiding positive traits will need reliable transformation and gene editing procedures that are still to be implemented in this genus. Moreover, we have shown a specific effect for SOR mutations in improving light-use efficiency. Indeed, besides the enhanced $^1O_2$ scavenging effect of SOR genotypes, an additional, still unknown, mechanism is needed to explain their higher growth rates in limiting-light conditions. Identification of this mechanism will be the subject of future research.

Materials and methods

Strains and culture conditions

Chlorella vulgaris WT strain was obtained from the SAG Culture Collection of Algae (Goettingen University, Germany, http://www.uni-goettingen.de/en/catalogue-of-strains/185049.html) as SAG strain number 211-11p. Cells were maintained on TAP-agar plates (Kropat et al., 2011) and grown in either minimal (BG-11) (Allen and Stanier, 1968) or rich (TAP) media. Shaken flasks (120 rpm) were illuminated from the top with 100 μmol photons m^{-2} s^{-1}, photoperiod of 16/8 h light/dark, 25 °C; irradiance was provided by warm-white LEDs (Epistar 35mil Chip High Power LED, warm white LEDE-P20B-DW, Wayjun Tech., Shenzhen, China). For all physiological and biochemical measurements, cultures were harvested during the logarithmic growth phase (~ $1{\cdot}10^8$ cells m L^{-1}). For short-term nitrogen-starvation experiments, cells were grown for 4 days in standard BG-11 medium containing excess nitrogen source ($NaNO_3$ 1.5 g L^{-1}) at an irradiance of 1400 μmol photons m^{-2} s^{-1}, 25 °C, with a photoperiod of 16/8 h light/dark; cells were then collected by centrifugation, washed twice with sterile water, and re-suspended at $1{\cdot}10^8$ cells mL^{-1} in a modified BG-11 medium with limiting N source ($NaNO_3$ 0.07 g L^{-1}) and further grown for 3 days.

Mutagenesis and screening protocols

C. vulgaris WT cells in liquid cultures were harvested by centrifugation at the exponential phase of growth (~ $1{\cdot}10^8$ cells mL^{-1}), re-suspended in fresh TAP medium to $5{\cdot}10^7$ cells mL^{-1}, and treated with ethyl methanesulfonate (EMS). The survival curve for mutagenesis with EMS was carried out to determine the mutagen concentration which resulted in around 5% of cells viability. Upon 2-h maintenance in the dark, to prevent light-activated DNA repair, cells were plated at 100-fold dilution on TAP-agar medium and exposed to 100 μmol photons m^{-2} s^{-1}. Single colonies appeared after 14 days. The ones showing a pale-green phenotype were identified by direct sight inspection, inoculated onto fresh minimal medium, grown in the light for seven days, and the Chl content per cell was determined. This procedure allowed to isolate the pale-green mutant strain PG-14. Chemical mutagenesis was repeated on the strain PG-14 to isolate singlet oxygen-resistant mutant strains. The photosensitizer Red Bengal (RB) was used as selection method: RB

is a chemical producing $^1O_2$ when exposed to white light (Fischer et al., 2012); thus, the screening of the mutants was performed by their resistance to the exogenous $^1O_2$. A wide range of concentrations of chemical were tested to find out the minimal concentration which inhibited grown of the PG-14 strain. SOR (singlet oxygen resistant) mutants were selected by plating mutagenized PG-14 cells on TAP-agar plates containing 12 μM RB, which were then exposed to 100 μmol photons m^{-2} s^{-1} to initiate the selection for resistant clones. $^1O_2$-resistance of selected mutants was tested by serial dilution of a concentrated culture (~ $5 \cdot 10^7$ cells mL^{-1}), spotted onto plates containing 12 μM RB and maintained in the light for several days. Estimation of resistance to exogenously generated $^1O_2$ was done by transferring aliquots of culture ($5 \cdot 10^7$ cells m L^{-1}) into a multi-well plate and adding RB (0–50 μM). Cells were grown for 24 h at 100 μmol m^{-2} s^{-1}, then 10 μL from each well were spotted on TAP-agar plates.

Cell count and pigment analysis

Cell density was measured using an improved Neubauer hemocytometer. Pigments were extracted from intact cells with 100% dimethyl-formamide. The supernatant of each sample was recovered after centrifugation (10 min at 15,000g, 4 °C), diluted in acetone and pigments were separated and quantified by HPLC (Gilmore and Yamamoto, 1991b).

Gel Electrophoresis and Immunoblotting

For SDS-PAGE and immunotitration analysis, cells were resuspended in Loading Buffer (5% glycerol, 1% SDS, 2.5% 2-mercaptoethanol, 0.1 M Tris, 0.1 M Tricine pH 8.45) and grinded in a tissue homogenizer (Precellys, Bertin, France) by adding a ceramic lysing matrix. The supernatant of each sample was recovered after centrifugation (10 min at 15,000g, 4 °C) and Chl content of extracts was determined. SDS-PAGE analysis was performed with the Tris-Tricine buffer system (Schägger and von Jagow, 1987). For immunotitration (Towbin et al., 1979), a range of total protein extract corresponding to 0.1–2.0 μg of Chl were loaded for each sample and electroblotted on nitrocellulose membranes. Proteins were detected with primary antibodies (home-made: α-CP43, α-Rubisco, α-LhcSR; from Agrisera: α-PsaA AS06-172100, α-Cyt *f* AS06-119, α-ATPase β subunit AS05-085) and an alkaline phosphatase-conjugated secondary antibody (Sigma-Aldrich A3687). Signal amplitude was quantified using the GelPro 3.2 software (Bio-Rad).

Measurements of photosynthetic activity

The oxygen evolution activity of the cultures was measured at 25 °C with a Clark-type O_2 electrode (Hansatech, UK) upon illumination with white light provided by a halogen lamp (Schott, Germany). Samples of 2 mL cell suspension (~ $5{\cdot}10^7$ cell m L−1) were loaded into the oxygen electrode chamber; 3 mM $NaHCO_3$ was added to the cell suspension prior to the O_2 evolution measurements to ensure electron transport was not limited by the carbon supply.

In vivo chlorophyll fluorescence analysis

Fluorescence induction kinetics was recorded with a home-built apparatus as previously described (Rappaport et al., 2007). Variable fluorescence was induced with a green light of 7 μmol photons m^{-2} s^{-1} at RT, on cells suspensions (~ $5{\cdot}10^7$ cells mL^{-1}) in BG-11 medium containing 100 μM DCMU. The reciprocal of time corresponding to two-thirds of the fluorescence rise (T2/3) was taken as a measure of the PSII functional antenna size (Malkin et al., 1981). Quantum efficiency of PSII (Fv/Fm) was measured on cell suspension, dark adapted for 20 min, with a PAM 101 fluorimeter (HeinzWalz, Germany). The light dependence of NPQ during photosynthesis was measured through Chl fluorescence on dark-adapted cell suspension at RT with a FluorCam 700MF (Photon Systems Instruments, Brno, Czech Republic); NPQ was calculated according to (Maxwell and Johnson, 2000) at steady-state photosynthesis (upon 20 min illumination).

Determination of the sensitivity to photooxidative stress

The extent of lipid peroxidation in cells was estimated by measuring malondialdehyde (MDA) formation, as an indirect quantification of lipid peroxides (Havaux et al., 2005). Quantitative evaluation was done by transferring 2 mL aliquots of WT and mutant cell suspensions (~ $5{\cdot}10^7$ cell mL^{-1}, in BG-11) into a 24-well culture plate, kept on a rotary shaker and illuminated for 2 days with high light (1400 μmol photons m^{-2} s^{-1}, 25 °C). Samples ($2{\cdot}10^5$ cells) were taken for analysis during a period of 48 h, and frozen in liquid nitrogen. MDA content of aliquots was quantified as previously described (Baroli et al., 2004).
The photobleaching kinetics of Chl cell content were measured on cell suspensions (~ $5{\cdot}10^7$ cell mL^{-1}, in of 14,000 μmol of photons m BG-11 + 0.03% w/v agarose) using actinic light intensities of 14,000 μmol of photons m^{-2} s^{-1} for 2 h; temperature of samples was maintained at 25 °C. During the illumination, the absorbance area between 600 and 750 was recorded; the initial and maximal absorbance were set, so the same absorbance area was used in the wavelength range 600 nm < λ < 750 nm for all the samples.

Growth analysis

Growth experiments were performed at 25 °C in a homebuilt photobioreactors, composed of glass cylinders with a maximum light path of 8 cm and a working volume of 1 liter each (Cazzaniga et al., 2014). Cultures were continuously mixed with a flux of air and CO_2. The ratio of compressed air and CO_2 was automatically adjusted to keep the pH of the medium within the range 6.8–7.2. Each autotrophic batch cultivation was carried out in duplicate. Illumination was provided by a panel of warm-white LEDs (Epistar 35mil Chip High Power LED, warm white LEDE-P20B-DW),

microalgae were exposed to an irradiance of 1,400 μmol photons m^{-2} s^{-1}, with a photoperiod of 16/8 h light/ dark. The parameters determined to monitor cell growth were cell number and dry biomass weight, for which the washed cell pellets were dried overnight in a lyophilizer. The inoculum size was $1 \cdot 10^6$ cell mL^{-1}.

Determination of total lipid content and lipid composition

Total lipids were extracted from 100 mg lyophilized biomass from 3 days nitrogen-starved cultures, homogenized by 4 cycles of 30 s at 8000 rpm, with a Precellys homogenizer (Bertin, France) using the extraction protocol by (Axelsson and Gentili, 2014), with a total of 3 mL methanol, 6 mL chloroform and a subsequent washing step with 4 mL water. Net total lipid amount was determined gravimetrically. To determine lipid composition, lyophilized biomass was extracted with a Soxhlet apparatus using CHCl3-hexane (2:1 v/v). The extract was evaporated under N_2 and weighted and resuspended in hexane. Fatty acid methyl esters (FAME) were obtained, after addition of an aliquot of the internal standard heptadecanoate, by treatment with MeOH-BF3 according to the method described by (Horwitz, 2000). The quantitative determination of FAME was obtained by gas chromatography using a flame ionization detector (FID-GC). A ZB5-MS 30-m column was used with the following temperature program: 60 °C for 1 min, then an increasing rate of 10 °C min^{-1} up to 180 °C, a second increase of 1 °C min^{-1} up to 230 °C, then 15 °C m in−1 to reach 290 °C. The injector temperature was 280 °C, the detector temperature was 280 °C; the carrier gas was He with a flow rate of 1 mL min^{-1}; splitless injection mode. Based on internal standard area, FAME from FFA, MAG, DAG and TAG were quantitatively estimated on an algae dry weight basis. Compounds were identified by both retention times, comparison of pure standards and gas chromatography coupled to mass spectrometry (GC–MS). Carrier gas was He with a constant flow of 1 mL min−1, transfer line temperature to MSD was 280 °C, ionization energy 70 eV, and full scan range 50–500 m/z.

Determination of antioxidant activity

Free radical scavenging activities of lyophilized algae, grown at an irradiance of 1400 μmol photons m −2 s −1, were determined using the radical species 2,2′-azinobis(3-ethylbenzothiazoline-6-sulfonic acid) ($ABTS^{\bullet+}$) assay as described by (Re et al., 1999). The reducing activity of ethanolic extracts was assessed using FRAP method (Benzie and Strain, 1996). FRAP was freshly prepared by mixing (8:1:1, v/v) 0.3 M acetate buffer (pH 3.6), 10 mM 2,4,6-tripyridyl-s-triazine (TPTZ) and 20 mM $FeCl_3$. All data are expressed as μmol Trolox Equivalents (TE) per g of WT alga. All measurements were repeated three times.

Statistics

Significance analysis was performed using either Student's t test or ANOVA test in GraphPad Prism software. Error bars represent the standard deviation.

Supplementary information

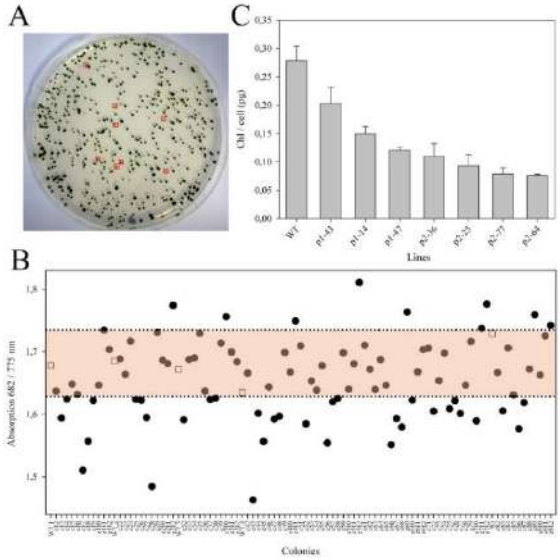

Fig.* | *S3.1.1. *Screening strategy used to isolate pale-green mutant of C. vulgaris. Upon chemical mutagenesis, cells were plated on BG-11 agar plates and exposed to 70 µmol photons m-2 s-1, 24°C. Single colonies (approximately, 25,000) appeared after 14 days (panel A). Colonies showing a pale-green phenotype were identified by direct sight inspection (90 colonies), then were picked to liquid minimal medium in microtiter plates, grown in the light for seven days, and the Chl content per cell was estimated by measuring absorption of cell suspensions at both 682 and 775 nm (panel B). WT cultures, used as internal standard, showed a 682/775 nm absorption ratio in between 1.63 and 1.73 (rose bar). Strains whose 682/775 ratio was below 1.63 (the lowest values measured for WT) were further selected. Total Chl content analysis was repeated on the most promising lines. This procedure allowed to isolate a group of pale-green mutants (7 lines, panel C).*

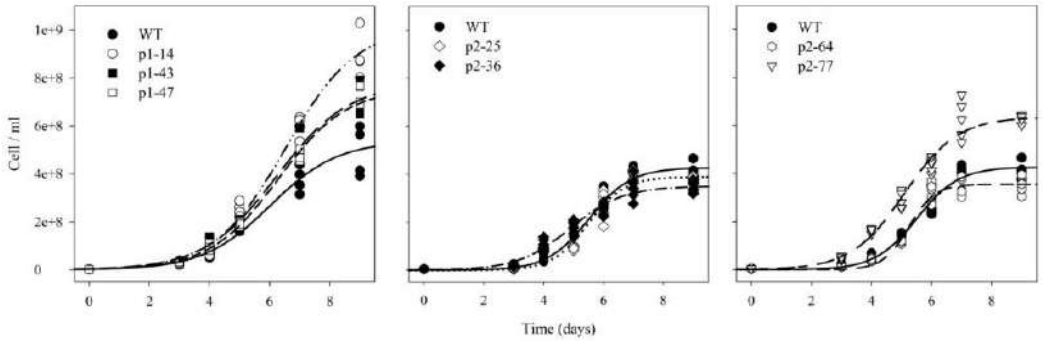

Fig.* | *S3.1.2. *Growth curves of WT and pale-green mutants of C. vulgaris, under autotrophic conditions. C. vulgaris WT was grown with pale-green mutants and the cell content was measured once a day. All experiments were performed in 1-L cylinders, illuminated with 450 µmol photons m^{-2} s^{-1}, 24°C. Growths were performed in a semi-batch system fed with air/CO_2 mix; the CO_2 supply was modulated in order to keep the pH of the medium always below 7.1. Each experimental point corresponds to a different sample; data are representative of two independent experiments. Initial inoculum: 1·10^6 cells ml^{-1}. This procedure allowed to identify PG-14 (isolate p1-14), the pale-green strain with the highest rate of growth, hereafter used.*

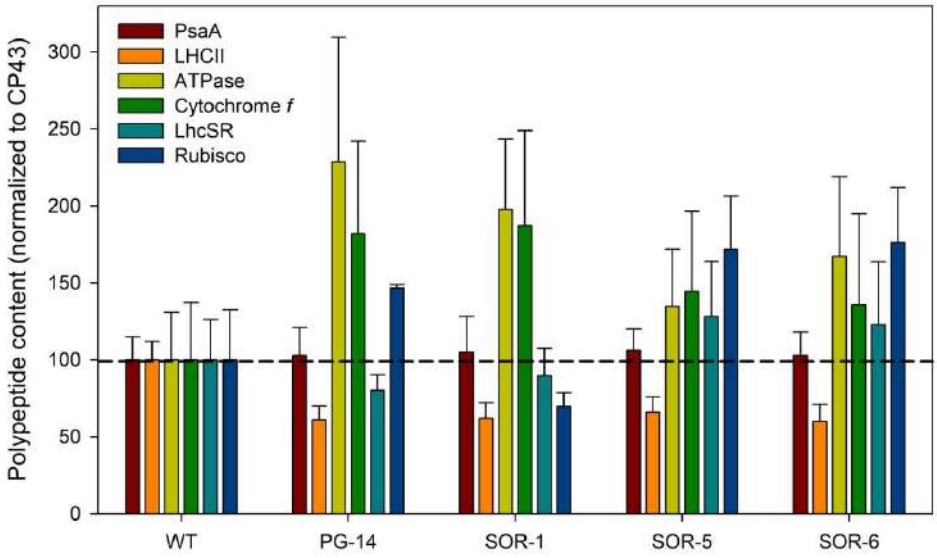

Fig. | S3.1.3. Immunotitration of major photosynthetic subunits. *Total proteins were extracted from WT and mutant cells, grown as reported in Figure 3.1.6. Proteins from mutant and control genotypes were fractionated by SDS-PAGE in the same slab gel. The abundance of each subunit in mutants was evaluated by densitometric analysis of western blot, normalized to the PSII core subunit CP43 and expressed as a percentage of the corresponding value in the WT. Data are reported as mean ± SD (n = 3).*

Table S3.1.1. Acyl chain composition of lipid fraction from WT and mutants PG-14 and SOR. *Data are expressed as mean ± SD, n = 3. Significantly different values (ANOVA test, $p < 0.05$), within the same column, are marked with different letters.*

	Fraction of acyl chains (%)											
	Pentadecanoic acid C15:0	7-10-Hexadecadienoic acid C16:2	7-10-13-hexadecatrienoic acid C16:3	9-hexadecatrienoic acid C16:3	Hexadecanoic acid C16:0	15-methylheptadecanoic acid C18:0	8-heptadecanoate C17:0	Linoleic acid C18:2	Oleic acid C18:1	Elaidic acid C18:1	Stearic acid C18:0	Total Fatty acid content (μg mg^{-1} DW)
WT	0.38 ± 0.01^{a}	6.97 ± 0.28^{a}	3.58 ± 0.95^{a}	1.45 ± 0.32^{a}	$18.22 \pm 0.61^{a,c}$	1.15 ± 0.27^{a}	0.79 ± 0.19^{a}	37.86 ± 0.31^{a}	27.72 ± 0.67^{a}	1.27 ± 0.07^{a}	0.62 ± 0.06^{a}	74.6 ± 2.5^{a}
PG-14	0.22 ± 0.01^{b}	4.50 ± 0.01^{b}	4.10 ± 0.01^{a}	1.17 ± 0.03^{a}	$17.98 \pm 0.09^{a,d}$	0.53 ± 0.01^{b}	0.77 ± 0.01^{a}	20.14 ± 0.02^{b}	46.98 ± 0.05^{b}	1.77 ± 0.03^{b}	1.83 ± 0.02^{b}	107.2 ± 0.6^{b}
SOR-1	0.30 ± 0.01^{c}	5.52 ± 0.02^{c}	3.90 ± 0.01^{a}	1.50 ± 0.04^{a}	18.69 ± 0.16^{c}	0.80 ± 0.04^{b}	0.83 ± 0.01^{a}	31.91 ± 0.07^{c}	33.95 ± 0.08^{c}	2.03 ± 0.02^{c}	0.57 ± 0.01^{a}	80.2 ± 1.5^{c}
SOR-5	$0.24 \pm 0.01^{d,b}$	$4.39 \pm 0.01^{d,b}$	$3.48 \pm 0.01^{a,b}$	1.19 ± 0.02^{a}	$18.57 \pm 0.14^{a,c}$	0.61 ± 0.02^{b}	0.79 ± 0.01^{a}	22.17 ± 0.04^{d}	45.20 ± 0.10^{d}	1.70 ± 0.05^{b}	1.66 ± 0.01^{c}	102.7 ± 0.5^{d}
SOR-6	$0.29 \pm 0.05^{c,d}$	$4.60 \pm 0.06^{b,d}$	4.21 ± 0.05^{a}	1.20 ± 0.07^{a}	$17.72 \pm 0.12^{a,d}$	0.64 ± 0.02^{b}	0.83 ± 0.01^{a}	20.95 ± 0.26^{e}	48.01 ± 0.33^{e}	0.29 ± 0.02^{d}	1.37 ± 0.01^{d}	102.8 ± 0.6^{d}

Abbreviations

β-CC: β-cyclocitral; Car: carotenoids; Chl: chlorophylls; DCMU: 3-(3,4-dichlorophenyl)-1,1-dimethylurea; dhA: dihydroactinidiolide; DW: dry weight; EL: excess light; EMS: ethyl metanesulfonate; Fv/Fm: maximal quantum yield of PSII; LHCI/II: light-harvesting complex of PSI/II; MDA: malondialdehyde; NPQ: non-photochemical quenching; Pmax: maximal photosynthetic rate; PAP: 3-phosphoadenosine-5-P; PAR: photosynthetic active radiation; PBR: photobioreactor; PG: pale green; PSI/II: photosystem I/II; RB: Red Bengal; ROS: reactive oxygen species; SOR: singlet oxygen resistant; WT: wild-type; ^{1}Chl*: singlet excited state of Chl; ^{3}Chl*: triplet excited state of Chl; $^{1}O_2$: singlet oxygen.

Authors' contributions

LD, SC and ZG performed identification and isolation of all the genotypes used; MB, SB and SC carried out the biochemical and photosynthetic characterization of strains and drafted the manuscript; GM and MEM carried out antioxidant assays and lipidomic analysis; LD and RB conceived the study, participated in its design and coordination and edited the manuscript. All authors read and approved the final manuscript.

Funding

Financial support for this work was provided by the Marie Curie Actions Initial Training Networks SE2B (H2020-MSCA-ITN-2015-GA N. 675006), the University of Verona (Fondo Ricerca di Base HuntingLight) and "Programma Operativo Regionale FSE 2014–2020" (Grant No. 1695-16-2216-2016) from Regione del Veneto.

Availability of data and materials

The datasets analyzed during the current study available from the corresponding author on reasonable request.

Competing interests

The authors declare that they have no competing interests.

3.2 High Carotenoid Mutants of *Chlorella vulgaris* Show Enhanced Biomass Yield under High Irradiance

plants

MDPI

Article

High Carotenoid Mutants of *Chlorella vulgaris* Show Enhanced Biomass Yield under High Irradiance

Zeno Guardini †, Luca Dall'Osto †, Simone Barera, Mehrdad Jaberi, Stefano Cazzaniga, Nicola Vitulo and Roberto Bassi *

Abstract: Microalgae represent a carbon-neutral source of bulk biomass, for extraction of high-value compounds and production of renewable fuels. Due to their high metabolic activity and reproduction rates, species of the genus *Chlorella* are highly productive when cultivated in photobioreactors. How- ever, wild-type strains show biological limitations making algal bioproducts expensive compared to those extracted from other feedstocks. Such constraints include inhomogeneous light distribution due to high optical density of the culture, and photoinhibition of the surface-exposed cells. Thus, the domestication of algal strains for industry makes it increasingly important to select traits aimed at enhancing light-use efficiency while withstanding excess light stress. Carotenoids have a crucial role in protecting against photooxidative damage and, thus, represent a promising target for algal domestication. We applied chemical mutagenesis to *Chlorella vulgaris* and selected for enhanced tolerance to the carotenoid biosynthesis inhibitor norflurazon. The NFR (norflurazon-resistant) strains showed an increased carotenoid pool size and enhanced tolerance towards photooxidative stress. Growth under excess light revealed an improved carbon assimilation rate of NFR strains with respect to WT. We conclude that domestication of *Chlorella vulgaris*, by optimizing both carotenoid/chlorophyll ratio and resistance to photooxidative stress, boosted light-to-biomass conversion efficiency under high light conditions typical of photobioreactors. Comparison with strains previously reported for enhanced tolerance to singlet oxygen, reveals that ROS resistance in *Chlorella* is promoted by at least two independent mechanisms, only one of which is carotenoid-dependent.

Keywords: microalgae; biomass; photoprotection; carotenoids; photooxidative stress; chloroplast; norflurazon

Introduction

Mass culture of microalgae in photobioreactors (PBRs) has gained interest in the past few decades. Beside small-scale traditional cultivations mainly aimed to human or animal feeding, commercial production of algae on a large scale has been identified as a renewable and environmentally sustainable strategy for feedstock production (Benedetti et al., 2018). Both microalgae and land plants catalyze photosynthetic reactions (Nelson and Ben-Shem, 2004), yet the simpler structure of microalgae enhances efficiency in solar energy conversion into biomass respect to plants (Chisti, 2008; Rodolfi et al., 2009; Weyer et al., 2010; Woittiez et al., 2017). Thus, cultivation of microalgae represents a promising source of biomass for many industrial applications, which include production of bioactive compounds, recombinant proteins, livestock feed, biofuels, organic fertilizer and biostimulants (Leu and Boussiba, 2014; Chew et al., 2017). Microalgae can grow in wastewater on marginal lands, thus avoiding competition for both arable land and water source with food crops (Scott et al., 2010). Furthermore, the high capacity for nitrogen and phosphorus removal, together with use of flue gas as a source of CO_2, makes phycoremediation a valuable circular-economy-based biorefinery (Christenson and Sims, 2011; Pittman et al., 2011).

The genus *Chlorella* includes fast-growing species, highly productive and easy to cultivate, exploited to a significant extent as food additives and nutraceuticals (Münkel et al., 2013). Carotenoids (Car) are currently the most important commercial product from microalgae successfully marketed (Borowitzka, 2013; Chen et al., 2019; Novoveská et al., 2019). These pigments are widely utilized as aquaculture feed additives, food colorants and ingredients for cosmetics; moreover, Car have biomedical applications, as anti-inflammatory agents due to their strong antioxidant properties (Benedetti et al., 2018). Xanthophylls (oxygenated Car) are antioxidants with a key role in protecting from ocular oxidative damage (Nwachukwu et al., 2016); indeed, the human macula lutea are rich in lutein and zeaxanthin, which help maintain eye health. β-carotene is commercially produced mainly from the halophilic alga *Dunaliella salina* through cultivation in ponds; however, microalgae are not yet used as a source of xanthophylls at an industrial scale (Leu and Boussiba, 2014). The latter and many other algae-based production processes require significant improvements in the high cost for PBRs management and in the efficiency at various process steps such as biomass recovery and product extraction (Chia et al., 2018). Moreover, limitations include biological constraints such as low efficiency of PAR (photosynthetically active radiation) utilization, especially under excess light (EL) conditions, which hinder the economic viability of algal products. The maximum theoretical efficiency of solar energy conversion into biomass has been reported to fall between 6% and 12% (Weyer et al., 2010; Tredici, 2014) while present-day production systems typically exhibit photosynthetic conversion efficiency of about 1% or below (Heaton et al., 2008; Rodolfi et al., 2009). Limits in biomass yield can be ascribed to a number of factors (Stephenson et al., 2011; Ooms et al., 2016), including inhomogeneous light distribution within a mass culture and photooxidative stress.

In particular, PAR efficiently drives photosynthesis under light-limiting conditions, while photoinhibition is observed upon exposure to irradiance exceeding plant capacity for electron transport, decreasing light-to-biomass conversion efficiency (Ruban et al., 2012). The high optical density of wild-type strains accounts for additional efficiency drop: a high chlorophylls (Chl)

content per cell is a valuable trait which maximizes the photon capture in the natural environment, while a large array of antenna complexes (light-harvesting complexes, LHCs) (Dall'Osto et al., 2015), binding Chl and Car (Fuciman et al., 2012), hampers biomass productivity in a PBR. Indeed, high cell concentration originates a steep light gradient which leaves inner cell layers below the compensation point (Formighieri et al., 2012), while sustained over-excitation of cells in the surface layers increases the yield of Chl triplet state (^{3}Chl*) and the consequent release of the reactive oxygen species (ROS) singlet oxygen ($^1O_2$). Photooxidative stress is a consequence of the formation of strongly oxidizing intermediates in different steps of the photosynthetic process, that inevitably leads to PSII photoinhibition and reduces net assimilation (Aro et al., 1993; Krieger-Liszkay et al., 2008). Domesticating microalgae for higher productivity in mass cultures requires introduction of traits aimed to relieve the light-use constraints (Vecchi et al., 2020). Among many, we chose two traits: (i) the optical density of algal cells and (ii) the photoprotection capacity. Decreasing overall absorption of PAR per unit volume of culture was shown to enhance light distribution in PBR and thus productivity (Melis, 2009). Whereas, increasing resistance to photooxidative stress is expected to prevent photoinhibition, thus increasing fitness (Külheim et al., 2002) and enhancing carbon gain (Zhu et al., 2004).

In the photosynthetic membranes, the photoprotective action of Car is well-established (Frank and Cogdell, 1996; Dall'Osto et al., 2013). Car participate in the antioxidant network of the chloroplast, aimed at the detoxification of ROS generated by light reactions: Car efficiently act by scavenging both O^{2-} and OH, and $^1O_2$ in thylakoids, thus preventing lipid peroxidation. Chl-binding complexes are protected against $^1O_2$ formation by Car, which catalyze quenching of ^{3}Chl* and results in Car triplets (^{3}Car*) formation, that safely decay to the ground state, producing heat (El-Agamey et al., 2004; Dall'Osto et al., 2012). Car biosynthesis is therefore a promising target to improve tolerance to photooxidative stress. In this work, we report on the isolation of *Chlorella vulgaris* mutant strains combining lower optical density and higher resistance to EL stress. Through chemical mutagenesis followed by selection on the carotenoid biosynthesis inhibitor norflurazon, we succeeded in the isolation of two pale green strains enriched in the antioxidant Car (NFR, norflurazon-resistant strains). Mutants exhibited higher biomass productivity in PBR, and were significantly more resistant to photooxidative damage than WT strain under very strong irradiance. Moreover, NFR strains in PBR showed further enhancement in productivity with respect to another *Chlorella* pale green mutant (Dall'Osto et al., 2019).

Overall, these results demonstrate that domestication of *C. vulgaris* for improved tolerance to photooxidation has the potential to generate strains with positive advantages in the artificial environment of a PBR. Moreover, comparison with strains previously obtained (Dall'Osto et al., 2019), which were selected for resistance to $^1O_2$, reveals that photoprotection in *Chlorella* is promoted by at least two independent mechanisms, only one of which is strengthened by Car overaccumulation.

Results

Isolation of NFR-3 and NFR-13, High Car Content Mutants of *Chlorella vulgaris*

Tolerance to high light stress is a desired trait for microalgal biotechnology (Day et al., 2012), being crucial for establishing efficient outdoor cultivation in low latitudes. Car biosynthesis represents an obvious target when aiming to enhance photosynthetic yield of microalgae under photooxidative conditions caused by EL. Indeed, Car contribute to the antioxidant network of the chloroplast, aimed to the detoxification of ROS, particularly $^1O_2$ generated by photosynthetic light reactions, thus preventing lipid peroxidation (Dall'Osto et al., 2014a), whereas the photoacclimation to high light involves Car up-regulation (Cordero et al., 2011). We used random mutagenesis and phenotypic screening to isolate *C. vulgaris* strains that combined a pale green phenotype with increased size of Car pool, these being traits expected to improve light conversion efficiency. Cells were subjected to two rounds of random chemical mutagenesis with EMS and mutants were selected for resistance to norflurazon, an inhibitor of carotenogenesis (Chamovitz et al., 1991). In a first selection step, approximately 5,000 mutagenized lines were screened and seven independent mutants were distinguished as putatively affected in Chl content per cell. Pale green strains were pooled, grown to enhance cell number, and submitted to a second treatment with EMS. Approximately 60,000 mutagenized lines were spread on BG-11 agar plates containing 4 μM norflurazon. 54 herbicide-resistant colonies (NFR, norflurazon-resistant) were obtained. Upon discarding mutants exhibiting either low growth or unstable resistance to the herbicide, 12 lines were selected, grown in liquid cultures, and the Car and Chl content per cell was determined after five days of growth under photoautotrophic conditions. Among the identified strains, lines NFR-3 and NFR-13 showed the highest Car content per cell, and were therefore selected for further analysis.

NFR lines showed a significant reduction of Chl content per cell (58% in NFR-3, 73% in NFR-13) (Table 3.1.1). The Chl a/b ratio was significantly higher in the mutants, with a value of 4.14/4.92 in NFR-3/-13 vs. 2.67 in WT. These data hint a reduction in the Chl b rich antenna complexes (LHC) in both mutants. Moreover, NFR-13 strain showed a stronger decrease in total Chl per cell and a higher Chl a/b ratio, thus suggesting that the Chl b-enriched antenna system was further decreased in this line respect to NFR-3.

Table 3.2.1 | Pigment content, PSII maximum quantum yield (Fv/Fm) and PSII functional antenna size of WT and mutants NRF*. Parameters were determined after 5 days of growth in minimal medium BG-11. Data are expressed as mean ± SD, n > 4. Significantly different values (ANOVA followed by Tukey's post-hoc test at a significance level of p < 0.05), within the same column, are marked with different letters.*

genotype	Chl / cell (pg)	Car / cell (fg)	Chl *a* / *b*	F_v / F_m	PSII antenna size ($T_{2/3}^{-1} \cdot 10^3$, ms^{-1})
WT	0.26 ± 0.03^a	57 ± 3^a	2.67 ± 0.22^a	0.67 ± 0.03^a	6.74 ± 0.49^a
NFR-3	0.11 ± 0.02^b	71 ± 3^b	4.14 ± 0.35^b	0.66 ± 0.03^a	4.32 ± 0.22^b
NFR-13	0.07 ± 0.01^c	65 ± 2^c	4.92 ± 0.46^c	0.65 ± 0.04^a	3.19 ± 0.42^c

Both NFR-3 and NFR-13 exhibited higher Car content per cell (+25% and +14%, respectively) respect to the WT strain (Table 3.2.1). Additional HPLC analysis of the Car composition of cell extracts (Table 3.2.2, Figure S3.2.1) revealed that carotenes and xanthophylls, while more abundant in NFR on a Chl basis, were maintained in similar relative abundance compared to WT.

Table 3.2.2 | HPLC analysis of pigment composition of WT and NFR mutants upon growth in either control or N-depleted media*. Pigment composition was determined after 5 days of growth in each medium. Cells were dark-adapted for 2 h before pigment extraction in dimethyl-formamide (DMFA). Data are expressed as mean ± SD, n = 3, and normalized to 100 Chls. Significantly different values (ANOVA followed by Tukey's post-hoc test at a significance level of p < 0.05), within the same column, are marked with different letters.*

					mol / 100 mol Chl						
	genotype	Car / cell (fg)	Chl *a* / *b*	Chl / Car	Neo	Viola	Anthera	Lute	Zea	α-Car	β-Car
control	**WT**	57 ± 3^{a}	2.7 ± 0.2^{a}	4.3 ± 0.1^{a}	2.8 ± 0.8^{a}	2.8 ± 0.7^{a}	0.1 ± 0.1^{a}	13.5 ± 1.7^{a}	1.3 ± 0.1^{a}	0.5 ± 0.1^{a}	1.9 ± 0.3^{a}
	NFR-3	71 ± 3^{b}	4.1 ± 0.3^{b}	1.6 ± 0.1^{c}	5.3 ± 1.3^{b}	8.9 ± 1.7^{b}	1.4 ± 0.2^{c}	37.3 ± 8.7^{c}	5.8 ± 1.1^{c}	0.8 ± 0.2^{a}	$4.9 \pm 1.0^{b,c}$
	NFR-13	65 ± 2^{c}	4.9 ± 0.4^{b}	1.0 ± 0.3^{d}	4.6 ± 0.5^{b}	15.5 ± 3.0^{c}	$2.0 \pm 0.5^{c,d}$	54.9 ± 5.0^{d}	7.9 ± 1.6^{c}	1.5 ± 0.2^{b}	$9.5 \pm 1.6^{c,d}$
N-depleted	**WT**	89 ± 4^{d}	2.8 ± 0.1^{a}	2.8 ± 0.1^{e}	3.9 ± 0.5^{b}	3.1 ± 0.4^{a}	1.1 ± 0.2^{c}	21.5 ± 0.3^{b}	2.9 ± 0.3^{b}	0.7 ± 0.1^{a}	2.9 ± 0.1^{b}
	NFR-3	121 ± 2^{e}	4.1 ± 0.1^{b}	0.9 ± 0.1^{d}	14.7 ± 1.1^{d}	18.8 ± 3.9^{e}	3.1 ± 0.8^{d}	52.9 ± 1.1^{d}	11.2 ± 0.8^{d}	1.8 ± 0.1^{b}	8.4 ± 0.1^{d}
	NFR-13	160 ± 8^{f}	4.8 ± 0.2^{b}	0.4 ± 0.1^{d}	27.7 ± 7.1^{e}	40.0 ± 0.6^{f}	4.7 ± 1.7^{d}	116.3 ± 2.6^{e}	21.9 ± 0.4^{e}	2.9 ± 0.2^{c}	19.8 ± 0.2^{e}

Further to the characterization of these mutants, we checked the effect of nitrogen starvation on Car accumulation, a treatment reported to increase Car content (Del Campo et al., 2007). When transferred from standard BG-11 to a modified BG-11 medium with limiting N source ($NaNO_3$ 0.8 mM), Car contents on a per cell basis increased in both NFR strains, by 1.7- and 2.5-fold, respectively, than standard BG-11, with the β,β-xanthophylls undergoing a preferential enhancement over α,β-xanthophylls and carotenes (Figures S3.2.1 and S3.2.2, Table 3.2.2).

Stoichiometry of Pigment–Protein Complexes and Photosynthetic Efficiency

To determine whether the mutation affected the PSII operating efficiency, Chl fluorescence measurements were carried out to quantify the capacity of the antenna system to transfer absorbed energy to RCs. All strains showed no significant differences in the maximal quantum yield of PSII photochemistry (Fv/Fm) (Table 3.2.1), suggesting that the PSII function was not worsened in NFR mutants despite the altered pigment composition. PSII functional antenna size was evaluated upon treatment of cells with DCMU (3-(3,4- dichlorophenyl)-1,1-dimethylurea), an inhibitor that blocks the plastoquinone binding site of PSII. In DCMU-treated cells, the rise time of Chl a fluorescence (Figure 3.2.1A) is inversely related to the antenna cross-section (Malkin et al., 1981; De Marchin et al., 2014). The T2/3−1 of the Chl fluorescence rise was reduced by ~36% in NFR-3 and by ~53% in NFR-13, with respect to WT (Table 3.2.1).

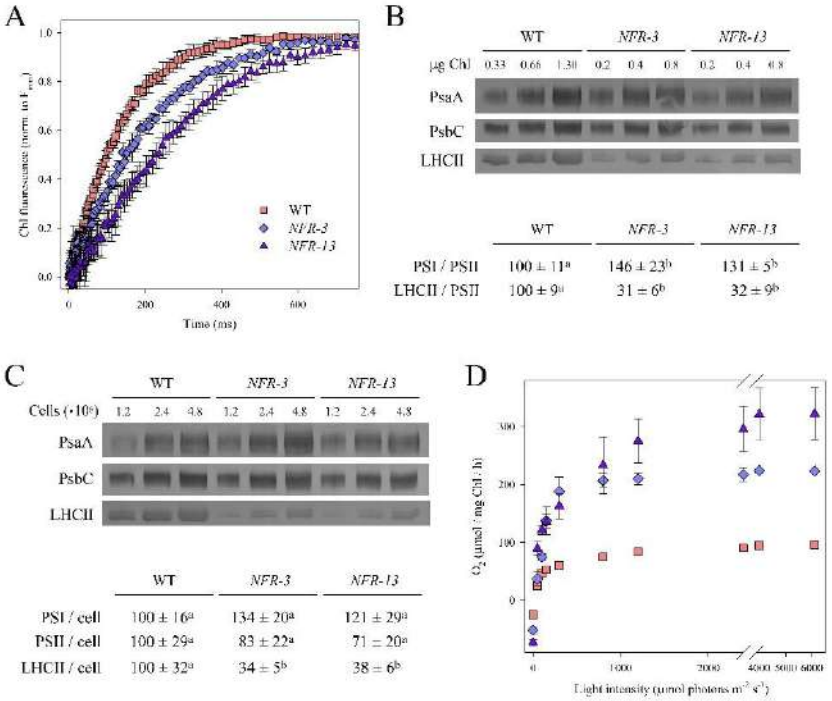

Fig. 3.2.1 | Characterization of C. vulgaris norflurazon-resistant (NFR) strains of Chlorella vulgaris. *(A) PSII functional antenna size. Variable Chl fluorescence was induced with a green light (15 µmol photons m−2 s−1), on dark-adapted cells of WT and NFR (about 1 × 10⁷ cells mL−1) in BG-11 medium supplemented with 50 µM DCMU. Data are expressed as mean ± SD, n = 10. The reciprocal of time needed for reaching two-thirds of the fluorescence rise (T2/3) was taken as a measure of the PSII functional antenna size (see Table 3.2.1). (B,C) Immunoblotting used for the quantification of photosynthetic subunits. (upper) Immunotitration was performed with antibodies directed against individual gene products: LHCII, the major light harvesting complex of PSII; the PSII core subunit PsbC (CP43); the PSI core subunit (PsaA). The amounts of Chls (panel B) and of cells (panel C) loaded for each lane are indicated. (lower) In each table, significantly different values (ANOVA followed by Tukey's post-hoc test at a significance level of p < 0.05), within the same row, are marked with different letters. (D) Light-saturation curves of photosynthesis, measured in cultures grown in BG-11 minimal medium. Data are expressed as mean ± SD, n = 4.*

These results were supported by quantification of LHC protein content. The abundance of selected photosynthetic subunits was assessed by immunotitration on cell extracts and expressed relative to WT, upon normalization to the PSII inner antenna CP43 content (Figure 3.2.1B). The LHCII/PSII ratio was reduced in both NFR mutants (68% vs. WT), while the PSI/PSII (PsaA/PsbC) ratio was significantly higher in mutants. When cultivated under limiting light conditions (70 µmol photons m^{-2} s^{-1}), both mutants showed a significant decrease in growth rate and a lower mean biomass production with respect to WT, consistent with the reduction in PSII antenna size (Figure S3.2.3).

The content in LHCII, PsbC and PsaA subunits was quantified on a per cell basis by immunotitration, and expressed as a percentage of the corresponding WT values. Figure 3.2.1C shows that LHCII content in NFR cells was significantly reduced vs. WT, while PSI and PSII contents were less affected.

The operation efficiency of the photosynthetic machinery was investigated in a wide range of irradiances, by measuring the light-saturation curve of photosynthesis in WT and NFR cells, grown under photoautotrophic conditions (Figure 3.2.1C). The rate of O_2 production rose as a function of light intensity within the range 0–1,000 μmol photons m^{-2} s^{-1}, showing a linear increase for WT and NFR lines at irradiances below 150 μmol photons m^{-2} s^{-1}.

The linear regressions of O_2 release vs. light intensity exhibited a slope of 0.71 ± 0.07 for WT, with a significant increase in NFR strains (1.27 ± 0.13 in NFR-3, 1.94 ± 0.29 in NFR-13), suggesting that the effective quantum yield of photosynthesis was enhanced in NFR mutants with respect to WT. Half-saturation of photosynthesis was reached at similar light intensity in WT and NFR-3 strains (approximately 110–130 μmol photons m^{-2} s^{-1}), while it was significantly higher in NFR-13 strain (Table 3.2.3). Values of Pmax, the maximum rate of light-induced O_2 evolution (photosynthesis net respiration), was reached around 2,000 μmol photons m^{-2} s^{-1} in WT strain, with a value of 96 ± 5 μmol O_2 mg Chl^{-1} h^{-1}; this value was significantly higher in NFR cells (225 ± 2 in NFR-3, 323 ± 45 in NFR-13). O_2 production rate was normalized on Chl content, yielding Pmax as a measure of the productivity for the two strains per unit Chl. The dark respiration rate on a per cell basis was the same in WT and mutant strains (Table 3.2.3). As a whole, these results point to an enhanced photosynthetic productivity of NFR mutants with respect to the WT.

Table 3.2.3 | Photosynthesis and respiration rates. *Parameters were measured on dark-adapted cell suspensions of WT and NFR strains, upon 5 days of photoautotrophic growth in BG-11 medium in low light conditions (70 μmol photons m−2 s−1, 25 ◦C). O2 evolution and consumption were measured with a Clark-type oxygen electrode (Oxygraph, Hansatech UK). Data are expressed as mean ± SD, n > 4. Significantly different values (ANOVA followed by Tukey's post-hoc test at a significance level of p < 0.05), within the same row, are marked with different letters.*

Parameters	WT	*NFR-3*	*NFR-13*
Half-saturation intensity (μmol photons m^{-2} s^{-1})	110 ± 24^{a}	128 ± 12^{a}	241 ± 73^{b}
P_{max} (μmol O_2 mg Chl^{-1} h^{-1})	96 ± 5^{a}	225 ± 2^{b}	323 ± 45^{c}
Respiration (μmol O_2 mg Chl^{-1} h^{-1})	25 ± 3^{a}	52 ± 7^{b}	73 ± 6^{c}
Respiration (fmol oxygen $cell^{-1}$ h^{-1})	6.4 ± 0.8^{a}	5.7 ± 0.7^{a}	5.1 ± 0.4^{a}
P_{max}/respiration (relative units)	3.9 ± 0.4^{a}	4.4 ± 0.5^{b}	4.4 ± 0.4^{b}

Phototolerance of WT and NFR Strains during EL Exposure

EL conditions lead microalgae to photooxidation: the enhanced release of $^1O_2$ (Prasad et al., 2016) results in lipid peroxidation, Chl bleaching and a consequent decline in the photosynthetic yield. Photoautotrophs have evolved a plethora of mechanisms aimed at limiting photo- damage; these include the tight regulation of Car pool size, which is increased in response to the EL stress (Del Campo et al., 2004). Therefore, the mutant strains NFR, due to a constitutive enhancement of Car content, are expected to counteract photooxidative conditions more efficiently, thus limiting photoinhibition.

To characterize the photooxidative stress experienced by WT and NFR mutants, cells were transferred from control conditions to strong irradiance (Figure 3.2.2). A well-known consequence of ROS release in the thylakoids is the peroxidation of unsaturated lipids, a reaction that releases malondialdehyde (MDA) as a by-product. When cultures were exposed to 1,400 µmol photons m^{-2} s^{-1}, at 24 °C for 24 h, rate of MDA release was ~5 times higher in WT cells with respect to NFR strains (Figure 3.2.2A), implying a significantly lower level of oxidative damage of the membranes in the mutants.

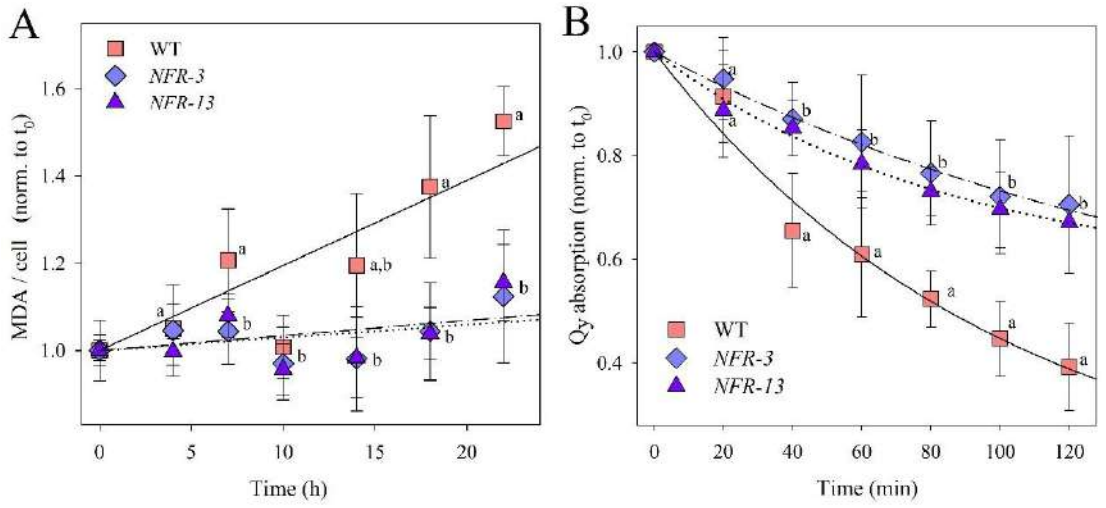

Fig. 3.2.2 | Photooxidation of C. vulgaris WT and NRF mutant genotypes under photooxidative stress. *(A) Cell suspensions of WT and mutant strains were treated with 1,400 µmol photons m−2 s−1 at 20 ◦C, and kinetics of malondialdehyde (MDA) formation were followed. MDA is an in- dex of membrane lipid peroxidation, and was quantified by HPLC as thiobarbituric reactive sub- stances. Slopes of the linear fit (proportional to the rate of MDA release) were 0.0195 ± 0.0056 (WT), 0.0029 ± 0.0024 (NFR-3), 0.0034 ± 0.0031 (NFR-13). (B) Cell suspensions were treated with strong white light (14,000 µmol photons m−2 s−1, 20 ◦C) and the amount of Chl was evaluated by measuring the absorption area in the region 600–750 nm. See Materials and Methods for details. Symbols and error bars show means ± SD, n = 4. Values marked with the same letters are not significantly different from each other within the same time point (ANOVA followed by Tukey's post-hoc test at a significance level of $p < 0.05$).*

We then analyzed cell suspensions of WT and mutant strains, by a time-course pigment bleaching upon transfer of cultures from low to extremely strong light (14,000 μmol photons m^{-2} s^{-1}, at 20 °C). In all cultures, the total cell Chl content decreased progressively upon EL treatment (Figure 3.2.2B); however, the rate of Chl bleaching was twice faster in WT respect to NFR strains.
To further investigate the photooxidative stress experienced by these genotypes, liquid cultures were grown photoautotrophically under very high irradiance (2,500 μmol photons m^{-2} s^{-1}, 24 °C), for 6 days in batch conditions. While the WT strain showed a long lag phase, NFR mutants exhibited a robust early growth phenotype, with NFR-13 culture displaying the faster growth rate (Figure S3.2.4). Among the mechanisms possibly underlying the higher biomass yield of NFR is the reduced optical density of culture, which allows for more homogeneous light distribution within the culture: indeed, pale-green mutants of different algal species (Kirst et al., 2012; Cazzaniga et al., 2014; Perin et al., 2015) possess an enhanced photosynthetic productivity with respect to the corresponding WT strain. Therefore, the *C. vulgaris* mutant PG-14 previously described (Dall'Osto et al., 2019) was included in the growth trial as internal control. The PG-14 mutant showed a growth kinetic and final biomass yield higher than WT (Figure S3.2.4), consistent with previous report (Dall'Osto et al., 2019). Growth enhancement of NFR strains with respect to WT was higher than with PG-14 under photooxidative conditions, thus suggesting higher productivity of NFR strains was caused not only by enhanced light diffusion in the culture, but also by higher tolerance to EL stress.

Biomass Productivity of WT and NFR Strains in Laboratory-Scale PBR

The above results are consistent with a higher tolerance to photooxidative damage of NFR strains with respect to WT, which implies mutant strains could have an improved biomass productivity in PBR dense cultures under elevated irradiances. Therefore, strains were cultivated photoautotrophically over a period of 6 days in a laboratory-scale PBR, a semi-batch cultivation system consisting of 1 L glass cylinders. Cells were grown in minimal medium (BG-11), illuminated with 1,400 μmol photons m^{-2} s^{-1} at 24 °C, under a day/night cycle of 16:8 h. Each cylinder was fed with a mix of air and CO_2, whose relative abundance was tuned in order to maintain the pH of the medium between 6.8 and 7.2. Both NFR mutants showed a faster growth rate with respect to WT (Figure 3.2.3), and cell concentration at day 6 was about 5 10^8 cells mL^{-1} in both mutants vs. 3.6 10^8 cells mL^{-1} in the WT (Figure 3.2.3).

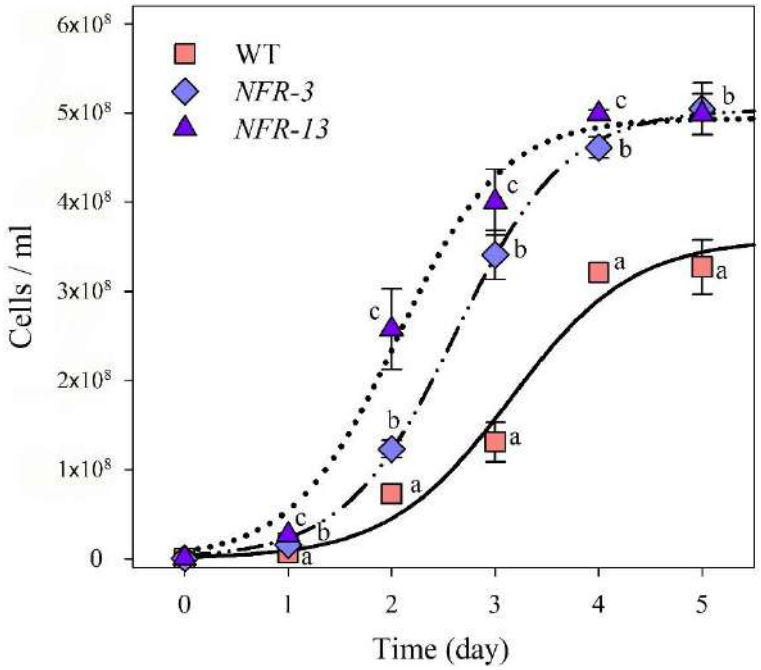

Fig. 3.2.3 | Growth curves of WT and mutant strains*. Growth of WT and NRF mutant lines was performed under photoautotrophic conditions, in 1-L cylinders, illuminated with 1400 µmol photons m⁻² s−1, 25 ◦C. Cultures were maintained in a semi-batch system fed with air/CO_2 mix; CO_2 supply was modulated in order to keep the pH of the medium always between 6.8 and 7.2. Symbols and error bars show means ± SD, n = 5. Values marked with the same letters are not significantly different from each other within the same time point (ANOVA followed by Tukey's post-hoc test at a significance level of p < 0.05).*

The specific growth rate (µ) for NFRs was higher than that obtained for the WT strain (Table 3.2.4). Furthermore, NFR mutant strains reached a biomass productivity of 0.56 g L^{-1} day^{-1}, which was significantly improved (+23%) with respect to the yield obtained in WT (0.43 g L^{-1} day^{-1}, see Table 3.2.4).

Table 3.2.4 | Growth parameters of WT and NFR strains, cultured in air/CO_2 bubbling system*. Biomass content was measured by determination of dry biomass accumulated at the end of the cultivation period, divided by the number of days of cultivation. µ, specific growth rate, was calculated from the slope of logarithmic cell concentration curve. Data are expressed as mean ± SD, n = 5. Significantly different values (ANOVA followed by Tukey's post-hoc test at a significance level of p < 0.05) are marked with different letters.*

genotype	Mean increase of biomass (g L^{-1} day^{-1})	µ (day^{-1})
WT	0.43 ± 0.03[a]	1.87 ± 0.08[a]
NFR-3	0.56 ± 0.03[b]	1.99 ± 0.04[b]
NFR-13	0.56 ± 0.01[b]	1.99 ± 0.02[b]

The higher photoresistance of NFRs could be ascribed to a number of mechanisms, which include the photoprotective Non-Photochemical Quenching (NPQ). NPQ catalyzes the safe dissipation of the excitation energy in excess as heat, and its amplitude is modulate by the size of the xanthophyll pool (Niyogi, 2000; Park et al., 2019). Once assessed at steady-state photosynthesis, NPQ amplitude showed negligible differences between WT and NFR strains, over all the light intensities tested (Figure 3.2.4A and Figure S3.2.4). Alternatively, resistance and/or recovery from photoinhibitory EL treatment could be improved in mutant strains. To verify this possibility, we treated cells for 3 h at 1,800 μmol photons m^{-2} s^{-1}, 24 °C, and measured Fv/Fm ratio. The extent of PSII photoinhibition was significantly higher in WT vs. NFR strains, with Fv/Fm values being 15% lower at the end of light treatment (Figure 3.2.4B); this is consistent with the milder oxidative damage experienced by the mutants (See Figure 3.2.2). However, recovery of Fv/Fm in low light (Figure 3.2.4B, inset) showed that all genotypes performed equally, implying that the higher productivity of NFR strains was not due to a strengthened PSII repair system.

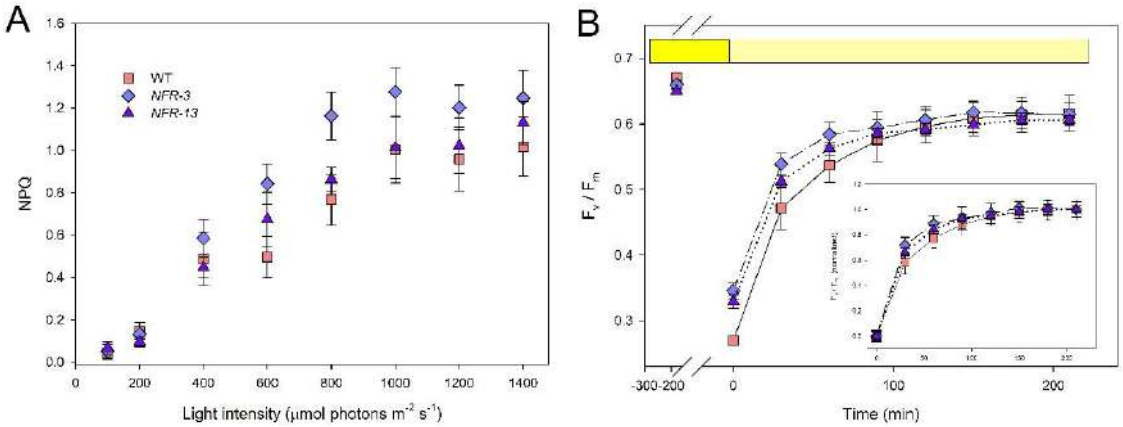

Fig. 3.2.4* | *Analysis of Chl fluorescence during photosynthesis under EL. *(A) Chl fluorescence was monitored in cultures dark-adapted for 2 h. Cell suspensions were illuminated for 25 min and the non-photochemical quenching (NPQ) was determined at the end of light treatment (i.e., during steady-state photosynthesis). (B) PSII quantum yield recovery after EL treatment was quantified on WT and NFR strains by measuring Fv/Fm recovery in low light (20 μmol photons m^{-2} s^{-1}, 24 ◦C, light yellow bar) upon 3 h of EL treatment (1800 μmol photons m^{-2} s^{-1}, 24 ◦C, yellow bar). (Inset) kinetics of Fv/Fm were zeroed at the end of the EL treatment and normalized to the maximum Fv/Fm during low light recovery. Data are expressed as mean ± SD, n = 4.*

Lipid Productivity under Nitrogen Starvation

Microalgae gained increasing interest as a feedstock for biofuel production. Thus, an analysis of oil content in WT and mutant strains is crucial to assess their potential for commercial-scale oil production. EL (Solovchenko et al., 2011) and nutrient deficiency (Hu et al., 2008) were recognized as stress factors which promote lipid accumulation in microalgae. Signaling involves photooxidative stress perception, while ROS and ROS-related by-products likely represent effector molecules, as suggested by the correlation between ROS level and lipid content in *C. vulgaris* cells (Menon et al., 2013). It comes that the higher resistance to photooxidative damages,

measured in NFR strains, might impair oil yield by affecting ROS-based crosstalk signals. Thus, the total lipid content was determined in WT and NFR strains. Microalgae were first grown in lab-scale PBR (see Figure 3.2.3) in nutrient-rich BG-11 medium, to attain high cell density, then were transferred to the same medium except that N was limiting (-95% N content than standard BG-11). After 11 days of growth, lipid content per DW was determined gravimetrically (Table S3.2.1). Lipid content in WT algae was about 25% of the dry biomass, while cells from both NFR lines had a significantly lower lipid fraction, in the amount of 16% of the dry biomass.

Genotypic Characterization of NFR Strains by Whole-Genome Sequencing

The complex regulation of EL adaptation mechanisms is poorly understood in microalgae and most key factors are still awaiting elucidation. Mutant strains represent valuable tools to identify the underlying genotypic traits. Therefore, the two high Car content mutants, as well as the corresponding WT strain, were investigated in a whole-genome re-sequencing approach in order to identify the genetic background of the phototolerant phenotypes. For the systematic identification of the mutation(s) responsible for the Car- accumulating phenotypes, we applied a workflow based on open-source bioinformatics tools. Sequencing the parental WT strain alongside NFR mutants enabled us to identify and remove common variants present in the WT background strain. Whole-genome sequencing was performed on an Illumina HiSeq platform. After trimming and quality filtering, the mean obtained coverage was 65.9X, 55.2X and 18.6X for the WT, NFR-3 and NFR-13 respectively. Percentage of the reads mapped to the reference genome were 99.4, 71.5, and 60.8% for WT, NFR-3, and NFR-13, respectively (Table 3.2.5).

Table 3.2.5 | Summary of whole-genome sequencing and read mapping for WT and two EMS-treated mutants.

Sample	Total number of reads produced	Total number of reads after trimming	Mapped reads	Mean fold coverage
WT	38,406,276	25,308,558	25,157,713	65.9X
NFR-3	37,378,884	28,743,282	20,555,916	55.2X
NFR-13	17,628,716	11,931,178	7,249,676	18.6X

After the filtering process and manual inspection with Integrated Genomics Viewer (IGV), we detected a total of 34 variations (SNPs and small INDELs, see also Figure S3.2.5) that differed between the mutants and parental WT. Variants are listed in Table 3.2.6, and discussed further ahead.

Table 3.2.6 | Identified variants that are specific for the respective mutant *(SS: Super-Scaffold; PO: Pilon Object; sub: substitution; noTP: no Transit Peptide; SP: Signal Peptide; mTP: mitochondrial Transit Peptide; cTP: chloroplast Transit Peptide; * indicates low confidence for SIFT algorithm prediction—see Materials and Methods for details).*

Mutant	Variant pos.	Ref/Alt		Region	CDS Effect [SIFT prediction]	TargetP	ChloroP	Putative gene function (gene ID)
NFR-13	SS_1:3929152	G	A	Exon	Missense sub. (Arg598Gln) [SIFT: Tolerated]	noTP	-	Predicted protein (g380)
NFR-13	SS_2:14375	G	A	Exon	Missense sub. (Arg150Cys) [SIFT: Deleterious]	noTP	-	RNA helicase, activating signal cointegrator 1 (g5804)
NFR-13/NFR-3	SS_2:5043375	G	C	Exon	Missense sub. (Gln67His) [SIFT: Tolerated]	noTP	-	Predicted protein (g2438)
NFR-13	SS_3:393571	G	A	Exon	Missense sub. (Arg470Cys) [SIFT: Deleterious*]	noTP	-	Serine/threonine-protein phosphatase 2A 65 kDa regulatory subunit A beta isoform-like (g2544)
NFR-13/NFR-3	SS_5:2569375	G	C	Exon	Missense sub. (Glu178Asp) [SIFT: Deleterious]	noTP	cTP	Glycerol-3-phosphate acyltransferase 3 (g4271)
NFR-13	SS_5:2624939	C	T	Exon	Missense sub. (Ser119Leu) [SIFT: Deleterious]	SP	-	Serine threonine- kinase receptor R831 (g4284)
NFR-3	SS_10:492953	G	A	Exon	Missense sub. (Arg233Cys) [SIFT: Deleterious]	noTP	-	S49 family peptidase (g6424)
NFR-13	SS_13:1005023	G	A	Exon	Missense sub. (Ala80Thr) [SIFT: Tolerated]	mTP	cTP	Acylamino-acid-releasing enzyme-like (g7937)
NFR-3	SS_14:552899	G	A	Exon	Missense sub. (Gly391Asp) [SIFT: Deleterious]	noTP	-	Biosynthetic arginine decarboxylase (g9015)
NFR-13	SS_14:1569725	C	T	Exon	Missense sub. (Ala6Thr) [SIFT: Deleterious*]	noTP	-	Hypothetical protein (g8357)
NFR-13/NFR-3	SS_18:1233529	G	A	Exon	Missense sub. (Gly1235Arg) [SIFT: Deleterious*]	noTP	-	Hypothetical protein (g9528)
NFR-13/NFR-3	SS_1:4651287	G	A	Exon	Synonymous sub.	noTP	-	cold shock domain-containing protein (g211)
NFR-13/NFR-3	SS_2:4256144	C	T	Exon	Synonymous sub.	noTP	-	haloalkane dehalogenase (g2220)
NFR-13/NFR-3	SS_2:4392343	C	G	Exon	Synonymous sub.	noTP	-	solute carrier family 25 member 44 (g2251)
NFR-13/NFR-3	SS_5:1173035	G	A	Exon	Synonymous sub.	noTP	-	Large subunit GTPase 1 (g3878)
NFR-13/NFR-3	PO_26F:57866	C	T	Exon	Synonymous sub.	noTP	-	Predicted protein (g10631)
NFR-3	SS _1:3944123	C	T	Intron	No	mTP	cTP	Methionyl-tRNA synthetase (g376)
NFR-13/NFR-3	SS_1:5342472	G	A	Intron	No	noTP	cTP	Cleavage and polyadenylation specificity factor subunit 1 (g15)
NFR-13/NFR-3	SS_2:4545066	G	A	Intron	No	noTP	-	Putative Xaa-Pro aminopeptidase 3 (g2293)
NFR-13/NFR-3	SS_2:4545075	G	A	Intron	No	noTP	-	Putative Xaa-Pro aminopeptidase 3 (g2293)
NFR-13/NFR-3	SS _3:1002678	A	G	Intron	No	SP	-	Hypothetical protein (g2664)
NFR-13/NFR-3	SS_5: 1971361	AG	A	Intron	No	noTP	-	MAU2 chromatid cohesion factor-like protein (g4126)
NFR-3	SS _5:2687539	G	C	Intron	No	noTP	cTP	Serine/threonine-protein kinase sepA (g4294)
NFR-13/NFR-3	SS_6: 1727681	TC	T	Intron	No	cTP	cTP	Water chloroplastic-like (g4763)
NFR-13/NFR-3	SS _13:303225	G	A	Intron	No	noTP	cTP	Allophanate hydrolase (g7748)
NFR-3	SS_13:1920503	G	A	Intron	No	noTP	-	U3 small nucleolar ribonucleoprotein protein IMP4 (g8749)
NFR-3	SS_7:737237	G	C	Intron	No	noTP	-	Sodium:proline symporter (g5015)
NFR-3	SS_8:332225	C	T	Intron	No	noTP	cTP	MFS general substrate transporter (g5411)
NFR-13	SS_1:269018	C	A	Splice region	No	noTP	-	Preprotein translocase subunit SecA (g1481)
NFR-13/NFR-3	SS_3:344676	G	A	Splice donor	Yes	noTP	-	E3 Ubiquitin-protein Ligase SP1 related [PTHR47568:SF2] (g2532)
NFR-13/NFR-3	SS_13:2646657	G	A	Splice region	No	cTP	cTP	S1 motif domain-containing protein (g8549)
NFR-13	SS_1:2991332	G	T	Intergenic	No	noTP	-	Upstream of: Nuclear/nucleolar GTPase 2 (g672); Nuclear transport receptor (g671)
NFR-13/NFR-3	SS_5:1304829	C	T	Intergenic	No	noTP	-	Upstream of predicted protein (g3913). Downstream of predicted protein (g3914)
NFR-3	SS1:3529923	A	AT	Intergenic	No	noTP	-	Downstream of transcription initiation factor IIB-2 (g501). Downstream of putative phosphatase 2C 35 (g500)

Discussion

Realization of microalgae potential to satisfy global demands requires a decrease of the current production costs for biomass. Among factors contributing to the price of bio-products purified from microalgae are energy and material inputs, as well as cellular content of the desired molecule (Gimpel et al., 2015). It comes that cost-effective production needs selection of strains with enhanced accumulation of a valuable compound. Moreover, productivity of the most common industrial strains is far lower than maximal theoretical estimations, suggesting that removing bottlenecks which limit biomass yield is crucial in strategies aiming to make algal biofactories profitable on an industrial scale.

Optimization of Light-Use Efficiency Enhances Biomass Yield

The inefficient use of light, due to high optical density of cultures, is among the factors which limit algal biomass production in the artificial conditions of a PBR. Indeed, it was shown that the biomass yield in PBRs increased with decreasing the light path, which allows for more homogeneous light distribution in the culture vessel (Richmond et al., 2003). Unfortunately, short light paths in flat-panel PBR limit the overall volume of culture and, thus, the economic viability of large-scale plants.

A number of studies have shown that biomass yield can be improved by optimizing optical features of algal cultures through genetic engineering approaches: targeting genes such as TLA1, which control antenna size in *Chlamydomonas reinhardtii*, resulted in higher biomass yield (Polle et al., 2003); random mutagenesis applied to species with a high industrial interest such as *C. sorokiniana* and *N. gaditana*, selected pale-green mutants which exhibited increased light-use efficiency (Cazzaniga et al., 2014; Perin et al., 2015). A similar approach was used in this work with *Chlorella vulgaris*, searching for low optical density traits to increase light penetration and light-to-biomass yield, in order to find out a background strain for further domestication projects.

Both NFR mutants are defective in PSII antenna size, consisting of a LHCII content of 31% (in NFR-3) and 32% (in NFR-13) with respect to WT (Figure 3.2.1B). Fluorescence induction in cells treated with DCMU confirmed that both NFR strains had a reduced PSII functional antenna size (Figure 3.2.1A).

Photosynthetic rate was significantly enhanced in both NFR strains; yet this effect was larger in the strain with lower cross-section (Table 3.2.3): indeed, the Pmax of NFR-3 was 134% larger than in WT at saturating irradiances, while that of NFR-13 increased by 236%, implying the reduction in antenna size enhanced photosynthetic yield. These results are consistent with those reported for *C. reinhardtii* tla1 and tla3 strains with truncated antenna system (Polle et al., 2003; Kirst et al., 2012).

Photooxidative stress caused by EL conditions is a major reason for yield reduction in algal cultures (Yang and Gao, 2003). Microalgae exposed to saturating light intensity undergo PSII damage, which must be repaired by de novo synthesis (Domingues et al., 2012). The process impairs the overall efficiency of light-to-biomass conversion efficiency, therefore, it should be minimized to achieve high productivity.

Moreover, cells in dense suspensions are rapidly mixed and experience a rapid shift from darkness to saturating light, and mixing rate on a ms time-scale can easily be achieved in tubular PBR (Carvalho et al., 2011). The consequent fluctuations in light intensity are faster than mechanisms required for counteracting EL stress, such as the activation of dissipative channels or the reversible phosphorylation of LHCII. Therefore, the repeating fluctuations between low and high light phases challenge the light acclimation capacity of the photosynthetic apparatus (Tikkanen et al., 2012). In this work, growth rates of cultures were measured in the long term under strong irradiance (2,500 μmol photons m^{-2} s^{-1}) in batch conditions (Figure S3.2.4). During 6 days of growth, the PG-14 strain we used as a reference with reduced antenna size and without

Car content enhancement (Dall'Osto et al., 2019) showed a 57% increase in productivity with respect to WT (see Figure S3.2.3B), meaning that a reduction of LHC per PSII by 40% (previously determined for this genotype) significantly improved the phototolerance of *C. vulgaris* cells. Interestingly, NFR mutations showed a further increased growth rate with respect to both WT and PG-14 under EL. We conclude that overaccumulation of Car and diminished optical density of the cultures have a synergistic effect in improving light-use efficiency under strong irradiance. As a consequence of the highly reactive excited states generated during oxygenic photosynthesis, algae have evolved a number of photoprotective mechanisms to limit damage to cell structures (Li et al., 2009b). These mechanisms are effective in (i) regulating either ^{1}Chl* (Ruban et al., 2012) or ^{3}Chl* state formation (Dall'Osto et al., 2012), thus, ROS release, or (ii) scavenging ROS (Havaux et al., 2007). The first group includes the energy dissipation events which diminish the excitation pressure on PSII, while the antioxidant network comprises scavenging enzymes and antioxidant molecules (Erickson et al., 2015), including the thylakoid-bound antioxidants Car which catalyze both quenching of ^{1}Chl* and ^{3}Chl* and scavenging of $^1O_2$.

NPQ is the main mechanism that regulates ^{1}Chl* lifetime (Kondo et al., 2017; Meagher et al., 2021), making it a candidate process underlying higher biomass yield of NFR strains. However, NPQ amplitude, once measured over a range of irradiances, was essentially the same in WT and NFR genotypes (Figure 3.2.4A), implying that differences in growth cannot be ascribed to changes in Chl quenching activity. A similar consideration applies to the activity of PSII repair (Figure 3.2.4B). The phototolerance of NFR mutants was significantly higher vs. WT. The observed lower lipid peroxidation and higher resistance to Chl photobleaching (Figure 3.2.2) suggest either a reduced ROS release or a more efficient scavenging activity of ROS in the chloroplasts. The latter appears as the most likely hypothesis, as the content in the Car antioxidants is far higher in NFR strains (Table 3.2.1). Indeed, mutants impaired in the accumulation of Cars, in both plants and algae, were unable to acclimate to high irradiance, and progressively lost photosynthetic capacity along with oxidation of pigment–protein complexes and accumulation of ROS (Baroli et al., 2004; Fiore et al., 2012).

In addition to enhanced antioxidant capacity, other mechanisms could improve light-to-biomass conversion efficiency in NFR strains. We expect a lower ROS release in mutant lines due to higher antioxidant capacity. Depending on its concentration, $^1O_2$ was shown to play a role as second messenger in cell signal transduction pathways, controlling a number of stress-response mechanisms (Ledford et al., 2007); e.g., in *C. reinhardtii*, specific promoter regions mediate transcriptional responses to $^1O_2$ (Shao et al., 2007; Fischer et al., 2009), while experience of a moderated $^1O_2$ level was shown to improve resistance of algal cells to harsher photooxidative stress (Ledford et al., 2007).

A number of plastid-derived signals were shown to be involved in the adaptation of cells to the light environment, including cleavage products of Car or intermediates of Car biosynthesis (Kleine and Leister, 2016). Indeed, under EL stress, oxidized by-products of β-carotene, such as β-cyclocitral (β-CC) and β-ionone, work as signaling molecules in plants, enhancing resistance to EL and other stresses (Ramel et al., 2012; D'Alessandro and Havaux, 2019). Release of Car

cleavage products was also described in cyanobacteria (García-Plazaola et al., 2017), thus suggesting these signal pathways are ubiquitous in the green lineage.

Interestingly, previous work showed that resistance to oxidative stress can also be obtained without any increase in Car/Chl ratio; this is the case of $^1O_2$-resistant (SOR) strains (Dall'Osto et al., 2019), the photoprotection capacity of which was significantly enhanced than WT strain, despite the pool of Car not being differentially affected in these genotypes upon light stress. However, SOR strains, when cultivated in the same lab-scale PBR here reported, at 1,400 μmol photons m^{-2} s^{-1}, stood out for higher mean biomass productivity than both NFR strains. These *C. vulgaris* genotypes can be ranked with respect to the light-to-biomass conversion efficiency as follows: WT < NFRs < SOR-5 = SOR-6 (Dall'Osto et al., 2019). In the condition of prolonged EL treatment of cultures tested here, our results point to a specific involvement of Car in the defense of the photosynthetic machinery against photooxidative damage. Data also imply that multiple mechanisms take part in photoprotecting algal cells: indeed, the EL resistance measured in SOR strains was not related to any increase in the size of the Car pool.

Influence of ROS-Resistance Traits on Stress-Induced Lipid Production

While sustained ROS release under EL causes lipid peroxidation, mild photooxidative stress conditions enhance lipid accumulation in oleaginous microalgae (Wase et al., 2014). The mechanism possibly underlying such response is a ROS signaling network that up-regulates the pathway of fatty acid biosynthesis (Guarnieri et al., 2011). Consistently, in *C. vulgaris*, a positive correlation between oil content and ROS level was found (Menon et al., 2013), while in *S. cerevisiae* the endoplasmic reticulum triggers development of lipid bodies upon perception of oxidative stress (Jacquier et al., 2011). Overall, evidence for a correlation between intracellular ROS level and abundance of TAGs is still limited and molecular details are missing. In the case of NFR strains, if ROS level promotes fatty acid biosynthesis by complex signaling pathways, then we might expect an inhibiting effect in the accumulation of oil due to the enhanced antioxidant activity of the mutants. Indeed, quantification of intracellular lipid content, upon short-term nitrogen-starvation treatment of cultures, supports this hypothesis: oil content was significantly reduced in both NFR strains (-35% vs. WT, see Table S3.2.1). Alternatively, such a change in lipid content could be a consequence of the missense amino acid substitution in Glycerol-3-phosphate acyltransferase 3 (Table 3.2.6, Figure S3.2.7), which is indeed involved in the terminal steps of triacylglycerol biosynthesis in the endoplasmic reticulum (see below).

NFR as Promising Car Producer Strains for Commercial Applications

The demand for nutraceuticals has been increasing over the last years. Microalgae contribute as being rich in proteins and bioactive compounds such as essential fatty acids, Car and vitamins. However, only a few microalgal species are currently commercialized as nutraceuticals (Leu and Boussiba, 2014). *Chlorella vulgaris* is among the few species approved by the European Food Safety Authority for human consumption. *Chlorella* biomass is widely used as food supplement or to enhance the nutritional value of food products (Sahni et al., 2019). However, organoleptic features of algal biomass, e.g., strong green color or grassy taste, might disappoint the consumer, preventing them from including supplemented food in their diet (Lafarga, 2019). Isolation of

mutant strains with altered pigmentation, e.g., higher Car/Chl ratio, does represent an alternative strategy for improving the qualities of algal biomass as food additive. Furthermore, forward genetic approach is of particular relevance in the food industry, since it avoids restrictions to GMO (Zimny et al., 2019).

In this work we developed two Chl-deficient strains of *Chlorella vulgaris* of interest for nutritional applications. The changes in color of NFR-3 and NFR-13 mutant strains in N-limited conditions (Figure S3.2.1) are due to a lower Chl content, and to a 70% and 146% increase in Car content, respectively, with respect to the standard BG-11 medium. Under photoautotrophic growth, both strains showed a significantly improved growth performance with respect to WT, reaching a concentration of 3.79 g FW L^{-1} (NFR-3) and 4.74 g FW L^{-1} (NFR-13) in batch conditions. Moreover, the improved growth rates were maintained even when scaled up in 1-L lab-scale PBR (Figure 3.2.3, Table 3.2.4), a result which support their feasibility as potential candidates for the food industry and for the development of novel food supplements.
The strains here described point to *C. vulgaris* as an attractive candidate for the production of xanthophylls: NFR-13 strain showed a volumetric lutein content of 40 mg L^{-1} under N-starvation, significantly higher than those reported for other lutein-producing strains grown under photoautotrophic conditions (Del Campo et al., 2000, 2004). Moreover, NFR-13 cultures showed a high specific growth rate (0.08 h^{-1}), thus, it represents a promising strain for the production of xanthophylls for commercial applications.

Whole-Genome Sequencing to Identify Gene(s) Responsible for the Enhanced Light-Use Efficiency in C. vulgaris

The phenotype of NFR strains is the product of one or more mutations which affect regulatory and metabolic processes of Car biosynthesis. Here, we identified genetic variants among which these mutations can be searched for, and suggest how these variations could alter gene function, yielding the observed phenotype of NFR-3 and NFR-13 mutants.

1. Glycerol-3-phosphate acyltransferase 3. A transversion (G to C) was observed at nucleotide 534 on the 6th exon. This results in missense amino acid substitution of a glutamic acid into an aspartic acid, a mutation shared by both NFR mutants, affecting a subunit involved in neutral lipid metabolism. Glutamic acid and aspartic acid are both acidic amino acids with side chains containing a carboxylic acid group which carries a full negative charge. In terms of interaction modes, both amino acids include ionic, van der Waals and H-bonds. However, glutamic acid differs from aspartic acid only in that its side chain is longer by one methylene group. This results in higher side chain flexibility in glutamic acid compared to aspartic acid whose side chain flexibility is moderate. Transmembrane topology prediction indicates that the site of mutation is at the boundary between cytoplasmic domain (residues 169–179) and the consecutive transmembrane region (residues 180–199). Multiple sequence alignments of top BLAST hits indicate that the last two residues of the cytoplasmic domain (E178 and R179) are conserved among green cut species (Figure S3.2.7). Glycerol-3-phosphate acyltransferase 3 is a key component of the diglyceride-3-phosphate synthesis pathway. Consistently, its activity has

been reported to be directly correlated to the amount of glycerophospholipids in *E. coli* cells (Janßen and Steinbüchel, 2014) and used as a target for membrane engineering to enhance production and accumulation of ß-carotene (Wu et al., 2017).

2. E3 Ubiquitin-protein Ligase SP1-related (PTHR47568:SF2) encoding sequence contains a splice donor variant and is shared by both mutants, NFR-3 and NFR-13. A transition (G to A) occurs at the first nucleotide of the second intron affecting canonical GT-AG splice site pairs. Group of E3 ubiquitin–protein ligases, including SP1 from *Arabidopsis* (UniProtKB: Q8L7N4), are involved in regulation of plastid's proteome via ubiquitination and subsequent degradation of translocon at the outer envelope membrane of chloroplasts (TOC) complexes (Ling et al., 2012). In addition, it promotes stress tolerance by depleting the chloroplast protein import apparatus, which limits photosystem assembly and the potential for ROS formation (Ling and Jarvis, 2015). Formighieri et al. (Formighieri et al., 2013) demonstrated that absence of ARSA1, a protein localized in the *C. reinhardtii* cytosol, led to a strongly decreased Chl content per cell; ARSA1 was shown to be required for optimal biogenesis of photosystems due to its involvement in the accumulation of TOC34, a component of the outer chloroplast membrane translocon complex. Interestingly, in both species, a mutation targeting a component interacting with TOC is associated with a pale green phenotype.

3. Serine/threonine-protein phosphatase 2A 65 kDa regulatory subunit A contains variation observed in NFR-13 mutant only. Transition mutation (C to T) results in substitution of an arginine by cysteine. 2A protein phosphatases are evolutionarily conserved and carry out multiple functions such as growth- and stress-related signaling, cell cycle regulation, vesicle trafficking, as well as regulation of the activities of a number of enzymes involved in key metabolic pathways (Farkas et al., 2007). The mutant 2A protein phosphatase in NFR-13 contains fatty acid desaturase domain (IPR005804) which is involved in the lipid metabolic process (GO:0006629).

4. Both NFR-3 and NFR-13 share an intronic variation on Allophanate hydrolase (g7748). In *Chlamydomonas reinhardtii*, allophanate hydrolase is involved in urea hydrolysis to produce ammonium depending on the source of nitrogen available (Park et al., 2015).

5. Another exonic mutation found only in NFR-3 targets biosynthetic arginine decarboxylase (g9015) involved in the polyamine biosynthesis pathway. In plants, polyamine accumulation was shown to correlate with Car content (Neily et al., 2011).

6. A missense amino acid substitution (Arg233Cys) was identified on S49 family peptidase (g6424) in NFR-3. The predicted protein contains peptidase_S49 domain (IPR002142) from residues 20–236. InterPro entry (IPR002142) describes proteolytic enzymes that exploit serine in their catalytic activity. The sequences of these ubiquitous enzymes are variously annotated in different taxonomic groups. In plants, these proteolytic sequences are annotated as Signal peptide peptidase A (SppA; protease IV; MEROPS identifier S49.001) which are involved in cleavage of signal peptides.

7. NFR-13 mutant contains a point mutation resulting in Ala80Thr on Acylamino-acid-releasing enzyme-like (g7937). Acylamino-acid-releasing enzymes have been identified and characterized in plants. They are found to be mainly localized in the stroma of chloroplasts, and are possibly involved in degradation of glycated/oxidized proteins, such as glycated RuBisCO (ribulose-1,5-bisphosphate carboxylase/oxygenase), and thus contribute to sustain the chloroplast antioxidative system (Nakai et al., 2012).

Lastly, 6 out of 34 identified variants lie within or in close proximity to gene bodies containing transcriptional or translational regulatory domains, namely, transcription initiation factor IIB-2 (g501, NFR-3), Nuclear/nucleolar GTPase 2 (g672, NFR-13), Nuclear transport receptor (g671, NFR-13), S1 motif domain-containing protein (g8549, NFR-3/NFR-13), U3 small nucleolar ribonucleoprotein protein IMP4 (g8749, NFR-3). In NFR-13, an amino acid substitution (Arg150Cys) on an RNA helicase (g5804) with U5 small nuclear ribonucleoprotein 200 kDa helicase domain (PTHR24075:SF5) is identified. This predicted protein is likely to be involved in spliceosome assembly, activation and disassembly (inferred from sequence similarity to UniProtKB:P32639).

Conclusions

Here we show that *C. vulgaris* mutagenesis and selection in the Car biosynthesis inhibitor norflurazon resulted in a significant increase in the size of the Car cellular pool. The mutant strains were more tolerant to EL conditions, as shown by reduced lipid peroxidation and pigment bleaching. Stress protection is probably due to the function of Car in preventing oxidative damage of membranes. Moreover, these strains showed an improved biomass productivity with respect to WT in mass cultures under EL conditions. Overall, our results show that a domestication strategy, focused on the modulation of both cell optical density and resistance to photooxidative stress, succeeded in the development of improved strains, which is of interest for industrial production. Although our genomic analysis cannot unequivocally identify the genetic origin of the phenotypes reported for NFR genotypes, we can tentatively propose that the mutation on Glycerol-3-phosphate acyltransferase 3, which is shared by NFR-13 and NFR-3 mutants, might be involved in the reduced accumulation of lipids upon N starvation (Table S3.2.1). Similarly, the mutation at the E3 Ubiquitin-protein Ligase SP1 might cause the pale green phenotype through its effect on TOC complex assembly. Experimental verification of these hypotheses will involve targeting these individual genes by either genome editing (Angstenberger et al., 2020) or tapping from the mutant collection (Li et al., 2019a) in the green algae relative species *Chlamydomonas reinhardtii*.

Materials and Methods

Strains and culture conditions.

Chlorella vulgaris WT strain was obtained from the SAG Culture Collection of Algae (Goettingen University, Germany, http://www.unigoettingen.de/en/catalogue-of-strains/185049.html (accessed on 1 May 2021)) as SAG strain number 211-11p. Cells were maintained on TAP agar plates (Kropat et al., 2011) and grown in either minimal (BG-11) [94] or rich (TAP) liquid media. Shaken flasks (120 rpm) and plates were illuminated from the top with 70 μmol photons m^{-2} s^{-1}, photoperiod of 16/8 h light/dark, 25 °C (control condition); irradiance was provided by warm-white LEDs (Epistar 35mil Chip High Power LED, warm white LEDE-P20B-DW, Wayjun Tech., Shenzhen, China). For nitrogen starvation experiments, cells were grown in the BG-11 medium containing excess nitrogen source ($NaNO_3$ 17 mM); they were then collected by centrifugation at the end of the logarithmic growth phase, washed twice with sterile water, and re-suspended in a modified BG-11 medium with limiting N source ($NaNO_3$ 0.8 mM). For physiological measurements, cultures were harvested during the logarithmic growth phase (about 1–3 10^7 cells mL^{-1}).

Mutagenesis and screening protocols.

Liquid cultures of *C. vulgaris* WT strain were harvested by centrifugation at the exponential phase of growth (~1 10^6 cells mL−1), re-suspended in fresh BG-11 medium to 5 10^7 cells mL^{-1}, and treated with 2.2% (w/v) of ethyl methanesulfonate (EMS). The survival curve for mutagenesis with EMS was carried out to determine the mutagen concentration which resulted in around 5–10% of cell viability. Upon 2 h maintenance in the dark, to prevent light-activated DNA repair, cells were plated at 100-fold dilution on minimal medium, and the inhibitor norflurazon (NF) was used as selection method. NF is a herbicide inhibiting the carotenogenic enzymes phytoene desaturase (Cordero et al., 2011). A wide range of concentrations of the chemicals were previously tested to find out the minimal concentration which inhibited grown of the WT strain. For the selection of NFR (norflurazon resistant) strains, mutagenized cells were spread on a solid minimal medium containing 4 μM NF and incubated at 70 μmol photons m^{-2} s^{-1} for 2 weeks; single colonies appeared after 14 days.

Cells were subjected to two rounds of random chemical mutagenesis with EMS. In a first selection step, lines were selected for pale green phenotype by direct sight inspection, then pale green strains were pooled, grown to enhance cell number, submitted to a second treatment with EMS, and mutants were selected for resistance to inhibition of Car biosynthesis.

Selected lines upon two rounds of mutagenesis were inoculated onto fresh minimal medium, grown in the light for seven days, and the Chl content per cell was determined. The herbicide-resistant colonies were sub-cultivated several times in liquid BG-11 medium containing 4 μM NF to check their resistance to the herbicide and further analyzed for Car and Chl content per cell and for growth rate.

Cell count and pigment analysis.

Cell density was measured using an improved Neubauer hemocytometer. Pigments were extracted from intact cells with 100% dimethyl-formamide (DMFA). The supernatant of each sample was recovered after centrifugation (10 min at 15,000 g, 4 ◦C), and pigments were separated and quantified by HPLC (Gilmore and Yamamoto, 1991b).

Gel Electrophoresis and Immunoblotting.

For SDS-PAGE and immunotitration analysis, cells were resuspended in Loading Buffer (5% glycerol, 1% SDS, 2.5% 2-mercaptoethanol, 0.1 M Tris, 0.1 M Tricine pH 8.45) and ground in a tissue homogenizer (Precellys, Bertin, France) by adding a ceramic lysing matrix. The supernatant of each sample was recovered after centrifugation (10 min at 15,000 xg, 4 °C) and Chl content of extracts was determined by fitting of the spectra of acetone extracts with the spectra of individual pigments (Croce et al., 2002a). SDS-PAGE analysis was performed with the Tris-Tricine buffer system (Schägger and von Jagow, 1987). For immunotitration (Towbin et al., 1979), a range of total protein extract corresponding to 0.25–1.0 μg of Chl were loaded for each sample and electroblotted on nitrocellulose membranes (Amersham Protran®, pore size 0.45 μm). Proteins were detected with primary antibodies (home-made, α-CP43 and α-LHCII; from Agrisera, α-PsaA AS06-172-100) and an alkaline phosphatase-conjugated secondary antibody (Sigma-Aldrich A3687). Signal amplitude was quantified using the GelPro 3.2 software (Bio-Rad).

Measurements of photosynthetic activity.

The oxygen evolution activity of the cultures was measured at 25 °C with a Clark-type O_2 electrode (Hansatech, UK) upon illumination with white light provided by a halogen lamp (Schott, Germany). Samples of 2 mL cell suspension (5 10^6 cell mL^{-1}) were loaded into the oxygen electrode chamber; 3 mM $NaHCO_3$ was added to the cell suspension prior to the O_2 evolution measurements to ensure electron transport was not limited by the carbon supply.

In vivo chlorophyll fluorescence analysis.

Fluorescence induction kinetics were recorded with a home-built apparatus, as previously described (Rappaport et al., 2007). Variable fluorescence was induced with a green light of 15 μmol photons m^{-2} s^{-1} at RT, on cells suspensions (1 10^7 cells mL^{-1}) in BG-11 medium containing 50 μM DCMU. The reciprocal of time corresponding to two-thirds of the fluorescence rise (T2/3) was taken as a measure of the PSII functional antenna size (Malkin et al., 1981; De Marchin et al., 2014). Maximum quantum efficiency of PSII (Fv/Fm) [100] was measured on cell suspension with a PAM 101 fluorimeter (Heinz-Walz, Effeltrich, Germany). The light dependence of NPQ was measured through Chl fluorescence with a Fluor-Cam 700MF (PSI, Drasov, Czech Republic), on cell suspension dark-adapted for 2 h at RT; NPQ was assessed at steady-state photosynthesis, upon 25 min illumination over a range of light intensities (100–1,400 μmol photons m^{-2} s^{-1}).

Determination of the sensitivity to photooxidative stress.

The extent of lipid peroxidation in cells was estimated by measuring malondialdehyde (MDA) formation, as an indirect quantification of lipid peroxides. Quantitative evaluation was done by transferring aliquots of WT and mutant cell suspensions in BG-11, corresponding to 4×10^6 cells mL^{-1}, into a 24-well culture plate, 2 mL total volume in each well, kept on a rotary shaker and illuminated for 2 days with high light (1,400 μmol photons m^{-2} s^{-1}, 20 °C). Samples ($2\ 10^5$ cells) were taken for analysis for a period of 48 h, and frozen in liquid nitrogen. MDA content of aliquots was quantified as previously described (Havaux et al., 2005).
The photobleaching kinetics of Chl cell content were measured on cell suspensions ($2\ 10^6$ cells mL^{-1}, in BG-11 + 0.03% w/v agarose) using actinic light intensities of 14,000 μmol of photons m^{-2} s^{-1} for 2 h; temperature of samples was maintained at 20 °C. During the illumination, the absorbance area between 600–750 nm was recorded; the initial and maximal absorbance were set, so the same absorbance area was used in the wavelength range 600 nm < λ < 750 nm for all the samples.

Growth analysis.

Growth experiments were performed at 25 °C in a home-built photobioreactor, composed of glass cylinders with a maximum light path of 8 cm and a working volume of 1 liter each (Cazzaniga et al., 2014). Cultures were continuously mixed with a flux of air and CO_2. The ratio of compressed air and CO_2 was automatically adjusted to keep the pH of the medium within the range of 6.8–7.2. Each autotrophic batch cultivation was carried out in duplicate. Illumination was provided by a panel of warm-white LEDs (Epistar 35mil Chip High Power LED, warm white LEDE-P20B-DW), microalgae were exposed to irradiance of 1,400 μmol photons m^{-2} s^{-1}, with a photoperiod of 16/8 h light/dark; batch cultivation was carried out in duplicate.

For cultivation under very strong irradiance (2500 μmol photons m^{-2} s^{-1}), illumination was provided by a panel of warm-white LEDs (Epistar 35mil Chip High Power LED, warm white LEDE-P20B-DW), microalgae shaked in flasks were exposed to an irradiance of 2500 μmol photons m−2 s−1, with a photoperiod of 16/8 h light/dark; batch cultivation was carried out in triplicate. The parameters determined to monitor cell growth were cell number and dry biomass weight, for which the washed cell pellets were dried overnight in a lyophilizer.

Determination of total lipid content.

Total lipids were extracted from 100 mg homogenized biomass (4 cycles of 30 s at 8,000 rpm, with a Precellys homogenizer, Bertin, France) using an extraction protocol by (Axelsson and Gentili, 2014), with a total of 3 mL methanol, 6 mL chloroform, and a subsequent washing step with 4 mL water. Net total lipid amount was determined gravimetrically.

Whole-genome sequencing and identification of unique mutations.

For DNA preparation, $2\ 10^8$ cells were collected by centrifugation, then resuspended in 1 ml TEN buffer (10 mM Tris-HCl pH 8.0, 100 mM EDTA, 150 mM NaCl), centrifuged (1,500 g, 2 min, 4 °C) and resuspended in 300 μL SDS-EB buffer (2% w/v SDS, 400 mM NaCl, 40 mM EDTA, 100 mM

Tris-HCl pH 8.0). Extraction by mechanical destruction was carried out by treating the suspensions in Precellys Homogenizer (Bertin Instruments) with 100 mg glass beads (8 cycles, 30 s each cycle, 8,000 rpm). Samples were treated with 700 µL phenol:chloroform:isoamyl alcohol (25:24:1), centrifuged (15,000 g, 5 min, 4 ◦C), then 2.5 volumes of ethanol and 0.11 volumes of Na-acetate 3M pH 5.5 were added to the supernatant. Upon incubation at -80 °C for 30 min, DNA was precipitated (15,000 g, 25 min, 4 °C) and washed twice with 600 µL ethanol. Pellets were resuspended in a small volume of 10 mM Tris-HCl buffer pH 8.0, treated with RNAse 10 µg/µL at 37 °C for 30 min, then DNA was further purified from RNA contaminants (NucleoSpin Plasmid, MACHEREY-NAGEL). DNA samples were quantified by Qubit 2.0 Fluorometer (Invitrogen, Carlsbad, CA, USA). Celero DNA-Seq Library Preparation Kit (Tecan Genomics, Redwood City, CA, USA) has been used for library preparation following the manufacturer's instructions. Final libraries were checked with both Qubit 2.0 Fluorometer (Invitrogen, Carlsbad, CA, USA) and Agilent 2100 Bioanalyzer DNA assay (Agilent technologies, Santa Clara, CA, USA). Libraries were then pooled for sequencing and sequenced in paired-end 125 bp mode on HiSeq2500 (Illumina, San Diego, CA, USA). Sequencing was outsourced (https://www.igatechnology.com, accessed on 1 May 2021).

Assessment of raw read quality was performed with FASTQC v0.11.9 (https://www.bioinformatics.babraham.ac.uk/projects/fastqc/, accessed on 1 May 2021). All sequences were trimmed with Trimmomatic v0.39 (Bolger et al., 2014). Alignments were performed with Burrows– Wheeler Aligner (BWA) v0.7.17 (Li and Durbin, 2009) using default parameters for paired-end reads and mapped to the recently published reference genome (Cecchin et al., 2019). Sorting and deduplication were performed with PicardTools v2.17.10 (http://broadinstitute.github.io/picard, accessed on 1 May 2021). Statistical analysis of BAM files was performed with QualiMap v2.2.2 (García-Alcalde et al., 2012). SNPs and small indels were called using the GATK Haplotype Caller v4.0.6.0 (Depristo et al., 2011) with ploidy set to 1. All the filtering processes were carried out using GATK SelectVariants and VariantFilteration tools. First, common SNPs between each mutant and the parental WT were removed from the dataset. The Quality by Depth filter with a cut-off of QD < 2.0 was used to filter out variants with low confidence. In addition, *Chlorella vulgaris* is haploid and heterozygous sites likely represent alignment or sequencing errors. Therefore, heterozygous variants in each sample with an allele frequency below 0.9 were removed. Finally, variants were manually inspected using the Integrated Genomics Viewer (IGV) v2.3 (Thorvaldsdóttir et al., 2013). SnpEff v4.3 (Cingolani et al., 2012) was used to retrieve the genomic context of each variant and predict the effect of the variants on gene function. Functional information for the identified genes was obtained through Blast2go analysis (Götz et al., 2008). Protein domains and motifs were predicted by InterPro and its associated software (Mitchell et al., 2019). SIFT 4G (Sorting Intolerant From Tolerant for Genomes) algorithm v2.0.0 (Vaser et al., 2015) was used to build SIFT4G database for *Chlorella vulgaris* genome. SIFT 4G annotator (https://github.com/pauline-ng/SIFT4G_Annotator, accessed on 1 May 2021) was used to annotate the VCF file. TargetP v2.0 (Armenteros et al., 2019) and ChloroP v1.1 (Emanuelsson et al., 1999) were used to detect sequence signals.

Supplementary Materials:

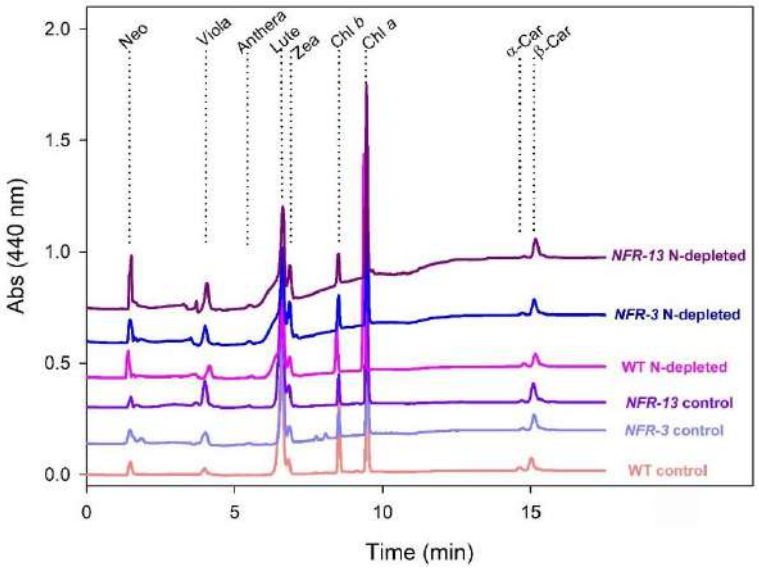

Fig. S3.2.1* | *Analysis of pigment content of WT and NFR cells, grown in either control or N-depleted media. *Pigment composition was determined after 5 days of growth in each medium (see Table 3.2.2). Separation of lipid-soluble pigments was based on HPLC analysis. Each chromatogram represents absorbance at 440 nm of pigments extracted in dimethyl-formamide from dark-adapted cells. Chromatograms were vertically shifted for better comparison.*

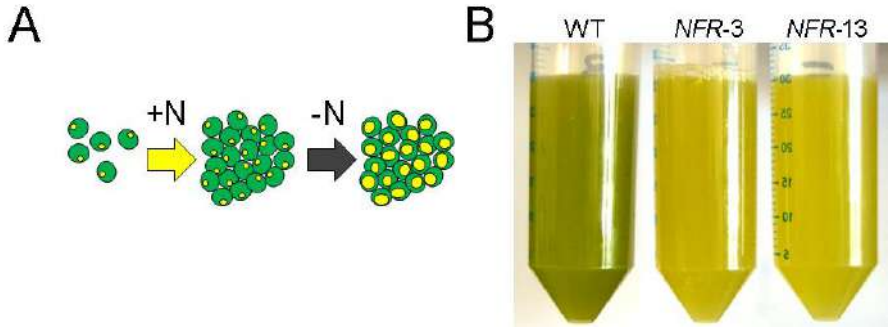

Fig. S3.2.2* | *Effect of nitrogen starvation on WT and NFR mutants. *(A) Cells were grown in BG-11 with 100% content of nitrogen (17 mM $NaNO_3$) till they reach saturation. Then the cells were collected by centrifugation and then resuspended in BG-11 with 5% content of nitrogen (0.8 mM $NaNO_3$). Yellow circles represent the intracellular content in lipophilic compounds, such as TAGs and carotenoids, whose accumulation is stimulated by factors such as irradiance and nutrient availability (Wase et al., 2014). (B) Appearance of the three genotypes at the end of the experiment, after 5 days of growth in N-depleted medium. All the lines were diluted at the same cellular concentration (2×10^7 cells mL^{-1}).*

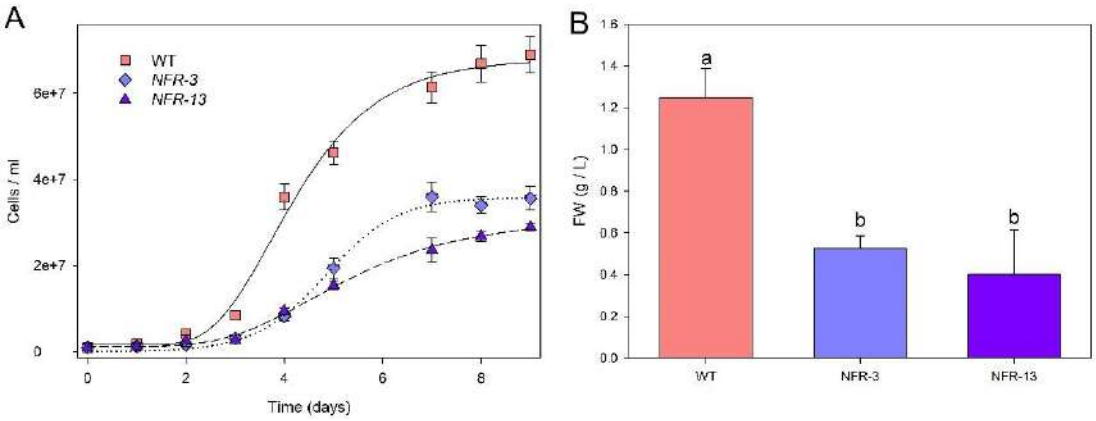

Fig. S3.2.3 | Growth of WT and NFR strains under low light conditions*. (A) Growth curves of WT and NRF mutant lines under photoautotrophic conditions, monitored as the cell number per ml culture. All experiments were performed in flasks with continuous stirring, illuminated with 70 µmol photons m^{-2} s^{-1}, 25 °C. Cell concentration at t0 was about 1 × 10^6 cells mL^{-1}. (B) Fresh weight (FW) of biomass collected after 9 days of growth. Symbols and error bars show means ± SD, n = 5. Values marked with different letters are significantly different from each other (ANOVA, p < 0.05).*

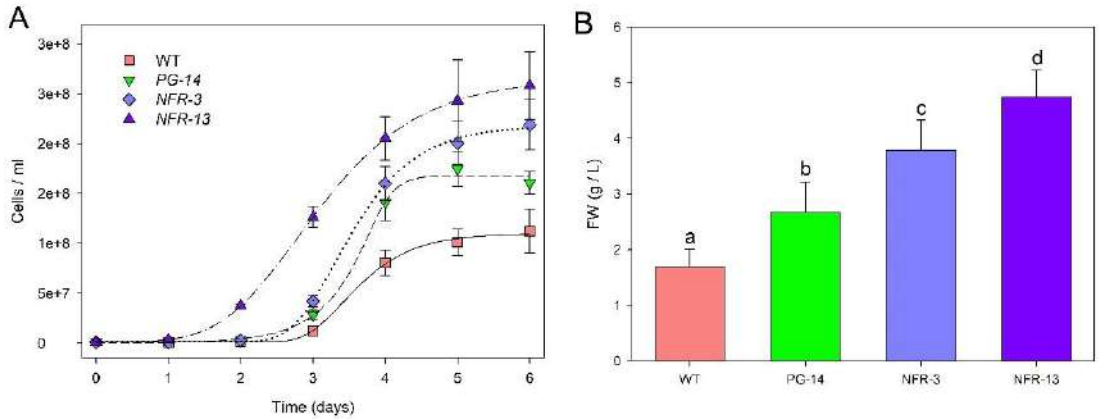

Fig. S3.2.4 | Photoautotrophic growth of WT and NFR strains under excess light conditions. *(A) Growth of WT and NRF mutant lines was monitored under autotrophic conditions, in flasks with continuous stirring, under strong light conditions (2,500 µmol photons m^{-2} s^{-1}, 25 °C), as the cell number per ml culture. At time 0, the cultures were switched from low light (70 µmol photons m^{-2} s^{-1}, 25 °C) to strong light conditions. Cell concentration at t0 was about 1 × 10^6 cells mL^{-1}.(B) fresh weight (FW) of biomass collected after 6 days of growth. Symbols and error bars show means ± SD, n = 5. Values mark ed with different letters are significantly different from each other (ANOVA, p < 0.05).*

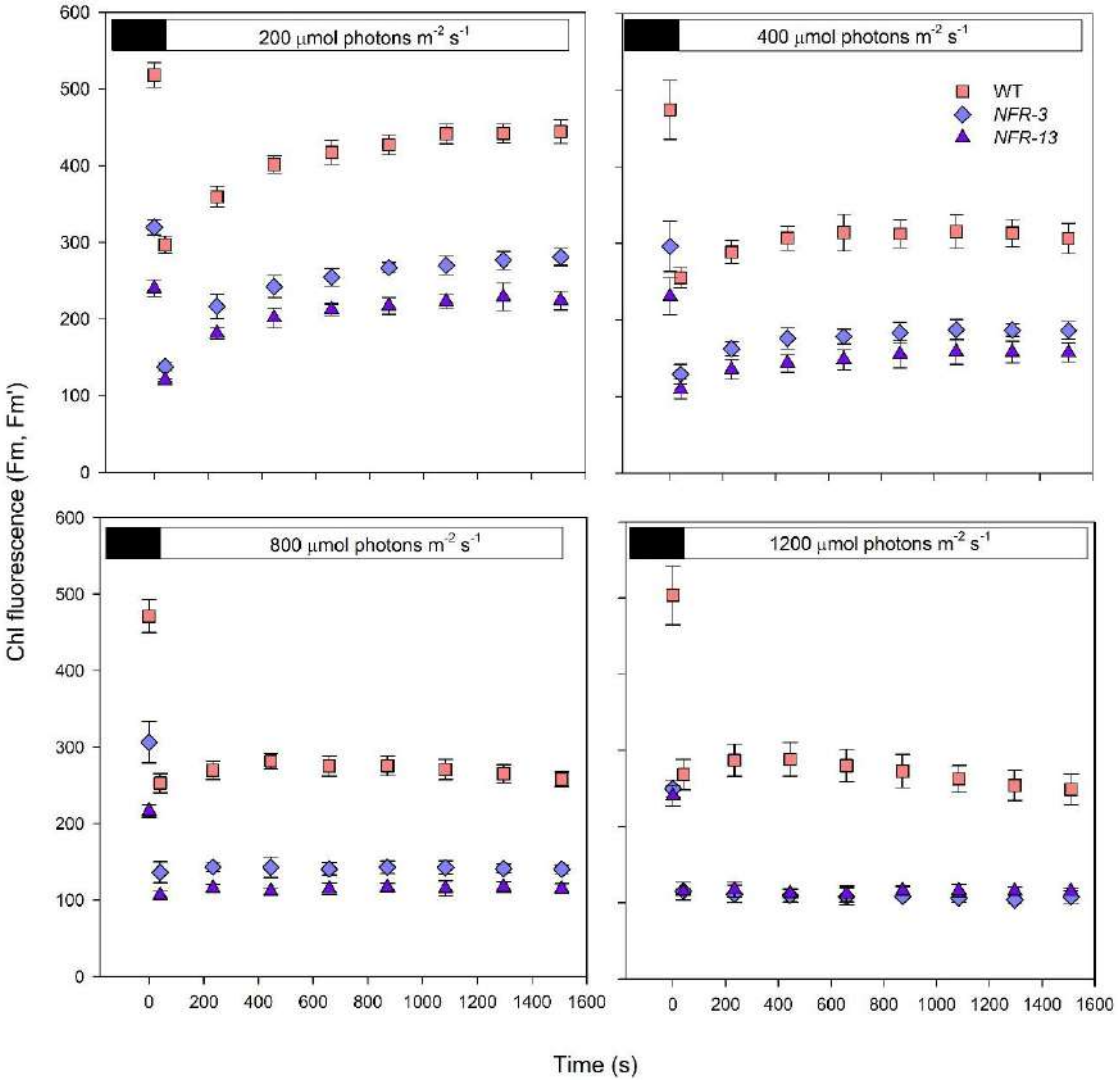

Fig. S3.2.5 | Analysis of room temperature Chl fluorescence during photosynthesis. *Chl fluorescence was monitored in cell suspensions from dark-adapted cultures (see methods for details). Cells were given 25 min of white light illumination, over a range of light intensities (white bar). Maximum fluorescence in the dark (Fm, dark bar) and in the light (Fm', white bar) are shown as means ± SD (n = 4).*

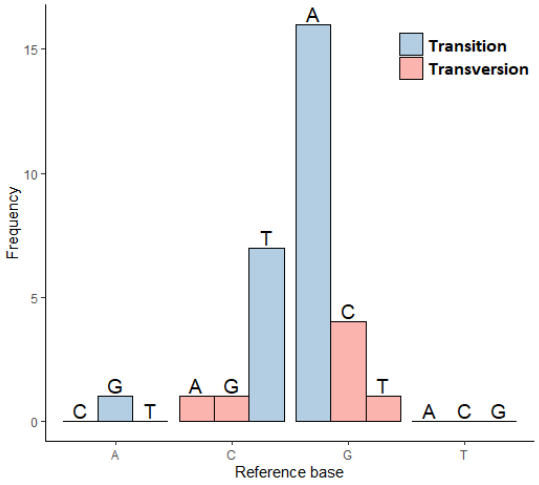

Fig. S3.2.6 | Frequency of base changes in NFR mutants. *EMS mutagenesis induces nucleotide transition, transversion, insertion and deletions. Higher frequency of G/C to A/T transition corresponds to the expected EMS mutagenesis outcome with transitions as the predominant type of mutations.*

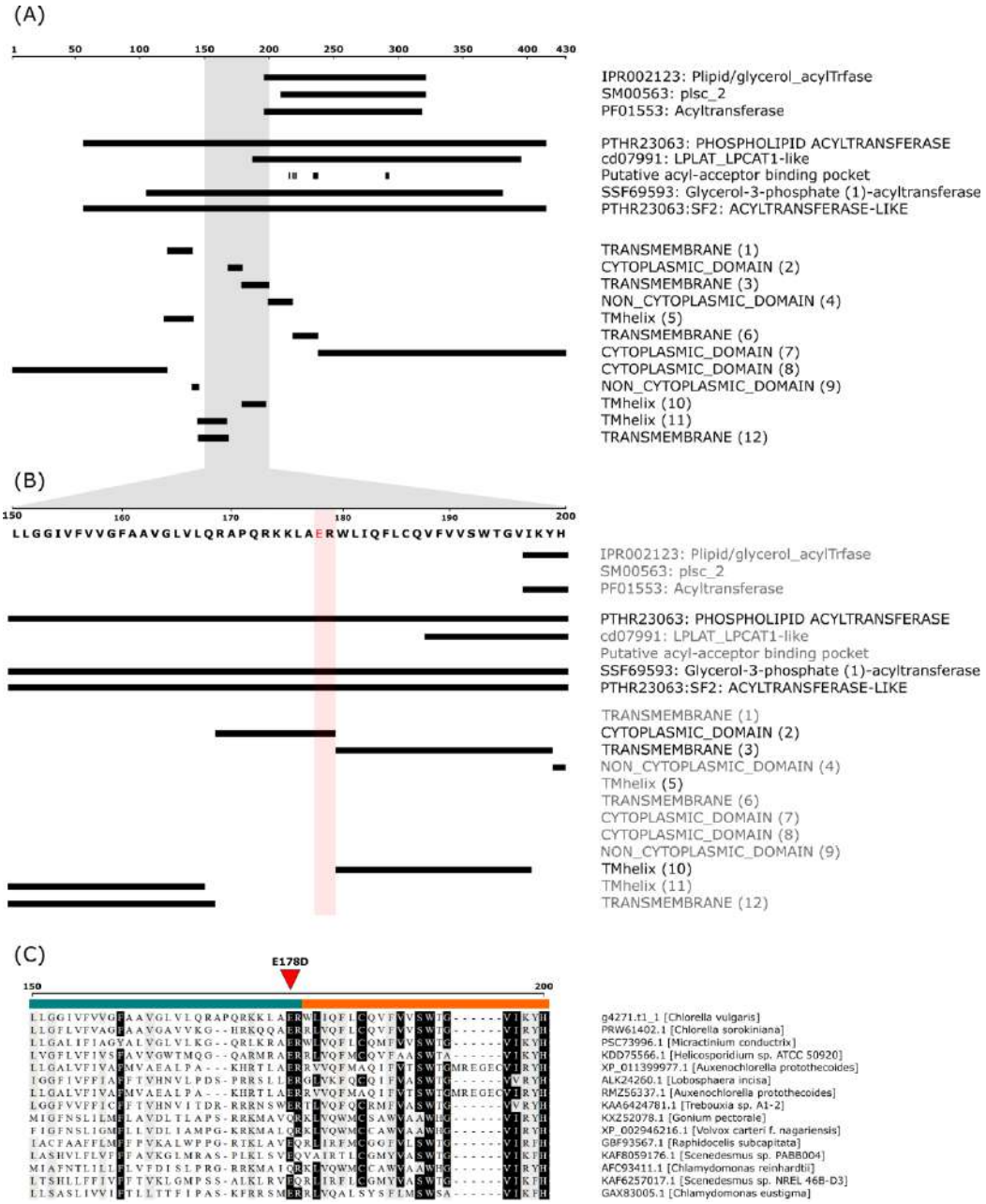

Fig. S3.2.7 | Schematic representation of Glycerol-3-phosphate acyltransferase 3 (g4271) and predicted domains. *(A) An overview of protein domains and motifs predicted by InterPro and its associated software. (B) The last two residues of the cytoplasmic domain are shaded light red (glutamic acid 178 and arginine 179). The site of mutation E178D overlaps with PANTHER entry PTHR23063:SF2, SUPERFAMILY entry SSF69593, and predicted cytoplasmic domain. (C) Amino acid sequence alignment of predicted cytoplasmic domain (2) and transmembrane domain (3) in Chlorella vulgaris Glycerol-3-phosphate acyltransferase 3 (g4271) and top BLAST hits in green algae (taxid:3041) with ≥75% coverage. The position of Glu178Asp mutation present in both NFR-13 and NFR-3 mutants is indicated by an inverted red triangle. The cytoplasmic domain in Chlorella vulgaris is indicated by teal color while the transmembrane domain is in orange. Black boxes indicate ≥80% sequence identity.*

Table S3.2.1 | Lipid content of algal biomass. *Total lipid content was determined gravimetrically on the dry biomass, from WT and mutant cultures grown for 7 days in nutrient-rich BG-11 medium (1400 µmol photons m−2 s−1, 25 ◦C) and then moved for further 4 days of growth in modified BG-11 medium with limiting N source. Data are expressed as mean ± SD, n = 4. Significant different values in oil content among genotypes (ANOVA test, p < 0.05) are marked with different letters.*

genotype	Total oil content (% DW)
WT	25.1 ± 2.7[a]
NFR-3	16.5 ± 3.0[b]
NFR-13	15.7 ± 1.1[b]

Author Contributions: L.D. and R.B. conceived this work. Z.G., S.C. and S.B. identified mutant lines and performed all biochemical and physiological characterizations under the supervision of R.B. and L.D. M.J. and N.V. performed the bioinformatic analysis. L.D. and R.B. wrote the manuscript with contributions from all the authors. All authors have read and agreed to the published version of the manuscript.

Funding: We acknowledge the financial support from the University-Industry Joint Projects "Industrialgae" (grant JPVR 2016). In addition, we acknowledge the support of the ENAC-2019 fund "Carburanti Alternativi per l'Aviazione Civile" and the grant PON for industrial research and experi- mental development ARS01_00881 "ORIGAMI" by the Italian Ministry of University and Research (MIUR).

Conflicts of Interest: The authors declare no conflict of interest.

4. Physiological characterization of *Arabidopsis* mutants devoid of trimeric LHCII

Chloroplasts of higher plants are organized into complex networks of membranes comprising linear (stroma lamellae) and appressed regions (grana). This highly organized architecture has been obtained through evolution, indeed membrane organization increases from cyanobacteria to higher plants (Trissl and Wilhelm, 1993). Photosynthetic complexes are embedded in thylakoids membrane and the mobile component are free to diffuse within the lipid layer (plastoquinone) or in the lumen (plastocyanin) (Lavergne and Joliot, 1991; Kirchhoff et al., 2011). Photosystems II and their antenna complexes (Lhcb) are segregated in the grana while PSI is mainly found in stroma lamellae. This physical separation is needed to maximize photosynthetic efficiency (more details in section 1.1.1 "*The Chloroplast*"). The role of specific Lhcb proteins in shaping the architecture of thylakoids has been investigated in chapter 4.1, by applying CRISPR-Cas9 genome editing to knock out *lhcb* genes. Our results showed that both monomeric and trimeric Lhcb proteins are needed stabilization of grana structures, with special functions mediated by the subunits Lhcb5 and Lhcb2. These results are of particular relevance because, to date, an accurate description of the gene products responsible for grana formation is not available and a mutant completely lacking the typical higher plants stroma-grana organization has never been described, although the absence of grana was previously reported for specific kinds of cells (e.g. bundle- sheath cells) (Bassi et al., 1995). In the second part of this chapter (Chapter 4.2) we carried out the physiological characterization of lines produced in chapter 4.1. We focused our attention on photoprotection, defining the role of both monomeric and trimeric complexes in the activation of Non Photochemical-Quenching and the specific contribution of the different component of PSII antenna system in higher-plants photo-tolerance.

This chapter is a manuscript in preparation.
A former version of the manuscript is available as preprint on BioRxiv: "Thylakoid grana stacking revealed by multiplex genome editing of LHCII encoding genes."

4.1 A recently evolved member among LHCII encoding genes controls grana stacking in land plant chloroplasts.

Zeno Guardini[1], Rodrigo L. Gomez[1], Roberto Caferri[1], Johannes Stuttmann[2], Luca Dall'Osto[1] and Roberto Bassi[1,*]

[1]Dipartimento di Biotecnologie, Università di Verona, Strada Le Grazie 15, 37134, Verona, Italy

[2]Institute for Biology, Department of Plant Genetics, Martin Luther University Halle-Wittenberg, Weinbergweg 10, 06120 Halle (Saale), Germany

[*]Corresponding author: roberto.bassi@univr.it

Running title: Lhcb2 regulates grana stacks dynamics in plants

Abstract

Land plants chloroplasts differ from those of green algae for a most conspicuous morphological feature: the stacking of their thylakoid membranes, hosting photosynthetic machinery, into grana, piles of vesicles paired by their stromal surface. Thylakoid coupling forms circular domains, which include Photosystem II and its antenna system. Photosystem I and ATPase are instead located in both grana end membranes and stroma membranes connecting grana stacks. Despite extensive research, the molecular basis of grana stacking still remains unclear. We have dissected the photosystem II antenna system and obtained genotypes lacking either the major trimeric antenna complex LHCII, or the monomeric antennas Lhcb4-6, or both. Electron microscopy showed that deletion of the antenna system caused a complete lack of grana, while deletion of specific LHC subgroups caused a 50% decrease in stacking. The Lhcb5 monomeric complex alone partially restored stacking, while the expression of Lhcb2 as the only Photosystem II antenna produced grana stacks with a very large diameter, which broke down upon light-dependent phosphorylation. The growth rate of genotypes was proportional to the level of stacking rather than to the antenna size of photosystem II. Cyclic electron transport was maintained in the lack of stacking, while excitation energy balance between photosystems and the repair efficiency of damaged Photosystem II were affected. We conclude that grana evolved for need of regulating energy balance between photosystems, in conditions typical of terrestrial canopy environment involving rapid changes in photon spectral distribution.

Keywords: chloroplast, thylakoids, grana, stroma membranes, stacking, LHC, LHCII, monomeric antennae, photosystem, photoprotection.

Introduction

The land plant chloroplast contains chlorophylls (Chl) and carotenoids (Car) within its inner membranes called thylakoids, as recognized already by Meyer in 1883 (Gunning et al., 2006). Its most distinctive feature is the organization into grana (Wietrzynski et al., 2020), a feature of land plant species (Heitz, 1936; Kyle et al., 1983; Iwai et al., 2018), which is absent in algae (Vallon et al., 1991). Grana are stacks of round, flattened vesicles (Granick and Porter, 1947) connected by pairs of unstacked membranes, called stromal membranes, intersecting grana at an angle, suggesting a helical arrangement (Paolillo and Reighard, 2011). Freeze-etching electron microscopy (EM) coupled to mutant analysis showed that the photosynthetic pigment-protein complexes of thylakoid membranes are compartimented: photosystem (PS) II particles in the appressed region of the grana (Simpson and Robinson, 1984; Armond and Arntzen, 1977); PSI and ATPase complexes hosted in stromal membranes (Armond et al., 1977; Simpson, 1982). Cytochrome (Cyt) *b*$_6$*f* complex was enriched in stromal domains and grana margins (Olive et al., 1986; Allred and Staehelin, 1985; Vallon et al., 1991). Biochemical and immunocytochemical analysis supported differential compartimentation of PSI and PSII (Anderson and Melis, 1983; Vallon et al., 1991), arguably for preventing excitation energy spillover from PSII to PSI, owing to the low energy chlorophyll spectral forms of plant PSI-LHCI (Murata, 1969). Since photosynthetic electron transport occurs linearly between PSs, the Plastoquinone (PQ) diffusion towards Cyt *b*$_6$*f* is restricted by PSII crowding in grana partitions (Lavergne and Joliot, 1991), thus limiting linear electron flow (LET) rate. Restriction of diffusion also applies to PSII damaged by photoinhibition, which need to reach the stromal domains in order to be repaired (Mattoo et al., 1989). Thus, the size of granal *vs.* stromal domains compromise between the positive effect of ensuring adequate excitation energy to both PSs and the negative effect of restricting PQ diffusion and PSII repair rate. This is consistent with PQ overreduction activating STN-7 and -8 kinases, which phosphorylates, respectively, the trimeric antenna (LHCII) subunits and the PSII core, yielding into reduced granal diameter (Hepworth et al., 2021) and diffusion of LHCII subunits, to PSI-LHCI. This boosts PSI photon cross section and oxidation of plastoquinol (PQH_2) (Kyle et al., 1983) causing kinase inactivation, balancing PSI *vs.* PSII activity (Goldschmidt-Clermont and Bassi, 2015). It was suggested that reduction of grana domains enhances the fraction of Cyt *b*$_6$*f* in stromal membranes and favors the dynamics of cyclic electron flow (CEF) and ATP synthesis to meet the NADPH/ATP ratio required for CO_2 fixation (Kramer and Evans, 2011). In this context it is important to clarify the mechanism of grana stacking. Reverse genetics and EM analysis yielded controversial results: intermittent light grown plants becomes LHCII-deficient and reduces their grana (Armond et al., 1976; Argyroudi-Akoyunoglou et al., 1971); yet, *chlorina f2* mutants, lack Chl *b*, depleted in LHCs and retained extensive grana stacks and photosystem lateral heterogeneity (Bassi et al., 1985; Kim et al., 2009). Grana were also retained in the *viridis115* barley mutants, lacking PSII core complex, and in the double mutant *viridis 115 x chlorina f2* (Simpson et al., 1989), suggesting that neither of the two major thylakoid components located in grana partitions (LHCII and PSII core) was essential for grana stacking. Chloroplasts lacking grana can be found in bundle sheath (BS) cells of maize leaves, with a reduced PSII activity and a low LHCII level (Bassi et al., 1995). Also, LHCII of BS exhibited a simpler polypeptide composition with respect to mesophyll chloroplasts suggesting that specific gene products within

LHC, rather than any member of the family, might be responsible for stacking (Bassi and Simpson, 1986). Here, we proceeded to the reverse genetic analysis of grana stacking by a combination of genome editing (GE) and EM. Previous work showed that PSII core complex-less plants (Campoli et al., 2009; Margulies, 1966; Belgio et al., 2014) enhance stacking, we focused on LHCs: genotypes lacking either monomeric or trimeric LHC gene products or both were produced and analyzed for stacking by transmission EM. In addition, Lhcb2, a minor component of trimeric LHCII, reported to be needed for state 1 - state 2 transitions (Pietrzykowska et al., 2014), was expressed as the only LHC component and found to induce the formation of extensive stacking in dark conditions, which were broken down upon light-induced phosphorylation. Our results show that a major role in thylakoid stacking is played by minority components of the PSII antenna system, namely Lhcb5 (CP26) and Lhcb2, which, respectively, mediate the constitutive and dynamic components of thylakoid stacking, which is required for efficient of PSII repair and balance of excitation energy; instead, it does not significantly change the rate of linear *vs.* cyclic electron transport.

Results

Construction of *Arabidopsis* genotypes with selectively reduced PSII antenna system by GE

The construction of *Arabidopsis thaliana* genotypes affected in LHC protein composition was performed from either the knock-out (ko) line *koLhcb3,* missing the Lhcb3 component of the major LHCII complex, or the *NoM koLhcb3* genotype, devoid of the *Lhcb4-6* genes encoding monomeric LHCs: Lhcb4 (CP29), CP26 and Lhcb6 (CP24) (Dall'Osto et al., 2017), as well as Lhcb3 (Supplementary Figure S4.1.1-A). To obtain the Lhcb-free genotype, CRISPR-Cas9 targeted mutagenesis strategy was implemented according to (Ordon et al., 2020): for each of the 5 *Lhcb1* and 3 *Lhcb2* genes, pairs of sg (single guide) RNAs were designed within coding sequences (Supplementary Figure S4.1.2, Table S4.1.1), with the aim of producing large DNA deletions, favoring DNA repair by non-homologous end-joining (NHEJ) (Malzahn et al., 2017). *Lhcb1* and *lhcb2* genes were separately targeted to get Lhcb1-less and Lhcb2-less plants, which were then crossed to obtain lines lacking both Lhcb1 and Lhcb2 proteins. We obtained either the *koLHCII* line (lacking all LHCII but retaining monomeric Lhcb4-6 proteins), or the *koLhcb* line, lacking both the monomeric and trimeric LHCs of PSII, by applying this procedure on *koLhcb3* or *NoM koLhcb3* genotypes. In both cases LHCI proteins were unaffected. The *low-LHCII* genotype was selected for the level of residual LHCII among the products of incomplete gene editing of both *Lhcb1* and *Lhcb2*: the two selected lines contain one LHCII trimer per monomeric PSII core complex (Supplementary Table S4.1.2). *NoM koLhcb1 koLhcb3* lines (*Lhcb2-only*) retained Lhcb2 as the unique PSII antenna (Supplementary Figure S4.1.1B, S4.1.2A).

Growth and pigment composition of LHC-depleted plants

Plants are shown in Figure 4.1.1A upon growth under light-limiting (LL) conditions (150 μmol photons m^{-2} s^{-1}, 8/16 h photoperiod, 24 °C). Wild type showed the best growth. *NoM* and the two *koLHCII* lines accumulated between 45% and 50% with respect to the wild type; while the growth of *koLhcb* was far more reduced: the two independent lines grew less than 3% with respect to the wild type based on fresh weight (FW) (Figure 4.1.1B). The Chls content per leaf surface behaved similar to the growth pattern although changes were far smaller: *NoM* showed 25% less Chl *vs.* the wild type, while *koLhcb* lines about 50% Chls when compared to *koLHCII* and 25% with respect to the wild type, implying the growth rate per pigment unit was higher in the presence of monomeric antenna proteins (Figure 4.1.1C). The pigment composition of the different genotypes reflected the abundance of their pigment-protein complexes. Thus, Chl *a*/*b* ratio was the lowest in *NoM* (3.28 vs 3.51 in the wild type), the highest in *koLhcb* (6.21) and intermediate in *koLHCII* (5.19), consistent with the lower Chl *b* content of monomeric Lhcbs vs LHCII (Table 4.1.1). LHCI complexes, unaffected in our genotypes, accounted for the residual Chl *b* content in *koLhcb*. The Chl/Car ratio ranged from 3.0 to 3.7 depending on LHC content (Table 4.1.1). β-carotene doubled in *koLhcb* with respect to the LHCII-rich wild type and *NoM* (Supplementary Table S4.1.3). *koLHCII* and *koLhcb* decreased Neoxanthin content by 60% and 80%, with a concomitant increase in Violaxanthin, owing to the preferential location of Neoxanthin in trimeric LHCII and its absence in PSI-LHCI complexes (Schiphorst and Bassi, 2020).

The major differences in growth between mutants might be due to either the large differences in PSII antenna size, thus limiting photon harvesting, and/or to defects in the electron transport chain induced by changes in the organization of the thylakoid membranes. We thus proceeded to grow plants at higher irradiance, to compensate for antenna size limitation, yet avoiding excess irradiation to circumvent photodamage. Figure 4.1.1D shows wild type and LHC mutant genotypes grown at moderately high light (HL, 350 μmol photons m^{-2} s^{-1}, 8/16 h photoperiod, 24°C). *NoM* and *koLHCII* grew similarly while *koLhcb* was far slower and grew as in control light light (150 μmol photons m^{-2} s^{-1}) (Figure 4.1.1B, D). Thus, enhancing irradiance did not complement for the decreased growth phenotype under LL conditions and, in some cases, made it even stronger. Thus, insufficient photon harvesting was unlikely the major cause of the differences in growth. Also, none of the lines were obviously photodamaged, or died at 350 μmol photons m^{-2} s^{-1}, suggesting that photoprotection was not dramatically reduced.

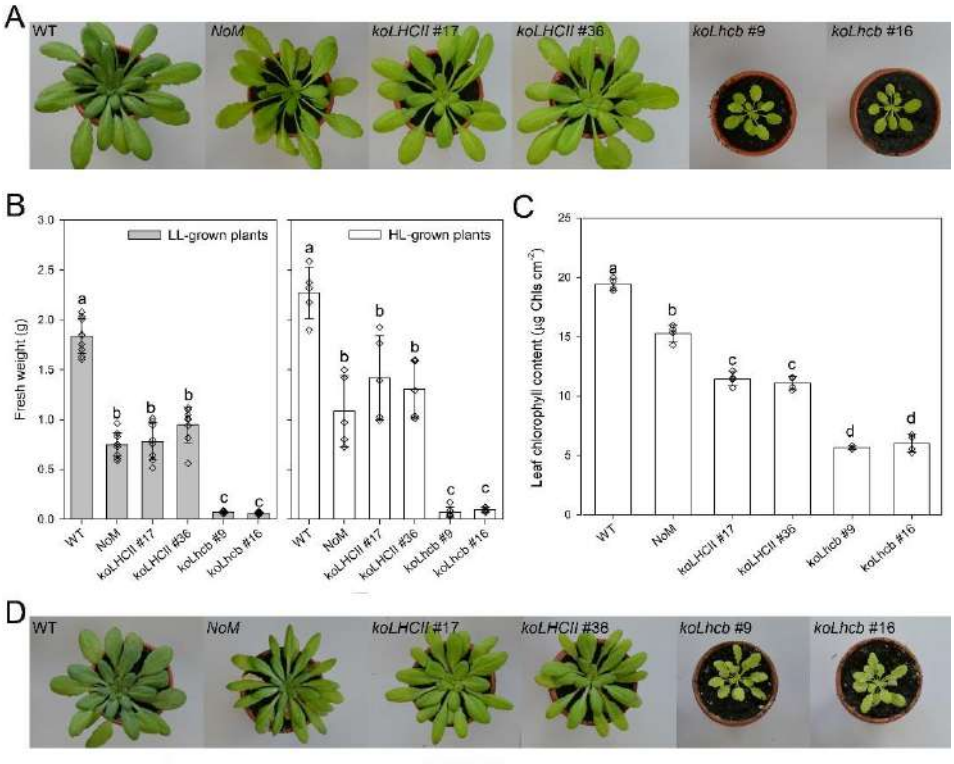

Figure 4.1.1. Phenotype of wild type and mutant plants. (A) *Plants were grown for 6 weeks at 150 µmol photons m^{-2} s^{-1}, 23 °C, 8/16 h light/dark (LL).* ***(B)*** *The fresh weight of all. Values are expressed as mean ± SD. [n = 9 (wild type, koLhcb #9, koLhcb #16), 10 (NoM), 8 (koLHCII #17, koLHCII #36)].* ***(C)*** *Leaf Chl content. koLhcb lines retained only 25% of Chl per area, while NoM and koLHCII retained 75% and 50%, respectively. Values are expressed as mean ± SD, n=4.* ***(D)*** *Plant growth for 6 weeks at 350 µmol photons m^{-2} s^{-1}, 23 °C, 8/16 h light/dark (HL). Values are expressed as mean ± SD. [n = 5 (wild type, NoM, koLHCII #17, koLHCII #36, koLhcb #16), 6 (koLhcb #9)]. NoM and koLHCII showed similar growth while koLhcb lines were much smaller, alike in control light (panel B). Leaf Chl content relative to the wild type remained essentially the same in LL vs HL (panel C). Values that are significantly different from the corresponding wild type (ANOVA followed by Tukey's post-hoc test at a significance level of $P < 0.05$) are marked with different letters. Experiments were repeated independently twice, with similar results.*

Table 4.1.1. Pigment content and fluorescence induction parameters determined for leaves of Arabidopsis WT and mutant lines. *At least five different plants were tested for each line. Chl/Car, molar ratio between chlorophylls (a + b) and carotenoids. Fresh weight refers to growth after 6 weeks under control conditions. Data are expressed as mean ± SD, n = 6 biologically independent leaves. Values marked with different letters are significantly different from each other within the column (ANOVA, followed by Tukey's post-hoc test at a significance level of P < 0.05). Experiments were repeated independently twice, with similar results.*

	Chl *a* / *b*	Chl / Car	µg Chl cm^{-2}	F_v / F_m
WT	3.51 ± 0.09^{a}	3.69 ± 0.21^{a}	19.4 ± 0.5^{a}	0.82 ± 0.01^{a}
npq4	3.40 ± 0.02^{a}	3.66 ± 0.13^{a}	21.1 ± 1.4^{a}	0.82 ± 0.01^{a}
NoM	3.28 ± 0.05^{a}	$3.45 \pm 0.09^{a,b}$	15.3 ± 0.74^{b}	0.61 ± 0.01^{b}
koLHCII #17	5.23 ± 0.11^{b}	3.37 ± 0.06^{b}	11.46 ± 0.55^{c}	0.76 ± 0.01^{c}
koLHCII #36	5.15 ± 0.10^{b}	3.34 ± 0.02^{b}	11.03 ± 0.58^{c}	0.76 ± 0.01^{c}
koLhcb #9	6.28 ± 0.15^{c}	3.12 ± 0.05^{c}	5.68 ± 0.15^{d}	0.50 ± 0.02^{e}
koLhcb #16	6.14 ± 0.22^{c}	3.09 ± 0.08^{c}	6.10 ± 0.76^{d}	0.54 ± 0.03^{e}
ch1	-	2.77 ± 0.02^{c}	6.55 ± 0.54^{d}	0.78 ± 0.01^{c}
ch1 koLhcb5	-	2.57 ± 0.02^{c}	4.50 ± 0.23^{e}	0.67 ± 0.01^{d}
lowLHCII #14	4.01 ± 0.22^{d}	3.01 ± 0.06^{b}	7.24 ± 0.87^{c}	0.52 ± 0.05^{e}
lowLHCII #32	$4.71 \pm 0.39^{b,d}$	2.98 ± 0.03^{b}	7.58 ± 1.01^{c}	0.55 ± 0.05^{e}
Lhcb2-only	3.96 ± 0.16^{e}	3.18 ± 0.11^{b}	9.77 ± 1.82^{c}	0.51 ± 0.02^{e}

Pigment-protein complexes and photosynthetic function in antenna mutants

The actual pigment-protein content of the genotypes as well as their supramolecular organization was investigated by non-denaturing Deriphat-PAGE upon solubilization with low (0,8%) α-DM. Consistent with previous reports (Dall'Osto et al., 2014c, 2017), the *NoM* genotype was depleted in PSII supercomplexes and over-accumulated the major trimeric antenna LHCII (Figure 4.1.2A). The trimeric LHCII band was completely absent in both *koLHCII* and *koLhcb* genotypes. These were also depleted of high molecular weight (MW) supercomplexes except for two bands migrating just above PSI-LHCI (BD1 and BD2). A faint green band (BD3) was detected migrating slightly below trimeric LHCII in both *koLHCII* and *koLhcb*, while a fourth band (BD4) was detected in both *koLHCII* and *koLhcb*, migrating alike the monomeric Lhcbs (Figure 4.1.2A). Biochemical and spectroscopical analyses revealed BD1 and BD2 being composed of PSI-LHCI complexes with different LHC complements, BD3 contained dimeric LHCI subunits, BD4 comprised monomeric Lhcbs in *koLHCII* and monomeric LHCIs in *koLhcb* (Supplementary Figure S4.1.3).

The functional antenna size of PSII from Chl fluorescence rise time in DCMU-treated leaves showed that *NoM* had nearly twice the capacity for PSII photon harvesting, compared to wild type, while *koLHCII* and *koLhcb* antenna size, scored 30% and 45% respectively, *vs.* the wild type (Figure 4.1.2B). The maximum quantum yield of photochemistry scored very high, i.e. 0.82 and

0.76 respectively, for wild type and *koLHCII*. Instead, *NoM* and *koLhcb* scored far lower: 0.62 and 0.51 respectively (Figure 4.1.2C).

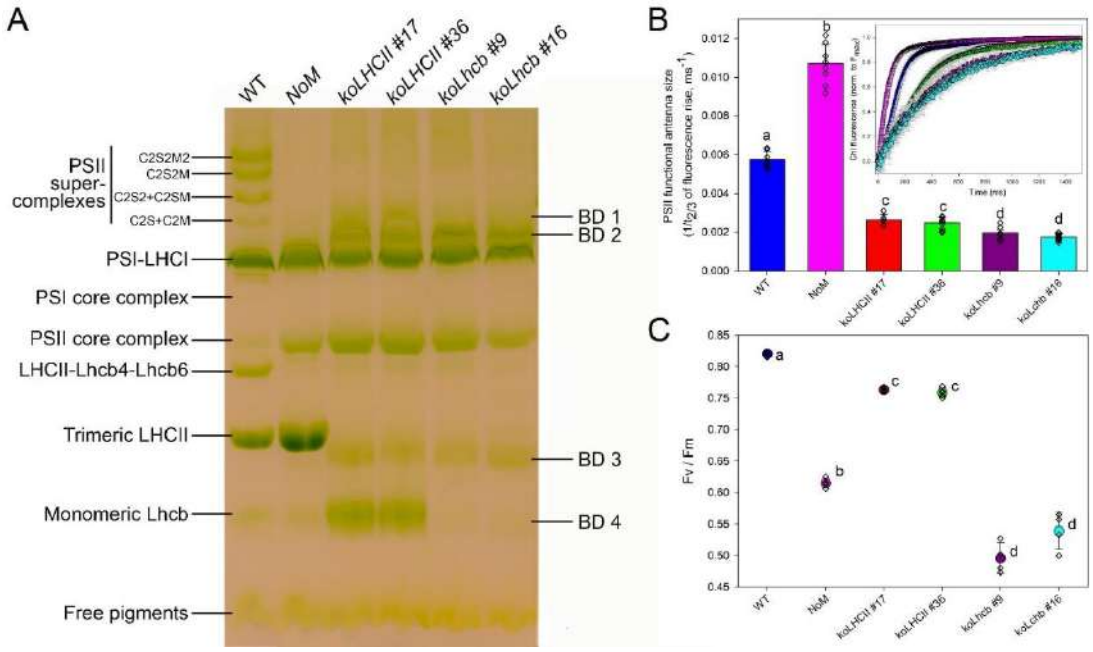

Figure 4.2.2. Biochemical and functional characterization of the photosynthetic apparatus of wild type and mutant plants. (A) *Non-denaturing Deriphat-PAGE of thylakoids upon solubilization with 0.8% α-DM, revealing pigment-protein complexes of wild type, NoM, koLHCII and koLhcb lines. Thylakoid proteins corresponding 20-35 μg of Chls were loaded in each lane. The composition of major bands is indicated based on previous reports, while that of bands BD1-BD4 was determined from absorption spectra and SDS-PAGE (Supplementary Figure S4.1.2).* ***(B)*** *PSII functional antenna size of wild type and mutants, measured at RT on leaves vacuum-infiltrated with 50 μM DCMU. The reciprocal of time corresponding to two-thirds of the fluorescence rise ($t_{2/3}^{-1}$) was taken as a measure of the PSII functional antenna size. Plants were dark-adapted for 30 min before measurements. Data are expressed as mean ± SD. [n = 7 (wild type, koLHCII #17, koLhcb #9), 9 (NoM), 10 (koLHCII #36), 8 (koLhcb #16)]. Values marked with different letters are significantly different from each other (ANOVA followed by Tukey's post-hoc test at a significance level of P < 0.05).* ***(C)*** *PSII maximal quantum yield (F_v/F_m) of wild type, NoM, koLHCII and koLhcb lines, measured on dark adapted leaves. Symbols and error bars show means ± SD . [n = 4 (wild type, koLhcb #9, koLhcb #16), 5 (NoM), 6 (koLHCII #17), 5 (koLHCII #36)]. Values that are significantly different (ANOVA followed by Tukey's post-hoc test at a significance level of P < 0.05) are marked with different letters. Experiments were repeated independently twice, with similar results.*

Thylakoid membranes organization

Antenna proteins of PSII are the most abundant components of thylakoid membranes, implying membrane organization could be affected in LHC-less genotypes. The trimeric LHCII complex has been proposed as the major determinant of grana stacking (Standfuss et al., 2005), domain segregation, and the basis for multiple regulation and biogenetic mechanisms essential in the challenging terrestrial environment, such as PSII repair cycle and state 1 - state 2 transitions. To verify the effect of LHCII abundance in the different genotypes, we have analyzed the extent of grana stacks by transmission EM (Figure 4.1.3A-G). All genotypes had chloroplasts with the same size in ultrathin sections (Figure 4.1.3H). Grana stacks were defined as made of at least three thylakoid appressions; the stacks diameter was approx. 450 nm and was found to be very similar between genotypes, only *NoM* showed a slightly larger grana diameter of approximately 550 nm (Figure 4.1.3I). However, see below for the special case of the *Lhcb2-only* genotype.

Grana were quantified by measuring the surface of membrane stacks *vs.* chloroplast area (Figure 4.1.3K). Wild type chloroplasts had about 18% of their section area occupied by grana, a value that was reduced to 11% in *koLHCII* and *NoM*. *koLhcb* was fully depleted grana stacks (<1% of stacked area, Figure 4.1.3K), while partial depletion of LHCII in the *lowLHCII* genotype yielded only a small recovery to 3%. We noticed that *koLHCII* retained more than 50% of its stacking ability, similar to *NoM* (Figure 4.1.3K), even though these two genotypes display highly diverse content in LHCs: *koLHCII* has 3 monomeric LHCs per PSII core, while *NoM* has 18, in form LHCII trimers per PSII core (this corresponds to 60% more respect to WT) (Dall'Osto et al., 2017). The stacking efficiency for a single LHC monomeric unit, is thus 6 times higher for monomeric LHCs respect to trimeric LHCII. When comparing *koLHCII* to *lowLHCII,* having the same LHC/PSII core stoichiometry monomers are 3 time more efficient in stacking. In all cases the number of events analyzed was statistically significant except for the case of *koLhcb*, because most of the chloroplasts did not contain any stacks (Figure 4.1.3J).

Possibly, one of the clearest effects on grana stacking in previous research was obtained by controlling the expression of CURT genes (Heinz et al., 2016). Supplementary Figure S4.1.4 shows that no major differences were observed in the abundance of CURT, suggesting LHCII abundance/composition controlled stacking independently form CURT, or LHCII was needed for CURT activity.

To identify whether a specific subunit, among monomeric LHCs, had a special role in stacking, we analyzed the *ch1* genotype devoid of CAO (Chl *a* oxygenase), which is known for a strongly reduced antenna size (Kim et al., 2009) because Lhcb proteins are destabilized in lack of Chl *b*. CP26, however, is particularly promiscuous for Chl *a vs.* Chl *b* binding (Croce et al., 2002a) and is retained and functional in *ch1* genotype (Havaux et al., 2007). Grana stacking in *ch1* and *ch1 koLhcb5* mutants (Figure 4.1.3F-G) showed that *ch1* had similar stacking as the *koLHCII* genotype (Figure 4.1.3K), suggesting that whatever induced stacking in *koLHCII* was still present in *ch1.* Instead, stacking was drastically reduced in the *ch1 koLhcb5* genotype (Figure 4.1.3G,K), implying that CP26, among monomeric LHCs, had a prominent function on grana formation. Again, the

chloroplast area and the diameter of grana in sections were very similar in *ch1* and *ch1 koLhcb5* genotypes with respect to the wild type and *koLHCII* (Figure 4.1.3H,I).

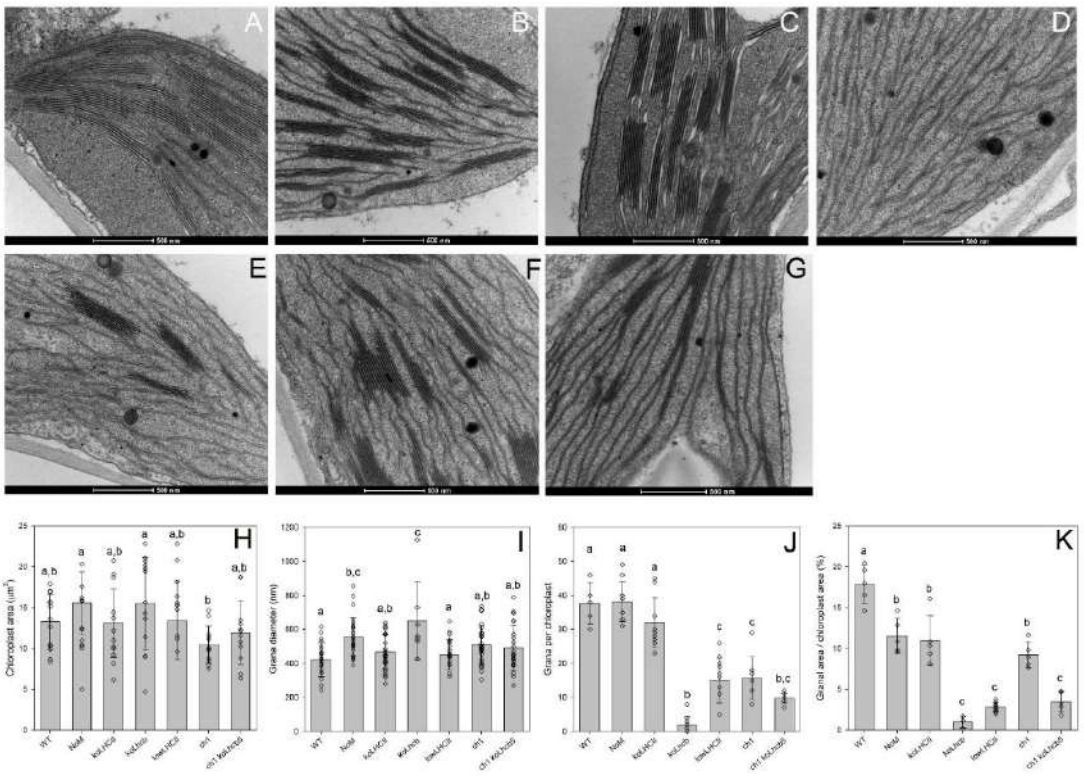

Figure 4.1.3. Transmission electron micrographs of plastids from leaf mesophyll cells of wild type and mutant lines. (A-D) *Plants grown in short-day conditions were dark-adapted for 2 hours before harvesting leaves, then samples were fixed, embedded, and observed in thin sections at different levels of magnification. Wild type (A), NoM (B) and koLHCII (C) showed a characteristic organization of stroma lamellae interconnecting grana, while the chloroplasts of koLhcb (D) lacked grana.* ***(E-G)*** *Micrograph of lowLHCII (E), ch1 (F) and ch1 koLhcb5 (G) chloroplasts.* ***(H-K)*** *Statistical analysis of the extent of the thylakoid stacking in the wild type, LHC KO lines and Chl b-less mutants ch1 and ch1 koLhcb5. Histograms report: (H) chloroplast area [n = 13 (wild type, koLhcb), 12 (NoM, koLHCII, lowLHCII, ch1, ch1 koLhcb5)]; (I) grana diameter [n = 22 (wild type, lowLHCII), 27 (NoM), 26 (koLHCII), 7 (koLhcb), 25 (ch1), 23 (ch1 koLhcb5)]; (J) grana per chloroplast [n = 5 (wild type), 10 (NoM, koLHCII, koLhcb, ch1 koLhcb5), 14 (lowLHCII), 8 (ch1),]; (K) granal area vs. chloroplast area [(n = 5 (wild type, NoM, koLHCII, ch1, ch1 koLhcb5), 3 (koLhcb), 12 (lowLHCII)]. Data are shown as mean ± SD. Values that are significantly different (ANOVA followed by Tukey's post hoc test at a significance level of P < 0.05) are marked with different letters. Experiments were repeated independently twice, with similar results.*

Lhcb2 controls changes in grana stacking during State 1 - State 2 transitions

Arabidopsis lines depleted on Lhcb2 proteins lacked state 1 - state 2 transitions (Pietrzykowska et al., 2014). The GE of *Lhcb1* in the *NoM koLhcb3* background (Supplementary Figure S4.1.1) produced a genotype retaining Lhcb2 as the only PSII antenna (Ordon et al., 2020). Wild type and mutant genotypes analyzed above showed grana diameters between 400 and 550 nm (Figure 4.1.3I) (Kirchhoff, 2019). Despite having a similar PSII-core/LHCII ratio (Supplementary Figure S4.1.1), the *Lhcb2-only* plants were striking different with respect to the *lowLHCII* lines because they showed a few, yet much larger, grana with a diameter up to 3 μm or even more (Figure 4.1.4A-C), spanning the chloroplast sections. We then proceeded to verify whether light exposure did affect thylakoid stacking. Dark-adapted leaves were illuminated with PSII light (200 μmol photons m^{-2} s^{-1}, 24°C, 60 min) to promote PQ over-reduction despite the small PSII antenna size of both *Lhcb2-only* and *lowLHCII* genotypes, thus Lhcb2 phosphorylation (Figure 4.1.4D). In *Lhcb2-only* chloroplasts large grana essentially broke down upon illumination, and the size distribution extended towards narrower diameters. In both *Lhcb2-only* and *lowLHCII* lines, grana length and level of stacking were significantly reduced by state 2 induction (Figure 4.1.4E-F).

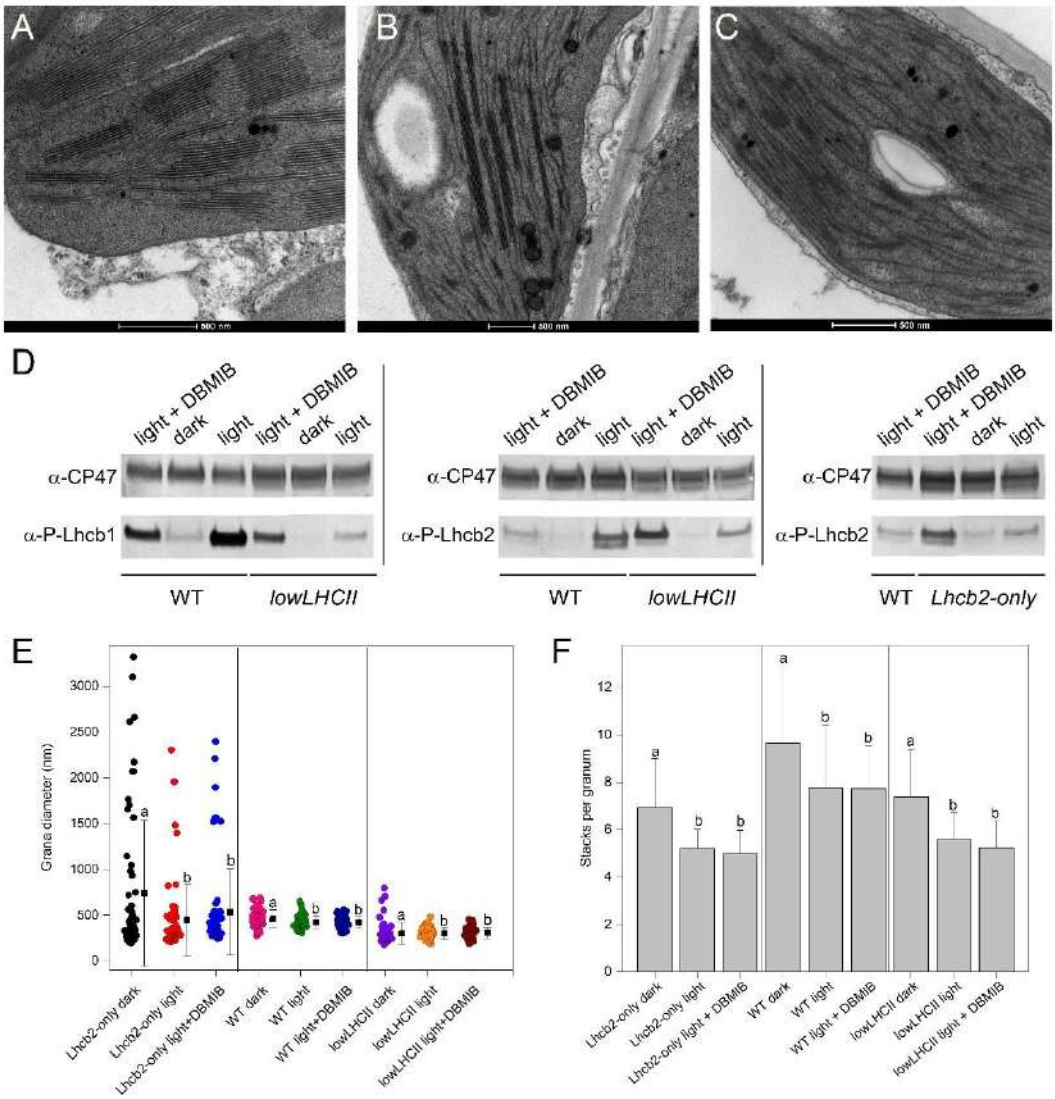

Figure 4.1.4. Changes in chloroplast ultrastructure of state 1- and state 2-adapted leaves. (A-C) *Leaves from wild type (A), Lhcb2-only (B) and lowLHCII (C) plants were subjected to 60 minutes of PSII light (200 μmol photons m^{-2} s^{-1}) to promote LHCII phosphorylation and transition to state 2. Reference samples included leaves either dark-adapted for 1 hours or exposed to PSII light upon vacuum-infiltration with 100 μM DBMIB to maximize PQ reduction thus LHCII phosphorylation. Leaf discs were then fixed, embedded, and observed in thin sections.* ***(D)*** *Leaf discs from the same treatments were snap frozen, then the phosphorylation level of Lhcb1/Lhcb2 was quantified by immunotitration, using α-Lhcb1-P and α-Lhcb2-P primary antibodies. Proteins corresponding to 0.8 μg of Chls (wild type sample) or 2.4 μg of Chls (mutant samples) were loaded for each sample. All samples were loaded on the same SDS-PAGE slab gel.* ***(E)*** *Statistical analysis of differences in grana diameter, in state 1 and state 2 [n = 60 (Lhcb2-only), 55 (wild type), 58 (lowLHCII)].* ***(F)*** *Statistical analysis of the average number of layers in grana stacks, in state 1 and state 2 (n = 30). Data (E, F) are expressed as mean ± SD. Values that are significantly different (ANOVA followed by Tukey's post-hoc test at a significance level of $P < 0.05$) are marked with different letters. Experiments were repeated independently twice, with similar results.*

Physiological consequences of thylakoid stacking for photosynthesis

Chloroplasts of unicellular algae do not show well-defined grana stacks, while cyanobacteria exhibit single membranes, showing that oxygenic photosynthesis can proceed without the need of thylakoid stacking (Mullineaux, 2005). Nevertheless, consequences of decreased level of stacking are clear from Figures 4.1.1 and 4.1.3: growth correlates well with the level of stacking, with the wild type showing both the maximal level of membrane stacking and the best growth. *NoM* and *koLHCII* exhibited intermediate level of both biomass yield and thylakoid stacking, while *koLhcb* had no grana and was severely impaired in growth. The functional reason(s) for the growth phenotype are unclear. Grana stacking has been suggested to affect (1) the repair of damaged PSII (Pribil et al., 2014; Mullineaux and Emlyn-Jones, 2005; Koochak et al., 2019; Hepworth et al., 2021) (2) the switch between CEF and LEF and/or (3) light-harvesting. We proceeded to evaluate whether the PSII repair rate was affected by thylakoid stacking. To this aim, leaves were treated with excess light to induce photoinhibition, as detected by F_v/F_m ratio, which was reduced to about 30% of initial values in all genotypes. The recovery of F_v/F_m was then followed under low light conditions (15 μmol photons m^{-2} s^{-1}, 24°C) favoring the PSII repair process (Mattoo et al., 1999). The results are shown in Figure 4.1.5A. Clearly, the wild type and *koLHCII* genotypes showed the same rate of PSII recovery. A similar dataset was published previously for the *NoM* genotype (Dall'Osto et al., 2020), showing no difference in the kinetic of recovery with respect to wild type plants. Instead, *koLhcb* healed its PSII activity to a much lower extent, suggesting that lateral heterogeneity between fully functional PSII in grana and PSII under repair in stroma-exposed margins might be necessary for a fully functional PSII repair cycle.
We then verified whether the different level of thylakoid stacking did affect regulation of LEF *vs.* CEF amplitudes.
We then measured Chl fluorescence and the kinetic of electrochromic shift (ECS) on leaves, as a measure of electrons and protons transfer in the photosynthetic apparatus, respectively (Figure 4.1.5B). The quantum yield of PSII photochemistry can be used to measure the electron released from PSII (LEF) in leaves under a different light. ECS kinetics can be used to estimate fluxes of protons through the thylakoids, upon steady-state actinic illumination (Cruz et al., 2005): ECS_t, the total amplitude of the ECS signal upon light-dark transition, measures the light-driven protonmotive force (pmf) across the membrane, while the ECS decay lifetime (gH^+) assesses the conductivity of the thylakoid ATPase to proton efflux. Under steady-state photosynthetic electron transport, the pmf produced by LEF alone can be estimated by the LEF/gH^+ ratio, a parameter termed pmfLEF (Avenson et al., 2005). It turned out that the slope of the linear relationship of pmfLEF *vs.* ECS_t was proportional to the stoichiometry of electron *vs*. proton transfer. Figure 4.1.5B shows that wild type and mutant plants produced approximately the same extent of pmf that can be accounted for by LEF only, thus suggesting a similar CEF amplitude in all genotypes.

Finally, the function of grana stacks, as for light-harvesting, consists in avoiding spill-over of excitons harvested by PSII-LHCII towards PSI-LHCI, which would unbalance the electron transport rate in favor of PSI and is obtained by partitioning PSI-LHCI and PSII-LHCII into two different domains of thylakoids. The F_m/F_0 ratio has been shown to be strongly reduced with respect to the high value of 5.56 observed in WT in the presence of spill-over of excitation energy

from PSII to PSI antenna systems. Indeed, genotypes with reduced grana stack scored far lower, with values of 2,0 in grana-less *koLhcb* (Table S4.1.4), closely reproducing the case of *Mantoniella squamata*, undergoing massive spill-over of PSII excitation energy to PSI (Wilhelm et al., 1989).

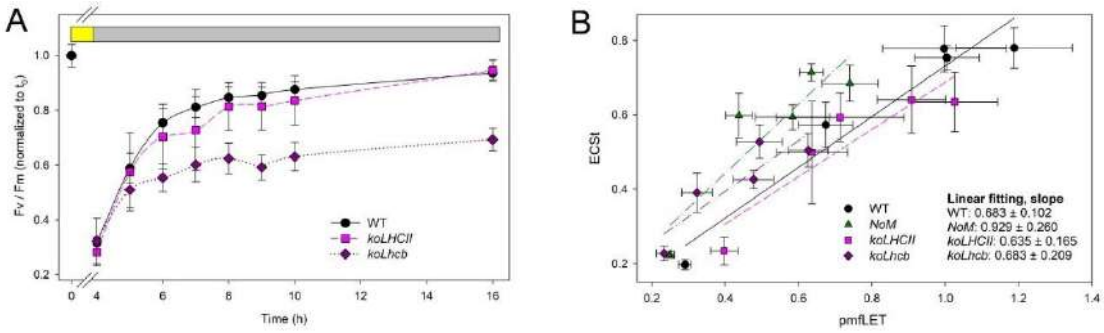

Figure 4.1.5. Biophysical characterization of the mechanisms regulating energy transduction reactions in thylakoids. (A) *PSII repair efficiency. Detached leaves were exposed to EL for 3 hours (wild type, 1100 µmol photons m^{-2} s^{-1}; koLHCII, 900 µmol photons m^{-2} s^{-1}; koLhcb, 750 µmol photons m^{-2} s^{-1} – yellow bar) at 4°C, to reduce PSII maximal quantum yield (F_v/F_m) to about 30% of the initial value. Recovery of F_v/F_m was performed at 15 µmol photons m^{-2} s^{-1}, 24°C (gray bar). koLhcb line showed a slower PSII repair kinetic compared to both wild type and koLHCII. Values are expressed as mean ± SD, n = 5.* ***(B)*** *Relationship between pmfLET and ECSt in wild type and mutant lines upon steady state illumination. All genotypes showed similar amplitude of total ECS as a function of LET, thus suggesting a similar amplitude of CEF. Values are expressed as mean ± SD, n = 4. Experiments were repeated independently twice, with similar results.*

Discussion

Grana stacks are the most conspicuous feature of plant chloroplasts, which attracted the attention of Mayer since 1883, when they were first reported (Gunning et al., 2006). The reasons for this interest is that grana are found in land plant, but are absent in algal chloroplast which, despite the obviously common function of chloroplasts through the species, do not have this highly structured multiple membrane layers, yet maintain differentiation between stacked and unstacked membrane domains (Trissl and Wilhelm, 1993).

The deletion of either the inner layer (monomeric), or the outer layer (trimeric) antenna complexes, or both, had a strong impact on growth rate which was maximal with depletion of monomeric antennas, while the deletion of trimeric LHCII, although causing a moderate decrease in growth, did not affect biomass accumulation as much as it could be predicted by the difference in antenna size (Figure 4.1.1A, B). This is particularly evident when comparing the *NoM* with the wild type: since *NoM* strongly over-accumulates LHCII, the antenna size of its PSII, as determined by fluorescence induction with DCMU, is larger than in wild type and yet its growth is decreased by 50% (Figure 4.1.2B). We conclude that monomeric LHCs have an essential role in the efficiency of excitation energy transfer from outer antenna to RC of PSII, consistent with the high F_0 values

previously reported for the *NoM* (Dall'Osto et al., 2014c). The higher-than-wild type PSII antenna size in *NoM* is at odd with its reduced growth, implying that factors other than ET to PSII RC are involved in growth retardation. The stronger loss of growth is observed in the absence of both antenna types. Growth retardation does not appear to be due to enhanced photodamage, because increasing photon fluence by a factor of three (Figure 4.1.1B, D) did not impair the growth rate of all the genotypes. The *koLhcb* plants, although not increasing their growth rate in HL, do not undergo photobleaching, implying growth was independent on light intensity and yet photoprotection is not crucial in growth retardation. It should be noted that the strongest gain in growth when comparing HL *vs*. LL was obtained in the *koLHCII* plants which retained monomeric LHCs (+80%), suggesting that these complexes are those best related to light use efficiency. The decrease in antenna size of the different phenotypes was associated to a higher PSII/PSI ratio (Figure 4.1.2A), a partial compensation for the reduced antenna size of PSII. Indeed, an enhanced PSII *vs*. PSI content and a low F_m/F_0 ratio has been observed in the alga *Mantoniella squamata* that lacks grana stacks and thylakoid lateral heterogeneity because of a simplified antenna system composed of a single LHCII-like protein (Rhiel and Mörschel, 1993), which is shared by PSI and PSII RCs, leading to spill-over of PSII excitation energy by PSI (Wilhelm et al., 1989). It has been reported that the extensive destacking of thylakoid membranes in the evergreen conifer, *Pinus sylvestris*, which is inferred to cause direct PSII-PSI interaction upon mixing thylakoid domains, allows for direct energy transfer from PSII to PSI, thus conferring photoprotection under high irradiance and low temperature. This effect was proposed to be a major component of the so-called "sustained quenching" mechanism enabling evergreen to stand winter conditions (Bag et al., 2020).

Based on evidence from basic photosynthetic parameters and the lesson from comparative analysis of thylakoid lateral heterogeneity in *Mantoniella*, *Pleurochloris*, *Chlorella* and higher plants (Trissl and Wilhelm, 1993; Bag et al., 2020), it could be hypothesized that by knocking out LHC genes we had both decreased the PSII antenna size and reduced the lateral heterogeneity between PSI and PSII, likely by causing de-stacking of thylakoid membranes.

Thylakoid stacking. Indeed, the EM analysis confirmed that the growth rate correlated to the extent of thylakoid stacking (Figure 4.1.3K), which was decreased by 30% in both *NoM* and *koLHCII* plants, implying that components of both monomeric and trimeric LHC proteins were involved in stabilizing grana partitions. The deletion of both PSII antenna types has a tremendous effect, in that only agranal chloroplasts were detected (Fig. 4.1.3D). The relevance of monomeric vs trimeric LHCs in eliciting grana stacking could be assessed by comparing the *lowLHCII* genotype, containing mostly Lhcb1 with little Lhcb2 gene products, with the *koLHCII*, retaining monomeric complexes endowed with the same total LHC antenna cmplement. Since the *lowLHCII* plants had approximatively 18% stacking as compared to the genotype retaining the three monomeric complexes (*koLHCII*), we conclude that the efficiency of monomeric antennas in causing stacking was 5-6 times higher with respect to trimeric LHCII. The analysis of chlorophyll b-less genotypes allowed to sort out which one, among the three inner antennae was critical for stacking. We took advantage of the early observation that the *ch1* mutant, in which a lack of Chl *b* de-stabilizes LHCs, retained a substantial level of stacking which closely matched the level found in *koLHCII* (Figure 4.1.3K) (Bassi et al., 1985). Loss of Chl *b* prevented accumulation of all

LHC proteins; yet, CP26 was retained (Havaux et al., 2004) because CP26 can bind Chl *a* at most of its Chl *b* binding sites (Croce et al., 2002a). When the *ch1 koLhcb5* double mutant was analyzed for thylakoid stacking, indeed, showed a sharp decrease (Figure 4.1.3J), implying that CP26 was a major determinant of grana formation. Last input, but not less impressive, was provided by the stacking phenotype of *Lhcb2-only* plants. Lhcb2 is present at low levels in thylakoids as compared to Lhcb1 and yet it was shown to be essential for state 1 - state 2 transitions (Pietrzykowska et al., 2014). State 1 - state 2 transitions caused thylakoid de-stacking upon phosphorylation-dependent migration of LHCII trimers, containing both Lhcb1 and Lhcb2, from grana to stroma membranes (Bassi et al., 1989; Hepworth et al., 2021). The huge grana stacks, far wider than in the wild type, evidenced in *Lhcb2-only* genotype (Fig. 4.1.4B) imply that Lhcb2 is prominent in mediating membrane appression into grana partitions. This was confirmed by the effect of inducing Lhcb2 phosphorylation with PSII light treatment (Figure 4.1.4D). Lhcb2 phosphorylation dramatically reduced the number of grana as well as their size (Figure 4.1.4B, C, E). We suggest that the grana remaining upon light treatment are promoted by un-phosphorylated LHCII. In a recent study (Albanese et al., 2020), the formation of dimeric PSII supercomplexes connected by their stromal side was studied as a proxy for thylakoid stacking, by cross-linking and proteomic analysis. Consistent with our finding, both the monomeric and the trimeric antenna were suggested to mediate the interaction between PSII supercomplexes. Nevertheless, the identity of the key gene products identified in that study (i.e. Lhcb1 and CP29) did not match our *in vivo* analysis. Although Lhcb1 and CP29 might well contribute to stacking, the genetic evidence shown here suggests that the major player in determining stacking and its regulation through phosphorylation are, indeed, the CP26 and the Lhcb2 components of the LHCII trimeric antenna. This difference in attribution might be ascribed to the use of the purified dimeric PSII supercomplex fraction which, although reminiscent of face-to-face stacking, it might represent a PSII population resistant to detergent treatment yet not fully representative of the general PSII organization in grana partitions. Indeed, the same research group has recently reported on alternative organization forms of the face-to-face dimeric complexes (Grinzato et al., 2020) and a recent high resolution study has identified two distinct conformations of the PSII C_2S_2 complex, one of which is consistent with grana stacking being stabilized by interactions between CP26 and a LHCII subunit (Caspy et al., 2021). Alternatively, the differences with respect to our reports might well be ascribed to the *in vivo vs. in vitro* analysis: accessibility of the cross-linkers to individual LHC complexes might not correspond to the strength of interactions they elicit as thylakoid stacking determinants (Crepin & Caffarri, 2018).

Functional significance of the granal stacking. In C3 plants and most green algae, the two PSs are well separated, making the possibility of exciton spilling from PSII antenna in a granal partition to PSI antenna pigments in the stroma-lamellae, rather small (Kirchhoff et al., 2007). This structural arrangement has the advantage of increasing the concentration of PSII, which is kinetically slower, by packing it densely in grana partitions and increasing the cooperativity between PSII RC beyond the obvious level of 2 defined by the dimeric organization of supercomplexes (Lavergne and Joliot, 1991; Lavergne and Trissl, 1995). The high PSII/PSI stoichiometry ratio and high F_m/F_0 ratio are in agreement with such good excitonic separation, which require state 1 - state 2 transitions in order to balance the turnover-rate when light is not

equally absorbed by the two PSs (Miller and Lyon, 1985). Moreover, the requirement for the CBB cycle and other metabolic uses of ATP/NADPH from the light phase of photosynthesis, is variable. Indeed, changes in CET *vs.* LET rates have been proposed to depend on state transitions and their effect in modulating the ratio between grana and stroma membranes (Hepworth et al., 2021). Finally, PSII is found in its fully functional state in grana partitions, while its repair process upon photoinhibition occurs in stroma membranes, where the machinery for disassembly of PSII core complex is located.

Physiological analysis in dependence of the extent of grana stacking showed that the efficiency of PSII repair process, i.e. the kinetic of recovery from photoinhibition, was severely affected in *koLhcb* as compared to *koLHCII* (Figure 4.1.5A). This effect could be due to the lack of monomeric LHCs in the former genotype or to the lack of grana. We favor the second hypothesis because the *NoM* genotype, although lacking monomeric LHCs, like *koLhcb*, shows recovery kinetic from photoinhibition as in the wild type (Dall'Osto et al., 2020). Instead, we did not observe any major differences in CET *vs.* LET depending on the level of grana stacking (Figure 4.1.5B): a strong change in the CET/LET ratio should be reflected in the slope of the electrochromic shift signal *vs.* protonmotive force, which was not observed since all genotypes behave similarly in this respect (Figure 4.1.5B).

Lastly, we consider the possibility of excitation energy being spilled over from PSII to PSI upon thylakoid de-stacking. According to previous work with systems showing high spill-over, i.e. the liken *Parmelia sulcata* (Slavov et al., 2013), the conifer *Pinus sylvestris* (Bag et al., 2020) and the primitive unicellular green alga *Mantoniella squamata* (Trissl and Wilhelm, 1993), a low F_m/F_0 ratio associated to the high PSII/PSI stoichiometry is the best indication of ongoing spill-over, as assessed by fast fluorescence spectroscopy at low temperature and DAS deconvolution (Slavov et al., 2013). We observed that *koLhcb* has a similarly low F_m/F_0 and PSII/PSI ratio as in *Mantoniella* while genotypes retaining significant level of stacking behaved like the wild type, i.e had high F_m/F_0 and PSII/PSI ~1 (Supplementary Table S4.1.4). It should be noted that the canonical method for assessing spill-over consists in showing an increase of P700 antenna size in DCMU-treated samples (Wilhelm et al., 1989). We have attempted this experiment with unconclusive results. Indeed, our mutants, parlicularly relevant being *koLhcb*, have a reduced cross section for photon absorption due to the very nature of the mutations applied: a PSII core complex binds 35 Chl *a* (Müh and Zouni, 2020), a figure that might be at the limit of detection for optically detected measurement since PSI-LHCI complex binds at least 145 Chls plus several LHCII complexes (Schiphorst et al., 2021). In order to fully verify the hypothesis of spill-over occurring differentially in our grana endowed *vs.* grana depleted genotypes, fast spectroscopy measurements need to be performed and will be the object of future studies. Yet the occurrence of this process in our grana-depleted genotypes is strongly consistent with data, namely the high F_m/F_0 ratio of *Mantoniella squamata* (Rhiel and Mörschel, 1993) and other photosynthetic systems without well defined compatimentation between PSI and PSII RC.

We conclude that thylakoid stacking is a characteristic of specific and lowly abundant Lhcb proteins, namely CP26 and, chiefly, Lhcb2. Indeed, while CP26 is conserved in algae, Lhcb2 cannot be traced back though the green lineage from land plants to green algae, which, in turn,

do not show highly structured multiple membrane layers (Alboresi et al., 2008). As for the major physiological functions associated to the evolution of grana, it is a more efficient PSII repair process, possibly due to the compartmentalization of the fully functional PSII separately from the damaged complex under repair and the energy separation of PSI from PSII antenna. Indeed, the evolution of red chlorophyll absorption forms upon land colonization has made the effect of spill-over far more deleterious for an equilibrated energy balance between PSs with respect to algae, whose PSI is depleted in red-forms and is, therefore, less efficient in draining excitation energy from connected antenna beds, according to Boltzmann's relation.

Materials and Methods

Plant materials.

Arabidopsis thaliana mutants *ch1*, *ch1 koLhcb5*, *koLhcb3* and *NoM* were obtained as previously described (Damkjaer et al., 2009; Havaux et al., 2007; Dall'Osto et al., 2014c). *NoM koLhcb3* was obtained by crossing single mutants and selecting progeny by immunoblotting. *koLHCII*, *Lhcb2-only*, *koLhcb* and *lowLHCII* lines were obtained by GE as reported in (Ordon et al., 2017, 2020). Plants were transformed (Zhang et al., 2006) with *Agrobacterium tumefaciens* (strain GV3101). Seedlings were tested for resistance to applications of the antibiotic hygromycin (25 mg l^{-1}). For each genotype, independent transformants (T1 generation) were self-fertilized, and absences of proteins were confirmed in the T3 generation by immunotitration.

Growth conditions.

Wild type and mutant genotypes were grown in soil, in a phytotron for 6 weeks at either 150 or 350 μmol photons m^{-2} s^{-1}, 23°C, 70% relative humidity, 8/16 h of day/night. All biochemical and physiological analyses were performed on plants prior to the onset of flowering. The growth of plants was determined by measuring the rosette fresh weight at the end of the growth cycle.
Membrane isolation. Stacked thylakoid membranes were isolated as previously described (Casazza et al., 2001).

Pigment analysis.
Pigments were extracted from leaf discs with 85% acetone buffered with Na_2CO_3, then separated and quantified by HPLC (Jasco Extrema LC-4000) as in (Gilmore and Yamamoto, 1991a).

Spectroscopy.
Absorption spectra were recorded at RT using an Aminco DW2000 spectrophotometer. Leaf pigment content was calculated from spectra of acetonic extracts (Croce et al., 2002a).

Electrophoresis and immunoblotting.

SDS-PAGE analysis of thylakoid proteins was performed using the Tris-Tricine buffer system (Schägger and von Jagow, 1987). For immunotitration (Towbin et al., 1979), proteins were detected with alkaline phosphatase-conjugated antibody (Sigma-Aldrich A3687). Primary antibodies used were: α-PsbB/CP47 (AS04 038), α-Lhcb1 (AS01 004), α-Lhcb2 (AS01 003), α-P-Lhcb1 (AS13 2704), α-P-Lhcb2 (AS13 2705) from Agrisera. Signal amplitude was quantified using the GelPro 3.2 software (Bio-Rad). Non-denaturing Deriphat-PAGE was performed as in (Guardini et al., 2020). SDS-PAGE analysis on complexes eluted from non-denaturing gel was performed using the Laemmli system as reported in (Crepin et al., 2020).

Analysis of Chl fluorescence.

Photosynthetic parameters (Baker, 2008) were measured on leaves at RT with a DUAL-PAM-100 equipment (Walz, GmbH). Variable fluorescence was measured in a home-built Chl fluorimeter, and induced by green light (Rappaport et al., 2007) (10 μmol photons m^{-2} s^{-1}) in dark adapted leaves, infiltrated with DCMU 50 μM. Steady state, light-induced pmf was estimated from changes in absorbance associated with the ECS at 520 nm (Livingston et al., 2010; Cruz et al., 2005), using a LED spectrophotometer (JTS10; Biologic Science Instruments).

Electron Microscopy and image analysis.

Transmission electron microscopy on leaf fragments was conducted using a FEI Tecnai T12 electron microscope operating at 100 kV accelerating voltage. Leaf fragments were fixed in 3% glutaraldehyde in 0.1 M cacodylate buffer pH 6.9. Analyses on EM images were conducted with ImageJ software (Schneider et al., 2012).

LHCII phosphorylation induction.

Leaves were dark adapted for 60 minutes prior to exposure to 200 μmol photons m^{-2} s^{-1} PSII light (orange) for 60 minutes at 24°C.

Statistics.

Statistical analyses were performed in SigmaPlot using One-way analysis of variance (ANOVA), means were separated with Tukey's post hoc test at a significant level of $P < 0.05$ (see the figure legends for details). Error bars represent the standard deviation.

Data availability.

Sequence data from this article can be found in the *Arabidopsis* Genome Initiative or GenBank/EMBL databases under accession numbers At1g29920 (*Lhcb1.1*), At1g29910 (*Lhcb1.2*), At1g29930 (*Lhcb1.3*), At2g34430 (*Lhcb1.4*), At2g34420 (*Lhcb1.5*), At2g05100 (*Lhcb2.1*), At2g05070

(*Lhcb2.2*), At3g27690 (*Lhcb2.3*), At5g54270 (*Lhcb3*), At5g01530 (*Lhcb4.1*), At3g08940 (*Lhcb4.2*), At4g10340 (*Lhcb5*), At1g44446 (*cao*). The KO lines used in the work were obtained from the NASC under the stock numbers N376476 (*koLhcb4.1*), N877954 (*koLhcb4.2*), N514869 (*koLhcb5*), N520342 (*koLhcb3*), N524295 (*ch1*).

Funding

The work was supported by grant RIBA 2017 to R.B. and grant PRIN 2017 (201795SBA3_004, HARVEST) to L.D.

Author contributions

R.B. and L.D. conceived the work and designed the experiments. R.B. performed EM analysis. Z.G. carried out the construction of mutants and performed their physiological characterization, together with L.D. and R.C., R.L.G. analyzed fluorescence kinetics and biochemically characterized mutant lines. J.S. developed and provided the CRISPR-Cas9 plasmids system. All authors contributed to writing the manuscript, discussed the results and commented on the manuscript.

Aknowledgements

We thank Pierre Joliot, Francis-André Wollman and Benjamin Bailleul (IBPC-Paris) for discussions and suggestions, the team of Electron Microscopy service at the University of Padua-department of Biology Vallisneri for excellent technical assistance. The authors declare no competing interests.

Supplemental Information

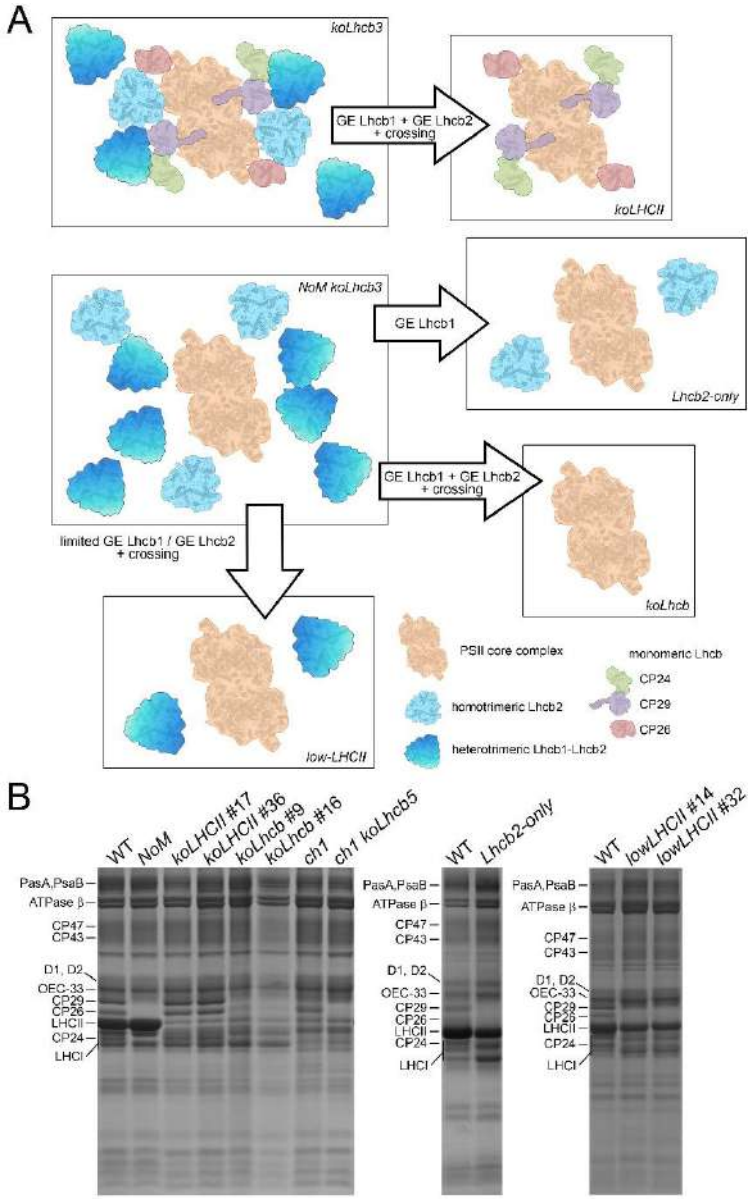

Supplementary Figure S4.1.1. Schematic diagram and protein composition of Arabidopsis LHC mutants produced in the present work. (A) *The NoM line was obtained as previously reported (Dall'Osto et al. 2017), and a T-DNA insertion in At5g54270 (Lhcb3; NASC N520342) was further introgressed. Specific sgRNA were selected and used for the deletion of either Lhcb1 or Lhcb2 genes (Ordon et al. 2020), in both koLhcb3 and NoM koLhcb3 genetic backgrounds. koLHCII and koLhcb lines were obtained by crossing koLhcb1 x koLhcb2 lines and selecting progeny by immunoblotting, while Lhcb2-only lines were obtained by deleting Lhcb1 genes in NoM koLhcb3 plants. low-LHCII lines were produced by crossing NoM koLhcb3 lines which underwent limited genome editing on Lhcb1 and Lhcb2 loci, then selecting in the progeny plants retaining ~30% of LHC content than parental genotype.* ***(B)*** *SDS–PAGE analysis of wild type (WT) and LHC mutant thylakoid proteins, performed with the Tris-Tricine buffer system. Selected apoprotein bands are marked.*

Supplementary Figure S2

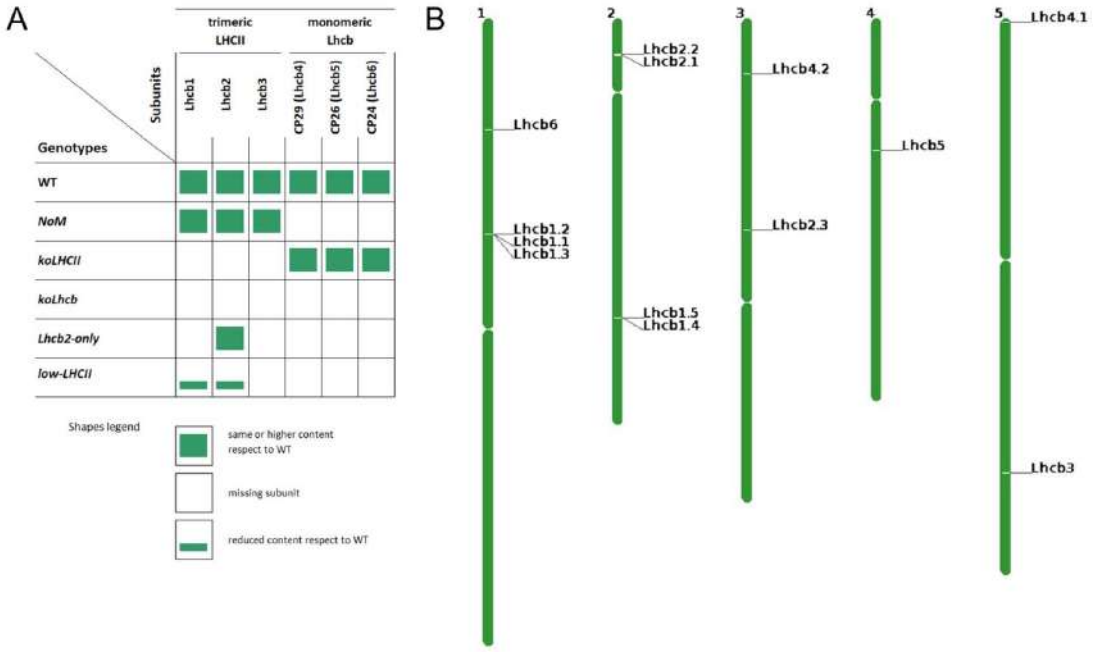

Supplementary Figure S4.1.2. *(A) Synopsis of LHC composition of the genotypes used in this work. (B) Distribution of Lhcb genes on the Arabidopsis genome, plotted using TAIR chromosome map utility (http://www.arabidopsis.org/jsp/ChromosomeMap/tool.jsp).*

Supplementary Figure S4.1.3

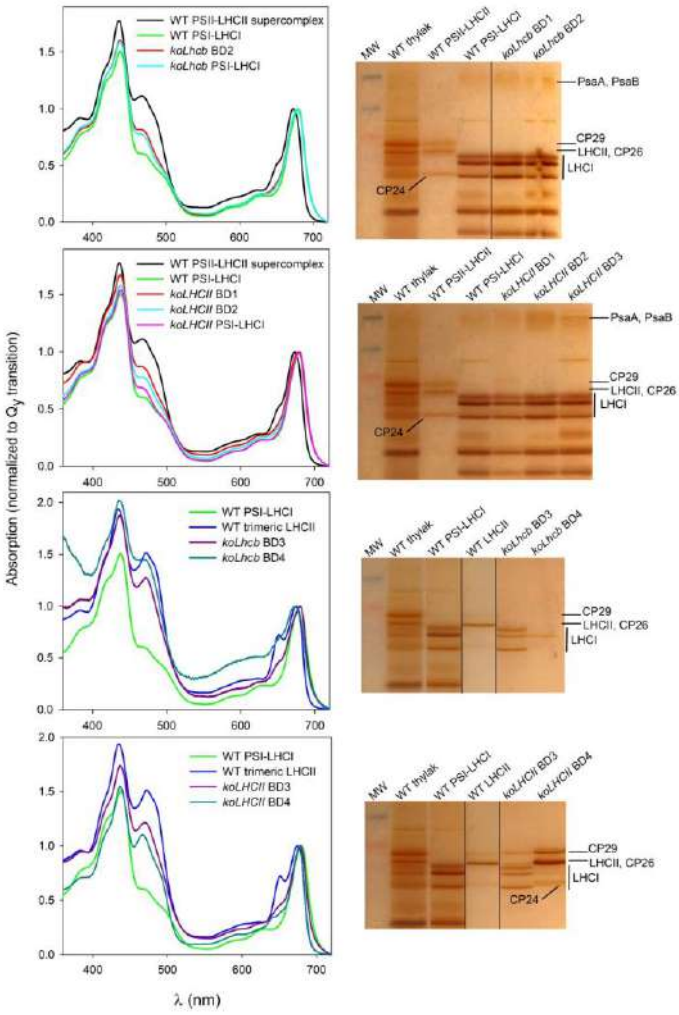

Supplementary Figure S4.1.3. Insights on the composition of pigment-binding complexes separated by non-denaturing Deriphat-PAGE (see Figure 4.1.2A). *Chl-binding complexes were extracted from acrylamide matrix and further characterized by absorption spectroscopy at RT (left column). Moreover, protein composition of selected bands was determined by SDS-PAGE and silver staining (right column). Fractions BD1 and BD2 contained PSI-LHCI supercomplexes with increasing LHC content, as determined by (i) the red–tail of the Q_y transition, and (ii) the lower Chl a/b ratio with respect to the PSI-LHCI supercomplex from WT thylakoids. In all these bands, major subunits identified were PsaA/PsaB (PSI core complex) and LHCI (PSI antennae). BD3 and BD4 from koLhcb contained LHCI, likely dimeric in BD3 (which indeed showed an electrophoretic mobility intermediate between trimeric LHCII and monomeric Lhcb), while monomeric in BD4. BD3 from koLHCII was enriched in LHCI subunits, but also contained dimeric states of Lhcb complex (CP29/CP26). In BD4 from koLHCII, the relative abundance of monomeric LHCI was reduced than BD3, while the monomeric Lhcb CP29, CP26 and CP24 were the major components.*

Supplementary Figure S4.1.4

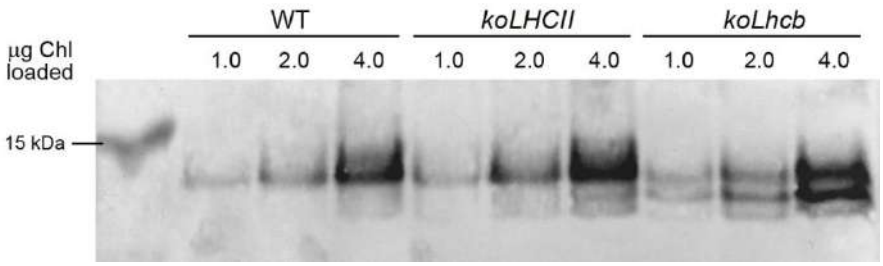

Supplementary Figure S4.1.4. Analysis of CURT1, the factor controlling curvature of thylakoid membranes at the margins and grana shaping. *Immunoblotting used for the quantification of the CURT1A subunits in the WT and mutant thylakoids. Proteins corresponding to 1.0, 2.0 and 4.0 µg of Chls were loaded for each sample. All samples were loaded on the same SDS-PAGE slab gel.*

Supplementary Tables

Supplementary Table S4.1.1. *Sequences of sgRNA used for genome editing.*

Target	sgRNA
Lhcb1.1 - Lhcb1.5	GGTTCACAGATCTTCAGCGA ATGGACCC AAGTACTTGACT TGTGGATAACTTCT AGCTCA GGCTACTCAAGTTATCCTCA GAAGCGGCCGTGTGACAATG AGAAGTTATCCACAGCAGGT GAGGACTTGCTTTACCCCGG AGGGGAGGAGAGAGCCATTG
Lhcb2.1 - Lhcb2.3	CGCAAGGTTGGTGTATCCGG TGGAGGGCTTGAGAGCCGTT CGCCCAAGACGCCCACCTTT AGACTTGACGGTACGACGCA AGGGCTTGACCCGCTTTACC GGATCAAGTTAGGGTTTCCG CCAACATTGCCCATCTACTG TCTGGGCTGTTCAAGTTGTG

Supplementary Table S4.1.2. Lhcb1 and Lhcb2 content of Arabidopsis lines lowLHCII and Lhcb2-only. *The abundance of Lhcb subunits was determined on independent lines by SDS–PAGE fractionation of thylakoid proteins and immunotitration with specific primary antobodies. Lhcb content was normalized (norm.) to that of the CP47 (PSII core) subunit. Data are expressed as mean ± s.d., n = 4 biologically independent samples. Values marked with different letters are significantly different from each other within the column (ANOVA followed by Tukey's post-hoc test at a significance level of P < 0.05).*

	Protein content (norm. to WT level)	
	Lhcb1	**Lhcb2**
WT	1.000 ± 0.046 [a]	1.000 ± 0.152 [a]
lowLHCII L1	0.192 ± 0.033 [b]	0.082 ± 0.026 [b]
lowLHCII L2	0.320 ± 0.096 [b]	0.077 ± 0.016 [b]
Lhcb2-only	nd	1.439 ± 0.218 [c]

Supplementary Table S4.1.3. Photosynthetic pigment composition of leaves from wild type and mutant lines. *Pigments were extracted from dark-adapted leaves with 85% acetone, separated and quantified by HPLC. Data are normalized to 100 Chl a + b molecules and are expressed as mean ± SD, n = 6 biologically independent samples.*

	Carotenoid content (normalized to 100 Chl *a* + *b*)			
	Neoxanthin	**Violaxanthin**	**Lutein**	**β-Carotene**
WT	3.7 ± 0.2	3.0 ± 0.4	12.8 ± 0.3	7.7 ± 0.2
NoM	4.0 ± 0.1	3.7 ± 0.4	13.9 ± 0.2	7.5 ± 0.2
koLHCII #17	1.6 ± 0.2	5.1 ± 0.2	11.6 ± 0.3	11.4 ± 0.4
koLHCII #36	1.8 ± 0.3	5.3 ± 0.4	11.6 ± 0.5	11.3 ± 0.1
koLhcb #9	0.7 ± 0.2	6.4 ± 0.3	11.2 ± 0.2	13.8 ± 0.3
koLhcb #16	1.0 ± 0.2	6.1 ± 0.4	11.7 ± 0.1	13.7 ± 0.3
ch1	1.6 ± 0.6	6.3 ± 0.6	14.6 ± 1.0	13.6 ± 0.7
ch1 koLhcb5	2.0 ± 0.8	6.0 ± 1.3	14.8 ± 0.5	16.2 ± 1.3
lowLHCII #14	2.3 ± 0.1	4.8 ± 0.4	11.7 ± 1.5	10.2 ± 2.0
lowLHCII #32	1.8 ± 0.6	5.1 ± 0.8	11.5 ± 1.8	12.3 ± 1.1
Lhcb2-only	1.8 ± 0.3	4.8 ± 0.5	11.3 ± 2.2	10.7 ± 1.8

Supplementary Table S4.1.4. PS stoichiometry and Chl fluorescence induction parameters determined for leaves of wild type and mutants. *PSI/PSII ratios were determined by immunotitration analysis with primary antibodies directed against the PSII core subunit PsbB (CP47) and the PSI core subunit PsaA. F_m/F_0 and F_v/F_m values were obtained by analysis of chlorophyll fluorescence measured at the Dual-PAM. The connectivity parameter J was determined from fast Chl fluorescence induction in DCMU-treated leaves, measured with green light (7 µmol m^{-2} s^{-1}). Values are shown as mean ± SD (biologically independent samples n = 3 for PSI / PSII ratio measurements, n ≥ 5 for Chl fluorescence analysis). Values for Mantoniella squamata were reported in (Trissl and Wilhelm, 1993).*

	PSI / PSII (PsaA / CP47)	F_v / F_m	F_m / F_0	J
WT	1.00 ± 0.04[a]	0.82 ± 0.01[a]	5.56 ± 0.31[a]	2.05 ± 0.24[a]
NoM	1.00 ± 0.06[a]	0.61 ± 0.01[b]	2.56 ± 0.07[b]	0.79 ± 0.13[b]
koLHCII #17	0.46 ± 0.07[b]	0.76 ± 0.01[c]	4.17 ± 0.17[c]	1.76 ± 0.07[a]
koLHCII #36	0.45 ± 0.04[b]	0.76 ± 0.01[c]	4.17 ± 0.17[c]	1.71 ± 0.10[a]
koLhcb #9	0.66 ± 0.07[c]	0.50± 0.02[e]	2.00 ± 0.08[e]	0.58 ± 0.25[b]
koLhcb #16	0.70 ± 0.05[c]	0.54 ± 0.03[e]	2.17 ± 0.14[e]	0.60 ± 0.39[b]
Mantoniella squamata (Trissl & Wilhelm, 1993)	0.4 - 0.65	0.5 - 0.6	1.5 - 2.5	nd

This chapter is a manuscript in preparation.

4.2 Mapping the photoprotective response in the Photosystem II antenna system

Zeno Guardini[a,1], Luca Dall'Osto[a,1], Roberto Caferri[a], Rodrigo L. Gomez[a] and Roberto Bassi[a,#]

[a]Dipartimento di Biotecnologie, Università di Verona, Strada Le Grazie 15, 37134 Verona, Italy

[1]These authors contributed equally to the work

[#]To whom correspondence should be addressed:

Roberto Bassi, E-mail: roberto.bassi@univr.it; phone +39 045 8027915; fax +39 045 8027929

The author responsible for distribution of materials integral to the findings presented in this article in accordance with the policy described in the Instructions for Authors is: Roberto Bassi (roberto.bassi@univr.it).

Running title: functional topology of non-photochemical quenching

Keywords: Photosynthesis, Non-photochemical quenching, photoprotection, LHCII, monomeric LHCs, PsbS, Zeaxanthin, Lutein

Abstract

Optimizing plant photosynthetic performance requires a close matching between harvesting and utilization of light energy. The fastest response to fluctuating irradiance is Non-Photochemical Quenching (NPQ) i.e. the dissipation of energy absorbed in excess into heat. NPQ is triggered in antenna proteins by thylakoid lumen acidification through protonation of PsbS: a sensor of lumenal pH. Which subunits, within light harvesting antenna, undergo quenching reactions and their relative photoprotective efficiency is the matter of intense debate. Here, we report on the characterization of *Arabidopsis* mutants lacking either moieties of PSII antenna: the trimeric LHCII (*koLHCII*), the monomeric LHC (*NoM*) or both (*koLhcb*), aimed at identifying the site(s) of the photoprotective responses. Residual NPQ activity was detected in all genotypes thus showing the contribution of the different Photosystem II components to the overall quenching. While trimeric LHCII accounted for the larger contribution to NPQ, monomeric LHCs showed the highest photoprotective activity under excess light. We conclude that assembly of Photosystem II supercomplexes including monomeric LHCs has a key role in preventing photoinhibition.

Introduction

Photosynthesis converts sunlight into chemical energy (ATP) and reducing power (NADPH), which ultimately drive CO_2 fixation into sugars. Photosystem (PS) II catalyzes the initial step of electron transport (ET) and is composed of a dimeric core complex, hosting the reaction center (RC) catalyzing water splitting into O_2, and an antenna system, enhancing photon cross section (Wei et al., 2016). Three monomeric subunits (Lhcb4, Lhcb5 and Lhcb6) bridges excitation energy transfer between the core and the trimeric LHCII (Lhcb1-3) located peripherally in the supercomplex (Su et al., 2017). LHCII is the most abundant pigment-binding protein on earth, coordinating chlorophyll (Chl) *a*, *b* and xanthophyll ligands, namely neoxanthin, violaxanthin (Vio) and lutein (Lut) (Liu et al., 2004). Under limiting irradiance LHCII enhances photon interception (Fuciman et al., 2012). Under excess-light (EL) conditions excitation energy outcompetes downstream metabolic reaction rate, thus enhancing the probability that unquenched singlet excited states of Chl (^{1}Chl*) transit to triplet state (^{3}Chl*), which reacts with O_2, leading to singlet oxygen ($^1O_2$) release and photoinhibition (Fischer et al., 2013; Kok, 1956). Fast-activated mechanisms, which dissipate excess ^{1}Chl* as heat to prevent oxidative damage, are collectively named as Non-Photochemical Quenching (NPQ) (Ruban, 2016). NPQ can convert up to 70% of absorbed photons into heat, resulting into a strong decrease of PSII quantum yield, detected as light-dependent Chl fluorescence decline (Ishida et al., 2014).

The overall NPQ process can be dissected into several components (Horton et al., 1996; Cazzaniga et al., 2013; Malnoë, 2018). The fastest component, qE (energy quenching), is activated within few seconds and requires (i) lumen acidification, (ii) protonation of the pH-sensor PsbS (Li et al., 2004), and is enhanced by the (iii) conversion of Vio into zeaxanthin (Zea) within the xanthophyll cycle (Niyogi et al., 2001).

The precise location of quenching center(s) has been investigated since the 1980s (for a review, see (Wilson and Ruban, 2020; Pinnola and Bassi, 2018)). Being PsbS a pigment-less protein (Dominici et al., 2002; Fan et al., 2015), the qE reaction occurs in the pigment-binding subunits of PSII, located in grana partitions (Havaux et al., 2007). The following evidences have located quenching sites among Lhcb subunits of PSII: (i) Lut and Zea, essential for NPQ activity, are LHCs ligands (Bassi et al., 1993; Niyogi et al., 2001) ; (ii) the pH-dependent trigger, PsbS, is an interactor of Lhcb proteins (Gerotto et al., 2015; Correa-Galvis et al., 2016); (iii) the amplitude of quenching is proportional to Lhcb/RC ratio (Havaux et al., 2007; Ware et al., 2015a). In addition to Lhcb proteins, a RC-type NPQ was transiently observed, being replaced by antenna quenching in later steps of light exposure (Finazzi et al., 2004), see (Belgio et al., 2012) for a contrasting report.

Identification of the site(s) of quenching reactions is complex due to the high number of *Lhcb* gene products in PSII. Fluorescence quenching can be induced *in vitro* during aggregation of purified antennae (Horton et al., 1991, 1996), suggesting aggregation could be the basis for qE *in vivo* (Ware et al., 2015b). Moreover, co-reconstitution of PsbS and LHCII was sufficient for quenching activity (Wilk et al., 2013). Monomeric LHCs have been suggested as quenching centers based on their high affinity for Zea (Morosinotto et al., 2002; Dall'Osto et al., 2005) leading to the proposal of two quenching sites (Q1 and Q2), located respectively in the LHCII complex and in the monomeric LHCs (Holzwarth et al., 2009).

Reverse genetics on *Arabidopsis* showed that the fastest phase of the quenching was missing in the *NoM* mutant, lacking monomeric LHCs (Dall'Osto et al., 2017). Since *koCP26* and *koCP24* mutants were unaffected (De Bianchi et al., 2008) while *koCP29* mimicked *NoM* (De Bianchi et al., 2011) the latter was assigned as the site for the fast qE component. The pigment cluster catalyzing quenching was then identified by mutation analysis *in vivo* as the Chl pair *a*603-*b*609 (a5-b5) plus the Car in site L2 (Guardini et al., 2020). Although slower, qE in *NoM* was robust, implying LHCII also hosts PsbS-dependent quenching (Dall'Osto et al., 2017) in its Lhcb1 component (Pietrzykowska et al., 2014). Based on NPQ analysis of antisense Lhcb1 lines, it was suggested that LHCII is the only site for qE quenching (Nicol et al., 2019) re-fueling the intense debate (Ruban and Wilson, 2020; Bassi and Dall'Osto, 2021).

Here, we applied genome editing technology to produce the first full LHCII knockout mutant with or without monomeric LHCs. Further, these genotypes were deleted in PsbS, lutein and zeaxanthin biosynthesis in order to characterize NPQ activity of each LHC knockout line. Analysis of these genotypes allowed quantifying the contributions of both monomeric and trimeric LHCs to qE activation. Last but not least, analysis of photoprotection showed that this essential function is not tightly related to the amplitude of quenching so that a small quenching activity in monomeric LHCs is more effective in photoprotection than a large quenching from LHCII.

.

Results

koLHCII and *koLhcb* are *Arabidopsis* mutants lacking, respectively, Lhcb1-3 and Lhcb1-6 PSII antenna subunits

The *koLHCII* and *koLhcb* genotypes have been obtained by genome editing as previously described ((Guardini et al., 2022), Table S4.2.1). Mutants *npq4* (devoid of PsbS), *NoM* (lacking all monomeric LHCs), *ch1* (unable to accumulate Chl *b*) and *ch1 koLhcb5* (devoid of Lhcb5 minor antenna) were also included in the characterization. When grown under controlled conditions (150 μmol photons m^{-2} s^{-1}, 23/19°C, 8/16 hours day/night), *NoM* and *koLHCII* exhibited a similar growth rate although significantly reduced respect to wild type and *npq4* plants, while *koLhcb* lines showed a far stronger growth retardation, similar to mutants *ch1 koLhcb5* and *ch1 koLhcb5 npq4*. The size of *ch1* plants was intermediate between that of *koLHCII* and *ch1 koLhcb5*, implying the presence of Lhcb5 enhanced light harvesting (Figure 4.2.1, Table 4.2.1). The level of selected thylakoid proteins, relative to the wild type PSII core content (PsbC), was determined by immunotitration analysis (Figure S4.2.1). *koLHCII* and *koLhcb* completely lacked Lhcb1-3 and Lhcb1-6 subunits, respectively, while Lhcb5 was present in substantial amounts in *ch1* (170% than wild type). The PSI (PsaA) content was significantly reduced in mutants depleted of LHCs, while ATPase β-subunit and Cytochrome *f* level was similar in all genotypes. The functional antenna size of the different genotypes (Figure S4.2.2, Table 4.2.1) reflected the abundance of their antenna complexes: it was the lowest in *koLhcb* and *ch1 koLhcb5* (-65% than wild type), the highest in *NoM* (+90%,(Dall'Osto et al., 2017)), intermediate in *ch1* and *koLHCII* (-55%).

PSII function during photosynthesis was studied by analyzing Chl fluorescence on leaves at increasing light intensities (Figure S4.2.3). The fraction of PSII in open state (qL) was higher in *koLHCII vs*. wild type when irradiance was below 500 μmol photons m^{-2} s^{-1}, and even higher in all other LHC-depleted mutants (*koLhcb*, *ch1 koLhcb5*) *vs*. wild type at all intensities tested, thus suggesting an imbalance in the distribution of excitation between the two PSs in LHC-depleted lines. Chl fluorescence yield (Φ_F) provides information about how excitation energy is partitioned during photosynthesis (Kramer et al., 2004; Ahn et al., 2008). The quantum yield of PSII photochemistry (Φ_{II}) in dark-adapted leaves was the lowest in *koLhcb* and intermediate in *koLHCII* and *ch1 koLhcb5 vs.* wild type; Φ_{II} showed a rapid drop at increasing irradiances, reaching similar values in all genotypes. The yield of dissipation by downregulation (Φ_{NPQ}) showed a rise with increasing light intensity to a value of 0.6 in wild type and *NoM*, 0.4-0.45 in *koLHCII* and *ch1 koLhcb6*, 0.2 in *koLhcb*. The yield of other non-photochemical, unregulated energy losses (Φ_{NO}) changed little with varying light in wild type leaves, while it showed a rise to 0.6 in *koLHCII* and *ch1 koLhcb6*, to 0.8 in *koLhcb*, thus suggesting limitations in the compensatory changes in Φ_{II} and Φ_{NPQ} at increasing irradiances, in these mutants. Depletion in LHC rises Φ_{NO} in dark-adapted leaves as effect of a higher emission (F_0), attributable either to a lower efficiency in driving photochemistry or to an higher contribution of PSI-associated Chl to the overall fluorescence (Franck et al., 2002).

Optimization of linear electron flow is ensured by relocation of LHC between PSs through the process of state transition (ST), whose activity was measured from the Chl fluorescence (F) change upon plastoquinone (PQ) reduction (Lunde et al., 2000) (Figure S4.2.4). WT and *npq4* leaves showed the same ST amplitude and kinetic, while the *NoM* fluorescence behaviour differed from the wild type showing higher fluorescence at the steady-state during illumination (F_s) with orange light, no changes in F_s amplitude (from PQ pool oxidation/reduction) upon switching on/off far-red light, and smaller amplitude of $\Delta F_m'$ upon reduction of PQ (qT, see methods) than in the wild type. In both *koLHCII* and *koLhcb* leaves, the PQ redox state was unaffected by far red light, and ST were missing. The steady-state F_s level during illumination with orange light was slightly higher in *koLHCII* and far higher in *koLhcb* leaves with respect to the wild type, which reflect the higher values of Φ_{NO}.

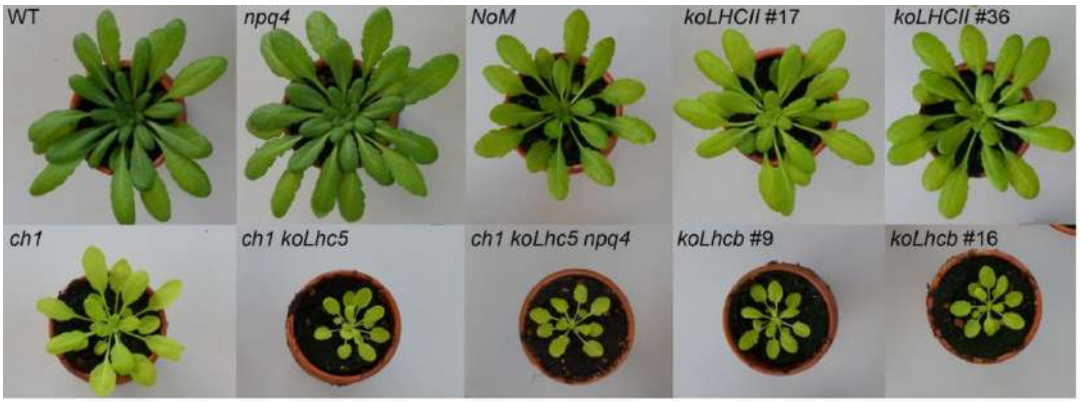

Figure 4.2.1. Phenotype of wild type and mutant plants. *Plants were grown for 6 weeks at 150 µmol photons m^{-2} s^{-1}, 23/19 °C, 8/16 h light/dark.*

Table 4.2.1. Pigment content and photosynthetic parameters determined for leaves of Arabidopsis WT, npq, ch1 and LHC mutant lines. *Values were measured in homozygous F3 or T3 plants; at least two lines were analysed for each mutant and five different plants were tested for each line. Chl/Car, molar ratio between chlorophylls (a + b) and carotenoids. Fresh weight refers to growth after 6 weeks under control conditions. Values of F_0 (minimal Chl fluorescence of PSII) were normalized to the corresponding Chl content per unit leaf surface (µg Chls cm^{-2}). All data are expressed as mean ± s.d., n = 5 biologically independent plants. Values marked with different letters are significantly different from each other within the column (ANOVA, followed by Tukey's post-hoc test at a significance level of P < 0.05). Experiments were repeated independently twice, with similar results.*

	Chl *a* / *b*	Chl / Car	µg Chl cm^{-2}	Fresh weight (g)	F_0 / Chl (norm. to WT)	F_v / F_m	1 / $t_{2/3}$ ($\cdot 10^{-3}$, ms^{-1})
WT	3.51 ± 0.09^{a}	3.69 ± 0.21^{a}	19.4 ± 0.5^{a}	2.03 ± 0.19^{a}	1.0 ± 0.08^{a}	0.82 ± 0.01^{a}	5.76 ± 0.42^{a}
npq4	3.40 ± 0.02^{a}	3.66 ± 0.13^{a}	21.1 ± 1.4^{a}	2.28 ± 0.46^{a}	0.83 ± 0.06^{a}	0.82 ± 0.01^{a}	6.07 ± 0.40^{a}
NoM	3.28 ± 0.05^{a}	3.45 ± 0.09^{a,c}	15.3 ± 0.74^{b}	0.75 ± 0.11^{b}	3.23 ± 0.26^{b}	0.61 ± 0.01^{b}	10.70 ± 0.98^{b}
ch1	-	2.77 ± 0.02^{b}	6.55 ± 0.54^{d}	0.30 ± 0.06^{c}	1.14 ± 0.14a	0.78 ± 0.01^{c}	2.48 ± 0.17^{c}
ch1 koLhcb5	-	2.57 ± 0.02^{b}	4.50 ± 0.23^{e}	0.07 ± 0.02^{d}	1.61 ± 0.22^{a,d}	0.67 ± 0.01^{d}	1.71 ± 0.21^{d}
ch1 koLhcb5 npq4	-	2.59 ± 0.08^{b}	3.87 ± 0.27^{e}	0.07 ± 0.02^{d}	1.75 ± 0.16^{a,d}	0.70 ± 0.02^{d}	1.75 ± 0.22^{d}
koLhcb #16	6.14 ± 0.22^{b}	3.09 ± 0.08^{d}	6.10 ± 0.76^{d}	0.06 ± 0.01^{d}	5.46 ± 0.88^{c}	0.54 ± 0.03^{e}	1.74 ± 0.18^{d}
koLhcb #9	6.28 ± 0.15^{b}	3.12 ± 0.05^{d}	5.68 ± 0.15^{d}	0.07 ± 0.01^{d}	5.18± 0.99^{c}	0.50± 0.02^{e}	1.95 ± 0.18^{d}
koLHCII #17	5.23 ± 0.11^{c}	3.37 ± 0.06^{c}	11.46 ± 0.55^{c}	0.78 ± 0.19^{b}	2.13 ± 0.28^{d}	0.76 ± 0.01^{c}	2.47 ± 0.31^{c}
koLHCII #36	5.15 ± 0.10^{c}	3.34 ± 0.02^{c}	11.03 ± 0.58^{c}	0.94 ± 0.18^{b}	2.18 ± 0.24^{d}	0.76 ± 0.01^{c}	2.66 ± 0.26^{c}

NPQ phenotype of LHC-depleted mutants

To evaluate the capacity of these genotypes to trigger NPQ, we first studied the main components of the mechanism, namely the abundance of the pH sensor PsbS, the activity of the xanthophyll cycle and the extent of thylakoid lumen acidification (Figure 4.2.2). The level of PsbS, relative to the PSII core content, was significantly reduced in both *koLHCII* and *koLhcb* mutants with respect to the wild type (-50%, Figure 4.2.2A).

The kinetic of de-epoxidation index, induced on leaves upon exposure at 1000 μmol photons m^{-2} s^{-1} at RT, was the same in *koLHCII* and wild type, while it resulted significantly higher in *koLhcb* leaves (Figure 4.2.2B). The total amplitude of the ECS signal (Cruz et al., 2005) was used to estimate the light-driven protonmotive force (pmf) across the thylakoids: it was the highest in wild type, significantly lower in *koLHCII* (-20%) and *koLhcb* (-35%), while half-saturation point of pmf was reached around 100 μmol photons m^{-2} s^{-1} in all genotypes (Figure 4.2.2C).

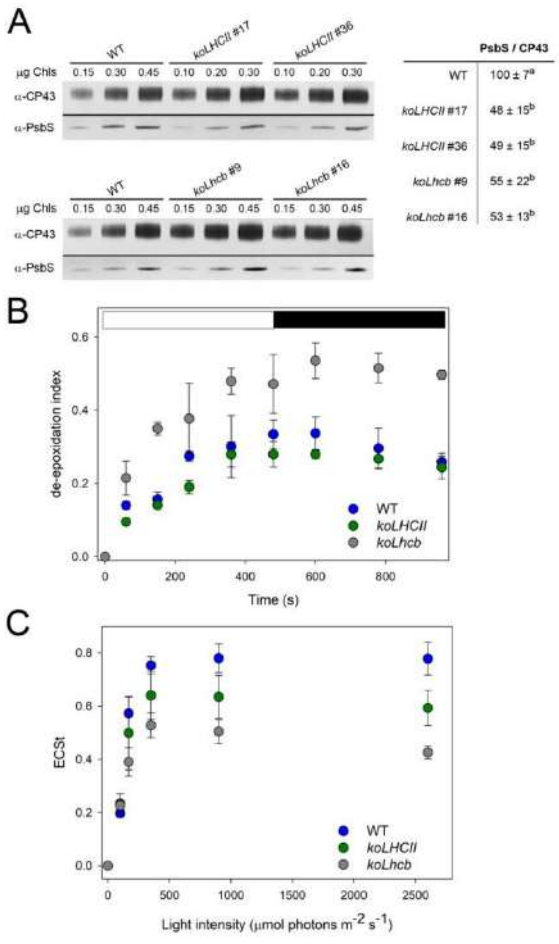

Figure 4.2.2. Analysis of the main factors controlling NPQ amplitude and kinetic. *(A) (left panel) Immunotitration of leaf extracts with α-PsbS and α-CP43 antibodies. PsbS content was normalized to the PSII core amount (PsbB content) and expressed with respect to the corresponding wild type value (right panel). Data are reported as mean ± s.d., n = 3 biologically independent samples. Values marked with different letters are significantly different from each other within the column (ANOVA followed by Tukey's post-hoc test at a significance level of P < 0.05). (B) Time course of Vio de-epoxidation in wild type and mutant plants. Dark-adapted leaf discs were illuminated at 1000 μmol photons m^{-2} s^{-1} (white actinic light) for 8 min, following 8 min of dark recovery; at different times, leaf discs were frozen in liquid nitrogen and total pigments extracted before HPLC analysis. White and black bars represent light and dark periods. (C) ECS_t vs. light intensity, measured at steady-state photosynthesis, is used to estimate the light-driven proton motive force across the thylakoids. All data are expressed as mean ± s.d. (n = 5).*

The NPQ activity of the different genotypes was investigated by measuring NPQ kinetic upon exposing dark-adapted leaves to EL (1000 μmol photons m^{-2} s^{-1}, see Figure 4.2.3). Wild type leaves showed two distinct phases in NPQ formation, a rapid phase that occurred within 1 min and was dependent on the formation of trans-thylakoid ΔpH, and a slower one that was shown to rely on zeaxanthin formation (Härtel et al., 1996; Niyogi et al., 1998). Upon a second illumination, preloading with Zea resulted in a much faster rise of quenching, thus showing that both components are triggered by lumen acidification. Consistently with previous report (Li et al., 2004), the *npq4* mutant displayed the lowest qE and the highest qI after both induction cycles. In *koLHCII* leaves, the severe reduction in NPQ affected both components of quenching, while a rapid relaxation after darkening was still evident in the mutant differently from *npq4* leaves, thus implying the presence of a qE component mediated by the monomeric LHCs (Figure 4.2.3A). In *koLhcb* leaves, formation of both phases of NPQ was far slower than *koLHCII*, and largely superimposable to the quenching kinetic of *ch1 koLhcb5 npq4* leaves. In *ch1* leaves, a rapidly-reversible quenching activity was detected, which was significantly higher than in *koLHCII*, while NPQ in *ch1 koLhcb5* was intermediate between *ch1* and *koLhcb* lines (Figure 4.2.3B) thus implying the residual antenna plays a key role in catalyzing NPQ. It is worth noting that in all these genotypes the kinetic of Zea accumulation was not hampered, it comes that reduced NPQ can be ascribed to either changes in the availability of Zea-binding sites or altered ΔpH.

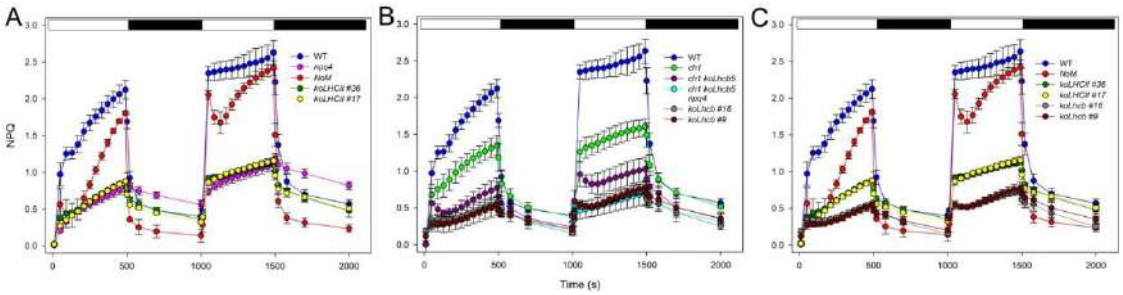

Figure 4.2.3. Kinetics of formation and relaxation of photoprotective energy dissipation in wild type, npq, ch1 and LHC mutant leaves*. NPQ kinetics were measured on selected genotypes during two consecutive periods of illumination with white light (1,000 μmol photons m^{-2} s^{-1}) at RT. White and black bars represent light and dark periods. Data are expressed as mean ± s.d., n = 4 biologically independent plants. Experiments were repeated independently twice, with similar results.*

To investigate *in vivo* the specific contribution of Zea, Lut and PsbS in determining NPQ activity, further genetic analysis was carried out. *Arabidopsis koLHCII* mutants devoid of Zea (*koLHCII npq1*), Lut (*koLHCII lut2*) or PsbS (*koLHCII npq4*) were produced by CRISPR-Cas9 genome editing. The effects of genome editing have been confirmed in T3 plants by immuno-titration with α-VDE and α-PsbS primary antibodies on leaf extracts, and by HPLC to verify the absence of either Lut in dark-adapted leaves or Zea in EL-treated leaves (Figure S4.2.5, Table S4.2.1, S4.2.2).
The effect of introducing the mutation *npq4* yielded into a full depletion of NPQ activity in *koLHCII* background (Figure 4.2.4A). The rapid phase of NPQ induction was still detectable in the genotypes *koLHCII npq1* and *koLHCII lut2* in both first and second illumination period (Figure 4.2.4B, C). The slower phase, still present in *npq1* leaves, was strongly reduced in *koLHCII npq1* plants, suggesting Zea-binding to residual monomeric LHCs modulated their activity in

quenching. Instead, the slower phase, present in *lut2* leaves, was reduced to the same level in both *koLHCII* and *koLHCII lut2* plants, implying Lut-binding sites active in NPQ were not present in monomeric LHCs.

Overall, the double illumination experiment confirmed that NPQ in a mutant retaining monomeric LHCs only was fully dependent on Zea and independent from Lut.

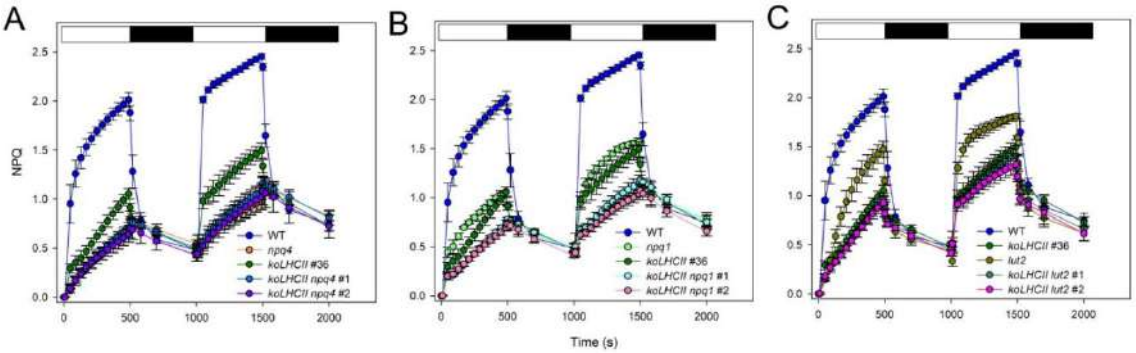

Figure 4.2.4. Kinetics of formation and relaxation of photoprotective energy dissipation in wild type and mutants koLHCII npq and koLHCII lut2. *NPQ kinetics were measured on leaves during two consecutive periods of illumination with white light (1,000 µmol photons m^{-2} s^{-1}) at RT. White and black bars represent light and dark periods. Data are expressed as mean ± s.d., n = 4 biologically independent plants. Experiments were repeated independently twice, with similar results.*

Investigating the photoprotection capacity of monomeric *vs.* trimeric LHC proteins

Previous work showed that both monomeric and trimeric LHC moieties contributed to the overall quenching activity of *Arabidopsis* leaves (De Bianchi et al., 2008; Dall'Osto et al., 2017). However, assessing the contribution of each quenching site to NPQ is not straight-forward due to the differences in the functional antenna size of individual genotypes. When considering the functional role of monomeric *vs*. trimeric LHCs in PSII photoprotection, we selected *Arabidopsis NoM koLhcb3* lines for the level of LHCII complement, obtained from incomplete editing of both Lhcb1 and Lhcb2 encoding genes. The LHC content was quantified by Coomassie-blue staining and densitometry, on a total of 16 lines selected based on their LHCII content, ranging from 0.004 to 0.028 nmol LHC / µg Chl of thylakoids. Their NPQ activity was measured (Figure S4.2.6) and expressed as their definite integrals over 8 min of actinic light window. Among these genotypes, we selected the two *lowLHCII* lines, which contained one LHCII trimer per monomeric PSII core complex, thus maintaining the PSII core/LHC protein stoichiometry.

Figure 4.2.5 shows that total NPQ of *koLhcb* rose upon different LHCII content. *koLHCII* lines showed NPQ activity significantly higher than *koLhcb* plants; however, when comparing the effect of accumulating LHC on NPQ activity, we could measure a significantly stronger effect of LHCII with respect to monomeric LHCs when stoichiometric (Figure 4.2.5, Figure S4.2.7).

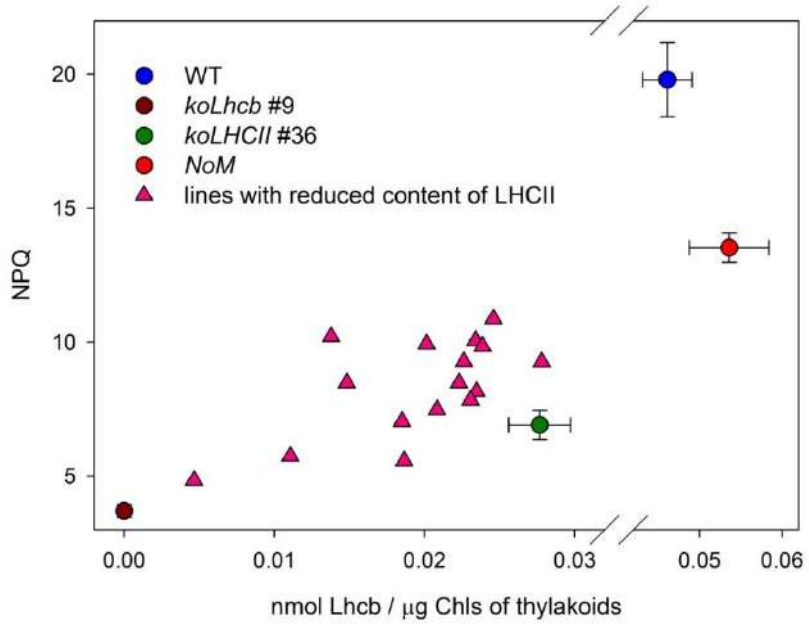

Figure 4.2.5. Correlation between NPQ amplitude and LHC content in plants expressing either monomeric LHC or trimeric LHCII only. *NPQ amplitude was measured in wild type and mutant plants devoid of specific LHC subunits (NoM, koLHCII, koLhcb), and in a segregating population obtained by NoM through the inactivation of multiple Lhcb1/Lhcb2 genes by Cas9-based nucleases (Figure S4.2.6A). For each plant: (i) LHC content was estimated by SDS–PAGE, Coomassie staining and densitometric analysis; (ii) definite integrals were calculated from NPQ curves in the range 0–8 min (Figure S4.2.6B). Data are expressed as mean ± s.d., n = 4 biologically independent plants. Each experimental point represents the LHCII content of the line and the definite integral from its NPQ traces. koLHCII leaves, which express only monomeric LHC, showed significantly lower NPQ amplitude that leaves expressing stoichiometric amount of LHCII (two-sided Student's t-test, P < 0.05).*

We then tested the photosensitivity of LHC-genome edited lines by monitoring maximal photochemical yield of PSII (F_v/F_m) during 6 hours under EL at low temperature (550 μmol photons m^{-2} s^{-1}, 4°C), a condition enhancing photooxidative stress (Figure 4.2.6). In wild type plants, F_v/F_m gradually decreased to 80% of the initial value. The F_v/F_m decline was significantly faster in *NoM* leaves with respect to those of *koLHCII* (photoinhibition $t_{1/2}$: 1.4 h for *NoM vs.* 1.9 for *koLHCII*). The *lowLHCII* lines resulted as the most photosensitive (photoinhibition $t_{1/2}$: 1.1 h). We conclude that the photoprotection in *koLHCII*, which appears to depend on the presence of monomeric LHCs, was significantly higher with respect to that in *lowLHCII* lines. This is in contrast with the observed higher quenching capacity associated to LHCII compared to monomeric Lhcb. These results are consistent with the Chl photobleaching kinetics of leaf discs exposed to stronger light (1800 μmol photons m^{-2} s^{-1}, 4°C) for 14 hours, which was effective in producing faster bleaching of *lowLHCII* discs with respect to *koLHCII*, whereas the wild type was the least affected (Figure S4.2.8).

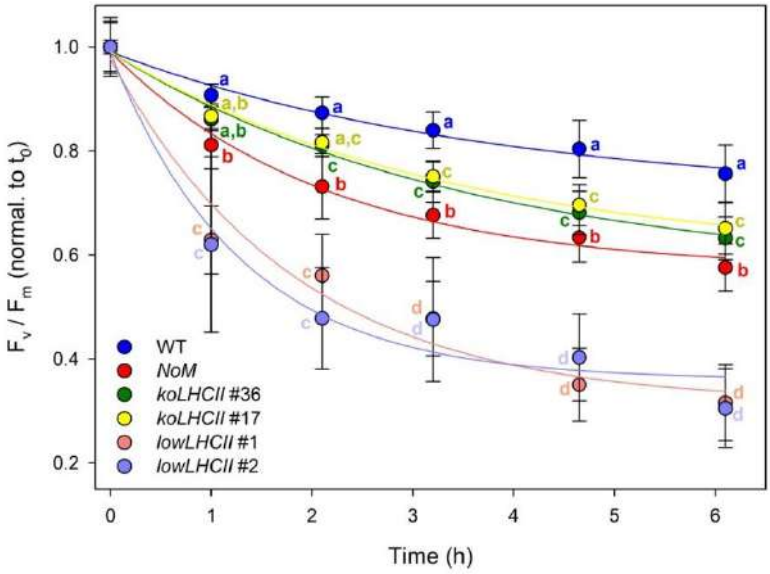

Figure 4.2.6. Photooxidation of wild type and LHC mutants exposed to excess light and low temperature. *PSII photoinhibition (F_v/Fm decay) was followed in wild type and antenna-depleted mutant (NoM, koLHCII, lowLHCII) plants, treated at 550 µmol photons m^{-2} s^{-1}, 4°C for 6 h. Data are expressed as mean ± s.d., n = 10 biologically independent samples, and all individual data points are shown. Values marked with different letters are significantly different from each other within the same time point (ANOVA followed by Tukey's post-hoc test at a significance level of P < 0.05).*

Discussion and conclusions

Tuning of photosynthetic light-use efficiency requires thylakoid lumen acidification, the pigment-less subunit PsbS and Chl *a*/*b*-xanthophyll binding LHC proteins where quenching occurs through modulation of either Chl/Chl or Chl/carotenoid interactions (Ruban, 2016). Redundancy within Lhcb subfamily is the main obstacle for the identification of quenching site(s); yet, the properties of gene products could be dissected by reverse genetics: previous work showed that depletion of either trimeric LHCII (Nicol et al., 2019) or monomeric LHCs (Dall'Osto et al., 2017) affected quenching activity. Nevertheless, the localization of quenching reactions incited a lively debate on whether quenching sites are hosted in LHCII only or in multiple sites (Nicol et al., 2021; Ruban and Wilson, 2020; Guardini et al., 2020; Bassi and Dall'Osto, 2021). Here, we characterized mutant lines devoid of specific Lhcb subgroups and, further, introduced mutations in qE-related genes, yielding to the following conclusions:

First, trimeric LHCII hosts PsbS-dependent quenching sites. The comparison of the NPQ activity of wild-type *vs. koLHCII* showed a decrease in quenching activity by approx. 68% (Figure 4.2.3). It is possible that this figure might be somehow overestimated because of the observed decrease in the level of PsbS and (ii) the amplitude of *pmf* per leaf surface (Figure 4.2.2) in the mutant. It is worth noting, however, that the reduced LHCII complement might well require less PsbS for saturation of PsbS-LHCII binding sites.

Second, monomeric LHCs contribute to NPQ. Indeed, the *koLhcb* lacking both trimeric LHCII and monomeric LHCs, undergoes a further decrease in the NPQ activity to ~22% of WT value (Figure

4.2.3). In this case PsbS content, the amplitude of *pmf* and the xanthophyll de-epoxidation index were comparable in *koLHCII vs*. *koLhcb* plants (Figure 4.2.2). Thus, we can reasonably conclude that the differences in NPQ between these genotypes originated from quenching site(s) located within the monomeric LHCs. Among those is the *a6*03-*a6*09-*a6*16 Chl cluster of CP29 (Lhcb4) (Guardini et al., 2020).

Third, CP26 contributes to the NPQ in *ch1* plants. This is evinced from the strong NPQ reduction in *ch1 koLhcb5 vs*. *ch1* (Figure 4.2.3). Indeed, these two genotypes showed a significant difference in PSII antenna size (Figure S4.2.2), implying CP26, the only Lhcb protein stable in the absence of Chl *b* (Croce et al., 2002a; Havaux et al., 2004) is excitonically connected to PSII RC. (De Bianchi et al., 2008) did not observe a reduced NPQ activity in *koCP26 vs.* WT, suggesting that CP26 might not be available for interaction with PsbS because of screening by LHCII interactors, which are missing in *ch1*. These results imply that Chl *b*-deficient mutant *ch1* cannot be used as reliable proxy for LHC-less plants.

Fourth, PSII core complex contributes to NPQ activity. Indeed, a rapidly reversible quenching was measured in *koLhcb* plants corresponding to ~22% of the level measured in WT (Figure 4.2.3), which is absent in *npq4.* This is consistent with a previous proposal (Finazzi et al., 2004) and with reports of direct interactions between PsbS and the core complex (Correa-Galvis et al., 2016; Haniewicz et al., 2013). We conclude that quenching reactions occur at multiple sites of the PSII supercomplex, in agreement with multi-site models for NPQ mechanism (Holzwarth et al., 2009; Farooq et al., 2018; Finazzi et al., 2004).

Our results support a model in which quenching originates from the interaction between PsbS and either minor or major LHC complexes rather than from aggregation of LHCII trimers disconnected from PSII supercomplexes (Horton et al., 1991). Indeed, NPQ activity is maintained, although to a different extent, whenever PsbS and Zea are present, including *koLHCII* and *koLhcb* genotypes which lack LHCII completely (Figure 4.2.4)

Interaction of PsbS with monomeric LHCs is expected to trigger conformational change(s), likely favored by the Vio/Zea exchange and by the formation of interactions between Chl *a* ligands and the xanthophyll in binding site L2 (Avenson et al., 2008; Ahn et al., 2008; Guardini et al., 2020). One additional PsbS interaction site is located in LHCII as shown by the null qE in the *NoM npq4* mutant (Dall'Osto et al., 2017). This interaction requires Zea, possibly located at the interface between PsbS and its LHCII interactor (Wilk et al., 2013). Topological analysis showed that induction of NPQ also involves dissociation of the $C_2S_2M_2$ supercomplex (Betterle et al., 2009; Johnson et al., 2011), while the robust quenching detected in *NoM*, lacking PSII supercomplexes, and in *lowLHCII* plants (Figure 4.2.4) supports the evidence that LHCII trimers are a site of quenching, irrespective from their assembly in PSII supercomplexes.

Thus, individual PsbS-dependent quenching reactions in mutants retaining subsets of PSII antenna system, either monomeric or trimeric LHCs, require Zea only for full expression of activity and are insensitive to the *lut2* mutation (Figure 4.2.4) (Dall'Osto et al., 2017). This is unexpected since Lut dependence of qE in plants has been well documented: *Arabidopsis lut2* mutant showed reduced qE and the *npq1 lut2* double mutant is null in qE (Niyogi et al., 2001).

Furthermore, over-accumulation of Lut in the *Arabidopsis szl1* mutant enhanced the amplitude of qE (Li et al., 2009a), suggesting that Lut ligands in LHCs play a direct role in quenching reactions. When focusing on the trimeric LHCII, we observe that Vio and Lut can substitute for each other in the same quenching site(s) as shown by the identical NPQ competent phenotype of the *NoM lut2* and *NoM* genotypes while the *NoM npq1* was severely affected (Dall'Osto et al., 2017). Since LHCII of *NoM* and *NoM lut2* differ for occupancy of xanthophyll binding sites L1 and L2 by Lut *vs.* Vio respectively, and yet they have the same Zea-dependent quenching activity, we conclude that the Zea dependent quenching effect is consequent to Zea binding to the site V1, the only site that undergoes Vio>Zea exchange in LHCII (Caffarri et al., 2001; Morosinotto et al., 2002). In order to explain the loss of Lut dependence in both *NoM* and *koLHCII* we can consider that the *lut2* mutation does affect trimerization of LHCII as well as formation of PSII supercomplexes (Lokstein et al., 2002) owing to a conformational change caused by Lut>Vio substitution in xanthophyll binding site L1 (Dall'Osto et al., 2005). If quenching is catalyzed by a PsbS-LHCII interaction (Nicol et al., 2021; Wilk et al., 2013) the monomerization of trimeric LHCII might either affect the interaction with PsbS directly, by modifying the strength of binding and/or by reducing the pigment bed size quenched by each PsbS-LHC complex with a given PsbS/LHC stoichiometry. Thus, Lut might support quenching by propagating it to neighbor LHC subunits and supercomplexes (Bennett et al., 2018). Instead, in monomeric LHCs, the identity of the pigment in L1 is not important for determining NPQ activity, as shown by unaltered qE activity in *koLHCII lut2* plants. This is consistent with the finding that in CP29 the pigment cluster Chls *a6*11 - Chl *a6*12 (a2) and Lut at site L1 is not essential for NPQ competence (Guardini et al., 2020). Also, the effect of *koLHCII lut2* mutations *in vivo* implies that at least one important component of qE cannot be ascribed to the process of LHCII clustering and aggregation (Johnson et al., 2011) mimicking the quenching *in vitro*, where Lut was proposed to be a quencher even in minor antennae (Ruban et al., 2007; Mozzo et al., 2008).

Quenching reactions are photoprotective (Bassi and Dall'Osto, 2021) and yet it can be asked whether the location of quenching sites within the antenna system might determine the level of photoprotection. A faster PSII photoinhibition rate was observed in *NoM vs.* wild type (Fig. 4.2.6), implying that monomeric LHCs were essential for efficient photoprotection and their function could not be compensated by over-accumulating trimeric LHCII. Moreover, monomeric LHCs hold specific function(s) crucial in optimising photoprotection. *NoM* sensitivity to photooxidation was associated to enhanced production of $^1O_2$ (Dall'Osto et al., 2020) from excess ^{1}Chl* in LHCIIs badly connected to the PSII core (Dall'Osto et al., 2014c). Conversely, xanthophylls bound to LHCs have enhanced $^1O_2$ scavenging activity (Johnson et al., 2007) making LHC-rich thylakoids more resistant to HL. In order to assess the relative importance of ROS scavenging *vs.* other protective mechanisms, we have produced the *lowLHCII* genotype. Indeed, *NoM* plants have up to 7 LHCII trimers per PSII core while *koLHCII* only have the equivalent of 1 trimer, i.e. three LHC monomers (Figure 6). The *lowLHCII* genotype was similar to *NoM* in not retaining monomeric LHCs and yet it had the same PSII/LHC stoichiometry as *koLHCII*. Since photosensitivity was ranked in the *lowLHCII* >> *NoM*> *koLHCII* > WT, we conclude that monomeric LHCs are far more effective in protecting PSII from photoinhibition as compared to LHCII. Possible mechanisms preventing photoinhibition include: (i) thermal dissipation of ^{1}Chl* by qE, (ii) scavenging of ROS

or (iii) quenching of ^{3}Chl* (Niyogi, 1999). We observed higher NPQ in *lowLHCII vs. koLHCII* suggesting qE was not the major protective component. Alternatively, (ii) we might hypothesize that monomeric LHCs may form a protective barrier surrounding the PSII core, thus preserving RC from either ROS or peroxy-lipids radicals produced in the peripheral LHCII or PSI. However, purified monomeric LHCs were more prone to photoxidation respect to LHCII (Dall'Osto et al., 2006), consistent with the higher efficiency of Chl to Car triplet transfer in trimeric LHCII (Mozzo et al., 2008). The increased efficiency in controlling ^{3}Chl* formation might be the mechanism that makes PSII more resistant to EL when binding monomeric LHCs. Beside β-carotene which has a crucial role in protecting P680 (Krieger-Liszkay et al., 2008; Telfer, 2002) xanthophylls bound to monomeric LHCs and surrounding the core could enhance phototolerance, possibly favoring loss of excitation energy over RC or draining of ^{3}Chl* energy from RC (Nayak et al., 2002).

In conclusion, we highlighted a specific role for monomeric LHCs in catalyzing qE and, to a greater extent, in providing efficient photoprotection when bound to PSII core. This accounts for the higher photosensitivity of plants in which minor antennae are replaced by LHCII, and confirm the existence of a specific protective effect of monomeric LHCs, besides qE energy quenching, which limits photoinhibition. We suggest the mechanism is related with Zea binding to monomeric LHCs, which was shown to modulate the yield of ^{3}Chl* *in vivo* and to prevent ROS release (Dall'Osto et al., 2012).

Methods

Plant material and growth conditions

Wild type plants of *Arabidopsis thaliana* (Col-0) and mutants *NoM*, *koLHCII*, *koLhcb*, *ch1*, *ch1 koLhcb5* and *npq4* were obtained as previously described (Li et al., 2000; Havaux et al., 2007; Dall'Osto et al., 2017; Guardini et al., 2022). Multiple mutant *ch1 koLhcb5 npq4* was isolated by crossing single mutants and selecting progeny by immunoblotting. *koLHCII npq4*, *koLHCII npq1*, *koLHCII lut2* lines were obtained by genome editing as reported in (Ordon et al., 2020). Plants were grown in a phytotron for 6 weeks at 150 μmol photons m^{-2} s^{-1}, 23°C, 70% humidity, 8/16 h of day/night.

Membrane isolation

Chloroplasts and stacked thylakoid membranes were isolated as previously described (Casazza et al., 2001)

Pigment analysis

To measure zeaxanthin accumulation, detached leaves were exposed to 1000 μmol photons m^{-2} s^{-1}, at room temperature (RT, 22°C). Pigments were extracted with 85% acetone buffered with Na_2CO_3, and quantified either by HPLC (Jasco Extrema LC-4000) as in (Gilmore and Yamamoto, 1991a) or from deconvolution of spectra of acetonic extracts (Croce et al., 2002a).

Spectroscopy

Absorption measurements were performed at RT using a SLM Aminco DW-2000 spectrophotometer. Light-induced pmf and ECS_t were estimated from changes in leaf absorbance at 520 nm (Livingston et al., 2010) with a JTS10 (Biologic Science Instruments).

Gel electrophoresis and immunoblotting

SDS-PAGE analysis was performed using the Tris-Tricine buffer system (Schägger and von Jagow, 1987). For immunotitration (Towbin et al., 1979), proteins were electroblotted on nitrocellulose membranes, then detected with alkaline phosphatase-conjugated antibody (Sigma-Aldrich A3687). Primary antibodies used were: α-PsbB/CP47 (AS04 038), α-Lhcb1 (AS01 004), α-Lhcb2 (AS01 003), α-Lhcb3 (AS01 002), α-ATPase (AS05 085), α-cytochrome *f* (AS20 4377), α-PsaA (AS06 172) from Agrisera; α-PsbS, α-Lhcb4, α-Lhcb5, α-Lhcb6 were home-made.

Analysis of Chl fluorescence

Chl fluorescence parameters were measured on leaves at RT with a Dual-PAM (Heinz-Walz) and calculated according to (Kramer et al., 2004; Baker, 2008) State transition experiments were performed according to established protocols (Lunde et al., 2000) The parameter qT (PSII cross-section changes) was calculated as (Fm′−Fm″) / Fm′ · 100, where Fm′/″ is the maximal fluorescence yield in state I/II. Fluorescence kinetics were measured in leaves vacuum-infiltrated with $3 \cdot 10^{-5}$ M DCMU and 100 mM sorbitol, the half-time of the fluorescence rise was taken as a measure of the functional antenna size of PSII (Malkin et al., 1981).

Determination of the sensitivity to photooxidative stress

Photooxidative stress was induced in detached leaves, exposed to excess light (550 μmol photons m^{-2} s^{-1}, 8°C, light provided by 150 W halogen lamp) following the decay kinetics of maximal quantum yield of PSII photochemistry (F_v/F_M) (Havaux et al., 2004) Photobleaching *in vivo* was induced in leaf discs at 1800 μmol photons m^{-2} s^{-1}, 8°C as reported in (Dall'Osto et al., 2012)

Statistics

Significance analysis was performed using either Student's *t* test or ANOVA in GraphPad Prism (see the figure legends for details).

Data availability

Sequence data from this article can be found in the *Arabidopsis* Genome Initiative or GenBank/EMBL databases under accession numbers At1g29920 *(Lhcb1.1*), At1g29910 (*Lhcb1.2*), At1g29930 (*Lhcb1.3*), At2g34430 (*Lhcb1.4*), At2g34420 (*Lhcb1.5*), At2g05100 (*Lhcb2.1*), At2g05070 (*Lhcb2.2*), At3g27690 (*Lhcb2.3*), At5g54270 (*Lhcb3*), At5g01530 (*Lhcb4.1*), At3g08940 (*Lhcb4.2*), At4g10340 (*Lhcb5*), At1g44446 (*cao*), At1g08550 (*npq1*), At1g44575 (*npq4*), At5g57030 (*lut2*). The KO lines used in the work were obtained from the NASC under the stock numbers N376476

(*koLhcb4.1*), N877954 (*koLhcb4.2*), N514869 (*koLhcb5*), N520342 (*koLhcb3*), N524295 (*ch1*). *npq4* mutant was kindly provided from K.K. Niyogi.

Funding

The work was supported by grant RIBA 2017 to R.B. and grant PRIN 2017 (201795SBA3_004, HARVEST) to L.D.

Author contributions

R.B. and L.D. conceived the work and designed the experiments. Z.G. carried out the construction of mutants and performed their biochemical and physiological characterization, together with L.D. and R.C. R.L.G. analyzed Chl fluorescence kinetics. All authors contributed to writing the manuscript, discussed the results and commented on the manuscript.

Supporting information

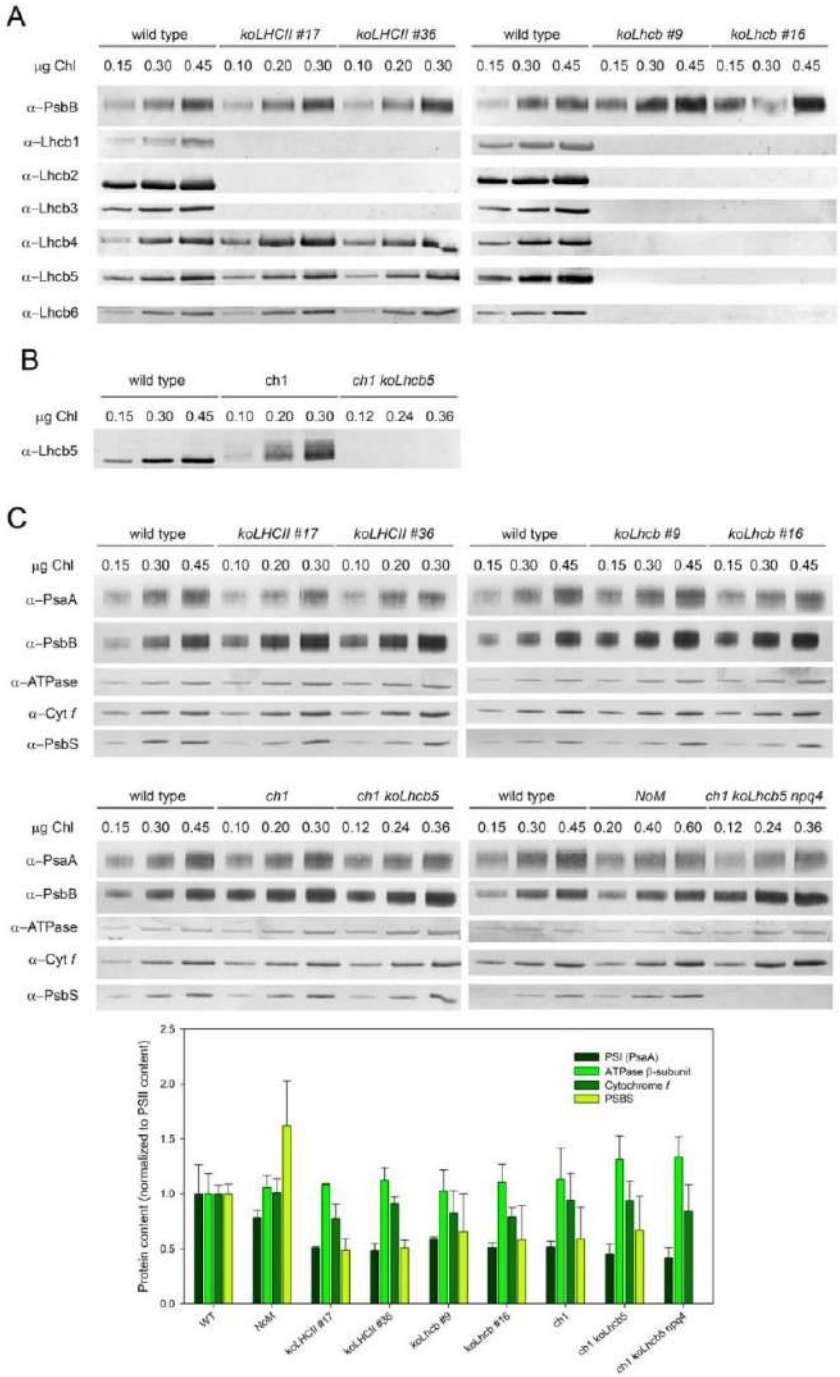

Figure S4.2.1. Immunoblotting used for the quantification of the major photosynthetic subunits in wild type and mutant thylakoids. *Immunoblot analysis was performed with antibodies directed against individual gene products: Lhcb proteins and the PSII core subunit PsbB (CP47) (panels A, B), and subunits of the major supercomplexes of thylakoids (PsaA, PsbB, cytochrome f, ATPase β subunit, panel C). Data of each subunits were normalized to the PSII core amount (PsbB content) and expressed with respect to the corresponding wild type value. The amounts of Chl loaded are indicated in each lane. Wild type and mutant samples were compared only when loaded on the same SDS–PAGE slab gel.*

Figure S4.2.2

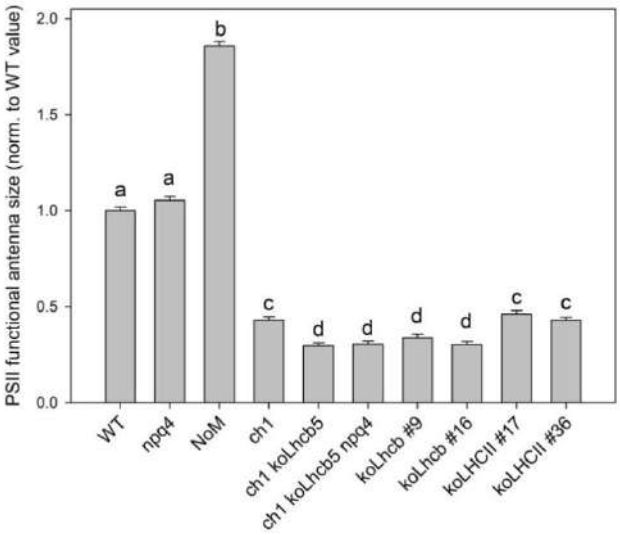

Figure S4.2.2. Functional antenna size of PSII, measured in wild type and mutant leaves. *Variable Chl fluorescence was induced at RT with a green light (15 μmol photons m^{-2} s^{-1}), on leaves vacuum-infiltrated with 30 μM DCMU. The reciprocal of time corresponding to two-thirds of the fluorescence rise ($t_{2/3}$) was taken as a measure of the PSII functional antenna size. Plants were dark-adapted for 30 min before each measurement. Data are expressed as mean ± S.D., n ≥ 8 biologically independent leaves. Values marked with different letters are significantly different from each other (ANOVA followed by Tukey's post-hoc test at a significance level of P < 0.05). Experiments were repeated independently twice, with similar results.*

Figure S4.2.3

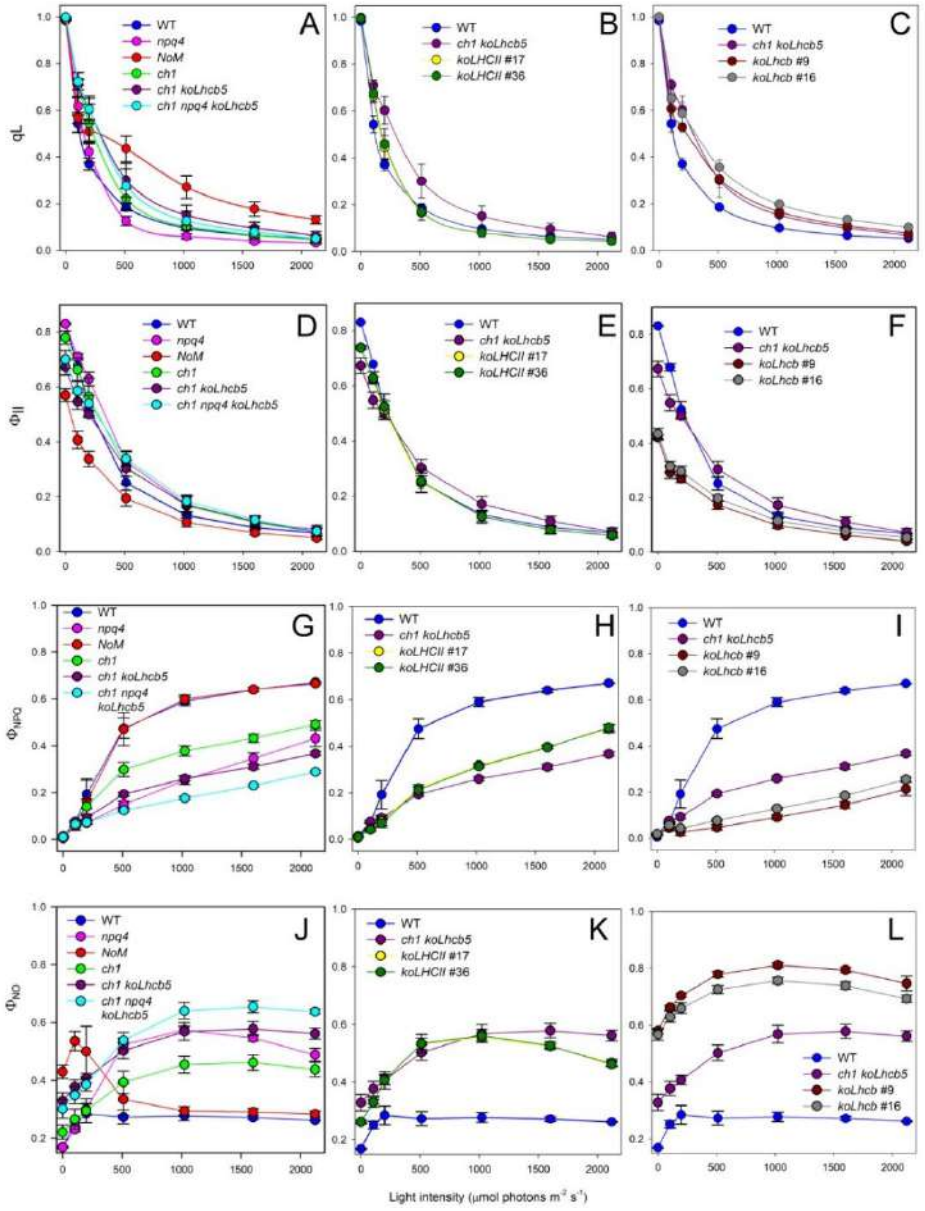

Figure S4.2.3. Analysis of Chl fluorescence and energy partitioning during photosynthesis in wild type and mutant leaves at RT. *(A-C) Light intensity dependence of the parameters qL, which reflects the redox state of the primary electron acceptor Q_A, thus the fraction of open PSII centers (qL=0, all centers are closed). (D-L) Light intensity dependence of quantum yield of PSII photochemistry (Φ_{II}, panels D-F), regulated quenching (Φ_{NPQ}, panels G-I) and unregulated quenching events (Φ_{NO}, panels J-L). Plants were dark-adapted for 30 min before measurements. Each value is expressed as mean ± s.d., n = 5 independent plants.*

Figure S4.2.4

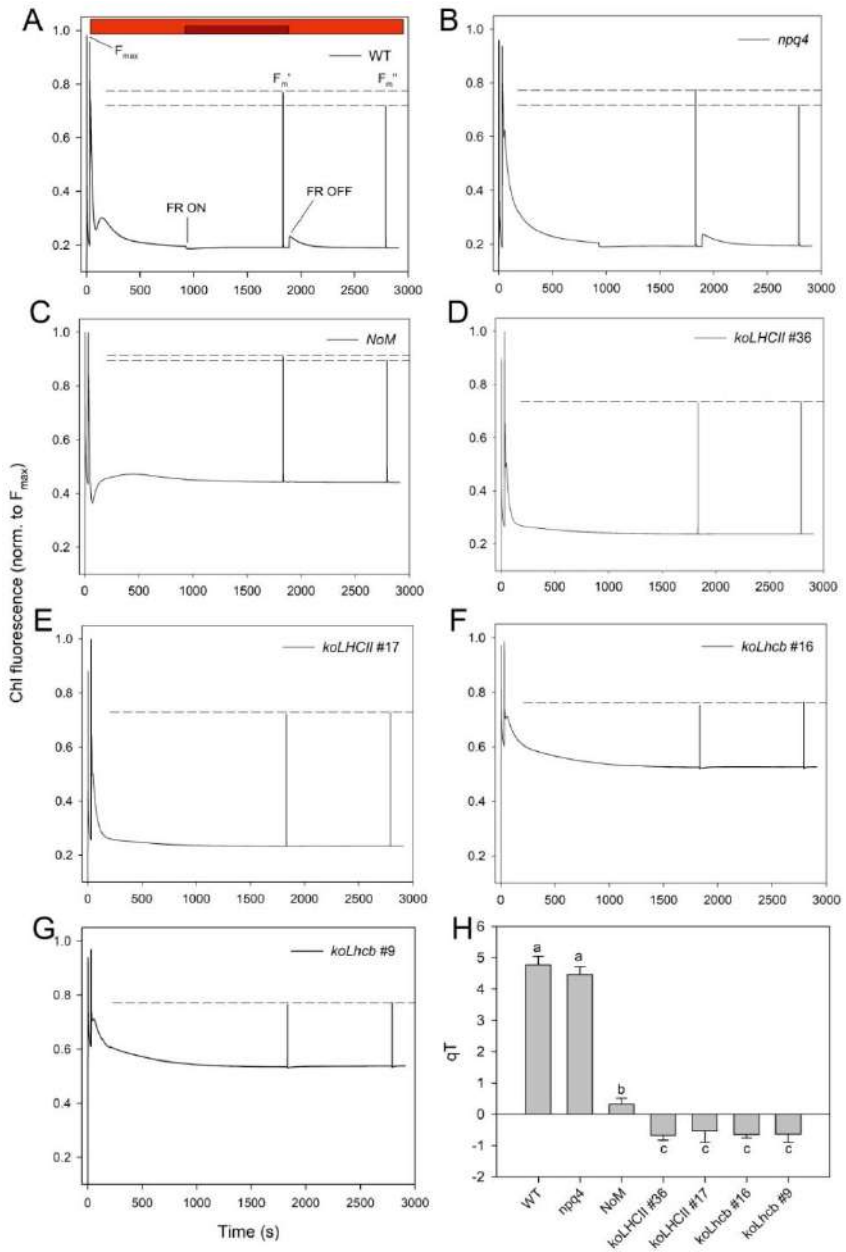

Figure S4.2.4. Measurement of state I - state II transition. *(A-G) Upon 1-h dark adaptation, wild type and mutant leaves were illuminated with red light (50 µmol photons m^{-2} s^{-1}, red bar) for 15 min to reach state II, then a far-red light (FR, dark-red bar) was superimposed on the red light to induce a transition to state I. F_{max}, and F_m levels in state I (F_m') and state II (F_m'') (see panel A) were determined by the application of a saturating light pulse (4000 µmol photons m^{-2} s^{-1}, 0.6 s). (H) The parameter qT (PSII antenna cross-section changes) was calculated as ($F_m' - F_m''$)/F_m'·100, where F_m'/'' is the maximal fluorescence yield in state I/II). Data are expressed as mean ± s.d., n = 3 biologically independent leaves. Values marked with different letters are significantly different from each other (ANOVA followed by Tukey's post-hoc test at a significance level of $P < 0.05$).*

Figure S4.2.5

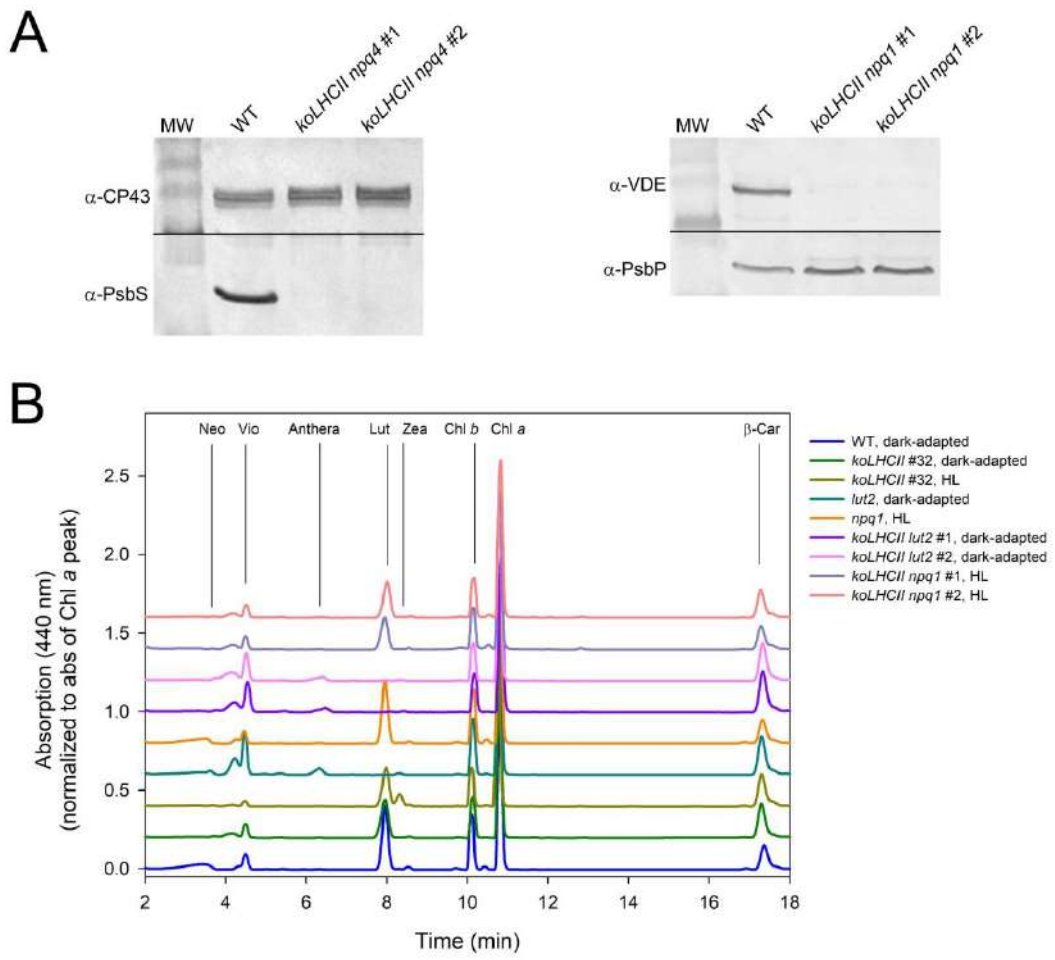

Figure S4.2.5. Characterization of koLHCII npq and lut2 lines. *Mutant lines were obtained by selection of the progeny from combining koLHCII with npq / lut2 single mutants by genome editing. (A) Immunoblotting used for the identification of koLHCII npq4 (left panel) and koLHCII npq1 (right panel). Immunoblot analysis was performed with antibodies directed against individual gene products: VDE (violaxanthin de-epoxidase), PsbS and the PSII core subunits PsbC (CP43) and PsbP; leaf extracts corresponding to ~2 μg of Chls were loaded for each sample. All samples were loaded on the same SDS–PAGE slab gel. (B) Analysis of pigment content of leaves from wild type and mutant plants. Separation of lipid-soluble pigments was based on HPLC analysis. Each chromatogram represents absorbance at 440 nm of pigments extracted from leaves either dark-adapted or exposed for 20 min to HL (550μmol photons m^{-2} s^{-1} at RT). Chromatograms were vertically shifted for better comparison. Peaks corresponding to the major pigment species are marked. HPLC experiments were repeated independently twice, with similar results.*

Figure S4.2.6

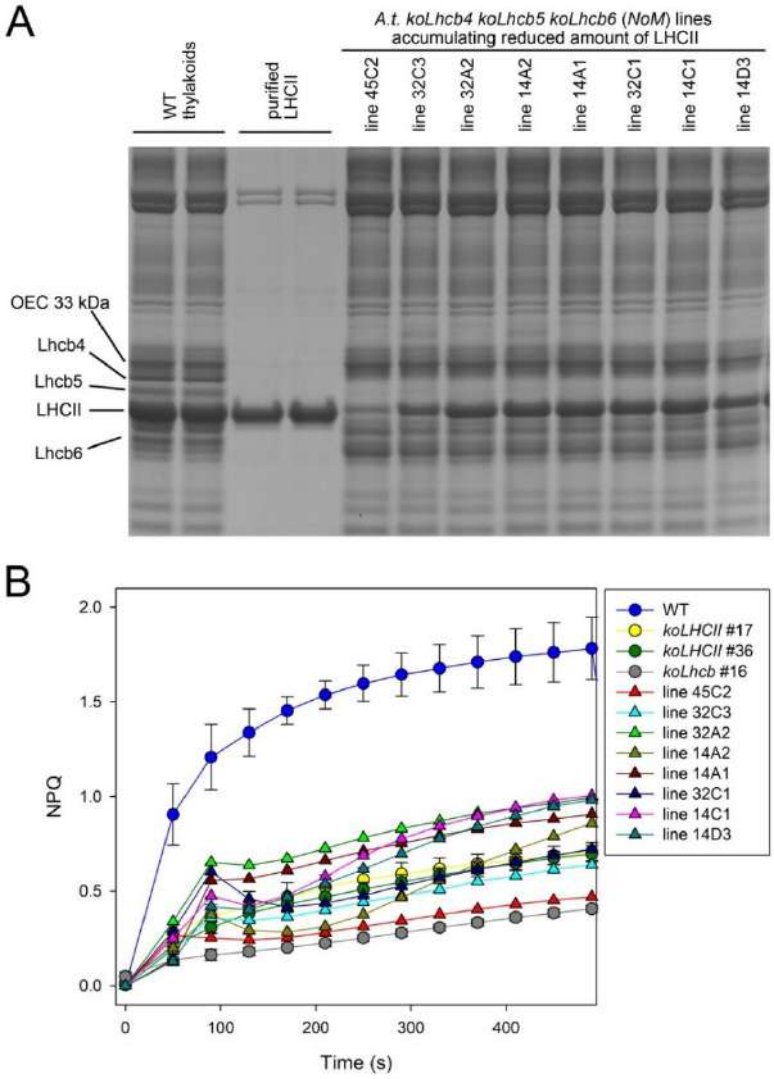

Figure S4.2.6. Characterization of NoM lines expressing a variable amount of the LHCII antenna. *(A) SDS–PAGE fractionation of purified LHCII and of thylakoid proteins from both WT and NoM lines expressing reduced amount of LHCII. The latter were obtained by a segregating population of A. thaliana NoM obtained from incomplete gene editing of both Lhcb1 and Lhcb2. Purified proteins and thylakoids corresponding to 4 µg and 10 µg of Chls, respectively, were loaded. The level of LHCII (mol protein / mol Chls of thylakoids) was determined by densitometry of Coomassie-stained gel. (B) Kinetics of formation and relaxation of photoprotective energy dissipation, measured following illumination of leaves with 1,000 µmol photons m^{-2} s^{-1} at RT. Lines WT, koLHCII L17 and L36, koLhcb L16: data are expressed as mean ± s.d., n = 4 biologically independent plants. Segregating population: each trace corresponds to a different plant. Experiments were repeated independently twice, with similar results.*

Figure S4.2.7

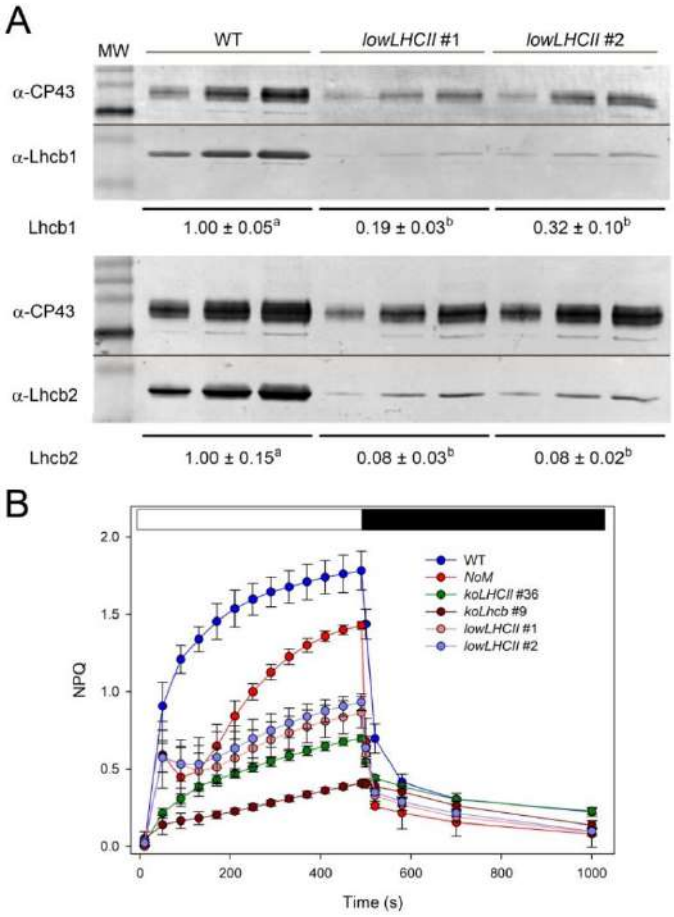

Figure S4.2.7. Characterization of lowLHCII lines. *(A) Immunoblotting used for the quantification of photosynthetic subunits in the wild type and lowLHCII thylakoids. lowLHCII lines were obtained from independent transformants (T1 generation, see Figure S4.2.6), that were self-fertilized and then homozygous lines were confirmed in the T3 generation. Immunoblot analysis was performed with antibodies directed against individual gene products: Lhcb1, Lhcb2 and the PSII core subunit PsbC (CP43); leaf protein extracts corresponding to 0.1, 0.25 and 0.5 μg of Chls were loaded for each sample. All samples were loaded on the same SDS–PAGE slab gel. Data of PSII antenna subunits were normalized to the core amount (PsbC content) and expressed with respect to the corresponding wild type value. Results of the immunotitration of thylakoid proteins are reported in the lower part of each filter. Values marked with different letters are significantly different from each other within the column (ANOVA followed by Tukey's post-hoc test at a significance level of $P < 0.05$). (B) Kinetics of formation and relaxation of photoprotective energy dissipation, measured following illumination of leaves with 1,000 μmol photons m^{-2} s^{-1} at RT. White and black bars represent light and dark periods. Data are expressed as mean ± s.d., n = 4 biologically independent plants. Experiments were repeated independently twice, with similar results.*

Figure S4.2.8

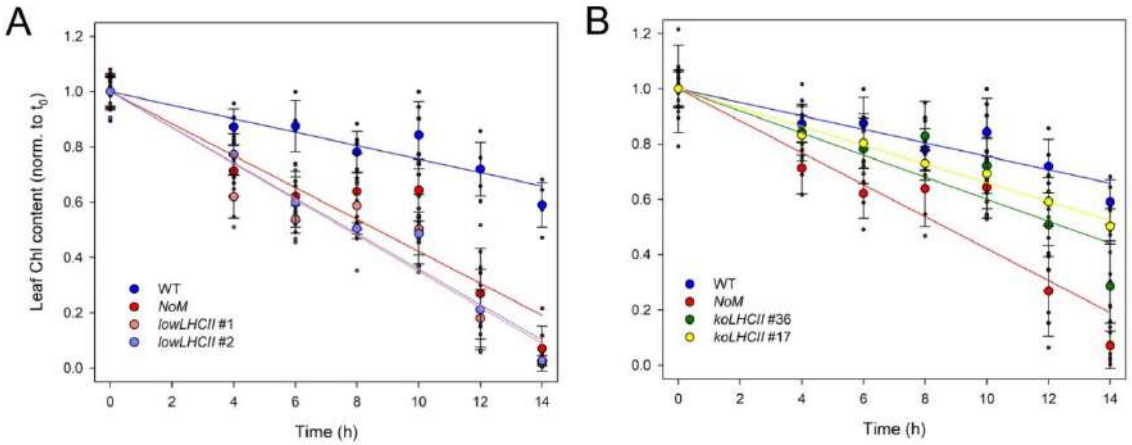

Figure S4.2.8. Photoprotective role of LHC. *Leaf discs on wet paper were treated at 1,800 µmol photons m^{-2} s^{-1} at 4°C, and kinetics of Chl bleaching were recorded. Experimental points were modeled with a linear regression. Statistical analysis (analysis of covariance) revealed that photobleaching was faster in NoM and lowLHCII leaves, which showed significantly higher photosensitivity than wild type (panel A, p = xy; differences between the slopes of mutants are not significant, p = xy); instead, koLHCII lines were more resistant than other mutants (panel B, differences between the slopes of NoM and koLHCII are significant, p = xy). Data are expressed as mean ± s.d., n = 5 biologically independent plants, and all individual data points are also shown.*

Table S4.2.1

Target	sgRNA
Lhcb1.1 - Lhcb1.5	GGTTCACAGATCTTCAGCGA
	ATGGACCC AAGTACTTGACT
	TGTGGATAACTTCT AGCTCA
	GGCTACTCAAGTTATCCTCA
	GAAGCGGCCGTGTGACAATG
	AGAAGTTATCCACAGCAGGT
	GAGGACTTGCTTTACCCCGG
	AGGGGAGGAGAGAGCCATTG
Lhcb2.1 - Lhcb2.3	CGCAAGGTTGGTGTATCCGG
	TGGAGGGCTTGAGAGCCGTT
	CGCCCAAGACGCCCACCTTT
	AGACTTGACGGTACGACGCA
	AGGGCTTGACCCGCTTTACC
	GGATCAAGTTAGGGTTTCCG
	CCAACATTGCCCATCTACTG
	TCTGGGCTGTTCAAGTTGTG
Psbs	GTTCCTCAAAAAATGGCCGG
	GAACTTTGGGCTGAGCCAAA
	CTTACTTCAGGCGTCACCGC
	CTCCGGTTGCACTACCATCT
carotene ε-cyclase (ε-CYC)	TGTAGTGTCAGAGCTAGCGG
	CGGTAGTGAGAGTTGTGTAG
	TTCCTTCGACAACTCCATGA
	TGTAGTGTCAGAGCTAGCGG
violaxanthin de-epoxidase (VDE)	AATCGAATACGGTCATGACA
	GCTGATCTCAGAACAACTGG
	CGACATTGGCTGCACAGGCA
	CATCTTGTATCCACCCACGA

Table S4.2.1. Target sites used for sgRNA design. *Sequences designed for Lhcb1 genes were the same reported in (Ordon et al., 2020).*

Table S4.2.2

	Chl a/b	Chl/Car	µg Chl / cm^2
WT	3.08 ± 0.08^{a}	4.32 ± 0.10^{a}	24.8 ± 1.7^{a}
npq1	3.07 ± 0.07^{a}	4.41 ± 0.11^{a}	28.4 ± 1.3^{b}
lut2	3.19 ± 0.08^{a}	5.22 ± 0.37^{b}	24.8 ± 2.2^{a}
koLHCII #36	$4.07 \pm 0.04^{b,c}$	$4.63 \pm 0.35^{a,b}$	14.0 ± 1.5^{c}
koLHCII npq1 #1	3.88 ± 0.19^{b}	4.28 ± 0.21^{a}	11.2 ± 1.4^{c}
koLHCII lut2 #1	4.18 ± 0.18^{c}	$4.62 \pm 0.83^{a,b}$	12.3 ± 1.5^{c}

Table S4.2.2. Pigment content determined for leaves of wild type, koLHCII, npq1 and lut2 lines*.Parameters were measured in T3 koLHCII npq1 and koLHCII lut2 plants. Chl/Car, molar ratio between chlorophylls (a + b) and carotenoids. Leaf Chl content refers to growth after 6 weeks under control conditions. Data are expressed as mean ± s.d., n = 5 biologically independent leaves. Values marked with different letters are significantly different from each other within the column (ANOVA, followed by Tukey's post test at a significance level of P < 0.05). Results displayed are representative of the independent lines.*

5. In vivo site-directed mutagenesis of Lhcb4 chlorophyll binding sites

NPQ is a photoprotective mechanism widely conserved among vascular plants. It has been studied for several years by many groups all around the world. The core components for qE activation are generally recognized as: transmembrane proton gradient in the thylakoid lumen, the molecular trigger PsbS, the xanthophylls cycle and the quenching centers, localized in the Lhcb subunits of PSII (Niyogi and Truong, 2013). In chapter 4 we confirmed the presence of at least two main quenching centers within PSII antenna system. The first one rapidly activated within monomeric Lhcb and a second one mediated by trimeric LHCII.

Among Lhcb we identified one catalytic cluster mediating fast qE activation within the monomeric Lhcb4. To do this, we applied a site-directed mutagenesis approach complementing koLhcb4 *Arabidopsis* plants with *lhcb4.1* gene isoforms mutated at the level of the triplets corresponding to specific Chl-binding residues. The cluster *a*603-*a*609-*a*616 and the xanthophyll in the site L2 resulted in having a major role in the qE activation mediated by Lhcb4 (Guardini et al., 2020)

In the second part of the chapter (5.2) we investigated how lack of a specific Chlorophyll within Lhcb4, namely Chl b614 results in an impaired thylakoid membrane organization, mainly due to the impaired accumulation of the monomeric complex Lhcb6.
In these lines the fluidity of membrane resulted affected and these mutants displayed: stunted growth, reduced plastoquinone diffusion and impaired ΔpH formation as previously observed in knock-out or knock-down lines for *lhcb6* (Kovács et al., 2006; De Bianchi et al., 2008). Lhcb6 is connected to the PSII-supercomplex by interacting with Lhcb4 (De Bianchi et al., 2011), thanks to the mutants described in chapter 5.2 we have been able to define the role of Chl b614 of Lhcb4 as docking site for Lhcb6. Mutant lines lacking Chl b614 show similar behaviors as koLhcb6 in: growth, NPQ and thylakoid supramolecular organization.

5.1 Identification of a pigment cluster catalysing fast photoprotective quenching response in CP29

nature plants

ARTICLES

https://doi.org/10.1038/s41477-020-0612-8

Check for updates

Identification of a pigment cluster catalysing fast photoprotective quenching response in CP29

Zeno Guardini, Mauro Bressan, Roberto Caferri, Roberto Bassi and Luca Dall'Osto ✉

Abstract

Non-photochemical quenching is the photoprotective heat dissipation of chlorophyll-excited states. In higher plants, two quenching sites are located in trimeric LHCII and monomeric CP29 proteins. Catalysis of dissipative reactions requires interactions between chromophores, either carotenoid, chlorophyll or both. We identified CP29 protein domains involved in quenching by complementing an *Arabidopsis* deletion mutant with sequences deleted in pigment-binding or pH-sensitive sites. Acidic residues exposed to the thylakoid lumen were found not essential for activation of thermal dissipation in vivo. Chlorophylls *a*603 (a5) and *a*616 were identified as components of the catalytic pigment cluster responsible for quenching reaction(s), in addition to xanthophyll L2 and chlorophyll *a*609 (b5). We suggest that a conformational change induced by acidification in PsbS is transduced to CP29, thus bringing chlorophylls *a*603, *a*609 and *a*616 into close contact and activating a dissipative channel. Consistently, mutations on putative protonatable residues, exposed to the thylakoid lumen and previously suggested to regulate xanthophyll exchange at binding site L2, did not affect quenching efficiency.

Introduction

Plants use light to drive electron transport from H_2O to nicotinamide adenine dinucleotide phosphate+, synthesize ATP and, ultimately, fix CO_2 into sugars (Nelson and Ben-Shem, 2004). The primary event consists of photon absorption by an array of chlorophylls (Chls) and carotenoids (Cars), organized into photosystems (PSs). Within each PS, a core complex hosts the electron carriers mediating charge separation while a peripheral light-harvesting (antenna) system expands its absorption cross-section (Van Amerongen and Croce, 2013). Although a large antenna is strategic for maximization of energy supply under limiting light, it causes excitation beyond the capacity for photochemical reactions in excess light conditions: unquenched singlet-excited states of Chl (^{1}Chl*) undergo intersystem crossing into triplets (^{3}Chl*), which react with O_2 to yield singlet oxygen ($^1O_2$) and ultimately result in photodamage (Krieger-Liszkay, 2005). Photosystem II (PSII) quantum efficiency is regulated by a set of inducible mechanisms, collectively referred to as non-photochemical quenching (NPQ), which dissipate most of the absorbed photons as heat (Ruban et al., 2012). Transduction of low luminal pH, caused by excess

irradiation, into activation of the fastest NPQ component, qE, requires PsbS, a pigment-less subunit localized in the grana, together with PSII (Li et al., 2004) (Dominici et al., 2002), implying that the events leading to quencher formation must be located in the pigment-binding subunits inter acting with PsbS. The PSII antenna system is arranged as an inner layer of mono- meric light-harvesting complexes (LHCs: Lhcb4/CP29, Lhcb5/ CP26 and Lhcb6/CP24) and an outer cluster of heterotrimeric LHCII (Lhcb1–3) which, together, form supercomplexes (Wei et al., 2016) that undergo dynamic changes depending on the light environment (Betterle et al., 2009). Reverse genetics identified two different qE mechanisms operating in different parts of the PSII antenna (Dall'Osto et al., 2017): monomeric LHCs contributing to the early phase of quenching, while the slower response is dependent on LHCII. *Arabidopsis thaliana* knockout (ko)Lhcb4 mutants exhibited markedly decreased qE, while mutants koLhcb5 and koLhcb6 were far less affected (De Bianchi et al., 2008, 2011), implying that Lhcb4 is crucial for qE response and that it a target of choice for analysis of quenching site architecture. The structures of Lhcb4 (Pan et al., 2011; Wei et al., 2016; Su et al., 2017) revealed several features, including the presence of 14 Chl and 3 xanthophyll binding sites. Here, to explore the molecular details of the quenching site in Lhcb4, we carried out a structure–function analysis by in vivo site-directed mutagenesis. Acidic residues exposed to the thylakoid lumen were not essential for activation of light-induced quenching activity. Chls *a*603 (a5) and *a*616 were identified as components of the catalytic pigment cluster responsible for quenching reaction(s), also including xanthophyll in L2 and Chl *a*609 (b5).

Characteristics of koLhcb4 plants complemented with the wild-type sequence Lhcb4.1

The fast component of NPQ increasing with illumination (Dall'Osto et al., 2017) is depleted in the NoM mutant, which lacks the three monomeric Lhcb proteins CP29, CP26 and CP24, while it retains a full complement of trimeric LHCII. Since koLhcb5 did not affect increase in NPQ (De Bianchi et al., 2008) while CP24 did not accumulate under conditions of excess light (Ballottari et al., 2007), CP29 plays a key role in the rapid qE response. Also, increased NPQ in the koLhcb5 koLhcb6 double mutant (Supplementary Fig. 5.1.1) can be ascribed to incomplete accumulation of CP29 (ref. (De Bianchi et al., 2011)). Quenching of Chl-excited states involves perception of changes in the luminal pH, and requires Chl and xanthophyll chromophore(s) for catalysis of quenching reactions. We therefore proceeded to create *A. thaliana* strains carrying CP29 mutated in specific sites, either sensing luminal pH or binding Chl ligands included in pigment clusters, with the target of identifying domains whose disruption negatively affects the ability to trigger NPQ. For this purpose, the gene Lhcb4.1 was amplified from *Arabidopsis* wild-type (WT) genomic DNA using primers designed to include both the promoter region and 389 base pairs (bp) down-stream of the stop codon. The genomic fragment was cloned in the vector pK7WG2 for *Agrobacterium*-mediated transformation. As a positive control for site-directed mutants, koLhcb4 *Arabidopsis* plants were transformed with the WT *A.t.*-Lhcb4.1 gene by floral dipping, and three independent kanamycin-resistant transgenic lines (Lhcb4.1 lines 12.1, 13.2 and 24.3) were selected based on the abundance of CP29 protein in leaf extracts. CP29 with the WT sequence accumulated in complemented lines at the same level as WT *Arabidopsis* (Fig. 5.1.1a). SDS–polyacrylamide gel electrophoresis (SDS–PAGE) analysis of thylakoid proteins confirmed that the gene product was targeted to thylakoid membranes (see Fig. 5.1.2a). Complemented lines showed Chl content per leaf area, Chl a/Chl b and Chl/Car ratios and a quantum efficiency of PSII (Fv/Fm), where Fv and

Fm indicate the variable and maximal fluorescence from dark-adapted leaves, respectively, measured after the application of a saturating flash indistinguishable from WT (Table 5.1.1), and all lines exhibited restoration of NPQ activity to WT level (Fig. 5.1.1b). Growth rate compared to WT was also maintained (Table 5.1.1), implying that the transformation process of koLchb4 plants with the WT CP29 sequence did not induce detectable effects other than restoration of the WT phenotype.

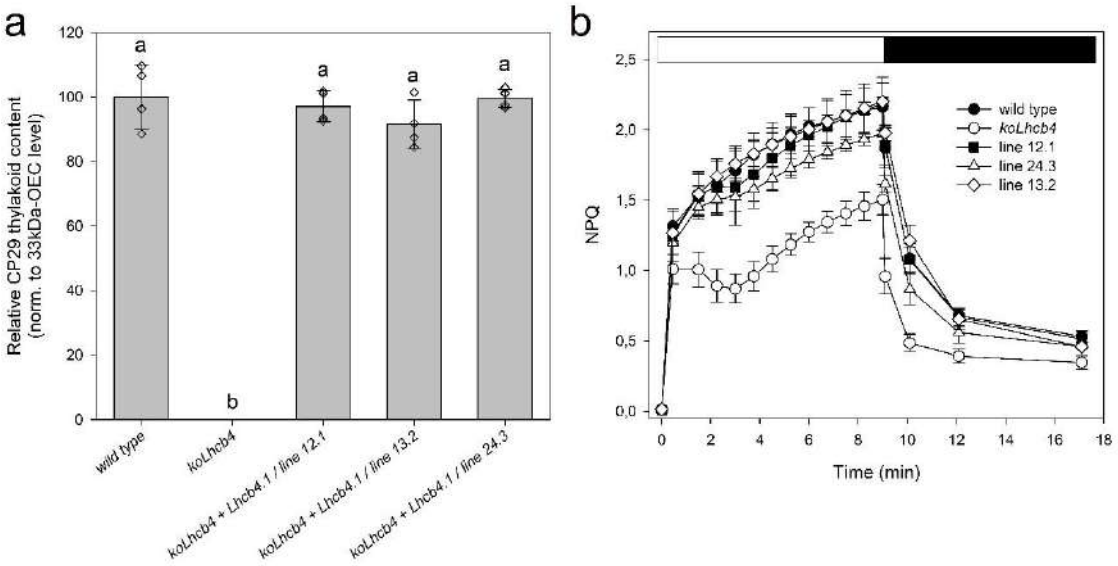

Fig. 5.1.1 | CP29 content and NPQ kinetics of lines complemented with Wt Lhcb4.1 gene from A. thaliana. a, *The abundance of CP29 was determined on three independent T3 lines by SDS–PAGE fractionation of thylakoid proteins, Coomassie staining and densitometry of selected protein bands. CP29 content was normalized (norm.) to that of the oxygen-evolving complex (OEC) 33-kDa subunit. Data are expressed as mean ± s.d., n = 4 biologically independent samples and all individual data points are shown. Values marked with different letters are significantly different from each other within the column (ANOVA followed by Tukey's post-hoc test at a significance level of P < 0.05).* ***b,*** *Kinetics of formation (white bar) and relaxation (black bar) of NPQ were carried out following illumination of leaves with 1,000 µmol photons m^{-2} s^{-1} at room temperature. Data are expressed as mean ± s.d., n = 4 biologically independent plants. Experiments were repeated independently twice, with similar results.*

Site-directed mutagenesis of candidate H+-binding sites exposed to the thylakoid lumen

Although the role of PsbS in sensing luminal pH is well established (Li et al., 2004), pH-sensing sites have been suggested in monomeric LHCs based on binding of the NPQ inhibitor DCCD to CP26 (ref. (Walters et al., 1996)) and CP29 (ref. (Pesaresi et al., 1997)). Protonation of acidic residues exposed to the lumen, namely D135, E140 and D143 in the loop between transmembrane helix C and the amphiphilic helix E, and residues D245 and D253 in the C-terminal region, was proposed to trigger local conformational changes thereby influencing the binding strength of xanthophyll L2 (ref (Pan et al., 2011)). Therefore, these residues were each mutated to their non-

protonatable N or Q homologues. In addition, the glutamate ligand of Chl b606 (b6) (Pesaresi et al., 1997) was edited into the non-protonatable residue Val. Supplementary Fig. 5.1.2 and Supplementary Table 5.1.1 summarize substitutions operated in the different residues to obtain the genotypes analysed in this work. Transgenic lines carrying these mutations were selected, and the accumulation level of CP29 was evaluated by SDS–PAGE and densitometry (Fig. 5.1.2a,b and Supplementary Table 5.1.1). In all lines, pigment composition, PSII quantum efficiency and growth rate were maintained at WT level (Table 5.1.1). In both triple (D135N E140Q D143N) and double (D245N D253N) mutants, CP29 accumulated as in the WT while a reduction to 41% compared to the WT level was caused by mutation E163V (Fig. 5.1.2a,b and Supplementary Table 5.1.1), suggesting that the amino acid substitution had affected protein stability. Nevertheless, NPQ activity was similar in all complemented lines compared to WT (Fig. 5.1.2c). We conclude that protonation of luminally exposed acidic residues in helix E, the E–C loop and the C ter- minus of CP29 is not a requirement for NPQ activity.

Site-directed mutagenesis of nine Chl-binding sites of *A. thaliana* CP29

We then proceeded to perform site-directed mutagenesis of specific residues involved in Chl binding at different sites. Supplementary Fig. 5.1.2a shows sequence comparison between Lhcb4 from spinach (Spinacia oleracea), whose Chl-binding residues have been identified by both X-ray crystallography (Pan et al., 2011) and single-particle cryo- electron microscopy (cryo-EM) (Wei et al., 2016), (Su et al., 2017), and Lhcb4.1 (hereafter called CP29) from *A. thaliana*, showing full conservation. Supplementary Fig. 5.1.2b displays the specific pigment-binding sites and Chl residues selected for mutagenesis, while Supplementary Table 5.1.1 summarizes the substitutions operated in the putative porphyrin-binding residues to obtain the genotypes analysed in this work. Axial ligands from six of ten Chl a molecules were identified as side chains of amino acid residues in spinach CP29 (refs. (Wei et al., 2016), (Pan et al., 2011)). Therefore, to remove the chromophore with minimal changes in protein structure we replaced Chl-binding residues with those found to be effective in allowing in vitro refolding of the recombinant protein with purified pigments, according to a previous report (Bassi et al., 1999). In the case of four Chl a sites, ligands other than amino acid side chains were reported, including backbone carbonyls (Chls *a*601 and *a*616), water molecules (Chl *a*604) and the phosphate group of phosphatidyl glycerol (Chl *a*611). In particular, Chls *a*601 and *a*616 were identified in the irregular coil structure of the long N-terminal domain (Wei et al., 2016); the central ligand of Chl *a*601 is the carbonyl of W26, while Chl *a*616 is located in the interfacial region with CP47 and coordinated by the backbone carbonyl of L80 (F92 in *Arabidopsis* Lhcb4.1). In an attempt to remove these two pigments, we mutated neighbouring residues 93 and 94 into bulky residues (Phe, Trp— see Supplementary Table 5.1.1) to cause steric hindrance within the Chl-binding pocket.

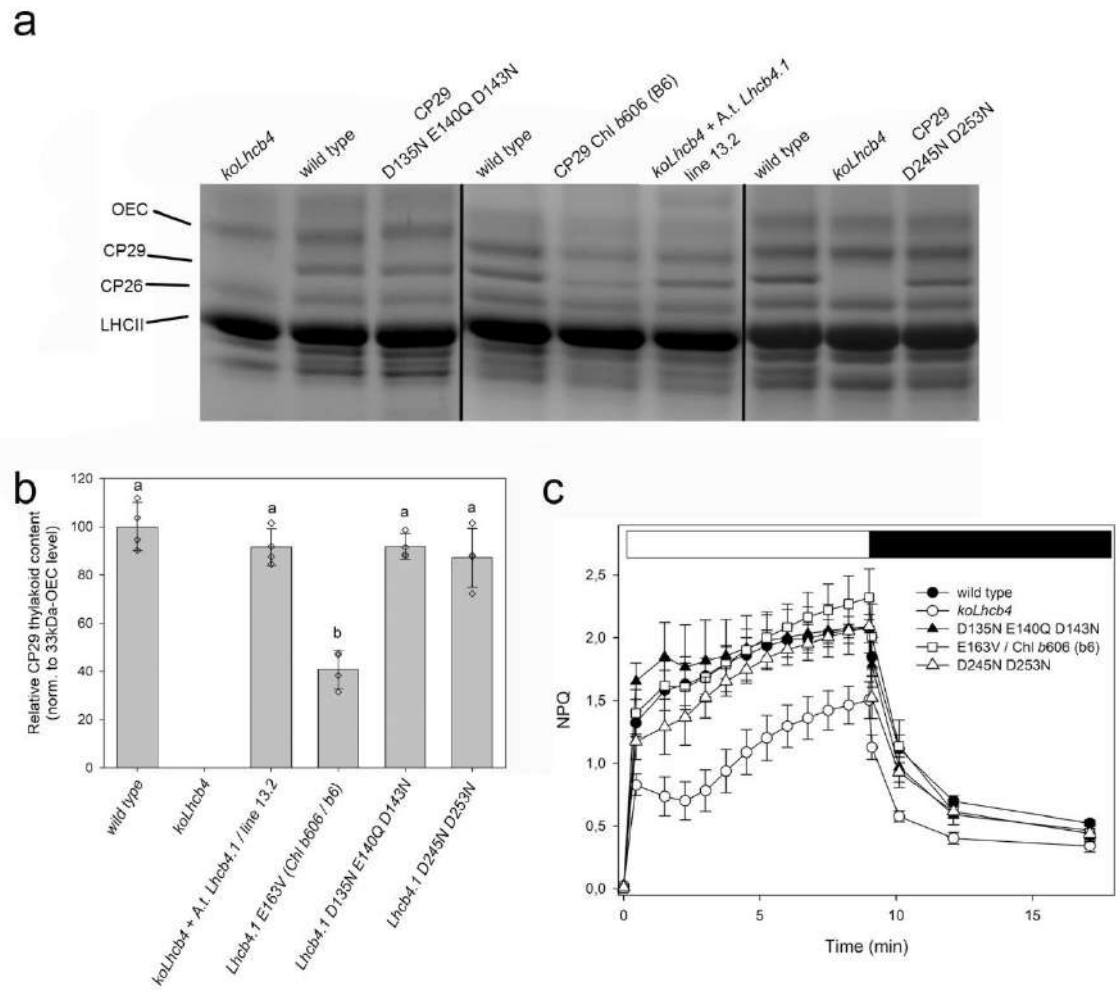

Fig. 5.1.2 | Characterization of Arabidopsis lines expressing CP29 isoforms mutated in putative protonatable sites. a, *SDS–PAGE fractionation of thylakoid proteins from WT, koLhcb4 and lines complemented with either WT or mutated CP29 isoforms (single-mutant E163V, double-mutant D245N D253N and triple-mutant D135N E140Q D143N).* ***b,*** *The level of CP29 was determined by densitometry of Coomassie-stained gel and normalized (norm.) to OEC 33-kDa subunit content. Data are expressed as mean ± s.d., n = 4 biologically independent samples and all individual data points are shown. Values marked with different letters are significantly different from each other within the column (ANOVA followed by Tukey's post-hoc test at a significance level of P < 0.05). Selected apoprotein bands are marked.* ***c,*** *Kinetics of formation and relaxation of photoprotective energy dissipation, measured following illumination of leaves with 1,000 µmol photons m−2 s−1 at room temperature. Data are expressed as mean ± s.d., n = 4 biologically independent plants. Experiments were repeated independently twice, with similar results. Results displayed are representative of the independent lines. A.t., A. thaliana.*

CP29 complementation efficiency and PSII organization in Chl-binding site mutants

All CP29 sequences described above were transformed into koLhcb4 *Arabidopsis* plants. For each mutation, independent lines containing a single gene insertion were identified in the T3 generation for resistance to applications of the antibiotic kanamycin. Genotypes obtained by complementation of koLhcb4 did not show significant growth rate reduction with respect to the WT under control lighting conditions (150 μmol photons m−2 s−1, 23 °C, 8/16 h day/night) nor altered Chl composition (Table 5.1.1), suggesting that no changes had occurred in the PSI/PSII ratio. In all genotypes, leaf xanthophyll and carotene contents were unaffected compared to the control genotype. The capacity for zeaxanthin (Zea) synthesis, a factor affecting NPQ activity, was evaluated by exposure of plants to excess light (1,000 μmol photons m^{-2} s^{-1}, 23 °C) for 15 min. Synthesis of Zea was identical in all lines produced in this work (Supplementary Table 5.1.2). koLhcb4 plants and some mutant lines obtained showed a significant decrease in Fv/Fm (see Table 5.1.1). To estimate the effects of mutations on CP29 protein levels, two to three transformant lines (T3 generation) for each mutation were selected based on their CP29 content (Fig. 5.1.3 and Supplementary Table 5.1.1). By comparison of transgenic lines to WT, genotypes could be assigned to one of three different groups based on their CP29 content.

Group 1: Chl *a*603 (a5, mutation H111N) and Chl *a*616 (mutations Q93Y and Q93F) binding sites. Mutations at these sites had little or no effect on accumulation of CP29, whose abundance was the same as in the WT and koLhcb4 lines complemented with WT CP29 sequence.

Group 2: Chls *a*601, *a*603 (a5, mutations H111F, H111L, H111W), *a*612 (a2), *a*613 (a3) and *a*616 (in the latter, mutations P94W and P94F) binding sites. Mutation in these sites yielded a reduced accumulation level of CP29 (20–80% reduction versus WT plants).

Group 3: Chls *a*602 (a4) and *a*610 (a1). No CP29 protein was detected when mutation targeted coordinating residues which, in addition to binding chromophores, formed ionic pairs stabilizing helix–helix interactions. An additional mutation lacking CP29 was E171F, affecting the Chl *a*609 (b5) binding site; mutation of Glu 171 into either Val, Tyr or Thr also yielded no accumulation of CP29.

The lack of CP29 protein suggests that mutation in Group 3 sites markedly impaired either folding or stability of the protein. We therefore did not analyse these genotypes further.

The organization of pigment–protein complexes in mutant lines was analysed by non-denaturing Deriphat–PAGE, following solubilization of stacked thylakoids with 0.8% dodecyl-α- d-maltopyranoside (α-DM) (Fig. 5.1.4). WT plants and koLhcb4 complemented with WT CP29 sequence showed the same fractionation pattern, composed of three major green bands at low molecular weight corresponding to free pigments (front, band B1), monomeric LHC proteins (at 30 kDa, B2) and trimeric LHCII (at~100 kDa, B3), respectively. Green bands with higher molecular weight were the CP29–CP24–LHCII supercomplex (B4), PSII core monomers (C, band B5) and dimers (C_2, band b6), the PSI–LHCI supercomplex (B7), and an additional four bands (B8–B11) composed of a dimeric PSII core with increasing molecular weight and antenna protein complements (Caffarri et al., 2009). In koLhcb4, complexes B4 and B8–11 were absent.

Complementation with mutant CP29 yielded partial recovery of bands depleted in koLhcb4: mutants *a*601 (W26F), *a*616 (Q93F) and *a*603 (a5, mutation H111N) recovered a WT pattern; mutants *a*603 (a5, mutations H111F, H111L and H111W) and *b*606 (b6) recovered B4, B8 and B9, while B10 and B11 were less abundant; mutants *a*612 (a2) and *a*613 (a3) were effective in recovering B8 and B9, but not B4, suggesting that mutations preferentially affected interactions with LHCII-M and CP24 versus CP47 in the PSII supercomplex.

Genotype (Chl / mutation)	Chl *a/b*	Chl / Car	µg Chl / cm^2	Fv / Fm	Fresh weight (g)
wild type	3.01 ± 0.15[a]	3.63 ± 0.14[a]	20.7 ± 1.7[a]	0.801 ± 0.005[a,d]	1.18 ± 0.19[a]
koLhcb4	2.78 ± 0.28[a]	3.75 ± 0.22[a]	19.8 ± 0.8[a]	0.752 ± 0.007[b]	0.96 ± 0.24[a]
koLhcb4 + Lhcb4.1 wild type	2.97 ± 0.16[a]	3.65 ± 0.14[a]	21.2 ± 1.2[a]	0.801 ± 0.007[a,d]	1.47 ± 0.42[a]
*a*601 / W26F	2.82 ± 0.22[a]	3.68 ± 0.22[a]	19.8 ± 1.2[a]	0.796 ± 0.018[a]	1.12 ± 0.33[a]
*a*602 (a4) / E108V & R215L	2.98 ± 0.16[a]	3.79 ± 0.11[a]	19.9 ± 1.1[a]	0.751 ± 0.005[b]	1.41 ± 0.27[a]
*a*603 (a5) / H111F	2.95 ± 0.15[a]	3.72 ± 0.12[a]	19.9 ± 1.8[a]	0.764 ± 0.007[b,c]	1.49 ± 0.55[a]
*a*603 (a5) / H111L	2.96 ± 0.05[a]	3.53 ± 0.07[a]	18.8 ± 1.1[a]	0.762 ± 0.004[b,c]	1.13 ± 0.31[a]
*a*603 (a5) / H111N	2.97 ± 0.05[a]	3.65 ± 0.09[a]	21.2 ± 0.9[a]	0.796 ± 0.010[a]	1.42 ± 0.36[a]
*a*603 (a5) / H111W	2.90 ± 0.05[a]	3.58 ± 0.10[a]	19.3 ± 1.9[a]	0.761 ± 0.009[b,c]	1.10 ± 0.37[a]
*b*606 (b6) / E163V	2.94 ± 0.14[a]	3.59 ± 0.10[a]	20.6 ± 1.1[a]	0.804 ± 0.018[d]	1.42 ± 0.24[a]
a609 (b5) / E171Y	2.92 ± 0.16[a]	3.61 ± 0.12[a]	19.9 ± 1.9[a]	0.754 ± 0.019[b]	1.28 ± 0.25[a]
*a*610 (a1) / E113L & E210V	2.98 ± 0.16[a]	3.76 ± 0.12[a]	21.2 ± 1.1[a]	0.746 ± 0.008[b]	1.43 ± 0.55[a]
*a*612 (a2) / H213Y	2.82 ± 0.24[a]	3.74 ± 0.26[a]	19.9 ± 0.9[a]	0.782 ± 0.004[c]	1.11 ± 0.19[a]
*a*612 (a2) / H213T	2.79 ± 0.14[a]	3.58 ± 0.20[a]	20.6 ± 1.2[a]	0.786 ± 0.010[c]	0.95 ± 0.26[a]
*a*613 (a3) / Q227L	2.86 ± 0.24[a]	3.63 ± 0.24[a]	19.6 ± 1.0[a]	0.746 ± 0.018[b]	1.04 ± 0.23[a]
*a*616 / Q93F	2.76 ± 0.19[a]	3.77 ± 0.22[a]	19.6 ± 0.8[a]	0.801 ± 0.006[a,d]	0.91 ± 0.12[a]
*a*616 / Q93Y	2.76 ± 0.16[a]	3.75 ± 0.22[a]	20.2 ± 0.6[a]	0.798 ± 0.002[a,d]	0.99 ± 0.18[a]
*a*616 / P94F	2.87 ± 0.25a	3.44 ± 0.17[a]	21.3 ± 0.9[a]	0.781 ± 0.004[c]	1.09 ± 0.11[a]
*a*616 / P94W	2.78 ± 0.23[a]	3.48 ± 0.21[a]	20.5 ± 1.5[a]	0.781 ± 0.006[c]	1.10 ± 0.19[a]
protonatable residues / D135N & E140Q & D143N	2.78 ± 0.14[a]	3.71 ± 0.11[a]	19.9 ± 0.4[a]	0.805 ± 0.010[d]	0.95 ± 0.14[a]
protonatable residues / D245N & D253N	3.03 ± 0.09[a]	3.55 ± 0.09[a]	20.1 ± 0.5[a]	0.781 ± 0.005[c]	1.34 ± 0.36[a]

Table 5.1.1 | Pigment content and fluorescence induction parameters determined for leaves of Arabidopsis wild type, koLhcb4 and lines expressing CP29 isoforms. *Parameters were measured in homozygous T3 plants containing a single copy Lhcb4.1 insertion. Two or three lines were analyzed for each site-directed mutant; at least four different plants were tested for each line. Fv/Fm, quantum yield of PSII; Chl/Car, molar ration between Chlorophylls (a+b) and Carotenoids. Fresh weight (g) refers to growth after six weeks in control conditions. Data are expressed as mean ± SD, n > 5. Values marked with the same superscript letters are not significantly different from each other, within the same column (ANOVA test, P < 0.05).*

Purification and characterization of CP29 isoforms

We then verified whether the pigment complement of mutant CP29 proteins was affected by the mutations—that is, whether the targeted chromophore was indeed lost. For this purpose, we purified CP29 from each genotype by ion-exchange chromatography according to a procedure previously described (Pan et al., 2013). Pigment content of the purified complexes was assessed both by fitting the acetonic extract spectra with spectra of individual Chl and Car species (Croce et al., 2000) and by high-performance liquid chromatography (HPLC). Figures for Chl a/b and Chl/Car ratios of complexes purified from control genotypes (WT plants and koLchb4

complemented with WT CP29 sequence) are consistent with a pigment complement of 14 Chl molecules (~10.2 Chl a and ~3.8 Chl b) and three Cars (Pan et al., 2011). Plants with CP29 purified from mutant lines *a*601 and *a*616 were essentially unaffected in regard to Chl a/b and Chl/Car ratio compared to the control samples, implying that no Chl or xanthophyll was lost (Supplementary Table 5.1.3). Indeed, the absorption spectra were indistinguishable from the WT (Fig. 5.1.5a–c). Because Chl *a*616, due to its peripheral position in the antenna, could be lost during purification, we analysed the absorption spectra and pigment composition of PSII supercomplexes from mutant plants (Supplementary Fig. 5.1.3). Since no differences were found between WT mutant complexes, we ruled out loss of Chl *a*616 during purification. Instead, both Chl a/b and Chl/Car ratios of CP29 from lines *a*603 (a5, mutations H111F, H111L and H111W), *a*612 (a2) and *a*613 (a3) were lower compared to WT, suggesting a selective loss of Chl a. Biochemical analysis (Supplementary Table 5.1.3) confirmed that mutation in sites *a*603 (mutations H111F, H111L and *H111W*), *a*612 and *a*613 yielded proteins lacking a Chl a chromophore. Also, the peak wavelength of the Qy transition (630–700 nm) was blue-shifted in these mutants (Fig. 5.1.5d–f,j–k), consistent with the loss of a Chl a ligand. By contrast, mutation H111N in site *a*603 did not exhibit the characteristics expected for a mutant with an empty Chl a site: namely, a blue-shifted Qy transition and lower Chl a/b ratio (Fig. 5.1.5l and Supplementary Table 5.1.3), suggesting that the Chl *a*603 ligand was retained in this specific mutant.

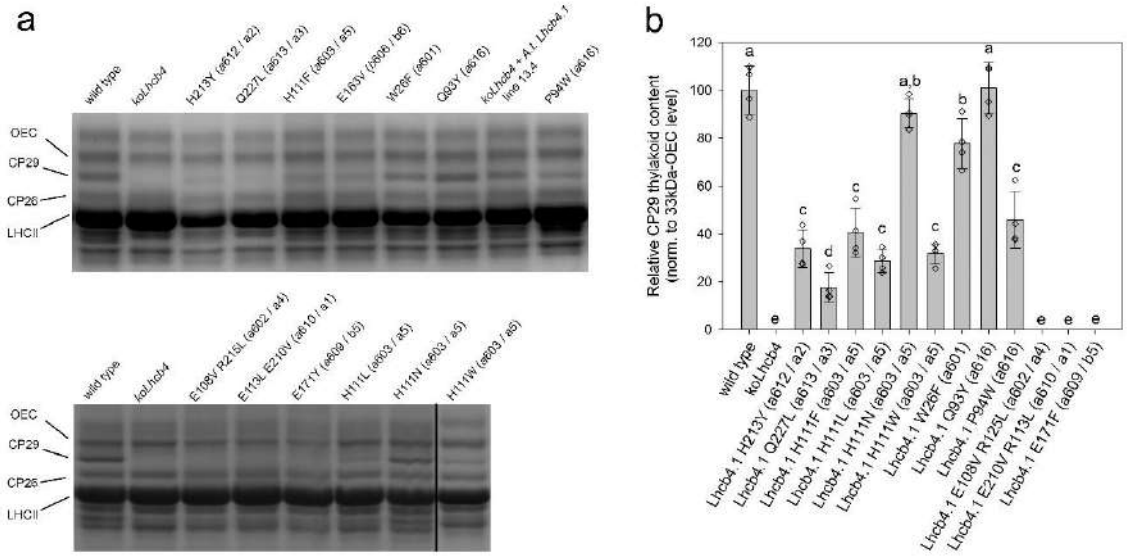

Fig. 5.1.3 | Characterization of Arabidopsis lines expressing Wt and mutant CP29 proteins. a, *SDS–PAGE analysis of thylakoid proteins from WT, koLhcb4 and plant lines expressing CP29 proteins. Selected apoprotein bands are marked. Thylakoid samples corresponding to 15 μg of Chls were loaded for each lane.* ***b,*** *The amount of CP29 was determined on selected lines by Coomassie blue staining of the gel and densitometric analysis. CP29 content was normalized (norm.) to that of the OEC 33-kDa subunit. Data are expressed as mean ± s.d., n = 4 biologically independent samples and all individual data points are shown. Values marked with different letters are significantly different from each other within the column (ANOVA followed by Tukey's post-hoc test at a significance level of P < 0.05). Experiments were repeated independently twice, with similar results*

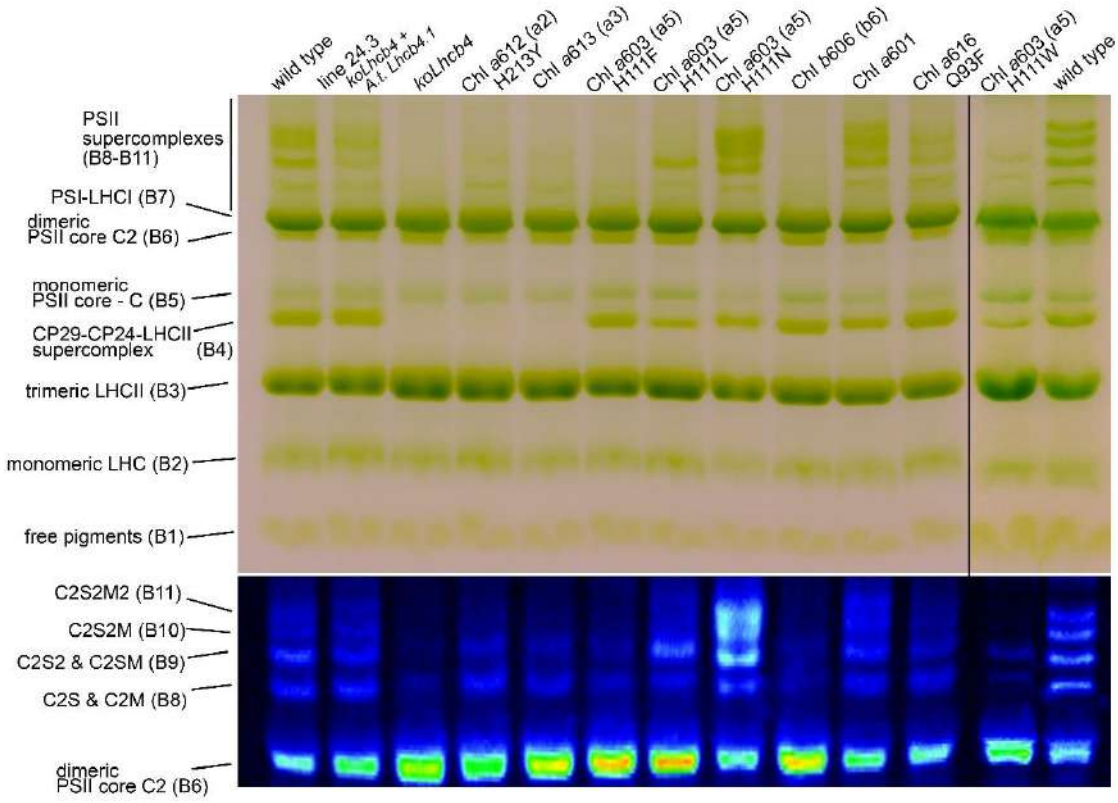

Fig. 5.1.4 | Organization of thylakoid pigment–protein complexes. Upper gel: *thylakoid pigment–protein complexes from WT, koLhcb4 and complemented lines were separated by non-denaturing Deriphat–PAGE following solubilization of membranes with 0.8% α-DM. Thylakoids (35 μg of Chls) were loaded in each lane. The composition of each band is indicated based on earlier work (Havaux et al., 2004).* ***Lower gel:*** *imaging of Chl fluorescence emission of pigment–protein complexes for enhanced detection of PSII supercomplexes. Experiments were repeated independently three times, with similar results.*

Absorption spectra of native complexes were further analysed to investigate the spectroscopic characteristics of missing Chls within the CP29 subunit. Spectra were normalized to the total area over Qy (630–700 nm) by assuming a Chl b/Chl a extinction ratio of 0.7 (Cinque et al., 2000), and WT minus mutant difference spectra were then calculated (Fig. 5.1.5g–i,l,m). Figure 5g shows the WT minus mutant Chl *a*612 (a2, mutation H213Y), the difference spectrum peaking at 679 nm with 11.5 nm full width at half maximum (FWHM), consistent with absorption by a single Chl a (Cinque et al., 2000). The case of three mutations to Chl *a*603 (a5, mutations H111F, H111L and H111W) was similar, with a 678-nm peak and 10.5 nm FWHM (Fig. 5.1.5i,m,n). Interestingly, in the case of mutation H111N/site Chl *a*603, the difference between WT and mutant spectra showed increased absorption in the red tail of the Qy transition at 685.6 nm, together with loss of a 674.8-nm form; no significant difference was observed in the Chl b absorption region (Fig. 5.1.5o). This is consistent with modulation of the spectroscopic properties of Chl a5 by mutation H111N: indeed, His versus Asn substitution is expected to decrease the distance between inter- acting Chls, with Asn having a lower steric hindrance compared with His, thus bringing Chl *a*603 (a5)

closer to Chl *a*609 (b5) and increasing excitonic interaction between neighbouring pigments. This was confirmed by low-temperature fluorescence emission spectra (Fig. 5.1.6): in mutant Chl *a*603 H111N, the emission peak was shifted from 680 to 682 nm; the difference between WT and mutant spectra showed loss at 675 nm, compensated by an increased emission at 689 nm. Mutant Chl *a*613 (a3, mutation Q227L) showed a major WT minus mutant absorption component at 678 nm and yet the spectral form was asymmetrical (Fig. 5.1.5j), suggesting that an additional spectral form peaking at 665 nm could also have been affected.

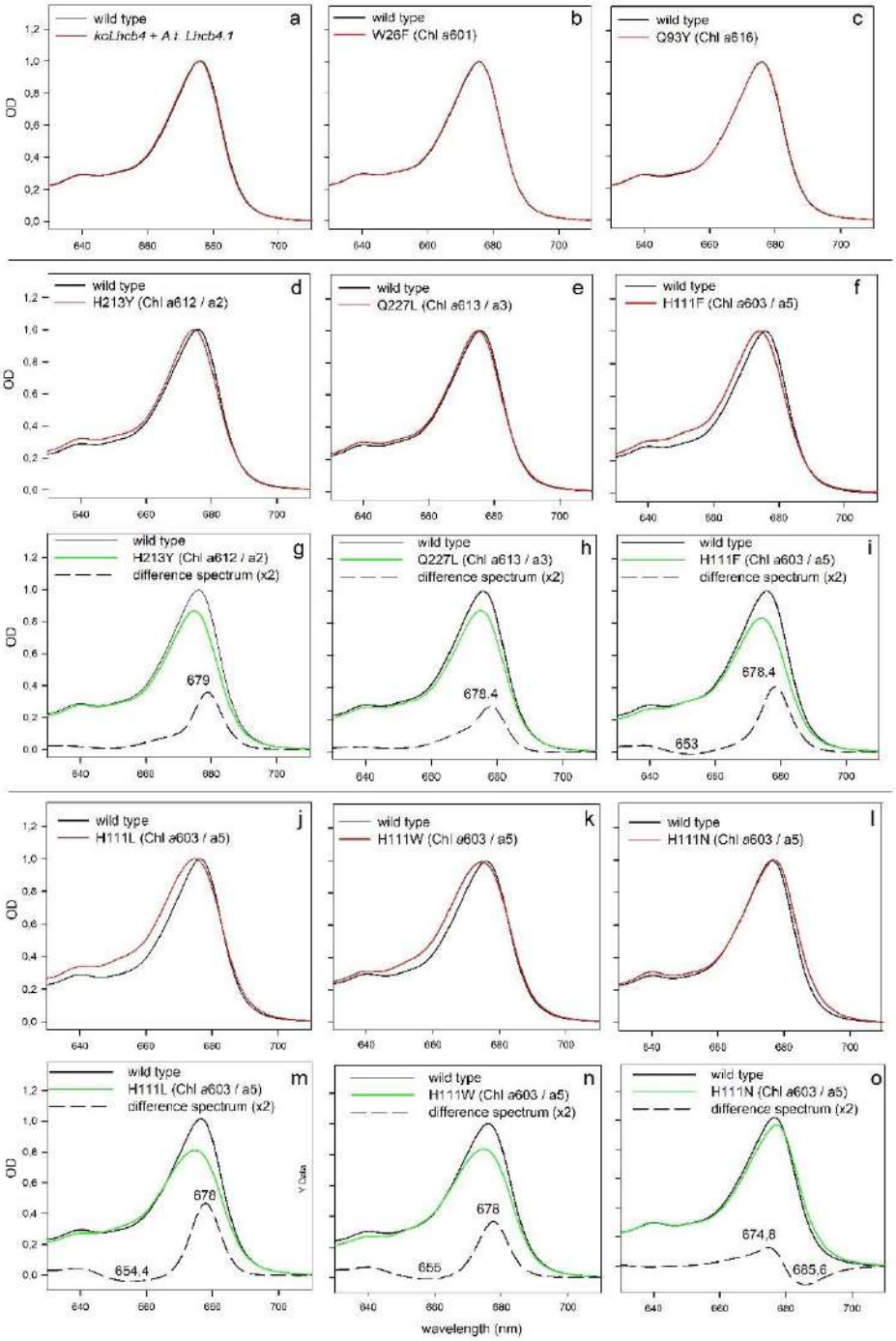

Fig. 5.1.5 | spectroscopic analysis of Wt and mutant CP29 purified holoproteins. a–o, *Absorption spectra of CP29 complex, purified from control genotypes (WT plants and koLhcb4*

*complemented with WT CP29 sequence (**a**)) and from lines expressing mutant isoforms of CP29 (**b–f,j–l**), were normalized to maximum absorption in the red region. Absorption spectra of complexes carrying mutations W26F (Chl a601 (b)), Q93Y (Chl a616 (**c**)) superimposed on that of WT, while CP29 purified from lines H213Y (Chl a612 (d)), Q227L (Chl a613 (e)) and H111F/L/W/N (Chl a603 (**f,j,k,l**)) showed spectroscopic changes. Absorption spectra of these mutants were then normalized to Chl content (**g–i,m–o**). The WT minus mutant difference spectrum therefore represents the absorption spectrum of the missing individual Chl molecule. Clear peaks in difference spectra were obtained for mutations affecting residues binding Chl a603 (H111F/L/W/N (**i,m–o**)), Chl a612 (H213Y (**g**)) and Chl a613 (Q227L (h)). Experiments were repeated independently three times, with similar results. OD, optical density.*

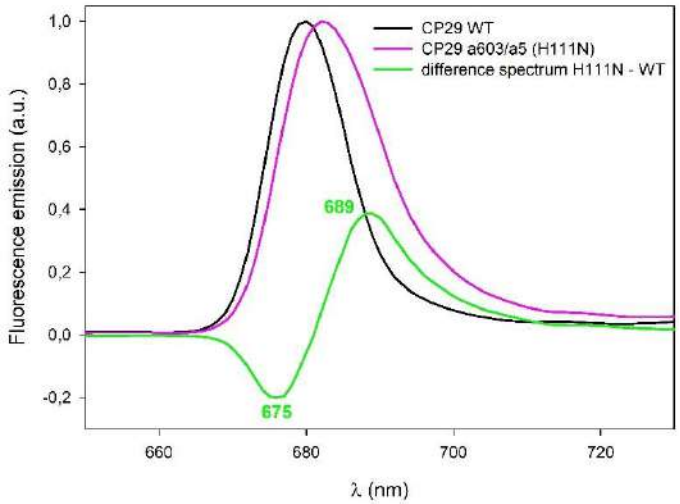

Fig. 5.1.6 | Fluorescence emission at 77 K of CP29 Wt and mutant a603/a5. *Spectra of WT and mutant H111N and difference spectrum are shown. Emission spectra were recorded following excitation at 470 nm and normalized to emission maximum. Experiments were repeated independently twice, with similar results. a.u., arbitrary units.*

NPQ activity of lines expressing WT and mutant CP29

Distribution of quenching sites within the pigment bed may be uneven: in some cases, WT level was obtained corresponding to two CP29 units per dimeric PSII core while, in others, CP29 accumulated to ~40% or even less compared to WT. This would imply a nonlinear relation between CP29 concentration and amplitude of quenching. Therefore, we then determined the dependence of quenching response versus CP29 content. We analysed different segregating T1 populations, obtained by complementing koLhcb4 *Arabidopsis* plants with WT Lhcb4.1 sequence. A total of 45 lines were selected based on CP29 content, ranging from 5 to 100% of WT level. Their NPQ activities were then assessed by pulse amplitude modulated (PAM) fluorometry and expressed as their respective definite integrals, calculated between 0 and 8 min of actinic light induction. Supplementary Fig. 5.1.4 shows the total NPQ increase compared to the value for koLhcb4 caused by different levels of complementation. NPQ amplitude showed a nonlinear relation to CP29 level, with 50% in NPQ increase obtained with ~30% CP29. We then measured

the NPQ amplitude of genotypes complemented with mutant CP29 (Fig. 5.1.7 and Supplementary Fig. 5.1.5). Mutations affecting Chls *a*601, *a*612 (a2) and *a*613 (a3) exhibited a dependence of total NPQ on CP29 content that was indistinguishable from WT, within experimental error. Instead, lines complemented with CP29 carrying mutations Q93Y and P94W (Chl *a*616 site), H111F, H111L, H111W and H111N (Chl *a*603/a5 site) showed NPQ activity significantly lower than WT. The extreme case was that of mutants H111F, H111L and H111W, whose NPQ activity closely matched that of koLhcb4 plants (Supplementary Fig. 5.1.5). Although there were essentially no effects found of the mutations on either photosynthetic yield or growth rate, it cannot be excluded that change in NPQ in H111L/F/W was the indirect result of a conformational change in mutated CP29: it might have increased, for example, the accessibility to proteases leading to lower accumulation. If this is the case, we might expect that substitution of WT by mutant CP29 isoforms altered the photochemical stability of PSII. To investigate this aspect, Fv/Fm was measured on intact chloroplasts isolated from WT and mutant plants at identical chlorophyll concentrations. Chloroplasts were maintained at room temperature and under low light (50-μE white light), under continuous stirring. Parameter b, obtained by fitting experimental points using a first- order exponential function $y = y0 + Aexp(-bx)$, can be used as a PSII stability index correlated to the rate of decline in PSII quantum yield. Treatment was continued for a further 6 h and yielded a simi- lar reduction in Fv/Fm on all genotypes tested, implying that mutations to CP29 did not impair PSII stability (Supplementary Fig. 5.1.6).

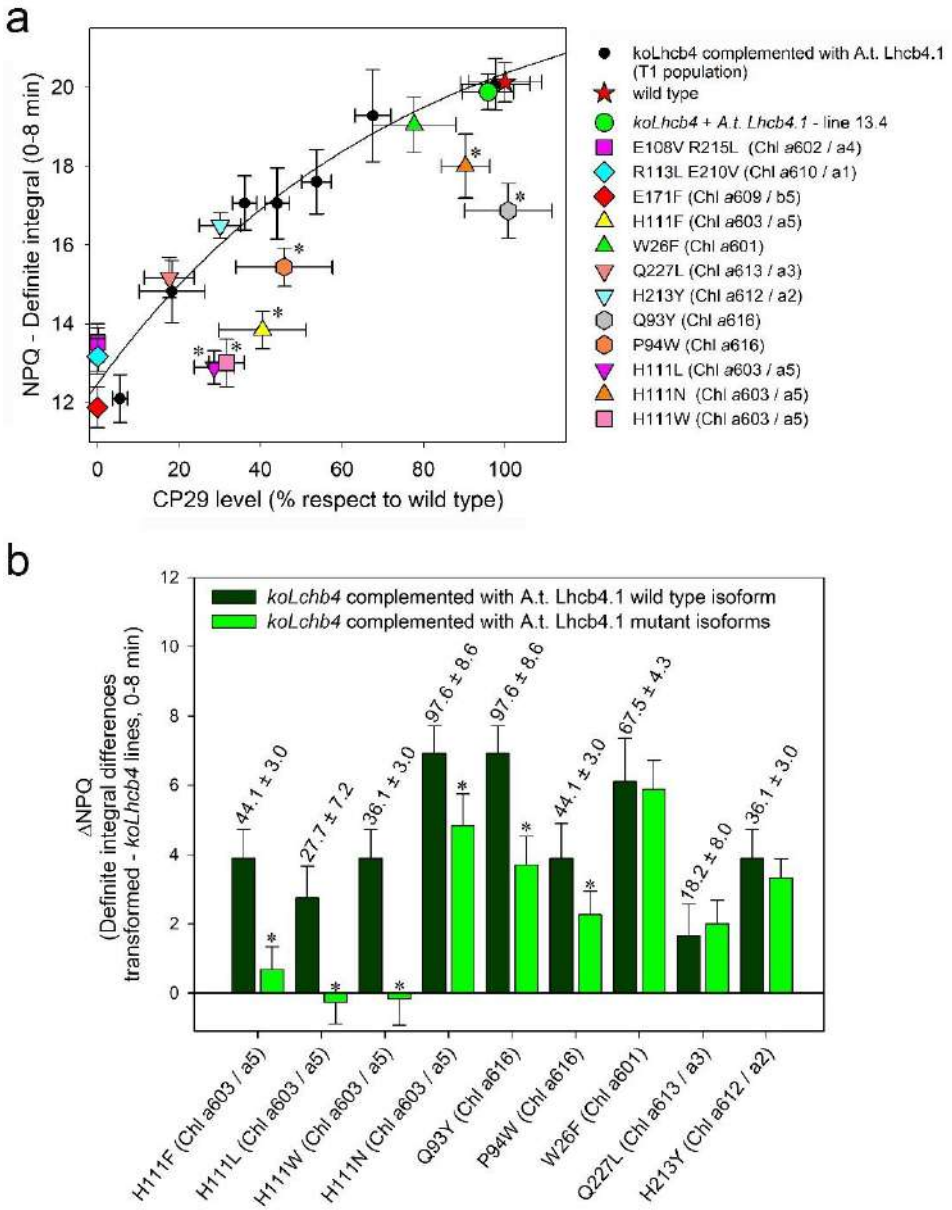

Fig. 5.1.7 | Correlation between NPQ amplitude and CP29 content in plants expressing either Wt or mutant CP29. a, *NPQ amplitude was measured in a segregating T1 population of A. thaliana koLhcb4 complemented with WT CP29. For each plant: (1) CP29 content was accurately estimated by SDS–PAGE, Coomassie staining and densitometric analysis, and plants were grouped by CP29 level; (2) definite integrals were calculated from NPQ curves in the range 0–8 min. For correlation analysis, experimental points (black circles) were modelled with an exponential function (f = y0+ a(1 – exp(–bx)) +c(1 – exp(–dx)), black line). Then, NPQ amplitude was measured on leaves from WT, koLhcb4 and independent T3 transgenic lines expressing either WT or mutant CP29 isoforms (see Supplementary Fig. 5.1.5). Data are expressed as mean ± s.d., n = 4 biologically independent plants. Each experimental point represents the CP29 content of the line and the definite integral from its NPQ traces. Leaves carrying mutations H111F, H111L, H111W and H111N (Chl a603), Q93Y and P94W (Chl a616) showed significantly lower NPQ amplitude (indicated by asterisks) than lines expressing WT CP29 (two- sided*

Student's t-test, P < 0.05). ***b,*** *Comparative analysis of differential NPQ amplitude (ΔNPQ) of selected genotypes. Plants from the segregating population, accumulating WT Lhcb4.1 to different levels, were grouped for CP29 level (see a). For each group of genotypes, ΔNPQ values were calculated by subtracting the mean NPQ definite integrals of koLhcb4 plants from those of transformed plants. ΔNPQ of mutant lines (light green) and that of lines expressing the same amount of WT CP29 (dark green) are shown. Numbers above bars denote mean CP29 content (percentage compared to WT) of the groups of T1 plants used as internal control. Data are expressed as mean ± s.d. Leaves carrying mutations on the Chl a603–a609–a616 cluster showed significantly lower ΔNPQ amplitude (indicated by asterisks) than those expressing the same level of WT CP29 (two-sided Student's t-test, P < 0.05). Data are representative of two independent experiments, with similar results*

Discussion

Among the Chl/xanthophyll pigment-proteins of PSII, two play a major role in the catalysis of quenching reactions based on reverse genetic analysis: CP29 and Lhcb1 (De Bianchi et al., 2011; Pietrzykowska et al., 2014; Dall'Osto et al., 2017), which are responsible for the very fast and slow components of qE, respectively (Dall'Osto et al., 2017). Triggering occurs following luminal acidification and the dissociation of LHCII-M and CP24 from PSII supercomplexes, thereby exposing CP29 to PsbS interaction8. Here, we verified whether (1) direct protonation of CP29, besides PsbS, is required for quenching, and (2) which Chl/xanthophyll chromophores in CP29 are involved in quenching reactions. The first question was addressed by mutating different groups of luminally exposed acidic residues, located respectively in helix E and the E–C loop (Pan et al., 2011), in the C-terminal portion of CP29, and the glutamate ligand of Chl b606 (b6) to non-protonatable homologues. In all cases, these mutations failed to impair the amplitude of NPQ (Fig. 5.1.2). This is to be compared to the effect of mutating luminally exposed residues E122 and E226 in PsbS, which abolished NPQ activity altogether (Li et al., 2004). We conclude that the protonation of these CP29 residues is not required for quenching reactions, while PsbS is probably the only protein responsible for luminal pH detection towards activation of NPQ (Li et al., 2004). In turn, the lack of pigment binding by PsbS (Fan et al., 2015) strongly suggests that a physical interaction of PsbS with CP29 is established for the conformational change induced by protonation to be transferred to CP29 (Sacharz et al., 2017). CP29 binds three xanthophylls, each in tight connection with several Chls a and which, in turn, are within 10–15 Å of Chl b ligands for efficient excitation energy transfer (Pan et al., 2013). The first pigment cluster is formed by lutein (Lut) in site L1–Chls *a*611–Chl *a*612 (a2), and was suggested as the site of quenching in LHCII (Ruban et al., 2007) and CP29 (Duffy et al., 2013). A second cluster, violaxanthin (Vio) L2–Chl *a*603 (a5)–Chl *a*609 (b5), was proposed as a charge-transfer (CT) quenching centre, following Vio–Zea exchange at site L2 (Ahn et al., 2008). Finally, neoxanthin (Neo) at site N1 is clustered with Chls *a*604–*b*608–*b*606 (b6). The latter cluster is not yet suggested as a quenching site, due to the unfavourable geometry of the Chl a/Neo arrangement (Pan et al., 2011) and the high NPQ activity observed in the *aba4* mutant lacking Neo (Dall'Osto et al., 2007a). In vivo measurements of *koLhcb4* genotypes complemented with mutant CP29 sequences showed that quenching in CP29 was not hampered by the removal of Chls *a*612 (a2), *a*613 (a3) or *b*606 (b6) (Figs. 5.1.2 and 5.1.7

and Supplementary Fig. 5.1.5), making it unlikely that they participate in quenching reactions. By contrast, the NPQ kinetic for mutant CP29–H111 (Chl *a*603 mutations H111F, H111L and H111W, a5) was indistinguishable from that of koLhcb4, despite the complemented mutant accumulating CP29 to 30–40% compared to WT, a level that ensured 75–85% of quenching activity with WT CP29 (Supplementary Fig. 5.1.4). The pigment composition and spectral properties of purified proteins CP29-H111F, CP29-H111L and CP29-H111W are consistent with the loss of a single Chl a ligand (Fig. 5.1.5), as evidenced by the WT minus mutant difference spectrum yielding a 678-nm peak and FWHM = 10.5 nm, corresponding to a single Chl a lacking strong interactions with nearby chromophores (Cinque et al., 2000). The Chl/Car ratio and HPLC analysis indicated no loss of xanthophylls (Supplementary Table 5.1.3), implying that Chl *a*603 (a5) is either responsible for the quenching reaction(s) per se or is part of a pigment cluster involved in the process. Structural studies (Wei et al., 2016), (Pan et al., 2011) have indeed shown that Chl *a*603 (a5)–Chl *a*609 (b5) and Vio bound to site L2 are part of a cluster of closely spaced chromophores in CP29. Chl *a*603 (a5) is closest (6.3 Å) to the polyene chain of Vio, with Chl *a*609 (b5) 9.4 Å further away. Unfortunately, all multiple mutations at the ionic pair coordinating Chl *a*609 (b5) yielded unstable forms of the protein, which did not accumulate in thylakoids, thus making impossible *in vivo* experimental verification of the role of Chl *a*609 (b5) in NPQ. Nevertheless, previous work with recombinant proteins refolded *in vitro* was effective in obtaining CP29 lacking either Chl *a*603 (a5) or *a*609 (b5). Both mutant proteins were impaired in their capacity to form carotenoid radical cations in their Zea-binding form (Ahn et al., 2008). The Chls *a*603–*a*609 pair is localized within the L2 domain and Chl *a*603 is roughly co-facial to, and centred along, the axis of the Zea-binding site, which is consistent with the requirements for CT quenching previously predicted by quantum chemistry calculations (Dreuw et al., 2003). Furthermore, Chls *a*603 (a5) and *a*609 (b5) are reported to be strongly coupled (Pan et al., 2011). The absence of CP29-dependent NPQ activity in plants carrying mutant CP29 lacking Chl *a*603 (a5), together with the concomitant loss of CT quenching in recombinant proteins Chl-a5 and Chl-b5 (Ahn et al., 2008), is consistent with quenching in CP29 being dependent on Chls *a*603 and *a*609, and with the catalytic site for quenching reactions comprising the xanthophyll in site L2 and the strongly coupled Chl pair (*a*603 and *a*609). Zea is a positive modulator of quenching (Niyogi et al., 1998; Dall'Osto et al., 2017), through binding to site L2 of monomeric LHCs, thus inducing a conformational change that enhances coupling between the Chl pair (Ahn et al., 2008) and activates CT quenching (Avenson et al., 2008). Nevertheless, our results do not prove conclusively that CP29-dependent quenching is catalysed through CT quenching per se (Holt et al., 2005). In fact, while the Zea$^{\bullet+}$ signal could be obtained in the isolated CP29–Zea complex, in vivo quenching also requires interaction with PsbS (Dall'Osto et al., 2017) thus enabling activation of quenching reactions other than CT quenching in the CP29–PsbS complex. Alternative hypotheses for quenching sites within LHCs have been proposed, including the possibility that quenching may occur by energy transfer between Chls *a*611 and *a*612 (a2) and Lut at site L1, based on quenching following aggregation with isolated LHCII in detergent solution (Ruban et al., 2007). In the case of CP29, this mechanism does not appear to be essential owing to the full NPQ competence of plants carrying mutant CP29 lacking either Chl *a*612 (a2) or Chl *a*613 (a3) (Fig. 5.1.7). We cannot exclude, however, that quenching proceeds in the Chls *a*611–*a*612–L1 pigment cluster in the case of LHCII, since this quenching component appears to be catalysed through a

different mechanism to that of monomeric complexes (Dall'Osto et al., 2017). Mutation H111N, though influencing neither the number nor composition of pigments bound to the complex, did promote the formation of red absorption forms in CP29 (Fig. 5.1.6), probably by inducing reorganization of chromophores in the *a*603–*a*609 cluster. We suggest that the main effect of this mutation is to reduce the distance between the two interacting Chls, thus promoting stronger excitonic interactions (Fig. 5.1.5o). Moreover, mutation H111N resulted in a significant decrease in NPQ (Fig. 5.1.7 and Supplementary Fig. 5.1.5) suggesting that orientation/distance between chromophores in the catalytic pigment cluster is crucial in regard to quenching efficiency. In principle, we cannot fully exclude that the loss of CP29-dependent NPQ activity in mutants H111W, H111L and H111F could have been the result of a conformation change in the protein rather than solely due to the loss of Chl *a*603 (a5). However, the decrease in NPQ in the H111N mutant retaining Chl *a*603, with a modified orientation/distance in respect to WT, supports that Chl *a*603 (a5) has a critical role in quenching reactions. Interestingly, all mutations targeting Chl *a*616 (Q93F/Y and P94F/W) failed to remove this chromophore (Fig. 5.1.5). Mutations on the P94 residue markedly influenced the accumulation level of CP29, down to 45% of WT, while mutations on residues Q93 did not reduce it (Supplementary Table 5.1.1). This could be ascribed to the more marked effect of a mutation in proline residue, a structurally planar residue, on the secondary structure of the protein, possibly affecting the binding affinity of the antenna to the PSII binding pocket. While mutations of residue Q93 versus P94 had distinct effects on the overall stability of CP29, both yielded a similar and significant reduction in NPQ activity (Fig. 5.1.7 and Supplementary Fig. 5.1.5). We suggest that both mutations affect the local environment of Chl *a*616. It is worth noting that Chl *a*616, the Chl a newly found by cryo-EM analysis (Wei et al., 2016), closely interacts with the Chl *a*603–*a*609 pair. Therefore, the results shown in Fig. 5.1.7 suggest that the catalytic pigment cluster responsible for quenching reaction extends to Chl *a*616. Overall, Chls *a*603, *a*609 and *a*616 probably form a cluster of chromophores that interact and promote energy quenching. Mutations on residues Q93 and P94 might affect the relative position of each component of the catalytic cluster, and thereby excitonic interactions within the cluster and the amplitude of quenching. Alternatively, the quenching reaction may be catalysed by the Chl *a*603–*a*609 dimer, with Chl *a*616 mediating photoprotective excitation energy transfer from the CP47 subunit of the PSII core complex to prevent over-excitation of PSII reaction centre. Distinguishing between these possibilities will require detailed spectroscopic analysis onfthe PSII–CP29 supercomplex.

Methods

Plant materials.

Arabidopsis thaliana koLhcb4 plants were obtained as previously described (De Bianchi et al., 2011). The coding region of the *A. thaliana lhcb4.1* gene was amplified by PCR on genomic DNA isolated from WT (Col-0) plants. The amplified fragment (−2,846 base pairs (bp), including 948 bp upstream of the transcriptional start site and 389 bp downstream of the stop codon) included both native promoters and regulatory sequences in the 3′-UTR region. The primers included attB sites facilitating cloning by the Gateway cloning system (Invitrogen).
Primer sequences were as follows:
forward,
5′-GGGGACAAGTTTGTACAAAAAAGCAGGCTTCTCGGAGATCGATTTGGAGAG-3′;
reverse,
5′-GGGGACCACTTTGTACAAGAAAGCTGGGTCCTATCATCGAATCTCCACGTTCA-3′.
The amplification product was recombined into plant destination vector pDONR221. Specific amino acidic residues (Supplementary Fig. 5.1.7a) were mutated by site-directed mutagenesis (QuickChange, Strategene) using specific primers (see Supplementary Table 5.1.4). Each mutated *lhcb4.1* gene was subcloned into pK7WG2 and then transformed into *koLhcb4* plants by *Agrobacterium*-mediated transfer DNA transformation (Zhang et al., 2006). Seedlings were screened for resistance to applications of the antibiotic kanamycin (50 mg L^{-1}). For each genotype, independent transformants (T1 generation, see Supplementary Table 5.1.5) were self-fertilized and homozygous lines were confirmed in the T3 generation. All codon changes were confirmed by sequencing of fragments amplified from genomic DNA (Supplementary Fig. 5.1.7b; www.eurofinsgenomics.eu).

Growth conditions.

WT and mutant genotypes were grown in soil, in a phytotron for 6 weeks at 150 μmol photons m^{-2} s^{-1}, 23 °C, 70% humidity, 8/16 h day/night. All biochemical and physiological analysis were carried out on plants before initiation of flowering.

Membrane isolation.

Stacked thylakoid membranes were isolated as previously described(Casazza et al., 2001).

Pigment analysis.

To measure Zea accumulation, detached leaves on wet paper were exposed to 1,000 μmol photons m^{-2} s^{-1} at room temperature (23 °C). Pigments were extracted from leaf discs with 85% acetone buffered with Na_2CO_3, separated and quantified by HPLC (Gilmore and Yamamoto, 1991b).

Protein isolation and purification.

For monomeric LHC preparations, 500 μg of membranes (in Chls) were solubilized at 0.5 mg mL^{-1} by the addition of an equal volume of 2.0% α-DM in 10 mM MES, pH 6.0. Solubilized samples

were centrifuged at 12,000g for 10 min, then fractionated by ultracentrifugation on a sucrose gradient in a SW40 rotor for 22 h at 4 °C at 40,000 r.p.m. Gradients were formed directly in the tube, by freezing at −80 °C and thawing at 4 °C a 0.5 M sugar solution containing 0.04% β-DM and 10 mM MES, pH 6.0. Green bands corresponding to monomeric LHCs were harvested, and then purification of CP29 was obtained by cation exchange chromatography as previously described (Pan et al., 2011).

Spectroscopy.

Absorption measurements were performed at room temperature using an SLM Aminco DW-2000 spectrophotometer, in 10 mM MES pH 6.0 and 0.04% β-DM. Fluorescence emission spectra were measured at 77 K using a Jobin–Yvon Fluoromax-3 spectrofluorometer. Samples were excited at 470 nm. Chl concentration was ~0.2 μg ml^{-1} in 60% glycerol, 10 mM MES, pH 6.0, and 0.04% β-DM.

Gel electrophoresis and immunoblotting.

SDS-PAGE analysis was performed using the Tris-Tricine buffer system (Schägger and von Jagow, 1987); Coomassie blue staining and densitometric analysis (Gel-Pro Analyzer, Biorad) were used to quantify protein levels in T3 lines. Non-denaturing Deriphat–PAGE was performed as previously described (Havaux et al., 2004). Immunotitration was carried out on leaf extract from T1 plants, to identify the most promising lines. Leaf extracts were loaded for each sample and electroblotted on nitrocellulose membranes. Proteins were then quantified using an α-Lhcb4 primary antibody made in-house (ImmunoGen: CP29 purified from Zea mays). A WT dilution series was used in each slab gel to plot the mutant content in CP29 in a sensible way. The signal was normalized to PSII core content by α-CP47 antibody (Agrisera, no. AS04038); detection was carried out by alkaline phosphatase-conjugated secondary antibody (Sigma-Aldrich, no. A3687).

Analysis of Chl fluorescence.

PSII function during photosynthesis was measured by Chl fluorescence on whole leaves at room temperature with a PAM 101 fluorimeter (Heinz Walz) according to ref. (Baker, 2008).

Statistics

. Statistical analysis was performed in GraphPad Prism using either Student's t-test or one-way analysis of variance (ANOVA), and means were separated with Tukey's post test at a significance level of $P < 0.05$ (see figure legends for details). Error bars represent s.d.

Reporting Summary

Further information on research design is available in the Nature Research Reporting Summary linked to this article.

Data availability.

Sequence data from this article can be found in the *Arabidopsis* Genome Initiative or GenBank/EMBL databases under accession nos. At5g01530 (Lhcb4.1) and At3g08940 (Lhcb4.2). The knockout lines used in the work were obtained from the Nottingham *Arabidopsis* Stock Centre under stock nos. N376476 (koLhcb4.1) and N877954 (koLhcb4.2).

Supplementary Information

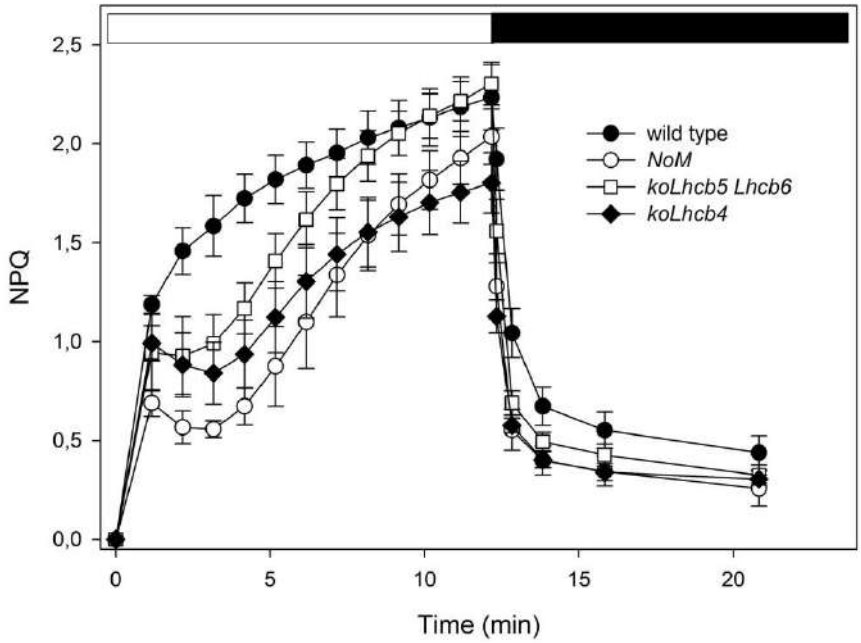

Supplementary Figure S5.1.1. Kinetics of the formation and relaxation of photoprotective energy dissipation. *Measurements of NPQ kinetics were carried out on wild-type, koLhcb4 and koLchb5 koLhcb6 leaves, upon illumination with 1000 µmol photons m^{-2} s^{-1} (white bar) and during dark relaxation (black bar), at RT. Data are expressed as mean ± SD, n = 4.*

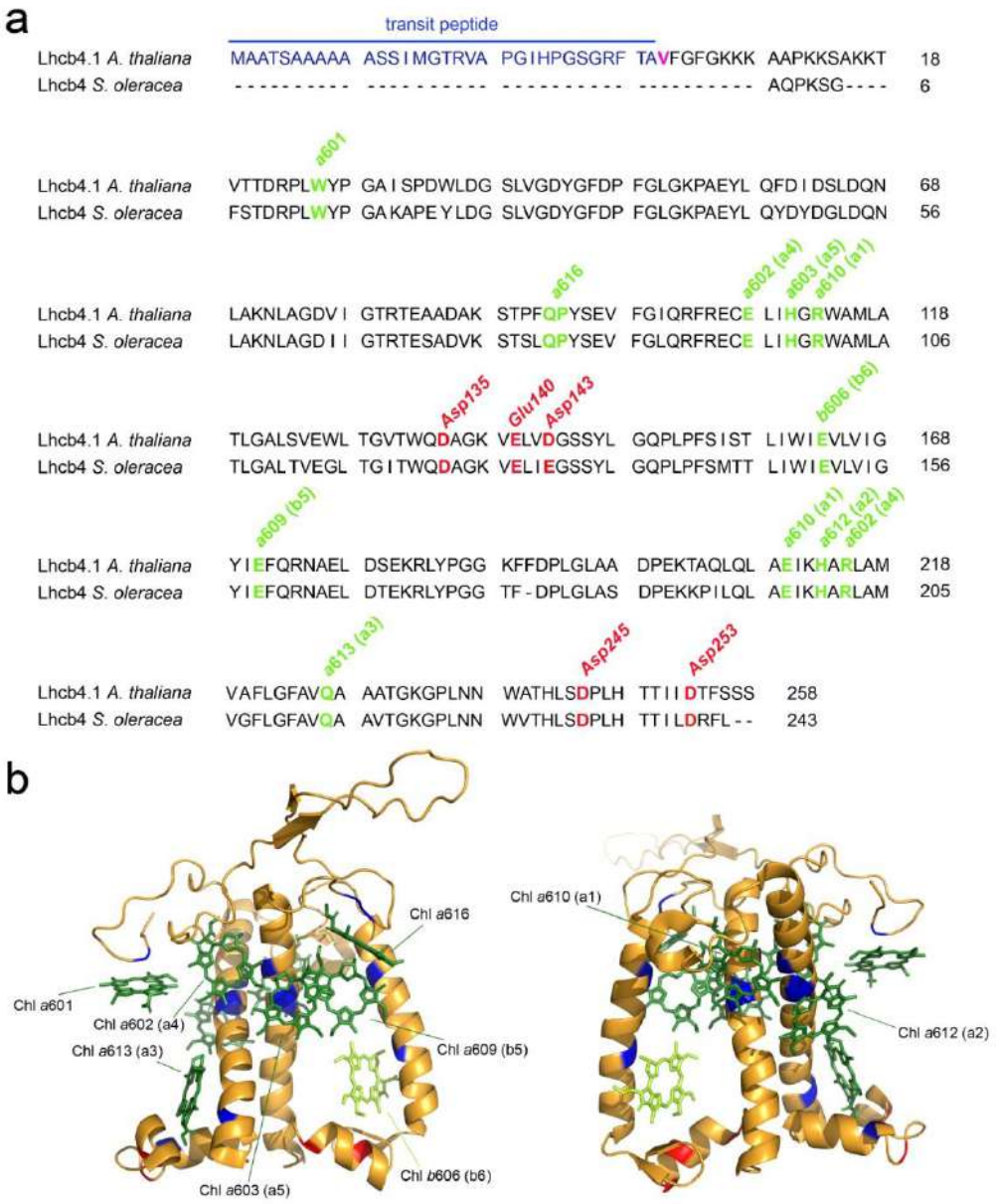

Supplementary Figure S5.1.2. Substitutions operated into the different residues in order to obtain the different mutant proteins. *(A) Sequence alignment of Lhcb4.1 protein of A. thaliana and Lhcb4 protein of S. oleracea. The amino termini of the Arabidopsis thaliana Lhcb4.1 is considered Val at position 33 (initiating Met is residue 1) as previously reported (Gómez et al., 2003). In the figure, the transit peptide (blue) and the amino termini (violet) are highlighted. The amino acid modified in this work include lumen-exposed protonatable residues in helix E and the E-C loop (red) and residues putatively binding Chl molecules (green, nomenclature from (Wei et al., 2016; Kühlbrandt et al., 1994)). (B) Stereo view of the overall structure of CP29 from spinach (Wei et al., 2016) showing Chls targeted in this study. For sake of clarity, the Chl phytyl chains are not shown. Dark green, Chl a; light green, Chl b; porphyrin-binding residues and lumen-exposed protonatable residues, modified in this work, are highlighted in blue and red, respectively.*

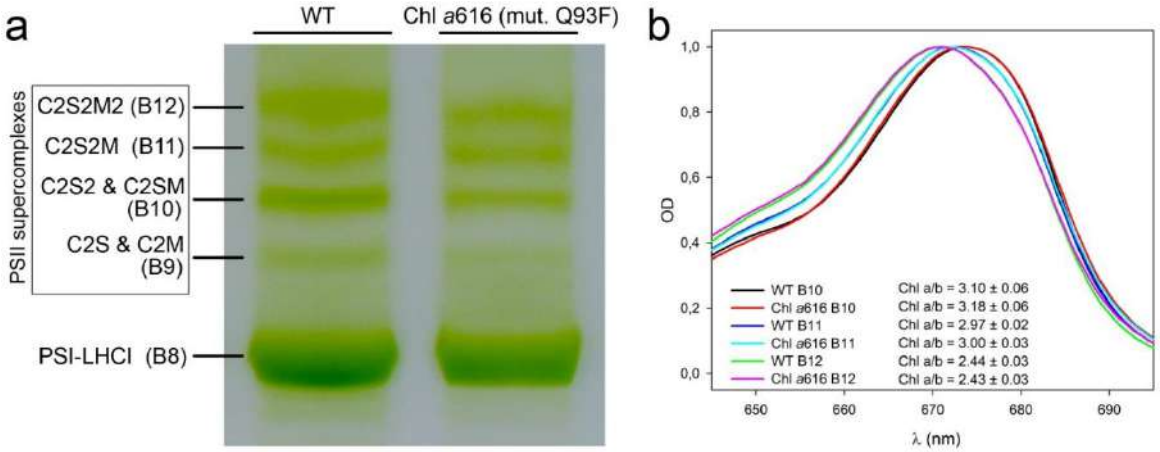

Supplementary Figure S5.1.3. Spectroscopic analysis of PSII supercomplexes purified from wild type and line Chl a616. *(A) Thylakoid pigment-protein complexes from wild type and line Chl a616, carrying mutation Q93F on CP29, were separated by non-denaturing Deriphat-PAGE, upon solubilization of membranes with 0.45% α-DM. The composition of each band is indicated (see also notes of Figure 5.1.4). (B) Selected green bands were excised and eluted, and absorption spectra of supercomplexes from wild type and line Chl a616 were normalized to the peak absorption in the Qy region. For each band analyzed, absorption spectrum of mutant complexes showed no major changes, respect to the corresponding band in wild type, Chl a/Chl b ratio of mutant complexes were indistinguishable from that of wild type.*

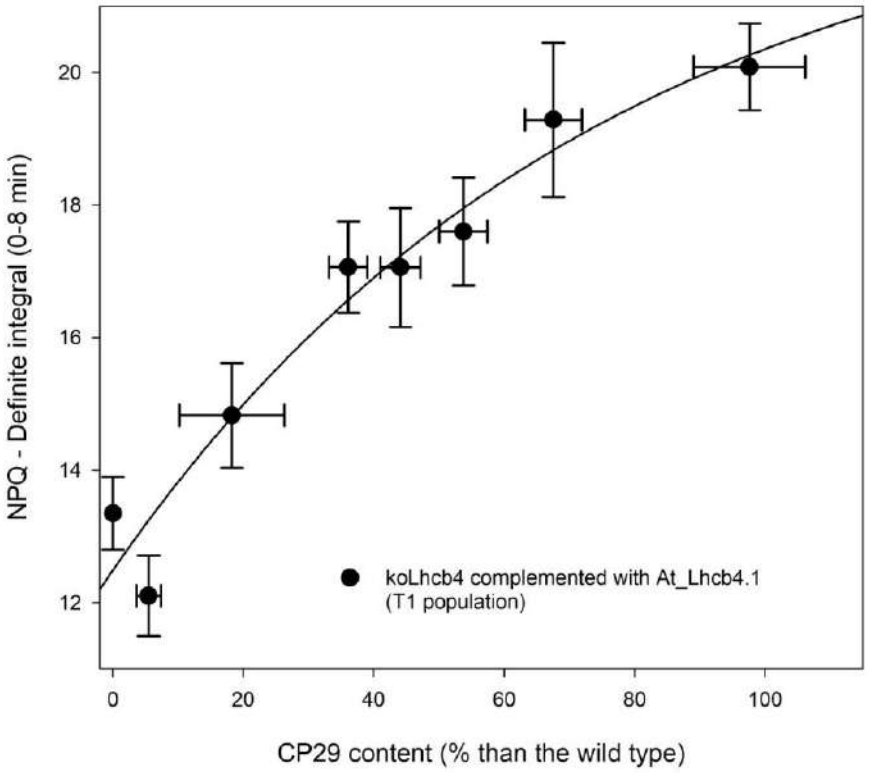

Supplementary Figure S5.1.4. Correlation between NPQ amplitude and CP29 content, in plants expressing the wild type Lhcb4.1 gene. *NPQ amplitude was measured on segregating T1 populations of Arabidopsis koLhcb4 complemented with wild type Lhcb4.1 isoform. For each plant, (i) the CP29 content was accurately estimated by SDS-PAGE, Coomassie blue staining and densitometric analysis. Plants were grouped for CP29 level, and (ii) definite integrals were calculated from NPQ curves in the range 0-8 minutes. For correlation analysis, experimental points (black circles) were modeled with an exponential function (f=y0+a*(1-exp(-b*x))+c*(1-exp(-d*x), black line). Then, NPQ amplitude was measured on leaves from wild type, koLhcb4 and independent T3 transgenic lines. Each experimental point represents the CP29 content of the line and the definite integral from its NPQ traces. At, Arabidopsis thaliana.*

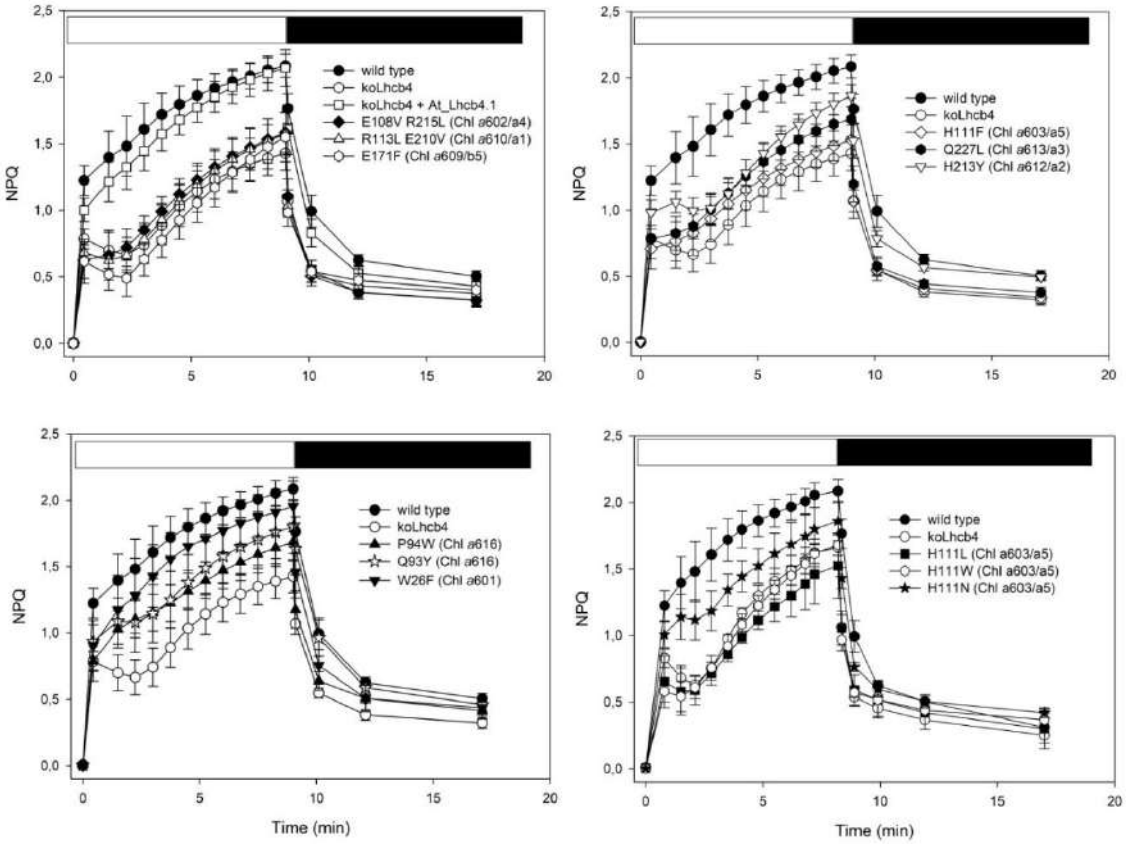

Supplementary Figure S5.1.5. Kinetics of the formation and relaxation of photoprotective energy dissipation. *Measurements of NPQ kinetics were carried out on leaves from wild-type, koLhcb4 and complemented lines, upon illumination with 1000 µmol photons m^{-2} s^{-1} (white bar) and relaxation in the dark (black bar) at RT. Each experimental point is the mean value obtained by measuring at least two independent T3 transgenic lines. Data are expressed as mean ± SD, n > 5.*

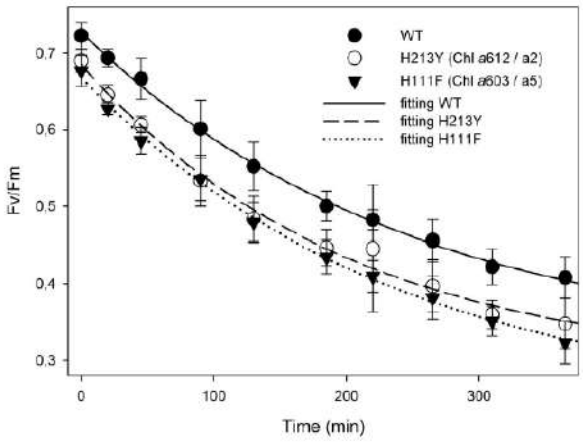

Fitting $y = y_0 + A \exp(-bx)$	y_0	A	b -10^3
WT	0.312 ± 0.021	0.416 ± 0.020	4.15 ± 0.41
H213Y (Chl a 612 / a2)	0.286 ± 0.024	0.399 ± 0.022	4.95 ± 0.61
H111F (Chl a603 / a5)	0.237 ± 0.021	0.431 ± 0.019	4.30 ± 0.40

Supplementary Figure S5.1.6. Kinetic of Fv/Fm decay measured on wild type, H213Y and H111F intact chloroplasts. *(upper figure) The decrease of maximal quantum yield of PSII Fv/Fm) was assessed in isolated chloroplasts during illumination (50 µmol photons m-2 s-1, white light, RT, stirring 200 rpm) for six hours. Data are shown as mean ± SD, n = 3 biologically independent samples. (lower table) Each dataset was fitted with an exponential function y = y0 + A e-bx, and the kinetic of quantum yield decay was assessed in the different genotypes by comparing parameters b, which describe the slope of exponential functions. Statistical analysis (two-sided Student's t-test, P < 0.05) showed this parameter was not significantly different in both mutants with respect to the corresponding wild type value.*

a


1 AATGGACTTG AAACATCACC AGATAACGCA GAGTTTAATA GATAAGATTA
51 GTAATCCTAC TCACCGTCAG ATGGATTTGT GAATCGATCC AACGGTCATA
101 ATCGTCTTTC CAAGATAGGC CAGCTCCGAA ACTCACCTCC ACGCATCTAT
151 AATCGTGTAT CAAGAAACGG ATCTTTCTTC TCTATCTTCT GAATATCACA
201 AAACCCAATT AGCCGGAGAT GGCCGCAACA TCCGCCGCTG CTGCAGCTGC
251 TTCTTCCATC ATGGGTACTC GGGTGGCTCC CGGTATCCAT CCCGGTTCAG
301 GTCGGTTCAC AGCCGTGTTC GGTTTCGGAA AGAAGAAGGC AGCTCCCAAA
W26
351 AAGAGTGCCA AAAAGACGGT GACTACGGAC CGGCCTCTTT GGTACCCAGG
401 CGCCATTTCT CCTGACTGGC TTGATGGTTC CTTGGTTGGA GATTACGGTT
451 TTGATCCCTT CGGTTTAGGC AAACCGGCCG AGTATCTTCA ATTCGATATC
501 GATTCACTAG ACCAGAATCT GGCTAAGAAC TTGGCCGGAG ACGTGATCGG
Q93 P94
551 AACCCGTACG GAAGCTGCCG ACGCCAAATC GACGCCGTTT CAGCCGTACA
E108 H111
601 GTGAGGTGTT CGGAATCCAG AGATTCAGGG AATGCGAACT CATCCACGGA
R113
651 CGGTGGGCGA TGCTCGCTAC TCTCGGCGCT CTCTCCGTCG AATGGCTTAC
D135
701 CGGCGTTACA TGGCAAGACG CTGGCAAGGT AACGCCACTC CCTTCTCCAC
751 TTGGATAATC GGTTATAAGT TAGTTATTTC GAAGATGCTA ATAAATTAGT
801 ATTCAAATAG TTGCGTTTGC GTTTGTTTGC GACTCAGATA GAAATGTATG
851 TACAATTTAG TTGATTTAGC GTTTGCTTTG GCGTCTGTCT CTCTCTCTTT
901 CTTACAGTTT GCGTTAGCAT TGGACTGTTT GAGTTTCTGT TCAGTCAAGA
951 ATATTCAAGT CTAGTGTTCA ATGAGTGATA TTTAAATATT AGTTGAAATG
E140 D143
1001 TTGTTATTCA ATCAGGTGGA GCTTGTAGAT GGATCGTCCT ACTTGGGGCA
E163
1051 GCCATTACCT TTCTCGATCT CGACATTGAT ATGGATCGAG GTGTTAGTGA
E171
1101 TCGGCTACAT CGAGTTCCAG CGCAACGCCG AGCTTGATTC GGAGAAGCGT
1151 TTATACCCCG GAGGCAAGTT CTTTGACCCG CTAGGTTTAG CGGCTGACCC
E210 H213 R215
1201 GGAGAAGACT GCTCAACTTC AGTTAGCTGA GATCAAGCAT GCACGTCTTG
Q227
1251 CGATGGTCGC CTTCTTGGGA TTCGCGGTTC AAGCGGCTGC AACAGGTAAA
D245
1301 GGTCCACTCA ACAATTGGGC TACTCACCTC AGTGATCCAC TCCACACCAC
D253
1351 CATCATCGAT ACCTTCTCCT CATCTTAA

Supplementary Figure S5.1.7. Genomic sequence of Lhcb4.1 of A. thaliana. *(a) Nucleotide sequence of A. thaliana Lhcb4.1 gene. In the figure, promoter sequence (blue), intron (red), triplets mutated in this work and the corresponding aminoacid (green) are highlighted. (b) Mutations verification on genomic DNA by Sanger sequencing of T3 plants. In each panel, upper sequence represents the wild type sequence, lower sequence the mutated form. Mutations W26F, Q93Y, P94W, E108V, H111F, H111L, H111W, H111N, D245N, D253N, R113L, D135N: forward sequencing. Mutations E140Q, D143N, E163V, E171F, E210V, H213Y, R215L, Q227L: reverse sequencing.*

Supplementary Table S5.1.1. Site-directed mutations in CP29 and their effects on antenna content in vivo. *CP29 protein level was measured by SDS-PAGE of thylakoid proteins, coomassie staining and densitometric analysis, on homozygous T3 plants containing a single copy Lhcb4.1 insertion. More than two lines were analyzed for each site-directed mutant, at least five different plants were tested for each line. Each mutant was designated by the sites as assigned by (Pan et al., 2011) and (Wei et al., 2016); in parenthesis, nomenclature by (Kühlbrandt et al., 1994). The targeted amino acid residues and their substitutions are shown. CP29 protein level is expressed as mean ± SD, n>4. Values marked with the same letters are not significantly different from each other within the column (ANOVA test, P < 0.05). nd, not detected.*

Sites[§]	AA residues in *Arabidopsis* CP29	Mutations	CP29 protein level (% than wild-type plants)
*a*601	Trp 26	W26F	77.7 ± 10.3[a]
*a*602 (a4)	Glu 108, Arg 215	E108V & R215L	nd
*a*603 (a5)	His 111	H111F	40.5 ± 10.7[b]
		H111L	28.6 ± 4.9[b]
		H111W	17.9 ± 6.5[c]
		H111N	90.3 ± 6.0[a,d]
*b*606 (b6)	Glu 163	E163V	40.8 ± 7.9[b]
*a*609 (b5)	Glu 171	E171V	nd
		E171Y	nd
		E171T	nd
		E171F	nd
*a*610 (a1)	Glu 210, Arg 113	R113L & E210V	nd
*a*612 (a2)	His 213	H213Y	30.1 ± 5.1[b]
		H213T	33.9 ± 7.9[b]
*a*613 (a3)	Gln 227	Q227L	17.6 ± 6.1[c]
*a*616	Gln 93	Q93F	109.1 ± 10.2[d]
		Q93Y	100.8 ± 10.7[d]
*a*616	Pro 94	P94F	49.3 ± 11.2[b]
		P94W	45.8 ± 11.8[b]
protonatable residues	Asp 135, Glu 140, Asp 143	D135N & E140Q & D143N	91.8 ± 5.4[d]
protonatable residues	Asp 245, Asp 253	D245N & D253N	87.1 ± 12.2[d]

[§]in parenthesis, Chl nomenclature by W. Kühlbrandt et al., Nature 367 (1994) 614–621

Supplementary Table S5.1.2. Photosynthetic pigment composition of leaves from wild type, koLhcb4 and complemented lines. *Pigment content was determined after leaves were illuminated for 15 min at 1000 µmol photons m^{-2} s^{-1}, RT, in homozygous T3 lines containing a single copy Lhcb4.1 insertion. Two lines were analyzed for each site-directed mutant. Data are normalized to 100 Chl a+b molecules and are expressed as mean ± SD (n = 6).*

Genotypes	mol pigment / 100 mol Chls					
	Neo	Vio	Ant	Zea	Lut	β-Car
wild type	4.8 ± 0.2	1.2 ± 0.1	0.5 ± 0.1	1.9 ± 0.2	12.9 ± 0.3	6.3 ± 0.5
koLhcb4	4.9 ± 0.2	1.0 ± 0.3	0.5 ± 0.1	2.0 ± 0.1	12.8 ± 0.3	5.9 ± 0.2
koLhcb4 + *Lhcb4.1* wild type	4.7 ± 0.3	1.2 ± 0.2	0.5 ± 0.1	1.8 ± 0.2	12.7 ± 0.3	6.5 ± 0.4
*a*601 / W26F	4.9 ± 0.3	1.1 ± 0.1	0.5 ± 0.1	2.2 ± 0.2	13.0 ± 0.6	5.4 ± 0.9
*a*602 (a4) / E108V & R215L	4.6 ± 0.2	0.9 ± 0.2	0.5 ± 0.1	1.9 ± 0.2	12.7 ± 0.3	6.2 ± 0.3
*a*603 (a5) / H111F	4.6 ± 0.3	1.1 ± 0.1	0.5 ± 0.1	1.8 ± 0.2	12.8 ± 0.4	6.4 ± 0.4
*a*603 (a5) / H111L	4.9 ± 0.2	0.9 ± 0.2	0.5 ± 0.1	1.9 ± 0.1	12.7 ± 1.6	5.9 ± 0.2
*a*603 (a5) / H111W	4.7 ± 0.1	0.9 ± 0.1	0.5 ± 0.1	1.8 ± 0.3	12.9 ± 0.4	5.8 ± 0.2
*a*603 (a5) / H111N	4.7 ± 0.3	1.1 ± 0.1	0.4 ± 0.1	1.8 ± 0.4	12.7 ± 0.6	6.0 ± 0.2
*b*606 (b6) / E163V	5.1 ± 0.2	1.2 ± 0.1	0.5 ± 0.1	1.9 ± 0.1	12.9 ± 0.4	7.1 ± 0.5
a609 (b5) / E171Y	5.0 ± 0.3	1.0 ± 0.1	0.6 ± 0.1	1.8 ± 0.1	13.0 ± 0.4	6.6 ± 0.4
*a*610 (a1) / E113L & E210V	4.4 ± 0.8	0.9 ± 0.2	0.5 ± 0.1	1.9 ± 0.1	12.7 ± 0.3	6.2 ± 0.4
*a*612 (a2) / H213Y	4.8 ± 0.4	1.1 ± 0.1	0.5 ± 0.1	2.1 ± 0.1	12.3 ± 0.6	6.0 ± 0.9
*a*612 (a2) / H213T	4.8 ± 0.2	1.2 ± 0.1	0.6 ± 0.1	2.1 ± 0.2	13.3 ± 0.6	5.8 ± 0.9
*a*613 (a3) / Q227L	4.9 ± 0.3	1.1 ± 0.1	0.5 ± 0.1	2.1 ± 0.4	12.9 ± 0.4	6.1 ± 0.5
*a*616 / Q93F	4.9 ± 0.2	1.3 ± 0.3	0.5 ± 0.1	2.0 ± 0.2	12.5 ± 0.4	5.8 ± 0.3
*a*616 / Q93Y	4.9 ± 0.3	1.3 ± 0.3	0.6 ± 0.1	1.9 ± 0.2	12.7 ± 0.7	5.5 ± 0.6
*a*616 / P94F	5.1 ± 0.3	1.1 ± 0.3	0.6 ± 0.1	2.2 ± 0.2	14.4 ± 1.1	5.5 ± 1.7
*a*616 / P94W	5.1 ± 0.3	1.1 ± 0.2	0.5 ± 0.1	2.2 ± 0.2	14.5 ± 0.9	5.6 ± 0.7
protonatable residues / D135N & E140Q & D143N	4.9 ± 0.3	1.2 ± 0.2	0.5 ± 0.1	1.9 ± 0.2	12.4 ± 0.4	6.2 ± 0.7
protonatable residues / D245N & D253N	4.8 ± 0.2	1.2 ± 0.1	0.6 ± 0.1	1.8 ± 0.2	12.2 ± 0.4	6.1 ± 0.2

Supplementary Table S5.1.3. Pigment composition of wild type purified CP29 and mutant isoforms. *Pigment content of the purified complexes was assessed by fitting spectra of the acetone extract with spectra of individual chromophores (Croce et al., 2000) combined with HPLC analysis. Data are expressed as no. of moles per mole of polypeptide, mean ± SD. Chl, chlorophyll; Neo, neoxanthin; Vio, violaxanthin; Lut, lutein.*

CP29 complex	Chl *a*	Chl *b*	Neo	Vio	Lut
wild type	10.2 ± 0.2	3.8 ± 0.2	1.1 ± 0.2	1.0 ± 0.1	1.3 ± 0.1
koLhcb4 + *Lhcb4.1* wild type	9.9 ± 0.2	4.1 ± 0.2	0.8 ± 0.1	0.9 ± 0.1	1.4 ± 0.1
*a*601 / W26F	9.8 ± 0.1	4.2 ± 0.1	1.1 ± 0.1	0.9 ± 0.1	1.3 ± 0.1
*a*603 (a5) / H111F	8.5 ± 0.1	4.5 ± 0.1	1.2 ± 0.1	0.8 ± 0.1	1.5 ± 0.1
*a*603 (a5) / H111L	9.2 ± 0.2	3.8 ± 0.2	1.0 ± 0.1	0.6 ± 0.1	1.5 ± 0.1
*a*603 (a5) / H111N	10.2 ± 0.1	3.8 ± 0.1	1.0 ± 0.1	1.0 ± 0.1	1.2 ± 0.1
*a*612 (a2) / H213Y	8.7 ± 0.1	4.3 ± 0.1	0.9 ± 0.1	0.8 ± 0.1	1.2 ± 0.2
*a*613 (a3) / Q227L	8.8 ± 0.1	4.2 ± 0.1	0.9 ± 0.1	0.8 ± 0.1	1.3 ± 0.1
*a*616 / Q93Y	9.9 ± 0.1	4.1 ± 0.1	0.9 ± 0.1	1.0 ± 0.1	1.3 ± 0.1

Supplementary Table S5.1.4. Sequences of oligonucleotide primers used for site-directed mutagenesis

Sites[§]	Mutations	primers	
		forward	reverse
*a*601	W26F	CGCCTGGGTAGAAAAGAGGCCGGTCCGTAGT	ACTACGGACCGGCCTCTTTTCTACCCAGGCG
*a*602 (a4)	E108V	CACCGTCCGTGGATGAGAACGCATTCCCTGAATCTC	GAGATTCAGGGAATGCGTTCTCATCCACGGACGGTG
	R215L	GGCGACCATCGCAAGAAGTGCATGCTTGATCTC	GAGATCAAGCATGCACTTCTTGCGATGGTCGCC
*a*603 (a5)	H111F	CATCGCCCACCGTCCGAAGATGAGTTCGCATTC	GAATGCGAACTCATCTTCGGACGGTGGGCGATG
	H111L	GCATCGCCCACCGTCCAAGGATGAGTTCGCATTC	GAATGCGAACTCATCCTTGGACGGTGGGCGATGC
	H111W	GCATCGCCCACCGTCCCCAGATGAGTTCGCATTCC	GGAATGCGAACTCATCTGGGGACGGTGGGCGATGC
	H111N	GCATCGCCCACCGTCCGTTGATGAGTTCGCATTC	GAATGCGAACTCATCAACGGACGGTGGGCGATGC
*b*606 (b6)	E163V	ATGTAGCCGATCACTAACACAACGATCCATATCAATGTCGAG	CTCGACATTGATATGGATCGTTGTGTTAGTGATCGGCTACAT
*a*609 (b5)	E171V	CGGCGTTGCGCTGGAAAACGATGTAGCCGATCAC	GTGATCGGCTACATCGTTTTCCAGCGCAACGCCG
	E171Y	CGGCGTTGCGCTGGAAATAGATGTAGCCGATCACT	AGTGATCGGCTACATCTATTTCCAGCGCAACGCCG
	E171T	GCTCGGCGTTGCGCTGGAAAGTGATGTAGCCGATCACTAAC	GTTAGTGATCGGCTACATCACTTTCCAGCGCAACGCCGAGC
	E171F	GTTAGTGATCGGCTACATCTTTTTCCAGCGCAACGCCGAGC	GCTCGGCGTTGCGCTGGAAAAAGATGTAGCCGATCACTAAC
*a*610 (a1)	R113L	TAGCGAGCATCGCCCAAAGTCCGTGGATGAGTTC	GAACTCATCCACGGACTTTGGGCGATGCTCGCTA
	E210V	CAAGACGTGCATGCTTGATAACAGCTAACTGAAGTTGAGC	GCTCAACTTCAGTTAGCTGTTATCAAGCATGCACGTCTTG
*a*612 (a2)	H213Y	GCGACCATCGCAAGACGTGCGAACTTGATCTCAGCTAACTGAA	TTCAGTTAGCTGAGATCAAGTTCGCACGTCTTGCGATGGTCGC
	H213T	CATCGCAAGACGTGCATACTTGATCTCAGCTAACT	AGTTAGCTGAGATCAAGTATGCACGTCTTGCGATG
*a*613 (a3)	Q227L	GTTGCAGCCGCAAGAACCGCGAATCCCAAGAAGGC	GCCTTCTTGGGATTCGCGGTTCTTGCGGCTGCAAC
*a*616	Q93F	CCTCACTGTACGGAAAAAACGGCGTCGATTTGGCGTCGG	CCGACGCCAAATCGACGCCGTTTTTTCCGTACAGTGAGG
	Q93Y	CTCACTGTACGGATAAAACGGCGTCGATTTGGCGTCG	CGACGCCAAATCGACGCCGTTTTATCCGTACAGTGAG
*a*616	P94F	GATTCCGAACACCTCACTGTAAAACTGAAACGGCGTCGATTTGGC	GCCAAATCGACGCCGTTTCAGTTTTACAGTGAGGTGTTCGGAATC
	P94W	CGAACACCTCACTGTACCACTGAAACGGCGTCGAT	ATCGACGCCGTTTCAGTGGTACAGTGAGGTGTTCG
protonatable residues	D135N	CGTTACCTTGCCAGCATTTTGCCATGTAACGCCGGTA	TACCGGCGTTACATGGCAAAATGCTGGCAAGGTAACG
	E140Q	GTAGGACGATCCATCTACAAGTTGCACCTGATTGAATAACAACAT	ATGTTGTTATTCAATCAGGTGCAACTTGTAGATGGATCGTCCTAC
	D143N	CAAGTAGGACGATCCATTTACAAGCTCCACCTGATTG	CAATCAGGTGGAGCTTGTAAATGGATCGTCCTACTTG
protonatable residues	D245N	GGCTACTCACCTCAGTAATCCACTCCACACCAC	GTGGTGTGGAGTGGATTACTGAGGTGAGTAGCC
	D253N	AGATGAGGAGAAGGTATTGATGATGGTGGTGTGGA	TCCACACCACCATCATCAATACCTTCTCCTCATCT

[§]in parenthesis, Chl nomenclature by W. Kühlbrandt et al., Nature 367 (1994) 614–621

Supplementary Table S5.1.5. Number of independent T1 plants. *Plants were identified by antibiotic resistance and further analyzed for CP29 content by immunotitration.*

Sites[§]	Mutations	Independent T1 plants (kanamycin resistant)
*a*601	W26F	22
*a*602 (a4)	E108V & R215L	18
*a*603 (a5)	H111F	20
	H111L	22
	H111W	17
	H111N	7
*b*606 (b6)	E163V	19
*a*609 (b5)	E171V	6
	E171Y	8
	E171T	13
	E171F	20
*a*610 (a1)	R113L & E210V	17
*a*612 (a2)	H213Y	20
	H213T	10
*a*613 (a3)	Q227L	21
*a*616	Q93F	32
	Q93Y	17
*a*616	P94F	14
	P94W	11
protonatable residues	D135N & E140Q & D143N	19
protonatable residues	D245N & D253N	8

[§]in parenthesis, Chl nomenclature by W. Kühlbrandt et al., Nature 367 (1994) 614–621

Supplementary Methods

Isolation of intact chloroplasts and analysis of Fv/Fm decay. Intact chloroplasts were isolated as previously described by Casazza A.P. and co-workers (Casazza et al., 2001), with the following modifications: 1.5 g of leaves were rapidly homogenized using mortar and pestle in 50 ml of grinding buffer (GB) devoid of protease inhibitors; the suspension was centrifuged at 2600 g for 3 min at 4°C, the pellet resuspended in 10 ml of resuspending buffer (RB) containing 0.3 M sorbitol, 2.5 mM EDTA, 5 mM $MgCl_2$, 10 mM $NaHCO_3$, 20 mM HEPES (pH 7.6) and 0.5% (w/v) fatty acids-free BSA. After centrifugation (2600 g for 3 min at 4 ◦C), the pellet was resuspended in 1 mL of RB, and chlorophyll content was quantified. Then, chloroplasts were diluted to 50 μg Chl/mL in measuring buffer (MB) containing 0.3 M sorbitol, 5 mM $MgCl_2$, 10 mM NaCl, 20 mM KCl, 30 mM Tricine/KOH (pH 8.0), 0.5% (w/v) fatty acids-free BSA, 5 mM ascorbic acid, 0.5 mM ATP, 100 μM methylviologen. Chloroplast suspensions were maintained in multi-wells, under stirring (200 rpm), at room temperature (24°C), illuminated with white light (50 μmol photons m^{-2} s^{-1}). Decay kinetics of maximal quantum yield of PSII photochemistry (Fv/Fm) was recorded during illumination to follow PSII photoinhibition; chloroplast suspensions were dark-adapted for 10 min before each measurement.

5.2 Loss of a single chlorophyll in CP29 triggers re-organization of the Photosystem II supramolecular assembly

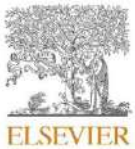

Contents lists available at ScienceDirect

BBA - Bioenergetics

journal homepage: www.elsevier.com/locate/bbabio

Loss of a single chlorophyll in CP29 triggers re-organization of the Photosystem II supramolecular assembly

Zeno Guardini [1], Rodrigo L. Gomez [1], Roberto Caferri, Luca Dall'Osto [*,1], Roberto Bassi [*,1]

Dipartimento di Biotecnologie, Università di Verona, Strada Le Grazie 15, 37134 Verona, Italy

Abstract

In land plants, both efficient light capture and photoprotective dissipation of chlorophyll excited states in excess require proper assembly of Photosystem II supercomplexes PSII-LHCs. These include a dimeric core moiety and a peripheral antenna system made of trimeric LHCII proteins connected to the core through monomeric LHC subunits. Regulation of light harvesting involves re-organization of the PSII supercomplex, including dissociation of its LHCII-CP24-CP29 domain under excess light. The Chl *a*603-*a*609-*a*616 chromophore cluster within CP29 was recently identified as responsible for the fast component of Non-Photochemical Quenching of chlorophyll fluorescence. Here, we pinpointed a chlorophyll-protein domain of CP29 involved in the macro-organisation of PSII-LHCs. By complementing an *Arabidopsis* knock-out mutant with CP29 sequences deleted in the residue binding chlorophyll *b*614 / b3-binding, we found that the site is promiscuous for chlorophyll *a* and *b*. By plotting NPQ amplitude *vs.* CP29 content we observed that quenching activity was significantly reduced in mutants compared to the wild type. Analysis of pigment-binding supercomplexes showed that the missing Chl did hamper the assembly of PSII-LHCs supercomplexes, while observation by electron microscopy of grana membranes highlighted the PSII particles were organized in two-dimensional arrays in mutant grana partitions. As an effect of such array formation electron transport rate between Q_A and Q_B reduced, likely due to restricted plastoquinone diffusion. We conclude that chlorophyll *b*614, rather being part of pigment cluster responsible for quenching, is needed to maintain full rate of electron flow in the thylakoids by controlling protein-protein interactions between PSII units in grana partitions.

Introduction

In land plants, sunlight drives photosynthetic electron transport, promotes synthesis of NADPH and ATP, and ultimately fuels CO_2 fixation into biomass. Light harvesting consists into photon absorption by arrays of chlorophylls (Chls) and carotenoids (Car), organized into photosystems (PS) within the thylakoid membranes. Each PS includes a core complex, where charge separation reactions are catalyzed, and a peripheral antenna system, composed by light-harvesting complexes (LHCs), which enhances the absorption cross section of the core (Croce and van Amerongen, 2020). The PSs are segregated in distinct domains of thylakoids with PSII located in grana partitions and PSI in grana margins as well as in the stromatic lamellae connecting grana stacks (Olive and Vallon, 1991; Kirchhoff, 2019). The tight packing of PSII-LHCs in stacked membranes allows for energy transfer between "closed" and "open" PSII reaction centres thus increasing light-use efficiency (Gaffron and Wohl, 1936; Lavergne and Trissl, 1995). A large antenna is crucial for maximizing photosynthesis in limiting light (LL); yet under excess light (EL) conditions, it results in excitation rate beyond the capacity for photochemical reactions. PSII over-excitation increases the yield of unquenched singlet excited states of Chl (^{1}Chl*) conversion into triplets (^{3}Chl*), as well as ROS (reactive oxygen species) release, which ultimately damages and inhibits the photosynthetic machinery (Krieger-Liszkay, 2005; Melis, 1999). In the ever-changing light environment experienced by plants, avoiding photosynthetic yield decline is therefore critical. During evolution, besides light capture, pressure for development of photoprotective mechanisms has shaped antenna machinery and its regulation (Bassi and Dall'Osto, 2021). These include the long-term reduction of PSII antenna size upon acclimation to EL, aimed at counteracting sustained over-excitation (Anderson, 1986; Kouřil et al., 2013). In the short term, this is complemented by state1-state2 transitions, by which a mobile LHCII fraction becomes reversibly associated to either PSI or PSII in order to balance energy distribution between PS (Allen, 1992; Galka et al., 2012). Additional mechanisms of photoprotection include NPQ (Non-Photochemical Quenching), which dissipates absorbed photons into heat (Ruban et al., 2012) and is catalysed in the antenna moiety of PSII. NPQ ensures fast adaptation of PSII quantum yield in response to changing irradiance. Among the kinetic components contributing to NPQ (Horton et al., 1996; Cazzaniga et al., 2013; Nilkens et al., 2010), qE is rapidly activated and relaxed (within 20-60 s), and is triggered by the over-acidification of the thylakoid lumen, thus working as a feedback control for PSII quantum yield. Transduction of the lumenal acidification into dissipative response requires PsbS (Li et al., 2004), a pigment-less protein in grana partitions (Fan et al., 2015) which undergoes protonation of two lumen-exposed acidic residues (Li et al., 2004), and a Chl-binding interactor(s) where quenching is activated to regulate the dissipative channel (Sacharz et al., 2017). Lastly, the Light harvesting moiety of PSII undergoes light-dependent reorganization with segregation of LHCII/CP24 domains detached from large supercomplexes found in low light (Johnson et al., 2011; Betterle et al., 2009; Kouřil et al., 2013).

Expression of qE requires PSII antenna proteins (Havaux et al., 2007) the products of the Lhcb gene family, binding Chl *a*, Chl *b* and xanthophylls. These are organized into two layers around dimeric PSII core complexes: the "major" LHCII antenna forms an outer layer of trimers made of combinations of Lhcb1, Lhcb2 and Lhcb3 gene products. These, in turn, are connected to core

complex by monomeric complexes Lhcb4 (CP29), Lhcb5 (CP26) and Lhcb6 (CP24) (Su et al., 2017). Depending on growth irradiance, PSII supercomplexes assumes different sizes: CP29 and CP26, together with LHCII-S (strongly bound) form C_2S_2 (Kouřil et al., 2012), whereas larger supercomplexes include the monomeric CP24 and the LHCII-M (moderately bound) trimer. Under low light conditions, antenna is furtherly enhanced by additional LHCII-L (loosely bound) trimers (van Oort et al., 2010; Kouřil et al., 2013).

Reverse genetics identified two distinct mechanisms for dissipation of photon energy absorbed in excess (EL), which operates at different protein domains in PSII antenna (Dall'Osto et al., 2017). Indeed, depletion of trimeric LHCII exhibited a reduction in NPQ by about 60% while deletion of monomeric LHCs resulted in a slower onset of NPQ induction, implying CP29 catalyses the fast- qE response upon dark-light transition(Dall'Osto et al., 2017), since plants devoid of both CP26 and CP24 were less affected (De Bianchi et al., 2008, 2011). Indeed, *in-vivo* site-directed mutagenesis of CP29 showed that Chl *a*603 (a5) and *a*616 chromophores were essential components of the catalytic pigment cluster, together with xanthophyll in L2 and Chl *a*609 (b5) (Guardini et al., 2020). CP29 also hosts an additional chromophore cluster, close to the lumenal surface, including the Chl *a*613 and Chl *b*614, coordinated by residues in the short amphipathic helix D. The 2.7Å resolution structure suggested these Chl participate in energy transfer pathway in PSII, with excitons from CP24 being received by CP29 through the interfacial Chl $b606_{CP24}$ – $b614_{CP29}$ at the lumenal side (Su et al., 2017). Based on molecular dynamics simulations (Ioannidis et al., 2016) it was suggested that membrane energization induces conformational change of the helix D domain, which correlates with Chl *b*614 macrocycle deformation likely to disrupt short range interactions with Chl *a*613, producing a quenching site (Papadatos et al., 2017).

Here, we explored the function of the Chl *a*613-*b*614 interaction at the luminal domain of CP29, by *in-vivo* site-directed mutagenesis of Chl *b*614. By modifying the pigment cluster coordinated by helix D, we found that NPQ amplitude in CP29-H242L plants was reduced respect to wild type. Also, loss of Chl *b*614 impaired light-use efficiency and growth rate, through affecting the supramolecular organisation of PSII and reducing PQ diffusion rate. We suggest the reduced quenching phenotype of the mutant was due to a pleiotropic effect on electron transport rate rather than to a disruption of quenching reactions within the Chl *a*613-*b*614 chromophore cluster.

Materials and Methods

Plant materials.

Arabidopsis thaliana knock-out (ko) mutants *koLhcb6* and *koLhcb4* plants (De Bianchi et al., 2008, 2011) and lines expressing Lhcb4.1 carrying specific mutation at the aminoacidic residue binding Chl *b*614 were obtained as previously described (De Bianchi et al., 2008, 2011; Guardini et al., 2020). The amplification product was cloned into a plant destination vector, pK7WG2. H242 amino acidic residue was mutated by site-directed mutagenesis (QuickChange, Strategene, for mutation H242L; Q5 site-directed mutagenesis, NEB, for mutations H242V and H242A) using specific primers (see Supplementary Table S5.2.3). Each mutated *Lhcb4.1* gene was transformed into *koLhcb4* plants by *Agrobacterium*-mediated transfer DNA transformation (Zhang et al., 2006). Seedlings were screened for resistance to applications of the antibiotic kanamycin (50 mg l^{-1}). For each genotype, independent transformants (T1 generation) were self-fertilized, and homozygous lines were confirmed in the T3 generation. All codon changes were confirmed by sequencing of fragments amplified from genomic DNA (www.eurofinsgenomics.eu).

Growth conditions

Wild type and mutant genotypes were grown in soil, in a phytotron for 6 weeks at 150 μmol photons m^{-2} s^{-1}, 23°C, 70% relative humidity, 8/16 h of day/night. All biochemical and physiological analyses were carried out on plants prior to initiation of flowering. The growth of plants was determined by measuring rosette fresh weight at the end of the growth experiments.

Membrane isolation

Stacked thylakoid membranes were isolated as previously described (Casazza et al., 2001). Grana membranes have been isolated from dark-adapted samples using α-dodecyl maltoside (α-DM) solubilisation of stacked thylakoids, as described in (Morosinotto et al., 2010).

Protein isolation and purification

Monomeric LHC preparations were obtained as previously described (Guardini et al., 2020).

Spectroscopy

Absorption measurements were performed at RT using an SLM Aminco DW-2000 spectrophotometer, in 10 mM MES pH 6.0 and 0.04% β-DM.

Gel electrophoresis and immunoblotting

SDS-PAGE analysis was performed using the Tris-Tricine buffer system (Schägger and von Jagow, 1987). *Coomassie* blue staining and densitometric analysis were used to quantify the level

of selected proteins (CP24, CP29, OEC 33kDa) in T3 lines. For immunotitration, thylakoid samples were loaded for each sample and electroblotted on nitrocellulose membranes. Proteins were detected with primary antibodies (from Agrisera, α-PsaA AS06 172, α-CP47 AS04 038) and an alkaline phosphatase-conjugated secondary antibody (Sigma-Aldrich A3687). CP29 content in transgenic lines was quantified using an α-CP29 primary antibody made in-house (immunogen: CP29 purified from *Z. mays*) (Guardini et al., 2020). Signal amplitude was quantified using the GelPro 3.2 software (Bio-Rad). Non-denaturing Deriphat-PAGE was performed as previously described (Havaux et al., 2004).

Analysis of Chl fluorescence

PSII function during photosynthesis was measured through Chl fluorescence on whole leaves at RT with a PAM 101 fluorimeter (Heinz-Walz) according to (Baker, 2008). Fluorescence induction kinetic curves (OJIP) were recorded on dark-adapted leaves using a 500 ms saturating pulse of red light (2000 μmol photons m^{-2} s^{-1}) with a DUAL-PAM-100 equipment (Walz, GmbH), set at resolution of 20 μs. The fluorescence decay kinetic traces used to estimate Q_A reoxidation were measured with the same equipment by applying a single turnover flash (40 μs, 8000 μmol photons m^{-2} s^{-1} red light) and following the fluorescence decay in the dark during 70 ms. Fluorescence decay traces were then normalized to the Fm at t=0 and then fitted to an exponential decay equation ($F = A1 * \exp(-t/\tau)$).

Electron Microscopy and Image Analysis

Electron microscopy on isolated grana membranes was conducted using an FEI Tecnai T12 electron microscope operating at 100 kV accelerating voltage. Membranes were isolated from 6-week-old wild type and mutant plants, grown under controlled conditions. Best grana patches, stained with 2% uranyl acetate, were analysed and PSII core positions were identified using ImageJ software (Schneider et al., 2012).

Statistics.

Statistical analysis was performed in GraphPad Prism using either Student's *t*-test or One-way analysis of variance (ANOVA) and means were separated with Tukey's post hoc test at a significant level of $P < 0.05$ (see the figure legends for details). Error bars represent the standard deviation.

Data availability

Sequence data from this article can be found in the *Arabidopsis* Genome Initiative or GenBank/EMBL databases under accession numbers At5g01530 (Lhcb4.1), At3g08940 (Lhcb4.2), At1g15820 (Lhcb6). The ko lines used in the work were obtained from the NASC under the stock numbers N376476 (*koLhcb4.1*), N877954 (*koLhcb4.2*), N577953 (*koLhcb6*).

Results

Characterization of koLhcb4 plants complemented with either wild type or mutant Lhcb4.1 sequences.

To the aim of studying the function of the C-terminal CP29 domain in triggering NPQ, we produced *Arabidopsis thaliana* lines carrying CP29 mutated in H242 residue binding Chl *b*614 (b3) which is part of the pigment cluster Chl *b*614-*a*613. To this purpose, the *Lhcb4.1* gene was amplified from *Arabidopsis* wild type genomic DNA and targeted by site-directed mutagenesis at the residue H242. Supplementary Figure S5.2.1A shows sequence alignment between Lhcb4 from *S. oleracea*, whose Chl-binding residues have been identified (Pan et al., 2011; Wei et al., 2016), and Lhcb4.1 (hereafter called CP29) from *A. thaliana*, showing full conservation. Supplementary Figure S5.2.1B shows the Chl-binding complex, highlighting the Chls *b*614-*a*613 at the C-terminal and their specific pigment-binding residues. Supplementary Table S5.2.1 summarizes the substitutions H242→L / A / V operated in order to obtain the genotypes analysed in this work.
Both wild type and mutant *Lhcb4.1* sequences were cloned in a vector for *Agrobacterium*-mediated transformation as previously described (Guardini et al., 2020) and *koLhcb4 Arabidopsis* plants were transformed by floral dipping. For each mutation, independent lines containing a single gene insertion were identified in the T3 generation for resistance to the antibiotic kanamycin. Then, transgenic lines were selected based on the abundance of CP29 protein upon SDS-PAGE analysis of thylakoid proteins, which also confirmed that all CP29 isoforms were targeted to thylakoid membranes (Figure 5.2.1A). CP29 with wild type sequence accumulated in complemented *Arabidopsis* lines at the same level as in wild type plants. Biomass accumulation of transformed plants was maintained when grown under control light conditions (150 μmol photons m^{-2} s^{-1}, 23°C, 8/16 day/night) (Figure 5.2.1B, Table 5.2.1); also Chl content per leaf area, Chl *a*/Chl *b* and Chl/Car ratios, and PSII quantum efficiency (F_v/F_m) were indistinguishable from wild type plants (Table 5.2.1), implying that the complementation of *koLhcb4* line with the Lhcb4.1 sequence fully restored wild type phenotype. Plants carrying mutations on Chl *b*614 (b3) binding site of CP29 (mutations H242L / V / A) had a negligible effect on accumulation of CP29, showing similar protein abundance than *koLhcb4* lines complemented with wild type *Lhcb4.1* (Figure 5.2.1A, Supplementary Table S5.2.1), thus suggesting that mutations did not impair either folding or stability of the protein. However, mutant genotypes did show a significant reduction in growth with respect to the wild type under control light conditions (Table 5.2.1).

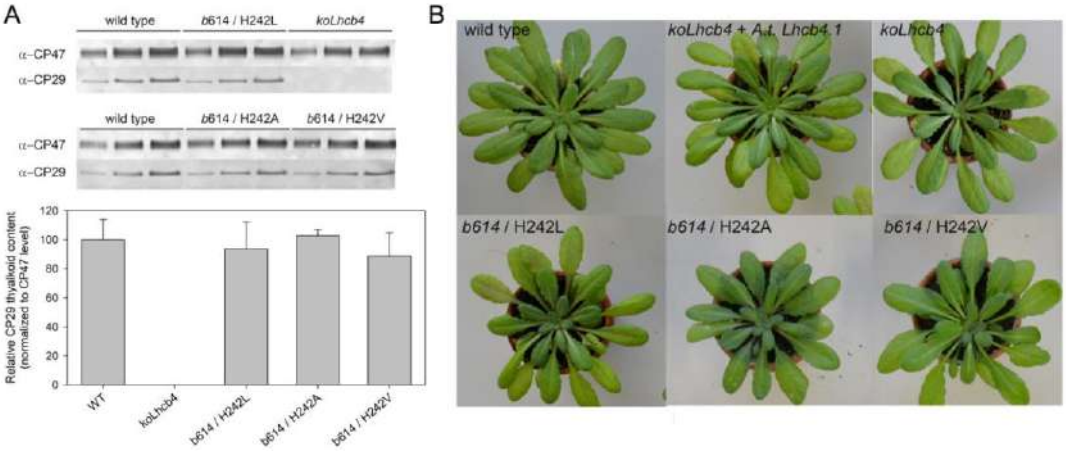

Fig. 5.2.1 | koLhcb4 plants complemented with either wild type or mutant Lhcb4.1 sequences. *(A) CP29 content of thylakoid membranes from wild type and mutant lines. The abundance of both CP29 and the PSII core subunit PsbB (CP47) was determined in KO mutants and independent T3 lines by immunotitration. Amounts of Chls loaded on the gel were 0.3, 0.6, and 0.9 µg. CP29 signal was normalized to that of CP47, and antenna content was expressed as a percentage of the corresponding wild type value. Data are expressed as mean ± SD, n = 3 biologically independent samples. Values marked with different letters are significantly different from each other (ANOVA followed by Tukey's post hoc test at a significant level of P < 0.05). Experiments were repeated independently twice with similar results. (B) Phenotype of wild type and mutant plants, grown for 6 weeks at 150 µmol photons m^{-2} s^{-1}, 23 °C, 8/16 h light/dark.*

Genotype (Chl / mutation)	Chl *a/b*	Chl / Car	µg Chl / cm^2	Fv / Fm	F_0 / Chl (norm. to wild type value)	Fresh weight (g)
wild type	$2.98 \pm 0.04^{a,b}$	3.61 ± 0.08^{a}	20.7 ± 1.7^{a}	0.816 ± 0.004^{a}	1.00 ± 0.04^{a}	2.38 ± 0.36^{a}
koLhcb4	2.89 ± 0.04^{a}	3.58 ± 0.03^{a}	19.8 ± 0.8^{a}	0.769 ± 0.014^{b}	1.34 ± 0.05^{b}	$1.62 \pm 0.26^{b,d}$
koLhcb4 + Lhcb4.1 wild type	$3.01 \pm 0.09^{a,b}$	3.67 ± 0.10^{a}	21.2 ± 1.2^{a}	0.815 ± 0.008^{a}	1.01 ± 0.05^{a}	$2.07 \pm 0.32^{a,b}$
koLhcb6	3.10 ± 0.06^{b}	3.66 ± 0.03^{a}	21.5 ± 3.1^{a}	0.749 ± 0.006^{b}	1.34 ± 0.05^{b}	0.97 ± 0.25^{c}
b 614 / H242L	$3.00 \pm 0.11^{a,b}$	3.66 ± 0.07^{a}	20.9 ± 0.5^{a}	0.770 ± 0.007^{c}	$1.29 \pm 0.09^{b,c}$	$1.22 \pm 0.36^{c,d}$
b 614 / H242A	$3.04 \pm 0.04^{a,b}$	3.60 ± 0.14^{a}	20.7 ± 1.2^{a}	0.772 ± 0.006^{c}	$1.25 \pm 0.14^{b,c}$	$1.35 \pm 0.29^{c,d}$
b 614 / H242V	3.08 ± 0.12^{b}	3.57 ± 0.17^{a}	20.4 ± 2.2^{a}	0.790 ± 0.005^{d}	1.16 ± 0.14^{c}	$1.33 \pm 0.19^{c,d}$

Table 5.2.1 | Pigment content and fluorescence induction parameters determined for leaves of Arabidopsis wild type and ko plants and lines expressing CP29 isoforms. *Parameters were measured in homozygous T3 plants containing a single copy Lhcb4.1 insertion. Two lines were analyzed for each site-directed mutant; at least four different plants were tested for each line. Fv/Fm, quantum yield of PSII; F_0, basal leaf fluorescence; Chl/Car, molar ration between Chlorophylls (a+b) and Carotenoids. Fresh weight (g) refers to growth after 6 weeks in control conditions. Data are expressed as mean ± SD (biologically independent leaves n = 5 for pigment analysis, n ≥ 6 for Chl fluorescence analysis, n ≥ 8 for FW determination). Values marked with different letters are significantly different from each other within the column (ANOVA followed by Tukey's post hoc test at a significant level of P < 0.05). Experiments were repeated independently twice with similar results.*

Purification and characterization of CP29 complexes

To verify whether Chl *b*614 was lost in mutant isoforms, we purified CP29 from control and H242L mutant plants by ion-exchange chromatography (Pan et al., 2011) and assessed pigment complement of the proteins both by fitting the spectra of acetonic extracts with spectra of individual Chl and Car species (Croce et al., 2000) and by HPLC analysis (Collin et al., 2008). Values of Chl *a*/*b* and Chl/Car ratios of CP29, purified from both wild type plants and native *Lhcb4.1* complemented lines, are consistent with a pigment complement of 14 Chls (~10.2 Chl *a* and ~3.8 Chl *b*) and 3 Cars (Su et al., 2017) (Supplementary Table S5.2.2). Instead, both Chl *a*/*b* and Car/Chl ratios of CP29 from line *b*614-H242L were higher compared to the wild type complex, suggesting a selective loss of Chl. Moreover, a blue-shift in the peak wavelength of the Q_y transition was in agreement with the loss of a Chl ligand (Figure 5.2.2A). To investigate the spectroscopic properties of the missing Chl, absorption spectra of wild type and mutant complexes were normalized to the total area over the Q_y transition, by assuming a Chl *b*/Chl *a* extinction ratio of 0.7 (Cinque et al., 2000), and CP29-wild type *minus* CP29-H242L difference spectra were then calculated (Figure 5.2.2B). The difference spectrum showed peaks at 639 nm and at 679 nm, consistent with the *b*614 site being promiscuous for Chl *b* and Chl *a*.

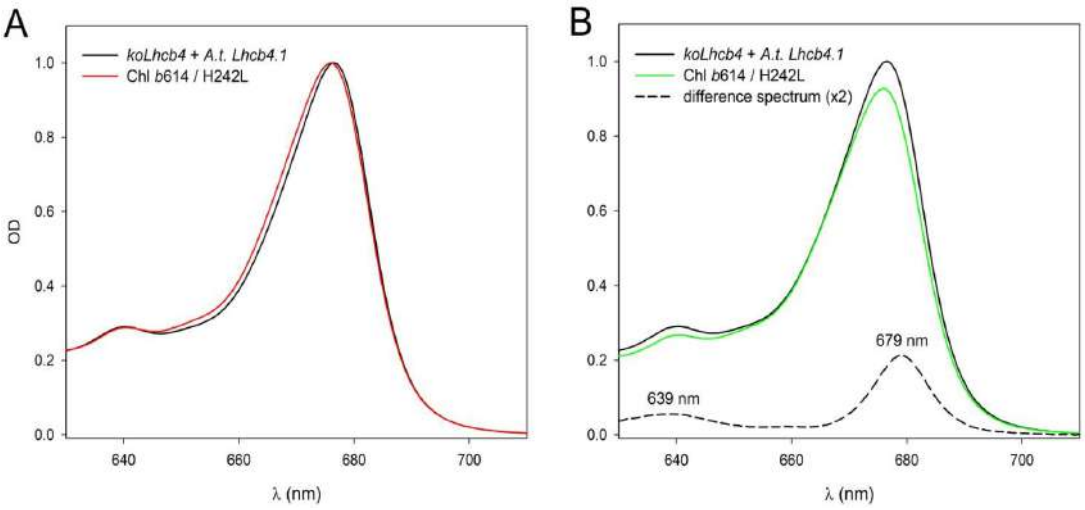

Fig. 5.2.2 | Spectroscopic analysis of wild type and mutant CP29 purified holoproteins. *(A) Absorption spectra of CP29 complex, purified from wild type plants (black line) and from lines expressing H242L mutant isoform of CP29 (red line) were normalized to the maximum absorption in the red region. Absorption spectra of complexes carrying the mutation, superimposed to that of wild type, showed spectroscopic changes. (B) The absorption spectrum of the mutant was then normalized to the Chl content (green line). The wild type minus mutant difference spectrum (dashed black line) therefore represents the absorption spectrum of the missing individual Chl molecule(s). Two clear peaks in the difference spectra were obtained for the mutant CP29. A.t., Arabidopsis thaliana.*

NPQ phenotype of plants expressing wild type or mutant CP29

Since Chl *b*614 has been suggested to be involved in a pH-induced conformational change in CP29 catalyzing energy dissipation (Papadatos et al., 2017; Ioannidis et al., 2016), we evaluated the capacity of different mutant lines to activate NPQ (Figure 5.2.3). Wild type plants, grown in control conditions, reached a NPQ of ~2 after 8 min of illumination at 1200 μmol photons m^{-2} s^{-1}, while induction of quenching in *koLhcb4* was slower and reached a lower amplitude (~1.3 at t = 8 min). *koLhcb4* lines complemented with native Lhcb4.1 isoform exhibited restoration of NPQ activity to wild type level. The NPQ pattern of the H242L line was peculiar: despite mutant plants expressing CP29 isoform to the same level as wild type plants (Figure 5.2.1A), their quenching activity closely matched that of *koLhcb4* plants (Figure 5.2.3A). Moreover, *koLhcb4 and* H242L plants showed a significant decrease in Fv/Fm, the maximum quantum efficiency of PSII, compared to wild type. A similar effect was observed in lines expressing CP29-H242A and CP29-H242V (Table 5.2.1). Thus, expression of isoforms devoid of Chl *b*614, to the same level as in wild type, failed to restore PSII quantum yield.

To further investigate the effect of Chl *b*614 depletion on NPQ, we determined the dependence of quenching response *vs.* CP29 content. We analysed two segregating T1 populations, obtained by complementing *koLhcb4 Arabidopsis* plants with either wild type or H242L *Lhcb4.1* sequence. A total of 45 plants were selected based on CP29 content, ranging from 0% to 90% of wild type level. Both NPQ (Figure 5.2.3B) and maximum quantum yield of PSII (Figure 5.2.3C) were then assessed by PAM fluorometry, and quenching activity was expressed as definite integrals of NPQ curves, calculated between 0 and 8 min of actinic light induction. In plants expressing wild type CP29, total NPQ area raised from a value of ~10 for *koLhcb4* to ~20, according to complementation levels. Instead, the NPQ amplitude of the lines complemented with mutant CP29 showed a more complex behaviour: total NPQ raised until CP29 content reached ~30% respect to wild type, then underwent a decline in which NPQ activity and CP29 level were inversely related (Figure 5.2.3B). The maximal quantum yield of PSII (Fv/Fm) increased from 0.77 (in *koLhcb4* plants) to 0.81 (wild type plants) upon wild type CP29 complementation (Figure 5.2.3C); in genotypes complemented with the H242L mutant sequence, Fv/Fm showed a non-linear relation with CP29 abundance: quantum yield underwent an initial rise from 0.75 to 0.78 (corresponding to ~30% CP29 abundance respect to wild type) then progressively decreased with higher level of CP29, yielding values closely matching the value in *koLhcb4* plants.

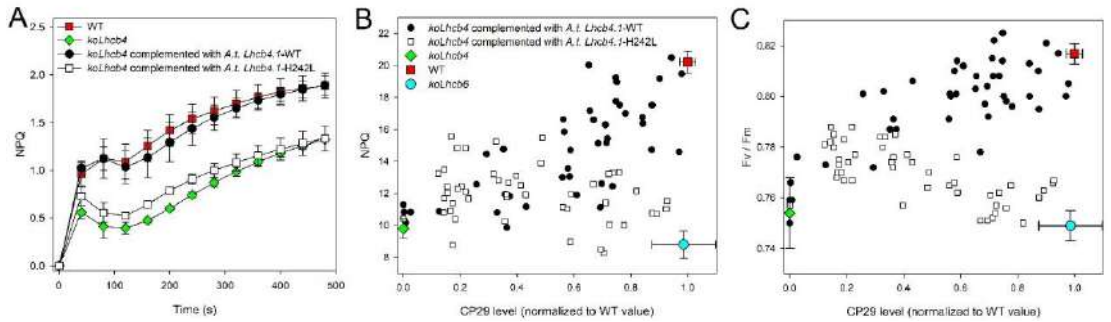

Fig. 5.2.3 | NPQ phenotype of plants expressing either wild type or H242L CP29. *(A) Kinetics of formation of photoprotective energy dissipation, measured upon illumination of leaves with 1200 µmol photons m^{-2} s^{-1}, at RT. Data are expressed as mean ± SD, n = 4 biologically independent plants. A.t., Arabidopsis thaliana. (B, C) Correlation between NPQ amplitude (B) or maximum PSII quantum yield (C) and CP29 content, in plants expressing either wild type or mutant CP29. Both NPQ amplitude and maximum PSII quantum yield (Fv/Fm values) was measured in a segregating T1 population of Arabidopsis thaliana koLhcb4 complemented with either wild type or CP29-H242L. For each plant, (i) the CP29 content was accurately estimated by SDS-PAGE, Coomassie staining and densitometric analysis, and (ii) Fv/Fm values were recorded or definite integrals were calculated for each plant from NPQ curves in the range from 0 to 8 minutes. Each experimental point represents the CP29 content of a plant and either the Fv/Fm value or the definite integral from its NPQ traces. Leaves carrying mutation showed clearly different NPQ or PSII quantum yield dependence on CP29 content than lines expressing wild type CP29 (analysis of covariance, $P < 0.05$). These data are representative of two independent experiments, with similar results. A.t., Arabidopsis thaliana.*

Organization and stoichiometry of Chl-binding complexes

To investigate the molecular basis of the reduced quenching activity and PSII quantum yield in H242L plants, thylakoid polypeptides abundance was analysed by SDS–PAGE (Figure 5.2.4A) and immunotitration (Figure 5.2.1A and S5.2.2). The ratio between PSI and PSII, as determined by immunotitration of PsaA and PsbB (CP47) subunits, was essentially the same in all genotypes (Supplementary Figure S5.2.2A). LHCII content was increased in *koLhcb4* plants in agreement with a previous report (De Bianchi et al., 2011), while abundance of CP26 and PsbS did not show major changes in any of the genotypes (Supplementary Figure S5.2.2B). The CP24 band was missing in *koLhcb4* plants. Indeed due to the absence of its docking site, i.e. CP29, CP24 undergoes proteolysis (De Bianchi et al., 2011). Consistently, complementation with wild type CP29 fully restored CP24 level. Instead, plants expressing the CP29-H242L isoform showed a strong reduction in CP24 content (Figure 5.2.4A, Supplementary Figures S5.2.2B). Such CP24 depletion was observed in all lines carrying CP29 lacking Chl *b*614, irrespective of the residues replacing the histidine H242 (Supplementary Figure S5.2.3), implying that the lack of Chl *b*614 is the major

cause affecting CP24 accumulation. In order to verify whether the mutation affected the organization of pigment–protein complexes in mutant plants, we analysed pigment-protein pattern by non-denaturing Deriphat–PAGE, upon solubilization of thylakoid membranes with 0.8% α-DM (Figure 5.2.4B). Wild type plants and genotypes complemented with the wild type *Lhcb4.1* sequence resulted in the same fractionation pattern, showing three major green bands at low MW corresponding to free pigments, monomeric Lhcb and trimeric LHCII, while bands at higher MW included the CP29-CP24-LHCII antenna supercomplex, monomeric and dimeric PSII core, and PSI-LHCI. The upper region of the gel contained PSII supercomplexes, which formed multiple bands including of a dimeric PSII core (C_2) with increasing antenna protein complements (LHCII trimers S and M) (Caffarri et al., 2009). In *koLhcb4*, the antenna supercomplex and all PSII supercomplexes were absent. *koLhcb6* plants and lines complemented with CP29-H242L showed the same pattern of green bands characterized by the missing of the CP29-CP24-LHCII antenna supercomplex, while the abundance of C_2S_2 PSII supercomplex was increased, implying that mutations to the Chl *b*614 binding site preferentially affected interactions of CP29 with LHCII-M and CP24 *vs.* CP47 in the PSII supercomplex.

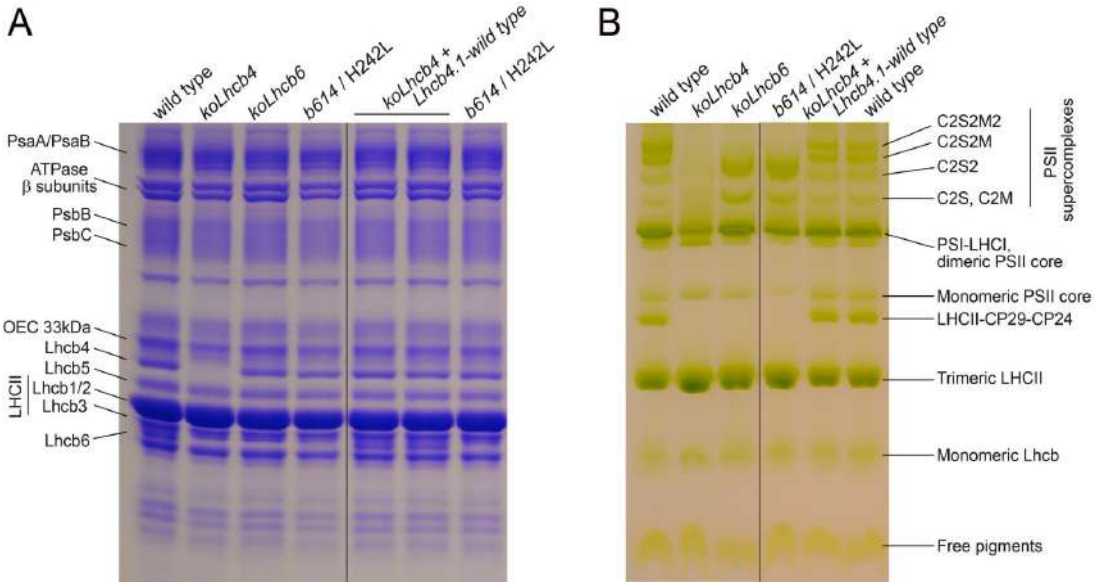

Fig. 5.2.4 | Characterization of the Arabidopsis lines expressing CP29-H242L isoform. *(A) SDS-PAGE fractionation of thylakoid proteins from wild type, koLhcb4, koLhcb6 and lines complemented with either wild type or mutated CP29 isoforms. (B) Organization of Chl-binding complexes of thylakoids. Pigment-protein complexes from wild type, koLhcb4, koLhcb6 and complemented lines were separated by non-denaturing Deriphat-PAGE, upon solubilization of membranes with 0.8% α-DM. Thylakoids (35 μg of Chls loaded in each lane. The composition of each band is indicated based on earlier works (Caffarri et al., 2009). Experiments were repeated independently two times with similar results. A.t., Arabidopsis thaliana.*

Lack of Chl *b*614 in CP29 altered the macro-organization of the PSII in the grana membranes

All results presented above suggest that reduced quenching activity in plants expressing mutant CP29 may be related to changes in the LHC complement. To further investigate this possibility, we analyzed the organization of PSII complexes in grana partitions by TEM. Indeed, a previous work had shown that altered PSII organization did impact both PSII quantum yield and photosynthetic electron transport (De Bianchi et al., 2008). To this aim, grana membranes were isolated by mild solubilization of stacked thylakoids with α-DM and observed after negative staining (Morosinotto et al., 2010). The procedure did yield circular patches of membranes (Supplementary Figure S5.2.4), consistent with their origin from grana stacks (Simpson, 1983). At high resolution, membranes from wild type plants (Figure 5.2.5A) revealed stain-excluding PSII core particles randomly distributed in a negative stain background (Simpson, 1979). PSII particles in wild type grana are spread at an average density of ~$13 \cdot 10^{-4}$ particles nm^{-2} (Figure 5.2.5G). Membranes from plants expressing high level of mutant CP29 were clearly different, showing highly ordered arrays of PSII particles (Figure 5.2.5D-F), yielding a particle density of ~$24 \cdot 10^{-4}$ particles nm^{-2} (Figure 5.2.5G), which is consistent with the formation of head-to-tail arrays of C_2S_2 supercomplexes (Supplementary Figure S5.2.5) (Onoa et al., 2014). A comparison of the two-dimensional arrays found in *koLhcb6* and CP29-H242L grana membranes, revealed that the crystal lattices were the same in the two samples (Supplementary Figure S5.2.6). Moreover, we calculated for each PSII core the average distance from its closest neighbor: PSII distribution in samples from CP29-H242L and *koLhcb6* showed an average distance between particles (~20 nm) significantly smaller than in wild type (Figure 5.2.5H).

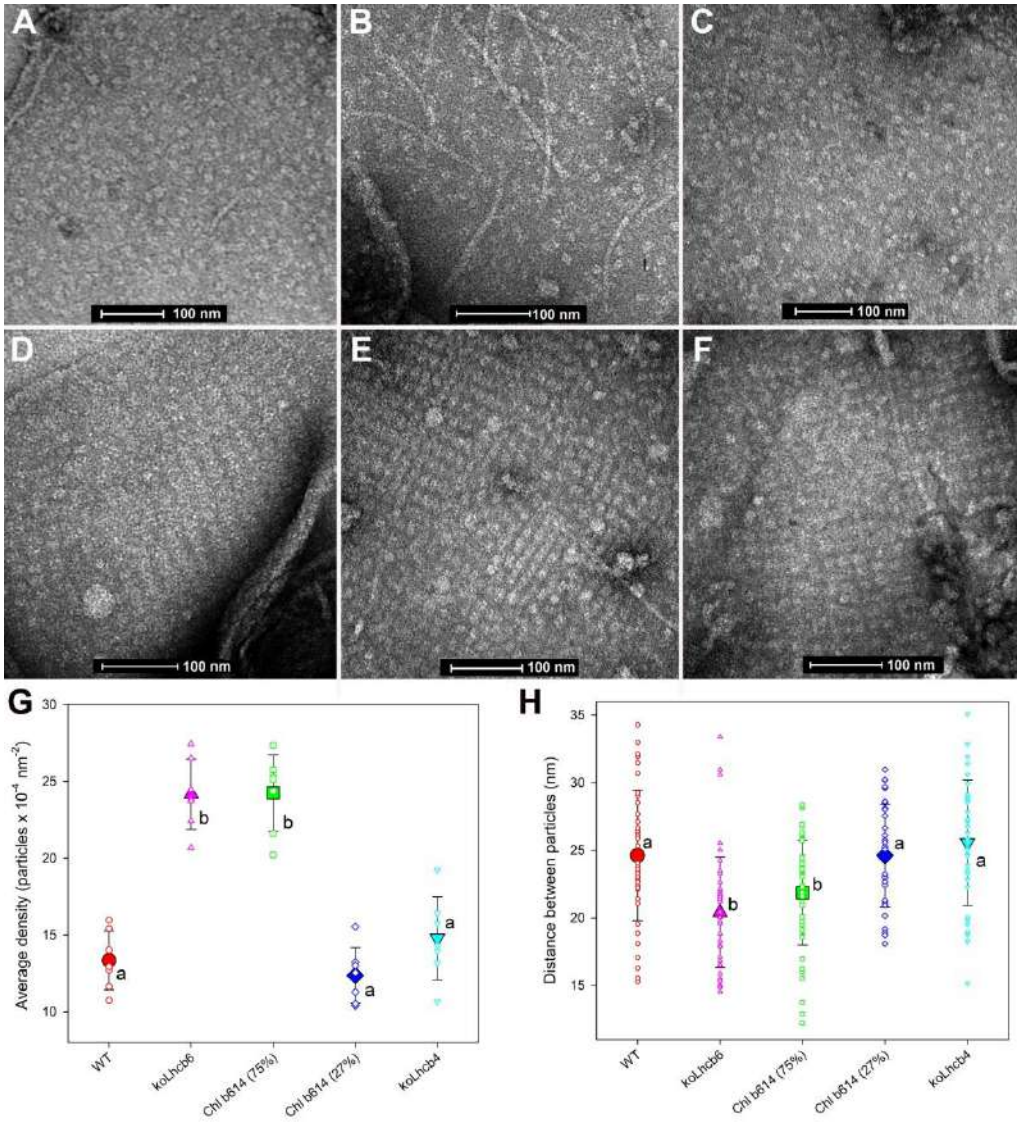

Fig. 5.2.5 | Electron microscopy of grana membranes isolated from wild type and mutant thylakoids. *EM of grana patches isolated from dark-adapted leaves of wild type (A) and koLhcb4 (B) plants, and koLhcb4 complemented with different level of the mutant CP29 isoform H242L, namely 27% than WT content (panel C) and 75% than WT content (panels D-F). Micrographs by negatively stained grana partition were carried out on preparations obtained by 0.32% α-DM solubilization of stacked thylakoids (see Materials and methods for details). The space bar represents 100 nm. (G, H) Average distance between nearest neighbours PSII tetrameric particles (G), and average density of tetrameric particles (H). Data are expressed as mean ± SD, and all individual data points are shown. Mean values marked with different letters are significantly different from each other (ANOVA followed by Tukey's post hoc test at a significant level of P < 0.05).*

Previous analysis (De Bianchi et al., 2008) showed restricted electron transport from Q_A to Q_B in plants devoid of CP24. To investigate whether Chl *b*614-depleted plants suffered from a similar limitation, fluorescence induction curves were recorded on dark-adapted leaves and the kinetic of the three rise steps 0-J, J-I and I-P (Strasser et al., 1995) was analysed for assessing rate of electron transport steps. *koLhcb6* and CP29-H242L leaves behaved similarly, showing an enhanced basal fluorescence (O) and a faster rise of the J-I phase with respect to control genotypes, while the I-P phase was slower (Figure 5.2.6A). This higher basal fluorescence level and the prevalence of the O-J rise on the induction kinetics suggest a restriction in $Q_A \rightarrow Q_B$ electron transport in these mutant genotypes. Moreover, the impairment in plastoquinone (PQ) reduction rates similarly affected *koLhcb6* and Chl *b*614-less plants. Furthermore, we assessed the Q_A re-oxidation efficiency by measuring Chl fluorescence decay on leaves upon applying a single turn-over flash: indeed, a saturating flash fully reduces Q_A and maximizes fluorescence emission, which then decays with a rate dependent on re-oxidation rate of Q_A, i.e. the rate of PQ diffusion to the Q_B site (Sane et al., 2003). Fluorescence decay kinetics were significantly slower in both *koLhcb6* and CP29-H242L plants with respect to control genotypes (Figure 5.2.6B), indicating that the access to the PSII Q_B site was restricted in these mutants. Again, no differences were observed between *koLhcb6* and Chl *b*614-less plants.

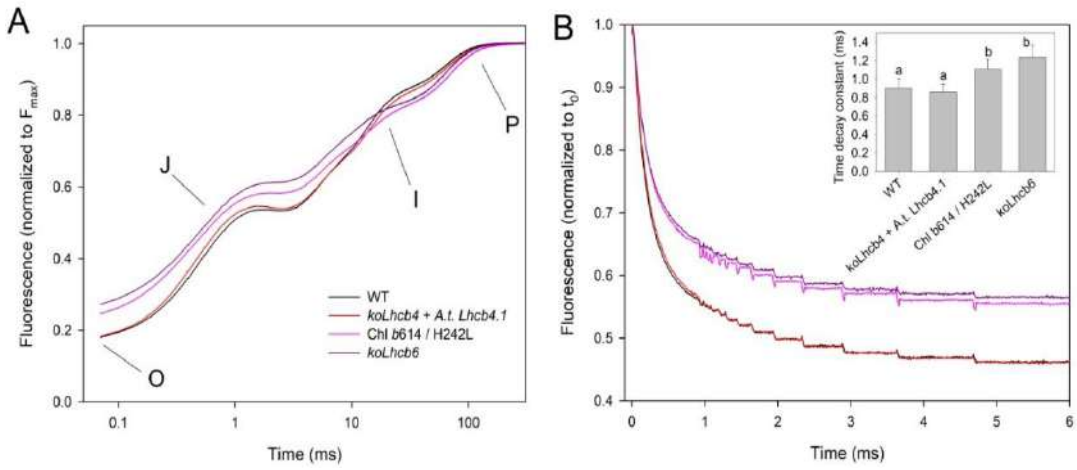

Fig. 5.2.6 | Functional analysis of PSII electron transport. *(A) PSII fluorescence rise was induced on dark-adapted leaf, using a saturating flash of red light (2000 µmol photons m^{-2} s^{-1}, 500 ms), and normalized to the F_{max} value. F_0 values increase in the order wild type < CP29-H242L < koLhcb6 < koLhcb4. Data are expressed as mean values of at least 12 fluorescence curves. (B) Chlorophyll fluorescence decay kinetics were measured after single turnover flash illumination in dark-adapted leaves, to estimate Q_A reoxidation kinetics. Experimental fluorescence curves were normalized to the corresponding F_{max} values and represent averages from 10-15 separate experiments. (inset) Each dataset was fitted with an exponential decay function $y = A0 + A1 \cdot exp(-t/\tau)$, and the Q_A reoxidation was assessed in the different genotypes by comparing time decay constants (τ) of the exponential decay of fluorescence. Values marked with different letters are significantly different from each other (ANOVA followed by Tukey's post hoc test at a significant level of $P < 0.05$).*

Discussion

Deleting Chl *b*614 (Chl b3) in CP29 did not affect polypeptide composition of the photosystems, except for the PSII monomeric antenna CP24, whose content was strongly reduced in all mutant lines. Plants expressing CP29 isoforms devoid of Chl *b*614 showed to be affected in several photosynthetic properties, including quenching activity, and a reduced growth, similarly to what shown in *koLhcb6* genotype, thus suggesting that photosynthetic phenotypes in transgenic lines are consequent to the altered LHC complement rather than to the missing chromophore. To investigate the mechanistic reasons for the above phenotypes, we studied both organization and function of the PSII antenna system in several *Arabidopsis* mutants, and assessed changes in Chl fluorescence kinetics, in pigment composition and in the supramolecular organization of PS.

The role of Chl *b*614 at the C terminus of CP29 in the assembly of PSII-LHC supercomplexes

As for the organization of the PSII peripheral antenna system, it appears to be affected in plants devoid of Chl *b*614 of CP29. Indeed, titration of the different Lhcb proteins with respect to PSII RC showed that the CP24 complex was strongly reduced in mutant lines despite CP29 was expressed to nearly wild type level (Figure 5.2.4, Supplementary Figures S5.2.2, S5.2.3). This implies that removal of a single chromophore at the C-terminus of CP29 decreases CP24 stability and/or binding affinity and suggests a key role of this domain in the docking for CP24 (Supplementary Figure S5.2.1A). Both CP29 and CP24 are part of the antenna CP29-CP24-LHCII-M supercomplex, which connects inner and outer antenna moieties of PSII (Su et al., 2017). Heterotrimeric LHCII-M includes Lhcb3, which interacts with CP29 and CP24 (Betterle et al., 2009; Caffarri et al., 2009) and is retained in plants missing Chl *b*614 (Figure 5.2.4). Moreover, LHCII is accumulated to wild type level (Figure 5.2.4). Thus, lack of $C_2S_2M_2$ supercomplex and retention of Lhcb3 in plants missing Chl *b*614 suggests a membrane topology similar to that previously found in *Arabidopsis koLhcb6* plants, in which a large part of the outer antenna formed by LHCII-M and LHCII-L was dissociated from PSII supercomplexes and formed LHCII-only domains that segregated from arrays of C_2S_2 particles (De Bianchi et al., 2008).
The efficiency of excitation energy transfer to the PSII RC was affected by depletion of Chl *b*614, as can be inferred by the analysis of the initial fluorescence level (F_0) significantly higher in all mutant lines, which affected F_v/F_m values (Table 5.2.1). In mutant lines we observed a biphasic trend in F_v/F_m values *vs*. level of CP29 complementation: PSII maximal quantum yield underwent an initial rise until 0.78 (corresponding to ~30% CP29) then progressively went down with CP29 content, reaching values closely matching that of *koLhcb6* plants (Figure 5.2.3C). We previously observed a decrease in F_v/F_m in mutants devoid of monomeric antennae, including *koLhcb6* (De Bianchi et al., 2008). This is a clear indication that the connection between the PSII core and the bulk trimeric LHCII was partially impaired in the mutants. Indeed, exciton equilibration between LHCII trimers was slower in the absence of monomeric LHCs, which decreased the probability of trapping by PSII RC and thus reduced PSII maximal quantum yield (Dall'Osto et al., 2014c). Such a decline in F_v/F_m values in lines expressing the isoform CP29-H242L was unexpected since complementation of *koLhcb4* mutant with either wild type or mutant CP29 devoid of specific

chromophores always exhibited a full restoration of F_v/F_m values (Guardini et al., 2020).
Such a discrepancy might be reconciled with the evidence that the topology of grana membranes, was affected by the missing chromophore at the C-terminal domain of CP29 (Figure 5.2.5). In grana membranes from the wild type, the distribution of tetrameric PSII particles was homogeneous through the whole surface. This is not the case for mutant expressing high levels of CP29-H242L, where portions of the grana are occupied by arrays of tetrameric particles with spacing consistent with a C_2S_2 composition. We conclude that the phenotype of CP29 H242L mutation can be ascribed to its reduced content in CP24. Indeed grana partitions in *koLhcb6* plants included LHCII-only domains that segregate from arrays of C_2S_2 particles (Kovács et al., 2006; De Bianchi et al., 2008). Consistently, the PSII arrays in *koLhcb6* and H242L lines were composed of C_2S_2 supercomplexes and have the same basic unit (Figures 5.2.4 and 5.2.5, Supplementary Figure S5.2.6). Since both *koLhcb6* and H242L had a full complement of LHCII trimers (Figure 5.2.4), we expected grana membranes of these genotypes, besides having arrays of C_2S_2 particles, to contain discrete patches of LHCII trimers that are interspersed by a few PSII core complexes. It comes that in discrete areas of their grana partitions, the LHCII/PSII core ratio is increased, and LHCII fluorescence is not efficiently quenched photochemically, thus affecting overall F_v/F_m value.

In plants missing Chl b614, low content of CP24 impaired PSII electron transport

Previous work with *koLhcb6* plants showed that a part of PSII was organized into arrays of C_2S_2 particles, which were absent in plants devoid of both CP29 and CP24 (De Bianchi et al., 2008), suggesting that the altered conformation of C_2S_2 particles in the double mutant prevents cooperative interactions into arrays. This is consistent with the lack of arrays in CP29-H242L mutant lines with low complementation of CP29 (Figure 5.2.5C). Instead, mutants which accumulated CP29 to higher level, showed a decrease in both F_v/F_m and growth rate, namely a photosynthetic phenotype similar to that of *koLhcb6* plants. Lack of CP24 in itself did not limit plant growth (PSII quantum yield is only marginally affected), rather *koLhcb6* membranes suffered for a restriction in PQH_2 diffusion from the PSII Q_B site to the cytochrome *b*$_6$*f* complex (De Bianchi et al., 2008), which indeed is the limiting step for photosynthetic ET (Joliot and Joliot, 1977). PSII arrays restricts protein dynamics and limits the PQ diffusion, due to tight packing of PSII particles (Morosinotto et al., 2010), thus allowing PQ diffusion only in boundary lipids tightly bound to membrane complexes (Tremolieres et al., 1994). The latter is consistent with the reduced growth of both *koLhcb6* and Chl *b*614-less plants (Supplementary Figure S5.2.7). The restriction in ET was confirmed by fluorescence induction in leaves, which appeared similarly affected in *koLhcb6* and CP29-H242L plants: the J-I and I-P phases, reflecting the reduction of acceptors downstream of PSII, were delayed in both mutant genotypes with respect to the wild type (Figure 5.2.6). Taken together these data are consistent with the observation that a restricted diffusion of PQH_2 between site Q_B and cytochrome *b*$_6$*f* increases Q_A reduction. Finally, the above hypothesis was confirmed by the measurement of Q_A reoxidation kinetic, which clearly showed a reduced rate of ET from Q_A to PQ pool in both mutants (Figure 5.2.6B).

The quenching phenotype of Chl b614-less plants originates by pleiotropic effects rather than by lack of function associated with the Chl cluster

The structure of PSII supercomplex from spinach suggested the Chl 614 of CP29 is a Chl *b*. It is worth mentioning that the structural differences between Chl *a* and *b* are too small to be reliably detected by electron crystallography and cryo-electron microscopy; even more difficult is the case of mixed occupancy. The pigment composition and spectral properties of purified proteins CP29-H242L are consistent with the loss of both Chl *a* and *b* ligand, as evidenced by the WT minus mutant difference spectrum yielding a 639 and 679 nm peaks (Figure 5.2.2, Supplementary Table S5.2.2). This result is consistent with the report of a mixed occupancy of site b3 in recombinant CP29 from spinach (Bassi et al., 1999).

Structural data from cryo-EM allowed to trace the potential energy transfer pathways within PSII, and to pinpoint Chl *b*614 in the excitation energy transferred (EET) network (Wei et al., 2016). The EET by CP24 was proposed to proceed through CP29 towards CP47. At the luminal side of CP24-CP29 interface, Chl *b*606 in CP24 and Chl *b*614 in CP29 are the closest Chl pair (Mg-to-Mg distance of 16.9 Å), making them the most likely candidates in EET. EET from LHCII-M to CP29 involves Lhcb3 and Chl *a*613 in CP29, while pigments at the interface between LHCII-M and CP24 are separated by too large a distance to allow efficient EET. Therefore, excitons from the peripheral LHCII are transferred to the PSII core mainly through CP29 and S-LHCII. It comes that selective removal of Chl *b*614 *in vivo* is not expected to deeply alter PSII EET network, beside the effect due to CP24 depletion; this is consistent with growth phenotype of plants expressing CP29-H242L, which is similar to that of *koLhcb6* (Supplementary Figure S5.2.5).

Reverse genetics analysis (Dall'Osto et al., 2017) revealed that CP29, together with LHCII, plays a major role in the catalysis of NPQ. Excitation energy quenching is triggered by the luminal acidification which promotes dissociation of LHCII-M-CP29-CP24 antenna complex, thereby exposing CP29 to PsbS interaction (Johnson et al., 2011; Betterle et al., 2009). Protonation of CP29 itself is not effective in promoting quenching since mutation of its lumenal-exposed acidic residues did not impair NPQ activity (Guardini et al., 2020). Instead, PsbS is required for luminal pH detection: mutation of its lumen-exposed glutamate residues prevents NPQ (Li et al., 2004) thus suggesting it undergoes a conformational change then transferred to CP29 and LHCII where quenching reaction occurs.

CP29 binds three xanthophylls and 13 Chls arranged in clusters, namely: (i) lutein in site L1–Chls *a*611–Chl *a*612 (a2), (ii) violaxanthin in site L2–Chl *a*603 (a5)–Chl *a*609 (b5)–Chl a616, and (iii) neoxanthin at site N1 clustered with Chls *a*604–*b*608–*b*606 (b6) (Pan et al., 2011). Clusters (i) and (ii) have been suggested as the site of quenching in LHCII and CP29 (Pan et al., 2013). Recently, mutation analysis *of Lhcb4 in vivo* showed that CP29-dependent NPQ activity resisted removal of Chls *a*612 and *a*613 (Guardini et al., 2020), implying these Chls are not involved in quenching reactions. Rather, plants devoid of Chl *a*603 had NPQ as in *koLhcb4*, implying that pigment cluster Chl *a*603 (a5)–Chl *a*609 (b5)–Chl *a*616 and xanthophyll bound to site L2 do catalyze the quenching reaction(s) in CP29. Alternative hypotheses for location of quenching sites within LHCs have been proposed, including molecular dynamics simulations, which suggested the protonation of carboxyl groups at the lumen side to be crucial in inducing a conformational change of the Chl *a*613 - *b*614 pair in the helix-D, to induce quenching (Ioannidis et al., 2016; Papadatos et al., 2017).

However, mutant lines here described showed that full complementation of koLhcb4 with the H242L mutant missing Chl *b*614, has NPQ activity identical to *koLhcb6* plants (Figure 5.2.3). Since H242L mutant lacks CP24, this implies that Chls pair at the C-terminus of CP29 are not involved in quenching reactions. This result is consistent with the site-directed mutagenesis of candidate protonatable sites exposed to the thylakoid lumen, namely acidic residues D245 and D253 located in helix D in the C-terminal portion of CP29 (Guardini et al., 2020) which did not affect NPQ respect to wild type plants. We conclude that a ΔpH-dependent conformational change of the helix D in CP29 is not a requirement for NPQ activity.

It is worth noting that a decrease in the photoactive PQ pool reduces NPQ activity as well (Pralon et al., 2019). Indeed, NPQ is triggered by low lumenal pH, and the major lumen acidification event is achieved by proton pumping upon PQH_2 oxidation by the cytochrome b_6f complex. We propose that NPQ phenotype, in plants missing Chl *b*614 of CP29, is mainly due to a decreased capacity for proton accumulation under EL. This is consistent with previous work with *koLhcb6* plants, which underlined the importance of supramolecular organization of PSII and protein–protein interaction between LHC subunits for the full expression of NPQ (Kovács et al., 2006). Furthermore, this is consistent with the NPQ phenotype of lines complemented with mutant CP29, which showed a complex behaviour (Figure 5.2.3B): quenching capacity raised until CP29 content reached ~25-35% than wild type level, then NPQ steadily decreased with increasing CP29 complementation, approaching NPQ value of *koLhcb6* plants when CP29 level approached that of wild type. When a large fraction of PSII is devoid of CP29, such as in the line accumulating 25% of CP29 wild type level (Figure 5.2.5C), no regular arrays of PSII were formed, and the fraction of PSII binding CP29 restored NPQ activity despite the lack of Chl *b*614. Instead, in line fully complemented with mutant CP29, interactions between C_2S_2 are promoted, thus leading to PSII array formation and restriction in ET NPQ inhibition.

Acknowledgments

The authors acknowledge the support of MIUR (grant 201795SBA3-PRIN2017 to L.D.), University of Verona (grant RB2018BASSIR "Ricerca di Base" to R.B.) and EEC (grant 675006-SE2B to R.B.).

Author contributions

R.B. and L.D. conceived the work and designed the experiments. Z.G. carried out the construction of mutants and performed their physiological characterization, together with L.D. and R.C. R.L.G. analyzed fluorescence quenching kinetics and biochemically characterized mutant lines. All authors contributed to writing the manuscript, discussed the results and commented on the manuscript.

Supplementary Results

Supplementary Figure S5.2.1

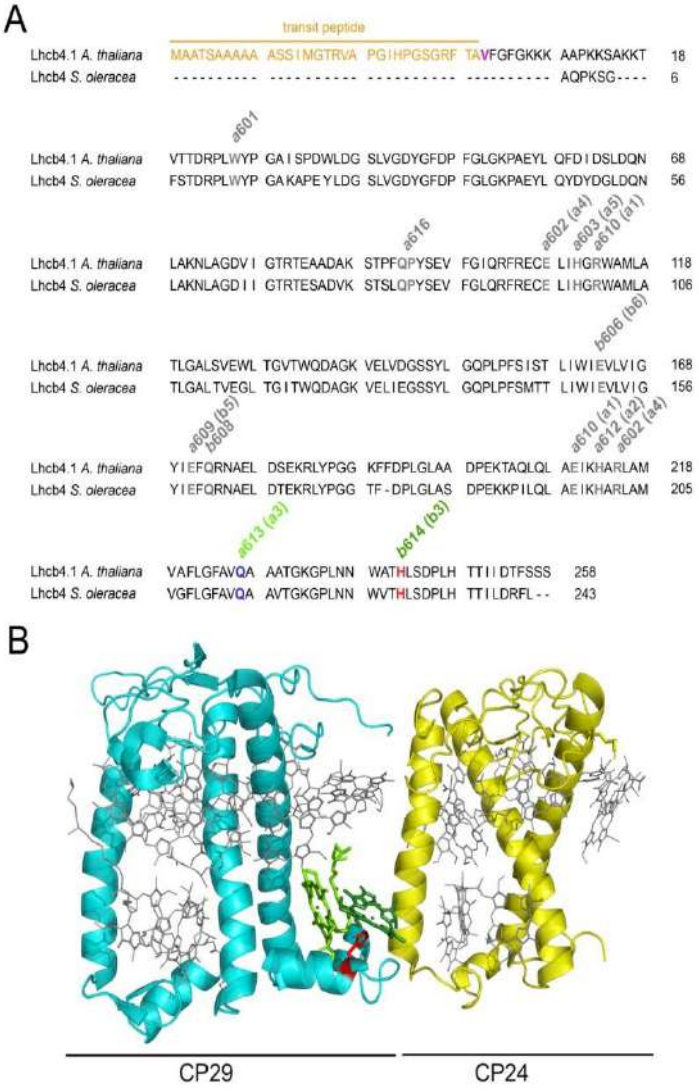

Fig. S5.2.1 | Substitutions operated into the H242 residue in order to obtain mutant lines devoid of Chl b614 in CP29. *(A) Sequence alignment of Lhcb4.1 protein of A. thaliana and Lhcb4 protein of S. oleracea. The amino termini of the Arabidopsis thaliana Lhcb4.1 is considered Val at position 33 (initiating Met is residue 1) (Gomez et al. 2003). In the figure, the transit peptide (orange) and the amino termini (violet) are highlighted. Pigment binding sites have been identified based on (Wei et al. 2016) and are highlighted in gray, the amino acid binding the interacting Chls a613 and b614 in blue (Q227) and red (H242), respectively. (B) Stereo view of the overall structure of CP29 from spinach (Su et al. 2017, PDB: 5XNL, cyan backbone), together with its interacting partner CP24 (yellow backbone), showing in dark green Chl b614 targeted in this study, and its interacting Chl a613 in light green. All the other Chls are in gray; in parenthesis, nomenclature by (Kühlbrandt et al. 1994).*

Supplementary Figure S5.2.2

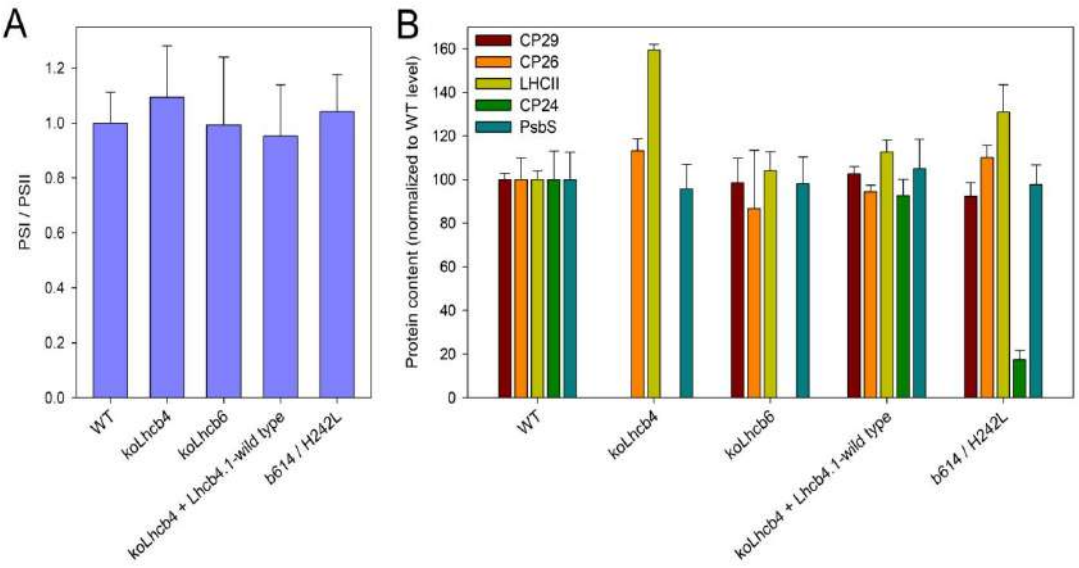

Fig. S5.2.2 | Polypeptide composition of thylakoid membranes from Arabidopsis wild type and mutant lines. *(A) PSI / PSII ratio. Immunotitration analysis was performed with antibodies directed against individual gene products, the PSII core subunit PsbB (CP47) and the PSI core subunit PsaA. Thylakoids corresponding to 0.25, 0.5, 0.75, and 1 μg of Chls were loaded for each sample. All samples were loaded on the same SDS-PAGE slab gel. (B) Quantification of PSII antenna subunits in wild type and mutant lines. The abundance of CP29, CP26, LHCII and CP24 was determined on three independent T3 lines by SDS–PAGE fractionation of thylakoid proteins, Coomassie staining and densitometry of selected protein bands. LHC content was normalized to that of the oxygen-evolving complex (OEC) 33-kDa subunit, and expressed as a percentage of the corresponding wild type content. Immunotitration analysis was performed with antibodies directed against PsbS. Data were normalized to the PSII core amount (PsbB content) and expressed as a percentage of the corresponding wild type content. Results are shown as mean ± SD, n = 3 biologically independent samples. A.t., Arabidopsis thaliana. Experiments were repeated independently twice with similar results.*

Supplementary Figure S5.2.3

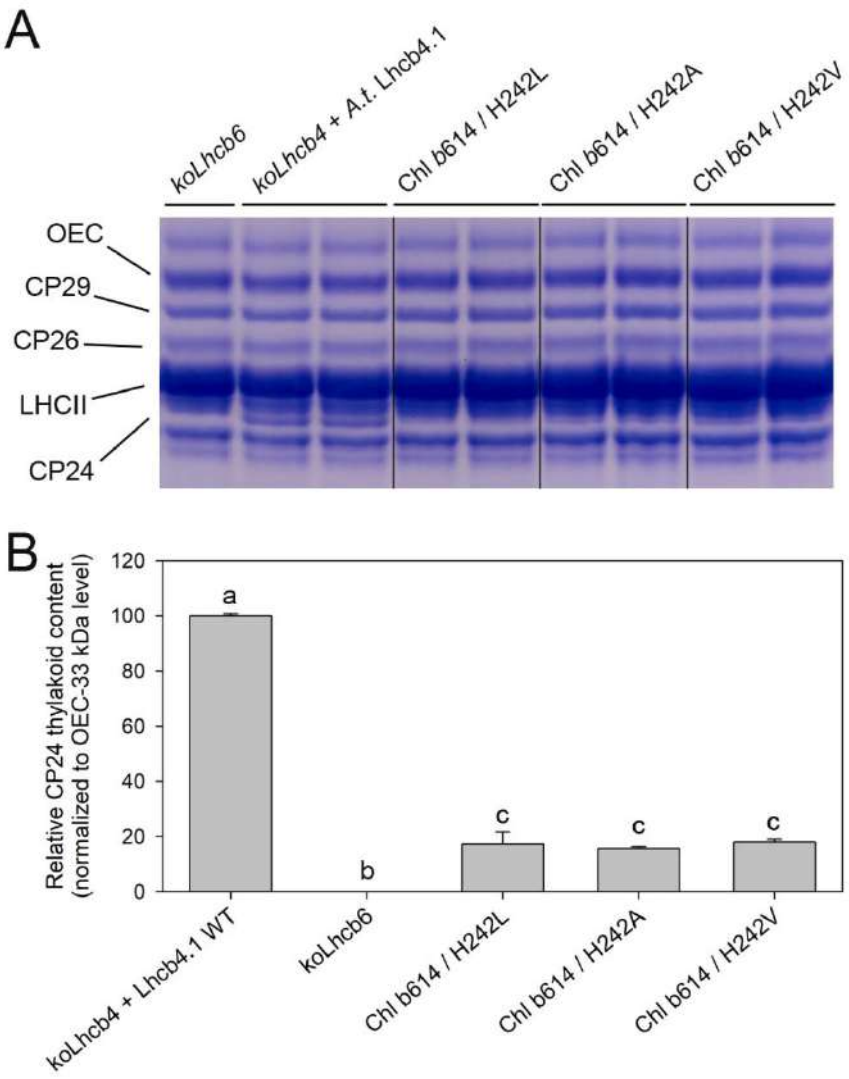

Fig. S5.2.3 | CP24 content of thylakoid membranes from wild type and mutant lines. (A) *SDS–PAGE fractionation of thylakoid proteins from koLhcb6 and lines complemented with either WT or mutated CP29 isoforms (b614 - H242L, H242A and H242V). Thylakoids were isolated from independent T3 lines* ***(B)*** *The abundance of CP24 was determined on SDS–PAGE fractionation by Coomassie staining and densitometry of selected protein bands. CP24 content was normalized to that of the oxygen-evolving complex (OEC) 33-kDa subunit. Data are expressed as mean ± s.d., biologically independent samples n = 3 for CP29-WT, 4 for Chl b614 mutants. Values marked with different letters are significantly different from each other within the column (ANOVA followed by Tukey's post-hoc test at a significance level of P < 0.05).*

Supplementary Figure S5.2.4

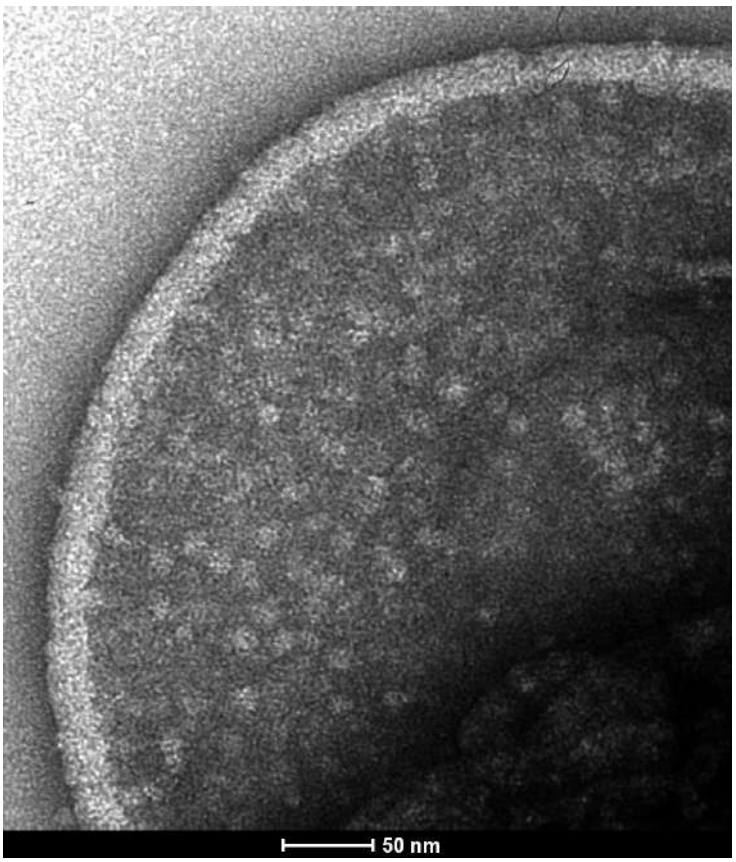

Fig. S5.2.4 | Micrograph of negatively stained grana partition preparation obtained by limited α-DM solubilization of stacked thylakoids. *See methods for details. WT and mutants yielded circular membrane patches of similar shape and size consistent with the diameter of grana stacks. The bar is 50 nm.*

Supplementary Figure S5.2.5

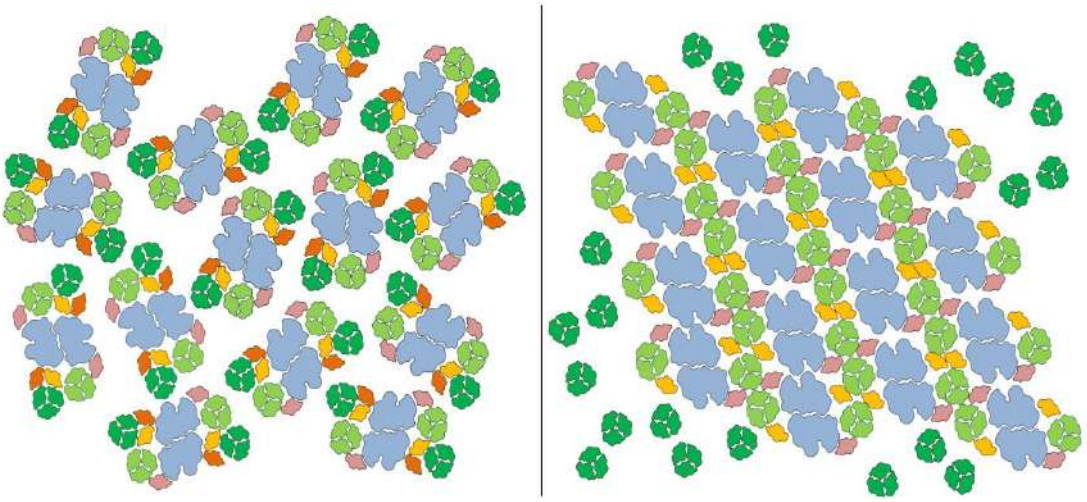

Fig. S5.2.5 | Effect of CP24/Chl b614 depletion on the supramolecular organization of PSII. *(left panel) Wild type grana contain the typical $C_2S_2M_2$ supercomplexes, which appear randomly distributed in the appressed membranes when observed by EM. (right panel) In the grana of both koLhcb6 (devoid of CP24 antenna) and CP29-H242L (missing Chl b614), head-to-tail binding of PSII lead to megacomplexes of C_2S_2 supercomplexes. S-LHCII trimers are light green, M-trimers are dark green, CP26 is rose, CP29 is yellow and CP24 is orange. Reaction center cores are in light blue.*

Supplementary Figure S5.2.6

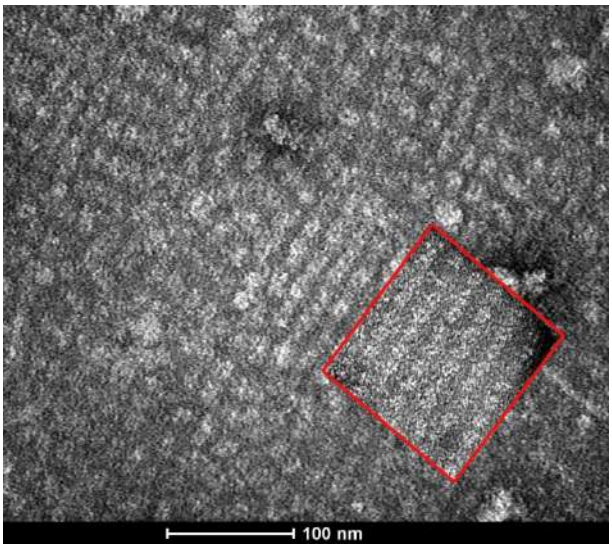

Fig. S5.2.6 | EM of negatively staining grana partition membranes obtained by partial solubilization with α-DM. *High-resolution micrographs show the distribution of stain-excluding tetrameric particles. A two-dimensional array from Arabidopsis koLhcb6 (red box) was superimposed on a larger array from the grana membranes of the CP29-H242L (see Figure 5.2.5), showing that the crystal lattice is identical in the two samples.*

Supplementary Figure S5.2.7

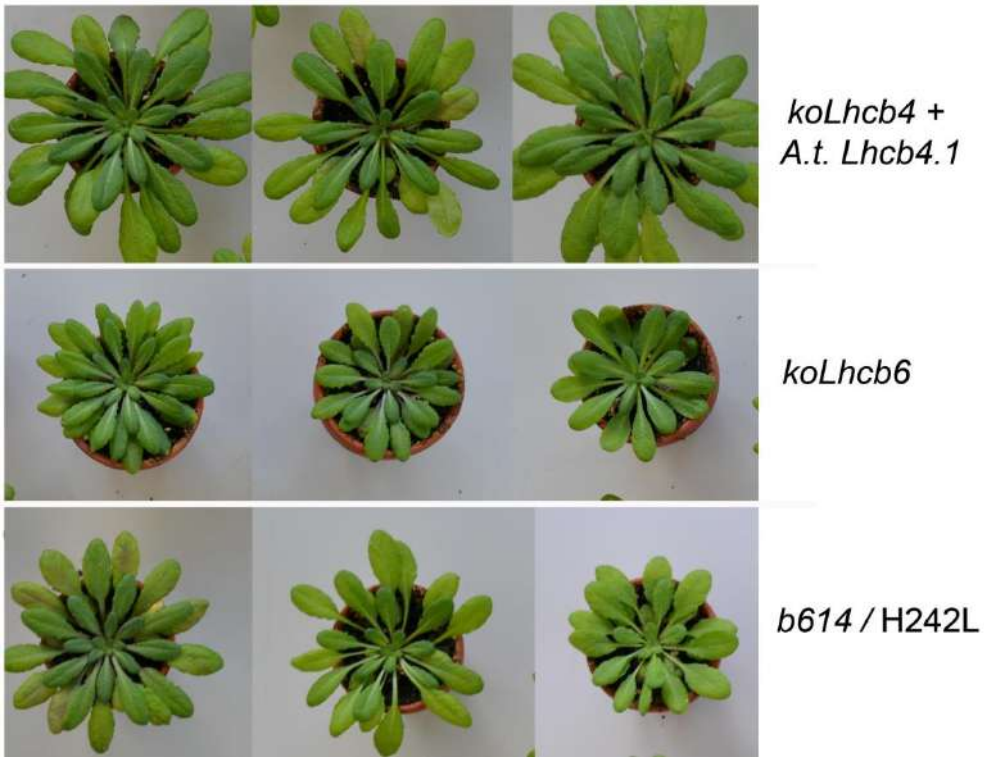

Fig. S5.2.7 | Phenotype of lines complemented with either WT or H242L Lhcb4.1 genes, in comparison with koLhcb6 plants. *Plants were grown for 6 weeks at 150 µmol photons m^{-2} s^{-1}, 23 °C, 8/16 h light/dark.*

Table S5.2.1 | Site-directed mutations in CP29 b614 site and their effects on antenna content in vivo. *CP29 protein level was measured by SDS-PAGE of thylakoid proteins, Coomassie staining and densitometric analysis, on homozygous T3 plants containing a single copy Lhcb4.1 insertion. At least five different plants were tested for each line. Each mutant was designated by the sites as assigned by (Pan et al. 2001; Wei et al. 2016). The targeted amino acid residue and their substitutions are shown. CP29 protein level is expressed as mean ± SD, n = 4 biologically independent samples. Values marked with different letters are significantly different from each other within the column (ANOVA followed by Tukey's post hoc test at a significant level of P < 0.05).*

Sites[§]	AA residues in *Arabidopsis* CP29	Mutations	CP29 protein level (% than *koLhcb4* + Lhcb4.1wild type plants)
*b*614	His 242	H242L	93.7 ± 18.7[a]
*b*614	His 242	H242A	102.8 ± 4.2[a]
*b*614	His 242	H242V	88.8 ± 16.1[a]

Table S5.2.2 | Pigment composition of wild type purified CP29 and mutant isoforms. *Pigment content of the purified complexes was assessed by fitting spectra of the acetone extract with spectra of individual chromophores combined with HPLC analysis. Data are expressed as number of moles per mole of polypeptide, mean ± SD, n = 3 biologically independent samples. Chl, chlorophyll; Neo, neoxanthin; Vio, violaxanthin; Lut, lutein.*

CP29 complex	Chl *a*	Chl *b*	Neo	Vio	Lut
wild type	10.2 ± 0.2	3.8 ± 0.2	1.1 ± 0.2	1.0 ± 0.1	1.3 ± 0.1
koLhcb4 + Lhcb4.1 wild type	9.9 ± 0.2	4.1 ± 0.2	0.8 ± 0.1	0.9 ± 0.1	1.4 ± 0.1
*b*614 / H242L	9.7 ± 0.1	3.3 ± 0.2	1.0 ± 0.1	1.0 ± 0.1	1.3 ± 0.1

Table S5.2.3 | Sequences of oligonucleotide primers used for site-directed mutagenesis.

Sites[§]	Mutations	primers	
		forward	reverse
*b*614	H242L	GGAGTGGATCACTGAGGAGAGTAGCCCAATTGTTG	CAACAATTGGGCTACTCTCCTCAGTGATCCACTCC
*b*614	H242A	TTGGGCTACTGCTCTCAGTGATC	TTGTTGAGTGGACCTTTAC
*b*614	H242V	TTGGGCTACTGTTCTCAGTGATCC	TTGTTGAGTGGACCTTTAC

6. Extended Conclusions

During my *Ph.D.* I focused my attention on Light Harvesting Complexes (Lhcb) of PSII. The main function of LHC is to increase light capture and regulate the transfer of excitation energy to the PSII reaction center. When energy absorbed by PSII overcomes the capacity of downstream reactions, this limit being exhacerbated by other stress factors, the over-excitation yields into production of reactive oxygen species and photo-oxidative damages to the chloroplast. LHCs evolved a number of mechanisms which are able to reduce the detrimental effects of over-excitation, the most important being the Non Photochemical Quenching (NPQ). Research activity in last decades revealed NPQ is a complex mechanism, regulated by multiple factors. During my work, I tried to shed light on the physiology of LHC system, which triggers NPQ response and regulates its amplitude, by applying a combination of reverse genetics and site-directed mutagenesis. LHC proteins are also key elements in the modeling of thylakoid membrane architecture. Therefore, I analyzed the organization of photosynthetic membranes in LHC knock-out mutants of *Arabidopsis thaliana*, with the aim to understand the molecular factors involved in the regulation of thylakoid stacking and the protein-protein interactions within the PSII supercomplex. Being critical components in the functioning of the photosynthetic apparatus, LHCs have been proposed as a promising target for the genetic engineering of both crops and massive cultures of microalgae (Ort et al., 2015). To this aim, we produced mutant strains of the green microalga *C. vulgaris* with reduced content of LHC proteins, in order to enhance growth rate under high-density conditions typical of industrial photobioreactors (PBR).

6.1. Light Harvesting Complexes as a target to improve light-to-biomass conversion efficiency

The isolation of *Chlorella vulgaris* mutants with reduced LHC content resulted in an enhanced light-to-biomass conversion efficiency under excess light conditions, with respect to the parental strain. This result is consistent with phenotypes observed in algal mutant strains carrying a truncated light harvesting system (Melis, 2009; Kirst et al., 2012; Cazzaniga et al., 2014; Perin et al., 2015). These pale-green phenotypes showed enhanced grow rate in PBR conditions, due to a better light distribution within the cultures. Despite such an important improvement, these strains are still not competitive for biofuel production, given the current low costs of fossil sources. To further increase productivity, a possible strategy was to enhance the resistance of these strains to excess light and limit photoinhibition, thus allowing cultivation at latitudes with strong irradiances. A direct evolution approach, based on EMS mutagenesis and selective pressure, allowed us to identify the mutant lines SOR (chapter 3.1) and NFR (chapter 3.2). Resulting genotypes showed both reduced antenna size and higher resistance to photo-oxidative stress than wild type strain, which resulted in better growth performances under PBR conditions. Taken together, our results reveal that the combination of ROS resistance and reduced Chl content represents a successful strategy towards the improvement of algal growth. Furthermore, the direct evolution of algal strains of industrial interest is an effective strategy to produce optimized strains without the need for genetic transformation, the latter being tricky in non-model organisms; in addition, transgenic organisms pose problems of public acceptance, and

require specific containment approaches, contributing to rise costs of both maintenance and scalability (Benedetti et al., 2018; Zimny et al., 2019)

6.2. Lhcb proteins participate in modeling the architecture of the thylakoid membranes.

The typical organization of thylakoid membranes, made of appressed stacks connected by stromatic lamellae, is affected by LHC composition. Previous evidences suggested that Lhcb proteins modulate the architecture of thylakoid membranes, in particular the dimensions and the shape of grana (Kim et al., 2009). To further investigate the relative contribution of the LHC members in shaping thylakoids architecture, we applied a CRISPR-Cas9 approach to *Arabidopsis thaliana* lines and got genotypes devoid of either LHCII (*koLHCII*) or the whole PSII antenna (*koLhcb)*. Results of chapter 4.1 revealed that both monomeric and trimeric Lhcb complexes are necessary to maintain the typical organization of thylakoids membranes of higher plants (grana-stroma lamellae). In particular, we highlighted the crucial role played by the low-abundant subunits Lhcb5 and Lhcb2.
Lhcb5 is highly conserved in green algae and higher plants and is implied in the stabilization of stacking layers, while Lhcb2 is a more recent evolutionary conquest which mediates the dynamics of grana upon illumination. This characteristic could have been fundamental in land colonization, allowing for better adaptation of plants in a completely different environment with respect to where photosynthetic organisms initially evolved. Moreover, the organization of thylakoids of higher plants was shown critical in the PSII repair cycle, which was negatively affected in grana-less *koLhcb* lines. It is worth noting that grana formation is a process that intrigued plant scientists for several years, while the genetic bases of such a structural feature has been never identified. For this reason, the results of chapter 4.1 could pave the way for further and deeper investigations in the field, e.g. identification of the LHC domains that contribute to the stacking.

6.3. Photoprotection in higher plants is mediated by both monomeric and trimeric Lhcb proteins

One of the main functions of LHC proteins, besides light-harvesting, is the protection of the photosynthetic apparatus, which is achieved throught the regulation of NPQ. It is generally accepted that activation of NPQ requires the pH sensing protein PsbS, zeaxanthin and chlorophylls bound to the PSII antenna complexes (Niyogi and Truong, 2013). Among Lhcb complexes, several have been proposed as quenching sites, comprising both monomeric and trimeric LHCs. While the role of trimeric LHCII as hosting the energy quencher is widely accepted, the involvement of monomeric Lhcb is still lively debated (Wilson and Ruban, 2020; Bassi and Dall'Osto, 2021). In this work we structurally pinpointed the quenching sites, confirming the role of trimeric LHCII as the main quencher of PSII and identifying the pigment cluster of Lhcb4 that contributes to photoprotective responses. We also confirmed the dependence of quenching responses on Zea and PsbS, in both monomeric and trimeric complexes, as previously proposed by (Dall'Osto et al., 2017). However, our results still leave a major open question: how do we explain the (lack of) effects of the *lut2* mutation on NPQ activity? In genotypes lacking either trimeric LHCII (*koLHCII)* or monomeric Lhcb (*NoM)* the introduction

of the *lut2* mutation did not affect the amplitue of quenching *in vivo*, while in wild type plants the absence of Lut strongly impacts on the quenching kinetics. Recent *in vitro* measurements on monomeric Lhcb1 suggested Chls *a*612 and *a*603, respectively connected to the Lut clusters in L1 and L2, as the most probable quenching centers (Agostini et al., 2021); moreover, (Ruban et al., 2007) detected Lut-dependent quenching even in monomeric LHC. While differences between *in vivo* and *in vitro* investigations should be considered with cautions, we can speculate that these two Chl can act as quenchers upon PsbS-LHCII interaction, possibly involving Zea molecules; in this case, the only role of Lut would be the maintenance of a correct conformation of the complex, rather than a direct participation to the quenching reaction.

To deeply understand the contribution of specific subunits, we carried out an *in vivo* site directed mutagenesis on the Chl binding sites of the monomeric Lhcb4, the most promising candidate among monomers in mediating qE (De Bianchi et al., 2011). The production and the *in vivo* investigation of mutant lines lacking single Chl represents an innovative and straightforward strategy to identify a specific cluster of pigments. Indeed, Chl *a*603-*a*609-*a*616 and the xanthophyll in L2 were identified as responsible for mediating qE activation in an intact photosynthetic environment (chapter 5.1). This result confirms that monomeric Lhcb participate in quenching reactions, as proposed in chapter 4.2. Using the same approach, we showed that lack of a single Chl induces a deep re-organization of the thylakoid complexes (chapter 5.2). Indeed, Chl *b*614 of Lhcb4 was found the docking site of Lhcb6 that, when unable to bind to the supercomplex, undergoes degradation (De Bianchi et al., 2008). CP24-less PSII resulted in the formation of array-like structures, affecting electron transport and plastoquinone diffusion (Kovács et al., 2006; De Bianchi et al., 2008) thus impacting on the growt rate. A recent structural study (Su et al., 2022) revealed a similar role played by Chls 617 and 618 of Lhca subunits in stabilizing the dimeric Lhca complex. These findings suggest that Chl can act as a molecular glue for PS subunits, thus shaping both strcture and function of the photosynthetic apparatus.

6.4. Further work and perspectives

By implementig *in vivo* site directed mutagenesis to the trimeric LHCII, which is already ongoing in our lab, we are confient to reach a deeper comprehension of the pigment cluster(s) responsible for NPQ response, as well as the specific contribution of Lut and Zea to the overall process. In *vivo* analysis could be coupled with modern single-molecule spectroscopy analysis performed on purified complexes embedded in nanodiscs (near-native membrane structures) together with specific xanthophylls and the trigger PsbS (Kondo et al., 2017; Son et al., 2020). This approach will constitute an important step toward the comprehension of the molecular basis of NPQ, which committed researchers for more than 30 years, and hold the potential of highly impacting on future developments in crops productivity (Kromdijk et al., 2016).

7. References:

Abdel-Raouf, N., Al-Homaidan, A.A., and Ibraheem, I.B.M. (2012). Microalgae and wastewater treatment. Saudi J. Biol. Sci. **19**: 257–275.

Adams, W.W., Demmig-Adams, B., Barker, D.H., and Kiley, S. (1996). Carotenoids and Photosystem II Characteristics of Upper and Lower Halves of Leaves Acclimated to High Light. Funct. Plant Biol. **23**: 669–677.

Agostini, A., Nicol, L., Da Roit, N., Bortolus, M., Croce, R., and Carbonera, D. (2021). Altering the exciton landscape by removal of specific chlorophylls in monomeric LHCII provides information on the sites of triplet formation and quenching by means of ODMR and EPR spectroscopies. Biochim. Biophys. Acta - Bioenerg. **1862**: 148481.

Ahn, T.K., Avenson, T.J., Ballottari, M., Cheng, Y.C., Niyogi, K.K., Bassi, R., and Fleming, G.R. (2008). Architecture of a charge-transfer state regulating light harvesting in a plant antenna protein. Science (80-.). **320**: 794–797.

Albanese, P., Manfredi, M., Marengo, E., Saracco, G., and Pagliano, C. (2019). Structural and functional differentiation of the light-harvesting protein Lhcb4 during land plant diversification. Physiol. Plant. **166**: 336–350.

Albanese, P., Tamara, S., Saracco, G., Scheltema, R.A., and Pagliano, C. (2020). How paired PSII–LHCII supercomplexes mediate the stacking of plant thylakoid membranes unveiled by structural mass-spectrometry. Nat. Commun. **11**.

Alboresi, A., Caffarri, S., Nogue, F., Bassi, R., and Morosinotto, T. (2008). In Silico and Biochemical Analysis of Physcomitrella patens Photosynthetic Antenna: Identification of Subunits which Evolved upon Land Adaptation. PLoS One **3**: e2033.

Alché, J. de D. (2019). A concise appraisal of lipid oxidation and lipoxidation in higher plants. Redox Biol. **23**.

Allen, J.F. (2003). Cyclic, pseudocyclic and noncyclic photophosphorylation: new links in the chain. Trends Plant Sci. **8**: 15–19.

Allen, J.F. (1992). How does protein phosphorylation regulate photosynthesis? Trends Biochem. **17**: 12–17.

Allen, M.M. and Stanier, R.Y. (1968). Growth and division of some unicellular blue-green algae. J Gen Micro. **51**: 199–202.

Allred, D.R. and Staehelin, L.A. (1985). Lateral distribution of the cytochrome b6/f and coupling factor ATP-synthetase complexes of chloroplast thylakoid membranes. Plant Physiol. **78**: 199–202.

Van Amerongen, H. and Croce, R. (2013). Light harvesting in photosystem II. Photosynth. Res. **116**: 251–263.

Amstutz, C.L., Fristedt, R., Schultink, A., Merchant, S.S., Niyogi, K.K., and Malnoë, A. (2020). An atypical short-chain dehydrogenase–reductase functions in the relaxation of photoprotective qH in Arabidopsis. Nat. Plants 2020 62 **6**: 154–166.

Anderson, J.M. (1986). Photoregulation of the composition, function and structure of thylakoid membranes. Ann.Rev.Plant Physiol. **37**: 93–136.

Anderson, J.M. and Melis, A. (1983). Localization of different photosystems in seperate regions of chloroplast membranes. Proc.Natl.Acad.Sci.USA **80**: 745–749.

Andersson, J., Wentworth, M., Walters, R.G., Howard, C.A., Ruban, A. V., Horton, P., and Jansson, S. (2003). Absence of the Lhcb1 and Lhcb2 proteins of the light-harvesting complex of photosystem II - Effects on photosynthesis, grana stacking and fitness. Plant J. **35**: 350–361.

Angstenberger, M., De Signori, F., Vecchi, V., Dall'Osto, L., and Bassi, R. (2020). Cell Synchronization Enhances Nuclear Transformation and Genome Editing via Cas9 Enabling Homologous Recombination in Chlamydomonas reinhardtii. ACS Synth. Biol. **9**: 2840–2850.

Argyroudi-Akoyunoglou, J.H., Feleki, Z., and Akoyunoglou, G. (1971). Formation of two chlorophyll-protein complexes during greening of etiolated bean leaves. Biochem. Biophys. Res. Commun. **45**: 606–614.

Armbruster, U. et al. (2014). Arabidopsis CURVATURE THYLAKOID1 proteins modify thylakoid architecture by inducing membrane curvature. Plant Cell **25**: 2661–2678.

Armenteros, J.J.A., Salvatore, M., Emanuelsson, O., Winther, O., Von Heijne, G., Elofsson, A., and Nielsen, H. (2019). Detecting sequence signals in targeting peptides using deep learning. Life Sci. Alliance **2**.

Armond, P.A. and Arntzen, C.J. (1977). Localization and Characterization of Photosystem II in Grana and Stroma Lamellae. Plant Physiol. **59**: 398–404.

Armond, P.A., Arntzen, C.J., Briantais, J.M., and Vernotte, C. (1976). Differentiation of chloroplast lamellae. Light harvesting efficiency and grana development. Arch. Biochem. Biophys. **175**: 54–63.

Armond, P.A., Staehelin, L.A., and Arntzen, C.J. (1977). Spatial relationship of photosysten I, photosystem II, and the light-harvesting complex in chloroplast membranes. J.Cell Biol. **73**: 400–418.

Aro, E.M., Virgin, I., and Andersson, B. (1993). Photoinhibition of Photosystem II. Inactivation, protein damage and turnover. Biochim. Biophys. Acta - Bioenerg. **1143**: 113–134.

Asada, K. (1999). The water-water cycle in chloroplasts: scavenging of active oxygens and dissipation of excess photons. Annu. Physiol Plant Mol.Biol. **50**: 601–639.

Asada, K., Kiso, K., and Yoshikawa, K. (1974). Univalent Reduction of Molecular Oxygen by Spinach Chloroplasts on Illumination. J. Biol. Chem. **249**: 2175–2181.

Avenson, T.J., Cruz, J.A., Kanazawa, A., and Kramer, D.M. (2005). Regulating the proton budget of higher plant photosynthesis. Proc. Natl. Acad. Sci. U. S. A. **102**: 9709–9713.

Avenson, T.J., Tae, K.A., Zigmantas, D., Niyogi, K.K., Li, Z., Ballottari, M., Bassi, R., and Fleming, G.R. (2008). Zeaxanthin radical cation formation in minor light-harvesting complexes of higher plant antenna. J. Biol. Chem. **283**: 3550–3558.

Axelsson, M. and Gentili, F. (2014). A single-step method for rapid extraction of total lipids from green microalgae. PLoS One **9**: e89643.

Baek, K., Kim, D.H., Jeong, J., Sim, S.J., Melis, A., Kim, J.S., Jin, E., and Bae, S. (2016). DNA-free two-gene knockout in Chlamydomonas reinhardtii via CRISPR-Cas9 ribonucleoproteins. Sci. Rep. **6**.

Bag, P., Chukhutsina, V., Zhang, Z., Paul, S., Ivanov, A.G., Shutova, T., Croce, R., Holzwarth, A.R., and Jansson, S. (2020). Direct energy transfer from photosystem II to photosystem I confers winter sustainability in Scots Pine. Nat. Commun. **11**.

Baker, N.R. (2008). Chlorophyll Fluorescence: A Probe of Photosynthesis In Vivo. Annu. Rev. Plant Biol. **59**: 89–113.

Ballottari, M., Dall'Osto, L., Morosinotto, T., and Bassi, R. (2007). Contrasting behavior of higher plant photosystem I and II antenna systems during acclimation. J. Biol. Chem. **282**: 8947–8958.

Ballottari, M., Govoni, C., Caffarri, S., and Morosinotto, T. (2004). Stoichiometry of LHCI antenna polypeptides and characterization of gap and linker pigments in higher plants Photosystem I. Eur. J. Biochem. **271**: 4659–4665.

Barera, S., Dall'Osto, L., and Bassi, R. (2021). Effect of lhcsr gene dosage on oxidative stress and light use efficiency by Chlamydomonas reinhardtii cultures. J. Biotechnol. **328**: 12–22.

Baroli, I., Gutman, B.L., Ledford, H.K., Shin, J.W., Chin, B.L., Havaux, M., and Niyogi, K.K. (2004). Photo-oxidative stress in a xanthophyll-deficient mutant of Chlamydomonas. J Biol Chem **279**: 6337–6344.

Bassham, J.A., Benson, A.A., and Calvin, M. (1950). THE PATH OF CARBON IN PHOTOSYNTHESIS VIII. THE ROLE OF MALIC ACID*.

Bassi, R., Croce, R., Cugini, D., and Sandonà, D. (1999). Mutational analysis of a higher plant antenna protein provides identification of chromophores bound into multiple sites. Proc. Natl. Acad. Sci. U. S. A. **96**: 10056–10061.

Bassi, R. and Dall'Osto, L. (2021). Dissipation of Light Energy Absorbed in Excess: The Molecular Mechanisms. Annu. Rev. Plant Biol. **72**: 47–76.

Bassi, R., Ghiretti Magaldi, A., Tognon, G., Giacometti, G.M., and Miller, K.R. (1989). Two-dimensional crystals of the photosystem II reaction center complex from higher plants. Eur. J. Cell Biol. **50**: 84–93.

Bassi, R., Marquardt, J., and Lavergne, J. (1995). Biochemical and fuctional properties of photosystem II in agranal membranes from maize mesophyll and bundle sheath chloroplasts. Eur.J.Biochem. **233**: 709–719.

Bassi, R., Pineau, B., Dainese, P., and Marquardt, J. (1993). Carotenoid-Binding Proteins of Photosystem-II. Eur.J.Biochem. **212**: 297–303.

Bassi, R. and Simpson, D.J. (1986). Differential expression of LHCII genes in mesophyll and bundle sheath cells of maize. Carlsberg Res. Commun. **51**: 363–370.

Bassi, R, Hinz, U., and Barbato, R. (1985). The role of the light harvesting complex and photosystem II in thylakoid stacking in the chlorina-f2 barley mutant. Carlsb. Res.Commun. **50_ _**: 347–367.

Belgio, E., Johnson, M.P., Jurić, S., and Ruban, A. V. (2012). Higher plant photosystem II light-harvesting antenna, not the reaction center, determines the excited-state lifetime - Both the maximum and the nonphotochemically quenched. Biophys. J. **102**: 2761–2771.

Belgio, E., Kapitonova, E., Chmeliov, J., Duffy, C.D.P., Ungerer, P., Valkunas, L., and Ruban, A. V. (2014). Economic photoprotection in photosystem II that retains a complete light-harvesting system with slow energy traps. Nat. Commun. **5**: 1–8.

Bellafiore, S., Barneche, F., Peltler, G., and Rochalx, J.D. (2005). State transitions and light adaptation require chloroplast thylakoid protein kinase STN7. Nature **433**: 892–895.

Benedetti, M., Vecchi, V., Barera, S., and Dall'Osto, L. (2018). Biomass from microalgae: The potential of domestication towards sustainable biofactories. Microb. Cell Fact. **17**: 1–18.

Bennett, D.I.G., Fleming, G.R., and Amarnath, K. (2018). Energy-dependent quenching adjusts the excitation diffusion length to regulate photosynthetic light harvesting. Proc. Natl. Acad. Sci. U. S. A. **115**: E9523–E9531.

Benzie, I.F.F. and Strain, J.J. (1996). The ferric reducing ability of plasma (FRAP) as a measure of "antioxidant power": the FRAP assay. Anal Biochem **239**: 70–76.

Bergantino, E., Segalla, A., Brunetta, A., Teardo, E., Rigoni, F., Giacometti, G.M., and Szabò, I. (2003). Light- and pH-dependent structural changes in the PsbS subunit of photosystem II. Proc. Natl. Acad. Sci. U. S. A. **100**: 15265–15270.

Berger, H., de Mia, M., Morisse, S., Marchand, C., Lemaire, S.D., Wobbe, L., and Kruse, O. (2016). A light switch based on protein S-nitrosylation fine-tunes photosynthetic light-harvesting in the microalga Chlamydomonas reinhardtii. Plant Physiol. **171**: pp.01878.2015.

Bernacchi, C.J., Portis, A.R., Nakano, H., Von Caemmerer, S., and Long, S.P. (2002). Temperature response of mesophyll conductance. Implications for the determination of Rubisco enzyme kinetics and for limitations to photosynthesis in vivo. Plant Physiol. **130**: 1992–1998.

Betterle, N., Ballottari, M., Zorzan, S., De Bianchi, S., Cazzaniga, S., Dall'Osto, L., Morosinotto, T., and Bassi, R. (2009). Light-induced dissociation of an antenna hetero-oligomer is needed for non-photochemical quenching induction. J. Biol. Chem. **284**: 15255–15266.

De Bianchi, S., Betterle, N., Kouril, R., Cazzaniga, S., Boekema, E., Bassi, R., and Dall'Osto, L. (2011). Arabidopsis mutants deleted in the light-harvesting protein Lhcb4 have a disrupted photosystem II macrostructure and are defective in photoprotection. Plant Cell **23**: 2659–2679.

De Bianchi, S., Dall'Osto, L., Tognon, G., Morosinotto, T., and Bassi, R. (2008). Minor antenna proteins CP24 and CP26 affect the interactions between photosystem II subunits and the electron transport rate in grana membranes of Arabidopsis. Plant Cell **20**: 1012–1028.

Björn, L.O., Papageorgiou, G.C., Blankenship, R.E., and Govindjee (2009). A viewpoint: Why chlorophyll a? Photosynth. Res. **99**: 85–98.

Bobik, K. and Burch-Smith, T.M. (2015). Chloroplast signaling within, between and beyond cells. Front Plant Sci. **6**: 781.

Bode, S., Quentmeier, C.C., Liao, P.N., Hafi, N., Barros, T., Wilk, L., Bittner, F., and Walla, P.J. (2009). On the regulation of photosynthesis by excitonic interactions between carotenoids and chlorophylls. Proc. Natl. Acad. Sci. U. S. A. **106**: 12311–12316.

Bolger, A.M., Lohse, M., and Usadel, B. (2014). Trimmomatic: a flexible trimmer for Illumina sequence data. Bioinformatics **30**: 2114–2120.

Bona, F., Capuzzo, A., Franchino, M., and Maffei, M.E. (2014). Semicontinuous nitrogen limitation as convenient operation strategy to maximize fatty acid production in Neochloris oleoabundans. Algal Res **5**: 1–6.

Bonente, G., Pippa, S., Castellano, S., Bassi, R., and Ballottari, M. (2012). Acclimation of Chlamydomonas reinhardtii to different growth irradiances. J. Biol. Chem. **287**: 5833–5847.

Borowitzka, M.A. (2013). High-value products from microalgae—their development and commercialisation. J. Appl. Phycol. 2013 253 **25**: 743–756.

Bos, I., Bland, K.M., Tian, L., Croce, R., Frankel, L.K., Van Amerongen, H., Bricker, T.M., and Wientjes, E. (2017). Multiple LHCII antennae can transfer energy efficiently to a single Photosystem I. Biochim.Biophys.Acta **1858**: 371–378.

Bressan, M., Bassi, R., and Dall'Osto, L. (2018). Light harvesting complex I is essential for Photosystem II photoprotection under variable light conditions in Arabidopsis thaliana. Environ. Exp. Bot. **154**: 89–98.

Britton, G., Liaaen-Jensen, S., and Pfander, H. (2004). Carotenoids Hand Book G. Britton, S. Liaaen-Jensen, and H. Pfander, eds (Birkhauser: Basel, Switzerland).

Brooks, M.D. and Niyogi, K.K. (2011). Use of a Pulse-Amplitude Modulated Chlorophyll Fluorometer to Study the Efficiency of Photosynthesis in Arabidopsis Plants. Methods Mol. Biol. **II**.

Brooks, M.D., Sylak-Glassman, E.J., Fleming, G.R., and Niyogi, K.K. (2013). A thioredoxin-like/β-propeller protein maintains the efficiency of light harvesting in Arabidopsis. Proc. Natl. Acad. Sci. U. S. A. **110**: E2733–E2740.

Buchanan, B.B., Gruissem, W., and Jones, R.L. (2015). Biochemistry & Molecular Biology of Plants. Second edi. A. society of P. Biologist, ed (Wiley Blackwell).

Caffarri, S., Croce, R., Breton, J., and Bassi, R. (2001). The Major Antenna Complex of Photosystem II Has a Xanthophyll Binding Site Not Involved in Light Harvesting. J. Biol. Chem. **276**: 35924–35933.

Caffarri, S., Croce, R., Cattivelli, L., and Bassi, R. (2004). A look within LHCII: Differential analysis of the Lhcb1-3 complexes building the major trimeric antenna complex of higher-plant photosynthesis. Biochemistry **43**: 9467–9476.

Caffarri, S., Kouřil, R., Kereïche, S., Boekema, E.J., and Croce, R. (2009). Functional architecture of higher plant photosystem II supercomplexes. EMBO J. **28**: 3052–3063.

Caffarri, S., Passarini, F., Bassi, R., and Croce, R. (2007). A specific binding site for neoxanthin in the monomeric antenna proteins CP26 and CP29 of Photosystem II. FEBS Lett. **581**: 4704–4710.

Caffarri, S., Tibiletti, T., Jennings, R., and Santabarbara, S. (2014). A Comparison Between Plant Photosystem I and Photosystem II Architecture and Functioning. Curr. Protein Pept. Sci. **15**: 296–331.

Del Campo, J.A., García-González, M., and Guerrero, M.G. (2007). Outdoor cultivation of microalgae for carotenoid production: Current state and perspectives. Appl. Microbiol. Biotechnol. **74**: 1163–1174.

Del Campo, J.A., Moreno, J., Rodríguez, H., Angeles Vargas, M., Rivas, J., and Guerrero, M.G. (2000). Carotenoid content of chlorophycean microalgae: factors determining lutein accumulation in Muriellopsis sp. (Chlorophyta). J. Biotechnol. **76**: 51–59.

Del Campo, J.A., Rodríguez, H., Moreno, J., Vargas, M.Á., Rivas, J., and Guerrero, M.G. (2004). Accumulation of astaxanthin and lutein in Chlorella zofingiensis (Chlorophyta). Appl. Microbiol. Biotechnol. **64**: 848–854.

Campoli, C., Caffarri, S., Svensson, J.T., Bassi, R., Stanca, A.M., Cattivelli, L., and Crosatti, C. (2009). Parallel pigment and transcriptomic analysis of four barley Albina and Xantha mutants reveals the complex network of the chloroplast-dependent metabolism. Plant Mol. Biol. **71**: 173–191.

Cantrell, M. and Peers, G. (2017). A mutant of Chlamydomonas without LHCSR maintains high rates of photosynthesis, but has reduced cell division rates in sinusoidal light conditions. PLoS One **12**: e0179395.

Carvalho, A.P., Silva, S.O., Baptista, J.M., and Malcata, F.X. (2011). Light requirements in microalgal photobioreactors: An overview of biophotonic aspects. Appl. Microbiol. Biotechnol. **89**: 1275–1288.

Casazza, A.P., Tarantino, D., and Soave, C. (2001). Preparation and functional characterization of thylakoids from Arabidopsis thaliana. Photosynth.Res. **68**: 175–180.

Caspy, I., Fadeeva, M., Mazor, Y., and Nelson, N. (2021). Structure of Dunaliella Photosystem II reveals conformational flexibility of stacked and unstacked supercomplexes. Preprint.

Cazzaniga, S., Dall'Osto, L., Kong, S.G., Wada, M., and Bassi, R. (2013). Interaction between avoidance of photon absorption, excess energy dissipation and zeaxanthin synthesis against photooxidative stress in Arabidopsis. Plant J. **76**: 568–579.

Cazzaniga, S., Dall'Osto, L., Szaub, J., Scibilia, L., Ballottari, M., Purton, S., and Bassi, R. (2014). Domestication of the green alga Chlorella sorokiniana: reduction of antenna size improves light-use efficiency in a photobioreactor. **7**.

Cazzaniga, S., Li, Z., Niyogi, K.K., Bassi, R., and Dall'Osto, L. (2012). The Arabidopsis szl1 mutant reveals a Critical role of β-carotene in photosystem I photoprotection. Plant Physiol. **159**: 1745–1758.

Cecchin, M., Marcolungo, L., Rossato, M., Girolomoni, L., Cosentino, E., Cuine, S., Li-Beisson, Y., Delledonne, M., and Ballottari, M. (2019). Chlorella vulgaris genome assembly and annotation reveals the molecular basis for metabolic acclimation to high light conditions. Plant J. **100**: 1289–1305.

Chamovitz, D., Pecker, I., and Hirschberg, J. (1991). The molecular basis of resistance to the herbicide norflurazon. Plant Mol. Biol. 1991 166 **16**: 967–974.

Chen, J.H., Chen, C.Y., Hasunuma, T., Kondo, A., Chang, C.H., Ng, I.S., and Chang, J.S. (2019). Enhancing lutein production with mixotrophic cultivation of Chlorella sorokiniana MB-1-M12 using different bioprocess operation strategies. Bioresour. Technol. **278**: 17–25.

Chen, M. and Blankenship, R.E. (2011). Expanding the solar spectrum used by photosynthesis. Trends Plant Sci. **16**: 427–431.

Chew, K.W., Yap, J.Y., Show, P.L., Suan, N.H., Juan, J.C., Ling, T.C., Lee, D.J., and Chang, J.S. (2017). Microalgae biorefinery: High value products perspectives. Bioresour. Technol. **229**: 53–62.

Chia, S.R., Chew, K.W., Show, P.L., Yap, Y.J., Ong, H.C., Ling, T.C., and Chang, J.S. (2018). Analysis of Economic and Environmental Aspects of Microalgae Biorefinery for Biofuels Production: A Review. Biotechnol. J. **13**: 1700618.

Chisti, Y. (2007). Biodiesel from microalgae. Biotechnol. Adv. **25**: 294–306.

Chisti, Y. (2008). Biodiesel from microalgae beats bioethanol. Trends Biotechnol **26**: 126–131.

Christenson, L. and Sims, R. (2011). Production and harvesting of microalgae for wastewater treatment, biofuels, and bioproducts. Biotechnol Adv **29**: 686–702.

Cingolani, P., Platts, A., Wang, L.L., Coon, M., Nguyen, T., Wang, L., Land, S.J., Lu, X., and Ruden, D.M. (2012). A program for annotating and predicting the effects of single nucleotide polymorphisms, SnpEff: SNPs in the genome of Drosophila melanogaster strain w1118; iso-2; iso-3. Fly (Austin). **6**: 80–92.

Cinque, G., Croce, R., and Bassi, R. (2000). Absorption spectra of chlorophyll a and b in Lhcb protein environment. In Photosynthesis Research, pp. 233–242.

Clark, D.A., Brown, S., Kicklighter, D.W., Chambers, J.Q., Thomlinson, J.R., and Ni, J. (2001). Measuring net primary production in forests: Concepts and field methods. Ecol. Appl. **11**: 356–370.

Clarke, J.E. and Johnson, G.N. (2001). In vivo temperature dependence of cyclic and pseudocyclic electron transport in barley. Planta 2001 2125 **212**: 808–816.

Clausen, C.H., Brooks, M.D., Li, T. De, Grob, P., Kemalyan, G., Nogales, E., Niyogi, K.K., and Fletcher, D.A. (2014). Dynamic mechanical responses of Arabidopsis thylakoid membranes during PSII-specific illumination. Biophys J **106**: 1864–1870.

Collin, V.C., Eymery, F., Genty, B., Rey, P., and Havaux, M. (2008). Vitamin E is essential for the tolerance of Arabidopsis thaliana to metal-induced oxidative stress. Plant Cell Environ. **31**: 244–257.

Colombo, G., Clerici, M., Garavaglia, M.E., Giustarini, D., Rossi, R., Milzani, A., and Dalle-Donne, I. (2016). A step-by-step protocol for assaying protein carbonylation in biological samples. J. Chromatogr. B Anal. Technol. Biomed. Life Sci. **1019**: 178–190.

Cordero, B.F., Obraztsova, I., Couso, I., Leon, R., Vargas, M.A., and Rodriguez, H. (2011). Enhancement of Lutein Production in Chlorella sorokiniana (Chorophyta) by Improvement of Culture Conditions and Random Mutagenesis. Mar. Drugs 2011, Vol. 9, Pages 1607-1624 **9**: 1607–1624.

Correa-Galvis, V., Poschmann, G., Melzer, M., Stuhler, K., and Jahns, P. (2016). PsbS interactions involved in the activation of energy dissipation in Arabidopsis. Nat. plants **2:15225**.

Crepin, A. and Caffarri, S. (2018). Functions and evolution of Lhcb isoforms composing LHCII, the major light harvesting complex of Photosystem II of green eukaryotic organisms. Curr. Protein Pept. Sci. **19**.

Crepin, A., Kučerová, Z., Kosta, A., Durand, E., and Caffarri, S. (2020). Isolation and characterization of a large photosystem I–light-harvesting complex II supercomplex with an additional Lhca1–a4 dimer in Arabidopsis. Plant J. **102**: 398–409.

Croce, R. and van Amerongen, H. (2020). Light harvesting in oxygenic photosynthesis: Structural biology meets spectroscopy. Science **369**.

Croce, R., Canino, G., Ros, F., and Bassi, R. (2002a). Chromophore organization in the higher-plant photosystem II antenna protein CP26. Biochemistry **41**: 7334–7343.

Croce, R., Cinque, G., Holzwarth, A.R., and Bassi, R. (2000). The Soret absorption properties of carotenoids and chlorophylls in antenna complexes of higher plants. Photosynth. Res. 2000 642 **64**: 221–231.

Croce, R., Morosinotto, T., Castelletti, S., Breton, J., and Bassi, R. (2002b). The Lhca antenna complexes of higher plants photosystem I. Biochim. Biophys. Acta - Bioenerg. **1556**: 29–40.

Cruz, J.A., Avenson, T.J., Kanazawa, A., Takizawa, K., Edwards, G.E., and Kramer, D.M. (2005). Plasticity in light reactions of photosynthesis for energy production and photoprotection. In Journal of Experimental Botany (J Exp Bot), pp. 395–406.

D'Alessandro, S. and Havaux, M. (2019). Sensing β-carotene oxidation in photosystem II to master plant stress tolerance. New Phytol. **223**: 1776–1783.

Dall'Osto, L., Bassi, R., and Ruban, A. (2014a). Photoprotective mechanisms: carotenoids.: 393–435.

Dall'Osto, L., Bressan, M., and Bassi, R. (2015). Biogenesis of light harvesting proteins. Biochim. Biophys. Acta **1847**: 861–71.

Dall'Osto, L., Caffarri, S., and Bassi, R. (2005). A mechanism of nonphotochemical energy dissipation, independent from PsbS, revealed by a conformational change in the antenna protein CP26. Plant Cell **17**: 1217–1232.

Dall'Osto, L., Cazzaniga, S., Bressan, M., Paleček, D., Žídek, K., Niyogi, K.K., Fleming, G.R., Zigmantas, D., and Bassi, R. (2017). Two mechanisms for dissipation of excess light in

monomeric and trimeric light-harvesting complexes. Nat. Plants **3**: 17033.

Dall'Osto, L., Cazzaniga, S., Guardini, Z., Barera, S., Benedetti, M., Mannino, G., Maffei, E.M., and Bassi, R. (2019). Combined resistance to oxidative stress and reduced antenna size enhance light-to-biomass conversion efficiency in Chlorella vulgaris cultures. Biotechnol. Biofuels **12**: 1–17.

Dall'Osto, L., Cazzaniga, S., Havaux, M., and Bassi, R. (2010). Enhanced photoprotection by protein-bound vs free xanthophyll pools: A comparative analysis of chlorophyll b and xanthophyll biosynthesis mutants. Mol. Plant **3**: 576–593.

Dall'Osto, L., Cazzaniga, S., North, H., Marion-Poll, A., and Bassi, R. (2007a). The Arabidopsis aba4-1 mutant reveals a specific function for neoxanthin in protection against photooxidative stress. Plant Cell **19**: 1048–1064.

Dall'Osto, L., Cazzaniga, S., Wada, M., and Bassi, R. (2014b). On the origin of a slowly reversible fluorescence decay component in the Arabidopsis npq4 mutant. Philos. Trans. R. Soc. B Biol. Sci. **369**.

Dall'Osto, L., Cazzaniga, S., Zappone, D., and Bassi, R. (2020). Monomeric light harvesting complexes enhance excitation energy transfer from LHCII to PSII and control their lateral spacing in thylakoids. Biochim. Biophys. Acta - Bioenerg. **1861**: 0–1.

Dall'Osto, L., Fiore, A., Cazzaniga, S., Giuliano, G., and Bassi, R. (2007b). Different roles of α- and β-branch xanthophylls in photosystem assembly and photoprotection. J.Biol.Chem. **282**: 35056–35068.

Dall'Osto, L., Holt, N.E., Kaligotla, S., Fuciman, M., Cazzaniga, S., Carbonera, D., Frank, H.A., Alric, J., and Bassi, R. (2012). Zeaxanthin protects plant photosynthesis by modulating chlorophyll triplet yield in specific light-harvesting antenna subunits. J.Biol Chem. **287**: 41820–41834.

Dall'Osto, L., Lico, C., Alric, J., Giuliano, G., Havaux, M., and Bassi, R. (2006). Lutein is needed for efficient chlorophyll triplet quenching in the major LHCII antenna complex of higher plants and effective photoprotection in vivo under strong light. BMC Plant Biol. **6**: 1–20.

Dall'Osto, L., Piques, M., Ronzani, M., Molesini, B., Alboresi, A., Cazzaniga, S., and Bassi, R. (2013). The Arabidopsis nox mutant lacking carotene hydroxylase activity reveals a critical role for xanthophylls in photosystem I biogenesis. Plant Cell **25**: 591–608.

Dall'Osto, L., Ünlü, C., Cazzaniga, S., and Van Amerongen, H. (2014c). Disturbed excitation energy transfer in Arabidopsis thaliana mutants lacking minor antenna complexes of photosystem II. BBA - Bioenerg. **1837**: 1981–1988.

Damiani, M.C., Popovich, C.A., Constenla, D., and Leonardi, P.I. (2010). Lipid analysis in Haematococcuspluvialis to assess its potential use as a biodiesel feedstock. Bioresour Technol **101**: 3801–3807.

Damkjaer, J., Kereiche, S., Johnson, M.P., Kovacs, L., a.z Kiss, Boekema, E.J., Ruban, A. V, Horton, P., and Jansson, S. (2009). The Photosystem II light-harvesting protein Lhcb3 affects the macrostructure of Photosystem II and the rate of state transitions in

Arabidopsis. Plant Cell **21**: 3245–3256.

Davey, M.W., Stals, E., Panis, B., Keulemans, J., and Swennen, R.L. (2005). High-throughput determination of malondialdehyde in plant tissues. Anal. Biochem. **347**: 201–207.

Davis, P.A. and Hangarter, R.P. (2012). Chloroplast movement provides photoprotection to plants by redistributing PSII damage within leaves. Photosynt.Res. **112**: 153–161.

Davison, P.A., Hunter, C.N., and Horton, P. (2002). Overexpression of beta-carotene hydroxylase enhances stress tolerance in Arabidopsis. Nature **418**: 203–206.

Day, J.G., Slocombe, S.P., and Stanley, M.S. (2012). Overcoming biological constraints to enable the exploitation of microalgae for biofuels. Bioresour. Technol. **109**: 245–251.

Dekker, J.P. and Boekema, E.J. (2005). Supramolecular organization of thylakoid membrane proteins in green plants. Biochim. Biophys. Acta - Bioenerg. **1706**: 12–39.

Deltcheva, E., Chylinski, K., Sharma, C.M., Gonzales, K., Chao, Y., Pirzada, Z.A., Eckert, M.R., Vogel, J., and Charpentier, E. (2011). CRISPR RNA maturation by trans-encoded small RNA and host factor RNase III. Nat. 2011 4717340 **471**: 602–607.

Demmig-Adams, B., Winter, K., Winkelmann, E., Krüger, A., and Czygan, F. -C (1989). Photosynthetic Characteristics and the Ratios of Chlorophyll, β-Carotene, and the Components of the Xanthophyll Cycle Upon a Sudden Increase in Growth Light Regime in Several Plant Species*. Bot. Acta **102**: 319–325.

Depristo, M.A. et al. (2011). A framework for variation discovery and genotyping using next-generation DNA sequencing data. Nat. Genet. 2011 435 **43**: 491–498.

Dexter, D.L. (1953). A Theory of Sensitized Luminescence in Solids. J. Chem. Phys. **21**: 836.

Ding, Z., GGalván-Ampudia, C.S., Demarsy, E., Łangowski, Ł., Kleine-Vehn, J., Fan, Y., Morita, M.T., Tasaka, M., Fankhauser, C., Offringa, R., and Friml, J. (2011). Light-mediated polarization of the PIN3 auxin transporter for the phototropic response in Arabidopsis. Nat. Cell Biol. **13**: 447–453.

Dogra, V. and Kim, C. (2020). Singlet Oxygen Metabolism: From Genesis to Signaling. Front. Plant Sci. **10**.

Domingues, N., Matos, A.R., da Silva, J.M., and Cartaxana, P. (2012). Response of the Diatom Phaeodactylum tricornutum to Photooxidative Stress Resulting from High Light Exposure. PLoS One **7**: e38162.

Dominici, P., Caffarri, S., Armenante, F., Ceoldo, S., Crimi, M., and Bassi, R. (2002). Biochemical properties of the PsbS subunit of photosystem II either purified from chloroplast or recombinant. J. Biol. Chem. **277**: 22750–22758.

Doudna, J.A. and Charpentier, E. (2014). The new frontier of genome engineering with CRISPR-Cas9. Science (80-.). **346**.

Dreuw, A., Fleming, G.R., and Head-Gordon, M. (2003). Chlorophyll fluorescence quenching by xanthophylls. Phys. Chem. Chem. Phys. **5**: 3247–3256.

Drop, B., Yadav K.n., S., Boekema, E.J., and Croce, R. (2014). Consequences of state transitions on the structural and functional organization of Photosystem i in the green alga Chlamydomonas reinhardtii. Plant J. **78**: 181–191.

Ducruet, J.M. (2003). Chlorophyll thermoluminescence of leaf discs: simple instruments and progress in signal interpretation open the way to new ecophysiological indicators. J.Exp.Bot. **54**: 2419–2430.

Ducruet, J.M. and Vavilin, D. (1999). Chlorophyll high-temperature thermoluminescence emission as an indicator of oxidative stress: perturbating effects of oxygen and leaf water content. Free Radic.Res. **31 Suppl**: S187--S192.

Duffy, C.D.P., Valkunas, L., and Ruban, A. V. (2013). Quantum mechanical calculations of xanthophyll-chlorophyll electronic coupling in the light-harvesting antenna of photosystem II of higher plants. J. Phys. Chem. B **117**: 7605–7614.

Dutta, S., Cruz, J.A., Jiao, Y., Chen, J., Kramer, D.M., and Osteryoung, K.W. (2015). Non-invasive, whole-plant imaging of chloroplast movement and chlorophyll fluorescence reveals photosynthetic phenotypes independent of chloroplast photorelocation defects in chloroplast division mutants. Plant J. **84**: 428–442.

Ehleringer, J. and Forseth, I. (1980). Solar Tracking by Plants. Science (80-.). **210**: 1094–1098.

El-Agamey, A., Lowe, G.M., McGarvey, D.J., Mortensen, A., Phillip, D.M., Truscott, T.G., and Young, A.J. (2004). Carotenoid radical chemistry and antioxidant/pro-oxidant properties. Arch. Biochem. Biophys. **430**: 37–48.

Ellis, R.J. (1979). The most abundant protein in the world. Trends Biochem. Sci. **4**: 241–244.

Emanuelsson, O., Nielsen, H., and Heijne, G. Von (1999). ChloroP, a neural network-based method for predicting chloroplast transit peptides and their cleavage sites. Protein Sci. **8**: 978–984.

Erickson, E., Wakao, S., and Niyogi, K.K. (2015). Light stress and photoprotection in Chlamydomonas reinhardtii. Plant J **82**: 449–465.

Escoubas, J.M., Lomas, M., LaRoche, J., and Falkowski, P.G. (1995). Light intensity regulation of cab gene transcription is signaled by the redox state of the plastoquinone pool. Proc. Natl. Acad. Sci. **92**: 10237–10241.

Fan, M., Li, M., Liu, Z., Cao, P., Pan, X., Zhang, H., Zhao, X., Zhang, J., and Chang, W. (2015). Crystal structures of the PsbS protein essential for photoprotection in plants. Nat. Struct. Mol. Biol. **22**: 729–735.

Farah, J., Rappaport, F., Choquet, Y., Joliot, P., and Rochaix, J.D. (1995). Isolation of a psaF-deficient mutant of Chlamydomonas reinhardtii: efficient interaction of plastocyanin with the photosystem I reaction center is mediated by the PsaF subunit. EMBO J. **14**: 4976–4984.

Farkas, I., Dombrádi, V., Miskei, M., Szabados, L., and Koncz, C. (2007). Arabidopsis PPP family of serine/threonine phosphatases. Trends Plant Sci. **12**: 169–176.

Farooq, S., Chmeliov, J., Wientjes, E., Koehorst, R., Bader, A., Valkunas, L., Trinkunas, G., and Van Amerongen, H. (2018). Dynamic feedback of the photosystem II reaction centre

on photoprotection in plants. Nat. Plants **4**: 225–231.

Finazzi, G., Johnson, G.N., Dall'Osto, L., Joliot, P., Wollman, F.A., and Bassi, R. (2004). A zeaxanthin-independent nonphotochemical quenching mechanism localized in the photosystem II core complex. Proc.Natl.Acad.Sci.U.S.A **101**: 12375–12380.

Fiore, A., Dall'Osto, L., Cazzaniga, S., Diretto, G., Giuliano, G., and Bassi, R. (2012). A quadruple mutant of Arabidopsis reveals a β-carotene hydroxylation activity for LUT1/CYP97C1 and a regulatory role of xanthophylls on determination of the PSI/PSII ratio. BMC Plant Biol. **12**: 1–15.

Fischer, B.B., Dayer, R., Schwarzenbach, Y., Lemaire, S.D., Behra, R., Liedtke, A., and Eggen, R.I.L. (2009). Function and regulation of the glutathione peroxidase homologous gene GPXH/GPX5 in Chlamydomonas reinhardtii. Plant Mol Biol **71**: 569–583.

Fischer, B.B., Hideg, É., and Krieger-Liszkay, A. (2013). Production, detection, and signaling of singlet oxygen in photosynthetic organisms. Antioxidants Redox Signal.

Fischer, B.B., Ledford, H.K., Wakao, S., Huang, S.Y.G., Casero, D., Pellegrini, M., Merchant, S.S., Koller, A., Eggen, R.I.L., and Niyogi, K.K. (2012). Singlet oxygen resistant 1 links reactive electrophile signaling to singlet oxygen acclimation in Chlamydomonas. Proc Natl Acad Sci USA **109**: E1302–E1311.

Flannery, S.E., Hepworth, C., Wood, W.H.J., Pastorelli, F., Hunter, C.N., Dickman, M.J., Jackson, P.J., and Johnson, M.P. (2021). Developmental acclimation of the thylakoid proteome to light intensity in *Arabidopsis*. Plant J. **105**: 223–244.

Flors, C., Fryer, M.J., Waring, J., Reeder, B., Bechtold, U., Mullineaux, P.M., Nonell, S., Wilson, M.T., and Baker, N.R. (2006). Imaging the production of singlet oxygen in vivo using a new fluorescent sensor, Singlet Oxygen Sensor Green. J.Exp.Bot. **57**: 1725–1734.

Formaggio, E., Cinque, G., and Bassi, R. (2001). Functional architecture of the major light-harvesting complex from higher plants. J. Mol. Biol. **314**: 1157–1166.

Formighieri, C., Cazzaniga, S., Kuras, R., and Bassi, R. (2013). Biogenesis of photosynthetic complexes in the chloroplast of Chlamydomonas reinhardtii requires ARSA1, a homolog of prokaryotic arsenite transporter and eukaryotic TRC40 for guided entry of tail-anchored proteins. Plant J. **73**: 850–861.

Formighieri, C., Franck, F., and Bassi, R. (2012). Regulation of the pigment optical density of an algal cell: filling the gap between photosynthetic productivity in the laboratory and in mass culture. J Biotechnol **162**: 115–123.

Förster, T. (1965). Delocalization excitation and excitation transfer. Mod. quantum Chem.

Förster, T. (1948). Zwischenmolekulare Energiewanderung und Fluoreszenz. Ann. Phys. **437**: 55-75 (published online 2004).

Franck, F., Juneau, P., and Popovic, R. (2002). Resolution of the Photosystem I and Photosystem II contributions to chlorophyll fluorescence of intact leaves at room temperature. Biochim. Biophys. Acta - Bioenerg. **1556**: 239–246.

Frank, H.A. and Cogdell, R.J. (1996). Carotenoids in Photosynthesis. Photochem. Photobiol. **63**:

257–264.

Freudenberg, R.A., Baier, T., Einhaus, A., Wobbe, L., and Kruse, O. (2021). High cell density cultivation enables efficient and sustainable recombinant polyamine production in the microalga Chlamydomonas reinhardtii. Bioresour. Technol. **323**.

Friedland, N., Negi, S., Vinogradova-Shah, T., Wu, G., Ma, L., Flynn, S., Kumssa, T., Lee, C.H., and Sayre, R.T. (2019). Fine-tuning the photosynthetic light harvesting apparatus for improved photosynthetic efficiency and biomass yield. Sci. Rep. **9**: 1–12.

Fuciman, M., Enriquez, M.M., Polívka, T., Dall'Osto, L., Bassi, R., and Frank, H.A. (2012). Role of xanthophylls in light harvesting in green plants: A Spectroscopic investigation of mutant LHCII and Lhcb pigment-protein complexes. J. Phys. Chem. B **116**: 3834–3849.

Gaffron, H. and Wohl, K. (1936). (GE) Theory of assimilation. Naturwissenschaften **24**: 81–90.

Galka, P., Santabarbara, S., Khuong, T.T.H., Degand, H., Morsomme, P., Jennings, R.C., Boekema, E.J., and Caffarri, S. (2012). Functional analyses of the plant photosystem I-light-harvesting complex II supercomplex reveal that light-harvesting complex II loosely bound to photosystem ii is a very efficient antenna for photosystem I in state II. Plant Cell **24**: 2963–2978.

García-Alcalde, F., Okonechnikov, K., Carbonell, J., Cruz, L.M., Götz, S., Tarazona, S., Dopazo, J., Meyer, T.F., and Conesa, A. (2012). Qualimap: evaluating next-generation sequencing alignment data. Bioinformatics **28**: 2678–2679.

García-Plazaola, J.I., Portillo-Estrada, M., Fernández-Marín, B., Kännaste, A., and Niinemets, Ü. (2017). Emissions of carotenoid cleavage products upon heat shock and mechanical wounding from a foliose lichen. Env. Exp Bot **133**: 87–97.

Gerotto, C., Franchin, C., Arrigoni, G., and Morosinotto, T. (2015). In vivo identification of Photosystem II Light Harvesting complexes interacting with Photosystem II subunit S. Plant Physiol. **168**: 1747--U1105.

Gilmore, A.M. and Yamamoto, H.Y. (1991a). Resolution of lutein and zeaxanthin using a non-endcapped, lightly carbon-loaded C18 high-performance liquid chromatographic column. J. Chromatogr. A **543**: 137–145.

Gilmore, A.M. and Yamamoto, H.Y. (1991b). Zeaxanthin Formation and Energy-Dependent Fluorescence Quenching in Pea Chloroplasts under Artificially Mediated Linear and Cyclic Electron Transport1. Plant Physiol. **96**: 635–643.

Gimpel, J.A., Henríquez, V., and Mayfield, S.P. (2015). In metabolic engineering of eukaryotic microalgae: Potential and challenges come with great diversity. Front. Microbiol. **6**: 1376.

Głowacka, K., Kromdijk, J., Kucera, K., Xie, J., Cavanagh, A.P., Leonelli, L., Leakey, A.D.B., Ort, D.R., Niyogi, K.K., and Long, S.P. (2018). Photosystem II Subunit S overexpression increases the efficiency of water use in a field-grown crop. Nat. Commun. **9**.

Goh, C.H., Jang, S., Jung, S., Kim, H.S., Kang, H.G., Park, Y. Il, Bae, H.J., Lee, C.H., and An, G. (2009). Rice phot1a mutation reduces plant growth by affecting photosynthetic responses to light during early seedling growth. Plant Mol. Biol. **69**: 605–619.

Golding, A.J. and Johnson, G.N. (2003). Down-regulation of linear and activation of cyclic electron transport during drought. Planta **218**: 107–114.

Goldschmidt-Clermont, M. and Bassi, R. (2015). Sharing light between two photosystems: mechanism of state transitions. Curr. Opin. Plant Biol. **25**: 71–78.

Gómez, S.M., Bil', K.Y., Aguilera, R., Nishio, J.N., Faull, K.F., and Whitelegge, J.P. (2003). Transit Peptide Cleavage Sites of Integral Thylakoid Membrane Proteins. Mol. Cell. Proteomics **2**: 1068–1085.

Gorman, A.A. and Rodgers, M.A.J. (1992). Current perspectives of singlet oxygen detection in biological environments. J Photochem Photobiol. **14**: 159–176.

Gotoh, E., Suetsugu, N., Yamori, W., Ishishita, K., Kiyabu, R., Fukuda, M., Higa, T., Shirouchi, B., and Wada, M. (2018). Chloroplast accumulation response enhances leaf photosynthesis and plant biomass production. Plant Physiol. **178**: 1358–1369.

Götz, S., García-Gómez, J.M., Terol, J., Williams, T.D., Nagaraj, S.H., Nueda, M.J., Robles, M., Talón, M., Dopazo, J., and Conesa, A. (2008). High-throughput functional annotation and data mining with the Blast2GO suite. Nucleic Acids Res. **36**: 3420–3435.

Granick, S. and Porter, K.R. (1947). THE STRUCTURE OF THE SPINACH CHLOROPLAST AS INTERPRETED WITH THE ELECTRON MICROSCOPE. Am. J. Bot. **34**: 545–550.

Grebe, S., Trotta, A., Bajwa, A.A., Suorsa, M., Gollan, P.J., Jansson, S., Tikkanen, M., and Aro, E.M. (2019). The unique photosynthetic apparatus of pinaceae: Analysis of photosynthetic complexes in Picea abies. J. Exp. Bot. **70**.

Grinzato, A., Albanese, P., Marotta, R., Swuec, P., Saracco, G., Bolognesi, M., Zanotti, G., and Pagliano, C. (2020). High-Light versus Low-Light: Effects on Paired Photosystem II Supercomplex Structural Rearrangement in Pea Plants. Int. J. Mol. Sci. **21**: 8643.

Gu, J., Zhou, Z., Li, Z., Chen, Y., Wang, Z., and Zhang, H. (2017). Rice (Oryza sativa L.) with reduced chlorophyll content exhibit higher photosynthetic rate and efficiency, improved canopy light distribution, and greater yields than normally pigmented plants. F. Crop. Res. **200**: 58–70.

Guardini, Z., Bressan, M., Caferri, R., Bassi, R., and Dall'Osto, L. (2020). Identification of a pigment cluster catalysing fast photoprotective quenching response in CP29. Nat. Plants **6**: 303–313.

Guardini, Z., Dall'Osto, L., Barera, S., Bassi, R., Jaberi, M., Cazzaniga, S., Vitulo, N., and Bassi, R. (2021). High Carotenoid Mutants of Chlorella vulgaris Show Enhanced Biomass Yield under High Irradiance.

Guardini, Z., Gomez, R.L., Caferri, R., Stuttmann, J., Dall'Osto, L., and Bassi, R. (2022). Thylakoid grana stacking revealed by multiplex genome editing of LHCII encoding genes. Preprint: 2021.12.31.474624.

Guarnieri, M.T., Nag, A., Smolinski, S.L., Darzins, A., Seibert, M., and Pienkos, P.T. (2011). Examination of triacylglycerol biosynthetic pathways via de novo transcriptomic and proteomic analyses in an unsequenced microalga. PLoS One **6**: e25851.

Gunning, B., Koenig, F., and Govindjee (2006). A Dedication to Pioneers of Research on Chloroplast Structure. In The structure and function of plastids, R.R. Wise and J.K. Hoober, eds (Springer: Dordrecht, The Netherlands), pp. xxiii–xxxi.

Haldrup, A., Naver, H., and Scheller, H.V. (1999). The interaction between plastocyanin and photosystem I is inefficient in transgenic Arabidopsis plants lacking the PSI-N subunit of photosystem. Plant J. **17**: 689–698.

Haldrup, A., Simpson, D.J., and Scheller, H.V. (2000). Down-regulation of the PSI-F Subunit of Photosystem I (PSI) in Arabidopsis thaliana: THE PSI-F SUBUNIT IS ESSENTIAL FOR PHOTOAUTOTROPHIC GROWTH AND CONTRIBUTES TO ANTENNA FUNCTION *. J. Biol. Chem. **275**: 31211–31218.

Hambourger, M., Moore, G.F., Kramer, D.M., Gust, D., Moore, A.L., and Moore, T.A. (2009). Biology and technology for photochemical fuel production. **38**: 25–35.

Haniewicz, P., De Sanctis, D., Buchel, C., Schroder, W.P., Loi, M.C., Kieselbach, T., Bochtler, M., and Piano, D. (2013). Isolation of monomeric photosystem II that retains the subunit PsbS. Photosynt.Res. **118**: 199–207.

Hankamer, B., Morris, E., Nield, J., Gerle, C., and Barber, J. (2001). Three-Dimensional Structure of the Photosystem II Core Dimer of Higher Plants Determined by Electron Microscopy. J. Struct. Biol. **135**: 262–269.

Hart, J.E., Sullivan, S., Hermanowicz, P., Petersen, J., Aranzazú Diaz-Ramos, L., Hoey, D.J., Łabuz, J., and Christie, J.M. (2019). Engineering the phototropin photocycle improves photoreceptor performance and plant biomass production. Proc. Natl. Acad. Sci. U. S. A. **116**: 12550–12557.

Härtel, H., Lokstein, H., Grimm, B., and Rank, B. (1996). Kinetic studies on the xanthophyll cycle in Barley leaves: Influence of antenna size and relations to nonphotochemical chlorophyll fluorescence quenching. Plant Physiol. **110**: 471–482.

Havaux, M. (2003). Spontaneous and thermoinduced photon emission: new methods to detect and quantify oxidative stress in plants. Trends Plant Sci. **8**: 409–413.

Havaux, M., Dall'Osto, L., and Bassi, R. (2007). Zeaxanthin has enhanced antioxidant capacity with respect to all other xanthophylls in arabidopsis leaves and functions independent of binding to PSII antennae. Plant Physiol. **145**: 1506–1520.

Havaux, M., Dall'Osto, L., Cuiné, S., Giuliano, G., and Bassi, R. (2004). The Effect of Zeaxanthin As the only Xanthophyll on the Structure and Function of the Photosynthetic Apparatus in Arabidopsis thaliana. J. Biol. Chem. **279**: 13878–13888.

Havaux, M., Eymery, F., Porfirova, S., Rey, P., and Dörmann, P. (2005). Vitamin E protects against photoinhibition and photooxidative stress in Arabidopsis thaliana. Plant Cell. **17**: 3451–3469.

Havaux, M. and Niyogi, K.K. (1999). The violaxanthin cycle protects plants from photooxidative damage by more than one mechanism. Proc.Natl.Acad.Sci.U.S.A **96**: 8762–8767.

Havaux, M. and Tardy, F. (1996). Temperature-dependent adjustment of the thermal stability of

photosystem II in vivo: possible involvement of xanthophyll-cycle pigments. Planta 1996 1983 **198**: 324–333.

Heaton, E.A., Dohleman, F.G., and Long, S.P. (2008). Meeting US biofuel goals with less land: the potential of Miscanthus. Glob. Chang. Biol. **14**: 2000–2014.

Heber, U. and Walker, D. (1992). Concerning a Dual Function of Coupled Cyclic Electron Transport in Leaves. Plant Physiol. **100**: 1621–1626.

Heinz, S., Rast, A., Shao, L., Gutu, A., Gügel, I.L., Heyno, E., Labs, M., Rengstl, B., Viola, S., Nowaczyk, M.M., Leister, D., and Nickelsen, J. (2016). Thylakoid membrane architecture in Synechocystis depends on CurT, a homolog of the granal CURVATURE THYLAKOID1 proteins. Plant Cell **28**: 2238–2260.

Heitz, E. (1936). Untersuchungen Über den Bau der Plastiden. Planta 1936 261 **26**: 134–163.

Hepworth, C., Wood, W.H.J., Emrich-Mills, T.Z., Proctor, M.S., Casson, S., and Johnson, M.P. (2021). Dynamic thylakoid stacking and state transitions work synergistically to avoid acceptor-side limitation of photosystem I. Nat. Plants **7**: 87–98.

Herrin, D.L., Battey, J.F., Greer, K., and Schmidt, G.W. (1992). Regulation of Chlorophyll Apoprotein Expression and Accumulation - Requirements for Carotenoids and Chlorophyll. J. Biol. Chem. **267**: 8260–8269.

Hobe, S., Förster, R., Klingler, J., and Paulsen, H. (1995). N-Proximal Sequence Motif in Light-Harvesting Chlorophyll a/b-Binding Protein Is Essential for the Trimerization of Light-Harvesting Chlorophyll alb Complex. Biochemistry **34**: 10224–10228.

Holt, N.E., Zigmantas, D., Valkunas, L., Li, X.P., Niyogi, K.K., and Fleming, G.R. (2005). Carotenoid cation formation and the regulation of photosynthetic light harvesting. Science (80-.). **307**: 433–436.

Holzwarth, A.R., Miloslavina, Y., Nilkens, M., and Jahns, P. (2009). Identification of two quenching sites active in the regulation of photosynthetic light-harvesting studied by time-resolved fluorescence. Chem. Phys. Lett. **483**: 262–267.

Horton, P., Ruban, A. V., Rees, D., Pascal, A.A., Noctor, G., and Young, A.J. (1991). Control of the light-harvesting function of chloroplast membranes by aggregation of the LHCII chlorophyll—protein complex. FEBS Lett. **292**: 1–4.

Horton, P., Ruban, A. V., and Walters, R.G. (1996). Regulation of light harvesting in green plants. Annu. Rev. Plant Physiol. Plant Mol. Biol. **47**: 655–684.

Horwitz, W. (2000). Official methods of analysis of AOAC international.

Hu, Q., Sommerfeld, M., Jarvis, E., Ghirardi, M., Posewitz, M., Seibert, M., and Darzins, A. (2008). Microalgal triacylglycerols as feedstocks for biofuel production: perspectives and advances. Plant J **54**: 621–639.

Huesemann, M.H., Hausmann, T.S., Bartha, R., Aksoy, M., Weissman, J.C., and Benemann, J.R. (2009). Biomass productivities in wild type and pigment mutant of Cyclotella sp (Diatom). Appl Biochem Biotechnol **157**: 507–526.

Ihnatowicz, A., Pesaresi, P., Varotto, C., Richly, E., Schneider, A., Jahns, P., Salamini, F., and Leister, D. (2004). Mutants for photosystem I subunit D of Arabidopsis thaliana: effects on photosynthesis, photosystem I stability and expression of nuclear genes for chloroplast functions. Plant J. **37**: 839–852.

Ioannidis, N.E., Papadatos, S., and Daskalakis, V. (2016). Energizing the light harvesting antenna: Insight from CP29. Biochim. Biophys. Acta - Bioenerg. **1857**: 1643–1650.

Ishida, S., Uebayashi, N., Tazoe, Y., Ikeuchi, M., Homma, K., Sato, F., and Endo, T. (2014). Diurnal and Developmental Changes in Energy Allocation of Absorbed Light at PSII in Field-Grown Rice. Plant Cell Physiol. **55**: 171–182.

Iwai, M., Roth, M.S., and Niyogi, K.K. (2018). Subdiffraction-resolution live-cell imaging for visualizing thylakoid membranes. Plant J. **96**: 233–243.

Jacquier, N., Choudhary, V., Mari, M., Toulmay, A., Reggiori, F., and Schneiter, R. (2011). Lipid droplets are functionally connected to the endoplasmic reticulum in Saccharomyces cere. J Cell Sci **124**: 2424–2437.

Janßen, H.J. and Steinbüchel, A. (2014). Fatty acid synthesis in Escherichia coli and its applications towards the production of fatty acid based biofuels. Biotechnol. Biofuels **7**: 1–26.

Jansson, S. (1999). A guide to the Lhc genes and their relatives in Arabidopsis. Trends Plant Sci. **4**: 236–240.

Jarvi, S., Suorsa, M., and Aro, E.M. (2015). Photosystem II repair in plant chloroplasts - Regulation, assisting proteins and shared components with photosystem II biogenesis. Biochim. Biophys. Acta-Bioenergetics **1847**: 900–909.

Jensen, P.E., Haldrup, A., Zhang, S., and Scheller, H.V. (2004). The PSI-O Subunit of Plant Photosystem I Is Involved in Balancing the Excitation Pressure between the Two Photosystems. J. Biol. Chem. **279**: 24212–24217.

Jin, H., Li, M., Duan, S., Fu, M., Dong, X., Liu, B., Feng, D., Wang, J., and Wang, H. Bin (2016). Optimization of light-harvesting pigment improves photosynthetic efficiency. Plant Physiol. **172**: 1720–1731.

Jinek, M., Chylinski, K., Fonfara, I., Hauer, M., Doudna, J.A., and Charpentier, E. (2012). A programmable dual-RNA-guided DNA endonuclease in adaptive bacterial immunity. Science (80-.). **337**: 816–821.

Johansson, E., Olsson, O., and Nyström, T. (2004). Progression and specificity of protein oxidation in the life cycle of Arabidopsis thaliana. J. Biol. Chem. **279**: 22204–22208.

Johnson, M.P., Goral, T.K., Duffy, C.D., Brain, A.P., Mullineaux, C.W., and Ruban, A. V (2011). Photoprotective energy dissipation involves the reorganization of Photosystem II light-harvesting complexes in the grana membranes of spinach chloroplasts. Plant Cell **23**: 1468–1479.

Johnson, M.P., Havaux, M., Triantaphylidès, C., Ksas, B., Pascal, A.A., Robert, B., Davison, P.A., Ruban, A. V., and Horton, P. (2007). Elevated Zeaxanthin Bound to Oligomeric LHCII Enhances the Resistance of Arabidopsis to Photooxidative Stress by a Lipid-

protective, Antioxidant Mechanism *. J. Biol. Chem. **282**: 22605–22618.

Joliot, P. (2003). Period-four oscillations of the flash-induced oxygen formation in photosynthesis. Photosynth. Res. **76**: 65–72.

Joliot, P. and Joliot, A. (1977). Evidence for a double hit process in photosystem II based on fluorescence studies. Biochim.Biophys.Acta **462**: 559–574.

Jones, C.S. and Mayfield, S.P. (2012). Algae biofuels: versatility for the future of bioenergy. Curr. Opin. Biotech. **23**: 346–351.

Jordan, P., Fromme, P., Witt, H.T., Klukas, O., Saenger, W., and Krauß, N. (2001). Three-dimensional structure of cyanobacterial photosystem I at 2.5 Å resolution. Nat. 2001 4116840 **411**: 909–917.

Kasahara, M., Kagawa, T., Oikawa, K., Suetsugu, N., Miyao, M., and Wada, M. (2002). Chloroplast avoidance movement reduces photodamage in plants. Nature **420**: 829–832.

Kim, C., Meskauskiene, R., Zhang, S., Lee, K.P., Ashok, M.L., Blajecka, K., Herrfurth, C., Feussner, I., and Apela, K. (2012). Chloroplasts of Arabidopsis are the source and a primary target of a plant-specific programmed cell death signaling pathway. Plant Cell. **24**: 3026–3039.

Kim, E.H., Li, X.P., Razeghifard, R., Anderson, J.M., Niyogi, K.K., Pogson, B.J., and Chow, W.S. (2009). The multiple roles of light-harvesting chlorophyll a/b-protein complexes define structure and optimize function of Arabidopsis chloroplasts: A study using two chlorophyll b-less mutants. Biochim. Biophys. Acta - Bioenerg. **1787**: 973–984.

Kim, J., Lee, S., Baek, K., and Jin, E.S. (2020). Site-Specific Gene Knock-Out and On-Site Heterologous Gene Overexpression in Chlamydomonas reinhardtii via a CRISPR-Cas9-Mediated Knock-in Method. Front. Plant Sci. **11**: 306.

Kim, J.Y.H., Kwak, H.S., Sung, Y.J., Choi, H. Il, Hong, M.E., Lim, H.S., Lee, J.-H., Lee, S.Y., and Sim, S.J. (2016). Microfluidic high-throughput selection of microalgal strains with superior photosynthetic productivity using competitive phototaxis. Sci. Rep. **6**: 21155.

Kim, S., Fujitsuka, M., and Majima, T. (2013). Photochemistry of singlet oxygen sensor green. J. Phys. Chem. B **117**: 13985–13992.

Kirchhoff, H. (2019). Chloroplast ultrastructure in plants. New Phytol. **223**: 565–574.

Kirchhoff, H., Haase, W., Haferkamp, S., Schott, T., Borinski, M., Kubitscheck, U., and Rögner, M. (2007). Structural and functional self-organization of Photosystem II in grana thylakoids. Biochim. Biophys. Acta - Bioenerg. **1767**: 1180–1188.

Kirchhoff, H., Hall, C., Wood, M., Herbstová, M., Tsabari, O., Nevo, R., Charuvi, D., Shimoni, E., and Reich, Z. (2011). Dynamic control of protein diffusion within the granal thylakoid lumen. Proc. Natl. Acad. Sci. U. S. A. **108**: 20248–20253.

Kirst, H., Gabilly, S.T., Niyogi, K.K., Lemaux, P.G., and Melis, A. (2017). Photosynthetic antenna engineering to improve crop yields. Planta **245**: 1009–1020.

Kirst, H., Garcia-Cerdan, J.G., Zurbriggen, A., Ruehle, T., and Melis, A. (2012). Truncated

photosystem chlorophyll antenna size in the green microalga Chlamydomonas reinhardtii upon deletion of the TLA3-CpSRP43 gene. Plant Physiol **160**: 2251–2260.

Kleine, T. and Leister, D. (2016). Retrograde signaling: organelles go networking. Biochim Biophys Acta **1857**: 1313–1325.

Klimmek, F., Sjodin, A., Noutsos, C., Leister, D., Jansson, S., Sjödin, A., Noutsos, C., Leister, D., and Jansson, S. (2006). Abundantly and Rarely Expressed Lhc Protein Genes Exhibit Distinct Regulation Patterns in Plants. Plant Physiol. **140**: 793–804.

Kok, B. (1956). On the inhibition of photosynthesis by intense light. Biochim.Biophys.Acta **21**: 234–244.

Kondo, T., Pinnola, A., Chen, W.J., Dall'Osto, L., Bassi, R., and Schlau-Cohen, G.S. (2017). Single-molecule spectroscopy of LHCSR1 protein dynamics identifies two distinct states responsible for multi-timescale photosynthetic photoprotection. Nat. Chem. 2017 98 **9**: 772–778.

Koochak, H., Puthiyaveetil, S., Mullendore, D.L., Li, M., and Kirchhoff, H. (2019). The structural and functional domains of plant thylakoid membranes. Plant J. **97**: 412–429.

Kouřil, R., Dekker, J.P., and Boekema, E.J. (2012). Supramolecular organization of photosystem II in green plants. Biochim. Biophys. Acta - Bioenerg. **1817**: 2–12.

Kouřil, R., Wientjes, E., Bultema, J.B., Croce, R., and Boekema, E.J. (2013). High-light vs. low-light: Effect of light acclimation on photosystem II composition and organization in Arabidopsis thaliana. **1827**: 411–419.

Kovács, L., Damkjær, J., Kereïche, S., Ilioaia, C., Ruban, A. V., Boekema, E.J., Jansson, S., and Horton, P. (2006). Lack of the light-harvesting complex CP24 affects the structure and function of the grana membranes of higher plant chloroplasts. Plant Cell **18**: 3106–3120.

Kramer, D.M. and Evans, J.R. (2011). The importance of energy balance in improving photosynthetic productivity. Plant Physiol. **155**: 70–78.

Kramer, D.M., Johnson, G., Kiirats, O., and Edwards, G.E. (2004). New fluorescence parameters for the determination of QA redox state and excitation energy fluxes. Photosynth. Res. **79**: 209–218.

Krieger-Liszkay, A. (2005). Singlet oxygen production in photosynthesis. J. Exp. Bot. **56**: 337–346.

Krieger-Liszkay, A., Fufezan, C., and Trebst, A. (2008). Singlet oxygen production in photosystem II and related protection mechanism (Springer Netherlands).

Kromdijk, J., Głowacka, K., Leonelli, L., Gabilly, S.T., Iwai, M., Niyogi, K.K., and Long, S.P. (2016). Improving photosynthesis and crop productivity by accelerating recovery from photoprotection. Science (80-.). **354**: 857–861.

Kropat, J., Hong-Hermesdorf, A., Casero, D., Ent, P., Castruita, M., Pellegrini, M., Merchant, S.S., and Malasarn, D. (2011). A revised mineral nutrient supplement increases biomass and growth rate in Chlamydomonas reinhardtii. Plant J. **66**: 770–780.

Kühlbrandt, W., Wang, D.N., and Fujiyoshi, Y. (1994). Atomic model of plant light-harvesting complex by electron crystallography. Nat. 1994 3676464 **367**: 614–621.

Külheim, C., Ågren, J., and Jansson, S. (2002). Rapid regulation of light harvesting and plant fitness in the field. Science (80-.). **297**: 91–93.

Kuttkat, A., Hartmann, A., Hobe, S., and Paulsen, H. (1996). The C-terminal domain of light-harvesting chlorophyll-a/b-binding protein is involved in the stabilisation of trimeric light-harvesting complex. Eur. J. Biochem. **242**: 288–292.

Kyle, D.J., Staehelin, L.A., and Arntzen, C.J. (1983). Lateral mobility of the light-harvesting complex in chloroplast membranes controls excitation energy distribution in higher plants. Arch.Biochem.Biophys. **222**: 527–541.

Laemmli, U.K. (1970). Cleavage of structural proteins during the assembly of the head of bacteriophage T4. Nature.

Lafarga, T. (2019). Effect of microalgal biomass incorporation into foods: Nutritional and sensorial attributes of the end products. Algal Res. **41**: 101566.

Langridge, P. (2014). Reinventing the Green Revolution by Harnessing Crop Mutant Resources. Plant Physiol. **166**: 1682–1683.

Lavergne, J. and Joliot, P. (1991). Restricted Diffusion in Photosynthetic Membranes. Trends Biochem. **16**: 129–134.

Lavergne, J. and Trissl, H.W. (1995). Theory of fluorescence induction in photosystem II: derivation of analytical expressions in a model including exciton-radical-pair equilibrium and restricted energy transfer between photosynthetic units. Biophys. J. **68**: 2474–2492.

Ledford, H.K., Chin, B.L., and Niyogi, K.K. (2007). Acclimation to singlet oxygen stress in Chlamydomonas reinhardtii. Eukaryot Cell **6**: 919–930.

Leu, S. and Boussiba, S. (2014). Advances in the Production of High-Value Products by Microalgae. Ind. Biotechnol. **10**: 169–183.

Li, H. and Durbin, R. (2009). Fast and accurate short read alignment with Burrows–Wheeler transform. Bioinformatics **25**: 1754–1760.

Li, X.-P., Bjo, O., Rkman, È., Shih, C., Grossman, A.R., Rosenquist, M., Jansson, S., and Niyogi, K.K. (2000). A pigment-binding protein essential for regulation of photosynthetic light harvesting.

Li, X. et al. (2019a). A genome-wide algal mutant library and functional screen identifies genes required for eukaryotic photosynthesis. Nat. Genet. 2019 514 **51**: 627–635.

Li, X.P., Gilmore, A.M., Caffarri, S., Bassi, R., Golan, T., Kramer, D., and Niyogi, K.K. (2004). Regulation of photosynthetic light harvesting involves intrathylakoid lumen pH sensing by the PsbS protein. J. Biol. Chem. **279**: 22866–22874.

Li, X.P., Muller-Moule, P., Gilmore, A.M., and Niyogi, K.K. (2002a). PsbS-dependent enhancement of feedback de-excitation protects photosystem II from photoinhibition. Proc.Natl.Acad.Sci.U.S.A **99**: 15222–15227.

Li, X.P., Phippard, A., Pasari, J., and Niyogi, K.K. (2002b). Structure-function analysis of photosystem II subunit S (PsbS) in vivo. In Functional Plant Biology (CSIRO PUBLISHING), pp. 1131–1139.

Li, Y., Liu, B., Zhang, J., Kong, F., Zhang, L., Meng, H., Li, W., Rochaix, J.D., Li, D., and Peng, L. (2019b). OHP1, OHP2, and HCF244 form a transient functional complex with the photosystem II reaction center. Plant Physiol. **179**: 195–208.

Li, Z., Ahn, T.K., Avenson, T.J., Ballottari, M., Cruz, J.A., Kramer, D.M., Bassi, R., Fleming, G.R., Keasling, J.D., and Niyogi, K.K. (2009a). Lutein Accumulation in the Absence of Zeaxanthin Restores Nonphotochemical Quenching in the Arabidopsis thaliana npq1 Mutant. Plant Cell **21**: 1798.

Li, Z., Wakao, S., Fischer, B.B., and Niyogi, K.K. (2009b). Sensing and Responding to Excess Light Excess light (EL): a relative term that describes the absorption of light that exceeds photosynthetic capacity. Annu. Rev. Plant Biol.

Liberton, M., Austin, J.R., Howard Berg, R., and Pakrasi, H.B. (2011). Insights into the complex 3-D architecture of thylakoid membranes in the unicellular cyanobacterium Cyanothece sp. ATCC 51142. Plant Signal. Behav. **6**: 566–569.

Ling, Q., Huang, W., Baldwin, A., and Jarvis, P. (2012). Chloroplast biogenesis is regulated by direct action of the ubiquitin-proteasome system. Science (80-.). **338**: 655–659.

Ling, Q. and Jarvis, P. (2015). Regulation of chloroplast protein import by the ubiquitin E3 ligase SP1 is important for stress tolerance in plants. Curr. Biol. **25**: 2527–2534.

Liu, Z., Yan, H., Wang, K., Kuang, T., Zhang, J., Gui, L., An, X., and Chang, W. (2004). Crystal structure of spinach major light-harvesting complex at 2.72 Å resolution. Nature **428**: 287–292.

Livingston, A.K., Cruz, J.A., Kohzuma, K., Dhingra, A., and Kramer, D.M. (2010). An arabidopsis mutant with high cyclic electron flow around photosystem i (hcef) involving the nadphdehydrogenase complex. Plant Cell **22**: 221–233.

Lokstein, H., Tian, L., Polle, J.E., and DellaPenna, D. (2002). Xanthophyll biosynthetic mutants of Arabidopsis thaliana: altered nonphotochemical quenching of chlorophyll fluorescence is due to changes in Photosystem II antenna size and stability. Biochim.Biophys.Acta **1553**: 309–319.

Long, S.P., Zhu, X.G., Naidu, S.L., and Ort, D.R. (2006). Can improvement in photosynthesis increase crop yields? Plant, Cell Environ. **29**: 315–330.

Lunde, C., Jensen, P.E., Haldrup, A., Knoetzel, J., and Scheller, H. V. (2000). The PSI-H subunit of photosystem I is essential for state transitions in plant photosynthesis. Nat. 2000 4086812 **408**: 613–615.

Malkin, S., Armond, P.A., Mooney, H.A., and Fork, D.C. (1981). Photosystem II photosynthetic unit sizes from fluorescence induction in leaves. Correlation to photosynthetic capacity. Plant Physiol. **67**: 570–579.

Malnoë, A. (2018). Photoinhibition or photoprotection of photosynthesis? Update on the (newly termed) sustained quenching component qH. Environ. Exp. Bot. **154**: 123–133.

Malnoë, A., Schultink, A., Shahrasbi, S., Rumeau, D., Havaux, M., and Niyogi, K.K. (2018). The plastid lipocalin LCNP is required for sustained photoprotective energy dissipation in arabidopsis. Plant Cell **30**: 196–208.

Malzahn, A., Lowder, L., and Qi, Y. (2017). Plant genome editing with TALEN and CRISPR. Cell Biosci. **7**: 1–18.

Maoka, T. (2020). Carotenoids as natural functional pigments. J. Nat. Med. **74**.

De Marchin, T., Ghysels, B., Nicolay, S., and Franck, F. (2014). Analysis of PSII antenna size heterogeneity of Chlamydomonas reinhardtii during state transitions. Biochim. Biophys. Acta - Bioenerg. **1837**: 121–130.

Margulies, M.M. (1966). Effect of Chloramphenicol on Formation of Chloroplast Structure and Protein During Greening of Etiolated Leaves of Phaseolus vulgaris. Plant Physiol. **41**: 992–1003.

Mattoo, A., K., Marder, J.B., and Edelman, M. (1989). Dynamics of the photosystem II reaction center. Cell **56**: 241–246.

Mattoo, A.K., Giardi, M.-T., Raskind, A., and Edelman, M. (1999). Dynamic metabolism of photosystem II reaction center proteins and pigments. Physiol. Plant. **107**: 454–461.

Maxwell, K. and Johnson, G.N. (2000). Chlorophyll fluorescence—a practical guide. J Exp Bot **51**: 659–668.

Meagher, E., Rangsrikitphoti, P., Faridi, B., Zamzam, G., and Durnford, D.G. (2021). Photoacclimation to high-light stress in Chlamydomonas reinhardtii during conditional senescence relies on generating pH-dependent, high-quenching centres. Plant Physiol. Biochem. **158**: 136–145.

Melis, A. (1999). Photosystem-II damage and repair cycle in chloroplasts: what modulates the rate of photodamage ? Trends Plant Sci. **4**: 130–135.

Melis, A. (2009). Solar energy conversion efficiencies in photosynthesis: minimizing the chlorophyll antennae to maximize efficiency. Plant Sci **177**: 272–280.

Menon, K.R., Balan, R., and Suraishkumar, G.K. (2013). Stress induced lipid production in Chlorella vulgaris: relationship with specific intracellular reactive species levels. Biotechnol Bioeng **110**: 1627–1636.

Miller, K.R. and Lyon, M.K. (1985). Do we really know why chloroplast membranes stack? Trends Biochem. Sci. **10**: 219–222.

Mitchell, A.L. et al. (2019). InterPro in 2019: improving coverage, classification and access to protein sequence annotations. Nucleic Acids Res. **47**: D351–D360.

Mitra, M., Kirst, H., Dewez, D., and Melis, A. (2012). Modulation of the light-harvesting chlorophyll antenna size in Chlamydomonas reinhardtii by TLA1 gene over-expression and RNA interference. Phil Trans R Soc B **367**: 3430–3443.

Moejes, F.W. et al. (2017). A systems-wide understanding of photosynthetic acclimation in algae and higher plants. J. Exp. Bot. **68**: 2667–2681.

Mojica, F.J.M., Díez-Villaseñor, C., García-Martínez, J., and Soria, E. (2005). Intervening sequences of regularly spaced prokaryotic repeats derive from foreign genetic elements. J. Mol. Evol. **60**: 174–182.

Monteith JL (1977). Climate and the efficiency of crop production in Britain. Philos. Trans. R. Soc. Lond. Ser. B **281**: 277–294.

Montillet, J.L., Cacas, J.L., Garnier, L., Montane, M.H., Douki, T., Bessoule, J.J., Polkowska-Kowalczyk, L., Maciejewska, U., Agnel, J.P., Vial, A., and Triantaphylides, C. (2004). The upstream oxylipin profile of Arabidopsis thaliana: a tool to scan for oxidative stresses. Plant J. **40**: 439–451.

Morosinotto, T., Ballottari, M., Klimmek, F., Jansson, S., and Bassi, R. (2005a). The Association of the Antenna System to Photosystem I in Higher Plants: COOPERATIVE INTERACTIONS STABILIZE THE SUPRAMOLECULAR COMPLEX AND ENHANCE RED-SHIFTED SPECTRAL FORMS *. J. Biol. Chem. **280**: 31050–31058.

Morosinotto, T., Baronio, R., and Bassi, R. (2002). Dynamics of chromophore binding to Lhc proteins in vivo and in vitro during operation of the xanthophyll cycle. J. Biol. Chem. **277**: 36913–36920.

Morosinotto, T., Mozzo, M., Bassi, R., and Croce, R. (2005b). Pigment-pigment interactions in Lhca4 antenna complex of higher plants photosystem I._ _. J. Biol. Chem. **280**: 20612–20619.

Morosinotto, T., Segalla, A., Giacometti, G.M., and Bassi, R. (2010). Purification of structurally intact grana from plants thylakoids membranes. J.Bioenerg.Biomembr. **42**: 37–45.

Mozzo, M., Dall'Osto, L., Hienerwadel, R., Bassi, R., and Croce, R. (2008). Photoprotection in the antenna complexes of photosystem II: role of individual xanthophylls in chlorophyll triplet quenching. J.Biol Chem. **283**: 6184–6192.

Müh, F. and Zouni, A. (2020). Structural basis of light-harvesting in the photosystem II core complex. Protein Sci. **29**: 1090–1119.

Müller, M.G., Lambrev, P., Reus, M., Wientjes, E., Croce, R., and Holzwarth, A.R. (2010). Singlet Energy Dissipation in the Photosystem II Light-Harvesting Complex Does Not Involve Energy Transfer to Carotenoids. Chemphyschem **11**: 1289–1296.

Müller, P., Li, X.P., and Niyogi, K.K. (2001). Non-Photochemical Quenching. A Response to Excess Light Energy. Plant Physiol. **125**: 1558–1566.

Mullineaux, C.W. (2005). Function and evolution of grana. Trends Plant Sci. **10**: 521–525.

Mullineaux, C.W. and Emlyn-Jones, D. (2005). State transitions: An example of acclimation to low-light stress. In Journal of Experimental Botany (J Exp Bot), pp. 389–393.

Münkel, R., Schmid-Staiger, U., Werner, A., and Hirth, T. (2013). Optimization of outdoor cultivation in flat panel airlift reactors for lipid production by Chlorella vulgaris. Biotechnol Bioeng **110**: 2882–2893.

Murata, N. (1969). Control of excitation transfer in photosynthesis. I. Light- induced change of chlorophyll a fluorescence in Porphyridium cruentum. Biochim.Biophys.Acta **172**: 242–

251.

Mustárdy, L. and Garab, G. (2003). Granum revisited. A three-dimensional model – where things fall into place. Trends Plant Sci. **8**: 117–122.

Nakai, A., Yamauchi, Y., Sumi, S., and Tanaka, K. (2012). Role of acylamino acid-releasing enzyme/oxidized protein hydrolase in sustaining homeostasis of the cytoplasmic antioxidative system. Planta **236**: 427–436.

Naqvi, K.R., Melo, T.B., Raju, B.B., Javorfi, T., Simidjiev, I., and Garab, G. (1997). Quenching of chlorophyll a singlets and triplets by carotenoids in light-harvesting complex of photosystem II: Comparison of aggregates with trimers. Spectrochim.Acta A **53**: 2659–2667.

Nawrocki, W.J., Liu, X., Raber, B., Hu, C., De Vitry, C., Bennett, D.I.G., and Croce, R. (2021). Molecular origins of induction and loss of photoinhibition-related energy dissipation qI. Sci. Adv. **7**: 1–14.

Nayak, L., Raval, M.K., Biswal, B., and Biswal, U.C. (2002). Topology and photoprotective role of carotenoids in photosystem II of chloroplast: a hypothesis. Photochem. Photobiol. Sci. **1**: 629–631.

Negi, S., Perrine, Z., Friedland, N., Kumar, A., Tokutsu, R., Minagawa, J., Berg, H., Barry, A.N., Govindjee, G., and Sayre, R. (2020). Light regulation of light-harvesting antenna size substantially enhances photosynthetic efficiency and biomass yield in green algae†. Plant J. **103**: 584–603.

Neilson, J.A.D. and Durnford, D.G. (2010). Structural and functional diversification of the light-harvesting complexes in photosynthetic eukaryotes. Photosynth. Res. **106**: 57–71.

Neily, M.H. et al. (2011). Enhanced polyamine accumulation alters carotenoid metabolism at the transcriptional level in tomato fruit over-expressing spermidine synthase. J. Plant Physiol. **168**: 242–252.

Nelson, N. and Ben-Shem, A. (2004). The complex architecture of oxygenic photosynthesis.

Nelson, N. and Yocum, C.F. (2006). Structure and Function of Photosystems I and II.

Nicol, L., Mascoli, V., van Amerongen, H., Croce, R., and Amsterdam, U. (2021). The quantitative contribution of different Photosystem II compartments to non-photochemical quenching in Arabidopsis. Preprint.

Nicol, L., Nawrocki, W.J., and Croce, R. (2019). Disentangling the sites of non-photochemical quenching in vascular plants. Nat. Plants **5**: 1177–1183.

Nield, J., Funk, C., and Barber, J. (2000). Supermolecular structure of photosystem II and location of the PsbS protein. Philos. Trans. R. Soc. London. Ser. B Biol. Sci. **355**: 1337–1344.

Nilkens, M., Kress, E., Lambrev, P., Miloslavina, Y., Müller, M., Holzwarth, A.R., and Jahns, P. (2010). Identification of a slowly inducible zeaxanthin-dependent component of non-photochemical quenching of chlorophyll fluorescence generated under steady-state conditions in Arabidopsis. Biochim. Biophys. Acta - Bioenerg. **1797**: 466–475.

Nisar, N., Li, L., Lu, S., Khin, N.C., and Pogson, B.J. (2015). Carotenoid Metabolism in Plants. Mol. Plant **8**: 68–82.

Niyogi, K., Shih, C., Soon Chow, W., Pogson, B., DellaPenna, D., and Björkman, O. (2001). Photoprotection in a zeaxanthin- and lutein-deficient double mutant of Arabidopsis. Photosynth. Res. **67**: 139–145.

Niyogi, K.K. (1999). PHOTOPROTECTION REVISITED: Genetic and Molecular Approaches. Annu. Rev. Plant Physiol. Plant Mol. Biol. **50**: 333–359.

Niyogi, K.K. (2000). Safety valves for photosynthesis. Curr. Opin. Plant Biol. **3**: 455–460.

Niyogi, K.K., Grossman, A.R., and Björkman, O. (1998). Arabidopsis mutants define a central role for the xanthophyll cycle in the regulation of photosynthetic energy conversion. Plant Cell **10**: 1121–1134.

Niyogi, K.K. and Truong, T.B. (2013). Evolution of flexible non-photochemical quenching mechanisms that regulate light harvesting in oxygenic photosynthesis. Curr. Opin. Plant Biol. **16**: 307–314.

Novoveská, L., Ross, M.E., Stanley, M.S., Pradelles, R., Wasiolek, V., and Sassi, J.F. (2019). Microalgal Carotenoids: A Review of Production, Current Markets, Regulations, and Future Direction. Mar. Drugs 2019, Vol. 17, Page 640 **17**: 640.

Nürnberg, D.J., Morton, J., Santabarbara, S., Telfer, A., Joliot, P., Antonaru, L.A., Ruban, A. V., Cardona, T., Krausz, E., Boussac, A., Fantuzzi, A., and William Rutherford, A. (2018). Photochemistry beyond the red limit in chlorophyll f–containing photosystems. Science (80-.). **360**: 1210–1213.

Nwachukwu, I.D., Udenigwe, C.C., and Aluko, R.E. (2016). Lutein and zeaxanthin: Production technology, bioavailability, mechanisms of action, visual function, and health claim status. Trends Food Sci. Technol. **49**: 74–84.

Oberhuber, W., Dai, Z.-Y., and Edwards, G.E. (1993). Light dependence of quantum yields of Photosystem II and CO z fixation in C 3 and C 4 plants* (Kluwer Academic Publishers).

Oey, M., Ross, I.L., Stephens, E., Steinbeck, J., Wolf, J., Radzun, K.A., Kügler, J., Ringsmuth, A.K., Kruse, O., and Hankamer, B. (2013). RNAi Knock-Down of LHCBM1, 2 and 3 Increases Photosynthetic H2 Production Efficiency of the Green Alga Chlamydomonas reinhardtii. PLoS One **8**: e61375.

Olive, J. and Vallon, O. (1991). Structural organization of the thylakoid membrane: freeze-fracture and immunocytochemical analysis. J.Electron Microsc.Tech. **18**: 360–374.

Olive, J., Vallon, O., Wollman, F.A., Recouvreur, M., and Bennoun, P. (1986). Studies on the Cytochrome B6/F Complex .2. Localization of the Complex in the Thylakoid Membranes from Spinach and Chlamydomonas-Reinhardtii by Immunocytochemistry and Freeze-Fracture Analysis of B6/F Mutants. Biochim. Biophys. Acta **851**: 239–248.

Onoa, B., Schneider, A.R., Brooks, M.D., Grob, P., Nogales, E., Geissler, P.L., Niyogi, K.K., and Bustamante, C. (2014). Atomic force microscopy of photosystem II and its unit cell clustering quantitatively delineate the mesoscale variability in Arabidopsis Thylakoids. PLoS One **9**: 101470.

Ooms, M.D., Dinh, C.T., Sargent, E.H., and Sinton, D. (2016). Photon management for augmented photosynthesis. Nat. Commun. 2016 71 **7**: 1–13.

van Oort, B., Alberts, M., de Bianchi, S., Dall'Osto, L., Bassi, R., Trinkunas, G., Croce, R., and Van Amerongen, H. (2010). Effect of antenna-depletion in Photosystem II on excitation energy transfer in Arabidopsis thaliana. Biophys. J. **98**: 922–931.

Van Oort, B., Van Grondelle, R., and Van Stokkum, I.H.M. (2015). A hidden state in light-harvesting complex II revealed by multipulse spectroscopy. J. Phys. Chem. B **119**: 5184–5193.

Op Den Camp, R.G.L., Przybyla, D., Ochsenbein, C., Laloi, C., Kim, C., Danon, A., Wagner, D., Hideg, É., Göbel, C., Feussner, I., Nater, M., and Apel, K. (2003). Rapid induction of distinct stress responses after the release of singlet oxygen in Arabidopsis. Plant Cell. **15**: 2320–2332.

Ordon, J., Bressan, M., Kretschmer, C., Dall'Osto, L., Marillonnet, S., Bassi, R., and Stuttmann, J. (2020). Optimized Cas9 expression systems for highly efficient Arabidopsis genome editing facilitate isolation of complex alleles in a single generation. Funct. Integr. Genomics **20**: 151–162.

Ordon, J., Gantner, J., Kemna, J., Schwalgun, L., Reschke, M., Streubel, J., Boch, J., and Stuttmann, J. (2017). Generation of chromosomal deletions in dicotyledonous plants employing a user-friendly genome editing toolkit. Plant J. **89**: 155–168.

Ort, D.R. et al. (2015). Redesigning photosynthesis to sustainably meet global food and bioenergy demand. Proc. Natl. Acad. Sci. U. S. A. **112**: 8529–8536.

Ort, D.R., Zhu, X., and Melis, A. (2011). Optimizing antenna size to maximize photosynthetic efficiency. Plant Physiol. **155**: 79–85.

Pan, X., Li, M., Wan, T., Wang, L., Jia, C., Hou, Z., Zhao, X., Zhang, J., and Chang, W. (2011). Structural insights into energy regulation of light-harvesting complex CP29 from spinach. Nat. Struct. Mol. Biol. **18**: 309–315.

Pan, X., Liu, Z., Li, M., and Chang, W. (2013). Architecture and function of plant light-harvesting complexes II. Curr. Opin. Struct. Biol. **23**: 515–525.

Pan, X., Ma, J., Su, X., Cao, P., Chang, W., Liu, Z., Zhang, X., and Li, M. (2018). Structure of the maize photosystem I supercomplex with light-harvesting complexes I and II. Science (80-.). **360**: 1109–1113.

Pandey, R., Sahu, A., and K, V.K. (2015). Studies on light intensity distribution inside an open pond photo-bioreactor. Bioprocess Biosyst. Eng.

Paolillo, D.J.J. and Reighard, J.A. (2011). ON THE RELATIONSHIP BETWEEN MATURE STRUCTURE AND ONTOGENY IN THE GRANA OF CHLOROPLASTS. https://doi.org/10.1139/b67-083 **45**: 773–782.

Papadatos, S., Charalambous, A.C., and Daskalakis, V. (2017). A pathway for protective quenching in antenna proteins of Photosystem II. Sci. Rep. **7**.

Park, J.J., Wang, H., Gargouri, M., Deshpande, R.R., Skepper, J.N., Holguin, F.O., Juergens,

M.T., Shachar-Hill, Y., Hicks, L.M., and Gang, D.R. (2015). The response of Chlamydomonas reinhardtii to nitrogen deprivation: a systems biology analysis. Plant J. **81**: 611–624.

Park, S., Steen, C.J., Lyska, D., Fischer, A.L., Endelman, B., Iwai, M., Niyogi, K.K., and Fleming, G.R. (2019). Chlorophyll–carotenoid excitation energy transfer and charge transfer in Nannochloropsis oceanica for the regulation of photosynthesis. Proc. Natl. Acad. Sci. **116**: 3385–3390.

Passos, F., Uggetti, E., Carrère, H., and Ferrer, I. (2014). Pretreatment of microalgae to improve biogas production: a review. Bioresour Technol **172**: 403–412.

Pearlstein, R.M. (1982). EXCITON MIGRATION AND TRAPPING IN PHOTOSYNTHESIS. Photochem. Photobiol. **35**: 835–844.

Peers, G. (2011). Enhancement of biomass production by disruption of light energy dissipation pathways.

Peers, G., Truong, T.B., Ostendorf, E., Busch, A., Elrad, D., Grossman, A.R., Hippler, M., and Niyogi, K.K. (2009). An ancient light-harvesting protein is critical for the regulation of algal photosynthesis. Nature **462**: 518–521.

Perin, G., Bellan, A., Segalla, A., Meneghesso, A., Alboresi, A., and Morosinotto, T. (2015). Generation of random mutants to improve light-use efficiency of Nannochloropsis gaditana cultures for biofuel production. Biotechnol Biofuels. **8**: 161.

Perrine, Z., Negi, S., and Sayre, R.T. (2012). Optimization of photosynthetic light energy utilization by microalgae. Algal Res. **1**: 134–142.

Pesaresi, P., Pribil, M., Wunder, T., and Leister, D. (2011). Dynamics of reversible protein phosphorylation in thylakoids of flowering plants: The roles of STN7, STN8 and TAP38. Biochim. Biophys. Acta-Bioenergetics **1807**: 887–896.

Pesaresi, P., Sandonà, D., Giuffra, E., and Bassi, R. (1997). A single point mutation (E166Q) prevents dicyclohexylcarbodiimide binding to the photosystem II subunit CP29. FEBS Lett. **402**: 151–156.

Pietrzykowska, M., Suorsa, M., Semchonok, D.A., Tikkanen, M., Boekema, E.J., Aro, E.M., and Jansson, S. (2014). The light-harvesting chlorophyll a/b binding proteins Lhcb1 and Lhcb2 play complementary roles during state transitions in Arabidopsis. Plant Cell **26**: 3646–3660.

Pinnola, A. and Bassi, R. (2018). Molecular mechanisms involved in plant photoprotection. Biochem. Soc. Trans. **46**: 467–482.

Pittman, J.K., Dean, A.P., and Osundeko, O. (2011). The potenrial of sustainable algal biofuel production using wastewater resources. Bioresour Technol **102**: 17–25.

Polle, J., Kanakagiri, S., and Melis, A. (2003). tla1, a DNA insertional transformant of the green alga Chlamydomonas reinhardtii with a truncated light-harvesting chlorophyll antenna size. Planta **217**: 49–59.

Porra, R.J., Thompson, W.A., and Kriedemann, P.E. (1989). Determination of accurate

extinction coefficients and simultaneous equations for assaying chlorophylls a and b extracted with four different solvents: verification of the concentration of chlorophyll standards by atomic absorption spectroscopy. Biochim. Biophys. Acta: 384–394.

Pralon, T., Shanmugabalaji, V., Longoni, P., Glauser, G., Ksas, B., Collombat, J., Desmeules, S., Havaux, M., Finazzi, G., and Kessler, F. (2019). Plastoquinone homoeostasis by Arabidopsis proton gradient regulation 6 is essential for photosynthetic efficiency. Commun. Biol. **2**.

Prasad, A., Ferretti, U., Sedlaová, M., and Pospíšil, P. (2016). Singlet oxygen production in Chlamydomonas reinhardtii under heat stress. Sci. Reports 2016 61 **6**: 1–13.

Prasad, A. and Pospíšil, P. (2011). Linoleic acid-induced ultra-weak photon emission from chlamydomonas reinhardtii as a tool for monitoring of lipid peroxidation in the cell membranes. PLoS One **6**: e22345.

Prasad, A., Sedlářová, M., and Pospíšil, P. (2018). Singlet oxygen imaging using fluorescent probe Singlet Oxygen Sensor Green in photosynthetic organisms. Sci. Rep. **8**.

Prasil, O., Adir, N., and Ohad, I. (1992). Dynamics of photosystem II : mechanism of photoinhibition and recovery process. Top. Photosynth. **11**: 295–348.

Pribil, M., Labs, M., and Leister, D. (2014). Structure and dynamics of thylakoids in land plants. J. Exp. Bot. **65**: 1955–1972.

Puzorjov, A. and McCormick, A.J. (2020). Phycobiliproteins from extreme environments and their potential applications. J. Exp. Bot. **71**: 3827–3842.

Qin, X., Suga, M., Kuang, T., and Shen, J.R. (2015). Structural basis for energy transfer pathways in the plant PSI-LHCI supercomplex. Science (80-.). **348**: 989–995.

Ramel, F., Birtic, S., Ginies, C., Soubigou-Taconnat, L., Triantaphylidès, C., and Havaux, M. (2012). Carotenoid oxidation products are stress signals that mediate gene responses to singlet oxygen in plants. Proc Natl Acad Sci USA **109**: 5535–5540.

Rappaport, F., Béal, D., Joliot, A., and Joliot, P. (2007). On the advantages of using green light to study fluorescence yield changes in leaves. **1767**: 56–65.

Re, R., Pellegrini, N., Proteggente, A., Pannala, A., Yang, M., and Rice-Evans, C. (1999). Antioxidant activity applying an improved ABTS radical cation decolorization assay. Free Radic. Biol Med **26**: 1231–1237.

Redekop, P., Rothhausen, N.N., Rothhausen, N.N., Melzer, M., Mosebach, L., Dülger, E., Bovdilova, A., Caffarri, S., Hippler, M., and Jahns, P. (2020). PsbS contributes to photoprotection in Chlamydomonas reinhardtii independently of energy dissipation. **1861**: 148183.

Rhiel, E. and Mörschel, E. (1993). The atypical chlorophyll a/b/c light-harvesting complex of Mantoniella squamata: molecular cloning and sequence analysis. Mol. Gen. Genet. MGG 1993 2403 **240**: 403–413.

Richmond, A., Cheng-Wu, Z., and Zarmi, Y. (2003). Efficient use of strong light for high photosynthetic productivity: interrelationships between the optical path, the optimal

population density and cell-growth inhibition. Biomol. Eng. **20**: 229–236.

Ritchie, H. and Roser, M. (2013). Crop Yields. OurWorldInData.org.

Roach, T., Na, C.S., Stöggl, W., and Krieger-Liszkay, A. (2020). The non-photochemical quenching protein LHCSR3 prevents oxygen-dependent photoinhibition in Chlamydomonas reinhardtii. J. Exp. Bot. **71**: 2650–2660.

Rochaix, J.-D. and Bassi, R. (2019). LHC-like proteins involved in stress responses and biogenesis/repair of the photosynthetic apparatus. Biochem. J. **476**: 581–593.

Rochaix, J.D. (2007). Role of thylakoid protein kinases in photosynthetic acclimation. FEBS Lett. **581**: 2768–2775.

La Roche, J., Van Der Staay, G.W.M., Partensky, F., Ducret, A., Aebersold, R., Li, R., Golden, S.S., Hiller, R.G., Wrench, P.M., Larkum, A.W.D., and Green, B.R. (1996). Independent evolution of the prochlorophyte and green plant chlorophyll a/b light-harvesting proteins. Proc. Natl. Acad. Sci. **93**: 15244–15248.

Rodolfi, L., Zittelli, G.C., Bassi, N., Padovani, G., Biondi, N., Bonini, G., and Tredici, M.R. (2009). Microalgae for oil: strain selection, induction of lipid synthesis and outdoor mass cultivation in a low-cost photobioreactor. Biotechnol Bioeng **102**: 100–112.

Ruban, A. V. (2016). Nonphotochemical chlorophyll fluorescence quenching: Mechanism and effectiveness in protecting plants from photodamage. Plant Physiol. **170**: 1903–1916.

Ruban, A. V. (2017). Quantifying the efficiency of photoprotection. Philos. Trans. R. Soc. B Biol. Sci. **372**.

Ruban, A. V., Berera, R., Ilioaia, C., Van Stokkum, I.H.M., Kennis, J.T.M., Pascal, A.A., Van Amerongen, H., Robert, B., Horton, P., and Van Grondelle, R. (2007). Identification of a mechanism of photoprotective energy dissipation in higher plants. Nature **450**: 575–578.

Ruban, A. V., Johnson, M.P., and Duffy, C.D.P. (2012). The photoprotective molecular switch in the photosystem II antenna.

Ruban, A. V and Wilson, S. (2020). The Mechanism of Non-Photochemical Quenching in Plants: Localization and Driving Forces. Plant Cell Physiol. **00**: 1–10.

Sacharz, J., Giovagnetti, V., Ungerer, P., Mastroianni, G., and Ruban, A. V. (2017). The xanthophyll cycle affects reversible interactions between PsbS and light-harvesting complex II to control non-photochemical quenching. Nat. Plants **3**: 16225.

Sahni, P., Aggarwal, P., Sharma, S., and Singh, B. (2019). Nuances of microalgal technology in food and nutraceuticals: a review. Nutr. Food Sci. **49**: 866–885.

Sakowska, K. et al. (2018). Leaf and canopy photosynthesis of a chlorophyll deficient soybean mutant. Plant Cell Environ. **41**: 1427–1437.

Sandmann, G. (2021). Diversity and origin of carotenoid biosynthesis: its history of coevolution towards plant photosynthesis. New Phytol. **232**: 479–493.

Sane, P. V, Ivanov, A.G., Hurry, V., Huner, N.P., and Oquist, G. (2003). Changes in the redox

potential of primary and secondary electron-accepting quinones in photosystem II confer increased resistance to photoinhibition in low-temperature-acclimated Arabidopsis. Plant Physiol **132**: 2144–2151.

Schägger, H. and von Jagow, G. (1987). Tricine-sodium dodecyl sulfate-polyacrylamide gel electrophoresis for the separation of proteins in the range from 1 to 100 kDa. Anal.Biochem. **166**: 368–379.

Scheller, H.V., Jensen, P.E., Haldrup, A., Lunde, C., and Knoetzel, J. (2001). Role of subunits in eukaryotic Photosystem I. Biochim. Biophys. Acta - Bioenerg. **1507**: 41–60.

Schiphorst, C., Achterberg, L., Go, R., Koehorst, R., Bassi, R., Amerongen, H. Van, Osto, L.D., Wientjes, E., and Biotecnologie, D. (2021). The role of light-harvesting complex I in excitation energy transfer from LHCII to photosystem I in Arabidopsis.: 1–12.

Schiphorst, C. and Bassi, R. (2020). Chlorophyll-Xanthophyll Antenna Complexes: In Between Light Harvesting and Energy Dissipation.: 27–55.

Schneider, C.A., Rasband, W.S., and Eliceiri, K.W. (2012). NIH Image to ImageJ: 25 years of image analysis.

Scott, S.A., Davey, M.P., Dennis, J.S., Horst, I., Howe, C.J., Lea-Smith, D.J., and Smith, A.G. (2010). Biodiesel from algae: challenges and prospects. Curr Opin. Biotechnol **21**: 277–286.

Sforza, E., Simionato, D., Giacometti, G.M., Bertucco, A., and Morosinotto, T. (2012). Adjusted light and dark cycles can optimize photosynthetic efficiency in algae growing in photobioreactors. PLoS One **7**.

Shang, B., Zang, Y., Zhao, X., Zhu, J., Fan, C., Guo, X., and Zhang, X. (2019). Functional characterization of GhPHOT2 in chloroplast avoidance of Gossypium hirsutum. Plant Physiol. Biochem. **135**: 51–60.

Shao, N., Krieger-Liszkay, A., Schroda, M., and Beck, C.F. (2007). A reporter system for the individual detection of hydrogen peroxide and singlet oxygen: its use for the assay of reactive oxygen species produced in vivo. Plant J **50**: 475–487.

Shen, G., Canniffe, D.P., Ho, M.Y., Kurashov, V., van der Est, A., Golbeck, J.H., and Bryant, D.A. (2019a). Characterization of chlorophyll f synthase heterologously produced in Synechococcus sp. PCC 7002. Photosynth. Res. **140**: 77–92.

Shen, L., Huang, Z., Chang, S., Wang, W., Wang, J., Kuang, T., Han, G., Shen, J.-R., and Zhang, X. (2019b). Structure of a $C_2S_2M_2N_2$-type PSII–LHCII supercomplex from the green alga Chlamydomonas reinhardtii. Proc. Natl. Acad. Sci.: 201912462.

Shi, L.X., Hall, M., Funk, C., and Schröder, W.P. (2012). Photosystem II, a growing complex: Updates on newly discovered components and low molecular mass proteins. Biochim. Biophys. Acta - Bioenerg. **1817**: 13–25.

Shikanai, T. and Yamamoto, H. (2017). Contribution of Cyclic and Pseudo-cyclic Electron Transport to the Formation of Proton Motive Force in Chloroplasts. Mol. Plant **10**: 20–29.

Shumbe, L., Bott, R., and Havaux, M. (2014). Dihydroactinidiolide, a high light-induced beta-carotene derivative that can regulate gene expression and photoacclimation in

Arabidopsis. Mol Plant. **7**: 1248–1251.

Shumbe, L., D'Alessandro, S., Shao, N., Chevalier, A., Ksas, B., Bock, R., and Havaux, M. (2017). METHYLENE BLUE SENSITIVITY 1 (MBS1) is required for acclimation of Arabidopsis to singlet oxygen and acts downstream of beta-cyclocitral. Plant Cell Env. **40**: 216–226.

Simpson, D.J. (1983). Freeze-fracture studies on barley plastid membranes. VI. Location of the P700-chlorophyll a-protein 1. Eur.J.Cell Biol. **31**: 305–314.

Simpson, D.J. (1979). Freeze-Fracture Studies on Barley Plastid Membranes .3. Location of the Light-Harvesting Chlorophyll-Protein. Carlsberg Res. Commun. **44**: 305–336.

Simpson, D.J. (1982). Freeze-fracture studies on barley plastid membranes V.viridis-n 34, a photosystem I mutant. Carlsb. Res. Commun. 1982 474 **47**: 215–225.

Simpson, D.J. and Robinson, S.P. (1984). Freeze-Fracture Ultrastructure of Thylakoid Membranes in Chloroplasts from Manganese-Deficient Plants. Plant Physiol. **74**: 735–741.

Simpson, D.J., Vallon, O., and von Wettstein, D. (1989). Freeze-fracture studies on barley plastid membranes: VIII. In viridis-115, a mutant completely lacking Photosystem II, oxygen evolution enhancer 1 (OEE1) and the α-subunit of cytochrome b-559 accumulate in appressed thylakoids. Biochim. Biophys. Acta - Bioenerg. **975**: 164–174.

Sivakumar, G., Xu, J., Thompson, R.W., Yang, Y., Randol-Smith, P., and Weathers, P.J. (2012). Integrated green algal technology for bioremediation and biofuel. Biores Technol **107**: 1–9.

Slattery, R.A. and Ort, D.R. (2015). Photosynthetic energy conversion efficiency: Setting a baseline for gauging future improvements in important food and biofuel crops. Plant Physiol. **168**: 383–392.

Slavov, C., Reus, M., and Holzwarth, A.R. (2013). Two Different Mechanisms Cooperate In The Desiccation-Induced Excited State Quenching In Parmelia Lichen. J. Phys. Chem. B **117**: 11326–11336.

Snow, A.A. and Smith, V.H. (2012). Genetically Engineered Algae for Biofuels: A Key Role for Ecologists. Bioscience **62**: 765–768.

Solovchenko, A., Khozin-Goldberg, I., Recht, L., and Boussiba, S. (2011). Stress-induced changes in optical properties, pigment and fatty acid content of Nannochloropsis sp: implications for non-destructive assay of total fatty acids. Mar. Biotechnol. **13**: 527–535.

Son, M., Pinnola, A., and Schlau-Cohen, G.S. (2020). Zeaxanthin independence of photophysics in light-harvesting complex II in a membrane environment. Biochim. Biophys. Acta - Bioenerg. **1861**.

Sonoike, K. (2011). Photoinhibition of Photosystem I. Physiol Plant **142_ _**: 56–64.

Standfuss, R., van Scheltinga, A.C.T., Lamborghini, M., and Kuhlbrandt, W. (2005). Mechanisms of photoprotection and nonphotochemical quenching in pea light-harvesting complex at 2.5A resolution. Embo J. **24**: 919–928.

Steen, C.J., Morris, J.M., Short, A.H., Niyogi, K.K., and Fleming, G.R. (2020). Complex Roles of

PsbS and Xanthophylls in the Regulation of Nonphotochemical Quenching in Arabidopsis thaliana under Fluctuating Light. J. Phys. Chem. B **124**: 10311–10325.

Stephenson, P.G., Moore, C.M., Terry, M.J., Zubkov, M. V., and Bibby, T.S. (2011). Improving photosynthesis for algal biofuels: toward a green revolution. Trends Biotechnol **29**: 615–623.

Strain, H.H., Thomas, M.R., and Katz, J.J. (1963). Spectral absorption properties of ordinary and fully deuteriated chlorophylls a and b. Biochim. Biophys. Acta **75**: 306–311.

Strasser, R.J., Srivastava, A., and Govindjee (1995). Polyphasic chlorophyll a fluorescence transient in plants and cyanobacteria. Photochem.Photobiol. **61**: 32–42.

Su, X. et al. (2017). Structure and assembly mechanism of plant C2S2M2-type PSII-LHCII supercomplex. Science (80-.). **357**: 815–820.

Su, X., Cao, D., Pan, X., Shi, L., Liu, Z., Dall'Osto, L., Bassi, R., Zhang, X., and Li, M. (2022). Supramolecular assembly of chloroplast NADH dehydrogenase-like complex with photosystem I from Arabidopsis thaliana. Mol. Plant.

Sueoka, N. (1960). MITOTIC REPLICATION OF DEOXYRIBONUCLEIC ACID IN CHLAMYDOMONAS REINHARDI. Proc. Natl. Acad. Sci.

Suetsugu, N. and Wada, M. (2007). Chloroplast photorelocation movement mediated by phototropin family proteins in green plants. Biol.Chem. **388**: 927–935.

Suga, M., Ozawa, S.I., Yoshida-Motomura, K., Akita, F., Miyazaki, N., and Takahashi, Y. (2019). Structure of the green algal photosystem I supercomplex with a decameric light-harvesting complex I. Nat. Plants **5**: 626–636.

Sun, X.M., Geng, L.J., Ren, L.J., Ji, X.J., Hao, N., Chen, K.Q., and Huang, H. (2018). Influence of oxygen on the biosynthesis of polyunsaturated fatty acids in microalgae. Bioresour Technol **250**: 868–876.

Suorsa, M., Jarvi, S., Grieco, M., Nurmi, M., Pietrzykowska, M., Rantala, M., Kangasjarvi, S., Paakkarinen, V., Tikkanen, M., Jansson, S., and Aro, E.M. (2012). Proton Gradient Regulation5 Is Essential for Proper Acclimation of Arabidopsis Photosystem I to Naturally and Artificially Fluctuating Light Conditions. Plant Cell **24**: 2934–2948.

Sztatelman, O., Waloszek, A., Banas, A.K., and Gabrys, H. (2010). Photoprotective function of chloroplast avoidance movement: _in vivo_ chlorophyll fluorescence study. J.Plant Physiol. **167**: 709–716.

Takahashi, S., Milward, S.E., Milward, D.Y.F., Chow, W.S., and Badger, M.R. (2009). How Does Cyclic Electron Flow Alleviate Photoinhibition in Arabidopsis? Plant Physiol. **149**: 1560–1567.

Takaichi, S. (2011). Carotenoids in algae: Distributions, biosyntheses and functions. Mar. Drugs **9**: 1101–1118.

Telfer, A. (2002). What is carotene doing in the photosystem II reaction centre? Philos. Trans. R. Soc. London. Ser. B Biol. Sci. **357**: 1431–1440.

Theis, J. and Schroda, M. (2016). Revisiting the photosystem II repair cycle. https://doi.org/10.1080/15592324.2016.1218587 **11**.

Thorvaldsdóttir, H., Robinson, J.T., and Mesirov, J.P. (2013). Integrative Genomics Viewer (IGV): high-performance genomics data visualization and exploration. Brief. Bioinform. **14**: 178–192.

Tibiletti, T., Auroy, P., Peltier, G., and Caffarri, S. (2016). Chlamydomonas reinhardtii PsbS protein is functional and accumulates rapidly and transiently under high light. Plant Physiol. **171**: 2717–2730.

Tikkanen, M. and Grebe, S. (2018). Switching off photoprotection of photosystem I – a novel tool for gradual PSI photoinhibition. Physiol. Plant. **162**: 156–161.

Tikkanen, M., Grieco, M., Nurmi, M., Rantala, M., Suorsa, M., and Aro, E.M. (2012). Regulation of the photosynthetic apparatus under fluctuating growth light. Philos. Trans. R. Soc. B Biol. Sci. **367**: 3486–3493.

Tjus, S.E., Møller, B.L., and Scheller, H.V. (1998). Photosystem I Is an Early Target of Photoinhibition in Barley Illuminated at Chilling Temperatures. Plant Physiol. **116**: 755–764.

Tjus, S.E., Scheller, H. V., Andersson, B., and Møller, B.L. (2001). Active Oxygen Produced during Selective Excitation of Photosystem I Is Damaging Not Only to Photosystem I, But Also to Photosystem II. Plant Physiol. **125**: 2007–2015.

Tokutsu, R., Fujimura-Kamada, K., Yamasaki, T., Matsuo, T., and Minagawa, J. (2019). Isolation of photoprotective signal transduction mutants by systematic bioluminescence screening in Chlamydomonas reinhardtii. Sci. Rep. **9**.

Tokutsu, R., Iwai, M., and Minagawa, J. (2009). CP29, a monomeric light-harvesting complex II protein, is essential for state transitions in Chlamydomonas reinhardtii. J. Biol. Chem. **284**: 7777–7782.

Towbin, H., Staehelin, T., and Gordon, J. (1979). Electrophoretic transfer of proteins from polyacrylamide gels to nitrocellulose sheets: Procedure and some applications. Proc. Natl. Acad. Sci. **76**: 4350–4354.

Townsend, A.J., Saccon, F., Giovagnetti, V., Wilson, S., Ungerer, P., and Ruban, A. V. (2018). The causes of altered chlorophyll fluorescence quenching induction in the Arabidopsis mutant lacking all minor antenna complexes. Biochim. Biophys. Acta - Bioenerg. **1859**: 666–675.

Trebst, A. and Depka, B. (1997). Role of carotene in the rapid turnover and assembly of photosystem II in Chlamydomonas reinhardtii. FEBS Lett. **400**: 359–362.

Tredici, M.R. (2014). Photobiology of microalgae mass cultures: understanding the tools for the next green revolution. http://dx.doi.org/10.4155/bfs.09.10 **1**: 143–162.

Tremolieres, A., Dainese, P., and Bassi, R. (1994). Heterogenous lipid distribution among chlorophyll-binding proteins of photosystem II in maize mesophyll chloroplasts. Eur.J.Biochem. **221**: 721–730.

Treves, H., Raanan, H., Finkel, O.M., Berkowicz, S.M., Keren, N., Shotland, Y., and Kaplan, A. (2013). A newly isolated Chlorella sp. from desert sand crusts exhibits a unique resistance to excess light intensity. FEMS Microbiol. Ecol. **86**: 373–380.

Triantaphylidès, C., Krischke, M., Hoeberichts, F.A., Ksas, B., Gresser, G., Havaux, M., Van Breusegem, F., and Mueller, M.J. (2008). Singlet oxygen is the major reactive oxygen species involved in photooxidative damage to plants. Plant Physiol **148**: 960–968.

Trissl, H.W. and Wilhelm, C. (1993). Why do thylakoid membranes from higher plants form grana stacks? Trends Biochem. Sci. **18**: 415–419.

Tsikas, D. (2017). Assessment of lipid peroxidation by measuring malondialdehyde (MDA) and relatives in biological samples: Analytical and biological challenges. Anal. Biochem. **524**: 13–30.

Vallon, O., Bulte, L., Dainese, P., Olive, J., Bassi, R., and Wollman, F.A. (1991). Lateral redistribution of cytochrome b6/f complexes along thylakoid membranes upon state transitions. Proc.Natl.Acad.Sci.U.S.A **88**: 8262–8266.

Vaser, R., Adusumalli, S., Leng, S.N., Sikic, M., and Ng, P.C. (2015). SIFT missense predictions for genomes. Nat. Protoc. 2015 111 **11**: 1–9.

Vavilin, D. V and Ducruet, J.-M. (1998). The origin of 115-130 degrees C thermoluminescence bands in chlorophyll-containing material. Photochem.Photobiol. **68**: 191–198.

Vecchi, V., Barera, S., Bassi, R., and Dall'Osto, L. (2020). Potential and challenges of improving photosynthesis in algae. Plants **9**.

Wada, M. (2013). Chloroplast movement. Plant Sci. **210**: 177–182.

Wada, M., Kagawa, T., and Sato, Y. (2003). Chloroplast movement. Ann.Rev.Plant Biol. **54**: 455–468.

Wada, M. and Kong, S.G. (2018). Actin-mediated movement of chloroplasts. J. Cell Sci. **131**.

Wahadoszamen, M., Berera, R., Ara, A.M., Romero, E., and Van Grondelle, R. (2012). Identification of two emitting sites in the dissipative state of the major light harvesting antenna. Phys. Chem. Chem. Phys. **14**: 759–766.

Wakabayashi, K., Misawa, Y., Mochiji, S., and Kamiya, R. (2011). Reduction-oxidation poise regulates the sign of phototaxis in Chlamydomonas reinhardtii. Proc. Natl. Acad. Sci. U. S. A. **108**: 11280–11284.

Walters, R.G., Ruban, A. V., and Horton, P. (1996). Identification of proton-active residues in a higher plant light-harvesting complex. Proc. Natl. Acad. Sci. U. S. A. **93**: 14204–14209.

Ware, M.A., Belgio, E., and Ruban, A. V. (2015a). Photoprotective capacity of non-photochemical quenching in plants acclimated to different light intensities. Photosynth. Res. **126**: 261–274.

Ware, M.A., Giovagnetti, V., Belgio, E., and Ruban, A. V. (2015b). PsbS protein modulates non-photochemical chlorophyll fluorescence quenching in membranes depleted of photosystems. J. Photochem. Photobiol. B Biol. **152**: 301–307.

Wase, N., Black, P.N., Stanley, B.A., and Dirusso, C.C. (2014). Integrated quantitative analysis of nitrogen stress response in Chlamydomonas reinhardtii using metabolite and protein profiling. J. Proteome Res. **13**: 1373–1396.

Wei, X., Su, X., Cao, P., Liu, X., Chang, W., Li, M., Zhang, X., and Liu, Z. (2016). Structure of spinach photosystem II-LHCII supercomplex at 3.2 Å resolution. Nature **534**: 69–74.

Weyer, K.M., Bush, D.R., Darzins, A., and Willson, B.D. (2010). Theoretical maximum algal oil production. Bioenergy Res. **3**: 204–213.

Whatley, J.M. and Whatley, F.R. (1981). CHLOROPLAST EVOLUTION. New Phytol. **87**: 233–247.

Whitney, S.M., Houtz, R.L., and Alonso, H. (2011). Advancing Our Understanding and Capacity to Engineer Nature's CO2-Sequestering Enzyme, Rubisco. Plant Physiol. **155**: 27–35.

Wientjes, E., Drop, B., Kouřil, R., Boekema, E.J., and Croce, R. (2013). During State 1 to State 2 Transition in Arabidopsis thaliana, the Photosystem II Supercomplex Gets Phosphorylated but Does Not Disassemble *. J. Biol. Chem. **288**: 32821–32826.

Wientjes, E., Roest, G., and Croce, R. (2012). From red to blue to far-red in Lhca4: How does the protein modulate the spectral properties of the pigments? Biochim. Biophys. Acta - Bioenerg. **1817**: 711–717.

Wietrzynski, W., Schaffer, M., Tegunov, D., Albert, S., Kanazawa, A., Plitzko, J.M., Baumeister, W., and Engel, B.D. (2020). Charting the native architecture of Chlamydomonas thylakoid membranes with single-molecule precision. Elife **9**: 1–18.

Wilhelm, C., Krämer, P., and Lenartz-Weiler, I. (1989). The energy distribution between the photosystems and light-induced changes in the stoichiometry of system I and II reaction centers in the chlorophyll b-containing alga Mantoniella squamata (Prasinophyceae). Photosynth. Res. 1989 203 **20**: 221–233.

Wilk, L., Grunwald, M., Liao, P.N., Walla, P.J., and Kühlbrandt, W. (2013). Direct interaction of the major light-harvesting complex II and PsbS in nonphotochemical quenching. Proc. Natl. Acad. Sci. U. S. A. **110**: 5452–5456.

Wilson, S. and Ruban, A. V. (2020). Rethinking the influence of chloroplast movements on non-photochemical quenching and photoprotection. Plant Physiol.: pp.00549.2020.

de Wit, M., Keuskamp, D.H., Bongers, F.J., Hornitschek, P., Gommers, C.M.M., Reinen, E., Martínez-Cerón, C., Fankhauser, C., and Pierik, R. (2016). Integration of Phytochrome and Cryptochrome Signals Determines Plant Growth during Competition for Light. Curr. Biol. **26**: 3320–3326.

Woittiez, L.S., van Wijk, M.T., Slingerland, M., van Noordwijk, M., and Giller, K.E. (2017). Yield gaps in oil palm: A quantitative review of contributing factors. Eur. J. Agron. **83**: 57–77.

Wu, T., Ye, L., Zhao, D., Li, S., Li, Q., Zhang, B., Bi, C., and Zhang, X. (2017). Membrane engineering - A novel strategy to enhance the production and accumulation of β-carotene in Escherichia coli. Metab. Eng. **43**: 85–91.

Xie, Y., Li, J., Ho, S.H., Ma, R., Shi, X., Liu, L., and Chen, J. (2020). Pilot-scale cultivation of Chlorella sorokiniana FZU60 with a mixotrophy/photoautotrophy two-stage strategy for efficient lutein production. Bioresour. Technol. **314**.

Yang, Y. and Gao, K. (2003). Effects of CO2 concentrations on the freshwater microalgae, Chlamydomonas reinhardtii, Chlorella pyrenoidosa and Scenedesmus obliquus (Chlorophyta). J. Appl. Phycol. 2003 155 **15**: 379–389.

Ye, Z.-P., Suggett, D.J., Robakowski, P., and Kang, H.-J. (2013). A mechanistic model for the photosynthesis-light response based on the photosynthetic electron transport of photosystem II in C 3 and C 4 species. New Phytol. **199**: 110–120.

Yen, H.-W., Hu, I.-C., Chen, C.-Y., Ho, S.-H., and Lee, D.-J. (2013). Microalgae-based biorefinery – From biofuels to natural products. Bioresour. Technol. **135**: 166–174.

Yilancioglu, K., Cokol, M., Pastirmaci, I., Erman, B., and Cetiner, S. (2014). Oxidative stress is a mediator for increased lipid accumulation in a newly isolated Dunaliella salina strain. PLoS One **9**: e91957.

Zamzam, N., Rakowski, R., Kaucikas, M., Dorlhiac, G., Viola, S., Nürnberg, D.J., Fantuzzi, A., Rutherford, A.W., and van Thor, J.J. (2020). Femtosecond visible transient absorption spectroscopy of chlorophyll-f-containing photosystem II. Proc. Natl. Acad. Sci. U. S. A. **117**: 23158–23164.

Zhang, S., Apel, K., and Kim, C. (2014). Singlet oxygen-mediated and EXECUTER-dependent signalling and acclimation of Arabidopsis thaliana exposed to light stress. Philosophical transactions of the Royal Society of London. Biol Sci **369**: 20130227.

Zhang, S. and Scheller, H. V (2004). Photoinhibition of Photosystem I at chilling temperature and subsequernt recovery in Arabidopsis thaliana. Plant Cell Physiol. **45**: 1595–1602.

Zhang, X., Henriques, R., Lin, S.-S., Niu, Q.-W., Chua, N.-H., Niu, W.-W., Chua, N.-H., Niu, Q.-W., and Chua, N.-H.H.N.-H. (2006). Agrobacterium-mediated transformation of Arabidopsis thaliana using the floral dip method. Nat. Protoc. **1**: 641–646.

Zhi, X., Han, Y., Mao, S., Wang, G., Feng, L., Yang, B., Fan, Z., Du, W., Lu, J., and Li, Y. (2014). Light spatial distribution in the canopy and crop development in cotton. PLoS One **9**: 113409.

Zhu, X.-G., Long, S.P., and Ort, D.R. (2010). Improving Photosynthetic Efficiency for Greater Yield. Annu. Rev. Plant Biol. **61**: 235–261.

Zhu, X.G., Long, S.P., and Ort, D.R. (2008). What is the maximum efficiency with which photosynthesis can convert solar energy into biomass? Curr.Opinion Biotech. **19_ _**: 153–159.

Zhu, X.G., Ort, D.R., Whitmarsh, J., and Long, S.P. (2004). The slow reversibility of photosystem II thermal energy dissipation on transfer from high to low light may cause large losses in carbon gain by crop canopies: a theoretical analysis. **55**: 1167–1175.

Zimny, T., Sowa, S., Tyczewska, A., and Twardowski, T. (2019). Certain new plant breeding techniques and their marketability in the context of EU GMO legislation – recent developments. N. Biotechnol. **51**: 49–56.